Iterative Source-Channel Decoding: Design and Optimization for Heterogeneous Networks

Von der Fakultät für Elektrotechnik und Informationstechnik
der Rheinisch-Westfälischen Technischen Hochschule Aachen
zur Erlangung des akademischen Grades eines
Doktors der Ingenieurwissenschaften genehmigte Dissertation

vorgelegt von

Diplom-Ingenieur

Laurent Schmalen

aus Luxemburg, Luxemburg

Berichter: Universitätsprofessor Dr.-Ing. Peter Vary
Universitätsprofessor Dr.-Ing. Gerd Ascheid

Tag der mündlichen Prüfung: 29. April 2011

AACHENER BEITRÄGE ZU DIGITALEN NACHRICHTENSYSTEMEN

Herausgeber:

Prof. Dr.-Ing. Peter Vary
Institut für Nachrichtengeräte und Datenverarbeitung
Rheinisch-Westfälische Technische Hochschule Aachen
Muffeter Weg 3a
52074 Aachen
Tel.: 0241-80 26 956
Fax.: 0241-80 22 186

Bibliografische Information der Deutschen Bibliothek
Die Deutsche Bibliothek verzeichnet diese Publikation in der Deutschen Nationalbibliografie; detaillierte bibliografische Daten sind im Internet über http://dnb.ddb.de abrufbar

1. Auflage Aachen:
Wissenschaftsverlag Mainz in Aachen
(Aachener Beiträge zu digitalen Nachrichtensystemen, Band 29)
ISSN 1437-6768
ISBN 3-86130-268-3

Wissenschaftsverlag Mainz
Süsterfeldstr. 83, 52072 Aachen
Tel.: 02 41 / 2 39 48 oder 02 41 / 87 34 34
Fax: 02 41 / 87 55 77
www.Verlag-Mainz.de

Herstellung: Druckerei Mainz GmbH,
Süsterfeldstr. 83, 52072 Aachen
Tel.: 02 41 / 87 34 34; Fax: 02 41 / 87 55 77
www.Druckservice-Aachen.de

Gedruckt auf chlorfrei gebleichtem Papier

"D 82 (Diss. RWTH Aachen University, 2011)"

Acknowledgments

This thesis was written during my time as research assistant at the *Institute of Communication Systems and Data Processing (IND)* at the *Rheinisch-Westfälische Technische Hochschule Aachen (RWTH Aachen University)*. I would like to take the opportunity to thank the people who contributed to the success of this work.

At first, I am deeply grateful to my supervisor Prof. Dr.-Ing. Peter Vary for his continuous support of my work by numerous ideas and suggestions and for encouraging me in my scientific interests. I am also indebted to Prof. Dr.-Ing. Gerd Ascheid for being the co-supervisor of this thesis and showing much interest in my work.

Furthermore, I want to thank all my colleagues for providing an enjoyable atmosphere and a pleasant working environment. I am particularly thankful to Dr.-Ing. Marc Adrat and Dr.-Ing. Thorsten Clevorn. The discussions with them have always been an indispensable source of inspiration. I also owe special thanks to Dr.-Ing. Christiane Antweiler, Dipl.-Ing. Moritz Beermann, Dipl.-Ing. Tobias Breddermann, Dipl.-Ing. Benedikt Eschbach, Dipl.-Ing. Matthias Pawig, and Dipl.-Ing. Matthias Rüngeler. Their proof-reading of parts of the manuscript resulted in many valuable improvements.

I would like to express my appreciation to the students who made significant contributions to my work. In particular, I would like to mention Dipl.-Ing. Yang Cui, Dipl.-Ing. Ulrich Engel, M. Sc. Enrique Monzó, Dipl.-Ing. Jan Reimes, Dipl.-Ing. Thomas Schlien, Dipl.-Ing. Matthias Tschauner, and Dipl.-Ing. Martin Volmer.

I would also like to thank the European Union for financing most of the work of this thesis and for giving me the opportunity to work in an international environment within the *FlexCode* project. I also wish to express my appreciation to Prof. W. Bastiaan Kleijn and his team at KTH Stockholm for many fruitful discussions, especially during my stay in their lab.

Finally, I want to thank my parents Aloyse and Mariette Schmalen for their continuous support over the years. I would also like to thank Joffrey, Julien, Luken, Michel, Philippe, and Yann for some unforgettable moments during my thesis. Dear Angela, thank you for your love, encouragement, patience, and understanding.

Stuttgart, May 2011 Laurent Schmalen

Abstract

The source-channel separation theorem postulated by Shannon has influenced the design of communication systems for multimedia content over the last decades: Source encoding and channel encoding are performed as two separate steps. However, the conditions of the separation theorem are almost never fulfilled in practical systems; a joint consideration of source and channel coding can thus be of special interest. Such a joint consideration with iterative decoding based on the Turbo principle has been found to be especially advantageous with regard to the realization of efficient multimedia communication systems.

In the first part of this thesis, the concept of Iterative Source-Channel Decoding (ISCD) is fundamentally extended and optimized, especially in view of a possible practical implementation. New design guidelines and optimization criteria lead to a flexible and versatile system design. Special care is taken to optimize the components such that a residual error rate, which shall be as low as possible, results. Besides an extended, iterative receiver architecture leading to an improved exploitation of the correlation between consecutive frames, a simple yet effective stopping criterion is presented. This stopping criterion leads to an ISCD system with incremental redundancy transmission. It is additionally shown how a complexity-reduced ISCD receiver can be designed by employing a novel way of signal quantization.

While the first part of this thesis treats the source encoding as given, it is consequently incorporated into the system design in the second part. As a novelty, an efficient method for the compression of parameter sources is introduced. This method shows the advantage of an easy adaptivity to varying transmission conditions. It is additionally shown how the ISCD concept can be applied for decoding *multiple descriptions* in order to improve the signal reconstruction quality in the presence of bit errors and packet losses. Besides optimized system designs, an innovative concept for the robust packet-based transmission of correlated source signals is presented.

All variants and proposals are thoroughly analyzed using theoretical methods, by convergence analysis, or with computer simulations. The contribution of this thesis is the improvement of the error robustness and the spectral efficiency of future digital multimedia communication systems.

Contents

Notations, Symbols & Abbreviations

Notations

A general baseband block diagram of the transmitter considered in most systems throughout this thesis is depicted in the following figure.

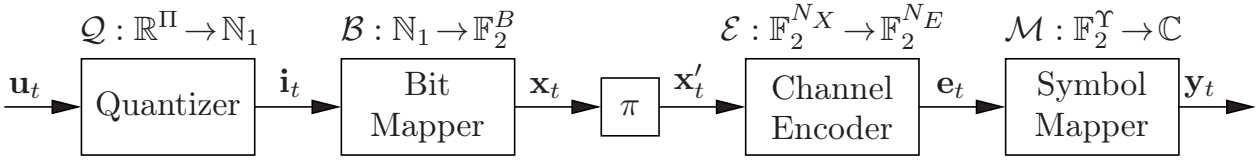

This is a simplified block diagram which highlights the connection of the different constituent blocks in the system considered in the bigger part of this thesis. The aim of this block diagram is to briefly introduce the utilized notation. The block diagram operates on a frame-by-frame index, with the discrete time (frame) index t. At time t, a vector of real-valued source parameters $\mathbf{u}_t$ is partitioned into Π-dimensional vectors $\mathbf{v}$ which are quantized by the quantizer $\mathcal{Q}$ to an index $i_{t,k}$, with $k \in \{1, \ldots, N_I\}$ denoting the position within the frame. All the quantizer indices of a frame are grouped in the vector $\mathbf{i}_t \in \mathbb{N}_1^{N_I}$. A bit pattern consisting of B bits is assigned to each quantizer index by the bit mapping function $\mathcal{B}$. The resulting bit stream is denoted $\mathbf{x}_t \in \mathbb{F}_2^{N_X}$, with $N_X = BN_I$. After interleaving by the permutation π, the interleaved vector $\mathbf{x}'_t$ results. The channel encoder $\mathcal{E}$ encodes $\mathbf{x}'_t$ to $\mathbf{e}_t \in \mathbb{F}_2^{N_E}$. In most cases, the size N_E of $\mathbf{e}_t$ is larger than the size N_X of $\mathbf{x}_t$ (and $\mathbf{x}'_t$). Prior to transmission over the channel, groups of Υ bits are mapped by the symbol mapping function to complex base band signal space points $y \in \mathbb{C}$. All signal space points of a frame are grouped in the vector $\mathbf{y}_t \in \mathbb{C}^{N_Y}$. Note that in the literature, the mapping function $\mathcal{M}$ is also commonly referred to as *modulation*.

Probabilities and Information Theoretical Values

Stochastical and information theoretical operators are denoted by sans serif letters.

X	random variables are represented by upper case letters
$\mathsf{Pr}\{X = x\}$	probability that the discrete random variable X takes on the value x
$\mathsf{P}(x)$	abbreviation for $\mathsf{Pr}\{X = x\}$, if there is no risk of confusion
$\mathsf{P}(x\|y)$	conditional probability that $X = x$, given the observation $Y = y$ abbreviation for $\mathsf{Pr}\{X = x\|Y = y\}$
$\mathsf{P}(x, y)$	joint probability, abbreviation for $\mathsf{Pr}\{X = x, Y = y\}$
$\mathsf{p}_X(x)$	probability density function of the (continuous) random variable X
$\mathsf{p}(x)$	abbreviation for $\mathsf{p}_X(x)$, if there is no risk of confusion
$\mathsf{p}(x\|y)$	conditional probability density function of X, given $Y = y$, abbrevation for $\mathsf{p}_{X\|Y}(x\|y)$
$\mathsf{p}(x, y)$	joint probability density function, abbreviation of $\mathsf{p}_{X,Y}(x, y)$
$\mathcal{N}$	the Gaussian distribution (mean μ, variance σ^2) is denoted by $\mathcal{N}(\mu, \sigma^2)$
$\sim$	distribution of a random variable, e.g., $X \sim \mathcal{N}(0, 1)$
$\mathsf{E}\{X\}$	expected value of random variable X, $\mathsf{E}\{X\} = \sum_x x \cdot \mathsf{P}(x)$ (X discrete) or $\mathsf{E}\{X\} = \int x \cdot \mathsf{p}(x)\,\mathrm{d}x$ (X continuous)
$\mathsf{H}(X)$	entropy of discrete random variable X, $\mathsf{H}(X) = -\sum_x \mathsf{P}(x) \operatorname{ld} \mathsf{P}(x)$
$\mathsf{H}(X, Y)$	joint entropy of discrete random variables X and Y, $\mathsf{H}(X, Y) = \sum_x \sum_y \mathsf{P}(x, y) \operatorname{ld} \mathsf{P}(x, y)$
$\mathsf{H}(X\|Y)$	conditional entropy of discrete random variable X given Y, $\mathsf{H}(X\|Y) = -\sum_y P(y) \cdot \mathsf{H}(X\|Y = y) = -\sum_x \sum_y \mathsf{P}(x, y) \operatorname{ld} \mathsf{P}(x\|y)$
$\mathsf{I}(X; Y)$	mutual information between X and Y, $\mathsf{I}(X; Y) = \mathsf{H}(X) - \mathsf{H}(X\|Y)$

Sets and Intervals

$\mathbb{X}$	blackboard bold letters are used to represent sets
$\|\mathbb{X}\|$	cardinality of a set $\mathbb{X}$, i.e., number of elements of $\mathbb{X}$
$\{x, y, \ldots\}$	set containing the elements $x, y, \ldots$, separated by commas
$[x; y]$	interval of all numbers between x and y with x and y included
$(x; y]$	interval of all numbers between x and y excluding x and including y
$[x; y)$	interval of all numbers between x and y including x and excluding y
$(x; y)$	interval of all numbers between x and y with x and y excluded

Vectors and Matrices

$\mathbf{x}$	Bold lower case letters are used to represent vectors
$\mathbf{X}$	Bold upper case letters are used to represent matrices
$\mathbf{x}^T$	Transposed vectors (and matrices) are indicated by a superscript ^{T}
$\dim \mathbf{X}$	dimension of a vector or matrix, format $\dim \mathbf{X} = \text{rows} \times \text{columns}$
$\|\mathbf{x}\|_0$	zero norm of $\mathbf{x}$, i.e., number of non-zero elements in $\mathbf{x}$
$\|\mathbf{x}\|_2$	Euclidean norm of $\mathbf{x}$, i.e., $\mathbf{x}^T\mathbf{x}$ if $\mathbf{x}$ is a column vector

Miscellaneous Mathematical Functions and Operators

$\mathcal{F}$	functions are denoted by calligraphic letters unless stated otherwise
$\circ$	composition of functions, $(\mathcal{G} \circ \mathcal{F})(x) = \mathcal{G}(\mathcal{F}(x))$
$\lfloor x \rfloor$	largest integer less than or equal to x
$\lceil x \rceil$	smallest integer greater than or equal to x
$\times$	the $\times$ operator replaced the $\cdot$ multiplication in multiline equations
$\wedge$	logical and
$\lessapprox$	approximately less than
$\gtrapprox$	approximately greather than
$\lessgtr$	less than, equal, or greather than
e	Euler constant, $\mathrm{e} \approx 2.7182$
exp	exponential function, $\exp(x) = \mathrm{e}^x$
erf	error function, $\mathrm{erf}(x) = \frac{2}{\sqrt{\pi}} \int_0^x \mathrm{e}^{-\chi^2} \, \mathrm{d}\chi$
erfc	complementary error function, $\mathrm{erfc}(x) = 1 - \mathrm{erf}(x)$
ln	natural logarithm, i.e., logarithm to the base e
ld	logarithm to the base 2, $\mathrm{ld}(x) = \log_2(x) = \frac{\ln(x)}{\ln(2)}$
lg	logarithm to the base 10, $\mathrm{lg}(x) = \log_{10}(x) = \frac{\ln(x)}{\ln(10)}$
$\max^\star$	Jacobian logarithm, $\max^\star(x, y) \doteq \ln(\mathrm{e}^x + \mathrm{e}^y) = \max(x, y) + \ln(1 + \mathrm{e}^{-\lvert x-y \rvert})$
mod	the function mod computes the remainder, i.e., $x \bmod n = x - n \cdot \lfloor \frac{x}{n} \rfloor$
rnd	rounding operator
$\binom{n}{k}$	binomial coefficient, $\binom{n}{k} = \frac{n!}{k!(n-k)!}$
*	a superscript star indicates the SDSD variables in the MDBM case
$\hat{x}$	estimated values are usually indicated by a hat

List of Principal Symbols

Latin Symbols

$\mathbf{0}$	matrix containing 0s at all positions
$\mathbf{1}$	matrix containing 1s at all positions
a	fading coefficient or attenuation factor of the channel model
A	auxiliary variable used in the description of SDSD
$\mathcal{A}(\cdot)$	area under an EXIT characteristic C, i.e., $\int_0^1 \mathsf{C}(\mathsf{I}^{[\mathrm{apr}]})\,\mathrm{d}\mathsf{I}^{[\mathrm{apr}]}$
b	single bit of the quantizer bit pattern
$b^\star$	single bit of a super bit pattern in multi-dimensional bit mappings
$b^{[\mathrm{D},\nu]}$	single bit of a bit pattern $\mathbf{b}^{[\mathrm{D},\nu]}$ of description ν (MDC case)
$b^{[\mathrm{NB}]}$	single bit of a bit pattern after natural binary bit mapping $\mathcal{B}^{[\mathrm{NB}]}$
$\mathbf{b}$	bit pattern for a quantizer index i, $\mathbf{b} = \mathcal{B}(i)$
$\mathbf{b}^\star$	super bit pattern for a quantizer super index $i^\star$
$\mathbf{b}^{[\mathrm{D},\nu]}$	bit pattern for a quantizer index i for description ν (MDC case)
$\mathbf{b}^{[\mathrm{NB}]}$	bit pattern after natural binary bit mapping $\mathcal{B}^{[\mathrm{NB}]}$
$\mathbf{b}^{[\mathrm{NB}]\star}$	super bit pattern after natural binary bit mapping $\mathcal{B}^{[\mathrm{NB}]}$
$\mathbf{b}^{[\mathrm{H},\theta]}$	bit pattern for a quantizer index i onb HARQ layer θ
B	number of bits that compose the bit pattern $\mathbf{b}$
$B^\star$	number of bits composing the super bit pattern $\mathbf{b}^\star$ of a super index $i^\star$
$\bar{B}$	average number of bits (per frame) composing the bit pattern $\mathbf{b}$
$B^{[\mathrm{H},\theta]}$	number of bits composing the bit pattern $\mathbf{b}^{[\mathrm{H},\theta]}$ of HARQ Layer θ
$B^{[\mathrm{D},\nu]}$	number of bits composing the bit pattern $\mathbf{b}^{[\mathrm{D},\nu]}$, description ν (MDC)
$B^{[\mathrm{NB}]}$	number of bits composing the natural binary bit pattern, $B^{[\mathrm{NB}]} \doteq \lceil \mathrm{ld}\, Q \rceil$
$B^{[\mathrm{NB}]\star}$	number of bits composing the natural binary super bit pattern $\mathbf{b}^{[\mathrm{NB}]\star}$
$\bar{\mathbf{b}}^{(\cdot)}$	possible bit pattern, element of the set $\mathbb{B}$
$\bar{\mathbf{b}}^{(\cdot)\star}$	possible super bit pattern, element of the set $\mathbb{B}^\star$
$\bar{\mathbf{b}}^{[\mathrm{D},\nu](\cdot)}$	possible bitpattern for description ν (MDC)
$\bar{b}^{(\cdot)}$	single bit of bit pattern $\bar{\mathbf{b}}^{(\cdot)}$
$\bar{b}^{(\cdot)\star}$	single bit of super bit pattern $\bar{\mathbf{b}}^{(\cdot)\star}$
$\bar{b}^{[\mathrm{D},\nu](\cdot)}$	single bit of possible bitpattern $\bar{\mathbf{b}}^{[\mathrm{D},\nu](\cdot)}$ for description ν (MDC)
$\mathcal{B}$	bit mapping of a quantizer index i to a bit pattern
$\mathcal{B}^{[\mathrm{NB}]}$	natural binary bit pattern representation of a quantizer index
$\check{\mathcal{B}}$	additional (possibly redundant) bit mapping, $\mathcal{B} = \check{\mathcal{B}} \circ \mathcal{B}^{[\mathrm{NB}]}$
$\mathcal{B}^{[\mathrm{H},\theta]}$	bit mapping corresponding to HARQ layer θ
$\mathcal{B}^{[\mathrm{D},\nu]}$	bit mapping for description ν in the MDC case
$\mathbb{B}$	set of all possible bit patterns
$\mathbb{B}^\star$	set of all possible super bit patterns (MDBM case)
$\mathbb{B}^{[\mathrm{D},\nu]}$	set of all possible bit patterns for description ν (MDC)
$\mathbb{B}_{\mathrm{red},q}^{[\mathrm{pos}]}$	reduced bit pattern set depending on spatially neighboring values
$\mathbb{B}_{\mathrm{red},q}^{[\mathrm{tim}]}$	reduced bit pattern set depending on temporally neighboring values

$\grave{\mathbb{B}}^{[\cdot]}_{\mathrm{red},q}$	set of bit pattern allowing a transition to pattern associated to $\bar{\mathbf{v}}^{(q)}$
$\mathbb{C}$	the set of complex numbers
$\mathcal{C}$	the channel function, models the transmission
C	variable denoting the EXIT characteristic
C_{CD}	variable denoting the EXIT characteristic of channel decoding
$\mathsf{C}_{\mathrm{CD,inn}}$	EXIT characteristic of inner channel decoding (SCCCs)
$\mathsf{C}_{\mathrm{CD,out}}$	EXIT characteristic of outer channel decoding (SCCCs)
$\mathsf{C}_{\mathrm{CD,irr}}$	EXIT characteristic of channel decoding with irregular codes
$\mathsf{C}_{\mathrm{CD,MDC}}$	EXIT characteristic of channel decoding in MDC-ISCD
C_{SD}	EXIT characteristic of SDSD
$\mathsf{C}_{\mathrm{SD,irr}}$	EXIT characteristic of SDSD with irregular bit mapping
$\mathsf{C}^{[\mathrm{bound}]}_{\mathrm{SD}}$	EXIT trajectory bound of SDSD
$\mathbf{c}_{\mathrm{SD}}$	vector containing Ξ sample points of the characteristic C_{SD}
$\mathbf{c}_{\mathrm{SD,inv}}$	vector containing Ξ sample points of the inverse characteristic $\mathsf{C}^{-1}_{\mathrm{SD}}$
$\mathbf{c}_{\mathrm{SD,irr}}$	vector containing Ξ sample points of the IBM characteristic $\mathsf{C}_{\mathrm{SD,irr}}$
$\mathbf{c}_{\mathrm{CD}}$	vector containing Ξ sample points of the characteristic $\mathsf{C}^{-1}_{\mathrm{CD}}$
$\mathbf{C}_{\mathrm{CD}}$	matrix containing the vectors $\mathbf{c}_{\mathrm{CD}}$ of several characteristics
$\mathbf{c}_{\mathrm{CD,inv}}$	vector containing Ξ sample points of the inverse characteristic $\mathsf{C}^{-1}_{\mathrm{CD}}$
$\mathbf{C}_{\mathrm{SD}}$	matrix containing the vectors $\mathbf{c}_{\mathrm{SD}}$ of several characteristics
$\mathfrak{C}_{\gamma}$	complexity increase factor in MDBM-SDSD ($\gamma^{\star}_{t,k}$, $\gamma^{[\mathrm{ext}]\setminus\chi,\star}_{t,k}$)
$\mathfrak{C}^{[\mathrm{ext}]}_{\mathrm{AK0}}$	complexity increase factor in MDBM-SDSD (extr. info., AK0)
$\mathfrak{C}^{[\mathrm{ext}]}_{\mathrm{AK1\text{-}INTER}}$	complexity increase factor in MDBM-SDSD (extr. info., AK1-INTER)
$\mathfrak{C}^{[\mathrm{ext}]}_{\mathrm{AK1\text{-}INTRA}}$	complexity increase factor in MDBM-SDSD (extr. info., AK1-INTRA)
$\mathfrak{C}^{[\mathrm{ext}]}_{\mathrm{AK1\text{-}NOPT}}$	complexity increase factor in MDBM-SDSD (extr. info., AK1-NOPT)
d	single elements of the difference vector $\mathbf{d}$
$\mathbf{d}$	difference vector
$d^{(1)}_{\mathcal{E}}$	Hamming weight of the impulse response of a convolutional code
$d_{\min}(\cdot)$	minimum distance of a code
D	delay operator
$\mathcal{D}$	multiple description index assignment function
$\mathbb{D}^{[\mathrm{D},\nu]}$	multiple description coding support set
$\mathcal{E}$	channel encoding function
e	single bit of the channel encoded bit pattern
$\mathbf{e}$	vector of channel encoded bits
$e^{[\mathrm{H},\theta]}$	single bit of outer-HARQ layer θ channel encoded vector
$\mathbf{e}^{[\mathrm{H},\theta]}$	vector of channel encoded bits of outer-HARQ layer θ
$e^{[\mathrm{D},\nu]}$	single bit of channel encoded vector of description ν (MDC case)
$\mathbf{e}^{[\mathrm{D},\nu]}$	vector of channel encoded bits of MDC description ν
$\check{\mathbf{e}}$	symbol mapper input vector, mapped to a modulation symbol y
E_{s}	average energy per channel symbol y
E_{b}	average energy per information bit

$\mathbb{F}_2$	the set of binary numbers, $\mathbb{F}_2 = \{0, 1\}$
$\underline{\mathcal{F}}_{\text{inv}}$	function interpolating sampling points of the inverse function
$\mathbf{G}^{[\text{BM}]}$	generator matrix describing the linear redundant bit mapping
$\mathbf{G}^{[\text{BM,HARQ}]}$	generator matrix describing overall HARQ redundant bit mapping
$\mathbf{G}^{[\text{H},\theta]}$	generator matrix describing layer θ of HARQ bit mapping
$\mathbf{G}^{[\text{D},\nu]}$	generator matrix of the linear redundant bit mapping of description ν
$\mathbf{G}_{\text{punc}}$	puncturing matrix of a convolutional code
$\mathbf{G}_{\text{punc}}^{[\text{CC,HARQ}]}$	puncturing matrix describing inner HARQ channel code puncturing
$\mathbf{G}^{[\text{CC}]}$	generator matrix describing the convolutional code
$\mathbb{G}^{[\text{CC}]}$	generator polynomials of a convolutional code
$\mathsf{H}(\cdot)$	entropy of a random variable
$\mathsf{H}_{\mathsf{C}}(\cdot, \cdot)$	cross-entropy of two random variables
$\mathbf{H}^{[\text{BM}]}$	parity check matrix of the linear redundant bit mapping
i	quantizer code book index, $i = \mathcal{Q}(\mathbf{v})$
$i^{[\text{CQ}]}$	quantizer code book index of the conditional quantizer
$i^{\star}$	quantizer super index, combination of Ψ indices i
$i^{[\text{D},\nu]}$	MDC quantizer index representing description ν
$i^{[\text{Model}]}$	quantizer indices corresponding to *FlexCode* model parameters
$i^{[\text{TC}]}$	quantizer indices corresponding to *FlexCode* transform coefficients
$\mathbf{i}$	vector of quantized code book indices
$\mathbf{i}^{[\text{D},\nu]}$	vector of (side) indices representing description ν
$\mathbf{i}^{[\text{Model}]}$	vector of *FlexCode* model parameter quantizer indices
$\mathbf{i}^{[\text{TC}]}$	vector of *FlexCode* transform coefficient quantizer indices
$\hat{\mathbf{i}}^{[\text{Model}]}$	estimated vector of *FlexCode* model parameter quantizer indices
$\hat{\mathbf{i}}^{[\text{TC}]}$	estimated vector of *FlexCode* transform coefficient quantizer indices
$\mathbb{I}$	set of possible quantizer indices, $\mathbb{I} \subset \mathbb{N}_1$
$\mathbb{I}^{\star}$	set of possible super quantizer indices if MDBMs are used
$\mathbb{I}^{[\text{CQ}]}$	set of possible quantizer indices in CQ, $\mathbb{I}_{t,k}^{[\text{CQ}]} \subseteq \mathbb{I}$
$\mathbb{I}^{[\text{D},\nu]}$	set of possible side quantizer indices of description ν (MDC case)
$\mathbb{I}_{\text{red},q}^{[\text{pos}]}$	reduced quantizer indices depending on spatially neighboring values
$\mathbb{I}_{\text{red},q}^{[\text{tim}]}$	reduced quantizer indices depending on temporally neighboring values
$\grave{\mathbb{I}}_{\text{red},q}^{[\text{pos}]}$	set of quantizer indices allowing a transition to the index q
$\grave{\mathbb{I}}_{\text{red},q}^{[\text{tim}]}$	set of quantizer indices allowing a transition to the index q
$\hat{\imath}$	estimated quantizer code book index
I	random process describing the quantizer code book indices
$I^{[\text{CQ}]}$	random process describing quantizer code book indices for CQ
$I^{\star}$	random process describing the quantizer super indices
$\hat{I}$	random process describing the estimated quantizer code book indices
$\mathcal{I}^{[\text{CQ}]}$	function mapping quantizer index to CQ index based on previous index
$\mathbf{I}$	identity matrix, e.g., $\mathbf{I}_4$ denotes the 4×4 identity matrix
I	mutual information between two random processes, e.g., $\mathsf{I}(X;Y)$

$\mathsf{I}^{[\mathrm{apr}]}$	mutual information between *a priori* L-values and bits X
$\mathsf{I}^{[\mathrm{ext}]}$	mutual information between extrinsic L-values and bits X
$\mathsf{I}^{[\mathrm{apr}]}_{\mathrm{SD}}$	mutual information between bits X and $\mathsf{L}^{[\mathrm{apr}]}_{\mathrm{SD}}$, $\mathsf{I}(X;\mathsf{L}^{[\mathrm{apr}]}_{\mathrm{SD}}(X))$
$\mathsf{I}^{[\mathrm{apr}]}_{\mathrm{SD,max}}$	maximum mutual information between bits X and $\mathsf{L}^{[\mathrm{apr}]}_{\mathrm{SD}}$
$\mathsf{I}^{[\mathrm{ext}]}_{\mathrm{SD}}$	mutual information between bits X and $\mathsf{L}^{[\mathrm{ext}]}_{\mathrm{SD}}$, i.e., $\mathsf{I}(X;\mathsf{L}^{[\mathrm{ext}]}_{\mathrm{SD}}(X))$
$\mathsf{I}^{[\mathrm{apr}]}_{\mathrm{CD}}$	mutual information between bits X and $\mathsf{L}^{[\mathrm{apr}]}_{\mathrm{CD}}$, i.e., $\mathsf{I}(X;\mathsf{L}^{[\mathrm{apr}]}_{\mathrm{CD}}(X))$
$\mathsf{I}^{[\mathrm{ext}]}_{\mathrm{CD}}$	mutual information between bits X and $\mathsf{L}^{[\mathrm{ext}]}_{\mathrm{CD}}$, i.e., $\mathsf{I}(X;\mathsf{L}^{[\mathrm{ext}]}_{\mathrm{CD}}(X))$
$\mathsf{I}^{[\mathrm{apr}]}_{\mathrm{CD,inn}}$	mutual information between bits X and $\mathsf{L}^{[\mathrm{apr}]}_{\mathrm{CD,inn}}$ in SCCCs
$\mathsf{I}^{[\mathrm{ext}]}_{\mathrm{CD,inn}}$	mutual information between bits X and $\mathsf{L}^{[\mathrm{ext}]}_{\mathrm{CD,inn}}$ in SCCCs
$\mathsf{I}^{[\mathrm{apr}]}_{\mathrm{CD,out}}$	mutual information between bits X and $\mathsf{L}^{[\mathrm{apr}]}_{\mathrm{CD,out}}$ in SCCCs
$\mathsf{I}^{[\mathrm{ext}]}_{\mathrm{CD,out}}$	mutual information between bits X and $\mathsf{L}^{[\mathrm{ext}]}_{\mathrm{CD,out}}$ in SCCCs
$\mathsf{I}_{\mathcal{C}}$	capacity of the channel $\mathcal{C}$
$\mathfrak{I}_{\mathrm{low}}$	Set containing the index positions of low importance
$\mathfrak{I}_{\mathrm{high}}$	Set containing the index positions of high importance
j	auxiliary variable used in various contexts
J	number of memory elements of a binary convolutional code
$\mathcal{J}$	J-function necessary for the computation of EXIT characteristics [tB01c]
k	position index of the quantizer input vectors and quantizer indices
$\mathfrak{k}$	substitution index used for describing MDBM index positions
K	generally used for normalization constants
L	L-value or *Log-Likelihood Ratio* (LLR)
$\boldsymbol{\mathsf{L}}$	notation for vectors of L-values, e.g., $\boldsymbol{\mathsf{L}}(x) = (\mathsf{L}(x_1), \mathsf{L}(x_2), \ldots)$
L_c	reliability value of the channel, $\mathsf{L}_c = 4a\frac{E_{\mathrm{S}}}{N_0}$ for an AWGN channel
$\mathsf{L}^{[\mathrm{apr}]}_{\mathrm{BL}}$	source *a priori* information (L-values) on bit level
$\boldsymbol{\mathsf{L}}^{[\mathrm{apr}]}_{\mathrm{BL}}$	vector of source *a priori* information (L-values) on bit level
$\mathsf{L}^{[\mathrm{apost}]}_{\mathrm{CD}}$	*a posteriori* information (L-values) at channel decoder output
$\mathsf{L}^{[\mathrm{apr}]}_{\mathrm{CD}}$	*a priori* information (L-values) at channel decoder input
$\mathsf{L}^{[\mathrm{apr}]}_{\mathrm{CD,inn}}$	*a priori* information (L-values) at inner channel dec. input (SCCCs)
$\mathsf{L}^{[\mathrm{apr}]}_{\mathrm{CD,out}}$	*a priori* information (L-values) at inner channel dec. input (SCCCs)
$\boldsymbol{\mathsf{L}}^{[\mathrm{apr}]}_{\mathrm{CD}}$	vector of *a priori* information at channel decoder input
$\boldsymbol{\mathsf{L}}^{[\mathrm{apr}]}_{\mathrm{CD,inn}}$	vector of *a priori* information at inner channel dec. input (SCCCs)
$\boldsymbol{\mathsf{L}}^{[\mathrm{apr}]}_{\mathrm{CD,out}}$	vector of *a priori* information at inner channel dec. input (SCCCs)
$\mathsf{L}^{[\mathrm{apr}]}_{\mathrm{SD}}$	*a priori* information (L-values) at channel decoder input
$\boldsymbol{\mathsf{L}}^{[\mathrm{apr}]}_{\mathrm{SD}}$	vector of *a priori* information at channel decoder input
$\boldsymbol{\mathsf{L}}^{[\mathrm{apr}]}_{\mathrm{SD,max}}$	vector of maximum reliable channel decoder *a priori* information
$\mathsf{L}^{[\mathrm{ext}]}_{\mathrm{CD}}$	extrinsic information (L-values) at channel decoder output
$\mathsf{L}^{[\mathrm{ext}]}_{\mathrm{CD,inn}}$	extrinsic information (L-values) at inner channel dec. output (SCCCs)
$\mathsf{L}^{[\mathrm{ext}]}_{\mathrm{CD,out}}$	extrinsic information (L-values) at inner channel dec. output (SCCCs)

$\mathsf{L}_{\mathrm{CD}}^{[\mathrm{ext}]}$	vector of extrinsic information at channel decoder output
$\mathsf{L}_{\mathrm{CD,inn}}^{[\mathrm{ext}]}$	vector of extrinsic information at inner channel dec. output (SCCCs)
$\mathsf{L}_{\mathrm{CD,out}}^{[\mathrm{ext}]}$	vector of extrinsic information at inner channel dec. output (SCCCs)
$\mathsf{L}_{\mathrm{SD}}^{[\mathrm{ext}]}$	extrinsic information (L-values) at SDSD output
$\mathbf{L}_{\mathrm{SD}}^{[\mathrm{ext}]}$	vector of extrinsic information at SDSD output
$\mathsf{L}_{\mathrm{CD}}^{[\mathrm{chan}]}$	channel-related input information (L-value) for the channel decoder
$\mathbf{L}_{\mathrm{CD}}^{[\mathrm{chan}]}$	channel-related information vector (L-values) for the channel decoder
ℓ	modulation symbol position index
m	number of symbols grouped to a code word in entropy coding
$\mathcal{M}$	mapping function, maps a group of bits to (complex) signal space points
$\mathcal{M}^{[\mathrm{BPSK}]}$	BPSK mapping functions, maps a bit to a bipolar value $y \in \{\pm 1\}$
M	number of considered states in the M-SDSD algorithm
$\mathbb{M}$	set containing the indices of the M best states in the M-SDSD algorithm
$M_{\mathcal{B}}$	number of different mappings used for optimizing irregular bit mappings
$M_{\mathcal{E}}$	number of different channel codes used for inner irregular channel codes
n	sample of (complex) channel noise
$\mathbf{n}$	vector of (complex) channel noise samples
N_0	power spectral density of the AWGN on the channel
$\mathbb{N}_0$	the natural numbers including zero, $\mathbb{N}_0 = \{0, 1, 2, \ldots\}$
$\mathbb{N}_1$	the natural numbers excluding zero, $\mathbb{N}_1 = \{1, 2, 3, \ldots\}$
N_E	number of channel encoded bits per frame
$N_E^{[\mathrm{D},\nu]}$	number of channel encoded bits for description ν (MDC-case)
N_I	number of quantization indices per frame
$N_I^{\star}$	number of super indices per frame if MDBMs are used
N_U	number of source parameters per frame
N_X	number of bits per frame
$N_X^{[\mathrm{H},\theta]}$	number of bits per frame per HARQ layer θ
$N_X^{[\mathrm{D},\nu]}$	number of bits per description ν (MDC case)
N_Y	number of (complex) modulation symbols per frame
$\mathfrak{N}$	number of transitions per update in the conditional quantizer
$\mathfrak{N}^{[\mathrm{tim}]}$	number of transitions per update if applied to inter-frame correlation
$\mathfrak{N}^{[\mathrm{pos}]}$	number of transitions per update if applied to intra-frame correlation
$\mathfrak{N}^{M}$	number of transitions per update if CQ is combined with M-SDSD
$\mathfrak{N}_{\max}^{M,\alpha}$	max. number of transitions/update in CQ-M-SDSD (forward rec.)
$\mathfrak{N}_{\max}^{M,\beta}$	max. number of transitions/update in CQ-M-SDSD (backward rec.)
N_{LMQ}	quantizer noise generated by LMQ quantization
N_{CQ}	quantizer noise generated by conditional quantization
$\mathbf{o}$	offset vector controlling the decoding tunnel in irregular bit mappings
O	complexity order of an algorithm
p	probability density function
P	(discrete) probability, short handed notation

Pr	(discrete) probability
$\widetilde{\mathsf{Pr}}$	logarithmic (discrete) probability, $\widetilde{\mathsf{Pr}}\{\cdot\} \doteq \ln \mathsf{Pr}\{\cdot\}$
P_{sys}	puncturing probability of the systematic output
$\mathbf{P}$	notation for vectors of probabilities, e.g., $\mathbf{P}(x) = (P(x_1), P(x_2), \ldots)$
P_{b}	bit error probability
$\mathsf{P}_{\text{b}}^{[\text{ext}]}$	bit error probability of the (hard-decided) extrinsic output
$\mathsf{P}_{\text{CD}}^{[\text{ext}]}$	extrinsic information (probability) at the channel decoder output
q	index used for addressing the quantizer code book entries
$q^\star$	super index for addressing the entries of the virtual super code book
Q	number of entries of the quantizer code book
$Q^{[\text{D},\nu]}$	side quantizer code book entries for description ν (MDC case)
$\mathcal{Q}$	quantizer for quantization of source parameters
$\mathcal{Q}_{\text{CQ}}$	symbol for the conditional quantizer function
r_{BC}	code rate of a (linear) block code
r_{BM}	coding rate of the bit mapping
$\mathbf{r}_{\text{BM}}$	vector grouping different bit mapping coding rates
$r_{\text{BM}}^{[\text{target}]}$	bit mapping target rate after irregular bit mapping
r_{CC}	coding rate of the channel encoder
$r_{\text{CC,eff}}$	effective channel encoder rate if desc. is lost in alternative MDC scheme
$\tilde{r}_{\text{CC}}$	inverse of the channel encoder coding rate
$\tilde{\mathbf{r}}_{\text{CC}}$	vector grouping the inverse of different channel coding rates, i.e., $1/r_{\text{CC}}$
r_{SC}	coding rate of source coding (comprising correlation and bit mapping)
$r_{\text{SC}}^{[\text{AK0}]}$	distribution related part of the source coding rate
$r_{\text{SC}}^{[\text{Mapping}]}$	mapping related part of the source coding rate
$r_{\text{SC}}^{[\text{Markov}]}$	Markov property related part of the source coding rate
$\mathbb{R}$	the set of real numbers
s	audio sample, input of the source encoder
$\mathbf{s}$	vector consisting of several audio samples, also denoted frame
$\hat{\mathbf{s}}$	estimated audio frame at the receiver
S	signal power of the source, $\mathsf{E}\{U^2\}$
S	design parameter of S-random interleavers
t	discrete time index of the considered frame
T_{ISCD}	EXIT trajectory of iterative source-channel decoding
T_{SCCC}	EXIT trajectory of serially concatenated convolutional codes
$\mathfrak{T}$	probability threshold for conditional quantization
u	single unquantized source parameter
$\mathbf{u}$	vector of unquantized source parameters
U	random variable describing the unquantized source parameter
$\tilde{u}$	intermediate uncorrelated Gaussian distributed source parameters
$\tilde{U}$	random variable describing the intermediate source parameters
$\hat{u}$	estimated source parameter at the receiver
$\hat{U}$	random variable describing the estimated source parameters

$\hat{\mathbf{u}}$	vector of estimated source parameters
$\mathbf{v}$	quantizer input vector
$\hat{\mathbf{v}}$	estimated quantizer reproduction vector
$\mathbb{V}$	quantizer code book, set of (multi-dimensional) reproduction levels
$\mathbb{V}_{\mathrm{red},q}^{[\mathrm{pos}]}$	reduced quantizer codebook depending on spatially neighboring values
$\mathbb{V}_{\mathrm{red},q}^{[\mathrm{tim}]}$	reduced quantizer codebook depending on temporally neighboring values
$\grave{\mathbb{V}}_{\mathrm{red},q}^{[\cdot]}$	set of code book entries allowing a transition to code book entry $\bar{\mathbf{v}}^{(q)}$
$\mathfrak{V}$	quantizer cell, region associated with the code book entry $\bar{\mathbf{v}}$
$\mathfrak{V}_{\mathrm{red},j}^{[\cdot],(q)}$	quantizer cell in conditional quantization
$\bar{\mathbf{v}}^{(q)}$	qth quantizer code book entry vector
$\bar{\mathbf{v}}_{\mathrm{red},j}^{[\cdot],(q)}$	reduced code book entry vector in conditional quantization
$\bar{v}^{(q)}$	qth quantizer code book entry in case of scalar quantization
$\bar{v}_{\mathrm{red},j}^{[\cdot],(q)}$	reduced code book entry (scalar case) in conditional quantization
w	weight resulting from the irregular code optimization
$\mathbf{w}$	vector containing the weights w from the irregular code optimization
$\mathbf{w}_{\mathrm{BM}}$	vector containing the bit mapping weights in joint irregular optimization
$\mathbf{w}_{\mathrm{CC}}$	vector containing the channel code weights in joint irregular optimization
x	single bit of the bit stream vector $\mathbf{x}$
X	random variable describing single bits of $\mathbf{x}$
$\mathbf{x}$	bit stream after bit mapping, composed of individual bit patterns $\mathbf{b}$
$\hat{\mathbf{x}}$	estimated bit stream after hard output channel decoding
$\mathbf{x}^{[\mathrm{H},\theta]}$	bit stream of layer θ after outer-HARQ bit mapping $\mathcal{B}^{[\mathrm{H},\theta]}$
$x^{[\mathrm{D},\nu]}$	single bit of the bit stream vector $\mathbf{x}^{[\mathrm{D},\nu]}$ (MDC case, description ν)
$\mathbf{x}^{[\mathrm{D},\nu]}$	bit stream of description ν after MDC
y	single (complex) signal space point
Y	random variable describing (complex) signal space points
$\mathbf{y}$	vector of (complex) signal space points
z	received, noisy (complex) signal space point
Z	random variable describing the received noisy signal space points
$\mathbf{z}$	vector of received, noisy (complex) signal space points
$\mathbb{Z}$	the set of integer numbers

Greek Symbols

α	symbol used for reliabilities in the SDSD forward recursion
$\alpha^{\star}$	symbol used for forward reliabilities in multi-dim. SDSD
$\tilde{\alpha}$	symbol used for logarithmic reliabilities in the SDSD forward recursion
$\alpha^{[\mathrm{pos}]}$	forward reliabilities (spatially) in the AK1-NOPT SDSD
$\alpha^{[\mathrm{pos}]\star}$	forward reliabilities (spatially) in the multi-dim. AK1-NOPT SDSD
$\tilde{\alpha}^{[\mathrm{pos}]}$	logarithmic forward reliabilities (spatially) in the AK1-NOPT SDSD
$\alpha^{[\mathrm{tim}]}$	forward reliabilities (temporally) in the AK1-NOPT SDSD
$\alpha^{[\mathrm{tim}]\star}$	forward reliabilities (temporally) in the multi-dim. AK1-NOPT SDSD

$\tilde{\alpha}^{[\mathrm{tim}]}$	logarithmic forward reliabilities (temporally) in the AK1-NOPT SDSD
β	symbol used for reliabilities in the SDSD backward recursion
$\tilde{\beta}$	symbol used for logarithmic reliabilities in the SDSD backward recursion
$\beta^{[\mathrm{pos}]}$	backward reliabilities (spatially) in the AK1-NOPT SDSD
$\beta^{[\mathrm{pos}]\star}$	backward reliabilities (spatially) in the multi-dim. AK1-NOPT SDSD
$\tilde{\beta}^{[\mathrm{pos}]}$	logarithmic backward reliabilities (spatially) in the AK1-NOPT SDSD
γ	receive reliability of a bit pattern in the SDSD
$\gamma^{[\mathrm{D},\nu]}$	bit pattern receive reliability of description ν in the MDC-SDSD
$\gamma^{\star}$	receive reliability of a super bit pattern in the multi-dim. SDSD
$\tilde{\gamma}$	logarithmic receive reliability of a bit pattern in the SDSD
$\tilde{\gamma}^{[\mathrm{D},\nu]}$	logarithmic receive reliability of description ν in the MDC-SDSD
$\gamma^{[\mathrm{ext}]\backslash\chi}$	extrinsic receive reliability for position (within bit pattern) χ
$\gamma^{[\mathrm{ext}]\backslash\chi,\star}$	extrinsic receive reliability for position (within super bit pattern) χ
$\tilde{\gamma}^{[\mathrm{ext}]\backslash\chi}$	extrinsic logarithmic receive reliability for position χ
$\gamma^{[\mathrm{D},\nu,\mathrm{ext}]\backslash\chi}$	extr. receive reliab. for position (in description ν bit pattern) χ
$\tilde{\gamma}^{[\mathrm{D},\nu,\mathrm{ext}]\backslash\chi}$	extr. log. receive reliab. for pos. (in description ν bit pattern) χ
δ	intra-frame correlation coefficient, $\delta = \mathsf{E}\{U_{t,\kappa}U_{t,\kappa-1}\}/\,\mathsf{E}\{U_{t,\kappa}^2\}$
ϵ	erasure probability
η	bit position index inside a channel encoded bit vector $\mathbf{e}$
Θ	Number of layers in HARQ-ISCD
θ	position index of the considered HARQ layer
κ	position index of the considered parameter
λ	multiplicative constants for setting up the source model
Λ	number of consecutive source frames grouped together for interleaving
μ	position index of the considered bit inside a bit pattern $\mathbf{b}$
μ_a	mean of the *a priori* L-values at the channel decoder input
μ_e	mean of the extrinsic L-values at the channel decoder output
ν	description index in *Multiple Description Coding* (MDC)
$\bar{\nu}$	defined as the "other" description in MDC, i.e., $\bar{\nu} \doteq 3 - \nu$
ξ	position index of the considered bit inside the bit vector $\mathbf{x}$
Ξ	number of sample points used to measure an EXIT characteristic
π	interleaver permutation function
Π	quantizer dimension
ρ	inter-frame correlation coefficient, $\rho = \mathsf{E}\{U_{t,\kappa}U_{t-1,\kappa}\}/\,\mathsf{E}\{U_{t,\kappa}^2\}$
σ_a	variance of *a priori* L-values at the channel decoder input
σ_e	variance of extrinsic L-values at the channel decoder output
Υ	number of bits per modulation symbol y
Φ	amount of previous frames considered in the improved inter-frame ISCD
χ	auxiliary variable used in various contexts
Ψ	dimension of the *Multi-Dimensional Bit Mapping* (MDBM)
ω	current iteration counter, $\omega \in \{1, \ldots, \Omega\}$
Ω	number of iterations performed at the receiver

List of Abbreviations

ACK	Acknowledge
AK0	A priori Knowledge of zeroth order (no correlation)
AK1	A priori Knowledge of first order (correlation)
AK1-INTER	A priori Knowledge of first order, inter-frame (correlation)
AK1-INTER-IMP	A priori Knowledge of first order, inter-frame improved
AK1-INTRA	A priori Knowledge of first order, intra-frame (correlation)
AK1-NOPT	A priori Knowledge of first order, near optimal estimation
AMR	Adaptive Multi-Rate
AMR-WB	Adaptive Multi-Rate Wideband
AR	Auto Regressive
ASIC	Application Specific Integrated Circuit
AWGN	Additive White Gaussian Noise
BCH	Bose-Chaudhuri-Hocquenghem
BCJR	Bahl, Cocke, Jelinek, Raviv
BEC	Binary Erasure Channel
BER	Bit Error Rate
BFI	Bad Frame Indicator
BICM	Bit Interleaved Coded Modulation
BICM-ID	Bit Interleaved Coded Modulation with Iterative Decoding
BM	Bit Mapping
BPSK	Binary Phase Shift Keying
BSA	Binary Switching Algorithm
BWE	BandWidth Extension
CC	Channel Code
CCSDS	Consultative Committee on Space Data Systems
CELP	Code Excited Linear Prediction
CESQ	Constrained Entropy Scalar Quantization
CE	Cross Entropy
CPU	Central Processing Unit
CRSQ	Constrained Resolution Scalar Quantization
CSI	Channel State Information
CQ	Conditional Quantization
CRC	Cyclic Redundancy Check
CUDA	Compute Unified Device Architecture
DSP	Digital Signal Processor
DVB	Digital Video Broadcasting
EDGE	Enhanced Data rates for GSM Evolution
EEC	Errors-and-Erasure Channel
EXIT	EXtrinsic Information Transfer
ETB	EXIT Trajectory Bound
FLC	Fixed Length Code
FPGA	Field Programmable Gate Array
GMM	Gaussian Mixture Model
GPRS	General Packet Radio Service

GPU	Graphical Processing Unit
GSM	Global System for Mobile Communications
HARQ	Hybrid Automatic Repeat reQuest
HSDPA	High Speed Downlink Packet Access
HSPA	High Speed Packet Access
HSUPA	High Speed Uplink Packet Access
IBM	Irregular Bit Mapping
IOWEF	Input Output Weight Enumerating Function
IRA	Irregular Repeat-Accumulate
IRBM	Incremental Redundant Bit Mapping
ISCD	Iterative Source-Channel Decoding
ISCM	Iterative Source-Coded Modulation
ISI	Inter-Symbol Interference
KLT	Karhunen-Loève Transform
LDPC	Low-Density Parity-Check
LLR	Log-Likelihood Ratio
LMQ	Lloyd-Max Quantizer
LP	Linear Prediction
LSB	Least Significant Bit
LSF	Line Spectral Frequency
LTE	Long Term Evolution
LUT	Look-Up Table
MAC	Multiply ACcumulate
MAP	Maximum A Posteriori
MDBM	Multi-Dimensional Bit Mapping
MDC	Multiple Description Coding
MDCC	Multiple Descriptions by Channel Coding
MDCT	Modified Discrete Cosine Transform
MDIA	Multiple Description Index Assignment
MDM	Multi-Dimensional Mapping
MELP	Mixed Excitation Linear Prediction
ML	Maximum Likelihood
MMSE	Minimum Mean Square Error
MP3	MPEG Audio Layer 3
MSB	Most Significant Bit
NACK	Not-Acknowledge
NAK	No A priori Knowledge
OFDM	Orthogonal Frequency Division Multiplexing
OPTA	Optimum Performance Theoretically Attainable
PCCC	Parallel Concatenated Convolutional Code
PDA	Personal Digital Assistant
pdf	Probability Density Function
PEG	Progressive Edge Growth
PIBC	Parameter Individual Block Code
PSNR	Parameter Signal-to-Noise Ratio

QoS	Quality of Service
RA	Repeat-Accumulate
RBM	Redundant Bit Mapping
RCPC	Rate-Compatible Punctured Convolutional
RSC	Recursive Systematic Convolutional
RNSC	Recursive Non-Systematic Convolutional
RPRSC	Randomly Punctured Recursive Systematic Convolutional
SCCC	Serially Concatenated Convolutional Code
SCR	Sign Change Ratio
SDM	Soft Demapper
SDR	Sign Difference Ratio
SDSD	Soft Decision Source Decoding
SER	Symbol Error Rate
SISO	Soft Input Soft Output
SNR	Signal-to-Noise Ratio
SOCC	Source Optimized Channel Code
SOVA	Soft Output Viterbi Algorithm
SPB	Sphere Packing Bound
SQP	Sequential Quadratic Programming
TDeC	Turbo DeCodulation
TLU	Table Look-Up
UEP	Unequal Error Protection
UMTS	Universal Mobile Telecommunications System
VLC	Variable Length Code
VoIP	Voice over IP
WiMAX	Worldwide Interoperability for Microwave Access
WLAN	Wireless Local Area Network

1

Introduction

The development of the radio telegraph system by Guglielmo Marconi has been one of the cornerstones of the modern information era. Without wireless communication, the rapid exchange of all types of information, indispensable for the effective functioning of most of nowadays economics, would be difficult. In fact, the increased mobility trend in today's business demands for widely available wireless and mobile voice and data communication.

The introduction of the *Global System for Mobile Communications* (GSM) standard has marked a considerable breakthrough in mobile wireless telephony. Following a rapid market penetration, mobile telephony suddenly became available to a high number of individuals. By the end of 2009, there were approximately 4.6 billion mobile cellular subscriptions, corresponding to 67% of the global population [ITU10]. Since 2006, the number of mobile subscriptions in Germany is higher than the number of its inhabitants [Bun08]. Even in the developing countries, the penetration is above the 50% mark [ITU10].

Following the success of mobile telephony, the desire to use mobile Internet related applications alongside voice services emerged. This led to the wish to be online at any time and everywhere. The GPRS and EDGE extensions to the GSM network were a first step towards the Internet access with mobile devices like phones, PDAs, or notebooks. The deployment of the *Universal Mobile Telecommunications System* (UMTS) network and its upcoming *Long Term Evolution* (LTE) extension has been an attempt to bridge the discrepancy between demand and supply of a fast access to the mobile Internet. The rise of the available data rates enables the possibility to transmit multimedia content like, e.g., audio and video, which becomes increasingly important.

Unfortunately, the achievable rate of a wireless data link is restricted by the fundamental limits formulated by Shannon [Sha48]. These limits are based on information theoretical considerations and give a nonconstructive proof of the maximum achievable transmission rate for noisy transmission channels. Following Shannon's seminal paper, it took the research community more than four decades to discover a practical coding scheme that is able to closely reach the fundamental limits. This milestone discovery, branded Turbo codes by its inventors [BGT93], has led to completely new

channel encoding and decoding paradigms, based on the iterative exchange of so-called *extrinsic* information.

The Turbo principle of exchanging extrinsic information is not only limited to channel decoding, but has later been applied to other components of the receiver chain, too. One example is the iterative evaluation of channel decoding and source decoding, denoted *Iterative Source-Channel Decoding* (ISCD) [Gör00, AVS01]. ISCD exploits the fact that most practical source encoders are unable to completely decorrelate the signal, as a consequence of delay and computational complexity constraints. The remaining natural redundancy is used in conjunction with possible artificial redundancy, introduced by the bit mapping, to generate extrinsic information which is iteratively refined in a loop between source decoder and channel decoder. After a certain number of iterations, an improved estimate (compared to the conventional non-iterative case) of the transmitted audio-visual signal can be generated.

In this thesis, the concept of ISCD is extended towards a flexible and practical implementation in heterogeneous networks. As predicted by Moore's law [Bro06], the computational power available in mobile devices increases exponentially. This enables the implementation of complex receivers like ISCD, boosting the performance as well as the coverage of mobile networks, thus indirectly reducing the capital investment of the network operators. Although the concept of ISCD is generally well understood, its implementation is still challenging. A great part of this thesis tries to overcome some of the drawbacks encountered when implementing practical ISCD schemes. These include the imprecise convergence prediction and the suboptimality of the source decoder in delay constrained ISCD systems, the need for unequal error protection, as well as the reduction of the error floor which leads to non-negligible symbol error rates even in good channel conditions. Furthermore, the use of incremental redundancy permits to increase the network throughput and thus indirectly the number of mobile users that can be served within the given bandwidth limitations.

As practical transmission schemes do not generally correspond to the simplified baseband models considered in earlier publications on ISCD, the concept is extended to include on the one hand *Multiple Description Coding* (MDC) – a source coding concept that is frequently used if packet losses are expected within heterogeneous networks. On the other hand, the substitution of entropy coding schemes, frequently employed in audio, image and video coding, by a more robust and versatile concept based on ISCD is examined.

Although the available computational power in mobile devices grows exponentially, the battery capacity does unfortunately not follow this increase. This fact, alongside the increasing awareness of the environmental resources by users and operators, necessitates the investigation of complexity reduction approaches. In this thesis, several complexity reduction approaches are presented. These include the limitation of the required receiver iterations as well as the introduction of complexity-reduced receiver components which do not alter the overall system complexity considerably.

Structure of the Thesis

In Chapter 2, *Iterative Source-Channel Decoding* (ISCD) is discussed in its historical context. ISCD denotes the realization of a Turbo-like receiver comprising the channel decoding and source decoding stages. A high-level introductory description of ISCD is given along with a justification of its use in today's multimedia codecs. ISCD is built upon the concept of Turbo-like codes. Therefore, Turbo codes which consist of parallel concatenated conventional codes are introduced and the more general class of Turbo-like codes is presented. The extension of the Turbo concept to other elements of the receiver chain is discussed and simulation results exhibit the superior performance of Turbo and Turbo-like codes compared to conventional channel coding schemes. Furthermore, the *EXtrinsic Information Transfer* (EXIT) chart technique [tB01c] is described, which permits a precise analysis of the convergence behavior of Turbo-like codes, and which has enabled a broad range of new system design methodologies.

Chapters 3 starts with an in-depth description of the ISCD system considered throughout this thesis. Simulation examples highlight the near-capacity performance of the ISCD scheme for correlated sources. It is shown how different types of correlation can be exploited and the applicability of ISCD is demonstrated in a real-world example. A technique based on EXIT charts to precisely estimate the *Symbol Error Rate* (SER) is given. It can be observed that in some cases, the EXIT charts do not permit to accurately predict the ISCD convergence behavior. A novel solution that overcomes this drawback is presented, leading to an improved convergence analysis that allows to forecast the number of necessary receiver iterations.

Furthermore, a new receiver concept is developed with the objective to overcome the suboptimality of the conventional delay-constrained ISCD receiver exploiting inter-frame correlation. Besides this new receiver concept, a transmitter based optimization technique for improving the decoding performance of ISCD is presented. This technique, denoted *Irregular Bit Mappings* (IBMs), optimizes the assignment of bit mappings to the different source parameters such that the decoding performance improves. Irregular bit mappings are a potent technique for system optimization and are one of the key innovations of this thesis. The inherent *Unequal Error Protection* (UEP) capabilities of IBMs are shown and the optimization is modified such that UEP can be taken into account if several source codec parameters have a higher influence on the reconstruction quality than others. This is the case in most modern speech, audio, image, and video codecs.

In several source codecs, the exact reconstruction of the parameters is indispensable for guaranteeing reconstruction of the source signal. However, optimized ISCD systems show in some cases an error floor, which means that a fraction of the parameters are still reconstructed erroneously, even in good channel conditions. The error floor is mainly influenced by the distance properties of the bit mapping in the source encoding stage. One of the key targets of this thesis is to reduce the error floor. For the achievement of this goal, it is shown how the selection of the bit mapping influences the error floor. The resulting loss in the waterfall region can be efficiently compensated by the use of a low complexity inner irregular code.

In certain cases, especially if small quantizer code books are employed, the use of a bit mapping with good Hamming distance properties is not always possible. In these cases, an elegant transmitter modification can be applied. The resulting innovative *Multi-Dimensional Bit Mappings* (MDBMs) permit to lower the error floor. Furthermore, the application of different stopping criteria to ISCD is studied and it is shown how a simple yet efficient *Hybrid Automatic Repeat reQuest* (HARQ) scheme can be realized for the transmission of source codec parameters with incremental redundancy.

Chapter 4 deals with the complexity reduction of one of the main elements of the ISCD receiver chain – the *Soft Decision Source Decoder* (SDSD). A first complexity reduction technique results from a transmitter based modification of the quantizer. This modification permits to construct an SDSD with considerably decreased complexity. A detailed analysis of the modified quantizer is given along with concrete and circumstantial complexity figures. A second complexity reduction approach, which is similar to known suboptimal channel decoding algorithms, prunes several improbable transitions at the receiver. It is of special interest that both algorithms can be combined which leads to the lowest overall complexity. It is highlighted how the combined algorithm can be used in a system with constrained computational resources to improve the overall performance by allowing more iterations.

In Chapter 5, the problem of error-resilient source compression is addressed. As the classical entropy coding schemes are generally prone to transmission errors, a novel alternative concept is proposed based on the ISCD system. In the design constraints of this concept, only near-lossless reconstruction is envisaged, because perfect reconstruction is not required in all speech or audio codecs, or can be neglected for certain parameters. The key aspect of ISCD-based source coding is that the compression can directly be incorporated into the system design. Novel guidelines for setting up either the irregular bit mapping, the irregular channel code, or both jointly, are derived. These guidelines can be elegantly formulated as linear programming or non-linear programming optimization problems that are numerically solvable. The different variants are finally compared amongst each other and with several state-of-the-art compression schemes.

Chapter 6 covers the robust transmission of *multiple descriptions*. *Multiple Description Coding* (MDC) is frequently used for the transmission of audio-visual content in packet-based networks prone to packet losses. First, SDSD is applied to multiple descriptions of correlated parameters and the achievable gains are quantified. It is additionally shown how iterative decoding can be applied to multiple descriptions and simulation results reveal that with an optimized system setup, large gains compared to the non-iterative approaches are possible. Using an EXIT chart based convergence analysis, the system settings are further optimized resulting in a novel setup which does not use any additional bit rate for dedicated channel coding, but guarantees good reconstruction over a wide range of channel qualities. The conventional MDC system without extra channel coding can be outperformed by several decibels with the proposed setup, if noise is expected on the transmission link.

Finally, a second innovative MDC approach based on ISCD is presented. In this case, the different descriptions are not generated by an *Multiple Description Index*

Assignment (MDIA), but by a convolutional code. The resulting system is denoted *Multiple Descriptions by Channel Coding* (MDCC). Investigations disclose that this methodology permits to fully reconstruct the signal if a description has been lost, as long as the source shows some minimum required correlation. Simulation results reveal that this novel system can operate close to the theoretical limit and is able to outperform the conventional multiple description techniques. Even in the presence of additive channel noise, the novel alternative system shows gains compared to the conventional scheme.

The driving influence for most of the innovations presented in this thesis has been the international *FlexCode* project, funded by the European Union. Many practical problems had its seeds within this project. Appendix A provides a brief high-level description of the *FlexCode* joint source-channel coding approach [BGK$^+$08c, KLK10]. Appendices B, C, and D contain various derivations required throughout the thesis. Appendix E addresses the problem of imperfect extrinsic information given perfect *a priori* knowledge of feed forward convolutional codes. Theoretical bounds of the attainable mutual information are derived. A complete summary of the SDSD equations in the probability and in the implementation-friendly logarithmic domain is given in Appendix F. Additionally, detailed complexity figures for the standard and the complexity reduced algorithms are given. The SDSD equations for the extension towards multiple descriptions are summarized in Appendix G in the probability as well as in the logarithmic domain.

Parts of the results of this thesis have been pre-published in the following references: [Sch05, SA05, CSS$^+$06, CSVA06, SCV07, SVAC07, ACS08, LSV08, SVCS08, SVC08, SSVC08, CSVA08a, TSV08, SVAC08, CSVA08b, SVA08, SSJ$^+$08, SSV08, LESV09, SV09, SV10a, SSV10, AAS$^+$10, CSVA10, SVCA10, SV10b, BSV11, SACV11]. These references are marked by an underlined label, i.e., [____], throughout the thesis.

2

Turbo-Like Codes & Transmission Systems

The discovery of Turbo codes in 1993 [BGT93, BG96] marked a breakthrough in the field of channel coding. Suddenly, channel coding close to the theoretical limits postulated by Shannon [Sha48] became possible with moderate computation complexity. The original Turbo concept is based on the parallel concatenation of relatively simple convolutional codes, separated by an interleaver. The key element of the outstanding performance of Turbo codes is on the one hand the use of an iterative decoder, which exchanges so-called *extrinsic* information between relatively simple component decoders, and on the other hand an interleaver which tries to ensure the statistical independence of the extrinsic information.

The Turbo concept of exchanging extrinsic information has revolutionized not only the field of channel coding, but has also been applied to other components of the receiver chain. Prominent examples possess iterative receivers which include demodulation, synchronization, equalization, and also source decoding, which is the focus of this thesis. The application of Turbo-like receivers and especially the introduction of convergence analysis tools like EXIT charts, has led to new design paradigms for transmission systems. Almost all new wireless and wireline transmission standards employ at least one iterative decoding loop at the receiver. Examples are UMTS [HT06], LTE [DPSB08], WiMAX [AGM07], WLAN 802.11n [IEE09], DVB-S2 [ETS09a], and DVB-T2 [ETS09b], to name only a few.

In this chapter, several basic channel coding notions are given first. As most building blocks of the subsequent chapters utilize either linear block codes or convolutional codes, they are briefly introduced in Sec. 2.1. The original Turbo code and the more general class of Turbo-like codes are introduced in Sec. 2.2. The EXIT chart technique for tracing the convergence of Turbo-like systems is highlighted in Sec. 2.3. Finally, the historical context of *Iterative Source-Channel Decoding* (ISCD) is given along with a high level block diagram in Sec. 2.4.

2.1 Linear Block and Convolutional Channel Codes

Linear Block Codes

Linear block codes describe one of the most basic channel coding techniques [Fri96, LC04, Moo05]. A code (row) vector $\mathbf{e}_t$ is obtained by the matrix multiplication

$$\mathbf{e}_t = \mathbf{x}_t \cdot \mathbf{G}$$

with $\mathbf{x}_t$ being the information (row) vector and $\mathbf{G}$ the generator matrix defining the code. The vectors $\mathbf{x}_t$ and $\mathbf{e}_t$ are defined as

$$\mathbf{x}_t = \left(x_{t,1}, x_{t,2}, \ldots, x_{t,\xi}, \ldots, x_{t,N_X}\right) \tag{2.1}$$

$$\mathbf{e}_t = \left(e_{t,1}, e_{t,2}, \ldots, e_{t,\eta}, \ldots, e_{t,N_E}\right) . \tag{2.2}$$

Thus, the generator matrix is of dimension $\dim \mathbf{G} = N_X \times N_E$ and the rate of the block code is defined as $r_{\mathrm{BC}} \doteq N_X/N_E$. The single components of $\mathbf{x}_t$, $\mathbf{G}$, and $\mathbf{e}_t$ are elements of the binary field $\mathbb{F}_2 \doteq \{0, 1\}$ or extension fields thereof. The latter case includes, e.g., the widely employed Reed-Solomon codes [RS60, WB94]. Besides the generator matrix $\mathbf{G}$, linear block codes are characterized by their parity check matrix $\mathbf{H}$, which defines the null space of $\mathbf{G}$ [Moo05]. Thus

$$\mathbf{e}_t \cdot \mathbf{H}^T = \mathbf{0}$$

holds for all valid code vectors $\mathbf{e}_t$ of a linear block code. A multitude of construction recommendations for linear block codes exist, with the most common being, e.g., *Bose-Chaudhuri-Hocquenghem* (BCH) codes, *Cyclic Redundancy Check* (CRC) codes, Reed-Muller codes, Golay codes [Ree54, LC04, Moo05], and the recently discovered capacity achieving (on binary input channels) polar codes [Ari09]. Tables of good block codes can be found in [MN77, Bro98].

Another important class of linear block codes are *Low-Density Parity-Check* (LDPC) codes, which have a sparse parity check matrix $\mathbf{H}$, i.e., $\mathbf{H}$ contains mostly zeros. LDPC codes have been invented in 1963 [Gal63], but have then been forgotten until 1996, when they were rediscovered by MacKay [MN96, MN97, Mac99]. LDPC codes are amongst the most powerful channel codes these days, especially for high code rates [Moo05], and compete with Turbo codes, each having their own advantages and disadvantages [Bee10]. LDPC codes which asymptotically reach the Shannon limit within a margin of 0.0045 dB can be constructed [CFRU01]. Decoding LDPC codes is usually performed using the suboptimal *belief propagation* algorithm [Pea88, CF02] or variants thereof, e.g., [ZF02, KK03, Bee10, BSV11].

Convolutional Codes

Convolutional codes were first introduced by Elias [Eli55] as an alternative to block codes and became extremely popular with the advent of the *Maximum Likelihood* (ML) Viterbi algorithm [Vit67, For73]. Besides the Viterbi algorithm, other decoding approaches exist, including the sequential decoder [WR61, AM84],

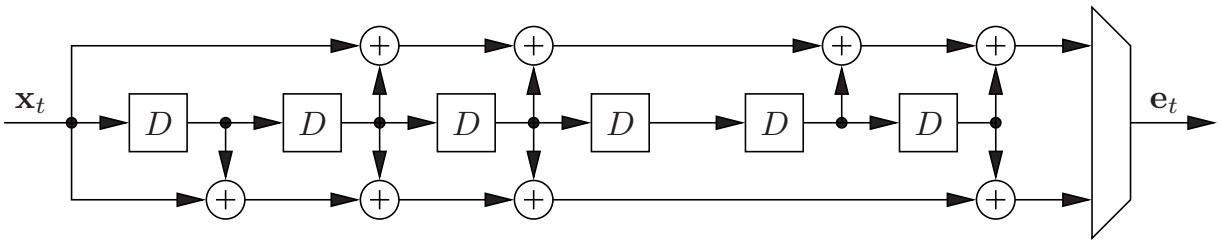

Figure 2.1: Feed forward convolutional code with $J = 6$, $\mathbb{G}^{[\mathrm{CC}]} = \{133, 171\}_8$, and rate $r_{\mathrm{CC}} = \frac{1}{2}$.

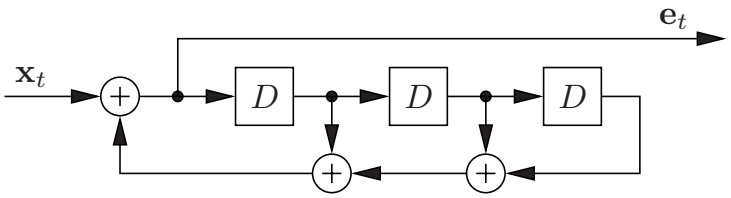

Figure 2.2: Recursive non-systematic convolutional code with $J = 3$, $\mathbb{G}^{[\mathrm{CC}]} = \{\frac{10}{17}\}_8$, and rate $r_{\mathrm{CC}} = 1$.

symbol-by-symbol *Maximum A Posteriori* (MAP) decoding with the *Bahl, Cocke, Jelinek, Raviv* (BCJR) algorithm [BCJR74], or (suboptimal) low-complexity decoders [And89, CFR01, Sch05]. An iterative decoding approach of convolutional codes has been studied in [SA05, SM06]. Iterative decoding of convolutional codes is especially beneficial for the class of self-doubly orthogonal convolutional codes [CHGB98, CHG03, CHH06].

Convolutional codes can be subdivided into the two main classes of feed forward and recursive convolutional codes and are mainly characterized by their rate $r_{\mathrm{CC}} \doteq \frac{N_X}{N_E}$ and their number of memory elements J (or their constraint length $J+1$). Figure 2.1 depicts an exemplary rate $r_{\mathrm{CC}} = \frac{1}{2}$ feed forward convolutional code with $J = 6$. The input and output vectors $\mathbf{x}_t$ and $\mathbf{e}_t$ are defined as in (2.1) and (2.2). Besides J, the code is characterized by its generator polynomials, which are commonly given in octal form. The upper output of the code in Fig. 2.1 can be described by a shift register with the generator polynomial $1 + D^2 + D^3 + D^5 + D^6$ [JZ99] which can be written as $(1\,0\,1\,1\,0\,1\,1)_2$ in binary form (with the LSB corresponding to the highest exponent of the polynomial) or as $(133)_8$ in octal representation. The generator of the considered code is written as $\mathbb{G}^{[\mathrm{CC}]} = \{133, 171\}_8$, describing both outputs. Note that the code depicted in Fig. 2.1 is often denoted "standard" code (see, e.g., [FH95]) as it is used in a variety of applications, for instance the Galileo deep space mission [LC88].

An example of a rate $r_{\mathrm{CC}} = 1$ *Recursive Non-Systematic Convolutional* (RNSC) code with $J = 3$ is given in Fig. 2.2. The generator for recursive codes is given in rational form with the numerator denoting the feed forward branch and the denominator the feedback branch. The generator of this code thus amounts to $\mathbb{G}^{[\mathrm{CC}]} = \{\frac{10}{17}\}_8$. An alternative description of recursive convolutional codes using Galois field arithmetic is given in [CSS+06].

A thorough review of convolutional codes and their properties can be found in [For70, JZ99]. Tables of good codes can be found in, e.g., [Lar73, DMW82, Pro00].

2.2 Turbo and Turbo-Like Channel Codes

2.2.1 Turbo Codes

A remarkable breakthrough in channel coding was the discovery of Turbo codes by Berrou, Glavieux and Thitimajshima [BGT93, BG96]. Using two *Parallel Concatenated Convolutional Codes* (PCCCs), separated by an interleaver and with an iterative decoder based on two BCJR blocks, channel coding close to the theoretical performance limit [Sha48] became possible with moderate computational complexity. The low decoding complexity combined with the extraordinary *Bit Error Rate* (BER) performance pushed Turbo codes into numerous applications [CHIW98, Ber03], such as, e.g., the *Universal Mobile Telecommunications System* (UMTS) [HT06], *Long Term Evolution* (LTE) [DPSB08], and *Worldwide Interoperability for Microwave Access* (WiMAX) [AGM07] wireless mobile radio standards.

Figure 2.3 depicts the encoder and decoder of the original (systematic) Turbo code of overall rate $r_{\mathrm{CC,Turbo}} = \frac{1}{3}$ as proposed in [BGT93, BG96]. Both convolutional codes are $r_{\mathrm{CC}} = 1$ identical codes with $J = 4$ and $\mathbb{G}^{[\mathrm{CC}]} = \{\frac{21}{37}\}_8$. A rate $r_{\mathrm{CC,Turbo}} = \frac{1}{2}$ code can be realized by alternatingly puncturing the output of the first and second encoder [BG96].

The iterative Turbo decoder is depicted in the right part of Fig. 2.3. It is assumed that the channel encoder output $\mathbf{e}_t$ is mapped to complex channel symbols $\mathbf{y}_t$, which are transmitted over a noisy channel, and that the noisy complex channel symbols $\mathbf{z}_t$ are received. The reliability of the channel transmission can be expressed in terms of channel transition *Probability Density Functions* (pdfs) $\mathsf{p}(z_{t,\ell}|y_{t,\ell})$. The symbol demapper computes the channel-related *a posteriori* L-values [HOP96]

$$\mathsf{L}_{\mathrm{CD}}^{[\mathrm{chan}]}(e_{t,\eta}) \doteq \ln\left(\frac{\mathsf{P}(e_{t,\eta}=0\,|\,\mathbf{z}_t)}{\mathsf{P}(e_{t,\eta}=1\,|\,\mathbf{z}_t)}\right), \tag{2.3}$$

with $\eta \in \{1,\ldots,N_E\}$ and $\mathbf{z}_t$ denoting the noisy vector of received channel symbols. In the case of a *Binary Phase Shift Keying* (BPSK) transmission (BPSK symbol

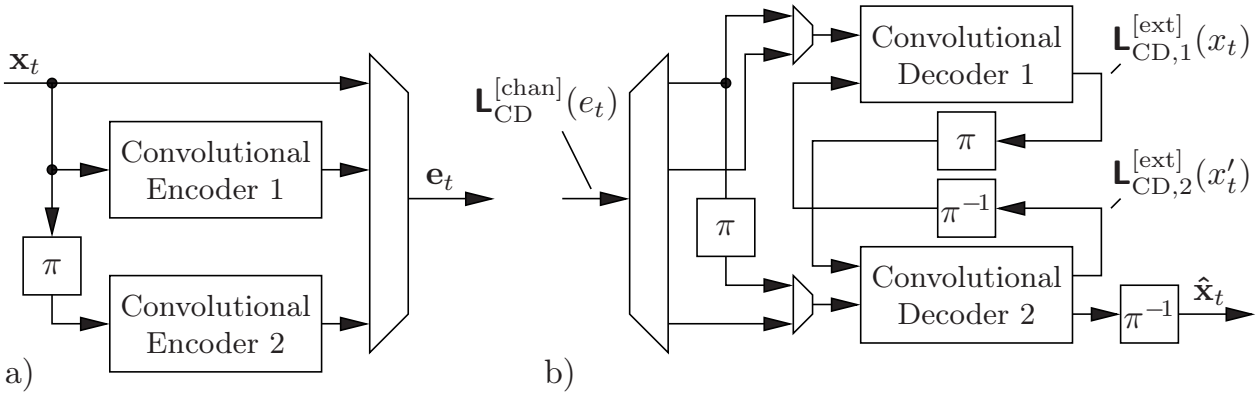

Figure 2.3: Turbo encoder (a) and Turbo decoder (b) as presented in [BGT93, BG96] consisting of two parallel concatenated convolutional codes. $\mathsf{L}_{\mathrm{CD}}^{[\mathrm{chan}]}(e_t)$ is a shorthand notation for the vector of L-values $\big(\mathsf{L}_{\mathrm{CD}}^{[\mathrm{chan}]}(e_{t,1}),\ldots,\mathsf{L}_{\mathrm{CD}}^{[\mathrm{chan}]}(e_{t,N_E})\big)$. Similarly, $\mathsf{L}_{\mathrm{CD},\chi}^{[\mathrm{ext}]}(x_t) \doteq \big(\mathsf{L}_{\mathrm{CD},\chi}^{[\mathrm{ext}]}(x_{t,1}),\ldots,\mathsf{L}_{\mathrm{CD},\chi}^{[\mathrm{ext}]}(x_{t,N_X})\big)$.

$y_{t,\eta} = \sqrt{E_\mathrm{s}}(1 - 2e_{t,\eta}))$ over a zero mean *Additive White Gaussian Noise* (AWGN) channel with attenuation a and known power spectral density $\sigma_n^2 = N_0/2$, the L-values $\mathsf{L}_{\mathrm{CD}}^{[\mathrm{chan}]}(e_{t,\eta})$ can also be written as [HOP96]

$$\mathsf{L}_{\mathrm{CD}}^{[\mathrm{chan}]}(e_{t,\eta}) = \ln\left(\frac{\mathsf{p}(z_{t,\eta}|e_{t,\eta}=0)}{\mathsf{p}(z_{t,\eta}|e_{t,\eta}=1)}\right) = 4a\frac{E_\mathrm{s}}{N_0}z_{t,\eta} = \frac{2aE_\mathrm{s}}{\sigma_n^2}z_{t,\eta} \doteq \mathsf{L}_c \cdot z_{t,\eta}\,, \tag{2.4}$$

with $z_{t,\eta} = a \cdot y_{t,\eta} + n_{t,\eta}$ and under the assumption that the bits $e_{t,\eta}$ are zero or one with equal probability. This latter assumption is usually valid for most well-designed communication systems (or can be provided by a scrambler).

As the code is systematic, there also exist channel-related L-values of the systematic bits $\mathbf{x}_t$, i.e., $\mathsf{L}_{\mathrm{CD}}^{[\mathrm{chan}]}(x_{t,\xi})$ with $\xi \in \{1,\ldots,N_X\}$, which are implicitly included in $\mathsf{L}_{\mathrm{CD}}^{[\mathrm{chan}]}(e_{t,\eta})$. The channel-related information $\mathsf{L}_{\mathrm{CD}}^{[\mathrm{chan}]}(e_{t,\eta})$ is also frequently denoted as *intrinsic* information. For the description of the frame-by-frame processing in the decoder, the single L-values $\mathsf{L}_{\mathrm{CD}}^{[\mathrm{chan}]}(e_{t,\eta})$ are grouped to a vector of L-values

$$\mathbf{L}_{\mathrm{CD}}^{[\mathrm{chan}]}(e_t) \doteq \left(\mathsf{L}_{\mathrm{CD}}^{[\mathrm{chan}]}(e_{t,1}),\ \mathsf{L}_{\mathrm{CD}}^{[\mathrm{chan}]}(e_{t,2}),\ \ldots,\ \mathsf{L}_{\mathrm{CD}}^{[\mathrm{chan}]}(e_{t,N_E})\right) \tag{2.5}$$

with N_E denoting the length of the vector $\mathbf{e}_t$.

At the decoder, the channel-related L-values are demultiplexed and the systematic part as well as the parity part of the first code are fed to the first convolutional decoder, which operates on the trellis of the corresponding *Recursive Systematic Convolutional* (RSC) code with $\mathbb{G}^{[\mathrm{CC}]} = \{1, \frac{21}{37}\}_8$. The decoder is based on the BCJR MAP algorithm [BCJR74, BDMP97] and usually a logarithmic implementation [RVH95, HOP96] (LogMAP decoder) is employed for numerical stability reasons. This first decoder computes *extrinsic* L-values $\mathbf{L}_{\mathrm{CD},1}^{[\mathrm{ext}]}(x_t)$, which are interleaved and fed to the second decoder as *a priori* information. Note that we use the short-hand notation $\mathbf{L}_{\mathrm{CD},1}^{[\mathrm{ext}]}(x_t)$, to represent vectors of L-values, with $\mathbf{L}_{\mathrm{CD},1}^{[\mathrm{ext}]}(x_t) = \left(\mathsf{L}_{\mathrm{CD},1}^{[\mathrm{ext}]}(x_{t,1}),\ldots,\mathsf{L}_{\mathrm{CD},1}^{[\mathrm{ext}]}(x_{t,N_X})\right)$. The second decoder also operates on the trellis of the $\mathbb{G}^{[\mathrm{CC}]} = \{1, \frac{21}{37}\}_8$ RSC code and uses the (interleaved) extrinsic information $\mathbf{L}_{\mathrm{CD},1}^{[\mathrm{ext}]}(x'_t)$ of the first decoder, the channel-related L-values of the parity bits generated by the second code, as well as the (interleaved) channel-related systematic L-values $\mathbf{L}_{\mathrm{CD}}^{[\mathrm{chan}]}(x'_t)$ to generate refined extrinsic information $\mathbf{L}_{\mathrm{CD},2}^{[\mathrm{ext}]}(x'_t)$, which is used as *a priori* information (after deinterleaving) in the subsequent iteration in the first decoder. After a fixed number of iterations Ω, the second decoder generates an estimate $\hat{\mathbf{x}}_t$ of the bit stream by taking the sign of the *a posteriori* L-values generated by the second decoder. The *a posteriori* L-values are given by (2.6) (see below).

The key element of the Turbo decoder is the use and the generation of extrinsic information in the component decoders. The extrinsic information $\mathsf{L}_{\mathrm{CD}}^{[\mathrm{ext}]}(x_{t,\xi})$ of a bit $x_{t,\xi}$ (with $\xi \in \{1,\ldots,N_X\}$) is the information carried by the bits surrounding $x_{t,\xi}$, as imposed by the code constraints [HLY02]. This means that no information directly concerning the data bit $x_{t,\xi}$ itself (i.e., also the intrinsic information $\mathsf{L}_{\mathrm{CD}}^{[\mathrm{chan}]}(x_{t,\xi})$ and

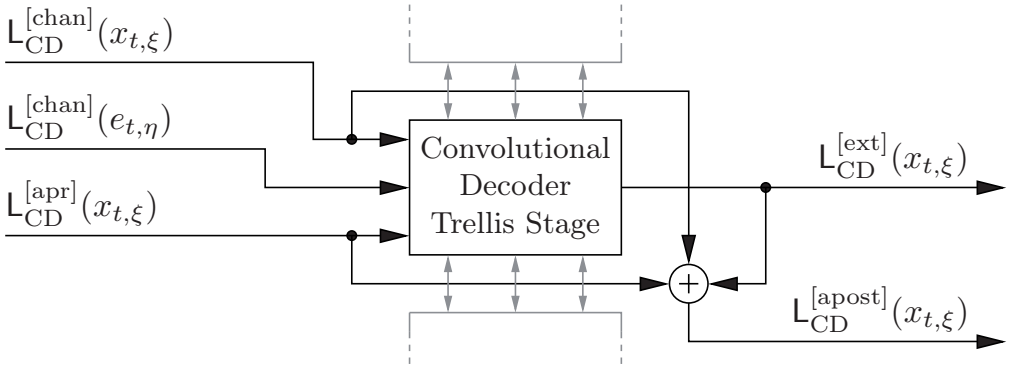

Figure 2.4: Relation between input L-values and extrinsic as well as *a posteriori* output L-values at the convolutional decoder (trellis) stage for the bit $x_{t,\xi}$.

optionally available bit-level source *a priori* information $\mathsf{L}_{\mathrm{BL}}^{[\mathrm{apr}]}(x_{t,\xi})$, characterizing a possible non-uniform distribution of the bit $x_{t,\xi}$) is part of the extrinsic information.

Figure 2.4 illustrates the relationships between the different kinds of information for one trellis stage (information bit at position ξ) of the convolutional code used in the above presented Turbo code. The input of the decoding stage is the (intrinsic) channel-related information of the systematic bit $\mathsf{L}_{\mathrm{CD}}^{[\mathrm{chan}]}(x_{t,\xi})$ and of the according parity bit $\mathsf{L}_{\mathrm{CD}}^{[\mathrm{chan}]}(e_{t,\eta})$ (rate $r_{\mathrm{CC}} = \frac{1}{2}$ systematic code). Additionally, *a priori* information $\mathsf{L}_{\mathrm{CD}}^{[\mathrm{apr}]}(x_{t,\xi})$ for the data bit under consideration is available. Within the Turbo decoder, this *a priori* information corresponds to the extrinsic output of the respective other component decoder and can also take into account a possible unequal distribution of the bit under consideration, e.g., $\mathsf{L}_{\mathrm{CD},1}^{[\mathrm{apr}]}(x_{t,\xi}) = \mathsf{L}_{\mathrm{CD},2}^{[\mathrm{ext}]}(x_{t,\xi}) + \mathsf{L}_{\mathrm{BL}}^{[\mathrm{apr}]}(x_{t,\xi})$. However, in most cases, the bits $x_{t,\xi}$ are assumed to be zero or one with equal probability. Therefore, the bit-level source *a priori* information is assumed to be zero in what follows, i.e., $\mathsf{L}_{\mathrm{BL}}^{[\mathrm{apr}]}(x_{t,\xi}) = 0$, leading to $\mathsf{L}_{\mathrm{CD},1}^{[\mathrm{apr}]}(x_{t,\xi}) = \mathsf{L}_{\mathrm{CD},2}^{[\mathrm{ext}]}(x_{t,\xi})$ and $\mathsf{L}_{\mathrm{CD},2}^{[\mathrm{apr}]}(x_{t,\xi}) = \mathsf{L}_{\mathrm{CD},1}^{[\mathrm{ext}]}(x_{t,\xi})$.

At the decoder output, the extrinsic information $\mathsf{L}_{\mathrm{CD}}^{[\mathrm{ext}]}(x_{t,\xi})$ and the *a posteriori* information $\mathsf{L}_{\mathrm{CD}}^{[\mathrm{apost}]}(x_{t,\xi})$ are related by [HOP96]

$$\mathsf{L}_{\mathrm{CD}}^{[\mathrm{apost}]}(x_{t,\xi}) = \mathsf{L}_{\mathrm{CD}}^{[\mathrm{ext}]}(x_{t,\xi}) + \mathsf{L}_{\mathrm{CD}}^{[\mathrm{apr}]}(x_{t,\xi}) + \mathsf{L}_{\mathrm{CD}}^{[\mathrm{chan}]}(x_{t,\xi})\,. \tag{2.6}$$

A completely new decoding paradigm emerged with the advent of Turbo codes and the utilization of extrinsic information. The concept of extrinsic message passing in channel decoding has later been applied to other channel coding concepts, such as *Serially Concatenated Convolutional Codes* (SCCCs) [BM96b], hybrid concatenated codes [DP97], or the concatenation of LDPC and convolutional codes [COV05], to name only a few.

2.2.2 Turbo-Like Channel Codes

Besides the parallel concatenation of convolutional codes, according to the original Turbo concept, the serial concatenation of interleaved channel codes with iterative decoding has proved to yield impressive results [BM96a, BM96b, BDMP98b,

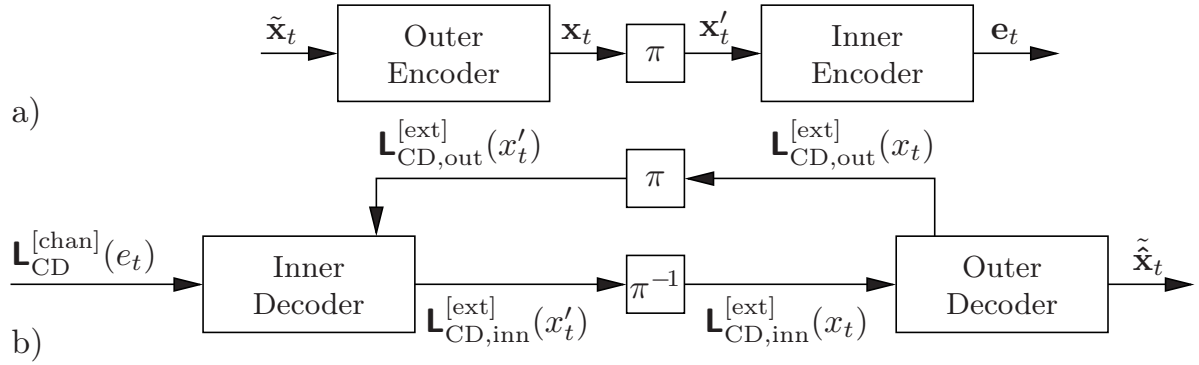

Figure 2.5: Encoder (a) and iterative decoder (b) for serially concatenated convolutional codes.

BMD03, Tüc04]. The concatenation of (interleaved) codes has been utilized prior to the invention of Turbo codes, for example the *Consultative Committee on Space Data Systems* (CCSDS) standard concatenation scheme is consisting of an outer Reed-Solomon code and an inner feed forward convolutional code of constraint length $J+1=7$ [CHIW98]. However, these codes were in general not decoded iteratively. In order to differentiate serially concatenated codes with iterative decoding from the original parallel concatenated Turbo codes, the expression *Turbo-like* codes has been introduced [DJM98, Jin01, Abb07].

Encoder and iterative decoder of Turbo-like serially concatenated codes are depicted in Fig. 2.5. The first encoder, denoted *outer encoder*, encodes $\tilde{\mathbf{x}}_t$ to $\mathbf{x}_t$, which is then encoded (after interleaving π) by the second encoder, denoted *inner encoder*, to $\mathbf{e}_t$. At the receiving side, the inner decoder generates the vector of extrinsic L-values $\mathsf{L}^{[\mathrm{ext}]}_{\mathrm{CD,inn}}(x'_t) = \big(\mathsf{L}^{[\mathrm{ext}]}_{\mathrm{CD,inn}}(x'_{t,1}), \ldots, \mathsf{L}^{[\mathrm{ext}]}_{\mathrm{CD,inn}}(x'_{t,N_X})\big)$ which is fed (after deinterleaving) to the outer decoder. Note that if the inner code is systematic, the vector of intrinsic systematic L-values $\mathsf{L}^{[\mathrm{chan}]}_{\mathrm{CD}}(x'_t)$ also need to be forwarded to the outer decoder [DP97]. Most inner codes in this thesis are non-systematic, which complies with the revelations that besides being recursive [KHC06], the inner code of a serially concatenated system should be of rate $r_{\mathrm{CC,inner}} \geq 1$ [AKtB02, AKtB04]. The doped [tB01b] and the *Randomly Punctured Recursive Systematic Convolutional* (RPRSC) [Tho07a, Tho07b] rate $r_{\mathrm{CC}} \geq 1$ convolutional codes contain, however, partly systematic bits, and care has to be taken to forward the intrinsic L-values of these bits to the outer decoder. Note that this connection is not depicted in Fig. 2.5 for simplicity.

The most widely known example for Turbo-like codes are *Serially Concatenated Convolutional Codes* (SCCCs). Besides SCCCs, the concatenation of other channel codes has also led to impressive results. One of the most prominent examples are *Repeat-Accumulate* (RA) codes, where the outer code consists of a simple repetition code and the inner code of an accumulator ($J=1$, $\mathbb{G}^{[\mathrm{CC}]} = \{\frac{2}{3}\}$ convolutional code) [DJM98]. RA codes with good performance can be designed for rates $\leq \frac{1}{3}$. Furthermore, the decoding complexity is kept relatively small due to the simplicity of the component codes [DP97, Jin01, Abb07]. The extension towards *Irregular Repeat-Accumulate* (IRA) codes leads to further performance improvements [JKM00, Abb07]. Another example is the concatenation of small block codes and convolutional codes [MIF06, Sch08, SSV08, SSV10].

Influence of Interleaving

The key element regarding the performance of Turbo and Turbo-like codes is the utilization of good interleavers. Common block interleavers lead to relatively poor performance if used for Turbo codes [HLY02, Cle06], as they are not able to sufficiently decorrelate the extrinsic information. The original Turbo code used a non-uniform interleaver which was crucial for the impressive performance [BG96]. Random or pseudo random interleaver constructions have proved to be a good choice for most system setups [HLY02]. A class of good random interleavers are the so called S-random interleavers [DP95a, DP95b, VY00] which have the property that the distance between S consecutive bits (before interleaving) is at least S after interleaving. Other interleaver designs which focus on reduced memory requirements and outperform the block interleaver are given in [HEM99a, HEM99b, HEM01].

If the amount of bits that have to be interleaved can vary from frame to frame, e.g., due to rate matching algorithms or the utilization of variable length codes, an interleaver which can cope with varying block lengths is often required. One example of such size-varying interleavers is the class of *prunable* S-random interleavers according to [FSB02]. Other prunable interleavers are given in [EH99, TDB07, DB05a, DB05b].

Turbo and Turbo-like codes are also subject to a phenomenon called *interleaver gain*, which is defined as the factor that decreases the bit error rate as a function of the interleaver size [BDMP98b]. It has been shown in [BDMP98b] that the interleaver gain can be higher for carefully designed SCCCs than for PCCCs.

Simulation Examples

Simulation results for several Turbo and Turbo-like codes are given in Fig. 2.6 for $r_{\mathrm{CC}} = \frac{1}{2}$ and $r_{\mathrm{CC}} = \frac{1}{3}$ codes and BPSK symbol mapping. In all cases, the size of information bits per frame amounts to $N_X = 10000$ bits. The PCCC is the original Turbo code of rate $r_{\mathrm{CC}} = \frac{1}{3}$; the rate $r_{\mathrm{CC}} = \frac{1}{2}$ version is achieved by alternatingly puncturing the parity bits [BGT93, BG96]. The SCCC for the rate $r_{\mathrm{CC}} = \frac{1}{2}$ case is the code designed in [tB00b] with an accumulator ($J = 1$, $\mathbb{G}^{[\mathrm{CC}]} = \{\frac{2}{3}\}_8$) as inner code and an RSC code with $J = 2$ and $\mathbb{G}^{[\mathrm{CC}]} = \{1, \frac{5}{7}\}_8$ as outer code. In the rate $r_{\mathrm{CC}} = \frac{1}{3}$ case, the outer code is replaced by an RSC code with $J = 3$ and $\mathbb{G}^{[\mathrm{CC}]} = \{1, \frac{10}{17}, \frac{10}{17}\}_8$. S-random interleavers ($\mathsf{S} = 15$) and $\Omega = 25$ decoding iterations have been used.

In addition to the PCCC and the SCCC, results for irregular LDPC codes constructed using the *Progressive Edge Growth* (PEG) algorithm [HEA01, HEA05] with degree distributions resulting from a density evolution optimization [CFRU01, CRU01, RSU01] are shown for comparison. Besides Turbo and Turbo-like codes, LDPC codes represent another important class of iteratively decodable codes that permit to closely reach the Shannon limit. The LDPC codes are decoded using standard belief propagation with $\Omega = 50$ iterations. Furthermore, simulation results of the convolutional code depicted in Fig. 2.1 are shown in the rate $r_{\mathrm{CC}} = \frac{1}{2}$ case. In the rate $r_{\mathrm{CC}} = \frac{1}{3}$ case, a convolutional code with $J = 6$ and $\mathbb{G}^{[\mathrm{CC}]} = \{133, 145, 175\}_8$ (maximum distance code [Pro00]) is used as reference. The theoretically achievable BER bound

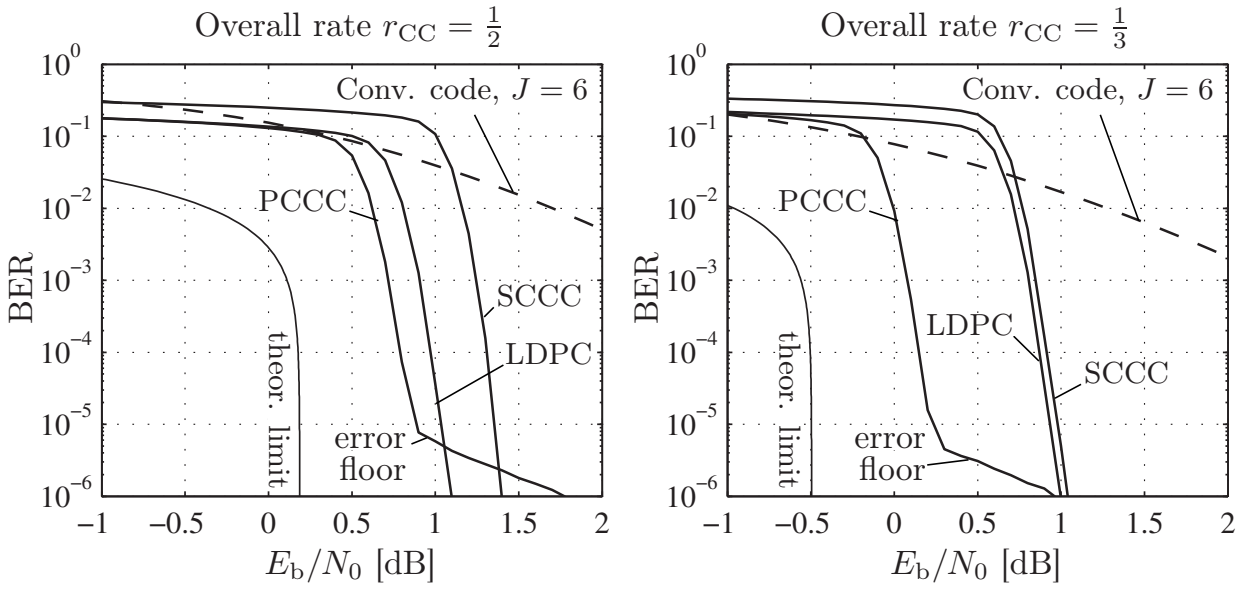

Figure 2.6: BER performance of different Turbo-like codes of overall coding rates $r_{\mathrm{CC}} = \frac{1}{2}$ and $r_{\mathrm{CC}} = \frac{1}{3}$ for information blocks of $N_X = 10000$ bits and $\Omega = 25$ decoding iterations ($\Omega = 50$ for the LDPC code) and the convolutional code depicted in Fig. 2.1 for BPSK symbol mapping.

for a successful transmission is also given, e.g., [Moo05, HH09]. This bound is obtained by combining the rate-distortion function [Ber71] of the binary source with the channel capacity [Sha48]. Note that E_{b} denotes the energy per information bit, i.e., $E_{\mathrm{b}} = E_{\mathrm{s}}/r_{\mathrm{CC}}$.

It can be seen that all three iteratively decoded codes outperform the conventional convolutional code. The PCCC shows the best waterfall performance, i.e., its BER starts to drop rapidly already for very low values of E_{b}/N_0. However, an error floor is visible. This means that at a certain channel quality, the BER does not drop rapidly anymore, but decreases slowly. The SCCC and the LDPC code do not show this error floor for the depicted bit error rates due to the better interleaver gain properties [BDMP98b] (however, an error floor is expected towards lower BER values [BDMP98b, Bee10]). Note that the SCCC considered here has a relatively low decoding complexity due to the very simple component codes. Figure 2.6 also confirms the statement that LDPC codes generally provide a better relative performance for higher coding rates [Moo05]. In the $r_{\mathrm{CC}} = \frac{1}{3}$ case, the LDPC code and the SCCC perform almost identically, while for $r_{\mathrm{CC}} = \frac{1}{2}$, the LDPC code outperforms the SCCC. Note that the simulated codes are not the best codes known, many advancements and improvements to PCCCs (e.g., [BGO$^+$07, BGOS09]), LDPC codes (e.g., [DM98]) and SCCCs (e.g., [Tüc04]) exist.

Unfortunately, the iteratively decodable codes do not perform equally well for all information block sizes N_X. A strong dependency of the BER performance with N_X which directly correlates with the interleaver size is observed [BDMP98a, BDMP98b, BMD03]. Simulation results for an information block length of $N_X = 100$ are given in Fig. 2.7 for the same codes as in Fig. 2.6. It becomes obvious that in this case, the conventional convolutional code is a good choice, as the BER performance is quite

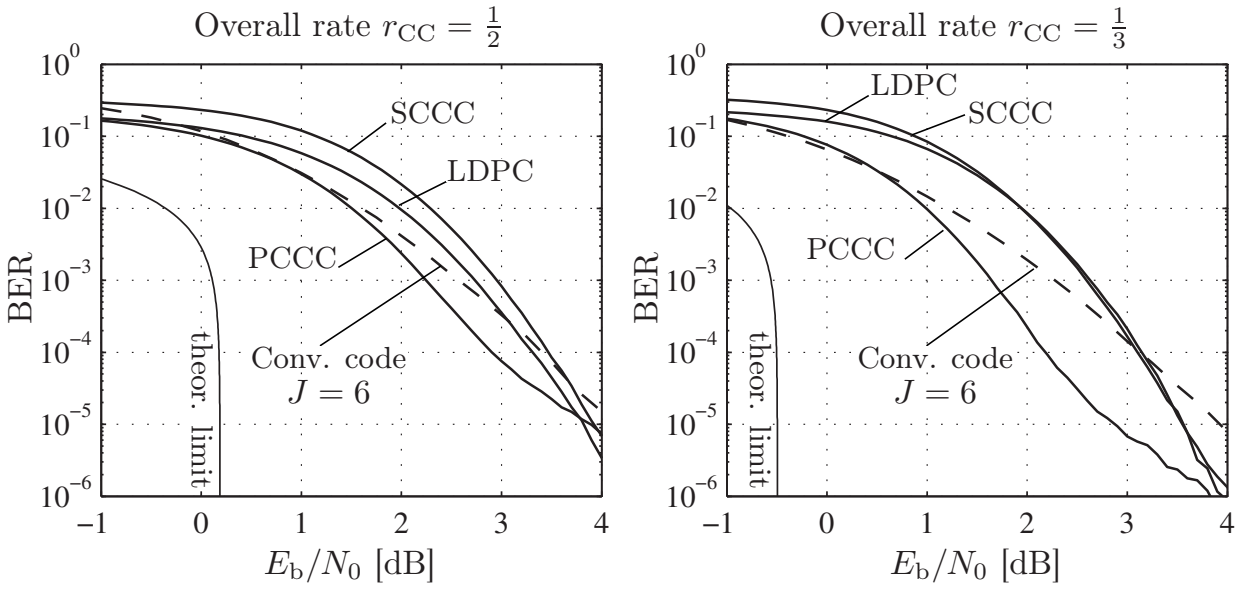

Figure 2.7: BER performance of different Turbo-like codes of overall coding rates $r_{\mathrm{CC}} = \frac{1}{2}$ and $r_{\mathrm{CC}} = \frac{1}{3}$ for information blocks of $N_X = 100$ bits and $\Omega = 25$ decoding iterations ($\Omega = 50$ for the LDPC code) and the convolutional code depicted in Fig. 2.1 for BPSK symbol mapping.

close to the one of the iteratively decodable codes, however, its decoding complexity is smaller. It can thus be concluded that the use of iteratively decodable codes is especially beneficial for large block lengths. In the case of a small block lengths ($N_X \approx 100$), the performance of these codes is comparable with conventional codes, such as convolutional codes.

2.2.3 Turbo-Like Receivers

The Turbo principle of exchanging extrinsic information between channel decoders has not only been applied to concatenated channel codes, but also to the complete receiver chain. Some of the most famous systems include the iterative decoding of *Bit Interleaved Coded Modulation* (BICM) [CTB98] (denoted *Bit Interleaved Coded Modulation with Iterative Decoding* (BICM-ID)) [LR97, LR99, CR01] and its extension towards *Orthogonal Frequency Division Multiplexing* (OFDM) [LSV08, NB08, LESV09], Turbo equalization [DJB95, TKS02, KST04], Turbo synchronization [NHD+03, GPH+07, HNL+07], iterative channel estimation and Turbo decoding [GLAV08], Turbo multiuser detection [Poo00, Poo04], but also *Iterative Source-Channel Decoding* (ISCD), which is introduced in Sec. 2.4. Systems employing more than one iterative loop and exploiting more than two code or receiver components also exist, e.g. [Tüc02, CBAV05, Cle06, OEAH07, SSVC08, NEO+08, OEA+09].

2.3 Convergence Analysis Using EXIT Charts

During the design of Turbo-like transmission schemes, a prediction of the convergence behavior is important in order to estimate the required number of iterations at the

receiver. If the code has converged, further iterations do not lead to substantial gains in terms of bit error rate. One useful tool to analyze and describe the information transfer between the two decoders with respect to the convergence analysis is the *EXtrinsic Information Transfer* (EXIT) chart [tB99a, tB99b, tB01c, tB01a]. EXIT charts visualize the mutual information [CT06] of the L-values exchanged in the iterative decoding process. Other convergence prediction tools include for instance SNR charts [DDP00]. A comparison of different convergence analysis tools is given in [TtBH02, Hag04], where it is revealed that EXIT charts are indeed the best choice known so far. EXIT charts have become a standard technique for designing and optimizing new coding schemes with iterative decoding. The behavior of a system can be accurately predicted by solely measuring the characteristics of the component decoders and selecting the configuration which leads to the best results. Thus, no extensive bit error rate simulations are necessary for judging the BER performance of a system setup. Examples of system optimizations based on EXIT charts are given, e.g., in [tB00a, tB00b, tB00c, tB01a, TH02, Tüc04, CGV04, AV05, AAC+06, CGV06, Tho07a, PYOH08, LESV09, NH09b, SACV11], to name only a few. In what follows, EXIT charts are described in the context of SCCCs [tB00c] which best resemble the ISCD system considered in the remainder of this thesis, however, the statements apply to all kinds of Turbo-like receivers and Turbo codes.

The idea of EXIT charts is to predict the behavior of the iterative decoder by solely considering the input/output relations of individual constituent decoders. EXIT charts make use of two key observations. First, the extrinsic L-values remain fairly uncorrelated from the respective channel observations over many iterations for large interleaver sizes. Second, the pdfs of the extrinsic output values $\mathsf{L}_{\mathrm{CD,inn}}^{[\mathrm{ext}]}(x_t)$ and $\mathsf{L}_{\mathrm{CD,out}}^{[\mathrm{ext}]}(x_t)$ (which are *a priori* input values for the subsequent decoding stage) approach Gaussian-like distributions with increasing number of iterations [tB01c]. Furthermore the distribution of $\mathsf{L}_{\mathrm{CD,inn}}^{[\mathrm{ext}]}(x_t)$ and $\mathsf{L}_{\mathrm{CD,out}}^{[\mathrm{ext}]}(x_t)$ is consistent, which means that mean μ_e and variance σ_e^2 of the distribution are linked by $\mu_e = \sigma_e^2/2$. Thus, the pdf of the extrinsic L-values can be modeled by (for the example of $\mathsf{L}_{\mathrm{CD,out}}^{[\mathrm{ext}]}(x_t)$)

$$\mathsf{p}_{\mathsf{L}_{\mathrm{CD,out}}^{[\mathrm{ext}]}(X)}(\chi|X=x) = \frac{1}{\sqrt{2\pi\sigma_e^2}} \exp\left(-\frac{1}{2\sigma_e^2}\left(\chi - \frac{\sigma_e^2}{2}(1-2x)\right)^2\right), \tag{2.7}$$

with $x \in \mathbb{F}_2$ and under the assumption of a bipolar representation (given by $1-2x$) [tB01c]. Note that time and position indices are omitted in (2.7) for simplicity.

Using the assumption of consistent Gaussian extrinsic (and thus also *a priori*) L-values (see (2.7)), and the fact that the extrinsic L-values of the outer decoder serve as *a priori* input $\mathsf{L}_{\mathrm{CD,inn}}^{[\mathrm{apr}]}(x_t)$ to the inner decoder (and vice versa), the mutual information $\mathsf{I}_{\mathrm{CD,inn}}^{[\mathrm{apr}]} \doteq \mathsf{I}(X; \mathsf{L}_{\mathrm{CD,inn}}^{[\mathrm{apr}]}(X))$ is obtained by

$$\mathsf{I}_{\mathrm{CD,inn}}^{[\mathrm{apr}]} \doteq \mathsf{I}(X; \mathsf{L}_{\mathrm{CD,inn}}^{[\mathrm{apr}]}(X)) = \mathcal{J}(\sigma_a) \tag{2.8}$$

with σ_a^2 denoting the variance of the consistent *a priori* L-values and with [tB01c]

$$\mathcal{J}(\sigma_a) \doteq 1 - \int_{-\infty}^{\infty} \frac{\exp\left(-\left(\chi - \frac{\sigma_a^2}{2}\right)^2 / (2\sigma_a^2)\right)}{\sqrt{2\pi}\sigma_a} \cdot \mathrm{ld}\left(1 + \exp(-\chi)\right) \mathrm{d}\chi \,. \tag{2.9}$$

The measurement of the EXIT characteristic C_{CD} of a channel decoder is performed as follows. First, a random vector $\mathbf{x}_t$ is generated. For a given $\mathsf{I}_{\mathrm{CD,inn}}^{[\mathrm{apr}]} \in [0;1]$, $\sigma_a = \mathcal{J}^{-1}(\mathsf{I}_{\mathrm{CD,inn}}^{[\mathrm{apr}]})$ is computed numerically. Using σ_a and $\mu_a = \pm\sigma_a^2/2$, a Gaussian random process is generated taking into account the (bipolar representation of the) outer encoded bits $\mathbf{x}_t$ under consideration. These random L-values then serve as *a priori* L-values for the channel decoder. Additionally, the noisy channel-related L-values $\mathsf{L}_{\mathrm{CD}}^{[\mathrm{chan}]}(e_t)$ need to be generated (by transmitting the encoded bits over the noisy channel under consideration) and fed to the inner decoder. Two separate histogram measurements of the extrinsic output (separate histograms for $x = 0$ and $x = 1$) are then used to numerically approximate the mutual information, using

$$\begin{aligned}\mathsf{I}_{\mathrm{CD,inn}}^{[\mathrm{ext}]} = \mathsf{I}(X; \mathsf{L}_{\mathrm{CD,inn}}^{[\mathrm{ext}]}(X)) = \frac{1}{2} \sum_{\forall x \in \mathbb{F}_2} \int_{-\infty}^{\infty} \mathsf{p}_{\mathsf{L}_{\mathrm{CD,inn}}^{[\mathrm{ext}]}(X)}(\chi | X = x) \\ \times \mathrm{ld}\left(\frac{2 \cdot \mathsf{p}_{\mathsf{L}_{\mathrm{CD,inn}}^{[\mathrm{ext}]}(X)}(\chi | X = x)}{\mathsf{p}_{\mathsf{L}_{\mathrm{CD,inn}}^{[\mathrm{ext}]}(X)}(\chi | X = 0) + \mathsf{p}_{\mathsf{L}_{\mathrm{CD,inn}}^{[\mathrm{ext}]}(X)}(\chi | X = 1)}\right) \mathrm{d}\chi\end{aligned} \tag{2.10}$$

and by replacing the integral with appropriate sums [tB01c]. The outcome of this procedure is a function $\mathsf{I}_{\mathrm{CD,inn}}^{[\mathrm{ext}]} = \mathcal{F}(\mathsf{I}_{\mathrm{CD,inn}}^{[\mathrm{apr}]})$, which is denoted EXIT characteristic. We denote this function $\mathsf{C}_{\mathrm{CD,inn}}$, i.e., $\mathsf{I}_{\mathrm{CD,inn}}^{[\mathrm{ext}]} = \mathsf{C}_{\mathrm{CD,inn}}(\mathsf{I}_{\mathrm{CD,inn}}^{[\mathrm{apr}]})$. Note that if the inner code is (partly) systematic, the channel-related L-values $\mathsf{L}_{\mathrm{CD}}^{[\mathrm{chan}]}(x_{t,\xi})$ of the systematic positions are added to the extrinsic output prior to the histogram measurements.

The same procedure can be applied to the outer decoder: Given a certain $\mathsf{I}_{\mathrm{CD,out}}^{[\mathrm{apr}]}$, consistent Gaussian distributed *a priori* L-values are generated and the according extrinsic output of the outer decoder is used in histogram measurements to get the outer decoder characteristic $\mathsf{C}_{\mathrm{CD,out}}$, with $\mathsf{I}_{\mathrm{CD,out}}^{[\mathrm{ext}]} = \mathsf{C}_{\mathrm{CD,out}}(\mathsf{I}_{\mathrm{CD,out}}^{[\mathrm{apr}]})$. Note that the characteristic of the outer decoder in Turbo-like systems is independent of the transmission channel quality. Channel-related L-values of the systematic bits (in the case of an inner systematic code) are included in the extrinsic output of the inner decoder for measuring the EXIT characteristics and are therefore not required at the input of the outer decoder (for the measurement of the EXIT characteristic).

Figure 2.8-a) shows the EXIT characteristic $\mathsf{C}_{\mathrm{CD,inn}}$ of the $J = 1$, $\mathbb{G}^{[\mathrm{CC}]} = \{\frac{2}{3}\}_8$ accumulator used as inner code in the SCCC considered for the simulation example in Fig. 2.6. It can be seen that the characteristic of this inner code is dependent on the channel quality E_s/N_0. Figure 2.8-b) depicts EXIT characteristics of different rate $r_{\mathrm{CC}} = \frac{1}{2}$ feed forward and RSC codes used as inner code in a SCCC for

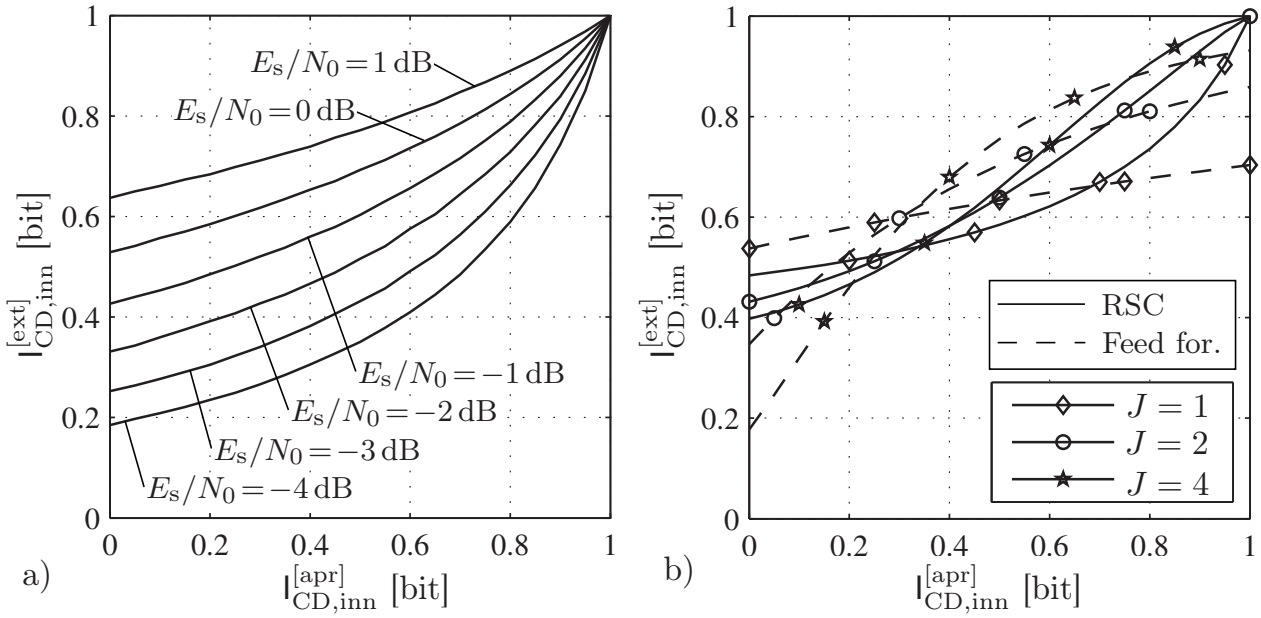

Figure 2.8: a) EXIT characteristics of the $r_{CC} = 1$, $J = 1$, $\mathbb{G}^{[CC]} = \{\frac{2}{3}\}_8$, accumulator for different channel qualities.
b) EXIT characteristics of several $r_{CC} = \frac{1}{2}$ feed forward and RSC codes for $E_s/N_0 = -5\,\text{dB}$.

	Feed forward	RSC
$J = 1$	$\mathbb{G}^{[CC]} = \{2, 3\}_8$	$\mathbb{G}^{[CC]} = \{1, \frac{2}{3}\}_8$
$J = 2$	$\mathbb{G}^{[CC]} = \{7, 5\}_8$	$\mathbb{G}^{[CC]} = \{1, \frac{5}{7}\}_8$
$J = 4$	$\mathbb{G}^{[CC]} = \{35, 23\}_8$	$\mathbb{G}^{[CC]} = \{1, \frac{23}{35}\}_8$

Table 2.1: Feed forward and Recursive Systematic Convolutional codes ($r_{CC} = \frac{1}{2}$) used in the right sub-plot of Fig. 2.8.

$E_s/N_0 = -5\,\text{dB}$. The utilized codes are summarized in Tab. 2.1. This case is especially important if an existing transmission system utilizing such a code shall be extended with an outer component. ISCD marks an example of such an extension. It can be seen that the feed forward codes are not able to generate $I^{[ext]}_{CD,inn} = 1\,\text{bit}$ for $I^{[apr]}_{CD,inn} = 1\,\text{bit}$. This means that even if perfectly reliable *a priori* information on the data bits is available, the decoder is unable to generate perfectly reliable extrinsic information. Reaching the $(1, 1)$ point in the EXIT chart is, however, crucial for a good performance of the Turbo-like system. This effect has already been observed in [tB01d]. A detailed analysis and theoretical bounds of the maximum attainable extrinsic mutual information are given in [SVAC07] and in App. E.

Figure 2.9-a) shows the complete EXIT chart analysis of the considered SCCC (see Fig. 2.6 for simulation results) for $E_b/N_0 = 1.3\,\text{dB}$ ($E_s/N_0 = -1.71\,\text{dB}$). To account for the iterative nature of the Turbo decoding algorithm, both decoder characteristics are plotted into a single diagram. However, the axes are swapped for the characteristic of the second decoder. Note that the characteristic $\mathsf{C}_{CD,out}$ is independent of the

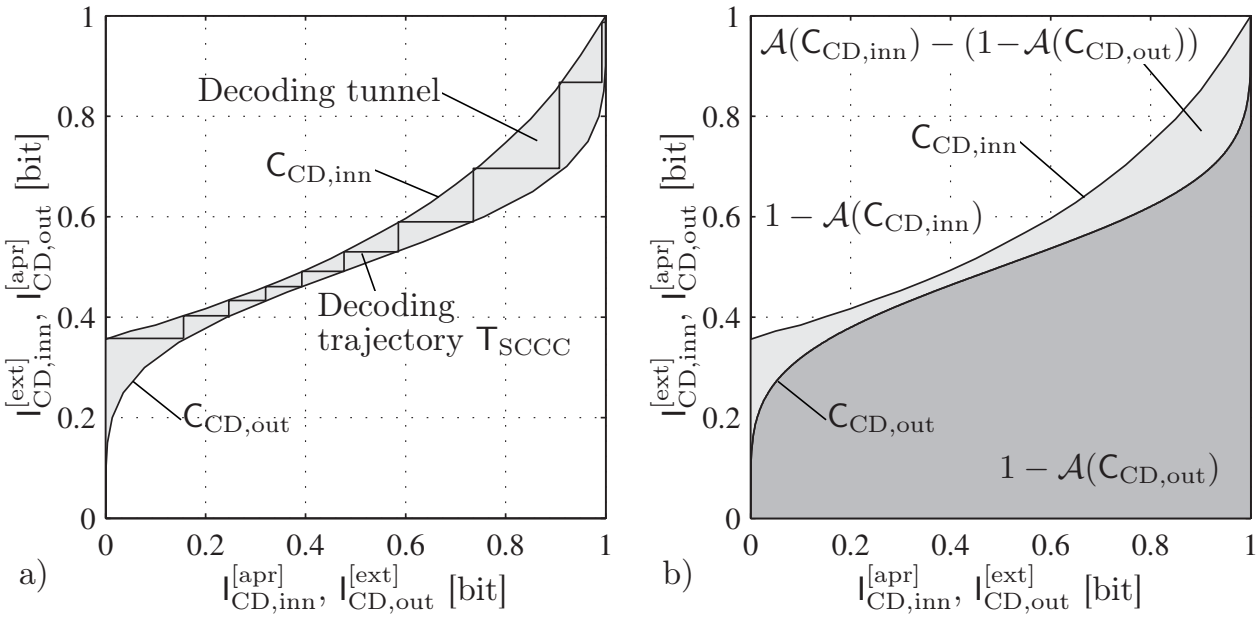

Figure 2.9: a) EXIT chart analysis of the SCCC used in Fig. 2.6 for $E_\mathrm{b}/N_0 = 1.3\,\mathrm{dB}$ ($E_\mathrm{s}/N_0 = -1.71\,\mathrm{dB}$), $r_{\mathrm{CC,inn}} = 1$, $J = 1$, $\mathbb{G}^{[\mathrm{CC}]} = \{\frac{2}{3}\}_8$ inner code, $r_{\mathrm{CC,out}} = \frac{1}{2}$, $J = 2$, $\mathbb{G}^{[\mathrm{CC}]} = \{1, \frac{5}{7}\}_8$ outer code.
b) Relation between the different areas in an EXIT chart.

channel quality. The exchange of mutual information in the actual decoder can also be measured and is visualized as a staircase-like decoding trajectory $\mathsf{T}_{\mathrm{SCCC}}$. Each step of $\mathsf{T}_{\mathrm{SCCC}}$ represents one decoding iteration. It can be seen that after $\Omega = 10$ iterations, the $(1, 1)$ point in the EXIT chart is reached for the given system setup, i.e., perfect (extrinsic) knowledge can be generated. This is confirmed by the simulation results in Fig. 2.6, where perfect decoding is possible at $E_\mathrm{b}/N_0 = 1.3\,\mathrm{dB}$.

Area Properties of EXIT Charts

A sufficient condition for successful iterative decoding is that an open decoding tunnel between both characteristics exists. A necessary but not sufficient condition for the existence of a decoding tunnel can be formulated using the area under the different characteristics of an EXIT chart. The necessary condition for successful decoding is that

$$\mathcal{A}(\mathsf{C}_{\mathrm{CD,inn}}) > 1 - \mathcal{A}(\mathsf{C}_{\mathrm{CD,out}}) \tag{2.11}$$

with

$$\mathcal{A}(\mathsf{C}_{\mathrm{CD}}) = \int_0^1 \mathsf{C}_{\mathrm{CD}}(\chi)\,\mathrm{d}\chi\,. \tag{2.12}$$

Figure 2.9-b) visualizes the different critical areas in an EXIT chart. The dark gray area represents $1-\mathcal{A}(\mathsf{C}_{\mathrm{CD,out}})$, while the light gray region represents the decoding tunnel. The area of the decoding tunnel thus amounts to $\mathcal{A}(\mathsf{C}_{\mathrm{CD,inn}}) - (1-\mathcal{A}(\mathsf{C}_{\mathrm{CD,out}}))$.

The areas under EXIT characteristics of components in a serially concatenated system exhibit different interesting properties [AKtB02, AKtB04]. One of these properties is the so-called *area property* of EXIT charts. The area property has been proved in [AKtB04] for arbitrary communication channels, however, the decoder *a priori* input has to be modeled by a *Binary Erasure Channel* (BEC). Observations suggest nonetheless that the property also holds for the Gaussian channels [Tüc04]. For the SCCC system, the area property can be formulated as [AKtB04]

$$\mathcal{A}\left(\mathsf{C}_{\mathrm{CD,out}}\right) = 1 - r_{\mathrm{CC,out}} \tag{2.13}$$

$$\mathcal{A}\left(\mathsf{C}_{\mathrm{CD,inn}}\right) \leq \frac{\mathsf{I}_{\mathcal{C}}}{r_{\mathrm{CC,inn}}}\,, \tag{2.14}$$

with $\mathsf{I}_{\mathcal{C}} \doteq \mathsf{I}(Y;Z)$ denoting the capacity of the transmission channel. Equality in (2.14) holds if the rate of the inner code $r_{\mathrm{CC,inn}} \geq 1$ [AKtB04]. In this case $\mathcal{A}(\mathsf{C}_{\mathrm{CD,inn}}) = \mathsf{I}_{\mathcal{C}}/r_{\mathrm{CC,inn}}$ and the area between both characteristics $(\mathcal{A}(\mathsf{C}_{\mathrm{CD,inn}}) - (1-\mathcal{A}(\mathsf{C}_{\mathrm{CD,out}})))$ is the so-called *rate loss* $\mathsf{I}_{\mathcal{C}} - r_{\mathrm{CC,out}}$. This implies that for a (decodable) capacity-achieving system, the area of the decoding tunnel asymptotically tends to zero, such that an infinite number of iterations (and an infinite block length) is required.

2.4 Iterative Source-Channel Decoding (ISCD)

Shannon's source-channel separation theorem [Sha48] states that if the minimum achievable source coding rate of a given source is below the channel capacity, the source can be reliably transmitted over the channel by performing appropriate encoding and decoding operations: therein, source and channel coding can be separated. The original theorem from Shannon holds for stationary and ergodic sources and channels and for asymptotically large block lengths. The result was extended to more general classes of sources and channels, for instance in [Dob63] and [Hu64], however, the condition of asymptotically large block lengths still has to be fulfilled. In [VVS94] and [VVS95], a simple example of a source not fulfilling the separation theorem has been shown. Vembu *et al.* conclude [VVS95] that care should be exercised before applying the separation theorem when dealing with non-stationary probabilistic models and they give more general conditions under which separation holds.

Shannon already showed the suboptimality of the separation theorem for multiuser systems in [Sha61], where an example of a correlated source transmitted over the two-way channel was provided [GEGP09]. Multiuser channels become increasingly important in the design of future mobile wireless networks for further increasing the spectral efficiency. A thorough analysis of the source-channel separability for multiuser channels is given in [GEGP09].

For the above-mentioned reasons, the joint consideration of source and channel coding needs to be considered for realizing transmission systems with good performance.

But also in more "traditional" cases, the constraints of the original separation theorem [Sha48] are almost never fulfilled. In state-of-the-art audio, image and video coding standards, delay and computational complexity restrictions imply the use of short block lengths. Some terms of residual redundancy typically remain in the source codec output due to these constraints and can be exploited at the receiver of a noisy communication system in order to increase the error robustness, e.g., [SB91, Fin98, FV01].

In the last decades, several techniques for joint source-channel coding have been introduced. The variety of these approaches can be divided into mainly two classes. In the first class, channel properties (like bit error rates) are utilized throughout the design of robust source encoding schemes, e.g., pseudo Gray coding [ZG90], channel optimized vector quantization [FV87, Far90, FV91], source optimized channel codes [Hei01b, HV05], or the selection of the optimum rate distribution between source and channel coding [HZ97, Hoc98]. The major drawback of all these approaches is that they have to be re-optimized for every specific channel condition. In the second class, source statistics (capturing the natural residual source redundancy) are exploited throughout channel (de)coding, which avoids re-optimization for every specific channel condition. Famous examples are unequal error protection [Hag88], source controlled channel decoding [Hag95, Hin01], and its application to, e.g., *Code Excited Linear Prediction* (CELP) [APF96] or *Mixed Excitation Linear Prediction* (MELP) encoded speech [FF03]. Joint source-channel coding approaches for JPEG2000 [TM01] image transmission are discussed in [FC06, FC10]. A compendium of (mostly non-iterative) joint source-channel coding techniques for video transmission can be found in [DK09].

Iterative Source-Channel Decoding (ISCD) [Gör00, HFSC00a, HFSC00b, AVS01, Gör01b, APV01, HG03, AV05, HAFH07, ACS08] can be considered as an advancement of source controlled channel decoding [Hag95, Hin01], where in each decoding step the source statistics are iteratively refined in a Turbo-like process. In the literature, ISCD has been applied to systems employing *Variable Length Codes* (VLCs) and *Fixed Length Codes* (FLCs).

Residual Source Redundancy

The key element of the ISCD approach is to exploit residual redundancy which is contained in the output parameters of the source encoder. As mentioned above, this is mostly due to delay and computational complexity constraints. However, a source encoder can also deliberately keep redundancy in the signal in order to increase the error robustness. If this redundancy is removed, for example by differential encoding, the decoder is prone to error propagation.

Figure 2.10 shows two examples of (measured) residual redundancy of source codec parameters. For this example, two of the model parameters of the *FlexCode* speech and audio encoder (see App. A) are considered. The measurements have been performed using German and English speakers of the NTT database [NA94] (male and female). Figure 2.10-a) shows the conditional inter-frame frequencies of occurrence

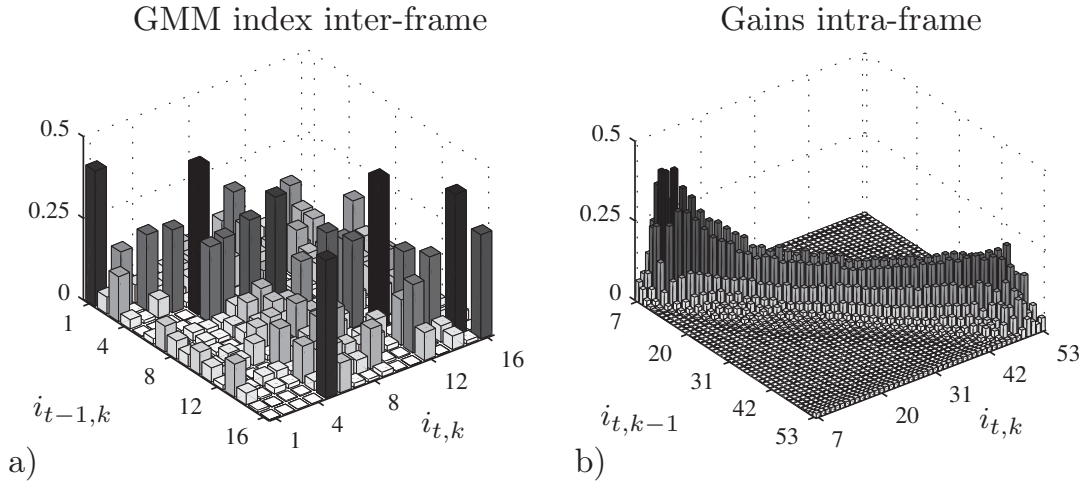

Figure 2.10: Residual redundancy of two model parameters of the *FlexCode* source encoder:
a) Conditional inter-frame frequencies of occurrence of the GMM index.
b) Conditional intra-frame frequencies of occurrence of the gain factors.

of the first quantizer index of each frame (frame index t). This first quantizer index, denoted $i_{t,1}$ (a detailed introduction to the notation is given in Sec. 3.1) represents the *Gaussian Mixture Model* (GMM) index, which is used to quantize the *Line Spectral Frequencys* (LSFs) (which represent the spectral amplitude of the signal segment) [Sam04, BGK+08a, BGK+08b, ZSN08]. Although looking quite chaotic at the first glance, subsequent indices show some correlation, as can be seen by a high number of very improbable transitions. Thus the residual redundancy of the GMM index can be effectively exploited within ISCD.

Figure 2.10-b) shows the intra-frame correlation of the gain factors. Note that each frame consists of four sub-frames with one gain factor for each sub-frame. The measured frequencies of occurrence are depicted and it can be seen that the gain factors are strongly correlated. Note that only a part of the histogram is depicted.

2.4.1 Baseband Block Diagram

Figure 2.11 depicts a generic baseband transceiver of a system employing ISCD. The time-discrete digitized counterpart of an analog source signal is partitioned into short time frames $\mathbf{s}_t$ which are labeled with the time (frame) index t. A generic source encoder extracts a bit vector $\mathbf{x}_t$ out of the source signal. If the employed source encoder is a so-called parametric source encoder, then it extracts a parameter vector $\mathbf{u}_t$ consisting of source codec parameters. For instance, in *Global System for Mobile Communications* (GSM) or UMTS speech communication, the parameter set comprises the coefficients of a filter describing the spectral envelope of a 20 ms speech segment, gain factors, as well as some other parameters representing the excitation of this filter. The generation of the bit stream is then performed using either FLCs, as in most speech codecs, or VLCs, as in one operation mode of the *FlexCode* codec and in most image and video codecs [TM01, DK09].

After interleaving, the resulting bit stream is channel encoded resulting in the bit vector $\mathbf{e}_t$. In this thesis, the utilized channel code is in most cases a convolutional code

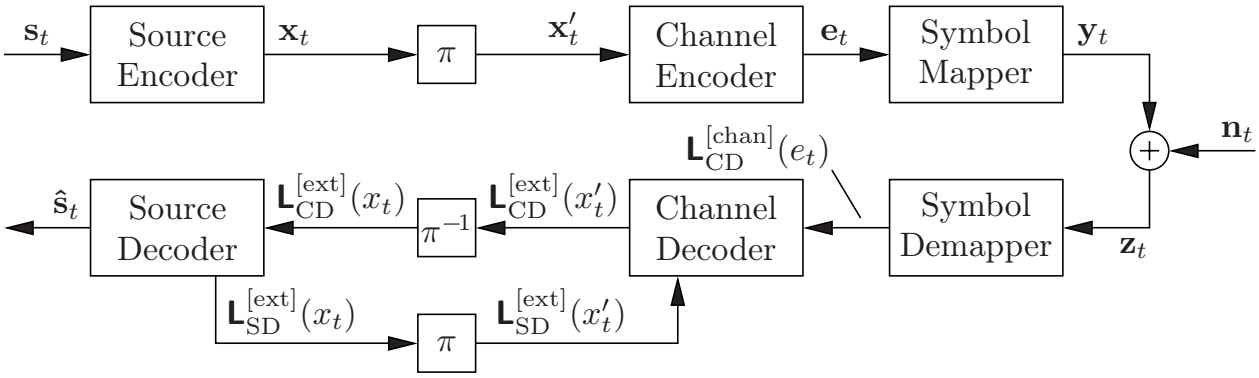

Figure 2.11: General baseband model of a transmission system employing ISCD.

according to Sec. 2.1, however, any channel code can be used as long as the respective decoder is able to generate the necessary extrinsic information. Besides convolutional codes, different channel coding concepts for ISCD (applied to FLCs or VLCs) have been presented in the literature, e.g., block codes [CAV06, CVA06b, ACS08], LDPC codes [PDLF05, LTV05, Sch06, SSVC08], or Turbo codes [LV02, JV08]. According to the design rule given in [KHC06], it follows that the channel code of a serially concatenated system like ISCD shall be recursive.

After channel coding, the bit vector $\mathbf{e}_t$ is mapped to complex signal space points $\mathbf{y}_t$, which are transmitted over the channel. Note that it can be beneficial to place a second (bit) interleaver between the channel coding and the symbol mapping stages if higher order modulation schemes are used and fading is expected to occur on the channel. This interleaver forms the basis of the BICM system [Zeh92, CTB98] and its extension BICM-ID [LR97, LR99, CR01]. As the goal of this thesis is to develop design methodologies and guidelines that are independent of the transmission channel and thus applicable also to other channel models and modulation schemes, we omit this second interleaver in the remainder of this thesis and consider non-fading AWGN channels (or block-fading, i.e., the fading remains constant for a complete frame) with BPSK mapping by way of example. The application of ISCD to other (fading) channel models such as, e.g., the Rayleigh channel, including higher order modulation has been demonstrated in, e.g., [CBAV05, Cle06, SSVC08, ACS08]. The verification of the applicability to channels with *Inter-Symbol Interference* (ISI) and their respective equalization is presented in [SCV07, Tho07c].

At the receiver, the symbol demapper generates the channel-related *a posteriori* L-values $\mathsf{L}_{\mathrm{CD}}^{[\mathrm{chan}]}(e_t)$ (see (2.3) and (2.4)), which are used to trigger the first channel decoding step. Subsequently, the (SISO) channel decoder and the (SISO) source decoder iteratively exchange extrinsic information $\mathsf{L}_{\mathrm{CD}}^{[\mathrm{ext}]}(x_t)$ and $\mathsf{L}_{\mathrm{SD}}^{[\mathrm{ext}]}(x_t)$. Note that in the case of a systematic channel code, the information fed to the source decoder has to contain the channel-related L-values $\mathsf{L}_{\mathrm{CD}}^{[\mathrm{chan}]}(x_{t,\xi})$ of those bit positions ξ corresponding to systematic bits. Furthermore, a potentially unequal distribution of the bits $x_{t,\xi}$ has to be taken into account. A detailed description of these latter cases is given in [Adr03, AV05, ACS08].

After a fixed number of iterations, the source decoder generates time-discrete estimates $\hat{\mathbf{s}}_t$ of the source samples. Note that in this general description of the baseband

system model, a generic source decoder is used. This source decoder can either process VLCs, FLCs, or even more exotic source coding schemes, such as, e.g., overcomplete source expansions [KM04, KM05].

2.4.2 ISCD for Variable-Length Codes

Output patterns of variable length typically result from entropy coding using for instance VLCs, applied after quantization, in order to increase the coding efficiency. Thus, ISCD can denote an iterative evaluation of VLCs and channel codes (e.g., [BH00, GFGR01, HN02, GS05]). Unfortunately, for systems employing VLCs, there exists the inherent problem of a synchronization loss in the case of transmission errors. ISCD shall mainly overcome this synchronization problem, and it serves for a proper segmentation of the reconstructed bit stream after channel decoding into data patterns of specific length, by using the inherent redundancy added by the VLC structure. The VLC code redundancy as well as the natural redundancy of the source has been exploited in an ISCD scheme in, e.g., [KT02a, KT02b, TK03, KT03, KT05, TK05, TK06, Tho07c, TK09]. This technique is, however, not in the focus of the present thesis. A thorough survey of ISCD for VLCs, based on Bayesian networks, can be found in, e.g., [GS05].

2.4.3 ISCD for Fixed-Length Codes

As most real world mobile communication systems demand constant bit rates, it is frequently recommended to include FLCs in the mobile and wireless profile, in spite of the higher coding efficiency of VLCs. In the case of FLCs, transmission errors affect only the bit pattern under consideration. A loss of synchronization can be avoided. Therefore, FLCs are used in systems like GSM, UMTS, or LTE. Most of the recent speech and audio codecs, like G.729.1 [ITU06] and G.718 [ITU08] employ FLCs, too.

ISCD can thus also be understood as iterative evaluation of FLCs and channel codes. First, FLCs offer the advantage of having a fixed rate. Second, it has been shown by an example in [Tho07a] that under certain circumstances, a less complex system designed with FLCs can outperform a system with VLCs, if ISCD is employed (for a given trade-off between coding efficiency and error robustness). A transmission scheme using ISCD for FLCs can be considered as a concatenation of a *Soft Input Soft Output* (SISO) channel decoder and a source decoder performing *Soft Decision Source Decoding* (SDSD)[1] [Fin98, FV01].

The benefits of ISCD for FLCs have already successfully been demonstrated for several applications. Perkert *et al.* have shown in [PKH01] that the error robustness of GSM speech transmission based on the full-rate speech codec can be improved by ISCD. Similar results have been achieved for the *Adaptive Multi-Rate* (AMR) and

[1] The acronym SDSD is also used to denote the *Soft Decision Source Decoder*. In earlier publications on ISCD, the soft decision source decoder was frequently denoted *SoftBit Source Decoder* (SBSD).

the *Adaptive Multi-Rate Wideband* (AMR-WB) speech codecs [HKH+00, HHSX00, OEAH07]. Besides speech and audio coding, ISCD has also successfully been applied to image and video transmission in [KG02, KGM04a, KGM04b, KGM06, NEO+08, PYOH08, NH09b, NH09a]. At this point it is important to mention that significant quality improvements have been achieved without any modification of the transmitter. Additional cross-layer considerations, taking into account the packet headers, are discussed in [BLV+10].

A speech and audio codec which has been designed to incorporate joint source-channel coding approaches including ISCD, is the *FlexCode* source-channel coding approach for heterogeneous networks [BGK+08a, BGK+08b, SVC08, SSV08, BGK+08c, SSJ+08, SSV10, KLK10]. The concept has been extended to the transmission of video in [BFF+09] and a real-time demonstrator was built [OV09]. Most of the results presented in the thesis at hand directly result from the development of the *FlexCode* paradigm, financed by the European Union under grant FP6-2002-IST-C 020023-2. A short introduction to the *FlexCode* source and channel coding concept is given in App. A.

In this thesis, only FLCs are considered, however, most results can easily be extended to VLCs, which provide a more general class of source codes (FLCs are a subset of VLCs) or other source coding schemes. A detailed description of the relevant parts of the baseband block diagram will be given in Sec. 3.1, together with a thorough description of the utilized notation.

3

Advances in Iterative Source-Channel Decoding

Iterative Source-Channel Decoding (ISCD), as introduced in Sec. 2.4, has proved to constitute an efficient and robust transmission scheme for delay constrained multimedia applications. In this chapter, the ISCD system utilized in this thesis is presented. Section 3.1 starts with a thorough review of the notation. Furthermore, the application of the *EXtrinsic Information Transfer* (EXIT) chart technique for convergence analysis is presented. Simulation examples show the performance of the basic ISCD system and an illustrative example gives hints to the principle of operation of the different utilized algorithms. In Sec. 3.2, the performance of the ISCD system exploiting inter-frame correlation is improved, especially for bad channel conditions, by a modified receiver structure. The overall performance of ISCD can be improved by introducing *Irregular Bit Mappings* (IBMs), as shown in Sec. 3.3, giving an elegant optimization technique using EXIT charts. The *Unequal Error Protection* (UEP) property of this approach is shown and the optimization is modified such that UEP can be directly incorporated into the design procedure. Two different remedies against a major problem of all ISCD schemes – the considerably high error floor – are presented in Sec. 3.4. Both are targeted at optimizing the Hamming distance of the bit mapping. In order to adaptively control the number of useful receiver iterations, different stopping criteria are applied to ISCD in Sec. 3.5. These are then applied in Sec. 3.6 to realize a *Hybrid Automatic Repeat reQuest* (HARQ) system which further improves the quality of the transmission if a feedback channel is available and several retransmissions of additional refinement information can be carried out.

3.1 Iterative Source-Channel Decoding

In this section, an in-depth introduction to the considered *Iterative Source-Channel Decoding* (ISCD) scheme is given. This introduction is based on [AV05, Cle06, ACS08]. Further details can be found in the references given throughout the description of the transmitter and the receiver.

3.1.1 Source Model

In most parts of this thesis, we consider the stationary source model depicted in Fig. 3.1. Instead of using the output of any specific source encoder, we use a Gauss-Markov source to model the source codec parameters, as introduced in [Hei01b]. A Gaussian source can efficiently be used to model the transform coefficients of transform-based source codecs (e.g., the *FlexCode* source coder utilizing a *Karhunen-Loève Transform* (KLT) or a *Modified Discrete Cosine Transform* (MDCT), see App. A.1) which can be assumed to be Gaussian due to the central limit theorem [PU02]. This source permits to model a Markov process with *inter-* and *intra-frame* correlation. The advantage of such a source is that on the one hand precisely repeatable Monte-Carlo simulations can be carried out and on the other hand the output of a wide range of source encoders can be modeled. The source model is based on N_U random number generators and a two-dimensional filter structure, as depicted in Fig. 3.1. In [Hei01b, HA08], it has been shown that this model is applicable, e.g., for the gain and LSF parameters of CELP speech codecs or for the gain factors of the MP3 codec. It is additionally applicable to model most of the parameters of the *FlexCode* source codec (see also App. A).

At (discrete) time instant t, the source model generates a frame $\mathbf{u}_t$ of unquantized source codec parameters with $\mathbf{u}_t = (u_{t,1}, \ldots, u_{t,N_U})$. Note that throughout this thesis we assume that the transmission starts at $t = 1$. The N_U random number generators compute samples $\tilde{u}_{t,\kappa}$ that are outcomes of the random process $\tilde{U}_{t,\kappa} \sim \mathcal{N}(0,1)$, $\forall t \in \mathbb{N}_1$, $\forall \kappa \in \{1, \ldots, N_U\}$. The source attempts to model a two-dimensional Markov process of first order. The statistical properties describing the source are the (temporal) inter-frame correlation coefficient

$$\rho \doteq \frac{\mathsf{E}\{U_{t,\kappa} U_{t-1,\kappa}\}}{\mathsf{E}\{U_{t,\kappa}^2\}} \qquad \forall \kappa \in \{1, \ldots, N_U\},\ \forall t \in \mathbb{N}_1 \setminus \{1\} \tag{3.1}$$

and the (spatial) intra-frame correlation coefficient

$$\delta \doteq \frac{\mathsf{E}\{U_{t,\kappa} U_{t,\kappa-1}\}}{\mathsf{E}\{U_{t,\kappa}^2\}} \qquad \forall \kappa \in \{2, \ldots, N_U\},\ \forall t \in \mathbb{N}_1\,. \tag{3.2}$$

Using the parameters ρ and δ, the multiplicative factors λ_1 and λ_2 can be set up such that the desired source properties are realized [Hei01b, HA08]:

$$\lambda_1 = \frac{\rho\left(1-\delta^2\right)}{1-\rho^2\delta^2} \tag{3.3}$$

$$\lambda_2 = \frac{\left(1-\rho^2\right)\delta}{\sqrt{\left(1-\rho^2\delta^2\right)\left(1+\rho^2\delta^2-\rho^2-\delta^2\right)}}\,. \tag{3.4}$$

Using λ_1 and λ_2, the factor

$$\lambda_3 = \frac{1-\lambda_1^2}{\sqrt{\lambda_2^2\left(1+\lambda_1^2\right) + \sqrt{4\lambda_1^2\lambda_2^4 + \left(1-\lambda_1^2\right)^2}}} \tag{3.5}$$

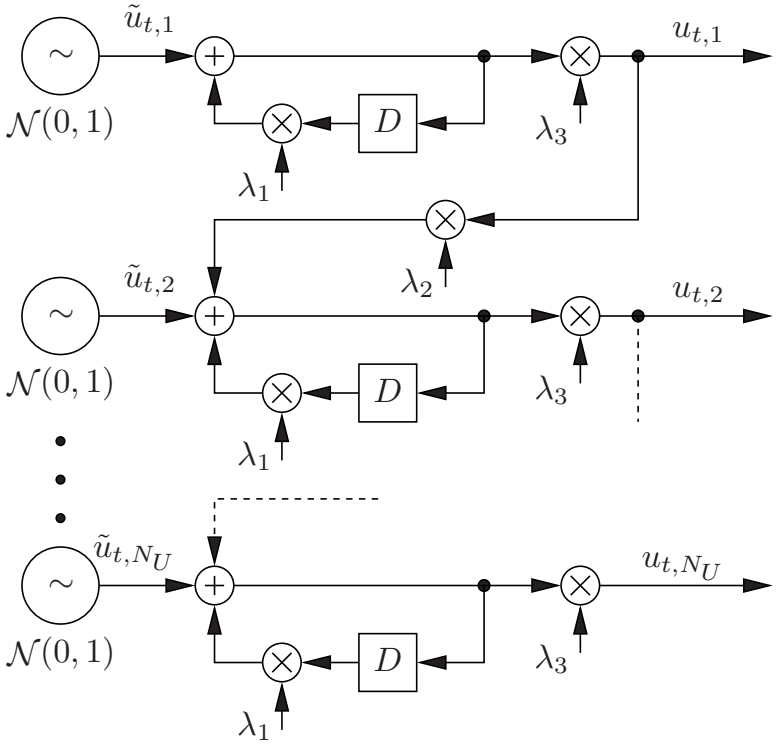

Figure 3.1: Source model generating temporally and spatially correlated parameters.

is determined such that $\mathsf{E}\{U_{t,\kappa}^2\} = 1$. Implementational details and derivations of the equations can be found in [Hei01a, Hei01b, HV05, HA08]. Two special cases can be considered:

- *Inter-frame* (temporal) correlation only, i.e., $\delta = 0$. In that case, $\lambda_1 = \rho$, $\lambda_2 = 0$, and $\lambda_3 = \sqrt{1-\rho^2}$. The connections between parallel branches are omitted (as $\lambda_2 = 0$) and the source model corresponds to the Gauss-Markov source utilized in, e.g., [Fin98, HHVH00, FV01, Gör01b, AV05, Cle06, ACS08].
- *Intra-frame* (spatial) correlation only, i.e., $\rho = 0$. In that case, $\lambda_1 = 0$, $\lambda_2 = \delta/\sqrt{1-\delta^2}$ and $\lambda_3 = \sqrt{1-\delta^2}$. The two-dimensional model then asymptotically approximates the Gauss-Markov model used for instance in [KT05, TK05, Tho07a, TSV08, SVAC08]. See [Hei01a] and [Hei01b] for an in-depth analysis of the asymptotic approximation.

3.1.2 Transmitter of the ISCD Scheme

The relevant part of the transmitter of a transceiving scheme with ISCD is depicted in Fig. 3.2. Digital communication systems for multimedia signals, such as, e.g., speech, audio, images, or video, often operate on a frame-by-frame basis, in order to keep the end-to-end delay reasonable. The source encoder is assumed to extract real-valued parameters from the multimedia signal. In real-world source encoders, these parameters are for example *Line Spectral Frequencies* (LSFs), gain factors, transform coefficients, pitch periods, and bit allocation information. For details, see for instance [JN84, Kon04, VM06]. These parameters are modeled by the source introduced in the previous section.

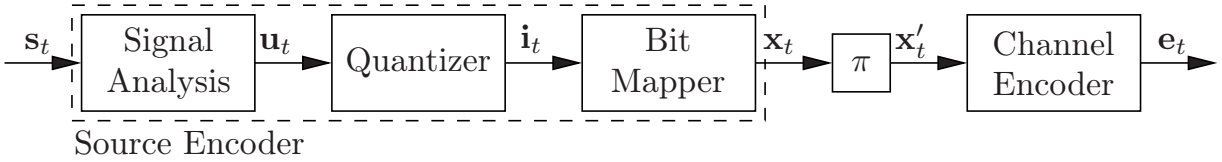

Figure 3.2: Baseband model for the transmitter of a scheme with ISCD.

Quantization

At time instant t, a source encoder generates a frame of N_U source codec parameters $\mathbf{u}_t = (u_{t,1}, \ldots, u_{t,\kappa}, \ldots, u_{t,N_U})$ with κ denoting the position in the frame. The frame $\mathbf{u}_t$ is quantized using either scalar or vector quantization. Therefore, the single entries of the vector $\mathbf{u}_t$ are grouped to $N_I \doteq \lceil N_U/\Pi \rceil$ sub-vectors $\mathbf{v}_{t,k} = (u_{t,(k-1)\Pi+1}, \ldots, u_{t,k\Pi})$, $k \in \{1, \ldots, N_I\}$ with Π denoting the quantizer dimension. In the case of scalar quantization, we have $\Pi = 1$, $k = \kappa$, and $\mathbf{v}_{t,k} = u_{t,\kappa}$. Each input vector $\mathbf{v}_{t,k}$ is individually quantized using the quantizer function

$$\begin{aligned} \mathcal{Q} &: \mathbb{R}^{\Pi} \to \mathbb{I} \doteq \{1, \ldots, Q\} \subset \mathbb{N}_1 \\ &\mathbf{v}_{t,k} \mapsto \mathcal{Q}(\mathbf{v}_{t,k}) = i_{t,k} \,. \end{aligned}$$

The quantizer function maps the input vector $\mathbf{v}_{t,k}$ to a quantizer index $i_{t,k}$ denoting the selected entry of the quantizer code book[1] $\mathbb{V} = \{\bar{\mathbf{v}}^{(1)}, \ldots, \bar{\mathbf{v}}^{(Q)}\} \subset \mathbb{R}^{\Pi}$. The quantizer function computes $i_{t,k} = \arg\min_{\forall q \in \mathbb{I}} \mathcal{D}_f(\bar{\mathbf{v}}^{(q)}, \mathbf{v}_{t,k})$, with $\mathcal{D}_f$ being an appropriate distance measure. For more details on scalar and vector quantization, see, e.g., [JN84, GN98, VM06]. Unless stated otherwise, all parameters are quantized with the same quantizer $\mathcal{Q}$ (with Q distinct code book entries) in this thesis. At the receiver, the quantization operation can be reverted by performing a so-called *Table Look-Up* (TLU) operation which selects the code book entry corresponding to the decoded index $\hat{\imath}_{t,k}$, i.e., $\mathcal{Q}^{-1}(\hat{\imath}_{t,k}) = \bar{\mathbf{v}}^{(\hat{\imath}_{t,k})}$. All quantization indices within a frame are grouped to a vector $\mathbf{i}_t = (i_{t,1}, \ldots, i_{t,N_I})$. The quantizer most frequently used throughout this thesis is the scalar *Lloyd-Max Quantizer* (LMQ) [Max60, Llo82, JN84], which minimizes the power of the quantization error.

Bit Mapping

To each quantizer index $i_{t,k}$ selected at time instant t and position k a unique bit pattern $\mathbf{b}_{t,k} \in \mathbb{B}_k \subseteq \mathbb{F}_2^{B_k}$ of B_k bits is assigned according to the *Bit Mapping* (BM)

$$\begin{aligned} \mathcal{B}_k &: \mathbb{I} \to \mathbb{B}_k = \left\{ \bar{\mathbf{b}}_k^{(1)}, \ldots, \bar{\mathbf{b}}_k^{(Q)} \right\} \subseteq \mathbb{F}_2^{B_k} \\ &i_{t,k} \mapsto \mathcal{B}_k(i_{t,k}) = \bar{\mathbf{b}}_k^{(i_{t,k})} = \mathbf{b}_{t,k} = (b_{t,k,1}, \ldots, b_{t,k,B_k}) \,. \end{aligned}$$

The single bits of the bit pattern $\mathbf{b}_{t,k}$ are denoted by $b_{t,k,\mu} \in \mathbb{F}_2$, with $\mu \in \{1, \ldots, B_k\} \subset \mathbb{N}_1$ denoting the μth entry of $\mathbf{b}_{t,k}$. The single bits of the entries

[1] In order to avoid confusion of the different indices, we use the superscript indexing notation $\bar{\mathbf{v}}^{(q)}$ to denote the qth entry of the quantizer code book.

$\bar{\mathbf{b}}_k^{(q)} = (\bar{b}_{k,1}^{(q)}, \ldots, \bar{b}_{k,\mu}^{(q)}, \ldots, \bar{b}_{k,B_k}^{(q)})$ are denoted by $\bar{b}_{k,\mu}^{(q)}$. Note that the bit mapping may differ from quantization index to quantization index within a frame; therefore $\mathcal{B}_k$, B_k, and $\mathbb{B}_k$ are indexed by the position k. Further note that the different entries $\bar{\mathbf{b}}_k^{(q)}$, $q \in \{1, \ldots, Q\}$, of the bit mapper codomain are superscript indexed by $^{(q)}$ in order to avoid confusion (see also the quantizer description). If $B_k > \operatorname{ld} Q$, the bit mapping is called *Redundant Bit Mapping* (RBM) as it introduces artificial redundancy: More bits than actually necessary are spent to represent a quantizer index. The bit mapping can always be considered to be the composite function $\mathcal{B}_k = \check{\mathcal{B}}_k \circ \mathcal{B}^{[\mathrm{NB}]}$, i.e., $\mathcal{B}_k(i_{t,k}) = \left(\check{\mathcal{B}}_k \circ \mathcal{B}^{[\mathrm{NB}]}\right)(i_{t,k}) = \check{\mathcal{B}}_k\left(\mathcal{B}^{[\mathrm{NB}]}(i_{t,k})\right)$ with $\mathcal{B}^{[\mathrm{NB}]} : \mathbb{I} \to \mathbb{F}_2^{B^{[\mathrm{NB}]}}$ denoting the natural binary bit mapping. $\mathcal{B}^{[\mathrm{NB}]}$ generates the natural binary representation of the index $i_{t,k}$ of length $B^{[\mathrm{NB}]} \doteq \lceil \operatorname{ld} Q \rceil$ according to $\mathcal{B}^{[\mathrm{NB}]}(i_{t,k}) = \mathbf{b}_{t,k}^{[\mathrm{NB}]} = \left(b_{t,k,1}^{[\mathrm{NB}]}, \ldots, b_{t,k,B^{[\mathrm{NB}]}}^{[\mathrm{NB}]}\right)$ with

$$b_{t,k,\mu}^{[\mathrm{NB}]} = \left\lfloor \frac{i_{t,k}}{2^{B^{[\mathrm{NB}]}-\mu}} \right\rfloor \bmod 2 = \left\lfloor \frac{i_{t,k}}{2^{B^{[\mathrm{NB}]}-\mu}} \right\rfloor - 2 \cdot \left\lfloor \frac{1}{2} \left\lfloor \frac{i_{t,k}}{2^{B^{[\mathrm{NB}]}-\mu}} \right\rfloor \right\rfloor, \; \forall \mu \in \{1, \ldots, B^{[\mathrm{NB}]}\}\,.$$

The second constituent position-dependent function of the mapping, $\check{\mathcal{B}}_k : \mathbb{F}_2^{B^{[\mathrm{NB}]}} \to \mathbb{B}_k$ can be regarded as being a (potentially non-linear) block code of rate $r_{\mathrm{BM},k} = B^{[\mathrm{NB}]}/B_k$. Two prominent examples of non-redundant mapping functions $\check{\mathcal{B}}_k$ are the Gray mapping [Gra53, JN84] and the pseudo-Gray mapping [ZG90]. The concept of redundant non-linear block codes employed as redundant bit mapping has been successfully utilized for the robust transmission of source codec parameters in, e.g., [Hei01b, HV05, CAV06, CVA06b]. Linear block codes as redundant bit mappings have been utilized in [Fin98, FHV99], therein denoted by *Parameter Individual Block Code* (PIBC). In that case, the function $\check{\mathcal{B}}_k$ can be described as a multiplication with a generator matrix $\mathbf{G}_k^{[\mathrm{BM}]}$, i.e., $\mathbf{b}_{t,k} = \mathbf{b}_{t,k}^{[\mathrm{NB}]} \cdot \mathbf{G}_k^{[\mathrm{BM}]}$, with $\dim \mathbf{G}_k^{[\mathrm{BM}]} = B^{[\mathrm{NB}]} \times B_k$. After the bit mapping, the N_I individual bit patterns $\mathbf{b}_{t,k}$ are grouped to a bit vector $\mathbf{x}_t \doteq (\mathbf{b}_{t,1}, \ldots, \mathbf{b}_{t,N_I}) = (x_{t,1}, \ldots, x_{t,\xi}, \ldots, x_{t,N_X})$. The size of the bit vector is $N_X \doteq \sum_{k=1}^{N_I} B_k$. The single bits $x_{t,\xi}$ of $\mathbf{x}_t$ are indexed by ξ. We furthermore define the average number of bits per pattern $\bar{B} \doteq \frac{1}{N_I} \sum_{k=1}^{N_I} B_k$. As the bit mapping is considered to be a code, the rate of the bit mapping is defined by

$$r_{\mathrm{BM}} = \frac{N_I \cdot \operatorname{ld} Q}{N_X} = \frac{N_I \cdot \operatorname{ld} Q}{\sum_{k=1}^{N_I} B_k} = \frac{\operatorname{ld} Q}{\bar{B}} \overset{\text{if } \operatorname{ld} Q = B^{[\mathrm{NB}]}}{=} \frac{N_I \cdot B^{[\mathrm{NB}]}}{\sum_{k=1}^{N_I} B_k} = \frac{B^{[\mathrm{NB}]}}{\bar{B}}\,. \tag{3.6}$$

Interleaving, Channel Coding, and Signal Space Mapping

After bit mapping, the bit vector $\mathbf{x}_t$ is permuted by a bijective interleaver function

$$\begin{aligned} \pi : \mathbb{F}_2^{N_X} &\to \mathbb{F}_2^{N_X} \\ \mathbf{x}_t &\mapsto \mathbf{x}'_t \end{aligned}$$

which maps the bit vector $\mathbf{x}_t$ of length N_X to an (interleaved) bit vector $\mathbf{x}'_t$ of the same length. In this thesis, we limit the interleaving to the present frame $\mathbf{x}_t$ in order

not to introduce any additional delay. The interleaving can also be performed for a sequence of Λ consecutive frames $(\mathbf{x}_{t-\Lambda+1}, \ldots, \mathbf{x}_t)$ [Adr03, AV05], however resulting in an additional delay of $\Lambda - 1$ time instants. This case is not considered in this thesis.

After interleaving, the channel encoder $\mathcal{E} : \mathbb{F}_2^{N_X} \rightarrow \mathbb{F}_2^{N_E}$, with $\mathbf{x}'_t \mapsto \mathcal{E}(\mathbf{x}'_t) = \mathbf{e}_t$, performs channel coding of rate $r_{\mathrm{CC}} = N_X/N_E$. The channel encoded bit vector $\mathbf{e}_t = (e_{t,1}, \ldots, e_{t,\eta}, \ldots, e_{t,N_E})$ consists of N_E bits $e_{t,\eta} \in \mathbb{F}_2$. In conventional transmission systems with non-iterative decoding, $r_{\mathrm{CC}} < 1$, i.e., $N_E > N_X$, usually holds. In Turbo-like systems designed for iterative decoding, the rate of the (inner) channel code can be $r_{\mathrm{CC}} = 1$ (e.g., [DP97, AV04b, AKtB04]) or even $r_{\mathrm{CC}} > 1$ with $N_E < N_X$ (e.g., [AKtB04, Tho07a, SV09, SV10a]). In this work, we frequently employ recursive convolutional codes of constraint length $J+1$ [JZ99, LC04] which are commonly used in publications on ISCD, e.g., [HG03, Gör01b, Gör07, AV05, OEA+09]. However, different channel codes can be used in the context of ISCD, for instance Turbo codes, *Low-Density Parity-Check* (LDPC) codes [SSVC08], the recently discovered capacity achieving polar codes [Ari09], or even simple small block codes [CVA06a].

The symbol mapper $\mathcal{M}$ (not depicted in Fig. 3.2) maps the sequence of bits $\mathbf{e}_t \in \mathbb{F}_2^{N_E}$ to a sequence of complex signal space points $\mathbf{y}_t = (y_{t,1}, \ldots, y_{t,\ell}, \ldots, y_{t,N_Y}) \in \mathbb{C}^{N_Y}$ of length N_Y. Therefore, the entries of $\mathbf{e}_t$ are grouped to $N_Y \doteq \lceil N_E/\Upsilon \rceil$ sub-vectors $\check{\mathbf{e}}_{t,\ell}$ with Υ denoting the number of bits assigned to a single modulation symbol. Each input vector is individually mapped using the mapping function $\mathcal{M} : \mathbb{F}_2^{\Upsilon} \rightarrow \mathbb{C}$, with $\check{\mathbf{e}}_{t,\ell} \mapsto \mathcal{M}(\check{\mathbf{e}}_{t,\ell}) = y_{t,\ell}$. The complex symbols $y_{t,\ell}$ are grouped to a vector $\mathbf{y}_t = (y_{t,1}, \ldots, y_{t,N_Y})$. As the modulation is not part of the ISCD system, we simplify matters and leave out modulation by assuming a simple *Binary Phase Shift Keying* (BPSK) transmission with $E_{\mathrm{s}} = 1$ for the encoded bits $e_{t,\eta}$. The mapping function then reduces to $\mathcal{M}^{[\mathrm{BPSK}]} : \mathbb{F}_2 \rightarrow \{\pm 1\}$, with $y_{t,\ell} = \mathcal{M}^{[\mathrm{BPSK}]}(e_{t,\eta}) = 1 - 2e_{t,\eta}$, i.e., $\Upsilon = 1$, $\ell = \eta$, and $N_Y = N_E$. In the context of ISCD, the symbol mapping can easily be extended to include higher order modulation schemes [CBAV05, Cle06, ACS08] and channel equalization [Tho07c, SCV07].

3.1.3 Receiver of the ISCD Scheme

After transmitting the modulation symbols $\mathbf{y}_t$ over the channel $\mathcal{C} : \mathbb{C} \rightarrow \mathbb{C}$, noisy values $\mathbf{z}_t = (z_{t,1}, \ldots, z_{t,N_Y}) = (\mathcal{C}(y_{t,1}), \ldots, \mathcal{C}(y_{t,N_Y}))$ are received. Using the channel transition *Probability Density Functions* (pdfs), the symbol demapper $\mathcal{M}^{-1}$ computes the vector of *a posteriori* L-values $\mathsf{L}_{\mathrm{CD}}^{[\mathrm{chan}]}(e_t) \doteq (\mathsf{L}_{\mathrm{CD}}^{[\mathrm{chan}]}(e_{t,1}), \ldots, \mathsf{L}_{\mathrm{CD}}^{[\mathrm{chan}]}(e_{t,N_E}))$. See also Sec. 2.2 for a detailed description of the short-hand notation $\mathsf{L}_{\mathrm{CD}}^{[\mathrm{chan}]}(e_t)$. In the case of a BPSK transmission over an *Additive White Gaussian Noise* (AWGN) channel, the *a posteriori* L-values $\mathsf{L}_{\mathrm{CD}}^{[\mathrm{chan}]}(e_{t,\eta})$ are given by (2.4).

If higher order modulation schemes with $\Upsilon > 1$ are employed, a *Soft Demapper* (SDM) [CTB98] has to be employed to generate the input L-values of the channel decoder according to the mapping function $\mathcal{M}$. Details in the context of ISCD are given for instance in [ACS08]. The aim of ISCD is to jointly exploit the channel-related L-values, the artificial channel coding redundancy, the artificial redundancy

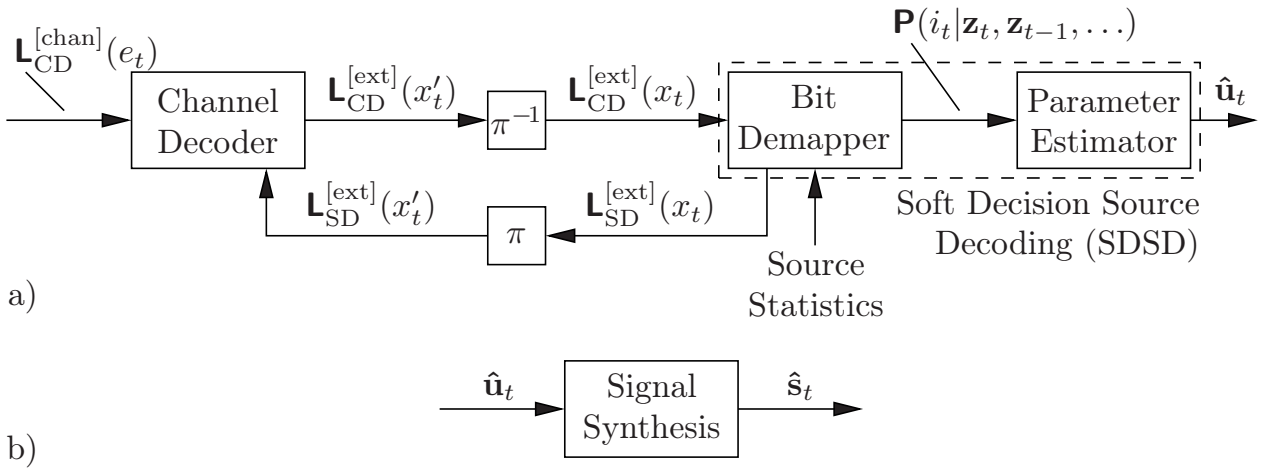

Figure 3.3: a) Baseband model of *Iterative Source-Channel Decoding* (ISCD).
b) Reconstruction of the source signal $\hat{\mathbf{s}}_t$.

possibly introduced by a redundant bit mapping as well as the natural residual source redundancy for approximating the *a posteriori* probabilities $\mathsf{P}(i_{t,k}|\mathbf{z}_t, \mathbf{z}_{t-1}, \ldots)$. For the attainment of this aim, a channel decoder and a *Soft Decision Source Decoder* (SDSD) iteratively exchange extrinsic information in a Turbo-like process [Gör00, AVS01, Gör01b, Adr03, Cle06, ACS08]. The baseband model of the ISCD receiver is depicted in Fig. 3.3. Only a brief description of the ISCD receiver is given here, a detailed description can be found in the literature.

Channel Decoding

The channel decoder utilized within the ISCD receiver accepts two different inputs. First, the channel related L-values $\mathbf{L}_{\mathrm{CD}}^{[\mathrm{chan}]}(e_t)$ are received once per frame. As the ISCD receiver operates on a frame-by-frame basis, the L-values of all transmitted symbols are grouped within a vector $\mathbf{L}(z_t|y_t) \doteq (\mathsf{L}(z_{t,1}|y_{t,1}), \ldots, \mathsf{L}(z_{t,N_Y}|y_{t,N_Y}))$ which is available to the channel decoder. The utilized channel decoder has to be a *Soft Input Soft Output* (SISO) version of a channel decoder. If, e.g., convolutional coding is employed, a SISO decoder [RVH95, BDMP97] based on the *Bahl, Cocke, Jelinek, Raviv* (BCJR) algorithm [BCJR74] is utilized. Alternatively, reduced-complexity variants like the *Soft Output Viterbi Algorithm* (SOVA) decoder [Hag95] can be used. Besides the channel-related input, the channel decoder requires the (interleaved) extrinsic output of the second component $\mathbf{L}_{\mathrm{SD}}^{[\mathrm{ext}]}(x'_t) = (\mathsf{L}_{\mathrm{SD}}^{[\mathrm{ext}]}(x'_{t,1}), \ldots, \mathsf{L}_{\mathrm{SD}}^{[\mathrm{ext}]}(x'_{t,N_X}))$ as additional input. The channel decoder computes extrinsic information $\mathsf{L}_{\mathrm{CD}}^{[\mathrm{ext}]}(x'_{t,\xi})$ for the single bits $x'_{t,\xi}$ of the frame $\mathbf{x}'_t$ which are grouped to a vector $\mathbf{L}_{\mathrm{CD}}^{[\mathrm{ext}]}(x'_t)$, deinterleaved, and fed to the SDSD. The extrinsic output of the channel decoder may contain parts of the channel-related L-values $\mathsf{L}_{\mathrm{CD}}^{[\mathrm{chan}]}(e_{t,\eta})$ if a systematic channel code is employed [ACS08] (see also Sec. 2.2).

Soft Decision Source Decoding

The SDSD module consists of two main parts: The *Bit Demapper* and the *Parameter Estimator*. The task of the bit demapper is to generate an extrinsic information vector

$\mathsf{L}_{\mathrm{SD}}^{[\mathrm{ext}]}(x_t)$ which is interleaved and fed back to the channel decoder for use in the subsequent iteration. The bit demapper therefore makes use of the (possibly redundant) bit mapping and the inherent residual or natural source redundancy of the quantizer indices $i_{t,k}$. The residual source redundancy needs to be known at the receiver in order to be exploitable. It can either be stored in fixed tables, transmitted over a side channel, mathematically modeled [KGM06], or estimated at the receiver [SVC07].

Throughout this thesis we distinguish four types of SDSD algorithms, differing in the type of redundancy that is exploited:

- The AK0 algorithm, which exploits the unequal distribution of quantizer indices, i.e., $\mathsf{P}(i_{t,k}) = \mathsf{Pr}\{I_{t,k} = i_{t,k}\}$.
- The AK1-INTER algorithm, which exploits the correlation of indices between consecutive frames, i.e., $\mathsf{P}(i_{t,k}|i_{t-1,k}) = \mathsf{Pr}\{I_{t,k} = i_{t,k}|I_{t-1,k} = i_{t-1,k}\}$. In this work, no additional delay from grouping frames (as proposed in [Adr03, AV05]) is tolerated (i.e., $\Lambda = 1$); therefore the AK1-INTER approach only considers the previous frame and no future frames.
- The AK1-INTRA algorithm, which exploits the correlation between indices within a single frame, i.e., $\mathsf{P}(i_{t,k}|i_{t,k-1}) = \mathsf{Pr}\{I_{t,k} = i_{t,k}|I_{t,k-1} = i_{t,k-1}\}$.
- The AK1-NOPT algorithm, which jointly exploits the correlation between consecutive frames and within a single frame, i.e., $\mathsf{P}(i_{t,k}|i_{t-1,k}) = \mathsf{Pr}\{I_{t,k} = i_{t,k}|I_{t-1,k} = i_{t-1,k}\}$ and $\mathsf{P}(i_{t,k}|i_{t,k-1}) = \mathsf{Pr}\{I_{t,k} = i_{t,k}|I_{t,k-1} = i_{t,k-1}\}$.

The latter algorithm is denoted by AK1-NOPT, because the underlying algorithm does not perform an optimal estimation of the correlated quantization indices based on $\mathsf{P}(i_{t,k}|i_{t-1,k}, i_{t,k-1})$ as described in [Hei01a, Hei01b], but only the *Near Optimal* (NOPT) estimation introduced in [Hin01, FHCS02] and analyzed in detail in [Adr03, APV04, HA08], which is based on $\mathsf{P}(i_{t,k}|i_{t-1,k})$ and $\mathsf{P}(i_{t,k}|i_{t,k-1})$. The advantage of the near optimal estimation compared to the optimal estimation is a reduction of the complexity demands from $O(Q^3)$ for the optimal estimator to $O(Q^2)$. Equations for all four types of SDSD are given in App. F in two different domains.

After a fixed number Ω of receiver iterations, the bit demapper computes a set of estimates of the *a posteriori* probabilities $\mathsf{Pr}\{I_{t,k} = q|\mathbf{z}_t, \mathbf{z}_{t-1}, \ldots\}$, $\forall k \in \{1, \ldots, N_I\}, q \in \mathbb{I}$. Using these probabilities, the quantizer reproduction vectors $\hat{\mathbf{v}}_{t,k}$ can be reconstructed using one of the following estimators:

- *Minimum Mean Square Error* (MMSE) estimation by considering all quantizer code book entries [MC78, Fin98]

$$\hat{\mathbf{v}}_{t,k} = \sum_{q=1}^{Q} \bar{\mathbf{v}}^{(q)} \cdot \mathsf{Pr}\{I_{t,k} = q|\mathbf{z}_t, \mathbf{z}_{t-1}, \ldots\}\,. \tag{3.7}$$

- *Maximum A Posteriori* (MAP) estimation by [Fin98]

$$\hat{\mathbf{v}}_{t,k} = \mathcal{Q}^{-1}(\hat{\imath}_{t,k}) = \bar{\mathbf{v}}^{(\hat{\imath}_{t,k})} \quad \text{with } \hat{\imath}_{t,k} = \arg\max_{\forall q \in \mathbb{I}} \mathsf{Pr}\{I_{t,k} = q|\mathbf{z}_t, \mathbf{z}_{t-1}, \ldots\}\,. \tag{3.8}$$

Finally, the estimated source parameter vector $\hat{\mathbf{u}}_t$ is obtained by concatenating all the estimated vectors $\hat{\mathbf{v}}_{t,k}$, i.e., $\hat{\mathbf{u}}_t = (\hat{\mathbf{v}}_{t,1} \cdots \hat{\mathbf{v}}_{t,N_I}) = (\hat{u}_{t,1} \cdots \hat{u}_{t,\kappa} \cdots \hat{u}_{t,N_U})$. Using $\hat{\mathbf{u}}_t$, the signal synthesis stage of the source decoder can reconstruct the audio-visual source signal $\hat{\mathbf{s}}_t$ (see Fig. 3.3-b)).

Quality Assessment Measures

The main quality assessment measure used throughout this thesis is the so-called *Parameter Signal-to-Noise Ratio* (PSNR),[2] which is defined as

$$\mathrm{PSNR} \doteq \frac{\mathsf{E}\left\{U^2\right\}}{\mathsf{E}\left\{(U-\hat{U})^2\right\}}\,, \tag{3.9}$$

with U (resp. $\hat{U}$) being the random variable describing the source parameters (resp. estimated source parameters) independently of position κ and time t.

If MAP estimation according to (3.8) is performed, another convenient quality assessment measure is the *Symbol Error Rate* (SER), which is defined by

$$\mathrm{SER} \doteq \mathsf{Pr}\{I \neq \hat{I}\}\,, \tag{3.10}$$

with I (resp. $\hat{I}$) being the random variable describing the quantizer indices (resp. estimated quantizer indices) independently of position κ and time t.

3.1.4 Simulation Examples

The performance of the ISCD system with different soft decision source decoders shall be compared in simulation examples. The source codec parameters are modeled by the source presented in Sec. 3.1.1 with inter-frame correlation coefficient $\rho = 0.9$ and intra-frame correlation coefficient $\delta = 0.9$. Such high correlation coefficients frequently occur in speech and audio codecs [Fin98, Hei01b, HA08]. The source emits $N_U = 250$ parameters per frame which are quantized by a $Q = 16$ level scalar LMQ, i.e., $N_I = N_U$. Bit patterns of $B_k = 8\,\mathrm{bits}$, $\forall k \in \{1, \ldots, N_I\}$ are assigned to the quantizer indices according to a repetition coded bit mapping. The generator matrix $\mathbf{G}_k^{[\mathrm{BM}]}$ generates a repetition code, i.e., $\mathbf{G}_k^{[\mathrm{BM}]} = (\mathbf{I}_4\ \mathbf{I}_4)$ with $\mathbf{I}_4$ denoting the 4×4 identity matrix. This repetition coded bit mapping has been found to result in a very good performance for $\rho = 0.9$ and AK1-INTER source decoding [CSVA08a, CSVA08b] and is in fact the optimal redundant bit mapping (in terms of decoding convergence) that is obtained by a systematic generator matrix $\mathbf{G}_k^{[\mathrm{BM}]}$ for the given setup (i.e., source properties, quantizer, and utilized channel code). This finding has been confirmed by performing a full search over all systematic generator matrices of size 4×8 and selecting the one which has convergence at the lowest channel quality.

[2] In image and video coding, the abbreviation PSNR is also often used for the *Peak Signal-to-Noise Ratio* which is defined as the ratio between the maximum possible power of a signal and the noise power.

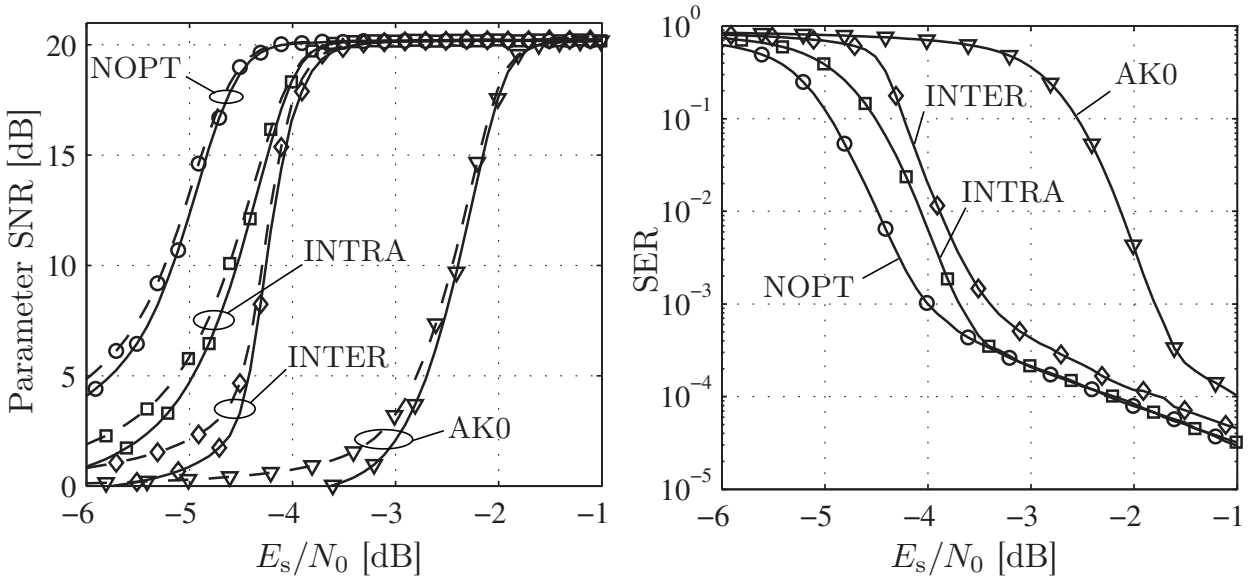

Figure 3.4: Comparison of different source decoders in ISCD with two-dimensional source correlation, $\rho = 0.9$, $\delta = 0.9$, LMQ scalar quantization, $N_I = 250$, $r_{\mathrm{BM}} = \frac{1}{2}$ repetition bit mapping, 8-state conv. code ($\mathbb{G}^{[\mathrm{CC}]} = \{\frac{10}{17}\}_8$), $\Omega = 25$ iterations. solid lines (——): MAP estimation dashed lines (– – –): MMSE estimation

After S-random interleaving with $\mathsf{S} = 15$ [DP95a, DP95b, VY00], a rate $r_{\mathrm{CC}} = 1$ recursive convolutional code with $J = 3$ and generator $\mathbb{G}^{[\mathrm{CC}]} = \{\frac{10}{17}\}_8$ is applied. The transmission is simulated using an AWGN channel with BPSK symbol space mapping.

In the first publications on ISCD, usually non-redundant bit mappings were used together with rate $r_{\mathrm{CC}} < 1$ convolutional codes. However, in [CAV06, CVA06b, KGM06, PYH07] it has been found that a redundant bit mapping can lead to significant improvements in terms of reconstruction PSNR. The related concept for the non-iterative case has been presented in [FHV99, Hei01b, HV05]. Utilizing redundant bit mappings together with $r_{\mathrm{CC}} = 1$ codes complies with the design rules for serially concatenated codes given in [BDMP98b, AKtB04]: The inner code shall be a recursive convolutional code (see also [KHC06]) and the outer code shall have a minimum Hamming distance ≥ 2. The repetition coded bit mapping realizes this constraint on the Hamming distance [CSVA08a]. The findings in [AKtB02, AKtB04] furthermore indicate that the inner code of a serially concatenated code shall be of rate $r_{\mathrm{CC}} \geq 1$ as a necessary condition for realizing a capacity-achieving system.[3]

Figure 3.4 shows the simulation results for the presented source and system settings. The left sub-plot depicts the reconstruction PSNR for the systems using either MMSE estimation according to (3.7) (dashed lines) or MAP estimation according to (3.8) (solid lines), plotted against the channel quality E_s/N_0. If MAP estimation is applied, the SER can be measured and it is depicted in the right sub-plot of Fig. 3.4. It can be clearly seen that the case exploiting *a priori* information of zeroth order (AK0) has the worst performance. Although exploiting the same amount of

[3]This fact has been proved in [AKtB04] for the case of a *Binary Erasure Channel* (BEC), but seems to be also true in the case of an AWGN channel, confirmed by observations.

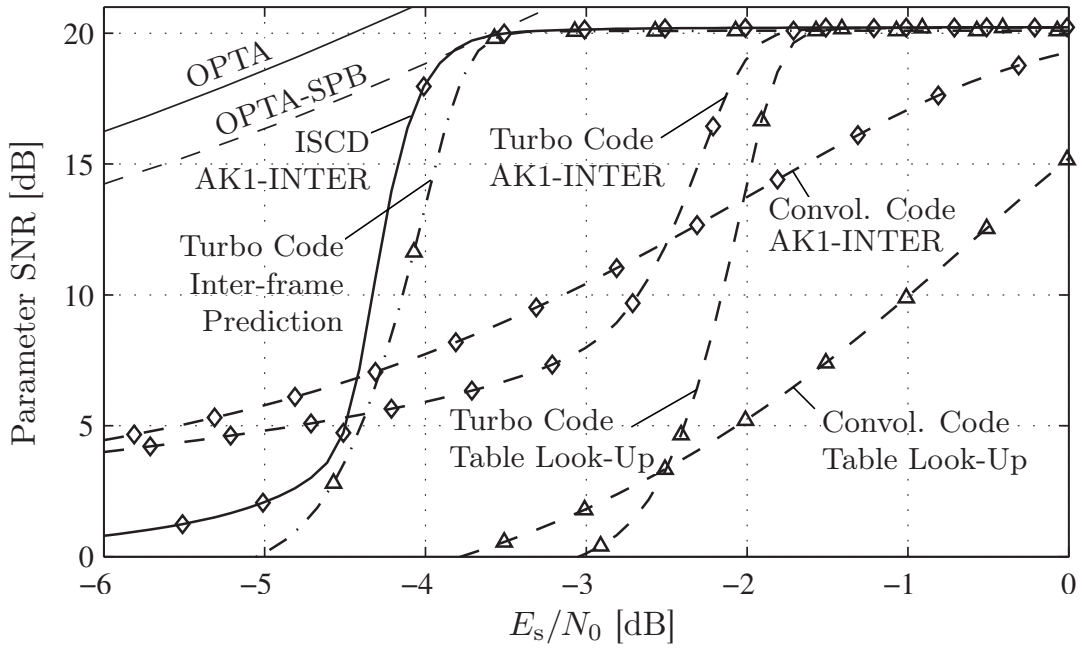

Figure 3.5: Comparison of conventional approaches using convolutional or Turbo codes with TLU or AK1-INTER SDSD, inter-frame prediction with Turbo code, and ISCD using repetition coded bit mapping and rate-1 channel coding ($\mathbb{G}^{[\mathrm{CC}]} = \{\frac{10}{17}\}_8$), $\rho = 0.9$, $\delta = 0$, $N_I = 250$, $N_E \approx 2000$, $\Omega = 25$ for all iterative decoders.

a priori information the AK1-INTRA case outperforms the AK1-INTER algorithm (in both cases, correlation coefficients of 0.9 are used). The reason for this is that AK1-INTER only exploits information from previous frames and not from future frames due to delay constraints. On the other hand, the AK1-INTRA decoder can perform a full forward/backward recursion using past and previous positions within a frame (see App. F), which explains the slightly better performance. As expected, the AK1-NOPT decoder, which jointly exploits inter- and intra-frame correlations shows the best performance. The performance of the AK1-NOPT (and the AK1-INTER) decoder could also be further enhanced by exploiting information of future frames (e.g., by grouping Λ frames prior to interleaving [Adr03]) and by using an optimal exploitation of the inter- and intra-frame correlations [Hei01a] instead of a near-optimal algorithm [APV04]. However, this modification introduces system delay and is thus not considered in this thesis. A modified receiver structure, which improves the decoding performance of the AK1-INTER (and the AK1-NOPT) algorithm without inducing any additional system delay, will be presented in Sec. 3.2.

The SER results in Fig. 3.4 reveal a considerably high error floor for all decoding algorithms. The reason for this is the relatively low Hamming distance of the outer repetition code with $d_{\min}(\mathbf{G}_k^{[\mathrm{BM}]}) = d_{\min}((\mathbf{I}_4\ \mathbf{I}_4)) = 2$, which is an indicator for the error floor, besides the interleaver size N_X [BDMP98b]. Solutions for reducing the error floor are given in Sec. 3.4.

In addition to comparing the different algorithms among each other, a comparison of ISCD and conventional algorithms designed according to the source-channel separation theorem [Sha48] is performed. We use a similar setting as for the previous

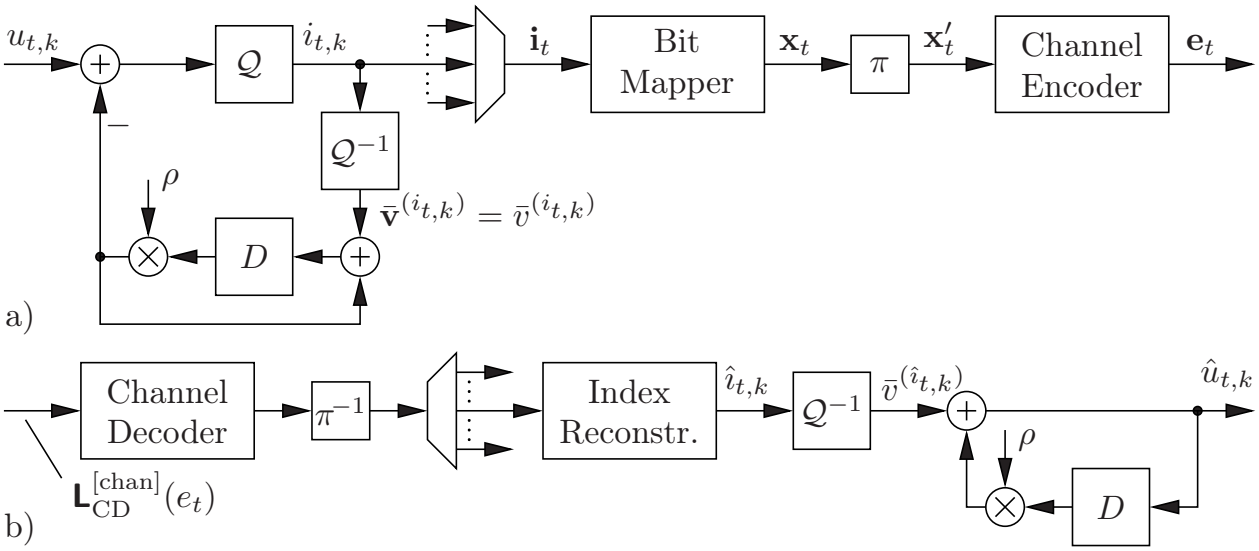

Figure 3.6: Baseband model of a transmitter and receiver of a scheme with scalar quantization and closed loop *Linear Prediction* (LP).

simulation examples, however, we assume that the source does not contain any intra-frame correlation, i.e., $\rho = 0.9$ and $\delta = 0$. All systems employ $Q = 16$ scalar LMQ. The first conventional system uses a *Recursive Systematic Convolutional* (RSC) code with $\mathbb{G}^{[\mathrm{CC}]} = \{1, \frac{13}{15}\}_8$ and a non-redundant natural binary bit mapping. The total number of transmitted bits amounts to $N_E = 2003$. At the receiver, the source symbols are reconstructed using either *Table Look-Up* (TLU) or SDSD with the AK1-INTER algorithm (as no intra-frame correlation is available). The simulation results are depicted in Fig. 3.5. Large improvements are possible if AK1-INTER source decoding is applied instead of a simple TLU. If the convolutional code is replaced by a rate $r_{\mathrm{CC}} = \frac{1}{2}$ Turbo code according to [BGT93, BG96] the performance of the system can be further enhanced and a PSNR of $\approx 20\,\mathrm{dB}$ can be retained for a broader range of channel qualities. Again, the application of AK1-INTER source decoding instead of a simple TLU is able to boost the overall system performance. The largest gains are observed if the previously introduced ISCD scheme with repetition coded bit mapping is used. The ISCD scheme is able to closely reach the theoretical performance limit given by the *Optimum Performance Theoretically Attainable* (OPTA) and OPTA-SPB bounds [Cle06, CSVA06]. The OPTA bound gives the theoretical limit for an infinite block length, while the OPTA-SPB takes into account the finite block size of $N_E \approx 2000\,\mathrm{bits}$ by using the *Sphere Packing Bound* (SPB) approximation [Sha59, DDP98a, DDP98b].

If the source shows inter-frame dependencies, these can also be removed using a differential encoder. A system which performs closed-loop *Linear Prediction* (LP) [JN84, VM06] using an optimal first order predictor for each scalarly quantized source parameter is depicted in Fig. 3.6. Due to the prediction gain, which can be used to improve the quantizer *Signal-to-Noise Ratio* (SNR) in the case of closed-loop prediction, the quantization can be performed using fewer quantizer reproduction levels. Thus, fewer bits N_X result after bit mapping, such that a better, lower-rate channel code can be used. In the present case, approximately 2.8 bits per parameter are necessary to achieve PSNR $\approx 20\,\mathrm{dB}$. This is realized by using a $Q = 8$ level scalar quantizer

for five consecutive parameters and a $Q = 4$ level quantizer for the sixth parameter and then repeating this pattern. In order to achieve $N_E \approx 2000$, a rate-$\frac{11}{31}$ channel code can then be applied. The channel code is realized by puncturing the original rate-$\frac{1}{3}$ Turbo code [BG96] according to the guidelines presented in [KM02, CRWC05]. The performance of this system comes close to the performance of ISCD, but is still outperformed by ISCD. Note that due to the recursive structure at the receiver, error propagation between consecutive frames is possible. This example shows the superiority of ISCD compared to conventional approaches with source-channel coding separation, but this shall neither be a general guideline nor a normal case. It has to be evaluated from case to case which system performs better under the given circumstances. A similar comparison with a closed-loop prediction scheme and *Source Optimized Channel Codes* (SOCCs) [HV05] has been presented in [AHV02]. MMSE decoding for differentially encoded parameters has been studied in [LK04, AL07b].

Figurative Example

In order to demonstrate the effects of ISCD and especially the effects of the four presented SDSD decoding algorithms, a figurative example is given. The two-dimensional source model delivers a still picture, which shows strong correlation in both the horizontal and the vertical direction. The image size is 512×512 pixels and thus the source emits $N_U = 512$ parameters per time instant t and a total number of 512 frames, i.e., $t \in \{1, 2, \ldots, 512\}$. In order to have a correspondence with the "geometry" of the source model given in Fig. 3.1, we employ the framing convention that each column of the picture represents one frame[4] $\mathbf{u}_t$. This convention is visualized in the upper left part of Fig. 3.7. Therefore, the image correlation in horizontal direction corresponds to inter-frame correlation while the correlation in vertical direction corresponds to intra-frame correlation.

The single pixels of the image are quantized using a $Q = 32$ level scalar quantizer, leading to $N_I = N_U = 512$. To each quantization level, bit patterns of $B_k = 10$ bits are assigned according to a $r_{\mathrm{BM}} = \frac{1}{2}$ bit mapping based on a repetition code with $\mathbf{G}_k^{[\mathrm{BM}]} = (\mathbf{I}_5\ \mathbf{I}_5)$. The same rate $r_{\mathrm{CC}} = 1$ convolutional code as in the first simulation example (see Fig. 3.4) is used. The transmission is simulated using an AWGN channel with BPSK symbol space mapping. The *a priori* information $\mathsf{P}(i_{t,k})$, $\mathsf{P}(i_{t,k}|i_{t-1,k})$, and $\mathsf{P}(i_{t,k}|i_{t,k-1})$ has been measured in advance (under the assumption of a stationary source) and stored in a table. Figure 3.7 depicts the results for AK0 and AK1-INTER decoding for $\Omega \in \{3, 10\}$ (AK0) or $\Omega \in \{1, 3, 10\}$ (AK1-INTER). Due to the bad channel quality ($E_{\mathrm{s}}/N_0 = -6.4\,\mathrm{dB}$), the AK0 algorithm is unable to reconstruct the image data. On the other hand, the AK1-INTER based SDSD can recover parts of the image by exploiting the inter-frame redundancies (i.e., the correlation in horizontal direction) although the source is not stationary, as assumed. Note that due to delay constraints, no information from future frames is used. It can clearly be seen how the algorithm tries to independently correct the different parameters (each parameter represents a row in the image).

[4] Note that in video coding, the term *frame* is also used to denoted a complete picture. In this figurative example, the term *frame* refers however only to a column of the picture.

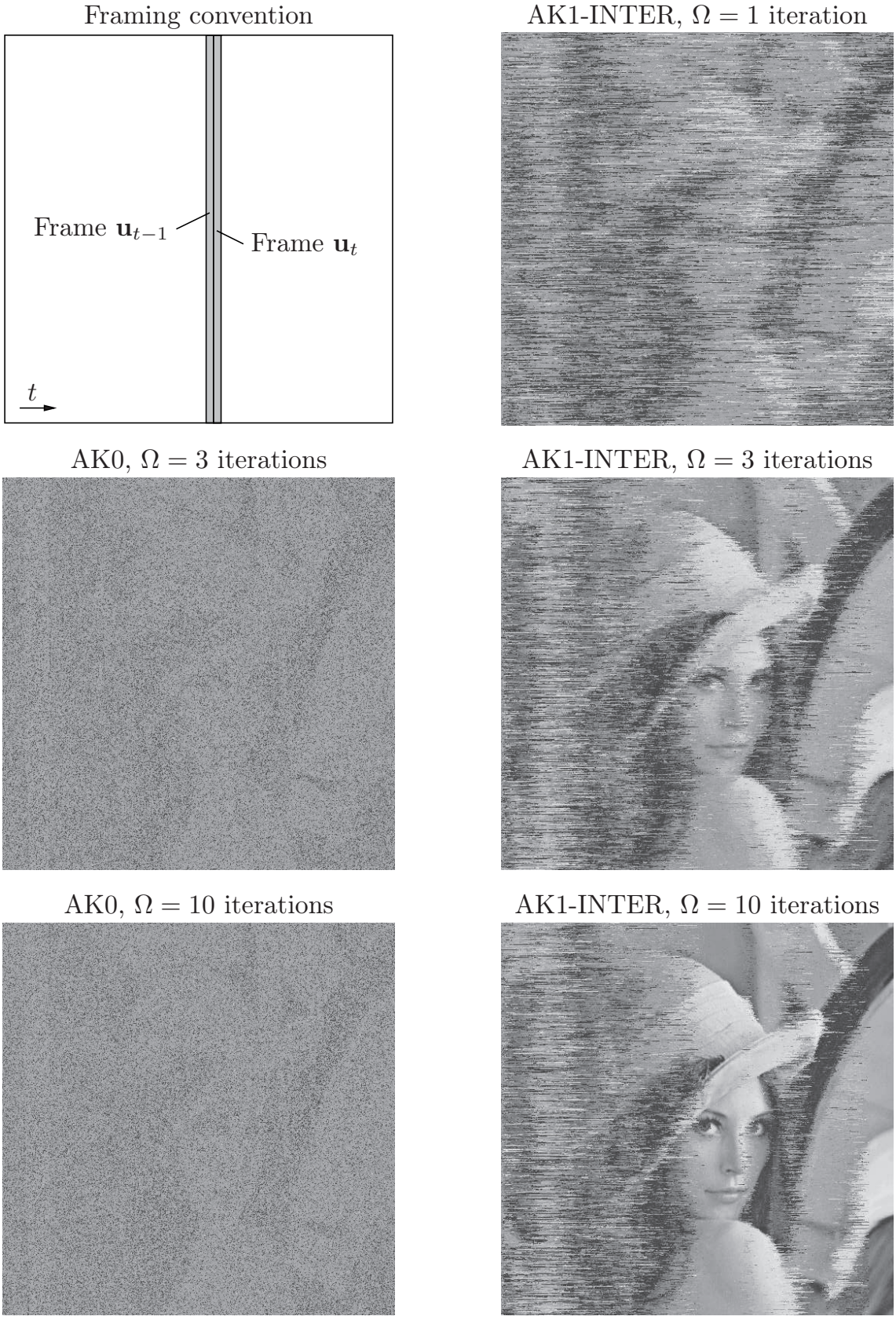

Figure 3.7: Figurative example of an image transmission using ISCD with coding rate $r_{\mathrm{BM}} = \frac{1}{2}$ repetition coded bit mapping, $Q = 32$, rate $r_{\mathrm{CC}} = 1$ channel coding ($\mathbb{G}^{[\mathrm{CC}]} = \{\frac{10}{17}\}_8$), AWGN channel with $E_{\mathrm{s}}/N_0 = -6.4\,\mathrm{dB}$, $N_I = 512$, AK0 and AK1-INTER decoding for $\Omega \in \{3, 10\}$ (AK0) or $\Omega \in \{1, 3, 10\}$ (AK1-INTER).

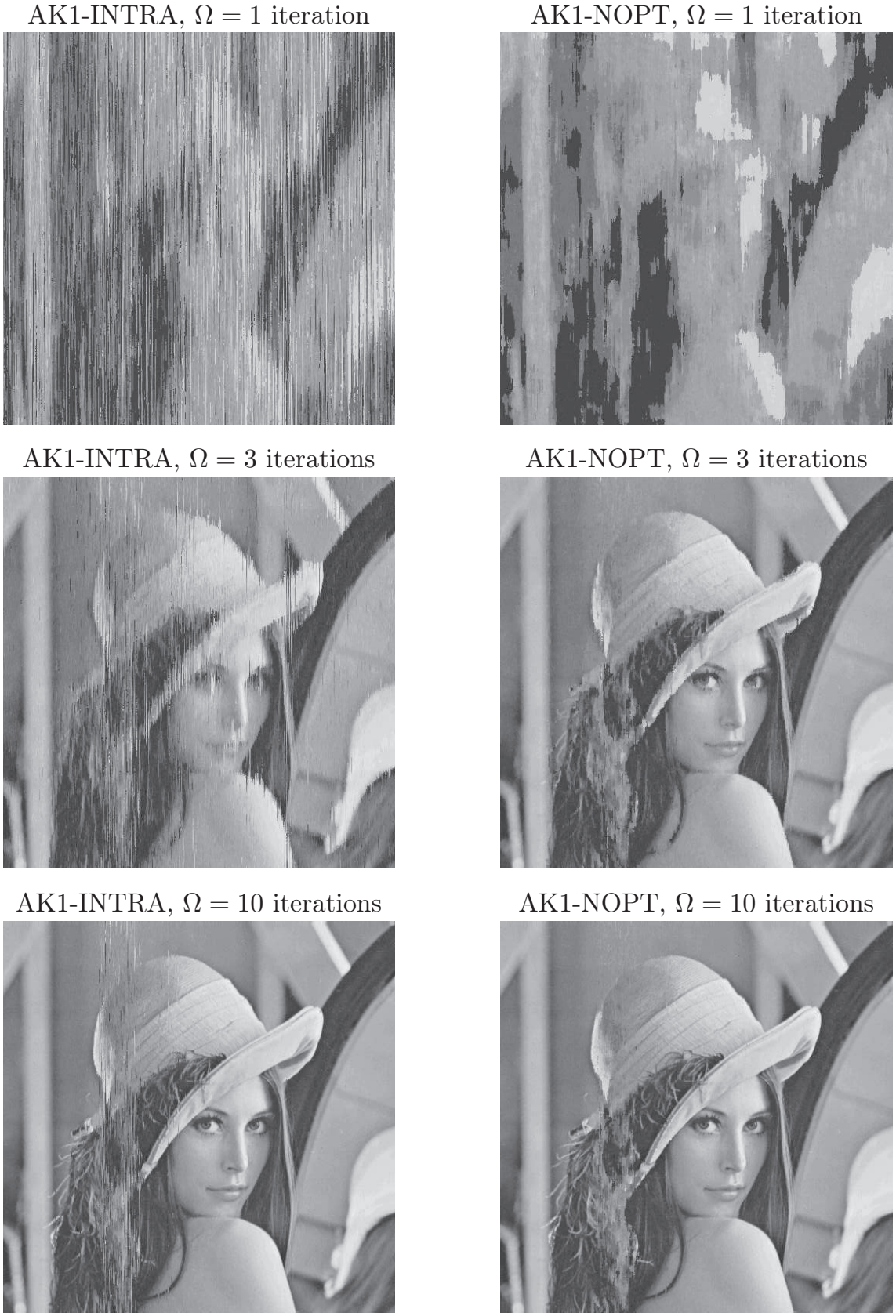

Figure 3.8: Figurative example of an image transmission using ISCD with coding rate $r_{\mathrm{BM}} = \frac{1}{2}$ repetition coded bit mapping, $Q = 32$, rate $r_{\mathrm{CC}} = 1$ channel coding ($\mathbb{G}^{[\mathrm{CC}]} = \{\frac{10}{17}\}_8$), AWGN channel with $E_\mathrm{s}/N_0 = -6.4\,\mathrm{dB}$, $N_I = 512$, AK1-INTRA and AK1-NOPT decoding for $\Omega \in \{1, 3, 10\}$.

Results for AK1-INTRA and AK1-NOPT are depicted in Fig. 3.8 for $\Omega \in \{1, 3, 10\}$. The decoding performance in the AK1-INTRA case is better than in the AK1-INTER case due to the full forward-backward algorithm that is carried out (see also Fig. 3.4). As the algorithm operates on a frame-by-frame basis, it can be clearly seen how the different frames (i.e., columns of the image) are recovered by the algorithm. If $\Omega = 10$, most frames have been recovered. As expected, the AK1-NOPT algorithm offers the best performance. After $\Omega = 3$ iterations, a very good estimate of the original image is obtained with only slight artifacts due to the joint exploitation of inter- and intra-frame redundancies. After $\Omega = 10$ iterations, the picture is almost fully recovered. Finally note that this is only an illustrative example of an image transmission to highlight the effects of ISCD and does not aim at presenting a technique for image transmission. However, an approach similar to the one presented in Chapter 5 may permit to implement a joint compression and protection scheme on the basis of ISCD.

Application Example

The applicability of ISCD shall be shown by means of an example. As already noticed in Sec. 2.4, the model parameters of the *FlexCode* source encoder contain a considerable amount of residual redundancy after source coding. This residual redundancy shall be utilized at the receiver to improve decoding of the model parameters, which are essential for reconstructing the remainder of a frame. The goal of this application example is to show that ISCD also works for very small block lengths.

In a first example, the $N_I = 30$ *FlexCode* model parameters (see Tab. A.2) are encoded with non redundant bit mappings according to [Gör03, AV05, CVA06c] resulting in $N_X = 108$ bits. The feed forward channel code of Fig. 2.1 ($J = 6$, $\mathbb{G}^{[\mathrm{CC}]} = \{133, 171\}_8$) is applied. At the receiver AK1-INTER decoding is applied to the GMM index, and AK1-NOPT decoding is applied to the gains, the pitch decay and the pitch refine parameters. No SDSD is performed for the pitch parameter ($Q = 14$) due to memory limitations. As the single LSFs are quantized with different resolution from frame to frame (but with a constant number of bits for all LSFs), a trick is applied: First, a bit stream is generated for the LSFs and then using this bit stream, "fake" LSFs with a constant number of bits per LSF are extracted. This constant number of bits is obtained by taking the maximum of the (variable) number of bits used to quantize each LSF. In this case, *a priori* information can be measured on "fake" LSF level and AK1-INTER SDSD can be applied. The *a priori* information has been measured using the NTT speech database [NA94] and it has been observed that even on the level of the "fake" LSFs, a certain amount of correlation is exploitable and the AK1-INTER algorithm can be employed.

Figure 3.9-a) shows simulation results for transmission with BPSK over an AWGN channel with an overall coding rate $r_{\mathrm{BM}} \cdot r_{\mathrm{CC}} = \frac{1}{2}$. As a reference, the hard decision decoding with natural binary bit mapping is given. It can be seen that the application of ISCD leads to quality improvements, especially in the second iteration. However, more than $\Omega = 3$ iterations are not beneficial in this case.

In a second experiment, all the parameters except the pitch are protected by a single parity check bit, leading to an interleaver size of $N_X = 138$. The channel code is a

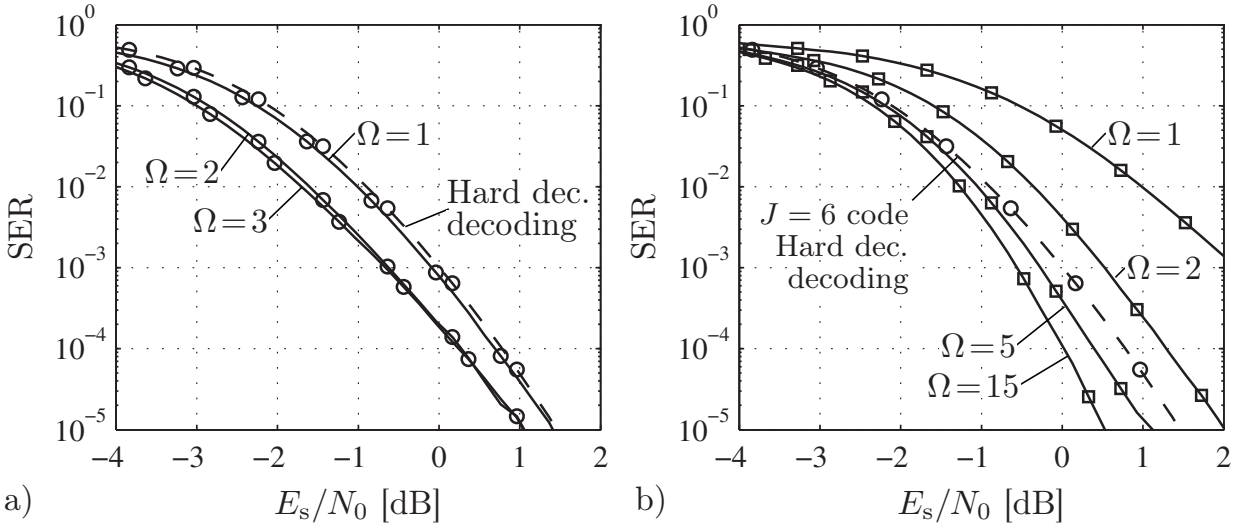

Figure 3.9: Application of ISCD to the transmission of the *FlexCode* model parameters over an AWGN channel with BPSK symbol mapping:

a) Non-redundant bit mappings, $J = 6$, $\mathbb{G}^{[\mathrm{CC}]} = \{133, 171\}_8$ feed forward convolutional code, $r_{\mathrm{BM}} \cdot r_{\mathrm{CC}} = \frac{1}{2}$.

b) Single parity check bit mapping, $J = 3$, $\mathbb{G}^{[\mathrm{CC}]} = \{\frac{15}{17}, \frac{13}{17}\}_8$ punctured RNSC code, $r_{\mathrm{BM}} \cdot r_{\mathrm{CC}} \approx \frac{1}{2}$.

$J = 3$ *Recursive Non-Systematic Convolutional* (RNSC) code with $\mathbb{G}^{[\mathrm{CC}]} = \{\frac{15}{17}, \frac{13}{17}\}_8$ punctured with the puncturing matrix

$$\mathbf{G}_{\mathrm{punc}} = \begin{pmatrix} 1 & 0 & 1 & 1 \\ 1 & 1 & 1 & 0 \end{pmatrix}$$

such that $r_{\mathrm{BM}} \cdot r_{\mathrm{CC}} \approx \frac{1}{2}$ holds. It can be seen in Fig. 3.9-b) that in this case more iterations can be exploited and if the computational complexity of $\Omega = 15$ iterations can be afforded, gains compared to the first approach (Fig. 3.9-a) for $\Omega = 3$) can be achieved for $E_s/N_0 > -0.3\,\mathrm{dB}$. The gains achievable by this second approach are especially important if low SERs of $\approx 10^{-5}$ are targeted. However, the system performs worse than the hard decision reference (taken from Fig. 3.9-a)) for a small number of iterations.

In [SSV08, SSV10], an LDPC code was used instead of a convolutional code for protecting the model parameters. LDPC codes have been chosen because of their inherent error detection capabilities, which facilitate the generation of a *Bad Frame Indicator* (BFI) necessary for error concealment. ISCD can also be applied in this case by using the LDPC-based ISCD approach highlighted in [SSVC08].

3.1.5 Source Coding Related Rates

The residual redundancy which is still present in the source codec parameters after source coding can be exploited within the ISCD system. Thus, it can be considered as some kind of additional inherent channel code. Therefore it can be advantageous

to know the rate of this implicit code and thus the real effective rate of the outer component in the ISCD system. According to [TK06, Tho07c] the total rate of the source code r_{SC} can be described by

$$r_{\mathrm{SC}} \doteq r_{\mathrm{SC}}^{[\mathrm{Markov}]} \cdot r_{\mathrm{SC}}^{[\mathrm{Mapping}]} = r_{\mathrm{SC}}^{[\mathrm{Markov}]} \cdot r_{\mathrm{SC}}^{[\mathrm{AK0}]} \cdot r_{\mathrm{BM}} \tag{3.11}$$

with

$$r_{\mathrm{SC}}^{[\mathrm{AK0}]} \doteq \frac{\mathsf{H}(I_{t,k})}{\mathrm{ld}(Q)} \qquad \text{and} \tag{3.12}$$

$$r_{\mathrm{SC}}^{[\mathrm{Markov}]}(t) \doteq \frac{\mathsf{H}(I_{1,1},\ldots,I_{1,N_I},\ldots,I_{2,1},\ldots,I_{2,N_I},\ldots,I_{t,1},\ldots,I_{t,N_I})}{t \cdot N_I \cdot \mathsf{H}(I_{t,k})}\,, \tag{3.13}$$

where $\mathsf{H}(I_{t,k})$ denotes the entropy of the random variable $I_{t,k}$ [CT06]. The detailed derivation of (3.12) and (3.13) can be found in [Tho07c]. Note that $r_{\mathrm{SC}}^{[\mathrm{Markov}]}(t)$ given by (3.13) is dependent on the time (or frame index) t. The transmission starts at $t = 1$ by definition and we assume that $\mathsf{H}(I_{t,k}) = \mathsf{H}(I) = \text{constant}$ for all t and k.

In the case of AK0 decoding, it is assumed that the indices $I_{t,k}$ are uncorrelated in time and position and it can thus easily be shown [Tho07c] that $r_{\mathrm{SC}}^{[\mathrm{Markov,AK0}]} = 1$. In the case of AK1-INTRA decoding, $r_{\mathrm{SC}}^{[\mathrm{Markov}]}(t)$ can be simplified to $r_{\mathrm{SC}}^{[\mathrm{Markov,INTRA}]}$ with [Tho07c]

$$r_{\mathrm{SC}}^{[\mathrm{Markov,INTRA}]} = \frac{\mathsf{H}(I_{t,k}) + (N_I - 1) \cdot \mathsf{H}(I_{t,k}|I_{t,k-1})}{N_I \cdot \mathsf{H}(I_{t,k})}\,, \qquad \text{and} \tag{3.14}$$

$$\lim_{N_I \to \infty} r_{\mathrm{SC}}^{[\mathrm{Markov,INTRA}]} = \frac{\mathsf{H}(I_{t,k}|I_{t,k-1})}{\mathsf{H}(I_{t,k})}\,. \tag{3.15}$$

Note that $r_{\mathrm{SC}}^{[\mathrm{Markov,INTRA}]}$ does not depend on the time t anymore, but only on the source properties and on the number N_I of quantizer indices per frame. It is shown in App. B.1 that in the case of AK1-INTER decoding, the value $r_{\mathrm{SC}}^{[\mathrm{Markov}]}(t)$ can be simplified to $r_{\mathrm{SC}}^{[\mathrm{Markov,INTER}]}(t)$ with

$$r_{\mathrm{SC}}^{[\mathrm{Markov,INTER}]}(t) = \frac{\mathsf{H}(I_{t,k}) + (t-1) \cdot \mathsf{H}(I_{t,k}|I_{t-1,k})}{t \cdot \mathsf{H}(I_{t,k})}\,, \qquad \text{and} \tag{3.16}$$

$$\lim_{t \to \infty} r_{\mathrm{SC}}^{[\mathrm{Markov,INTER}]}(t) = \frac{\mathsf{H}(I_{t,k}|I_{t-1,k})}{\mathsf{H}(I_{t,k})}\,. \tag{3.17}$$

If both spatial and temporal correlation are present (i.e., $\rho > 0$ and $\delta > 0$), it is shown in App. B.2 that $r_{\mathrm{SC}}^{[\mathrm{Markov,OPT}]}(t)$ amounts to

$$\begin{aligned} r_{\mathrm{SC}}^{[\mathrm{Markov,OPT}]}(t) = {} & \frac{(N_I - 1)(t-1)\mathsf{H}(I_{t,k}|I_{t-1,k}, I_{t,k-1}) + (t-1)\mathsf{H}(I_{t,k}|I_{t-1,k})}{t \cdot N_I \cdot \mathsf{H}(I_{t,k})} \\ & + \frac{(N_I - 1)\mathsf{H}(I_{t,k}|I_{t,k-1}) + \mathsf{H}(I_{t,k})}{t \cdot N_I \cdot \mathsf{H}(I_{t,k})} \end{aligned} \tag{3.18}$$

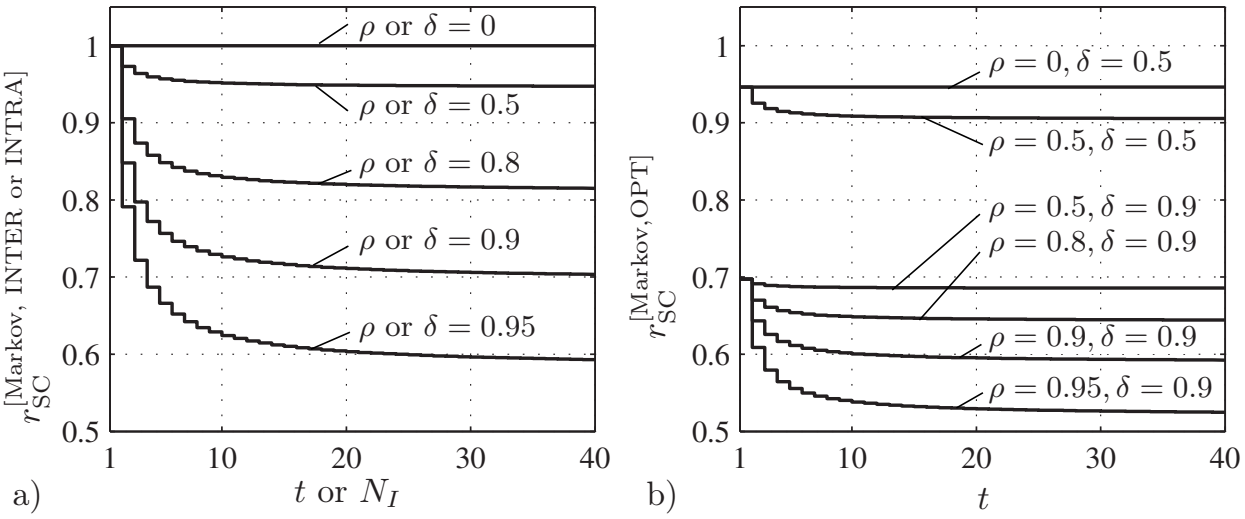

Figure 3.10: Source coding rates for different types and amounts of correlation.
a) Source coding rates $r_{\mathrm{SC}}^{[\mathrm{Markov,INTER}]}$ and $r_{\mathrm{SC}}^{[\mathrm{Markov,INTRA}]}$ as a function of t (resp. N_I).
b) Source coding rate $r_{\mathrm{SC}}^{[\mathrm{Markov,OPT}]}$ as a function of t with $N_I = 250$ for different combinations of ρ and δ.

with

$$\lim_{t\to\infty} r_{\mathrm{SC}}^{[\mathrm{Markov,OPT}]}(t) = \frac{(N_I-1)\mathsf{H}(I_{t,k}|I_{t-1,k}, I_{t,k-1}) + \mathsf{H}(I_{t,k}|I_{t-1,k})}{N_I \mathsf{H}(I_{t,k})} \tag{3.19}$$

$$\lim_{N_I\to\infty}\lim_{t\to\infty} r_{\mathrm{SC}}^{[\mathrm{Markov,OPT}]}(t) = \frac{\mathsf{H}(I_{t,k}|I_{t-1,k}, I_{t,k-1})}{\mathsf{H}(I_{t,k})}\,. \tag{3.20}$$

Note that (3.18) is in fact not valid for AK1-NOPT decoding, but only for the optimal decoding algorithm as described in [Hei01a, HA08]. The AK1-NOPT approach, which is a suboptimal approximation of the optimal decoding algorithm, offers however results comparable to the optimal decoder [ASHV00, APV04, HA08].

Figure 3.10 depicts the effects of (3.14), (3.16), and (3.18) for different amounts of correlation. As (3.14) and (3.16) generate the same results by exchanging time and position, both results are depicted in Fig. 3.10-a). If no correlation is exploited, $r_{\mathrm{SC}}^{[\mathrm{Markov}]} = 1$, as expected. It can be seen that the limit in (3.15) is a good approximation of (3.14) for $N_I > 30$. If AK1-INTER decoding shall be used, Fig. 3.10-a) indicates that during the first $t < 30$ frames after resetting the source at $t = 1$, the decoding is less reliable, as the source exhibits a higher correlation-related coding rate (see also Fig. 3.7 for a confirmation of this fact). This behavior is of high practical relevance, especially if the decoding assumes a short-time stationary source with sudden changes of the statistics. Such a situation can happen for instance in speech codecs if, e.g., an abrupt transition from a voiced to an unvoiced speech segment occurs. In this case, the statistics of certain parameters (e.g., the pitch period) may be subject to sudden changes.

Figure 3.10-b) shows the behavior of $r_{\mathrm{SC}}^{[\mathrm{Markov,OPT}]}$ if temporal and spatial correlation is available. Additional correlation improves the overall system quality due to the

decreased correlation-related coding rate. It can again be noticed that the correlation-related rate is larger in the first frames after a source reset, resulting in a poorer overall system performance.

3.1.6 EXIT Chart Analysis of ISCD

A powerful analysis tool for an easy comparison of different system setups and for assessing the convergence performance of ISCD are *EXtrinsic Information Transfer* (EXIT) charts [tB99a, tB01c, AvAV03, ABCV05], introduced in Section 2.3. Many optimizations and performance improvements of ISCD have been obtained by using EXIT charts, e.g., [AV04b, AV05, AVC05, AAC+06, CVA06b, KGM06, ACBV06, SVCS08, TSV08, CSVA08a].

Figure 3.11 shows EXIT charts for all four decoding algorithms of the simulation example in Fig. 3.4. In the AK0 case, the characteristics C_{CD} (channel decoder) and C_{SD} (soft decision source decoder) intersect for a low mutual information ($\mathsf{I}_{\mathrm{SD}}^{[\mathrm{apr}]} < 0.2\,\mathrm{bit}$). However, as the decoding trajectory $\mathsf{T}_{\mathrm{ISCD}}$ in the blow-up sub-plot in the EXIT

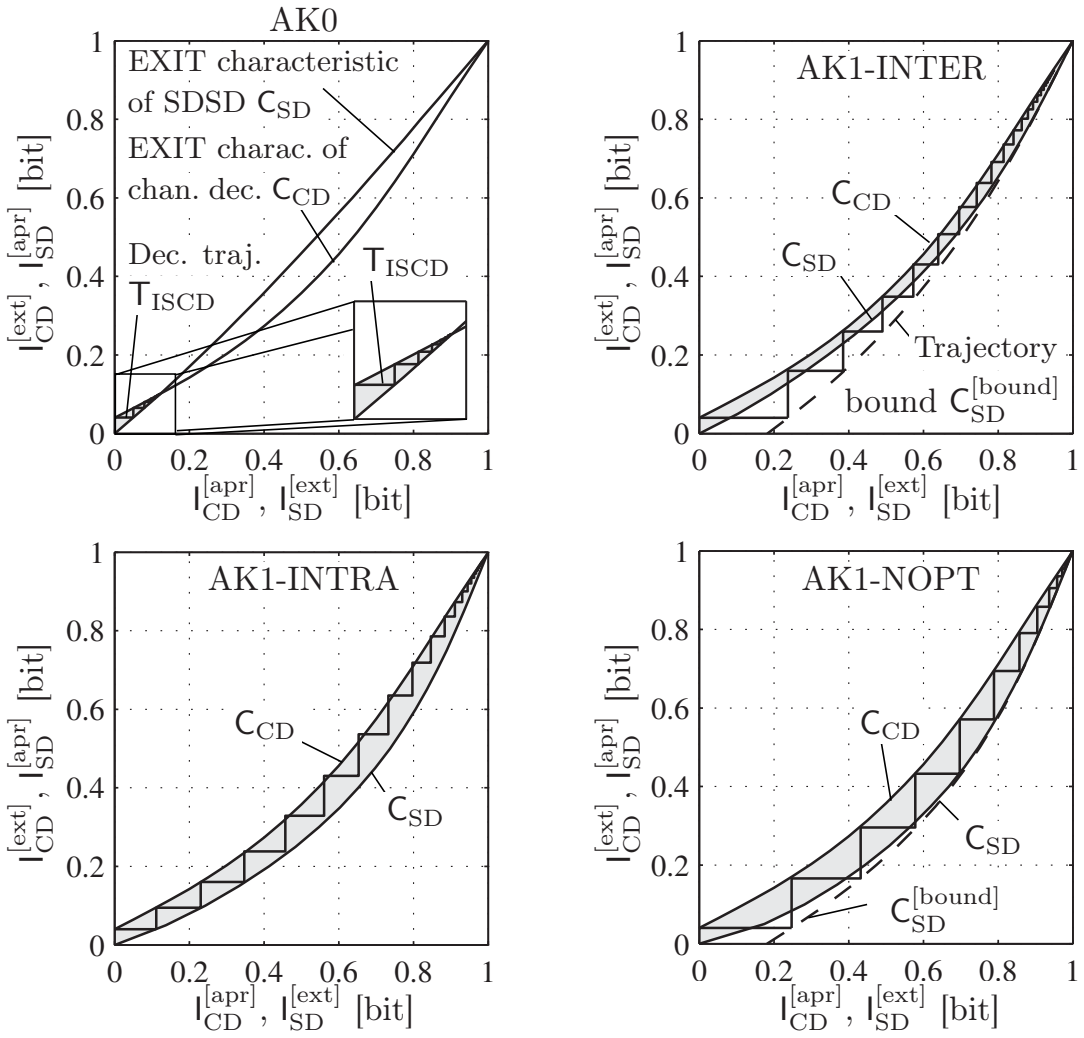

Figure 3.11: EXIT chart analysis for the simulation example of Fig. 3.4 at a channel quality of $\frac{E_{\mathrm{s}}}{N_0} = -4\,\mathrm{dB}$.

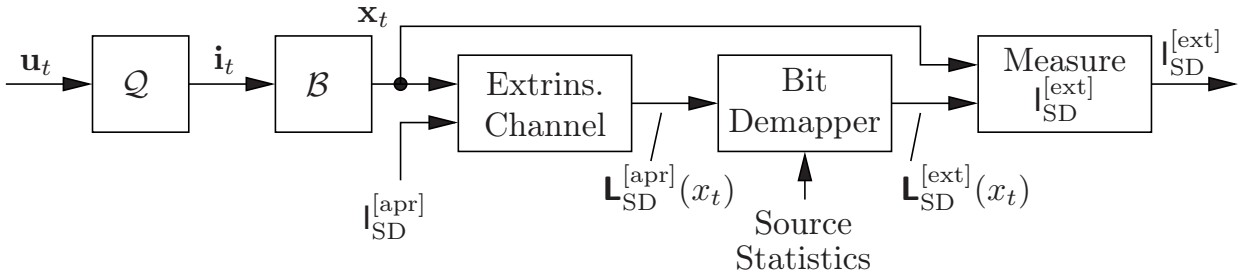

Figure 3.12: Block diagram for measuring the EXIT characteristics of SDSD.

chart indicates, the iterative processing helps to slightly improve the performance with $4-5$ iterations, compared to the non-iterative case. For all the other cases, a decoding tunnel exists and iterative decoding permits to reach the end of the tunnel, i.e., $\mathsf{I}_{\mathrm{SD}}^{[\mathrm{ext}]} = 1\,\mathrm{bit}$. As already observed in [CSVA08a, CSVA08b], the characteristic C_{SD} of the repetition coded bit mapping with $r_{\mathrm{BM}} = \frac{1}{2}$ matches the characteristic C_{CD} of the utilized rate $r_{\mathrm{CC}} = 1$ channel code very well for AK1 decoding. For the given channel quality of $E_{\mathrm{s}}/N_0 = -4\,\mathrm{dB}$ a decoding tunnel is present in all three AK1 cases. As expected, the decoding tunnel for the AK1-NOPT case is the widest for the given channel conditions, as both inter- and intra-frame correlations are exploited.

In the case of AK1-INTER and AK1-NOPT decoding, the characteristic C_{CD} is significantly exceeded by the decoding trajectory $\mathsf{T}_{\mathrm{ISCD}}$, especially during the first iterations. This behavior renders the EXIT characteristic of SDSD useless for predicting the behavior after a given amount of iterations (however, the intersection with the channel decoder characteristic is still useful for predicting convergence). The reason for this behavior has already been outlined in [ACBV06, SACV11] and is briefly revised here.

Figure 3.12 depicts the block diagram for measuring the EXIT characteristics of SDSD. Note that in contrast to the block diagram for the measurement of the inner convolutional code (see also App. E), no channel related knowledge is available at the bit demapping stage. It is assumed in this work that in the case of a systematic channel code, the channel-related L-values $\mathsf{L}_{\mathrm{CD}}^{[\mathrm{chan}]}(e_t)$ are included in the extrinsic output of the inner decoder, as described in Sec. 2.3.

The extrinsic information of the AK1-INTER algorithm is computed by (see also App. F.1) [AVS01, Adr03]

$$\mathsf{L}_{\mathrm{SD}}^{[\mathrm{ext}]}(b_{t,k,\mu}) = \ln \frac{\sum_{q=1}^{Q} \left(1-\bar{b}_{k,\mu}^{(q)}\right) \gamma_{t,k}^{[\mathrm{ext}]\setminus\mu}(q) \sum_{\tilde{q}=1}^{Q} \mathsf{Pr}\{I_{t,k}=q|I_{t-1,k}=\tilde{q}\}\alpha_{t-1,k}(\tilde{q})}{\sum_{q=1}^{Q} \bar{b}_{k,\mu}^{(q)} \gamma_{t,k}^{[\mathrm{ext}]\setminus\mu}(q) \sum_{\tilde{q}=1}^{Q} \mathsf{Pr}\{I_{t,k}=q|I_{t-1,k}=\tilde{q}\}\alpha_{t-1,k}(\tilde{q})}, \quad (3.21)$$

with $\alpha_{t-1,k}(\tilde{q})$ denoting the forward reliabilities of the BCJR algorithm [BCJR74] and $\gamma_{t,k}^{[\mathrm{ext}]\setminus\mu}(q)$ denoting the extrinsic channel-related reliabilities of the bit pattern $\bar{\mathbf{b}}_k^{(q)}$ without considering the bit at position μ. Details on the computation of $\alpha_{t-1,k}(\tilde{q})$ and $\gamma_{t,k}^{[\mathrm{ext}]\setminus\mu}(q)$ are given in App. F.1.

Due to the inter-frame relationship, the value $\mathsf{L}_{\mathrm{SD}}^{[\mathrm{ext}]}(b_{t,k,\mu})$ depends on $\alpha_{t-1,k}(\tilde{q})$ which has been computed at the previous frame (at time instant $t-1$). The value $\alpha_{t-1,k}$ is updated once per frame, after Ω iterations have been carried out, according to

$$\alpha_{t,k}(q) = \frac{1}{\mathrm{K}} \cdot \gamma_{t,k}(q) \cdot \sum_{\tilde{q}=1}^{Q} \mathsf{Pr}\{I_{t,k}=q | I_{t-1,k}=\tilde{q}\} \cdot \alpha_{t-1,k}(\tilde{q}) \,, \tag{3.22}$$

with the normalization constant K and the channel-related reliability $\gamma_{t,k}(q)$. If ISCD with $\Omega > 1$ iterations is employed, the update of $\alpha_{t-1,k} \rightarrow \alpha_{t,k}$ is performed at the end of the iterative process. If the iterative process has converged, highly reliable extrinsic information $\mathbf{L}_{\mathrm{CD}}^{[\mathrm{ext}]}(x_t)$ is available at the input of the bit demapper, which is then used to compute highly reliable $\gamma_{t,k}$. Highly reliable signifies that $\gamma_{t,k}(i_{t,k}) \rightarrow 1$ and $\gamma_{t,k}(q) \rightarrow 0$, $\forall q \in \mathbb{I} \setminus \{i_{t,k}\}$. Therefore, $\alpha_{t,k}$ is as well highly reliable. It is then stored and used at time $t+1$ to compute $\mathsf{L}_{\mathrm{SD}}^{[\mathrm{ext}]}(b_{t+1,k,\mu})$. In the first iterations of the frame at time $t+1$, the input L-values $\mathbf{L}_{\mathrm{CD}}^{[\mathrm{ext}]}(x_{t+1})$ are however relatively unreliable. In the computation of the EXIT chart however, the SDSD is only executed once per frame. Thus, the value $\alpha_{t-1,k}$ is updated using input L-values $\mathbf{L}_{\mathrm{SD}}^{[\mathrm{apr}]}(x_t)$ that have the same reliability as those that are used for computing the extrinsic information. This signifies that the EXIT chart does not suitably model the behavior of the ISCD system exploiting inter-frame correlation, especially during the first iterations.

To overcome this mismatch, a solution leading to so-called *EXIT Trajectory Bounds* (ETBs) has been proposed in [AAS+10, SACV11]. In order to compute the ETB, we use the maximum attainable *a priori* mutual information $\mathsf{I}_{\mathrm{SD,max}}^{[\mathrm{apr}]}$, which, if a decoding tunnel is present, amounts to $\mathsf{I}_{\mathrm{SD,max}}^{[\mathrm{apr}]} = \mathsf{H}(X)$. If the characteristics of SDSD and channel decoder intersect, it is convenient to use the SDSD *a priori* mutual information at the intersection point as $\mathsf{I}_{\mathrm{SD,max}}^{[\mathrm{apr}]}$. After completing the measurement of the SDSD EXIT characteristic as depicted in Fig. 3.12, new *a priori* information $\mathbf{L}_{\mathrm{SD,max}}^{[\mathrm{apr}]}(x_t)$ is computed based on the mutual information $\mathsf{I}_{\mathrm{SD,max}}^{[\mathrm{apr}]}$ (i.e., consistent Gaussian L-values are computed as defined in Sec. 2.3). Using this information, the bit demapper is executed a second time to compute the now more reliable $\alpha_{t,k}$ which are then stored and used in the evaluation of (3.21) for the frame $t+1$. This simulates the behavior of a fully converged system. The resulting curve is denoted by $\mathsf{C}_{\mathrm{SD}}^{[\mathrm{bound}]}$ and is depicted in Fig. 3.11 for the AK1-INTER and AK1-NOPT cases (which exploit inter-frame correlation). It can be seen that the trajectory bound is a good indicator for predicting the behavior of the different iterations in ISCD. Note that the ETB is only useful to predict the behavior of the decoding trajectory $\mathsf{T}_{\mathrm{ISCD}}$ and not for predicting at which channel quality the system converges.

SER Prediction Using EXIT Charts

According to [tB01a], the bit error rate P_{b} of the outer coded bits can be estimated using

$$\mathsf{P}_{\mathrm{b}} \approx \frac{1}{2} \operatorname{erfc}\left(\sqrt{\frac{1}{8}\left(\left[\mathcal{J}^{-1}\left(\mathsf{I}_{\mathrm{SD}}^{[\mathrm{apr}]} \right) \right]^2 + \left[\mathcal{J}^{-1}\left(\mathsf{I}_{\mathrm{SD}}^{[\mathrm{ext}]} \right) \right]^2 \right)} \right) , \tag{3.23}$$

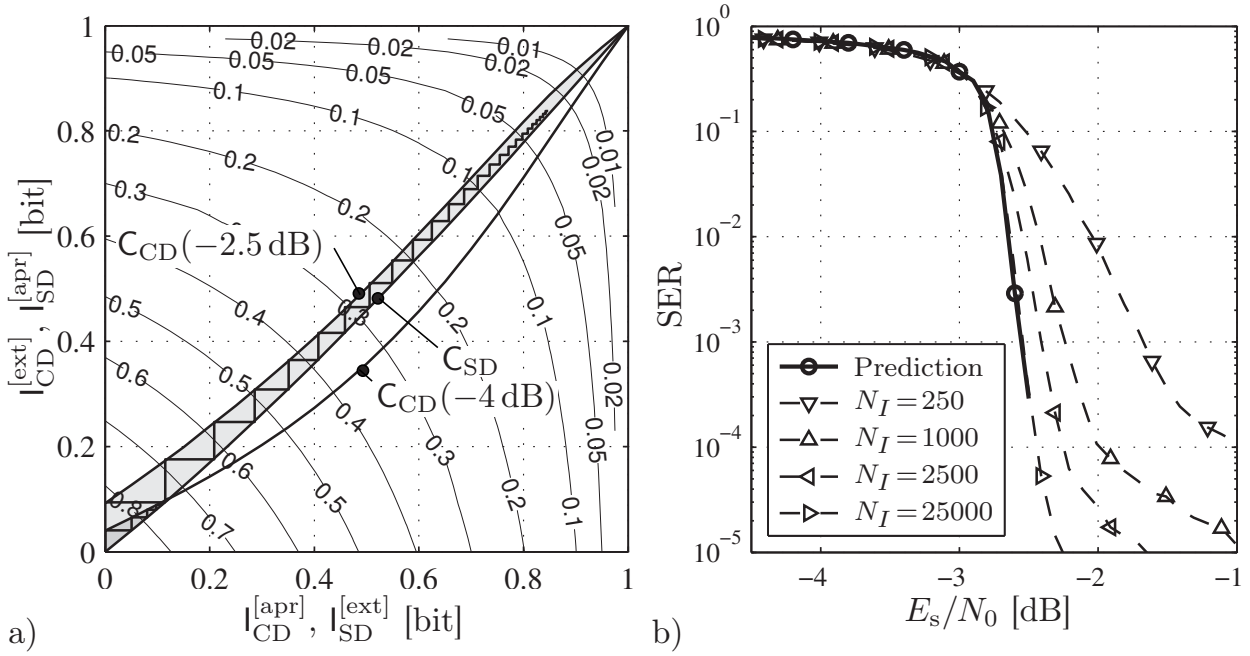

Figure 3.13: SER estimation using EXIT charts. System settings as in Figs 3.4 and 3.11, AK0 decoding only.

a) EXIT charts with SER contour lines and decoding trajectories for $E_s/N_0 = -4\,\text{dB}$ (intersection) and $E_s/N_0 = -2.5\,\text{dB}$ for $\Omega = 25$.

b) Estimated (solid line ——) and measured (dashed lines – – –) SER results for ISCD with $\Omega = 25$ and $N_I \in \{250, 1000, 2500, 25000\}$.

with $\mathcal{J}(\cdot)$ according to (2.9). Using (3.23), the SER of the index at position k can directly be expressed as

$$\mathsf{P}_s = 1 - (1 - \mathsf{P}_b)^{B_k^{[NB]}} \quad . \tag{3.24}$$

Equations (3.24) and (3.23) can be used to estimate the SER after ISCD. Two cases can be distinguished: If both characteristics intersect, convergence is not possible and the intersection point marks the maximum attainable mutual information, which can be used in (3.23) and (3.24) to approximate the SER. If, on the other hand, an open decoding tunnel is present, the maximum attainable mutual information has to be obtained by assuming an optimal decoding trajectory with Ω iterations. The endpoint of this trajectory marks the maximum attainable mutual information. If inter-frame correlation is exploited (by the AK1-INTER or AK1-NOPT algorithms), the *EXIT Trajectory Bound* (ETB) has to be used for determining the maximum mutual information for SER prediction after Ω iterations. Finally note that the EXIT chart requirements have to be fulfilled for a precise SER prediction, i.e., the frame size has to be infinite ($N_I \to \infty$). In realistic system setups with finite N_I, a loss in the SER (or the *Bit Error Rate* (BER), respectively) is observed [tB00a, tB01a, tB01c, tB01d, Tüc03, Tüc04].

Figure 3.13-a) shows the EXIT chart of the AK0 case of Fig. 3.11. Additionally, contour lines showing the correspondence between $(I_{SD}^{[apr]}, I_{SD}^{[ext]})$ and the SER. The EXIT characteristics and (measured) decoding trajectories for two different channel

conditions ($E_s/N_0 = -4\,\text{dB}$ and $E_s/N_0 = -2.5\,\text{dB}$) are also given. Figure 3.13-b) shows the predicted SER curve (solid line ——) as well as measured SER results (dashed lines – – –) for $N_I \in \{250, 1000, 2500, 25000\}$ in the AK0 case. The other simulation settings are the same as in Fig. 3.4. As expected, the SER predication is able to predict the waterfall behavior very well and a good correspondence is achieved for large interleaver lengths (here $N_I = 25000$ with an interleaver length of $N_X = 2 \cdot 10^5$). For smaller block lengths, an indispensable performance loss in terms of SER or E_s/N_0 has to be tolerated which increases with decreasing N_I. Further note that the SER prediction presented in this chapter is not capable of predicting the error floor [BDMP98b]. Error floor prediction can be efficiently performed using the union bound [DDPM95, BDMP98a, BDMP98b, DJM98, BMD03, Abb07].

Area Properties of EXIT Charts

The area properties given in Sec. 2.3 also hold in the context of ISCD. Equations (2.13) and (2.14) can be written as

$$\mathcal{A}\left(\mathsf{C}_{\text{SD}}\right) = 1 - r_{\text{SC}} \tag{3.25}$$

$$\mathcal{A}\left(\mathsf{C}_{\text{CD}}\right) \leq \frac{\mathsf{I}_{\mathcal{C}}}{r_{\text{CC}}}\,. \tag{3.26}$$

Again, equality in (3.26) holds if $r_{\text{CC}} \geq 1$ [AKtB04]. The area between both characteristics and thus the rate loss amounts to $\mathsf{I}_{\mathcal{C}} - r_{\text{SC}}$. Notice, as equality in (3.26) only holds for inner codes of rates ≥ 1, this has implications for the convolutional code used in the ISCD system.

Table 3.1 shows the source coding related rates r_{SC} and $1 - \mathcal{A}(\mathsf{C}_{\text{SD}})$ for four different decoding algorithms (and convenient source setups). In the AK0 and AK1-INTRA case, it can be observed in the example that (3.25) is fulfilled (i.e., $\mathcal{A}(\mathsf{C}_{\text{SD}}) = 1 - r_{\text{SC}}$, or $r_{\text{SC}} = 1 - \mathcal{A}(\mathsf{C}_{\text{SD}})$, respectively), however, this is not the case for AK1-INTER and AK1-NOPT decoding. The reason is that the latter two algorithms do not consider information from future frames and thus do not fully exploit the Markov property (and are thus suboptimal). However, the value $1 - \mathcal{A}(\mathsf{C}_{\text{SD}}^{[\text{bound}]})$ seems to coincide well (based on observations) with r_{SC}. There is a slight difference between r_{SC} and $1 - \mathcal{A}(\mathsf{C}_{\text{SD}}^{[\text{bound}]})$ in the AK1-NOPT case which is due to the fact that the AK1-NOPT algorithm is only an approximation of the optimal decoding algorithm. Therefore,

Source setup	r_{SC}	SDSD algorithm	$1 - \mathcal{A}\left(\mathsf{C}_{\text{SD}}\right)$	$1 - \mathcal{A}\left(\mathsf{C}_{\text{SD}}^{[\text{bound}]}\right)$
$\rho = 0$, $\delta = 0$	0.47	AK0	0.47	—
$\rho = 0.9$, $\delta = 0$	0.33	AK1-INTER	0.38	0.33
$\rho = 0$, $\delta = 0.9$	0.33	AK1-INTRA	0.33	—
$\rho = 0.9$, $\delta = 0.9$	0.28	AK1-NOPT	0.32	0.30

Table 3.1: Comparison between source coding related rates r_{SC} and areas of SDSD EXIT characteristics in Fig. 3.11 for different source setups.

the area difference $\mathcal{A}(\mathsf{C}_{\mathrm{SD}}^{[\mathrm{bound}]}) - \mathcal{A}(\mathsf{C}_{\mathrm{SD}})$ indicates which rate loss can be expected by not considering the information from future frames. Note that $\mathsf{C}_{\mathrm{SD}}^{[\mathrm{bound}]}$ only exists for those decoders exploiting inter-frame correlation, i.e., AK1-INTER and AK1-NOPT. For further information on the area properties of SDSD EXIT characteristics, see [ABCV05, ACBV06].

3.2 Improved Inter-Frame Decoding

As already noticed in Secs. 3.1.3, 3.1.5 and 3.1.6, the presented ISCD receiver, which exploits inter-frame correlation (i.e., $\rho > 0$, $\delta = 0$) using the AK1-INTER SDSD algorithm, cannot fully exploit the assumed Markov property of the parameters due to delay constraints. Only information from preceding frames is utilized, as the future frames are not yet available at the receiver during decoding of a frame at time instant t. This results in the forward-only algorithm explained in depth in App. F.1.

In order to improve the inter-frame based decoding, we propose the receiver depicted in Fig. 3.14, which is compatible to the transmitter depicted in Fig. 3.2. The proposed receiver performs individual channel decoding of $\Phi + 1$ frames received at the (past) time instants $t, t-1, \ldots, t-\Phi$. After deinterleaving, a forward-backward SDSD [Adr03, AV05, ACS08] can then perform the complete inter-frame forward-backward algorithm on the $\Phi+1$ considered frames and generate extrinsic information for each of the $\Phi + 1$ channel decoders. After a fixed number of Ω iterations, only the parameter vector $\hat{\mathbf{u}}_t$ of the current frame is estimated. No re-estimation of the previous frames is performed as this would imply an additional delay in the complete transceiver chain. Note that the extrinsic information computed at the output of the SDSD after Ω iterations has to be saved as it can be reutilized in the subsequent frames as initial *a priori* knowledge in the first execution of the channel decoder.

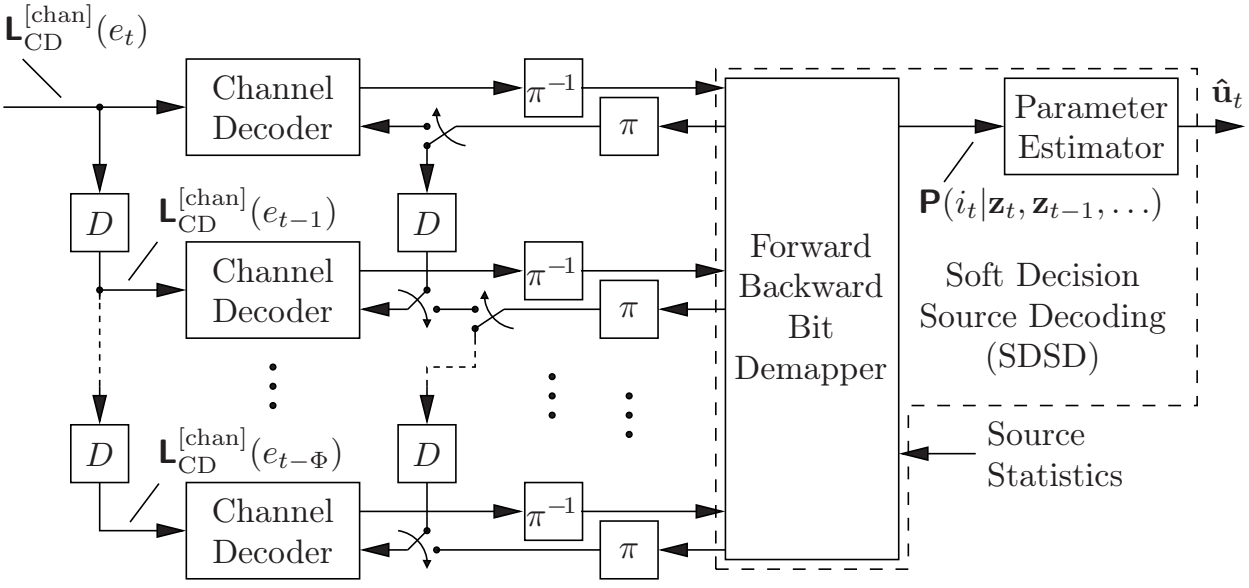

Figure 3.14: Proposed receiver for improved inter-frame based ISCD utilizing the forward-backward AK1-INTER-IMP algorithm and introducing no additional delay.

This is indicated by the switches in Fig. 3.14, which forward the extrinsic output of the SDSD to the memory after Ω iterations and then from the memory to the channel decoder in the first channel decoder execution of the subsequent frame. During the ISCD iterations, all switches are in the "horizontal" position. The situation shown in Fig. 3.14 occurs after Ω iterations and at the beginning of each frame, prior to the first channel decoder execution.

The forward-backward equations can be directly obtained from [Adr03, AV05, ACS08]. The equations of the improved inter-frame decoding algorithm (denoted AK1-INTER-IMP) given here are based on the description of the AK1-INTER algorithm in App. F.1. The forward and backward recursions of the decoding algorithm are given by ($\forall k \in \{1, \ldots, N_I\}$)

$$\alpha_{t',k}(q) = \frac{\gamma_{t',k}(q)}{\mathrm{K}_2} \sum_{\tilde{q}=1}^{Q} \mathsf{Pr}\{I_{t',k} = q | I_{t'-1,k} = \tilde{q}\} \alpha_{t'-1,k}(\tilde{q}) \doteq \frac{\gamma_{t',k}(q) A_{t',k}(q)}{\mathrm{K}_2} \tag{3.27}$$

$$\beta_{t'-1,k}(q) = \frac{1}{\mathrm{K}_3} \sum_{\tilde{q}=1}^{Q} \gamma_{t',k}(\tilde{q}) \mathsf{Pr}\{I_{t',k} = \tilde{q} | I_{t'-1,k} = q\} \beta_{t',k}(\tilde{q}) \tag{3.28}$$

with the initialization ($\forall q \in \mathbb{I}, k \in \{1, \ldots, N_I\}$)

$$\alpha_{0,k}(q) = \alpha_{-1,k}(q) = \cdots = \alpha_{-\Phi,k}(q) = \mathsf{Pr}\{I_{0,k} = q\} \tag{3.29}$$

because the overall transmission starts at $t = 1$. At the beginning of the decoding of each frame (time t), the factors $\beta_{t,k}$ are initialized with $\beta_{t,k}(q) = 1$, $\forall q \in \mathbb{I}, \forall k \in \{1, \ldots, N_I\}$. The forward recursion is carried out for all considered frames $t' \in \{t - \Phi, \ldots, t\}$, while the backward recursion is only carried out for the past frames $t-1, \ldots, t-\Phi$. Extrinsic information is obtained for all bits of all indices of all $\Phi + 1$ considered frames ($t' \in \{t - \Phi, \ldots, t\}$) by

$$\mathsf{L}_{\mathrm{SD}}^{[\mathrm{ext}]}(b_{t',k,\mu}) = \ln \frac{\sum_{q=1}^{Q} \left(1 - \bar{b}_{k,\mu}^{(q)}\right) \cdot \gamma_{t',k}^{[\mathrm{ext}]\setminus\mu}(q) \cdot \beta_{t',k}(q) \cdot A_{t',k}(q)}{\sum_{q=1}^{Q} \bar{b}_{k,\mu}^{(q)} \cdot \gamma_{t',k}^{[\mathrm{ext}]\setminus\mu}(q) \cdot \beta_{t',k}(q) \cdot A_{t',k}(q)}. \tag{3.30}$$

The *a posteriori* probabilities required for the estimation (by either (3.7) or (3.8)) are given by

$$\mathsf{Pr}\{I_{t,k} = q | \mathbf{z}_t, \mathbf{z}_{t-1}, \ldots\} = \frac{1}{\mathrm{K}_1} \cdot \alpha_{t,k}(q) \qquad \forall q \in \mathbb{I}\,. \tag{3.31}$$

Note that only the factors $\alpha_{t,k}$ are utilized in the *a posteriori* probabilities for the estimation, as only the values of the current frame t are estimated, and for this frame, $\beta_{t,k}(q) = 1$ by initialization. Further note that $\alpha_{t',k}(q)$ is continuously updated (initialization only for $t = 0$) while $\beta_{t',k}(q)$ is re-initialized in each decoding step.

The idea of the proposed decoder is to refine the extrinsic information of the SDSD for the past frames $t-1$, $t-2$, ..., by using the information from the current frame t.

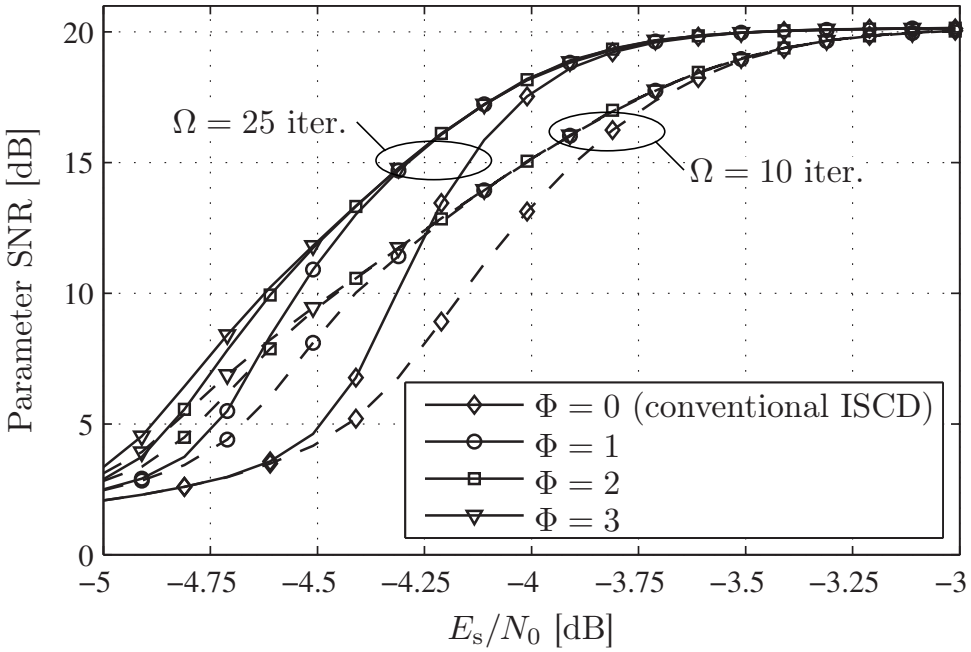

Figure 3.15: Parameter SNR performance of ISCD with improved inter-frame decoding for a source with $\rho = 0.9$, $\delta = 0$, scalar LMQ ($Q = 16$), $N_I = 250$, $r_{\mathrm{BM}} = \frac{1}{2}$ repetition bit mapping, rate $r_{\mathrm{CC}} = 1$ convolutional code ($J = 3$, $\mathbb{G}^{[\mathrm{CC}]} = \{\frac{10}{17}\}_8$), MMSE estimation.

Using this refined information, the channel decoders of the past frames can generate improved extrinsic information which, in the subsequent forward-backward SDSD execution, can improve the factors $\alpha_{t,k}(q)$ used for estimating the parameters in the current frame.

Figure 3.15 depicts simulation results for the proposed scheme for a similar setup as in Sec. 3.1.4. A source containing only inter-frame correlation, i.e., $\delta = 0$, is employed. The improved algorithm is applied with $\Phi \in \{1, 2, 3\}$ and compared to the conventional ISCD approach (i.e., $\Phi = 0$). Bit mapping and channel coding as in Sec. 3.1.4 are utilized. In all cases, $\Omega = 10$ or $\Omega = 25$ iterations are carried out at the receiver and the parameters are reconstructed using MMSE estimation. Figure 3.15 reveals that the proposed algorithm outperforms the conventional ISCD receiver. Already for $\Phi = 1$, a significant improvement is obtained. Increasing Φ leads to further improvements. It is noteworthy to mention that the overall decoding complexity linearly scales with Φ.

It is to be noted that the algorithm improves the decoding of the old frames $t - 1, t - 2, \ldots$ by taking into account imformation for future frames. However, the estimates of previous frames cannot be updated due to delay constraints and the estimate of the current frame can still not take into account information from future frames (see (3.31)). The proposed receiver mainly updates the extrinsic information, which supports the channel decoder of the previous frames to generate better extrinsic information for use within the SDSD. However, the performance obtained using a full forward-backward algorithm taking into account all past and future frames cannot be reached.

The proposed approach can also directly be adapted to the AK1-NOPT algorithm, which utilizes the identical temporal forward recursion as the AK1-INTER approach. Simulation results for AK1-NOPT decoding are not shown in this section as the behavior is similar to the AK1-INTER case. However, the expected gains are smaller, as the overshooting effect in the AK1-NOPT case is not as pronounced as in the AK1-INTER case (see also Fig. 3.11 and Sec. 3.1.6).

3.3 Irregular Redundant Bit Mappings

It is known that a necessary condition for the inner (channel) code of a capacity-achieving serially concatenated system is that it should be of rate $r_{\mathrm{CC}} \geq 1$ [AKtB04, Tho07a] (see also Sec. 3.1.6). If this inner (channel) code is fixed, the outer code can be matched quite well to the inner code using the principles of irregular codes [TH02, Tüc04] by making use of EXIT charts [tB01c]. Irregular codes, originally proposed for convolutional codes, use several component codes of different rates in one block (e.g., by changing the puncturing rule) to obtain a "good" outer code. The concept of irregular codes is based on the fact that the EXIT characteristic of the resulting code corresponds to the weighted sum of the component codes' characteristics (where the weights correspond to the fractions of code bits being encoded by the corresponding component code). An optimization algorithm that searches for optimum weights in order to get an (almost) perfectly matching characteristic can be formulated [TH02]. With this concept, capacity achieving codes can easily be found. Furthermore, it easily becomes possible to adapt the code and the rates to changing transmission parameters. This is essentially important in flexible source and channel coders that can adapt on the fly to varying channel and network conditions.

The concept of irregularity can be successfully applied to the ISCD system [SVCS08][5] by modifying the (redundant) bit mapping to get so-called *Irregular Bit Mappings* (IBMs). A similar approach for ISCD with *Variable Length Codes* (VLCs) has been introduced in [MWN+07, MWN+08]. These irregular bit mappings extend the concept of redundant bit mappings [AVC05, CAV06, CVA06b, KGM06, PYH07]. As already mentioned, redundant bit mappings with a minimum Hamming distance $d_{\min} \geq 2$ are necessary for guaranteeing good convergence properties and interleaver gains for the ISCD system [KGM06]. IBMs are an extension of the concept of irregular codes. As stated in Section 3.1.2, the bit mapping for the index $i_{t,k}$ comprises a *Parameter Individual Block Code* (PIBC) of rate $r_{\mathrm{BM},k} = B^{[\mathrm{NB}]}/B_k$. Instead of using the same amount of bits B_k for each parameter to achieve an overall r_{BM} outer encoding, we use the concept of irregular codes and vary B_k for each parameter, while keeping the overall rate r_{BM} constant. This allows the optimization of the bit mappings and to get an SDSD EXIT characteristic that matches the channel decoder's characteristic considerably well. The concept of irregularity can also be employed for optimizing the signal space mappings $\mathcal{M}$ in *Orthogonal Frequency Division Multiplexing* (OFDM) systems, e.g., [LSV08, LESV09].

[5] In [SVCS08], irregular bit mappings were denoted as *irregular index assignments*.

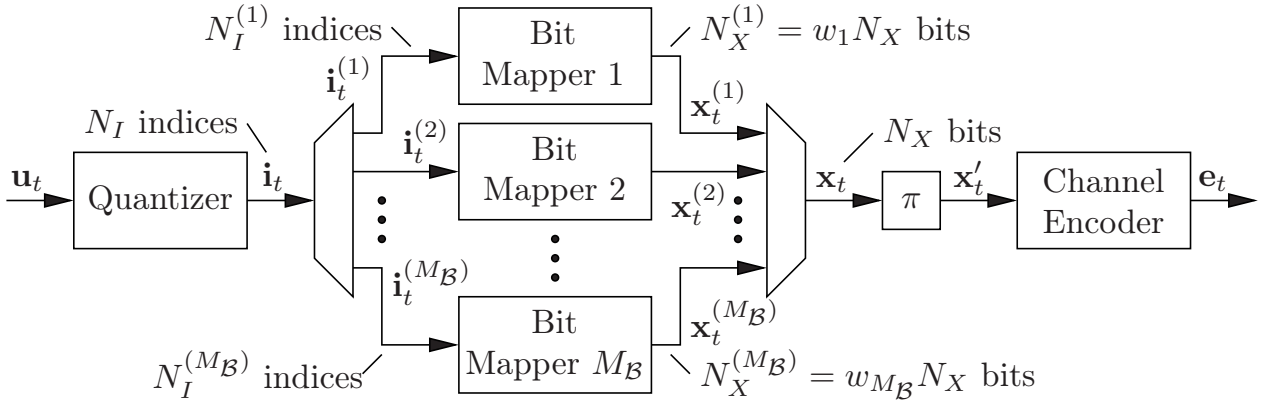

Figure 3.16: Baseband model for the transmitter of a scheme with irregular bit mappings.

The baseband block diagram of the ISCD transmitter with irregular bit mappings is given in Fig. 3.16. Instead of utilizing the same bit mapping for all indices within a frame, it is assumed that the redundant bit mappings $\mathcal{B}_k$ can be chosen from a set of $M_\mathcal{B}$ different bit mappings, i.e., $\mathcal{B}_k \in \{\mathcal{B}^{(1)}, \ldots, \mathcal{B}^{(M_\mathcal{B})}\}$. In order to perform irregular bit mapping, the vector $\mathbf{i}_t$, containing N_I quantizer indices, is split into $M_\mathcal{B}$ different sub-vectors $\mathbf{i}^{(j)}$, $j \in \{1, \ldots, M_\mathcal{B}\}$, having $N_I^{(j)}$ entries each, with $\mathbf{i}_t = (\mathbf{i}_t^{(1)}, \mathbf{i}_t^{(2)}, \ldots, \mathbf{i}_t^{(M_\mathcal{B})})$. Each sub-vector $\mathbf{i}_t^{(j)}$ is encoded using the redundant bit mapping $\mathcal{B}^{(j)}$ of rate $r_{\mathrm{BM}}^{(j)}$. Note that the rate of the $M_\mathcal{B}$ bit mappings can be different from bit mapping to bit mapping. Each bit mapping generates a bit vector $\mathbf{x}_t^{(j)}$ of $N_X^{(j)} = N_I^{(j)} B^{[\mathrm{NB}]} / r_{\mathrm{BM}}^{(j)}$ bits. The bit vector $\mathbf{x}_t$ of size N_X is obtained by concatenating all $\mathbf{x}_t^{(j)}$, i.e., $\mathbf{x}_t = (\mathbf{x}_t^{(1)}, \mathbf{x}_t^{(2)}, \ldots, \mathbf{x}_t^{(M_\mathcal{B})})$. We furthermore define that each bit mapping $\mathcal{B}^{(j)}$ generates a fraction $w_j N_X = N_X^{(j)}$ of the total number of output bits. The goal of the irregular bit mapping optimization is the selection of $N_I^{(j)}$ such that the reconstruction quality (e.g., in terms of parameter SNR) is maximized.

In the following, the optimization problem originally introduced by Tüchler [TH02, Tüc04] is applied to the irregular bit mapping. The EXIT characteristic of a specific bit mapping $\mathcal{B}^{(j)}$ shall be denoted by $\mathsf{C}_{\mathrm{SD}}^{(j)}$. The characteristic $\mathsf{C}_{\mathrm{SD}}^{(j)}$ is measured using Ξ sample points which are stored in the column vector $\mathbf{c}_{\mathrm{SD}}^{(j)}$. The matrix $\mathbf{C}_{\mathrm{SD}} \doteq \left(\mathbf{c}_{\mathrm{SD}}^{(1)} \cdots \mathbf{c}_{\mathrm{SD}}^{(M_\mathcal{B})}\right)$, with $\dim \mathbf{C}_{\mathrm{SD}} = \Xi \times M_\mathcal{B}$, contains all the $M_\mathcal{B}$ different SDSD characteristics. The column vector $\mathbf{c}_{\mathrm{CD,inv}}$ contains Ξ sample points of the inverse channel decoder characteristic $\mathsf{C}_{\mathrm{CD}}^{-1}$, measured at the channel quality for which the system is optimized. This channel quality usually is set to be slightly above the channel quality where successful decoding is still possible for the given rate constraints (Shannon limit), such that the optimized system is capacity-achieving due to the narrow decoding tunnel (see area properties in Secs. 2.3 and 3.1.6). The goal of the optimization is the determination of a weight vector $\mathbf{w} = (w_1, w_2, \ldots, w_{M_\mathcal{B}})^T$. The different characteristics $\mathsf{C}_{\mathrm{SD}}^{(j)}$ are multiplied by the weights w_j and then summed up. The resulting characteristic $\mathsf{C}_{\mathrm{SD,irr}}$ is the superposition of the weighted characteristics, i.e., $\mathsf{C}_{\mathrm{SD,irr}} = \sum_{j=1}^{M_\mathcal{B}} w_j \mathsf{C}_{\mathrm{SD}}^{(j)}$ or equivalently $\mathbf{c}_{\mathrm{SD,irr}} = \mathbf{C}_{\mathrm{SD}} \cdot \mathbf{w}$. The weighting factors need to fulfill the constraints $\sum_{j=1}^{M_\mathcal{B}} w_j = 1$ and $0 \leq w_j \leq 1$, $\forall j \in \{1, \ldots, M_\mathcal{B}\}$.

The $M_{\mathcal{B}}$ distinct rates are grouped in a vector $\mathbf{r}_{\mathrm{BM}} = (r_{\mathrm{BM}}^{(1)}, \ldots, r_{\mathrm{BM}}^{(M_{\mathcal{B}})})^T$, with $r_{\mathrm{BM}}^{(j)}$ denoting the rate of the bit mapping $\mathcal{B}^{(j)}$, $j \in \{1, \ldots, M_{\mathcal{B}}\}$. The overall target rate of the bit mapping is denoted by $r_{\mathrm{BM}}^{[\mathrm{target}]}$. The overall rate of the bit mapping corresponds to the weighted rates of the different $\mathcal{B}^{(j)}$. Therefore $\sum_{j=1}^{M_{\mathcal{B}}} w_j r_{\mathrm{BM}}^{(j)} = r_{\mathrm{BM}}^{[\mathrm{target}]}$ has to be fulfilled. Finally, the optimized characteristic $\mathsf{C}_{\mathrm{SD,irr}}$ shall not intersect the inverse characteristic of the channel decoder and an open decoding tunnel has to be present, i.e., $\mathbf{C}_{\mathrm{SD}} \cdot \mathbf{w} > \mathbf{c}_{\mathrm{CD,inv}}$.

Finding the optimized bit mapping according to [TH02, Tüc04] results in the least squares optimization [SVCS08]

$$\mathbf{w}_{\mathrm{opt}} = \arg\min_{\mathbf{w}} \left\| \mathbf{C}_{\mathrm{SD}} \cdot \mathbf{w} - \mathbf{c}_{\mathrm{CD,inv}} \right\|_2 \tag{3.32}$$

subject to

$$\mathbf{C}_{\mathrm{SD}} \cdot \mathbf{w} > \mathbf{c}_{\mathrm{CD,inv}} + \mathbf{o}\,, \tag{3.33}$$

$$\begin{pmatrix} \mathbf{r}_{\mathrm{BM}}^T \\ \mathbf{1}_{1\times M_{\mathcal{B}}} \end{pmatrix} \cdot \mathbf{w} = \begin{pmatrix} r_{\mathrm{BM}}^{[\mathrm{target}]} \\ 1 \end{pmatrix}, \tag{3.34}$$

$$0 \le w_j \le 1, \qquad \forall j \in \{1, \ldots, M_{\mathcal{B}}\}\,, \tag{3.35}$$

with $\mathbf{1}_{1\times M_{\mathcal{B}}}$ denoting the row vector containing $M_{\mathcal{B}}$ "1"s and $\mathbf{o}$ denoting an offset vector controlling the width of the decoding tunnel. The operator ">" in (3.33) denotes the element-wise comparison, i.e., all elements of the left-hand-side vector have to be larger than the corresponding elements in the right-hand-side vector. The operator $\|\cdot\|_2$ builds the Euclidean norm [GMW91]. The number of iterations and thus the decoding complexity can be controlled by adjusting $\mathbf{o}$. The optimization problem (3.32) can be solved using numerical algorithms (e.g., [GMW81, TH02]). A detailed description of the solution to a similar problem is given in Sec. 3.4.1.

The optimization yields $\mathbf{w}_{\mathrm{opt}}$, which contains the weighting factors of the different EXIT characteristics. The vector $\mathbf{w}_{\mathrm{opt}}$ also determines the fraction of bits $w_j N_X$ that result after encoding by bit mapping $\mathcal{B}^{(j)}$, $\forall j \in \{1, \ldots, M_{\mathcal{B}}\}$. From these fractions $w_j N_X = w_j N_I \bar{B}$, the corresponding $N_I^{(j)}$ (number of quantizer indices encoded by $\mathcal{B}^{(j)}$) can be determined by [SVCS08]

$$N_I^{(j)} = \mathrm{rnd}\left[w_j N_I \bar{B} \frac{r_{\mathrm{BM}}^{(j)}}{B^{[\mathrm{NB}]}} \right] = \mathrm{rnd}\left[w_j N_I \frac{r_{\mathrm{BM}}^{(j)}}{r_{\mathrm{BM}}^{[\mathrm{target}]}} \right] \qquad \forall j \in \{1, \ldots, M_{\mathcal{B}}\}\,, \tag{3.36}$$

with "rnd" being an appropriate rounding operation ensuring $\sum_{j=1}^{M_{\mathcal{B}}} N_I^{(j)} = N_I$.

3.3.1 Simulation Example

The capabilities of irregular bit mappings shall be demonstrated by a simulation example. We use the same source and quantization settings as in Section 3.1.4. The repetition coded bit mapping [CSVA08a, CSVA08b] utilized in the example in Section 3.1.4 allows near-capacity decoding capabilities for the given setup. However, if

different setup parameters like correlation coefficients ρ and δ, or the overall coding rate r_{BM} are modified, the repetition coded bit mapping might not be an optimal selection anymore. For instance, if the coding rate is decreased from $r_{\mathrm{BM}} = \frac{1}{2}$ to $r_{\mathrm{BM}} = \frac{1}{3}$ while maintaining $r_{\mathrm{CC}} = 1$, the repetition coded bit mapping generator matrix becomes $\mathbf{G}_k^{[\mathrm{BM}]} = (\mathbf{I}_4\ \mathbf{I}_4\ \mathbf{I}_4)$, $\forall k \in \{1, \ldots, N_I\}$. In this case, the EXIT characteristics C_{SD} and C_{CD} do not match as well as for $r_{\mathrm{BM}} = \frac{1}{2}$ and a performance loss is observed. One possibility to overcome this loss is to use a generator matrix $\mathbf{G}_k^{[\mathrm{BM}]}$ which results in better EXIT characteristics. A search over the EXIT characteristics of all possible systematic generator matrices results in $\binom{2^4-1+8-1}{8} = \binom{2^4+6}{8} = 319770$ possible combinations (all possible $12 - 4 = 8$ combinations with repetition out of $2^4 - 1$ non-zero column vectors, as only parity positions are considered) [BSMH05]. As the generation of 319770 EXIT characteristics consumes a considerable amount of computational power and the search space is still limited by only considering linear bit mappings, a different method has to be utilized. Besides IBMs, a *Binary Switching Algorithm* (BSA), as employed for example in [AV05], could be used. However, in that case, still a lot of computations have to be carried out and the algorithm could get stuck in a local minimum. Therefore, we show how to improve the performance by using IBMs.

In order to generate the different constituent bit mappings $\mathcal{B}^{(j)}$, a mother generator matrix $\mathbf{G}_{\mathrm{mother}}^{[\mathrm{BM}]}$ with $\dim \mathbf{G}_{\mathrm{mother}}^{[\mathrm{BM}]} = 4 \times 25$ is used to generate $M_{\mathcal{B}} = 21$ different bit mappings $\mathcal{B}^{(j)}$ of rates $r_{\mathrm{BM}}^{(j)} = 4/(4+j)$, $\forall j \in \{1, \ldots, M_{\mathcal{B}} = 21\}$. The different mappings $\mathcal{B}^{(j)}$ are generated by using the first $j + 4$ columns of $\mathbf{G}_{\mathrm{mother}}^{[\mathrm{BM}]}$. In this example we use the following systematic mother generator matrix [BV10]

$$\mathbf{G}_{\mathrm{mother}}^{[\mathrm{BM}]} = \begin{pmatrix} 1\,0\,0\,0\,1\,0\,1\,1\,1\,0\,1\,1\,1\,0\,1\,1\,1\,0\,1\,1\,1\,0\,1\,1\,1 \\ 0\,1\,0\,0\,1\,1\,0\,1\,1\,1\,0\,1\,1\,1\,0\,1\,1\,1\,0\,1\,1\,1\,0\,1\,1 \\ 0\,0\,1\,0\,1\,1\,1\,0\,1\,1\,1\,0\,1\,1\,1\,0\,1\,1\,1\,0\,1\,1\,1\,0\,1 \\ 0\,0\,0\,1\,1\,1\,1\,1\,0\,1\,1\,1\,0\,1\,1\,1\,0\,1\,1\,1\,0\,1\,1\,1\,0 \end{pmatrix}. \tag{3.37}$$

The fifth column of $\mathbf{G}_{\mathrm{mother}}^{[\mathrm{BM}]}$ ensures that for $B_k = B + 1$, a minimum Hamming distance $d_{\min} = 2$ is guaranteed according to the guidelines of [CAV06, CVA06b, KGM06, PYH07]. The subsequent columns ensure a higher Hamming distance $d_{\min}$ for $j > 2$.

Example: The quantizer index $i = 11$ shall be encoded by the bit mapping $\mathcal{B}^{(3)}$ of rate $r_{\mathrm{BM}}^{(3)} = \frac{4}{4+3} = \frac{4}{7}$, generated using $\mathbf{G}_{\mathrm{mother}}^{[\mathrm{BM}]}$. The generator matrix $\mathbf{G}^{[\mathrm{BM}](3)}$ is obtained by using the first $3 + 4 = 7$ columns of $\mathbf{G}_{\mathrm{mother}}^{[\mathrm{BM}]}$, i.e.,

$$\mathbf{G}^{[\mathrm{BM}](3)} = \begin{pmatrix} 1\,0\,0\,0\,1\,0\,1 \\ 0\,1\,0\,0\,1\,1\,0 \\ 0\,0\,1\,0\,1\,1\,1 \\ 0\,0\,0\,1\,1\,1\,1 \end{pmatrix}. \tag{3.38}$$

The natural binary representation of $i = 11$ (with $B^{[\mathrm{NB}]} = 4$) corresponds to $\mathbf{b}^{[\mathrm{NB}]} = (1\ 0\ 1\ 1)$, leading to $\mathbf{b} = \mathbf{b}^{[\mathrm{NB}]} \cdot \mathbf{G}^{[\mathrm{BM}](3)} = (1\ 0\ 1\ 1\ 1\ 0\ 1)$.

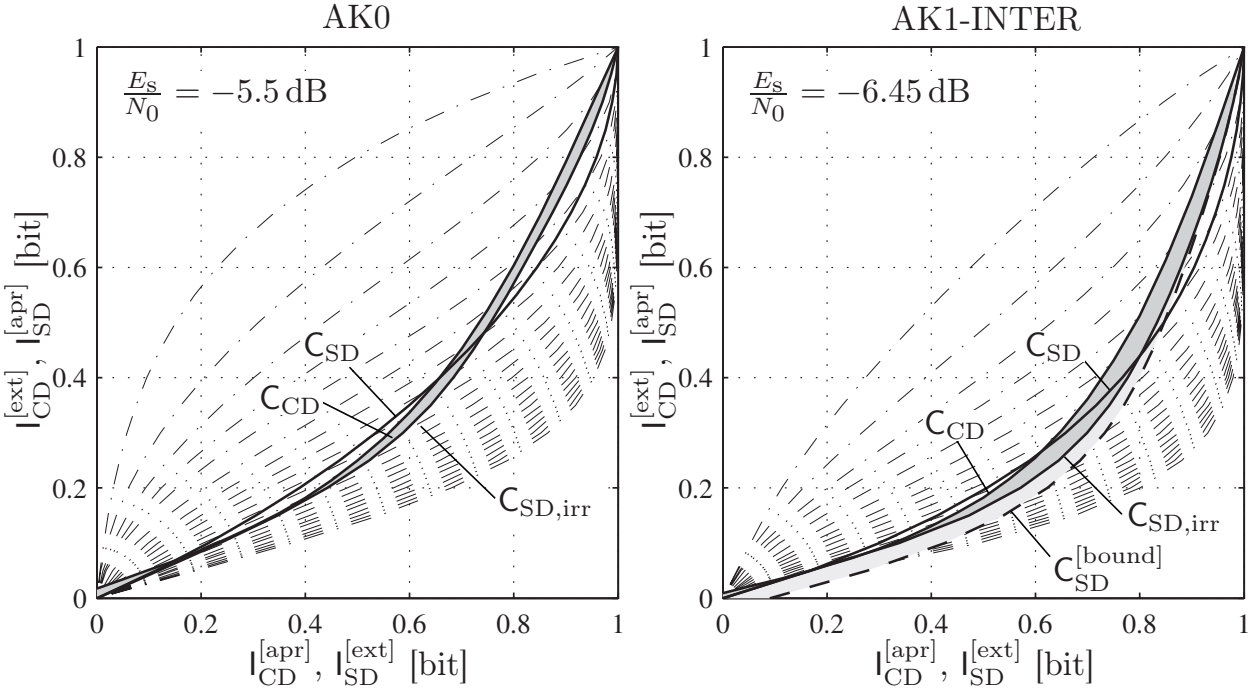

Figure 3.17: EXIT chart analysis for the simulation example using irregular bit mappings for AK0 and AK1-INTER decoding. The dash-dotted lines represent the characteristics $\mathsf{C}_{\text{SD}}^{(j)}$ of the $M_{\mathcal{B}} = 21$ different constituent bit mappings generated using $\mathbf{G}_{\text{mother}}^{[\text{BM}]}$ given by (3.37) for $Q = 16$ ($B^{[\text{NB}]} = 4$) and $\rho = 0.9$.

The characteristics $\mathsf{C}_{\text{SD}}^{(j)}$ of the different $\mathcal{B}^{(j)}$ are depicted in Fig. 3.17 for the cases of AK0 (left sub-plot) and AK1-INTER (right sub-plot) decoding. Note that the AK1-INTRA and AK1-NOPT plots show a similar behavior. The top-most characteristic is $\mathsf{C}_{\text{SD}}^{(1)}$ (for $r_{\text{BM}}^{(1)} = \frac{4}{5}$) and the bottom-most characteristic is $\mathsf{C}_{\text{SD}}^{(21)}$ (for $r_{\text{BM}}^{(21)} = \frac{4}{25}$). The channel decoder characteristics are measured at the channel quality at which the system shall be optimized, i.e., slightly above capacity. This channel quality can for instance be found by computing the source related rates r_{SC} (see Section 3.1.5) and comparing them with the channel capacity or by choosing the channel quality such that $1 - \mathcal{A}(\mathsf{C}_{\text{SD}})$ is slightly smaller than $\mathcal{A}(\mathsf{C}_{\text{CD}})$.

Setting the target rate to $r_{\text{BM}}^{[\text{target}]} = \frac{1}{3}$ and solving (3.32) leads to the irregular bit mapping with characteristic $\mathsf{C}_{\text{SD,irr}}$. The resulting numbers of indices to be encoded by a certain mapping $\mathcal{B}^{(j)}$ (found using (3.36)) are given in Table 3.2 for all four decoding algorithms for the given source settings. It can be seen in Fig. 3.17 that especially in the AK0 case, a very good matching characteristic can be found with a very narrow decoding tunnel. In the AK1-INTER case, the characteristic $\mathsf{C}_{\text{SD,irr}}$ does not match C_{CD} very well resulting in a capacity loss. This is due to the pronounced "boomerang"-like shape of C_{CD} which complicates the curve fitting, as all the constituent $\mathsf{C}_{\text{SD}}^{(j)}$ have slightly different shapes. A remedy would be either the use of a different generator matrix $\mathbf{G}_{\text{mother}}^{[\text{BM}]}$ (leading to different $\mathsf{C}_{\text{SD}}^{(j)}$), or the use of a different channel code. Furthermore, irregular inner and outer codes [MH09a, MH09b, SVCA10] could be used to jointly optimize the channel code and the bit mapping. This latter approach will be utilized in Sec. 5.1.3 to realize near-lossless source compression.

j		1	2	3	4	6	11	14	16	17	20	21
$r_{\mathrm{BM}}^{(j)}$		$\frac{4}{5}$	$\frac{4}{6}$	$\frac{4}{7}$	$\frac{4}{8}$	$\frac{4}{10}$	$\frac{4}{15}$	$\frac{4}{18}$	$\frac{4}{20}$	$\frac{4}{21}$	$\frac{4}{24}$	$\frac{4}{25}$
AK0	$N_I^{(j)}$	12		167						1		70
AK1-INTER	$N_I^{(j)}$		151		22			1				76
AK1-INTRA	$N_I^{(j)}$	15	155						1			79
AK1-NOPT	$N_I^{(j)}$	128	32			1					67	22

Table 3.2: Assignment of quantizer indices to the different mappings $\mathcal{B}^{(j)}$ for the simulation example ($Q = 16$, $B^{[\mathrm{NB}]} = 4$, $r_{\mathrm{BM}}^{[\mathrm{target}]} = \frac{1}{3}$, $\rho = 0.9$, $\delta = 0.9$, $r_{\mathrm{CC}} = 1$ convolutional code with $J = 3$ and $\mathbb{G}^{[\mathrm{CC}]} = \{\frac{10}{17}\}_8$), with $j \in \{1, \ldots, 21\}$ and $\sum_{j=1}^{M_{\mathcal{B}}} N_I^{(j)} = N_I = 250$ and $N_X = 3000$ bits after encoding. Note that only those j that are also used (i.e., those with non-zero weights w_j in at least one case) are given for clarity reasons.

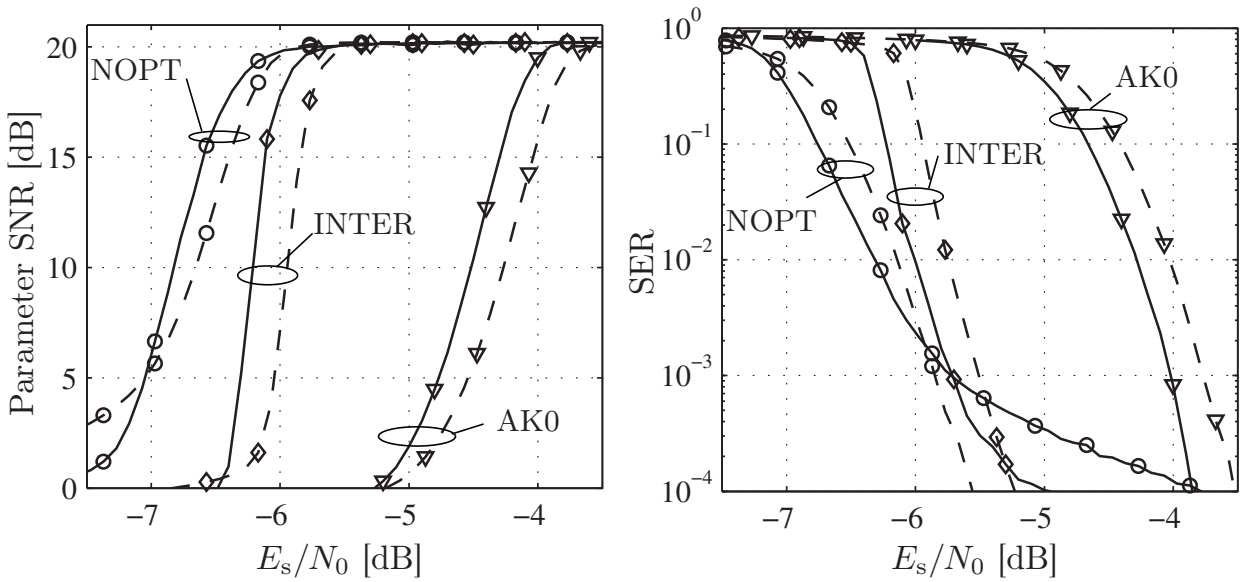

Figure 3.18: Comparison between repetition coded bit mapping (dashed lines – – –) and irregular bit mappings (solid lines ——) of Table 3.2 for $r_{\mathrm{BM}}^{[\mathrm{target}]} = \frac{1}{3}$, other settings as in Fig. 3.4, $\Omega = 25$ iterations, AK0, AK1-INTER, or AK1-NOPT decoding. MAP estimation

Figure 3.18 depicts simulation results for the irregular bit mappings given in Table 3.2 for a target rate $r_{\mathrm{BM}}^{[\mathrm{target}]} = \frac{1}{3}$. The same source and quantizer settings as in Section 3.1.4 are used. For clarity, only the results obtained with AK0, AK1-INTER, and AK1-NOPT source decoders are depicted for MAP estimation. The curves obtained with the regular repetition coded bit mappings are depicted as reference (dashed lines – – –). It can be seen that a gain of $\approx 0.2\,\mathrm{dB}$ can be achieved by using IBMs (see also EXIT charts in Fig. 3.17). However, especially for AK1-INTER and AK1-NOPT decoding, a higher error floor is observed. Thus, if low symbol error rates are a design criterion it can be advantageous to employ the regular bit

mapping despite having a worse waterfall behavior. The error floor is due to the narrow decoding tunnel and the quite small interleaver length of $N_X = 3000$ bits. For larger interleavers, the residual SER is expected to decrease [Tüc03, Tüc04]. Additional simulation examples for $r_{\mathrm{BM}}^{[\mathrm{target}]} = \frac{1}{2}$ and a different $\mathbf{G}_{\mathrm{mother}}^{[\mathrm{BM}]}$ can be found in [SVCS08, SVC08, SSV08, SACV11].

3.3.2 Unequal Error Protection on Parameter Level

It can be observed that the utilization of irregular bit mappings automatically introduces *Unequal Error Protection* (UEP) on parameter level.[6] If audio-visual signals are transmitted, UEP is often beneficial as some source codec parameters are more sensitive to errors than others. For instance, an error in a gain factor in speech and audio codecs can cause sudden large, subjectively annoying amplitude changes ("click" sounds). Transmission errors in other parameters, like the residual signal in speech codecs, cause less severe distortions. A higher symbol error rate, or a lower PSNR respectively, can be tolerated for those parameters if, in exchange, the more important parameters are better protected. The optimization of the irregular bit mapping is modified such that the UEP properties of the source can be taken into account in the proposed system.

The proposed ISCD system with irregular bit mappings inherently possesses unequal error protection capabilities. It can be observed that the indices which are assigned to the high-rate mappings have a slightly lower PSNR (or higher SER) after decoding than the indices which are assigned to the low-rate mappings. This is visualized in Fig. 3.19 where the SER after AK0 decoding has been measured for each of the $N_I = 250$ indices within a frame in the simulation example described in Section 3.3.1 at channel qualities of $E_{\mathrm{s}}/N_0 \in \{-4.6\,\mathrm{dB}, -4.5\,\mathrm{dB}, -4.2\,\mathrm{dB}\}$. The utilized irregular bit mapping is summarized in Table 3.2. The allocation of indices to bit mappings has been defined as follows: The first parameters of the block are encoded using the high-rate bit mappings and the indices towards the end of the block are encoded using the low-rate bit mappings. It can be seen that the indices which are encoded with lower rate bit mappings show a lower SER than those indices encoded with high rate bit mappings. Note that this behavior is best visible in the waterfall region. This region is quite narrow in the simulation example in Section 3.3.1, however, if fewer iterations are performed at the receiver (for instance due to complexity constraints), the waterfall region can be wider.

During system design, it is therefore advantageous to employ the low-rate bit mappings for those indices that are more sensitive to transmission errors. On the other hand the high-rate bit mappings can be utilized for those indices where decoding failures result in a minor subjective quality degradation in the reconstructed signal.

[6] Note that in channel coding, UEP also often refers to unequal error protection on bit level, which can be used for instance to allow a better protection of the *Most Significant Bits* (MSBs) of a bit pattern against transmission errors. Such a scheme can be realized for example using *Rate-Compatible Punctured Convolutional* (RCPC) codes [Hag88]. In this section, we focus however on UEP on parameter level as the design target is the estimation and reconstruction of quantizer indices, i.e., source codec parameters.

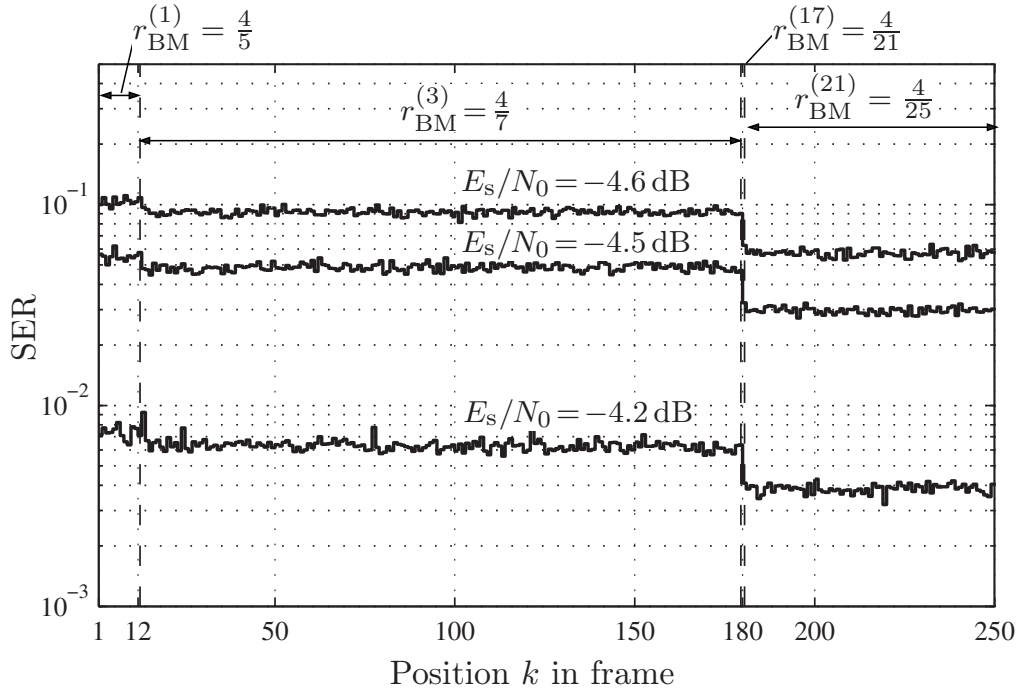

Figure 3.19: Symbol error rate of each symbol position, irregular bit mapping example of Fig. 3.18, AK0 decoding, MAP estimation, $N_I = 250$, $\Omega = 25$, $E_\mathrm{s}/N_0 \in \{-4.6\,\mathrm{dB}, -4.5\,\mathrm{dB}, -4.2\,\mathrm{dB}\}$.

If the source properties are known, the optimization of the irregular bit mappings can also be modified such that the UEP requirements of the source are incorporated into the optimization as additional constraints. Without loss of generality, we define two importance classes $\mathfrak{I}_\mathrm{low}$ and $\mathfrak{I}_\mathrm{high}$. The results given below can easily be extended to more than two importance classes. The importance class $\mathfrak{I}_\mathrm{low}$ is a set containing the indices to be encoded with the high-rate bit mappings (i.e., those indices where a higher amount of errors can be tolerated) while $\mathfrak{I}_\mathrm{high}$ contains the indices to be encoded with the low-rate bit mappings (i.e. the indices requiring stronger error protection).

For deriving the modified optimization problem, let us assume that the $M_\mathcal{B}$ different bit mappings $\mathcal{B}^{(j)}$ $\forall j \in \{1, \ldots, M_\mathcal{B}\}$ are ordered with descending corresponding rates, i.e., $r_\mathrm{BM}^{(j)} > r_\mathrm{BM}^{(j+1)}$, $\forall j \in \{1, \ldots, M_\mathcal{B} - 1\}$. Let us further define j_lim such that $r_\mathrm{BM}^{(j)} > r_\mathrm{BM}^{[\mathrm{target}]}$, $\forall j \in \{1, \ldots, j_\mathrm{lim}\}$ and $r_\mathrm{BM}^{(j)} \leq r_\mathrm{BM}^{[\mathrm{target}]}$, $\forall j \in \{j_\mathrm{lim} + 1, \ldots, M_\mathcal{B}\}$. If all the indices in $\mathfrak{I}_\mathrm{low}$ are encoded with $\mathcal{B}^{(1)}, \ldots, \mathcal{B}^{(j_\mathrm{lim})}$, we get

$$\sum_{j=1}^{j_\mathrm{lim}} N_I^{(j)} = \frac{N_I}{r_\mathrm{BM}^{[\mathrm{target}]}} \sum_{j=1}^{j_\mathrm{lim}} w_j r_\mathrm{BM}^{(j)} \stackrel{!}{=} |\mathfrak{I}_\mathrm{low}| \tag{3.39}$$

by utilizing (3.36) and neglecting the rnd operation. $|\mathfrak{I}_\mathrm{low}|$ denotes the cardinality of $\mathfrak{I}_\mathrm{low}$. Similarly, we can write

$$\sum_{j=j_\mathrm{lim}+1}^{M_\mathcal{B}} N_I^{(j)} = \frac{N_I}{r_\mathrm{BM}^{[\mathrm{target}]}} \sum_{j=j_\mathrm{lim}+1}^{M_\mathcal{B}} w_j r_\mathrm{BM}^{(j)} \stackrel{!}{=} |\mathfrak{I}_\mathrm{high}|\,. \tag{3.40}$$

The constraints (3.39) and (3.40) can be loosened for the given setup. Not exactly $|\mathfrak{I}_{\text{high}}|$ indices need to be encoded with the low-rate mappings, it only has to be assured that at least $|\mathfrak{I}_{\text{high}}|$ indices are well protected. This then leads to the least squares optimization of the redundant bit mappings incorporating specific UEP, which can be written as

$$\mathbf{w}_{\text{opt}} = \arg\min_{\mathbf{w}} \left\| \mathbf{C}_{\text{SD}} \cdot \mathbf{w} - \mathbf{c}_{\text{CD,inv}} \right\|_2 \tag{3.41}$$

subject to

$$\mathbf{C}_{\text{SD}} \cdot \mathbf{w} > \mathbf{c}_{\text{CD,inv}} + \mathbf{o}\,, \tag{3.42}$$

$$\begin{pmatrix} \mathbf{r}_{\text{BM}}^T \\ \mathbf{1}_{1\times M_{\mathcal{B}}} \end{pmatrix} \cdot \mathbf{w} = \begin{pmatrix} r_{\text{BM}}^{[\text{target}]} \\ 1 \end{pmatrix}, \tag{3.43}$$

$$0 \le w_j \le 1, \qquad \forall j \in \{1, \ldots, M_{\mathcal{B}}\} \tag{3.44}$$

$$\sum_{j=j_{\text{lim}}+1}^{M_{\mathcal{B}}} w_j r_{\text{BM}}^{(j)} \ge r_{\text{BM}}^{[\text{target}]} \frac{|\mathfrak{I}_{\text{high}}|}{N_I}\,. \tag{3.45}$$

Note that (3.41) with the constraints (3.42)-(3.45) reduces to the case without UEP (given by (3.32)-(3.35)) if $|\mathfrak{I}_{\text{high}}| = 0$ (general case). Prior to the optimization it has to be assured that $|\mathfrak{I}_{\text{high}}|$ is well chosen, such that the solution space is not empty. In the extreme case, i.e., $|\mathfrak{I}_{\text{high}}| = N_I$, two possibilities exist: First, if any of the $M_{\mathcal{B}}$ mappings is of rate $r_{\text{BM}}^{[\text{target}]}$, the optimization leads to a regular bit mapping; second, if none of the $M_{\mathcal{B}}$ mappings is of rate $r_{\text{BM}}^{[\text{target}]}$, no valid solution to (3.41)-(3.45) exists. Finally note that if N_I is unknown during the optimization (i.e. the general case is considered) the constraint (3.45) can also be formulated such that certain fractions of parameters fall into either importance class (i.e., the fraction $|\mathfrak{I}_{\text{high}}|/N_I$ is specified), as given in [SSV08].

3.4 Error Floor Reduction

The simulation example in Fig. 3.4 shows a considerably high error floor in terms of *Symbol Error Rate* (SER). This error floor is due to the properties of the (serially concatenated) ISCD transmitter: It is mainly characterized by the interleaver size N_X and the *Input Output Weight Enumerating Function* (IOWEF) (and thus also the Hamming distance) of the outer component code [BDMP98b]. In what follows, two different approaches for optimizing the Hamming distance of the outer component code are presented.

3.4.1 Distance Optimized Bit Mapping

One method to increase the distance is to utilize a different outer code with better distance properties (as the repetition code only exhibits $d_{\min} = 2$). For the given

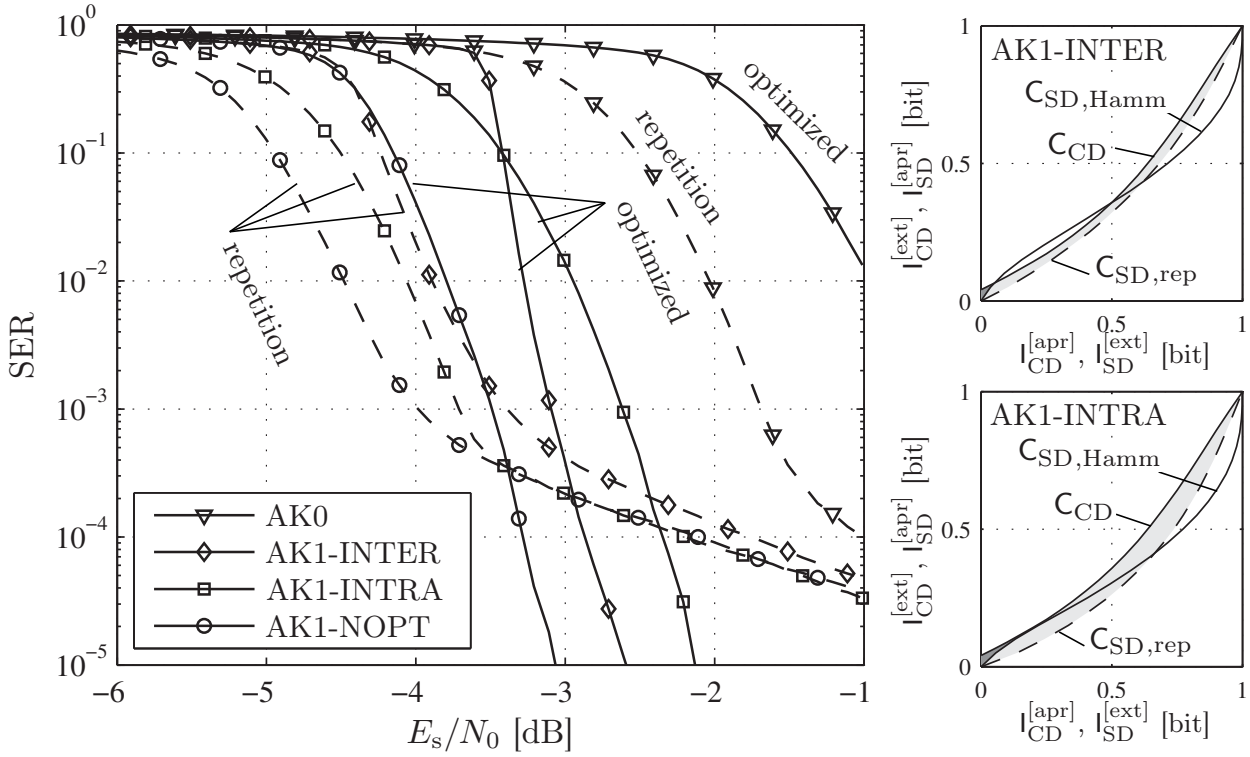

Figure 3.20: Comparison of the effect of different block code based redundant bit mappings with different source decoders in ISCD with $\rho = 0.9$, $\delta = 0.9$, LMQ scalar quantization, $N_I = 250$, $r_{\mathrm{BM}} = \frac{1}{2}$ repetition bit mapping, 8-state conv. code ($\mathbb{G}^{[\mathrm{CC}]} = \{\frac{10}{17}\}_8$), $\Omega = 25$, EXIT charts at $E_s/N_0 = -4\,\mathrm{dB}$.
dashed (– – –): repetition code solid (——): Hamming dist. optimized

setup $B^{[\mathrm{NB}]} = 4$, $r_{\mathrm{BM}} = \frac{1}{2}$, i.e., $B_k = 8$, there exists only a single linear block code of maximum Hamming distance $d_{\min} = 4$ with generator matrix $\mathbf{G}_k^{[\mathrm{BM}]} = (\mathbf{I}_4 \;\; \mathbf{1}_{4\times4} - \mathbf{I}_4)$ with $\mathbf{1}_{4\times4}$ denoting the 4×4 all-1 matrix [MN77, Bro98]. This matrix has been used in [SSV08] due to its special structure as encoding is possible using a simple circuit. A similar matrix (with several systematic repetitions) has also been used in [NH09b].

Figure 3.20 shows the comparison between both mappings. By increasing the distance by a factor of 2, the error floor is significantly lowered (no error floor is visible in the most interesting range of SER $> 10^{-5}$). However, the waterfall has been shifted by 0.7 - 1 dB towards higher values of E_s/N_0. This can be explained by the EXIT charts also depicted on the right-hand side of Fig. 3.20 (for the AK1-INTER and AK1-INTRA cases). While the characteristic of the repetition code $\mathsf{C}_{\mathrm{SD,rep}}$ and the channel decoder characteristic C_{CD} have well matching shapes, the Hamming distance optimized code exhibits a characteristic $\mathsf{C}_{\mathrm{SD,Hamm}}$ with a distinct curvature.

One way to overcome this problem is to search for a different rate $r_{\mathrm{CC}} = 1$ inner recursive convolutional code. The concept of IBMs cannot be applied as its usage would imply a lower $d_{\min}$. In fact, as higher rate bit mappings have to be used in IBMs together with lower rate bit mappings, these higher rate bit mappings naturally have a lower $d_{\min}$ (for the present example), and therefore lower the effective distance. If $d_{\min} = 4$ of the optimized BM should be retained, a different inner code has to

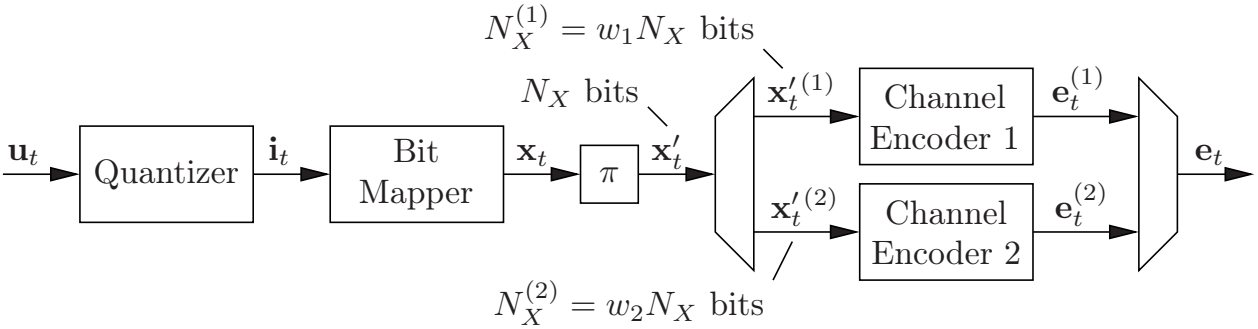

Figure 3.21: Baseband model for the transmitter with an irregular channel code.

be used. An elegant way to design a very well matching inner code is to apply the concept of irregular codes [TH02, Tüc04] to the inner code [Tho07c, TSV08, MH09a, MH09b, SV10a] as well.

The irregular inner codes presented in [Tho07c, TSV08] are based on *Randomly Punctured Recursive Systematic Convolutional* (RPRSC) codes. In this example, we show the optimization using more simple non-punctured codes. The codes shall also be selected such that the overall decoding complexity of the channel decoder is reduced. Maunder *et al.* also employ non-punctured rate $r_{\mathrm{CC}} = 1$ codes in [MH09a, MH09b]. Due to the curved shape of the SDSD EXIT characteristic, it can be challenging to find well matching rate-1 recursive convolutional codes. Note again that the inner code should be of rate-1 [AKtB04] and recursive [KHC06] for capacity achieving ISCD systems.

In order to demonstrate that a system with irregular codes does not need to be complex, we show a very simple system employing an inner irregular code consisting of $M_{\mathcal{E}} = 2$ convolutional codes. This encoder is depicted in the baseband model of Fig. 3.21. The interleaved bit vector $\mathbf{x}'_t$ is partitioned into $\mathbf{x}'^{(1)}_t$ and $\mathbf{x}'^{(2)}_t$ according to $\mathbf{x}'_t = (\mathbf{x}'^{(1)}_t, \mathbf{x}'^{(2)}_t)$. The irregular inner encoder then encodes the sub-vector $\mathbf{x}'^{(1)}_t$ consisting of $N_X^{(1)} \doteq w_1 N_X$ bits with the first code and the sub-vector $\mathbf{x}'^{(2)}_t$ consisting of $N_X^{(2)} \doteq w_2 N_X$ bits with the second code. The goal of the inner code optimization is to find a weight vector $\mathbf{w} = (w_1, w_2)^T$. In this example, the first convolutional code is a rate $r_{\mathrm{CC}} = 1$ RNSC code with memory $J = 2$ and octal generator $\mathbb{G}^{[\mathrm{CC}]} = \{\frac{7}{6}\}_8$, while the second RNSC code of rate $r_{\mathrm{CC}} = 1$ has $J = 1$ and $\mathbb{G}^{[\mathrm{CC}]} = \{\frac{2}{3}\}_8$ (accumulator). Both codes can be represented by a trellis diagram with either 4 or 2 states, respectively. This means that the (channel decoding) complexity is more than halved compared to the $J = 3$ code previously used. In the case of two component codes, the optimization problem can thus be formulated as [TH02, TSV08]

$$\mathbf{w}_{\mathrm{opt}} = \arg\min_{\mathbf{w}} \left\| \mathbf{C}_{\mathrm{CD}} \cdot \mathbf{w} - \mathbf{c}_{\mathrm{SD,inv}} \right\|_2 \tag{3.46}$$

subject to

$$\mathbf{C}_{\mathrm{CD}} \cdot \mathbf{w} > \mathbf{c}_{\mathrm{SD,inv}} + \mathbf{o}\,, \tag{3.47}$$

$$\mathbf{1}_{1\times 2} \cdot \mathbf{w} = 1, \tag{3.48}$$

$$0 \le w_j \le 1, \qquad \forall j \in \{1, \ldots, M_{\mathcal{E}} = 2\}\,. \tag{3.49}$$

SDSD Algorithm	Optimization E_s/N_0	w_1	w_2
AK0	$-2.75\,\mathrm{dB}$	0.386	0.614
AK1-INTER	$-4.2\,\mathrm{dB}$	0.574	0.426
AK1-INTRA	$-4.9\,\mathrm{dB}$	0.489	0.511
AK1-NOPT	$-5.2\,\mathrm{dB}$	0.838	0.162

Table 3.3: Optimum weights $\mathbf{w}_{\mathrm{opt}}$ for the inner irregular code with $M_{\mathcal{E}} = 2$ codes with $\mathbb{G}_1^{[\mathrm{CC}]} = \{\frac{7}{6}\}_8$ and $\mathbb{G}_2^{[\mathrm{CC}]} = \{\frac{2}{3}\}_8$ for four different SDSD algorithms ($\rho = 0.9$, $\delta = 0.9$).

The matrix $\mathbf{C}_{\mathrm{CD}}$ contains Ξ sample points of both channel decoder characteristics and $\mathbf{c}_{\mathrm{SD,inv}}$ contains Ξ sample points of the inverse SDSD characteristic $\mathsf{C}_{\mathrm{SD}}^{-1}$. The offset vector $\mathbf{o}$ can control the width of the decoding tunnel. Constraint (3.47) ensures an open decoding tunnel while constraints (3.48) and (3.49) guarantee the validity of the weights $\mathbf{w} = (w_1 \; w_2)^T$. As all component codes are of identical rate, no additional rate constraint needs to be considered. For a detailed description of irregular inner codes, the reader is referred to Section 5.1.2 and to [TSV08].

The optimization yields optimum weights $\mathbf{w}_{\mathrm{opt}}$ which are summarized in Table 3.3 for the four distinct SDSD algorithms. Note that the optimization is performed at different channel qualities, depending on the algorithm used. Figure 3.22 depicts the simulation results. Significant gains are observed compared to the regular $J = 3$ code. Although the waterfall region starts at slightly higher channel qualities than for the repetition coded bit mapping [CSVA08a], the error floor is significantly reduced. Furthermore, the algorithmic complexity of the channel decoder is also reduced, due to the smaller number of trellis states. Depending on the target SER, the proposed system can outperform the example system presented in Section 3.1.4 (for SER $\lessapprox 10^{-3}$).

The considered inner irregular code is also used in the *FlexCode* channel coder to protect the transform coefficients. As the bit assignment of the transform coefficients can change from frame to frame, resulting in a different SDSD EXIT characteristic, the channel code has to be set up on a frame-by-frame basis. For this reason, the simple inner irregular code presented in this example is best suited for this application. In what follows, the optimization is shown in detail. The optimum vector $\mathbf{w}'$ fulfilling constraint (3.48) is found by [TH02]

$$\mathbf{w}' = \mathbf{w}_0 - \left(\mathbf{C}_{\mathrm{CD}}^T \mathbf{C}_{\mathrm{CD}}\right)^{-1} \mathbf{1}_{2\times 1} \left(\mathbf{1}_{1\times 2} \left(\mathbf{C}_{\mathrm{CD}}^T \mathbf{C}_{\mathrm{CD}}\right)^{-1} \mathbf{1}_{2\times 1}\right)^{-1} (\mathbf{1}_{1\times 2}\mathbf{w}_0 - 1) \quad (3.50)$$

with

$$\mathbf{w}_0 = \left(\mathbf{C}_{\mathrm{CD}}^T \mathbf{C}_{\mathrm{CD}}\right)^{-1} \mathbf{C}_{\mathrm{CD}}^T \mathbf{c}_{\mathrm{SD,inv}} \quad (3.51)$$

denoting the optimum solution of the unconstrained problem (3.46). Note that only matrices of maximum size 2×2 need to be inverted in (3.50) and (3.51) thus leading to a very low computation complexity of the optimization. Further note that no offset vector $\mathbf{o}$ is used in the *FlexCode* setup, as a worse channel quality than actually present is assumed for the optimization. In this case, the least squares optimization

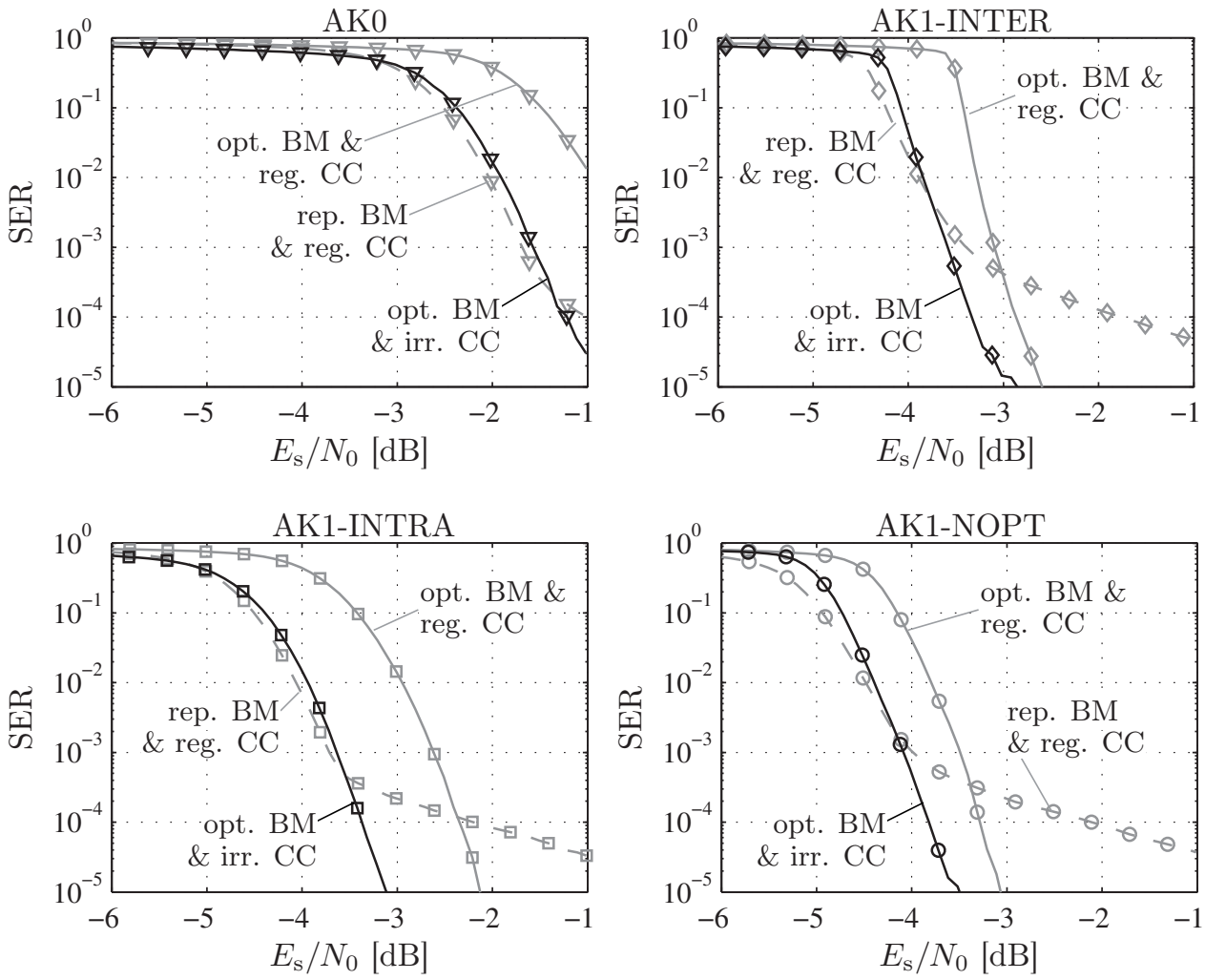

Figure 3.22: Comparison of a regular channel code ($J = 3$ and $\mathbb{G}^{[\mathrm{CC}]} = \{\frac{10}{17}\}_8$) and an irregular code built from $M_{\mathcal{E}} = 2$ convolutional codes, $\Omega = 25$, MAP estimation, other simulation settings as in Figs. 3.4 and 3.20.
dashed gray (– – –): repetition code and regular channel code
solid gray (——): Hamming distance optimized, regular code
solid black (——): Hamming distance optimized, irregular code.

ensures that there is always an equally wide decoding tunnel if the actual channel quality is considered.

Using $\mathbf{w}'$, which only fulfills the constraint (3.48), the optimum solution can be found by a steepest descent approach [GMW81, GMW91] by exploiting the fact that $\frac{\partial}{\partial \mathbf{w}} \|\mathbf{C}_{\mathrm{CD}}\mathbf{w} - \mathbf{c}_{\mathrm{SD,inv}}\|_2 = 2(\mathbf{C}_{\mathrm{CD}}\mathbf{w} - \mathbf{c}_{\mathrm{SD,inv}})$ [TH02]. The steepest descent approach is an iterative algorithm, where in each iteration the gradient (multiplied with a small enough step size) is subtracted from $\mathbf{w}'$. In the present case, the gradient $\frac{\partial}{\partial \mathbf{w}} \|\mathbf{C}_{\mathrm{CD}}\mathbf{w} - \mathbf{c}_{\mathrm{SD,inv}}\|_2$ as well as the gradients corresponding to the (convex) constraint (3.49) need to be considered. The resulting weights are subsequently used as $\mathbf{w}_0$ in (3.50) to compute a new $\mathbf{w}'$ for the next iteration. The optimum vector $\mathbf{w}_{\mathrm{opt}}$ is either obtained after a fixed number of iterations or if the frame-to-frame variation of $\|\mathbf{C}_{\mathrm{CD}}\mathbf{w} - \mathbf{c}_{\mathrm{SD,inv}}\|_2$ is sufficiently small. A faster converging algorithm can be found

in, e.g., [TH02], however, it has been found that the steepest descent approach is sufficiently fast in the *FlexCode* case.

3.4.2 Multi-Dimensional Bit Mappings

Increasing the Hamming distance of the redundant bit mapping is not always possible, especially if the amount of quantization levels Q is small. The Hamming distance of the bit mapping is upper bounded by the Singleton bound with $d_{\min} \leq B_k - \operatorname{ld} Q + 1$ (see, e.g., [Rot06]). If $\operatorname{ld} Q = B^{[\mathrm{NB}]}$, then the Singleton bound can also be expressed as $d_{\min} \leq B_k - B^{[\mathrm{NB}]} + 1 = 1 + B^{[\mathrm{NB}]}(\frac{1}{r_{\mathrm{BM},k}} - 1)$. For example, if $Q = 4$ (i.e., $B^{[\mathrm{NB}]} = 2$) and $r_{\mathrm{BM}} = 1/2$, $d_{\min}$ is bounded by $d_{\min} \leq 3$. However, linear block codes over $\mathbb{F}_2$ of size 2×4 only achieve $d_{\min} \leq 2$ (which can be confirmed by a full search over all linear codes).

In order to achieve higher distances $d_{\min}$ without modifying the rate $r_{\mathrm{BM},k}$ and Q, a different approach has to be considered. Following the Singleton bound with constant $r_{\mathrm{BM},k}$, increasing $d_{\min}$ results in larger codes. Unfortunately, the size of the code is limited by Q. In order to be able to utilize larger codes, *Multi-Dimensional Bit Mappings* (MDBMs), which group several quantizer indices to one *super index* and utilize a larger code as redundant bit mapping, can be used. This larger code allows a larger Hamming distance $d_{\min}$ and thus results in a lower error floor.

This approach is similar to the concept of *Multi-Dimensional Mappings* (MDMs), originally considered for trellis-coded modulation [FGL+84, Wei87, PDL+90] and later applied to *Bit Interleaved Coded Modulation with Iterative Decoding* (BICM-ID) [TN04, SWM04, SWBM05, SWM05, GBB05] and modulation for fading channels [CD09, WKM10]. A multi-dimensional code has also been successfully used in [CAV06, CVA06a, CVA06b, Cle06, ACS08] as an inner component of *Iterative Source-Coded Modulation* (ISCM) and *Turbo DeCodulation* (TDeC) systems.

The application of MDBMs is straightforward at the transmitter side: Ψ consecutive quantizer indices $i_{t,k}, \ldots, i_{t,k+\Psi-1}$ are grouped to a super index $i^{\star}_{t,k'}$, $k' = \lceil k/\Psi \rceil$ with

$$i^{\star}_{t,k'} = 1 + \sum_{j=1}^{\Psi} \left(i_{t,(k'-1)\Psi+j} - 1 \right) Q^{\Psi-j} \tag{3.52}$$

and $i^{\star}_{t,k'} \in \mathbb{I}^{\star} \doteq \{1, \ldots, Q^{\Psi}\}$. A frame then contains a total number of $N_I^{\star} \doteq \lceil N_I/\Psi \rceil$ super indices. To the super index $i^{\star}_{t,k'}$, the natural binary representation $\mathbf{b}^{[\mathrm{NB}]\star}_{t,k'}$ consisting of $B^{[\mathrm{NB}]\star} \doteq \Psi \cdot B^{[\mathrm{NB}]}$ bits is assigned, followed by the (possibly) redundant bit mapping. After bit mapping, $N_I^{\star}$ super bit patterns $\mathbf{b}^{\star}_{t,k'}$, $k' \in \{1, \ldots, N_I^{\star}\}$ of $B^{\star}_{k'}$ bits result. As in the one-dimensional case, $\mathbf{b}^{\star}_{t,k'} \in \mathbb{B}^{\star}_{k'} \subseteq \mathbb{F}_2^{B^{\star}_{k'}}$, with $\mathbb{B}^{\star}_{k'} \doteq \{\bar{\mathbf{b}}^{(1)\star}_{k'}, \ldots, \bar{\mathbf{b}}^{(Q^{\Psi})\star}_{k'}\}$.

Because the rate r_{BM} of the bit mapping is constrained to a fixed value, the condition $\sum_{k=1}^{N_I} B_k = \sum_{k'=1}^{N_I^{\star}} B^{\star}_{k'}$ has to hold. If we assume, without loss of generality, that all

bit patterns are encoded with the same rate r_{BM} (regular bit mapping), then we get from the Singleton bound

$$d_{\min}^{\star} \leq 1 + B^{[\mathrm{NB}]\star}\left(\frac{1}{r_{\mathrm{BM}}} - 1\right) = 1 + \Psi \cdot B^{[\mathrm{NB}]}\left(\frac{1}{r_{\mathrm{BM}}} - 1\right) \tag{3.53}$$

resulting in (for the highest theoretically attainable minimum distances)

$$\left(d_{\min}\right)_{\max} = 1 + B^{[\mathrm{NB}]}\left(\frac{1}{r_{\mathrm{BM}}} - 1\right) \leq 1 + \Psi \cdot B^{[\mathrm{NB}]}\left(\frac{1}{r_{\mathrm{BM}}} - 1\right) = \left(d_{\min}^{\star}\right)_{\max} . \tag{3.54}$$

Thus, choosing MDBMs with dimensions $\Psi > 1$ allows to (theoretically) increase the Hamming distance of the outer component code in the serially concatenated system.

Finally note that using MDBMs together with scalar quantizers ($\Pi = 1$) can also be interpreted as using $\Pi = \Psi$ dimensional vector quantization together with (one-dimensional) bit mappings. The (separable) code book of this resulting vector quantizer is composed of the original scalar code book in each dimension. However, as it is often not possible to change the quantizer (as the source codec is given and fixed), MDBMs have to be used for achieving higher distances $d_{\min}$ of the outer code.

Receiver Modifications

In order to be able to decode MDBMs, the SDSD has to be modified accordingly. The different kinds of decoding algorithms have to be considered separately, however, the first steps are common to all four algorithms. The factors $\gamma_{t,k}(q)$ and $\gamma_{t,k}^{[\mathrm{ext}]\setminus m}(q)$ given by (F.2) and (F.4) have to be replaced by $\gamma_{t,k'}^{\star}(q^{\star})$ and $\gamma_{t,k'}^{[\mathrm{ext}]\setminus m,\star}(q^{\star})$, according to

$$\gamma_{t,k'}^{\star}(q^{\star}) \doteq \prod_{\mu=1}^{B_{k'}^{\star}} \left(1 + \exp\left(-\left(1 - 2 \cdot \bar{b}_{k',\mu}^{(q^{\star})\star}\right) \cdot \mathsf{L}_{\mathrm{CD}}^{[\mathrm{ext}]}(b_{t,k',\mu}^{\star})\right)\right)^{-1} \tag{3.55}$$

$$\gamma_{t,k'}^{[\mathrm{ext}]\setminus\chi,\star}(q^{\star}) \doteq \prod_{\substack{\mu=1 \\ \mu\neq\chi}}^{B_{k'}^{\star}} \left(1 + \exp\left(-\left(1 - 2 \cdot \bar{b}_{k',\mu}^{(q^{\star})\star}\right) \cdot \mathsf{L}_{\mathrm{CD}}^{[\mathrm{ext}]}(b_{t,k',\mu}^{\star})\right)\right)^{-1} . \tag{3.56}$$

Equation (3.55) has to be evaluated for each distinct $q^{\star} \in \{1, \ldots, Q^{\Psi}\}$. Equation (3.56) has to be evaluated for each distinct pair of $(q^{\star}, \chi)$, with $\chi \in \{1, \ldots, B_{k'}^{\star}\}$.

Unfortunately, the usage of MDBMs increases the complexity of SDSD. If $B_k = B = \text{const.}$ (regular bit mapping) and $N_I^{\star} = \lceil N_I/\Psi \rceil = N_I/\Psi$, a total number of $N_I^{\star} Q^{\Psi} (B^{\star})^2 = N_I \Psi Q^{\Psi} B^2$ multiplications are required for computing all $\gamma_{t,k}^{\star}(q^{\star})$ and $\gamma_{t,k}^{[\mathrm{ext}]\setminus\chi,\star}(q^{\star})$ of a frame. The standard SDSD only requires $N_I Q B^2$ multiplications (see App. F.3.1 for a detailed derivation of the complexity figures). This corresponds to an increase of the number of multiplications per frame by a factor of $\mathfrak{C}_{\gamma} \doteq \Psi Q^{\Psi-1}$ common to all MDBM decoders. As the complexity increase grows exponentially with Ψ, the selection of a small dimension Ψ is suggested in order to keep the receiver moderate in its complexity. In what follows, the different flavors of the MDBM-SDSD are explained in detail. The corresponding MDBM-SDSD variables are also annotated by a superscript * for a better differentiation.

AK0: If only *a priori* knowledge of order zero is exploited (i.e., no correlation), the AK0 SDSD algorithm can be utilized. In this case, the extension towards MDBM is straightforward by exploiting the fact that consecutive parameters in a frame at instant t are statistically independent

$$\mathsf{Pr}\{I^{\star}_{t,k'} = q^{\star}\} = \prod_{j=1}^{\Psi} \mathsf{Pr}\{I_{t,\Psi(k'-1)+j} = q_j\} \qquad \text{with } q^{\star} = 1 + \sum_{j=1}^{\Psi} (q_j - 1) Q^{\Psi - j} \,. \quad (3.57)$$

Because of the invertible one-to-one mapping $q^{\star} \mapsto (q_1, \ldots, q_{\Psi})$ given by (3.52), (3.57) can be evaluated and used within SDSD, which now does not operate on single index level anymore, but on super index level. The product has to be performed over all $B^{\star}_k$ bits of the super bit pattern. Accordingly, (F.6) has to be adapted by replacing the probability of occurrence of the quantizer index by (3.57) and by using $\gamma^{[\mathrm{ext}]\setminus m,\star}_{t,k}(q^{\star})$. The computation of the extrinsic information requires Q^{Ψ} *Multiply ACcumulate* (MAC) operations per bit instead of Q. This corresponds to an increase by a factor of $\mathfrak{C}^{[\mathrm{ext}]}_{\mathrm{AK0}} \doteq Q^{\Psi-1}$.

AK1-INTER: In the case of inter-frame correlation, the different indices within a frame are statistically independent. This allows to write the conditional inter-frame *a priori* probabilities of the super indices as

$$\mathsf{Pr}\{I^{\star}_{t,k'} = q^{\star} | I^{\star}_{t-1,k'} = \tilde{q}^{\star}\} = \prod_{j=1}^{\Psi} \mathsf{Pr}\{I_{t,\Psi(k'-1)+j} = q_j | I_{t-1,\Psi(k'-1)+j} = \tilde{q}_j\} \quad (3.58)$$

with $q^{\star} = 1 + \sum_{j=1}^{\Psi} (q_j - 1) Q^{\Psi - j}$ and $\tilde{q}^{\star} = 1 + \sum_{j=1}^{\Psi} (\tilde{q}_j - 1) Q^{\Psi - j}$. In this case, the SDSD complexity is also increased. The factors $A^{\star}_{t,k}(q^{\star})$ (intermediate result of the temporal forward recursion) require $Q^{2\Psi}$ MAC operations while the computation of the temporal forward recursion $\alpha^{\star}_{t,k}(q^{\star})$ requires Q^{Ψ} multiplications per super index. However, the operations only need to be carried out $N^{\star}_I$ times per frame. Thus, in the forward recursion, the number of MAC operations increases by a factor of $\frac{1}{\Psi} Q^{2(\Psi-1)}$ while the number of multiplications increases by a factor of $\frac{1}{\Psi} Q^{(\Psi-1)}$. The number of MAC operations per bit required for computing the extrinsic information increases from Q to Q^{Ψ}.

AK1-INTRA: In contrast to the AK0 and AK1-INTER cases, the different indices within a frame are not independent anymore if intra-frame correlation is exploited. In this case, the *a priori* probabilities on super index level can be expressed as

$$\mathsf{Pr}\{I^{\star}_{t,k'} = q^{\star} | I^{\star}_{t,k'-1} = \tilde{q}^{\star}\} = \quad (3.59)$$

$$\mathsf{Pr}\{I_{t,\Psi(k'-1)+1} = q_1 | I_{t,\Psi(k'-2)+\Psi} = \tilde{q}_{\Psi}\} \prod_{j=2}^{\Psi} \mathsf{Pr}\{I_{t,\Psi(k'-1)+j} = q_j | I_{t,\Psi(k'-1)+j-1} = q_{j-1}\}$$

with $q^\star = 1 + \sum_{j=1}^{\Psi}(q_j - 1)Q^{\Psi-j}$ and $\tilde{q}^\star = 1 + \sum_{j=1}^{\Psi}(\tilde{q}_j - 1)Q^{\Psi-j}$. The proof of (3.59) is given in App. C.

The complexity increase in this case is again comparable to the AK1-INTER case as the forward recursion is basically identical and there is an additional backward recursion whose complexity scales by the same factor as the complexity of the forward recursion (see AK1-INTER case). For the computation of extrinsic information, Q^Ψ multiplications (instead of Q) are necessary in addition to the Q^Ψ MACs.

AK1-NOPT: As the AK1-NOPT algorithm basically combines the temporal recursion of the AK1-INTER algorithm with the spatial forward and backward recursions of the AK1-INTRA case, the adaptation is straightforward. In the computation of $\alpha_{t,k'}^{[\mathrm{pos}]\star}(q^\star)$ and $\beta_{t,k'}^{[\mathrm{pos}]\star}(q^\star)$, the expression $\mathsf{Pr}\{I_{t,k'}^\star = q^\star | I_{t,k'-1}^\star = \tilde{q}^\star\}$ of (3.59) has to be used, while the computation of $\alpha_{t,k'}^{[\mathrm{tim}]\star}(q^\star)$ necessitates the use of $\mathsf{Pr}\{I_{t,k'}^\star = q^\star | I_{t-1,k'}^\star = \tilde{q}^\star\}$ from (3.58). The complexity scaling is again similar to the three previously presented cases.

The implication of the complexity considerations beforehand is that the computational complexity of MDBM roughly increases by $Q^{\Psi-1}$. For this reason, the dimension Ψ (with $\Psi \geq 2$) should be kept as small as possible. Already with $\Psi = 2$, a considerable decrease of the error floor due to the higher $d_{\min}$ (in the case of a well-chosen RBM) can be observed, as will be shown below by a simulation example.

Simulation Example

The capabilities of MDBMs shall be demonstrated by a simulation example. The source setup of Section 3.1.4 is used with $Q = 4$ level scalar LMQ. The overall coding rate of the bit mapping shall be $r_{\mathrm{BM}} = 1/2$. In the one-dimensional case, the number of linear block codes with Hamming distance $d_{\min} \geq 2$ is limited due to the small dimension of the generator matrix (here 2×4). For the example, we use either the repetition code (i.e., $\mathbf{G}_k^{[\mathrm{BM}]} = (\mathbf{I}_2\ \mathbf{I}_2)$, $\forall k \in \{1, \ldots, N_I\}$) or the multiple parity check code (i.e., $\mathbf{G}_k^{[\mathrm{BM}]} = (\mathbf{I}_2\ \mathbf{1}_{2\times 2})$, $\forall k \in \{1, \ldots, N_I\}$). The minimum distance of these codes is $d_{\min} = 2$. In fact, for the given settings, only generator matrices with $d_{\min} = 2$ can be found.

In order to increase the possible Hamming distance of the bit mapping, a multi-dimensional bit mapping with $\Psi = 2$ is employed. The utilized generator matrix is the same as used in Section 3.4.1, i.e., $\mathbf{G}_{k'}^{[\mathrm{BM}]} = (\mathbf{I}_4\ \ \mathbf{1}_{4\times 4} - \mathbf{I}_4)$. Again, a block consists of $N_I = 250$ quantizer indices ($N_I/\Psi = 125$ super indices). The utilized convolutional codes are the $J = 3$, $r_{\mathrm{CC}} = 1$ RNSC code with $\mathbb{G}^{[\mathrm{CC}]} = \{\frac{10}{17}\}_8$ and additionally in the MDBM case, a low-complexity $r_{\mathrm{CC}} = 1$ RNSC code with $J = 1$ and $\mathbb{G}^{[\mathrm{CC}]} = \{\frac{2}{3}\}_8$. This code corresponds to the accumulator used in *Repeat-Accumulate* (RA) and *Irregular Repeat-Accumulate* (IRA) codes [DJM98, JKM00, Abb07].

Simulation results are given in Fig. 3.23. It can be observed that the systems employing the one-dimensional bit mapping suffer from a high error floor, which also

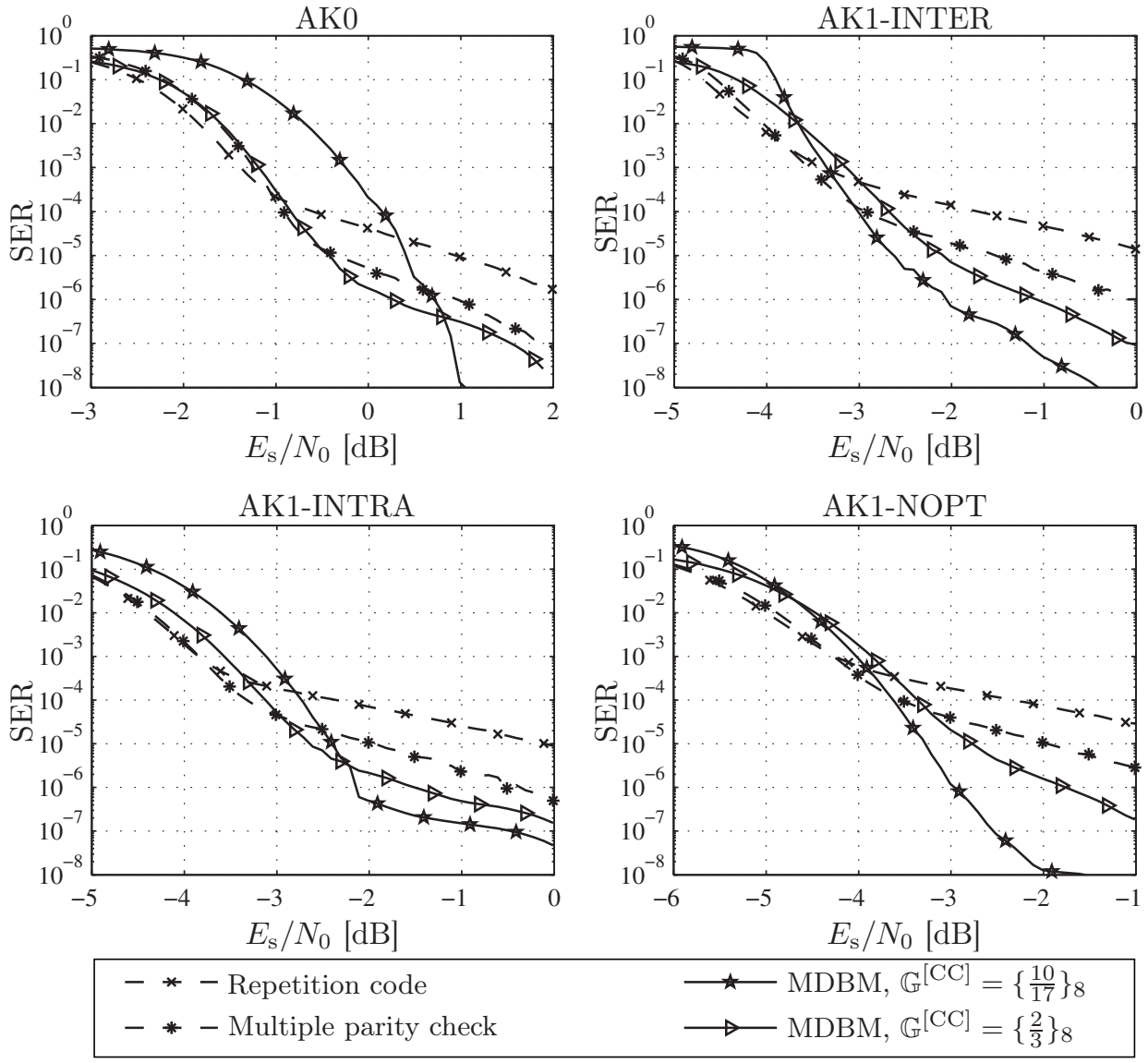

Figure 3.23: Comparison of different source decoders with and without *Multi-Dimensional Bit Mappings* (MDBMs) with $\rho = 0.9$, $\delta = 0.9$, scalar LMQ, $Q = 4$, $N_I = 250$, $r_{\text{BM}} = \frac{1}{2}$ bit mapping, $J = 3$, $r_{\text{CC}} = 1$ convolutional code ($\mathbb{G}^{[\text{CC}]} = \{\frac{10}{17}\}_8$) or $J = 1$, $r_{\text{CC}} = 1$ convolutional code ($\mathbb{G}^{[\text{CC}]} = \{\frac{2}{3}\}_8$), $\Omega = 25$ iterations, MAP estimation.

depends on the generator matrix used for the bit mapping. The repetition coded bit mapping suffers from the highest error floor. This is mainly due to the fact that the repetition code leads to two code words with Hamming weight two, while the multiple parity check code generates a single code word with Hamming weight two. If the dimension of the bit mapping is increased to $\Psi = 2$ and a bit mapping generator matrix with $d_{\min} = 4$ is employed, the error floor can be considerably reduced. However, as in Section 3.4.1, a shift of the waterfall region towards better channel qualities is observed. This shift can be compensated by utilizing different channel codes as, for instance, the irregular inner code of Section 3.4.1. In this Section, we have shown that a simple accumulator can improve the waterfall behavior, at the expense of a slightly higher error floor than in the $J = 3$ case.

3.5 Stopping Criteria

If iterative receivers like ISCD are employed, a simple measure to reduce the decoding complexity is to limit the number of iterations to the necessary amount. Usually the number of iterations is set up for the worst case degradation scenario, for example, utilizing the EXIT chart technique (see Sections 2.3 and 3.1.6). In good channel conditions, perfect reconstruction, i.e., convergence, might already be achieved after a small number of iterations. In bad channel conditions, carrying out a high number of iterations does not lead to noticeable reconstruction improvements as no EXIT decoding tunnel is open. The *stopping criterion* determines if the algorithm has converged, and stops the iterative process at the receiver in that case. Such a stopping criterion is extremely important in mobile applications where the reduction of the power consumption is one of the main optimization targets.

Stopping criteria have to be divided into two groups:

- Early stopping criteria, which stop the decoding process in bad channel conditions, i.e., if the EXIT characteristics intersect and perfect reconstruction is not possible, even using a high number of iterations;
- Late stopping criteria, which detect convergence in good channel conditions and stop iterating if no further corrections by the decoder are expected.

One of the easiest late stopping criteria can be realized by employing an additional outer pure error detecting code, for instance, a *Cyclic Redundancy Check* (CRC) code [SSA99]. This approach is for instance used in the *Long Term Evolution* (LTE) communication system. However, as this method requires the transmission of additional CRC bits, it is not further considered here.

In the literature, a plurality of different heuristic late stopping criteria have been presented [Moo05], some of them also possessing early termination capabilities:

- The *Cross Entropy* (CE) stopping criterion [HOP96] for parallel concatenated Turbo codes approximates the cross-entropy of the output of both component decoders and uses a heuristic to judge if the iterations should be stopped. This scheme possesses inherent early stopping, however it is also the computationally most complex one. This scheme can easily be adapted to ISCD. After each SDSD decoding step (iteration ω), the cross-entropy between input and output L-values of the SDSD is approximated by [HOP96]

$$\mathsf{H}_\mathsf{C}(\omega) \approx \sum_{\xi=1}^{N_X} \frac{\left(\mathsf{L}_{\mathrm{SD}}^{[\mathrm{ext}],\omega}(x_\xi) - \mathsf{L}_{\mathrm{SD}}^{[\mathrm{ext}],\omega-1}(x_\xi)\right)^2}{\exp\left(\left|\mathsf{L}_{\mathrm{SD}}^{[\mathrm{ext}],\omega}(x_\xi) + \mathsf{L}_{\mathrm{CD}}^{[\mathrm{ext}],\omega}(x_\xi)\right|\right)}$$

  with $\mathsf{L}_{\mathrm{SD}}^{[\mathrm{ext}],\omega}(x_\xi)$ denoting the extrinsic L-value at iteration ω and $\mathsf{L}_{\mathrm{SD}}^{[\mathrm{ext}],0}(x_\xi) = 0$. The iteration stops if $\mathsf{H}_\mathsf{C}(\omega) < 10^{-3} \cdot \mathsf{H}_\mathsf{C}(1)$. Note that always two or more iterations are performed with this criterion.

- The *Sign Change Ratio* (SCR) [SLF99] criterion compares the signs of the extrinsic output of the outer decoder at iteration ω with the corresponding signs of the previous iteration $\omega - 1$ and aborts if the number of sign changes is below a certain threshold. This scheme also possesses inherent early stopping capabilities and also always performs two or more iterations.

- The *Sign Difference Ratio* (SDR) algorithm [WWE00] requires less storage than the SCR approach, as only the amount of sign differences between input L-values and extrinsic output L-values is considered. Decoding stops if the number of sign differences is below a certain threshold. This scheme only realizes late stopping.

The disadvantage of these three methods is that they are based on heuristics and require a stopping threshold which has to be determined empirically. Depending on the threshold the stopping performance or even the overall system performance may be subject to considerable variations. For this reason we propose a different, non-heuristic, simple yet effective stopping criterion. Other heuristic approaches, based on thresholds are given, e.g., in [BA04, LW07].

The constraint of the proposed system is that the bit mapping in the ISCD system is a redundant bit mapping based on a linear block code. This is not a very tough constraint as it has been found that the best-performing ISCD systems all employ such a bit mapping (see, e.g., [KGM06, Tho07a, PYH07, ACS08, CSVA08a]). In this case, the bit mapping of a quantizer index (or super index) can be represented by a generator matrix $\mathbf{G}_k^{[\mathrm{BM}]}$. In this case, also a parity check matrix $\mathbf{H}_k^{[\mathrm{BM}]}$ such that $\mathbf{G}_k^{[\mathrm{BM}]} \cdot (\mathbf{H}_k^{[\mathrm{BM}]})^T = \mathbf{0}$ exists and a well-known concept from LDPC codes [Gal63, Mac99] can be applied: After each SDSD decoding step, a hard decision of the outer extrinsic information is performed and it is verified if the check equations are fulfilled (i.e., if the multiplication of the hard decision with $\mathbf{H}_k^{[\mathrm{BM}]}$ is the all-zero vector) [HCC01]. If this is the case for all $k \in \{1, \ldots, N_I\}$, the iterative process can be aborted. A total number of $B_k - B^{[\mathrm{NB}]}$ check equations per parameter can be evaluated. This late termination scheme, which will be denoted by PARITY in the following, has been successfully applied to ISCD in [SVCS08]. A different stopping criterion for ISCD based on heuristics has been presented in [BIV10].

In order to compare the different stopping criteria, we furthermore introduce the genie bound (the GENIE stopping criterion), where the receiver has knowledge about the transmitted (super) indices and aborts decoding if the MAP estimated parameters correspond to the transmitted ones. This gives a performance bound as the amount of utilized iterations cannot be lower without deteriorating the decoding performance (in terms of SER or PSNR).

The performance of the different stopping criteria is compared in a simulation example. The thresholds of the three heuristic algorithms CE, SCR, and SDR are chosen as proposed in the original publications [HOP96, SLF99, WWE00]. The ISCD setup is identical to Section 3.4.1: The redundant bit mapping is either a repetition code or the Hamming distance optimized code, the inner code is the $J = 3$ RNSC code,

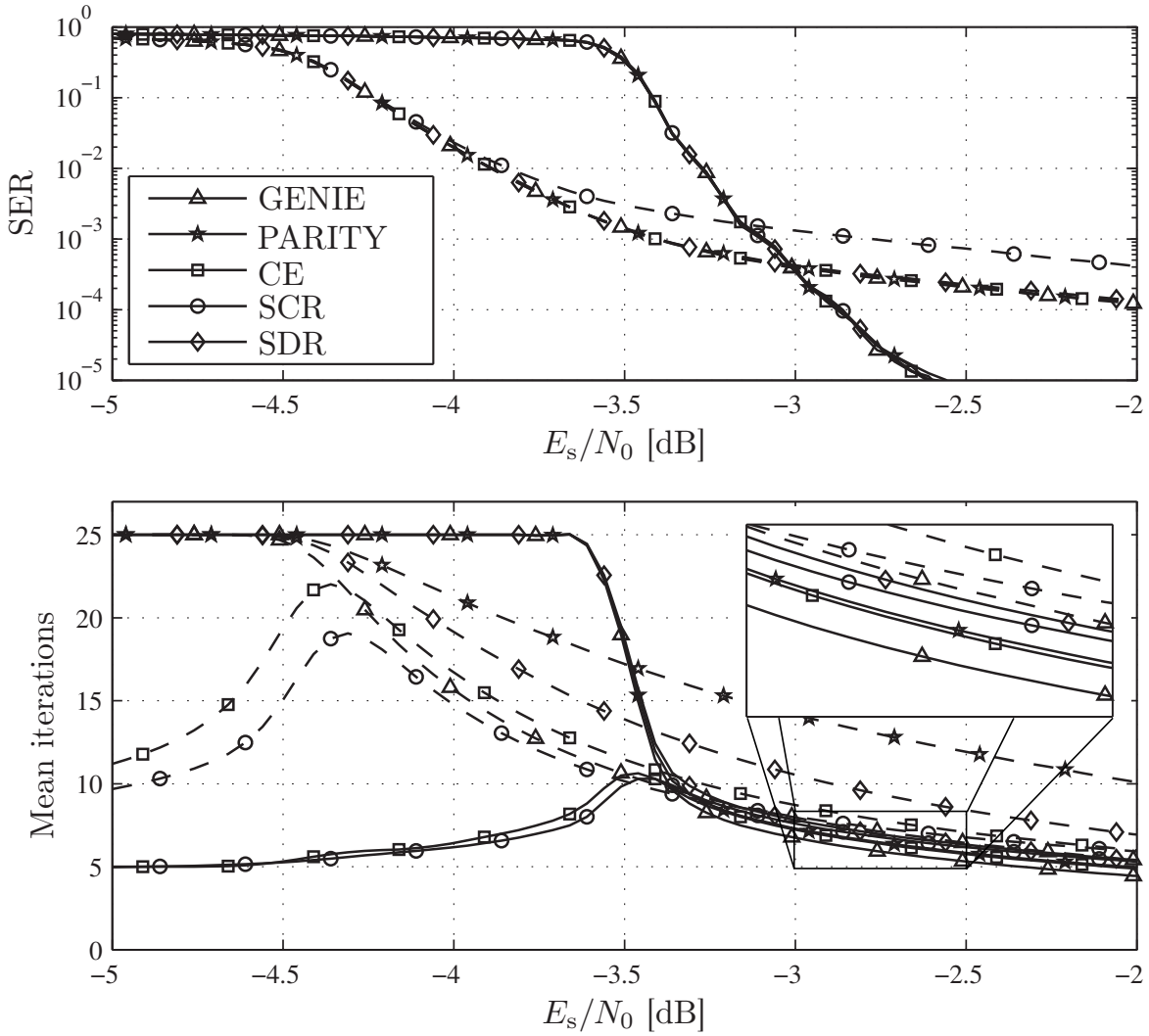

Figure 3.24: Comparison of different stopping criteria for ISCD with AK1-INTER decoding, regular channel code ($J = 3$ and $\mathbb{G}^{[\mathrm{CC}]} = \{\frac{10}{17}\}_8$), $\Omega_{\max} = 25$, MAP estimation, other simulation settings as in Figs. 3.4 and 3.20.
dashed (– – –): Repetition coded bit mapping.
solid (——): Hamming distance optimized bit mapping.

and we only consider AK1-INTER decoding for simplicity. The maximum number of iterations is fixed to $\Omega_{\max} = 25$. The simulation results are depicted in Fig. 3.24.

As expected, both the CE and SCR criteria allow early stopping, thus also reducing the number of iterations in bad channel conditions. It can furthermore be seen that the behavior of the stopping criteria is largely dependent on the considered approach. First, the case of the repetition coded bit mapping is considered. In this case, the SER performance of all stopping criteria is almost identical with the exception of the SCR scheme, which leads to a considerably higher error floor. In good channel conditions, the SCR also leads to the lowest number of iterations, followed by the CE approach, which is thus the best compromise (good SER performance and low number of iterations). The non-heuristic approach evaluating the parity check equations leads to the highest number of iterations.

On the other hand, the results of the Hamming distance optimized code are quite different. Again, the CE scheme offers the best performance in terms of number of iterations, however, it is very closely followed by the PARITY approach. The advantage of this latter approach is that the complexity of the stopping criterion is largely reduced and it is not based on a heuristic, which may need to be adapted depending on the system setup.

In order to also realize early stopping with the late-only stopping algorithms presented above, the heuristic presented in [LW07] could additionally be included. However, as this method introduces another threshold which has to be determined empirically, we do not consider it in this work. In the context of LDPC codes, the number of iterations can be further reduced by extending the PARITY stopping criterion with *forced convergence* [ZPBF04].

3.6 Hybrid ARQ Techniques

A common technique to increase the robustness of a transmission is the *Hybrid Automatic Repeat reQuest* (HARQ) protocol [CC84, Wic95], which is, e.g., part of the UMTS HSPA extension [HT06] and of the emerging LTE standard [DPSB08]. With HARQ, the receiver checks for example by means of a CRC if a packet was received without errors. Upon detection of an error, a retransmission is requested. If the retransmission contains (artificial) redundancy differing from the original transmission, e.g., other parity bits of a *Rate-Compatible Punctured Convolutional* (RCPC) code [Hag88], this is called incremental redundancy [Man74, Wic95].

If a feedback channel is available, HARQ can also be applied to the transmission of source encoded data such as speech, audio, or video. For example, speech transmission via HSDPA and HSUPA is investigated in [3GP07]. The application of HARQ to ISCD has been highlighted in [CSVA10] for the realization of a powerful transmission scheme of source codec parameters exhibiting residual redundancy. The application of HARQ is usually built around a stopping criterion, which can be either a CRC [SSA99] or one of the stopping criteria given in Sec. 3.5. In what follows, we utilize the PARITY stopping criterion [SVCS08], introduced in Sec. 3.5.

In this section, two different HARQ approaches for ISCD are compared:

- A conventional approach, where the different versions of incremental redundancy are generated by an RCPC code. This is similar to the HARQ approach utilized in the LTE standard. The ISCD transceiver corresponds to the one presented in Secs. 3.1.2 and 3.1.3 with the only difference that the output of the channel encoder is split into several chunks with one of them being initially transmitted. At the receiver, the encoded bits which have not been transmitted initially, are assumed to be erased by the channel. If, after a certain amount of iterations Ω, the stopping criterion is not fulfilled, a *Not-Acknowledge* (NACK) is sent back to the transmitter, which can then schedule the next chunk of bits for transmission.

This process is repeated until either the maximum number of retransmissions is reached or the frame is correctly decoded. In the latter case, the receiver sends an *Acknowledge* (ACK) signal to the transmitter to signal the error-free reception of the frame. This approach is subsequently denoted as *inner-HARQ*, as the incremental redundancy is generated by the inner component of the transmission chain.

- A novel approach, presented in [CSVA10], which extends the concept of RBMs to novel *Incremental Redundant Bit Mappings* (IRBMs), i.e., the incremental redundancy is generated directly in the source encoder and is exploited by the SDSD. The channel code remains unmodified and is identical for all (re)transmissions, allowing to utilize a rate $r_{\mathrm{CC}} \geq 1$ channel code for realizing a capacity-achieving system [AKtB04]. Again, the PARITY stopping criterion is utilized at the transmission to request a retransmission or to signal the error-free reception of a frame. This approach is denoted by *outer-HARQ* in the following.

Transmitter and Receiver of Outer-HARQ ISCD

Figure 3.25 depicts the baseband model of the novel outer-HARQ transmitter extension for ISCD. The HARQ control unit is connected to the feedback channel and toggles retransmissions if a NACK command is received. The bottom part of the transmitter in Fig. 3.25, which corresponds to the initial transmission, represents the classical ISCD scheme. This bottom part is indexed by $\theta = 1$. If the transmission of the initial layer was unsuccessful (NACK received), the control unit triggers the transmission of the next layer $\theta = 2$. This is repeated until either an ACK is received or the maximum layer count $\theta = \Theta$ is reached. Each layer is encoded using an individual bit mapping $\mathcal{B}^{[\mathrm{H},\theta]}$. Without loss of generality, we assume in this section that each quantizer index is encoded using the same bit mapping, i.e., $\mathcal{B}_k^{[\mathrm{H},\theta]} = \mathcal{B}^{[\mathrm{H},\theta]}$ (no irregular bit mappings). The bit mapping, as proposed in [CSVA10], is built from an overall

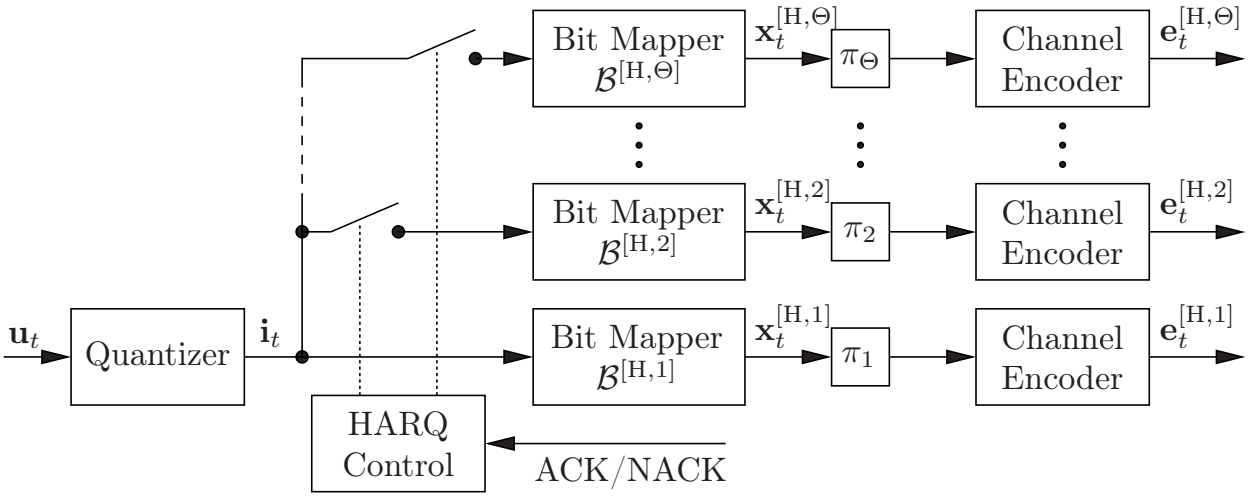

Figure 3.25: ISCD transmitter baseband model for the outer-HARQ scheme with Θ transmission layers.

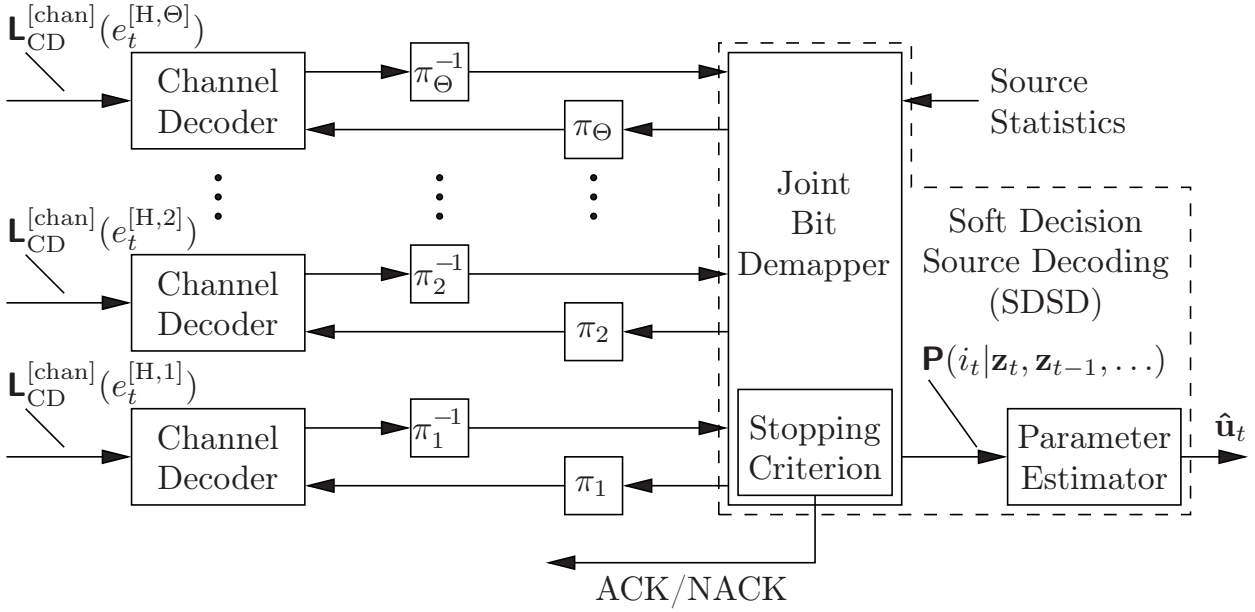

Figure 3.26: ISCD receiver baseband model for the outer-HARQ scheme with Θ transmission layers.

generator matrix $\mathbf{G}^{[\mathrm{BM,HARQ}]}$ of dimension $\dim \mathbf{G}^{[\mathrm{BM,HARQ}]} = B^{[\mathrm{NB}]} \times \sum_{\theta=1}^{\Theta} B^{[\mathrm{H},\theta]}$ which is composed as

$$\mathbf{G}^{[\mathrm{BM,HARQ}]} = \left(\mathbf{G}^{[\mathrm{H},1]} \; \mathbf{G}^{[\mathrm{H},2]} \; \cdots \; \mathbf{G}^{[\mathrm{H},\Theta]} \right) , \tag{3.60}$$

with $\mathbf{G}^{[\mathrm{H},\theta]}$ ($\dim \mathbf{G}^{[\mathrm{H},\theta]} = B^{[\mathrm{NB}]} \times B^{[\mathrm{H},\theta]}$) denoting the generator matrix of layer θ. The bit pattern generated at layer θ for quantizer index $i_{t,k}$ is given by $\mathbf{b}_{t,k}^{[\mathrm{H},\theta]} = \mathbf{b}_{t,k}^{[\mathrm{NB}]} \cdot \mathbf{G}^{[\mathrm{H},\theta]}$. The individual bit patterns $\mathbf{b}_{t,k}^{[\mathrm{H},\theta]}$ of length $B^{[\mathrm{H},\theta]}$ are grouped to the bit vector $\mathbf{x}_t^{[\mathrm{H},\theta]}$ of length $N_I \cdot B^{[\mathrm{H},\theta]}$ (regular bit mapping), interleaved, channel encoded, and transmitted over the channel. As the sizes of the resulting bit streams $\mathbf{x}_t^{[\mathrm{H},\theta]}$ may differ, the interleaver size of each layer has to be adapted accordingly. In the following, we assume that each layer is encoded using an identical channel code. However, in an actual system design, this latter constraint can be loosened in order to optimize the overall performance.

The receiver baseband model of the outer-HARQ ISCD scheme is depicted in Fig. 3.26. Upon reception of a certain layer θ, an iterative process between MAP channel decoder and the joint bit demapper is triggered. Note that also iterations between demapper and the channel decoder of previously received layers are carried out, as the newly received layer might contain information that can help improve channel decoding of lower layers (see also Sec. 3.2). The receiver can be built using a joint SDSD due to the use of a specially designed bit mapping (see below). The SDSD is configured such that only the sub-matrix $(\mathbf{G}^{[\mathrm{H},1]} \cdots \mathbf{G}^{[\mathrm{H},\theta]})$ of the already received layers is considered. Only extrinsic information for those bits that correspond to already received layers need to be computed and fed back to the corresponding channel decoder. Note that due to this outer-HARQ structure, easy parallelization of the individual channel decoders and (de-)interleavers is possible. Further note that the utilized stopping

criterion at the receiver is not fixed to be the PARITY criterion, but any of the criteria introduced in Sec. 3.5 can be used.

Simulation Example

The capabilities of the proposed outer-HARQ scheme are demonstrated by a simulation example. A system consisting of a base layer with overall rate $r_{\mathrm{BM}} \cdot r_{\mathrm{CC}} = \frac{1}{2}$ for the initial transmission is considered. The system shall allow up to 3 retransmissions ($\Theta = 4$). The same source and quantizer settings as in Sec. 3.1.4 are utilized, with the exception that $\delta = 0$ in this example, i.e., no intra-frame redundancy is present. The utilized matrix $\mathbf{G}^{[\mathrm{BM,HARQ}]}$ has been found using a heuristic search (with limited search space) and is given by

$$\mathbf{G}^{[\mathrm{BM,HARQ}]} = \left(\begin{array}{cccccccc|cccc|cccc|cccc} 1 & 0 & 0 & 0 & 0 & 1 & 1 & 1 & 1 & 1 & 1 & 1 & 0 & 1 & 0 & 1 & 1 & 1 & 1 & 1 \\ 0 & 1 & 0 & 0 & 1 & 0 & 1 & 1 & 1 & 1 & 0 & 1 & 0 & 0 & 1 & 1 & 1 & 1 & 1 & 1 \\ 0 & 0 & 1 & 0 & 1 & 1 & 0 & 1 & 1 & 1 & 0 & 0 & 1 & 1 & 0 & 1 & 1 & 1 & 1 & 1 \\ 0 & 0 & 0 & 1 & 1 & 1 & 1 & 0 & 1 & 1 & 1 & 0 & 1 & 0 & 1 & 1 & 1 & 1 & 1 & 0 \\ \underbrace{\hphantom{00000000}} & & & & & & & & \underbrace{\hphantom{0000}} & & & & \underbrace{\hphantom{0000}} & & & & \underbrace{\hphantom{0000}} & & & \\ \multicolumn{8}{c}{\mathbf{G}^{[\mathrm{H},1]}} & \multicolumn{4}{c}{\mathbf{G}^{[\mathrm{H},2]}} & \multicolumn{4}{c}{\mathbf{G}^{[\mathrm{H},3]}} & \multicolumn{4}{c}{\mathbf{G}^{[\mathrm{H},4]}} \end{array} \right) . \tag{3.61}$$

The matrix is designed such that $\mathbf{G}^{[\mathrm{H},1]}$ results in the distance optimized mapping given in Sec. 3.4.1 in order to realize a low error floor. The size of the interleavers of the different layers correspond to the sizes of the encoded bit streams, with $N_X^{[\mathrm{H},1]} = 2000$ and $N_X^{[\mathrm{H},2]} = N_X^{[\mathrm{H},3]} = N_X^{[\mathrm{H},4]} = 1000$. Channel encoding is performed by identical $r_{\mathrm{CC}} = 1$ accumulators, i.e., RNSC codes with $J = 1$ and $\mathbb{G}^{[\mathrm{CC}]} = \{\frac{2}{3}\}$.

At the receiver, AK1-INTER SDSD is performed and a maximum of $\Omega = 15$ iterations are executed before requesting a retransmission. Note that upon reception of an enhancement layer, the iterations are carried out again for all previously received layers as new information may be passed from the joint bit demapper to the individual channel decoders. Also note that upon reception of a new retransmission, the extrinsic information of all previous (re)transmissions is not reset but reused and further refined. More complex iteration schemes could be developed, but we restrict the example to this simple one. For simplicity, all control information, such as the ACK/NACK on the feedback channel, is assumed to be error-free. Furthermore, no frames or retransmissions are discarded due to a failed validity check after the last retransmission. All frames are considered in the final parameter estimation and contribute to the simulation results.

A realization of a conventional inner HARQ system with a punctured convolutional code serves for comparison. The bit mapping in this reference system is the Hamming distance optimized mapping given in Sec. 3.4.1. The punctured convolutional code is based on a rate $r_{\mathrm{CC}} = \frac{1}{3}$ RSC mother code with memory $J = 3$ and generator $\mathbb{G}^{[\mathrm{CC}]} = \{1, \frac{10}{17}, \frac{15}{17}\}_8$. The utilized HARQ puncturing matrix is given by

$$\mathbf{G}_{\mathrm{punc}}^{[\mathrm{CC,HARQ}]} = \begin{pmatrix} 2 & 3 & 2 & 3 & 2 & 3 & 2 & 3 \\ 1 & 1 & 1 & 1 & 1 & 1 & 1 & 1 \\ 4 & 0 & 4 & 0 & 4 & 0 & 4 & 0 \end{pmatrix} . \tag{3.62}$$

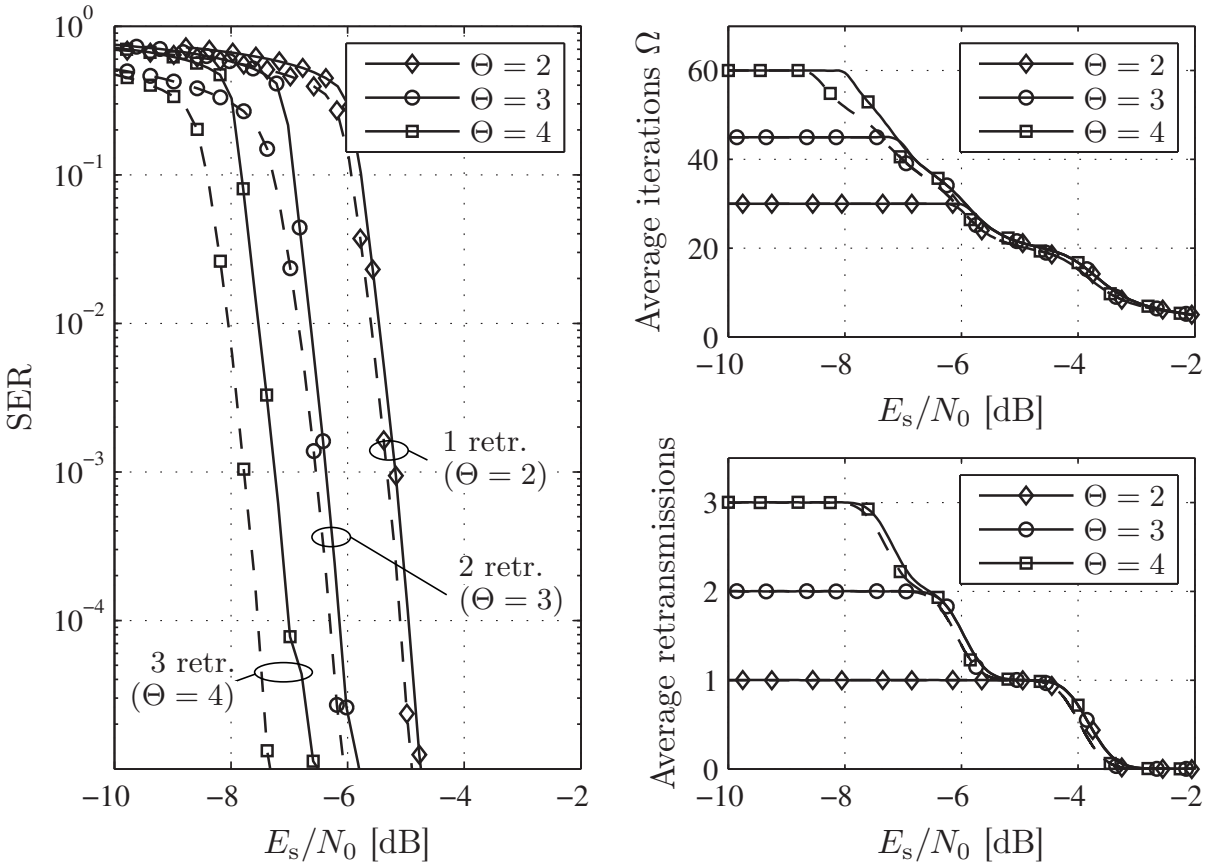

Figure 3.27: Comparison of different outer and inner HARQ with ISCD, source with $\rho = 0.9$, $\delta = 0$, AK1-INTER SDSD, MAP estimation, $\Theta \in \{2, 3, 4\}$, $\Omega = 15$ per layer before requesting retransmission.
dashed (– – –): Inner-HARQ solid (——): Outer-HARQ

The width of $\mathbf{G}_{\text{punc}}^{[\text{CC,HARQ}]}$ corresponds to the puncturing period and the height corresponds to the number of outputs of the convolutional code with the first output being the systematic one. A zero in $\mathbf{G}_{\text{punc}}^{[\text{CC,HARQ}]}$ signifies that the corresponding output is not transmitted at all. An entry > 0 signifies that the output is assigned to the corresponding HARQ layer. This means that the base layer corresponds to the non-optimized system given in Sec. 3.4.1 (regular rate $r_{\text{CC}} = 1$ convolutional code). The layers $\theta = 2$ and $\theta = 3$ are obtained by transmitting additional systematic bits while layer $\theta = 4$ adds bits from the second non-systematic output of the code. The format of $\mathbf{G}_{\text{punc}}^{[\text{CC,HARQ}]}$ is an extension of the puncturing matrices given in [Hag88].

Figure 3.27 shows the simulation results of both aforementioned system configurations. The left plot depicts the SER, while the right plots depict the average number of iterations and the average requested retransmissions. The simulation has been carried out for $\Theta = 2$ (1 retransmission), $\Theta = 3$ (2 retransmissions) and $\Theta = 4$ (3 retransmissions). If only 1 or 2 retransmissions are considered, the difference between both setups is very small. However, if up to 3 retransmissions are considered, the proposed outer-HARQ scheme is outperformed by the RCPC-based approach. The reason for this is that for very low channel qualities ($E_s/N_0 < -7\,\text{dB}$), the inner rate $r_{\text{CC}} = 1$ decoder can not cope with the channel noise anymore and all support

from the outer component can not lead to improvements (intersection in the EXIT chart). The channel decoder of the inner-HARQ approach can generate reliable extrinsic information even in bad conditions due to the additionally transmitted (partly) systematic bits, which support channel decoding. Finally, it can be concluded that a system combining both approaches (generating retransmissions by the outer and the inner component) might be a good choice as both advantages can be combined (error robustness in bad channel conditions and easy parallelization of the channel coding component).

Based on the outer-HARQ system depicted in Figs. 3.25 and 3.26, a more general adaptive and hierarchical transmission system for heterogeneous networks can be established. This advanced system utilizes especially designed bit mappings and interleavers such that portions of the bit stream can be discarded in the case of network bottlenecks. This approach is not to be confused with the *Multiple Description Coding* (MDC) approach which is discussed in Chapter 6. In the MDC case, arbitrary parts of the bit stream can be discarded, while in the hierarchical setup a base layer and extension layers exist. In this latter case, the control unit needs to take special care when discarding bits.

3.7 Conclusions

In this chapter, the ISCD concept has been fundamentally extended and novel design guidelines and optimizations have been given. After a thorough description of the transmitter and the receiver of the employed ISCD scheme, its performance has been demonstrated by figurative examples and simulation examples including the application to a real-world source coding platform.

The novel ETB has been proposed in this chapter as a remedy to the imprecise prediction of the required number of iterations with EXIT charts if inter-frame correlation is exploited. Directions on how to utilize the EXIT chart to precisely predict the SER behavior of ISCD have been given. Moreover, a novel receiver architecture has been proposed which aims at overcoming the suboptimal performance of ISCD if correlation between consecutive frames is exploited and delay constraints exist. The novel receiver better exploits the interrelations between consecutive frames in the iterative loop without violating the delay constraints.

The key design aspect of ISCD is the bit mapping between the quantizer indices and their respective bit patterns. A powerful ISCD scheme based on the novel *Irregular Bit Mappings* (IBMs) is introduced in this chapter. Irregular signifies in this context that the different parameters within a frame can be encoded using different bit mappings. Irregular bit mappings allow a powerful system optimization based on the EXIT chart technique and permit the design of capacity-achieving ISCD systems. It has been furthermore revealed how *Unequal Error Protection* (UEP) on parameter level can be systematically realized using irregular bit mappings by a reformulation of the optimization problem.

As several known ISCD systems showing good waterfall performance have the drawback of an observable error floor, several alternative methods for reducing this error floor have been studied in this chapter. It has been demonstrated that the error floor can be substantially lowered by a careful selection of the bit mapping. A carefully designed low-complexity inner irregular convolutional code can overcome the degraded waterfall performance of such bit mappings. This code can also be efficiently employed in the *FlexCode* source-channel encoder for the robust transmission of the transform coefficients. If small quantizer code books are employed, a bit mapping leading to low error floors is often not available. In this case, we have proposed *Multi-Dimensional Bit Mappings* (MDBMs), where several consecutive quantizer indices are grouped to multi-dimensional super indices, thus increasing the search space for beneficial (in terms of a low error floor) bit mappings. The improved error floor performance of ISCD with MDBMs has been confirmed by simulation examples.

In order to have an automatic control of the number of executed iterations, several stopping criteria, which detect convergence and only execute as many receiver iterations as necessary, have been compared in this chapter. Simulations have revealed that our novel proposed scheme, which is based on the parity check matrix of the redundant bit mapping, performs close to the optimum given by a genie bound and can outperform several known heuristic stopping criteria which have approximately equal computational demands. Finally, the proposed stopping criterion has been used to realize two ISCD-based HARQ schemes. In this case, the transmitter does not repeat the frame if a decoding failure occurs, but incrementally transmits additional parity symbols that help decoding the current frame.

4

Implementation and Complexity Reduction

In this chapter, several approaches for the complexity reduction of *Iterative Source-Channel Decoding* (ISCD) are presented. The complexity can be reduced by either reducing the complexity of the channel decoder or the complexity of *Soft Decision Source Decoding* (SDSD). In what follows we focus on the latter, as a variety of approaches for reducing the channel decoder complexity already exist, e.g., [FA98, WM04, CV05, STPM09]. The execution of the SDSD can be computationally quite demanding, especially if large quantizer code books are employed. In non-iterative transmission systems it is possible to execute the SDSD only for the most significant bits, as proposed in [LK03]. However, if such a source decoder is utilized in an ISCD transmission scheme, the source decoder can then only generate extrinsic information for the most significant bits, leading to a suboptimal performance.

If the SDSD complexity shall be reduced, it has to be distinguished between pure receiver-based approaches like reduced-search source decoding [SVA08] and approaches modifying the whole transmission chain such that a receiver with lower computational complexity can be built. An example of the latter approach is the concept of conditional quantization [SVAC08]. Conditional quantization exploits the correlation of the quantizer indices during the quantization process. Both approaches can also be combined for a further reduction of the decoding complexity.

4.1 Conditional Quantization

In order to realize a complexity-reduced ISCD receiver, we propose a transmitter-based modification which supports low-complexity SDSD. It has been observed that quite a high number of certain pairs of consecutive quantizer indices $(i_{t-1,k}, i_{t,k})$ or $(i_{t,k-1}, i_{t,k})$, depending on the source correlation ρ and δ, occur with small probability. If the transmitter can be modified in such a way that these transitions are not allowed, the SDSD does not need to consider all possible transitions anymore, thus reducing the decoding complexity. This modification leads to the concept of

Conditional Quantization (CQ) [SVAC08], which enables a very efficient realization (in terms of computational complexity) of the SDSD. In what follows, the concept of conditional quantization is formally described. The modification of the SDSD is highlighted in Sec. 4.1.1 while the effects on the reconstruction quality are studied in Sec. 4.1.2. Although we present the concept for a first order Markov model only, the extension to higher order Markov models is straightforward.

If $\mathbb{V}$ denotes the original quantizer code book, let $\mathfrak{V} = \{\mathfrak{V}^{(1)}, \ldots, \mathfrak{V}^{(Q)}\}$ denote the set of all quantization cells. A single quantization cell ($1 \leq q \leq Q$) is defined by

$$\mathfrak{V}^{(q)} = \left\{ \mathbf{v} \in \mathbb{R}^{\Pi} : |\mathbf{v} - \bar{\mathbf{v}}^{(q)}| < |\mathbf{v} - \bar{\mathbf{v}}^{(j)}|,\ \forall\, \bar{\mathbf{v}}^{(j)} \in \mathbb{V}, \bar{\mathbf{v}}^{(j)} \neq \bar{\mathbf{v}}^{(q)} \right\}. \tag{4.1}$$

Conditional quantization exploits the correlation between successive samples in such a way that the quantization of the current value $\mathbf{v}_{t,k}$ depends on the previously quantized value with index $i_{t,k-1}$ (intra-frame) or $i_{t-1,k}$ (inter-frame). For quantizing the current vector $\mathbf{v}_{t,k}$, the conditional quantizer only considers code book entries $\bar{\mathbf{v}}^{(q)} \in \mathbb{V}$ for which the conditional probabilities $\mathsf{P}(\bar{\mathbf{v}}^{(q)}|\bar{\mathbf{v}}^{(i_{t-1,k})})$ or $\mathsf{P}(\bar{\mathbf{v}}^{(q)}|\bar{\mathbf{v}}^{(i_{t,k-1})})$ are above a certain threshold $\mathfrak{T}$. Depending on the type of correlation that is expected (inter- or intra-frame or both), the threshold is applied considering spatially or temporally neighboring input vectors.

For the description of conditional quantization, we define a set of reduced code books

$$\mathbb{V}^{[\mathrm{pos}]}_{\mathrm{red},j} = \left\{ \bar{\mathbf{v}}^{(q)} \in \mathbb{V} : \mathsf{Pr}\left\{ I_{t,k} = q | I_{t,k-1} = j \right\} \geq \mathfrak{T} \right\} \tag{4.2}$$

$$\mathbb{V}^{[\mathrm{tim}]}_{\mathrm{red},j} = \left\{ \bar{\mathbf{v}}^{(q)} \in \mathbb{V} : \mathsf{Pr}\left\{ I_{t,k} = q | I_{t-1,k} = j \right\} \geq \mathfrak{T} \right\}. \tag{4.3}$$

The superscripts $^{[\mathrm{pos}]}$ and $^{[\mathrm{tim}]}$ in (4.2) and (4.3) indicate that the reduced code books exploit either spatial intra-frame ($^{[\mathrm{pos}]}$) or temporal inter-frame ($^{[\mathrm{tim}]}$) correlation. The conditional quantizer uses the reduced code book $\mathbb{V}^{[\cdot]}_{\mathrm{red},j}$ (either (4.2) or (4.3) depending on the predominant type of correlation) to quantize the input vector $\mathbf{v}_{t,k}$ if the neighboring vector has been quantized to $i_{t-1,k} = j$ (or $i_{t,k-1} = j$). Let $|\mathbb{V}^{[\cdot]}_{\mathrm{red},j}|$ denote the cardinality of $\mathbb{V}^{[\cdot]}_{\mathrm{red},j}$, i.e., the number of entries in the reduced code book $\mathbb{V}^{[\cdot]}_{\mathrm{red},j}$. The single entries of $\mathbb{V}^{[\cdot]}_{\mathrm{red},j}$ are denoted by $\bar{\mathbf{v}}^{[\cdot],(q)}_{\mathrm{red},j}$, $q \in \{1, \ldots, |\mathbb{V}^{[\cdot]}_{\mathrm{red},j}|\}$. The total number of transitions in an update step of the original SDSD (spatial forward or backward recursion, temporal forward recursion) amounts to Q^2 and is reduced to

$$\mathfrak{N}^{[\cdot]} \doteq \sum_{q=1}^{Q} |\mathbb{V}^{[\cdot]}_{\mathrm{red},q}| \leq Q^2 \tag{4.4}$$

by conditional quantization. This (reduced) number of transitions is directly linked to the complexity of the source decoder as shall be seen in Sec. 4.1.1. If it is obvious whether CQ is applied in inter- or intra-frame direction, the superscripts $^{[\mathrm{tim}]}$ or $^{[\mathrm{pos}]}$ are omitted and $\mathfrak{N}$ is used instead of $\mathfrak{N}^{[\mathrm{tim}]}$ or $\mathfrak{N}^{[\mathrm{pos}]}$ for simplicity. Let $\mathbb{B}^{[\cdot]}_{\mathrm{red},j}$ denote the set of all bit patterns assigned to the reduced code book $\mathbb{V}^{[\cdot]}_{\mathrm{red},j}$. Furthermore, in

order to simplify the description of the decoding algorithm, we define

$$\grave{\mathbb{V}}^{[\mathrm{pos}]}_{\mathrm{red},j} = \left\{ \bar{\mathbf{v}}^{(q)} \in \mathbb{V} : \bar{\mathbf{v}}^{(j)} \in \mathbb{V}^{[\mathrm{pos}]}_{\mathrm{red},q} \right\} \tag{4.5}$$

to be the set of all code book entries $\bar{\mathbf{v}}^{(q)}$ allowing a transition $(I_{t,k-1} = q) \rightarrow (I_{t,k} = j)$. Similarly, we define

$$\grave{\mathbb{V}}^{[\mathrm{tim}]}_{\mathrm{red},j} = \left\{ \bar{\mathbf{v}}^{(q)} \in \mathbb{V} : \bar{\mathbf{v}}^{(j)} \in \mathbb{V}^{[\mathrm{tim}]}_{\mathrm{red},q} \right\} . \tag{4.6}$$

Again, $\grave{\mathbb{B}}^{[\cdot]}_{\mathrm{red},j}$ denotes the set of assigned bit patterns to the entries of $\grave{\mathbb{V}}^{[\cdot]}_{\mathrm{red},j}$. Similarly, the sets $\mathbb{I}^{[\mathrm{pos}]}_{\mathrm{red},j}$, $\mathbb{I}^{[\mathrm{tim}]}_{\mathrm{red},j}$, $\grave{\mathbb{I}}^{[\mathrm{pos}]}_{\mathrm{red},j}$, $\grave{\mathbb{I}}^{[\mathrm{tim}]}_{\mathrm{red},j}$ contain the conditional quantizer indices.

Note that the utilization of conditional quantization also modifies the *a priori* knowledge of first order which is exploited in the source decoder. As the reduced code books possibly contain fewer entries than the original code book, the conditional probabilities (for inter-frame correlation) $\mathsf{Pr}\{I^{[\mathrm{CQ}]}_{t,k} = \mathcal{Q}^{-1}_{\mathrm{CQ}}(\bar{\mathbf{v}}^{[\mathrm{tim}],(q)}_{\mathrm{red},j}) | I^{[\mathrm{CQ}]}_{t-1,k} = \mathcal{Q}^{-1}_{\mathrm{CQ}}(\bar{\mathbf{v}}^{(j)})\} \geq \mathsf{Pr}\{I_{t,k} = \mathcal{Q}^{-1}(\bar{\mathbf{v}}^{(q)}) | I_{t-1,k} = \mathcal{Q}^{-1}(\bar{\mathbf{v}}^{(j)})\}$ with equality if and only if $\mathbb{V}^{[\cdot]}_{\mathrm{red},j} = \mathbb{V}$. The code book indices of the conditional quantizer are denoted by $i^{[\mathrm{CQ}]}_{t,k}$ and the corresponding random process by $I^{[\mathrm{CQ}]}_{t,k}$. The proof of this inequality is contained in the proof of Theorem D.2 in App. D. Similarly, the *a priori* probabilities change in the case of intra-frame correlation. These modified *a priori* probabilities have to be accounted for in the SDSD implementation.

4.1.1 Soft Decision Source Decoder Implementation

The modifications to the SDSD in order to be compatible with the conditional quantizer are straightforward. In the AK0 case, no complexity reduction is achieved by CQ as no correlation is exploited. In all the other cases, the complexity reduction is due to the reduction of state transitions in the forward (and backward, if available) recursion from Q^2 to $\mathfrak{N}$. For the equations and a detailed complexity analysis of the SDSD, we refer to App. F. For the example of the spatial forward and backward recursions in AK1-INTRA decoding, equations (F.18) and (F.20) modify to [SVAC08]

$$\alpha_{t,k}(q) = \frac{\gamma_{t,k}(q)}{\mathrm{K}_2} \sum_{\forall \tilde{q} \in \grave{\mathbb{I}}^{[\mathrm{pos}]}_{\mathrm{red},q}} \mathsf{Pr}\left\{ I^{[\mathrm{CQ}]}_{t,k} = q \mid I^{[\mathrm{CQ}]}_{t,k-1} = \tilde{q} \right\} \cdot \alpha_{t,k-1}(\tilde{q}) \tag{4.7}$$

$$\beta_{t,k-1}(q) = \frac{1}{\mathrm{K}_3} \sum_{\forall \tilde{q} \in \mathbb{I}^{[\mathrm{pos}]}_{\mathrm{red},q}} \gamma_{t,k}(\tilde{q}) \cdot \mathsf{Pr}\left\{ I^{[\mathrm{CQ}]}_{t,k} = \tilde{q} \mid I^{[\mathrm{CQ}]}_{t,k-1} = q \right\} \cdot \beta_{t,k}(\tilde{q}) \, , \tag{4.8}$$

with the normalization constants K_2 and K_3. The summations affected by conditional quantization in the other algorithms (AK1-INTER and AK1-NOPT) are to be changed accordingly. As the recursions in the original algorithm have to be carried out for all Q code book entries, the total complexity of the individual sums thus amounts

to Q^2 *Multiply ACcumulate* (MAC) operations. In the reduced complexity version of the algorithm, (4.7) and (4.8) still have to be evaluated for all Q entries, however, the summations are only performed for $|\grave{\mathbb{I}}^{[\mathrm{pos}]}_{\mathrm{red},q}|$ or $|\mathbb{I}^{[\mathrm{pos}]}_{\mathrm{red},q}|$ transitions (or $|\grave{\mathbb{I}}^{[\mathrm{tim}]}_{\mathrm{red},q}|$ and $|\mathbb{I}^{[\mathrm{tim}]}_{\mathrm{red},q}|$, respectively). This signifies that the complexity of each sum is reduced from Q^2 operations to $\mathfrak{N}$ according to (4.4). A thorough complexity evaluation and figures for all relevant cases are given in App. F.3.2.

4.1.2 Performance Evaluation of Conditional Quantization

As in (4.1), quantization cells for the conditional quantizer according to

$$\mathfrak{V}^{[\cdot],(q)}_{\mathrm{red},j} = \left\{\mathbf{v} \in \mathbb{R}^{\Pi} : |\mathbf{v} - \bar{\mathbf{v}}^{(q)}| < |\mathbf{v} - \bar{\mathbf{v}}^{(j')}|,\ \forall\, \bar{\mathbf{v}}^{(j')} \in \mathbb{V}^{[\cdot]}_{\mathrm{red},j}, \bar{\mathbf{v}}^{(j')} \neq \bar{\mathbf{v}}^{(q)}\right\} \tag{4.9}$$

can be defined for $q \in \{1, \ldots, |\mathbb{V}^{[\cdot]}_{\mathrm{red},j}|\}$ and $j \in \mathbb{I} \doteq \{1, \ldots, Q\}$. In what follows, we concentrate on the case with inter-frame correlation. However, the findings can immediately be applied to the intra-frame case by exchanging time and position indices. For a given stationary source with (two-dimensional) joint *Probability Density Function* (pdf) $\mathsf{p}_{U_{t,k},U_{t-1,k}}(u_{t,k}, u_{t-1,k}) = \mathsf{p}_{U_{t,k}|U_{t-1,k}}(u_{t,k}|u_{t-1,k}) \cdot \mathsf{p}_{U_{t-1,k}}(u_{t-1,k})$ the quantization noise in the case of scalar conditional quantization amounts to (e.g. [JN84, VM06, SVAC08])

$$N_{\mathrm{CQ}} = \tag{4.10}$$
$$\sum_{\forall \bar{v}^{(j)} \in \mathbb{V}} \sum_{\forall \bar{v}^{[\mathrm{tim}],(q)}_{\mathrm{red},j} \in \mathbb{V}^{[\mathrm{tim}]}_{\mathrm{red},j}} \int_{\mathfrak{V}^{(j)}} \int_{\mathfrak{V}^{[\mathrm{tim}],(q)}_{\mathrm{red},j}} \left(\zeta_1 - \bar{v}^{[\mathrm{tim}],(q)}_{\mathrm{red},j}\right)^2 \mathsf{p}_{U_{t,k},U_{t-1,k}}(\zeta_1, \zeta_0)\, \mathrm{d}\zeta_1\, \mathrm{d}\zeta_0\,.$$

Note that we restrict ourselves in the following to the scalar case, which is commonly used throughout this thesis. The extension towards vector quantization is obtained by increasing the dimensionality of the integration in (4.10). The quantization noise is determined by considering all possible previous samples $\bar{v}^{(j)} \in \mathbb{V}$ and then calculating the quantization noise amount of the pair $(\bar{v}^{(j)}, \bar{v}^{[\mathrm{tim}],(q)}_{\mathrm{red},j})$ with $\bar{v}^{[\mathrm{tim}],(q)}_{\mathrm{red},j} \in \mathbb{V}^{[\mathrm{tim}]}_{\mathrm{red},j}$ by solving the double integral in (4.10) and by summing over all combinations of $(\bar{v}^{(j)}, \bar{v}^{[\mathrm{tim}],(q)}_{\mathrm{red},j})$. Equation (4.10) allows us to numerically (or analytically, depending on the source pdf) evaluate the reconstruction quality of conditional quantization.

As an example, we assume that the source realizes a zero mean and unit variance Gauss-Markov process of first order according to Section 3.1.1 with inter-frame correlation ρ and no intra-frame correlation ($\delta = 0$). The two-dimensional joint distribution of the source amounts to (e.g., [VM06])

$$\mathsf{p}_{U_{t,k},U_{t-1,k}}(u_{t,k}, u_{t-1,k}) = \frac{1}{2\pi\sqrt{1-\rho^2}} \cdot \exp\left(-\frac{u^2_{t,k} + u^2_{t-1,k} - 2\rho u_{t,k} u_{t-1,k}}{2\,(1-\rho^2)}\right). \tag{4.11}$$

In order to evaluate conditional quantization, two measures are important. First, the number of transitions $\mathfrak{N}$ according to (4.4) is an indication of the complexity reduction

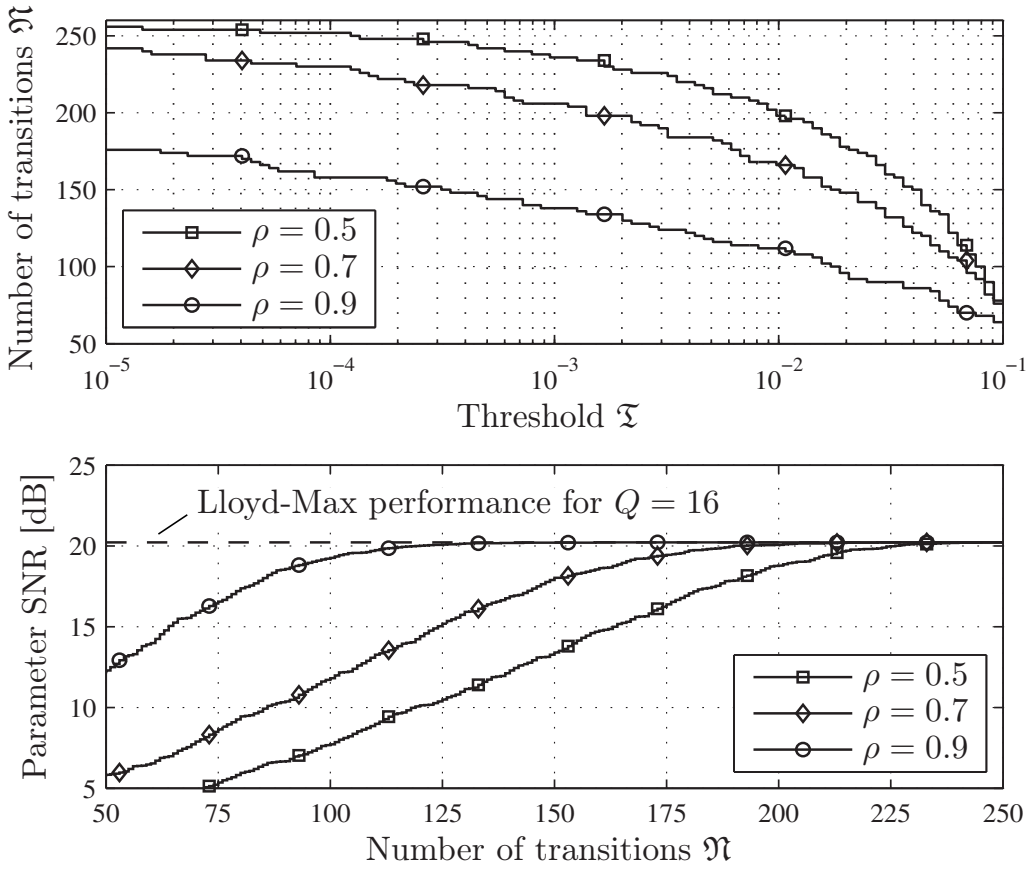

Figure 4.1: Impact of *Conditional Quantization* (CQ) on the number of transitions $\mathfrak{N}$ per SDSD recursion and on the parameter SNR performance for the source model of Sec. 3.1.1 with $\rho \in \{0.5, 0.7, 0.9\}$, $\delta = 0$ and scalar $Q = 16$ scalar LMQ.

as the number of operations performed within SDSD linearly scales with $\mathfrak{N}$. On the other hand, if too many transitions are forbidden by CQ, the reconstruction quality is affected. Therefore, it is interesting to see the behavior of the *Parameter Signal-to-Noise Ratio* (PSNR) performance if the conditional quantizer reduces the number of transitions. The PSNR can be evaluated by using (4.10) for expressing the conditional quantizer noise (in the scalar case).

The upper sub-plot of Fig 4.1 depicts the number of transitions $\mathfrak{N}$ as a function of the threshold $\mathfrak{T}$ for $\rho \in \{0.5, 0.7, 0.9\}$ and $Q = 16$ quantizer levels for the aforementioned source. As it is expected intuitively, a higher correlation ρ leads to a lower number of retained transitions $\mathfrak{N}$, i.e., transitions having a high conditional probability.

In order to evaluate how much the signal quality is affected by conditional quantization, (4.10) is evaluated for the same source and the PSNR after quantization is determined as a function of $\mathfrak{N}$. The original code book $\mathbb{V}$ is assumed to be the optimum *Lloyd-Max Quantizer* (LMQ) code book [JN84]. The results are depicted in the lower sub-plot of Fig. 4.1 for $Q = 16$. It can be seen that for $\rho = 0.9$ the number of transitions can be halved (i.e., from $Q^2 = 256$ to $\mathfrak{N} \approx 128$) without affecting the PSNR considerably. Additional illustrations on CQ can be found in [SVAC08].

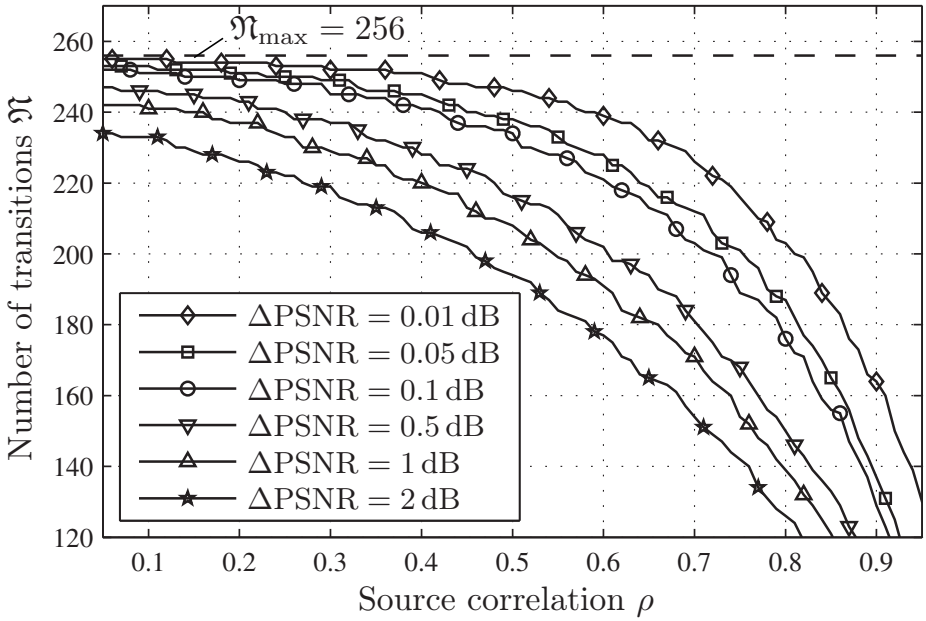

Figure 4.2: Number of allowed transitions $\mathfrak{N}$ in the conditional quantizer as a function of the source correlation ρ (Gauss-Markov source of Sec. 3.1.1 with $\delta = 0$) and for different allowed quantizer reconstruction quality losses ΔPSNR.

Figure 4.2 shows the possible reduction of the number of allowed transitions if a certain loss in the quantizer reconstruction quality can be tolerated. This loss is expressed as (logarithmic) difference ΔPSNR between the signal quantized with LMQ and the signal quantized with CQ based on the LMQ code books. This reduction of the number of transitions is computed for different values of the source correlation ρ (again, $\delta = 0$). As expected, the reduction potential is limited for small values of ρ, with a steep decrease of the number of transitions for $\rho > 0.7$.

Note that although we gave equations and an example for the case of inter-frame correlation, the results can be ported directly to the case of intra-frame correlation. If two-dimensional correlation is exploited by the AK1-NOPT algorithm, two cases have to be distinguished. If $\delta > \rho$, then CQ shall be applied based on the intra-frame correlation (denoted by *intra-frame CQ*), as in this case a forward and a backward recursion have to be carried out at the receiver and the number of transitions can be reduced from $2Q^2$ (Q^2 for either forward and backward recursion) to $2\mathfrak{N}^{[\mathrm{pos}]}$. On the other hand, if $\rho > \delta$ it has to be evaluated if the savings by applying CQ to the temporal correlation (denoted by *inter-frame CQ*), leading to a reduction from totally $3Q^2$ operations to $2Q^2 + \mathfrak{N}^{[\mathrm{tim}]}$, exceed the savings by applying CQ to the spatial correlation with a reduction from $3Q^2$ operations to $Q^2 + 2\mathfrak{N}^{[\mathrm{pos}]}$. For the exemplary case of $\rho = 0.9$ and a tolerated $\Delta\mathrm{PSNR} = 0.1\,\mathrm{dB}$, the overall number of transitions considered in the case where CQ is applied to the inter-frame correlation is $2Q^2 + \mathfrak{N}^{[\mathrm{tim}]} = 641$ (with the values taken from Fig. 4.2). If CQ is applied to the intra-frame correlation, then the overall number of transitions is reduced to $Q^2 + 2\mathfrak{N}^{[\mathrm{pos}]}$ and it can be observed that for $\delta \geq 0.75$, the transition reduction (and thus also the complexity reduction) is larger than in the inter-frame case. This means that special care has to be carried out when designing a system with conditional quantization for spatial and temporal

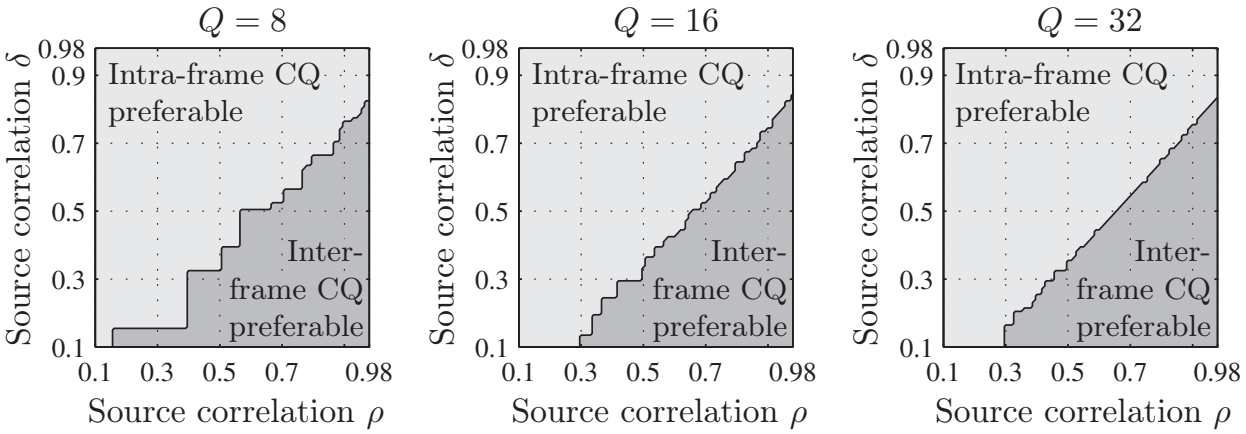

Figure 4.3: Regions of preferability (in terms of resulting computational complexity) for the application of inter-frame or intra-frame conditional quantization for the source model introduced in Sec. 3.1.1, three different quantizers (LMQ with $Q \in \{8, 16, 32\}$) and an allowed distortion $\Delta\mathrm{PSNR} = 0.1$.

correlation. For three exemplary quantizer configurations (LMQ, $Q \in \{8, 16, 32\}$) and the two-dimensional source model introduced in Sec. 3.1.1, Fig. 4.3 depicts the regions where either inter- or intra-frame conditional quantization is preferable.

If the optimum algorithm for exploiting inter- and intra-frame correlation according to [Hei01a, HA08] is used for SDSD, a "two-dimensional" CQ, which is conditioned on $(i_{t-1,k}, i_{t,k-1})$ can be utilized. However, as this optimum SDSD is not considered in this thesis for complexity reasons, the "two-dimensional" CQ is not examined here. As the (near-optimum) AK1-NOPT algorithm exploits independent spatial and temporal recursions, independent concurrent inter- and intra-frame CQ could be used. However, in that case, while quantizing a parameter, it could be that the resulting code book $\mathbb{V}^{[\mathrm{pos}]}_{\mathrm{red},i_{t,k-1}} \cap \mathbb{V}^{[\mathrm{tim}]}_{\mathrm{red},i_{t-1,k}} = \emptyset$, preventing quantization. Due to the independent spatial and temporal receiver processing in the AK1-NOPT case, we therefore choose to apply CQ in either spatial or temporal direction, depending on the correlation coefficients ρ and δ.

4.1.3 Improvement of the Waterfall Behavior

The application of conditional quantization can be interpreted as an additional functional block between quantizer and bit mapper. This block represents the function $\mathcal{I}^{[\mathrm{CQ}]}_{t,k} : \mathbb{I} \to \mathbb{I}$ with $i_{t,k} \mapsto i^{[\mathrm{CQ}]}_{t,k} = \mathcal{I}^{[\mathrm{CQ}]}_{t,k}(i^{[\mathrm{CQ}]}_{t,k})$, depending on the previous index $i_{t-1,k}$ (or $i_{t,k-1}$). Thus, the conditional quantizer can also be described by $\mathcal{Q}_{\mathrm{CQ}} = \mathcal{I}^{[\mathrm{CQ}]}_{t,k} \circ \mathcal{Q}$. From an information theoretic point of view, the effect of this additional function in the transmitter chain is a reduction of the (conditional) entropies $\mathsf{H}(I^{[\mathrm{CQ}]}_{t,k}) \leq \mathsf{H}(I_{t,k})$, and $\mathsf{H}(I^{[\mathrm{CQ}]}_{t,k}|I^{[\mathrm{CQ}]}_{t-1,k}) \leq \mathsf{H}(I_{t,k}|I_{t-1,k})$ (inter-frame CQ) or $\mathsf{H}(I^{[\mathrm{CQ}]}_{t,k}|I^{[\mathrm{CQ}]}_{t,k-1}) \leq \mathsf{H}(I_{t,k}|I_{t,k-1})$ (intra-frame CQ). The proof of these propositions can be found in App. D.

It can furthermore be observed that the reduction of the conditional entropy $\mathsf{H}(I^{[\mathrm{CQ}]}_{t,k}|I^{[\mathrm{CQ}]}_{t-1,k})$ (or $\mathsf{H}(I^{[\mathrm{CQ}]}_{t,k}|I^{[\mathrm{CQ}]}_{t,k-1})$) is larger than the reduction of the entropy

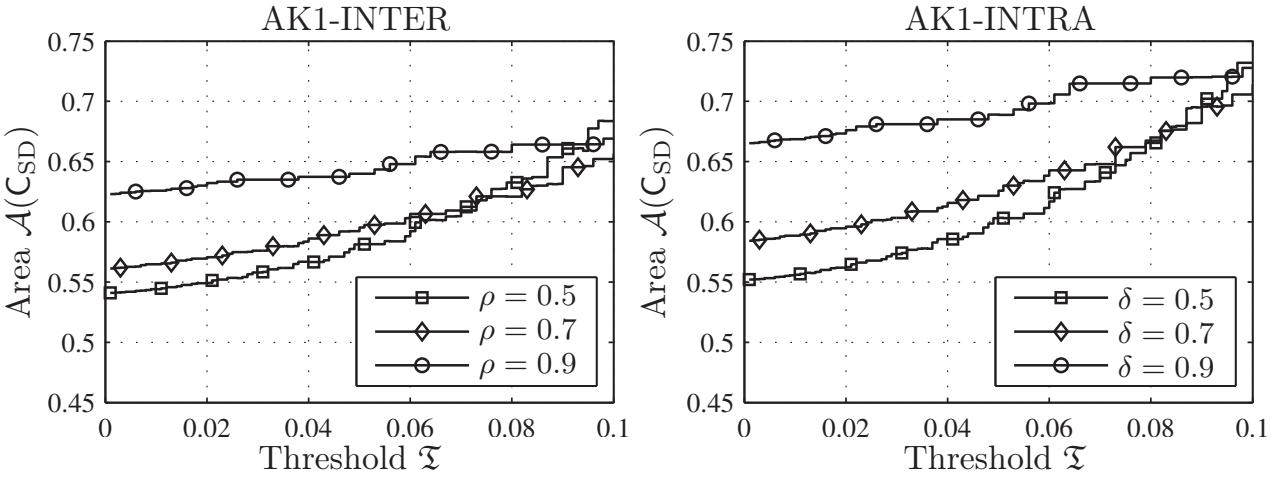

Figure 4.4: Impact of CQ on the area $\mathcal{A}(\mathsf{C}_{\mathrm{SD}})$ underneath the SDSD EXIT characteristic for inter- and intra-frame CQ with AK1-INTER or AK1-INTRA decoding, respectively, based on $Q = 16$ scalar LMQ with $r_{\mathrm{BM}} = 1/2$ repetition coded bit mapping ($B_k = 8$).

$\mathsf{H}(I_{t,k}^{[\mathrm{CQ}]})$, at least if a Gauss-Markov source with LMQ is used. This observation signifies that the source-coding related rate r_{SC} (in the asymptotic case), as given in Sec. 3.1.5, is decreased by CQ. A direct consequence of a reduced rate r_{SC} is an increase of the system capacity, i.e., successful transmission can be achieved in worse channel conditions E_{s}/N_0 with CQ than without CQ. However, the disadvantage is a decrease in the reconstruction quality PSNR. These findings go along with the *Optimum Performance Theoretically Attainable* (OPTA) limit given in [CSVA06], which indicates that the reconstruction performance is decreased if a successful transmission shall be achieved at worse channel qualities. This effect has already been observed in the case of CQ in [SVAC08] and it has been shown by an example that indeed the area $\mathcal{A}(\mathsf{C}_{\mathrm{SD}})$ underneath the SDSD EXIT characteristic is increased, which is clear as $\mathcal{A}(\mathsf{C}_{\mathrm{SD}}) = 1 - r_{\mathrm{SC}}$. This increase of $\mathcal{A}(\mathsf{C}_{\mathrm{SD}})$ (decrease of r_{SC}) directly leads to a shift of the waterfall behavior towards lower channel qualities. Figure 4.4 shows the increase of the area $\mathcal{A}(\mathsf{C}_{\mathrm{SD}})$ (and thus implicitly the decrease of r_{SC}) as a function of the CQ threshold $\mathfrak{T}$ for inter-frame CQ (with $\rho \in \{0.5, 0.7, 0.9\}$ $\delta = 0$, and AK1-INTER decoding) and intra-frame CQ (with $\rho = 0$, $\delta \in \{0.5, 0.7, 0.9\}$, and AK1-INTRA decoding).

The waterfall shifting effect is also visualized by means of a simulation example in the upcoming Sec. 4.1.4.

4.1.4 Simulation Example

In order to demonstrate the capabilities of conditional quantization within ISCD, we utilize the system settings presented in Sec. 3.1.4 together with CQ. For simplicity, we only employ AK1-INTER decoding, however, the results are similar for all other decoding algorithms [SVAC08]. The employed thresholds are $\mathfrak{T} \in \{0.0001, 0.0002, 0.0005, 0.001, 0.002, 0.001, 0.05, 0.04, 0.03, 0.02, 0.01\}$ with respective number of transitions $\mathfrak{N}^{[\mathrm{tim}]} \in \{158, 156, 146, 138, 134, 120, 112, 96, 90, 86, 84\}$ (see

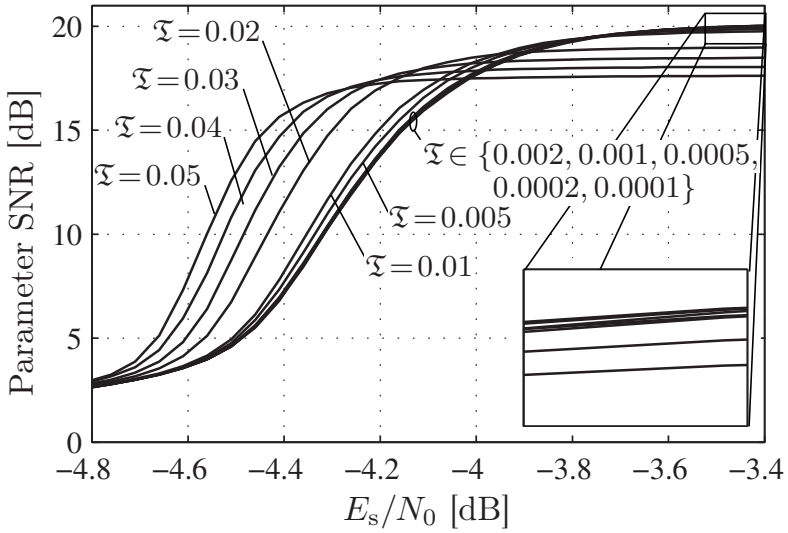

Figure 4.5: Comparison of different values of $\mathfrak{T}$ in ISCD with CQ for $\rho = 0.9$, $\delta = 0$, scalar LMQ, $N_I = 250$, $r_{\mathrm{BM}} = \frac{1}{2}$ repetition bit mapping, 8-state conv. code ($\mathbb{G}^{[\mathrm{CC}]} = \{\frac{10}{17}\}_8$), $\Omega = 25$ iterations, AK1-INTER decoding, MMSE estimation.

Fig. 4.1, $\rho = 0.9$). The simulation results given in Fig. 4.5 indicate that for $\mathfrak{T} \leq 0.01$ and the given system settings, the PSNR performance is more or less identical (with a small performance loss in terms of PSNR as predicted) to the conventional ISCD system. For $\mathfrak{T} > 0.01$ (i.e., if $\mathfrak{N} < 112$), a huge discrepancy of the PSNR behavior is observed. This corresponds to the results predicted in the bottom part of Fig. 4.1 where the performance started to drop rapidly for $\mathfrak{N} \lessapprox 112$. As predicted in Sec. 4.1.3, the waterfall is indeed shifted towards the range of lower E_s/N_0 conditions due to the decreased source-coding related rate r_{SC}. Further simulation results of CQ can be found in Sec. 4.4.

4.2 Reduced Search SDSD (M-SDSD)

The conditional quantization (CQ) approach presented in Section 4.1 has the limitation that the transmitter has to be modified in order to allow a low-complexity SDSD implementation at the receiver. However, ISCD has originally been proposed as a receiver-only technique to improve decoding of quantized source codec parameters in the presence of channel noise [AVS01, Gör01b, ACS08]. Thus, usually the transmitter cannot be modified. For this reason, we propose a receiver-only approach to reduced the SDSD complexity, called M-SDSD [SVA08]. This approach is similar to the well-known M-algorithm [And89, FA98, WM04], or related approaches [CFR01], known from channel decoding. The M-algorithm [FA98] can be successfully applied to the decoding of convolutional codes in order to reduce the complexity. Another successful field of application is channel equalization of *Inter-Symbol Interference* (ISI)-channels [WM04]. The application of a similar reduction technique to ISCD has also been introduced in [Adr03]. We show that the number of operations can be considerably reduced by only slightly affecting the overall system performance.

The SDSD in fact is a variant of the *Bahl, Cocke, Jelinek, Raviv* (BCJR) algorithm [BCJR74] operating on a fully developed trellis [ACS08]. Each state corresponds to a quantizer code book index (or a bit pattern, respectively). The state transitions correspond to the possible transitions $I_{t-1,k} \rightarrow I_{t,k}$ (or $I_{t,k-1} \rightarrow I_{t,k}$ respectively). The M-SDSD algorithm is characterized by its value M. During the forward recursion of the SDSD (from position k to $k+1$ in the spatial update), the M best states of the trellis diagram are selected, i.e., the M different indices for which $\alpha_{t,k}(q)$, $q = 1, \ldots, Q$ has the largest value. Let $\mathbb{M}_{t,k}$ contain the M quantizer indices with the largest $\alpha_{t,k}(q)$, i.e., $|\mathbb{M}_{t,k}| = M$ and $\alpha_{t,k}(q) \geq \alpha_{t,k}(j)$ holds $\forall q \in \mathbb{M}_{t,k}, \forall j \in \mathbb{I} \setminus \mathbb{M}_{t,k}$. Alternatively, we define

$$\mathbb{M}_{t,k} \doteq \left\{ q \in \mathbb{I} : \boldsymbol{\chi}_{\text{opt}} = \arg\max_{\forall \boldsymbol{\chi} \in C_M^Q} \sum_{j=1}^{Q} \chi_j \alpha_{t,k}(j) \wedge \chi_{\text{opt},q} = 1 \right\} \tag{4.12}$$

with the combination set $C_M^Q \doteq \{\boldsymbol{\chi} = (\chi_1, \chi_2, \ldots, \chi_Q) : \chi_j \in \mathbb{F}_2 \wedge \sum_{j=1}^{Q} \chi_j = M\}$ containing all $\binom{Q}{M}$ combinations of states, stored as Q-dimensional vectors with M ones each.

The forward and backward recursions of the M-SDSD then modify to (for the example of AK1-INTRA decoding)

$$\alpha_{t,k}(q) = \frac{\gamma_{t,k}(q)}{\mathrm{K}_2} \sum_{\forall \tilde{q} \in \mathbb{M}_{t,k-1}} \mathsf{Pr}\{I_{t,k} = q | I_{t,k-1} = \tilde{q}\} \cdot \alpha_{t,k-1}(\tilde{q}) \,, \quad \forall q \in \mathbb{I} \tag{4.13}$$

$$\beta_{t,k-1}(q) = \frac{1}{\mathrm{K}_3} \sum_{\forall \tilde{q} \in \mathbb{M}_{t,k}} \gamma_{t,k}(\tilde{q}) \mathsf{Pr}\{I_{t,k} = \tilde{q} | I_{t,k-1} = q\} \cdot \beta_{t,k}(\tilde{q}) \,, \quad \forall q \in \mathbb{M}_{t,k-1} \,. \tag{4.14}$$

After having executed the forward recursion (4.13), a new set $\mathbb{M}_{t,k}$ can be computed by searching the M best values $\alpha_{t,k}(q)$. These sets have to be stored as they are used subsequently within the backward recursion (4.14). The sum in (4.14) is performed over all M indices contained in $\mathbb{M}_{t,k}$, however, only those $\beta_{t,k-1}(q)$ which have been retained in the forward recursion (those within $\mathbb{M}_{t,k-1}$) are considered (so-called *living states*), following the guidelines given in [FA98].

The operations performed in (4.13) and (4.14) are illustrated in the trellis representations in Fig. 4.6 for $M = 6$ and $Q = 16$. Figure 4.6-a) illustrates the considered transitions in the forward recursion (4.13). The set of M best states $\mathbb{M}_{t,k-1} = \{6, 7, 8, 9, 10, 12\}$ is given and MQ operations are performed to compute $\alpha_{t,k}(q)$, $\forall q \in \mathbb{I}$. After this step, a new set $\mathbb{M}_{t,k}$ can be obtained by selecting the M states having the highest values of $\alpha_{t,k}(q)$. In the exemplary case, we assume that $\mathbb{M}_{t,k} = \{4, 7, 8, 9, 11, 12\}$. In the backward recursion (4.14), of course only those transitions from the states in $\mathbb{M}_{t,k}$ to the states in $\mathbb{M}_{t,k-1}$ need to be considered. This is depicted in Fig. 4.6-b). Thus, the backward recursion (4.14) only needs to be carried out for M^2 different combinations.

In the AK1-INTRA case, the number of state transitions thus reduces from $2Q^2$ to $QM + M^2$ (forward recursion and backward recursion). In the AK1-INTER case, only

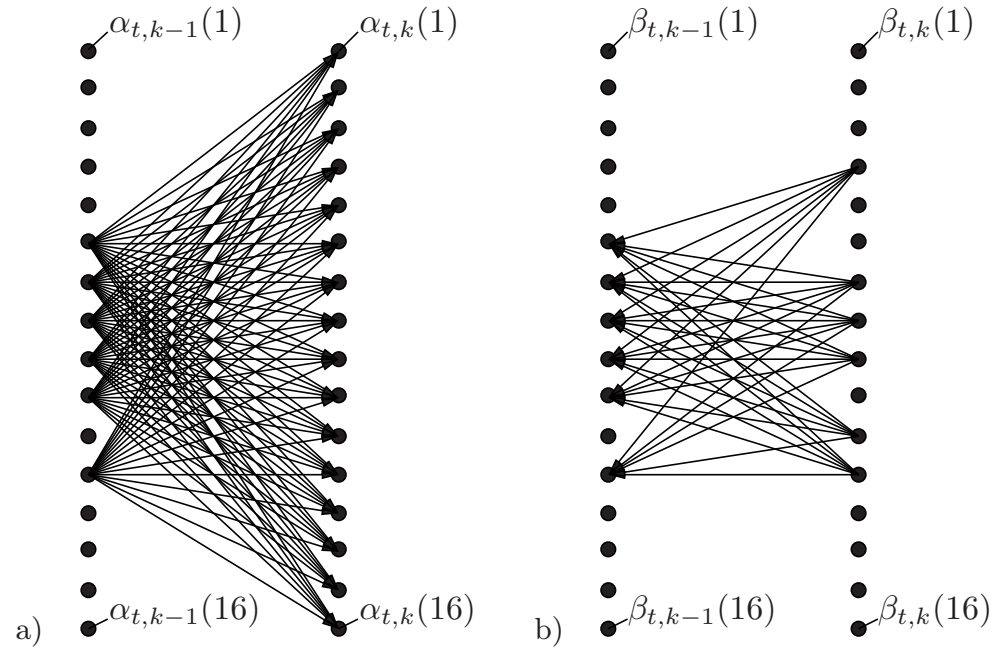

Figure 4.6: Exemplary trellis representations for the computations performed in the forward and backward recursions of the AK1-INTRA M-SDSD algorithm ($M = 6$)
a) forward recursion trellis representation, $\mathbb{M}_{t,k-1} = \{6, 7, 8, 9, 10, 12\}$.
b) backward recursion trellis representation, $\mathbb{M}_{t,k-1} = \{6, 7, 8, 9, 10, 12\}$ and $\mathbb{M}_{t,k} = \{4, 7, 8, 9, 11, 12\}$.

a forward recursion is carried out, requiring the consideration of QM transitions. In the AK1-NOPT case, we define the following strategy: After the temporal update (F.33) (or (F.74), respectively) from $t-1$ to t, the M best states are computed and stored in the sets $\mathbb{M}_{t,k}$, $\forall k \in \{1, \ldots, N_I\}$. Using these sets, the spatial updates (F.29) and (F.30) can be carried out using the retained states in $\mathbb{M}_{t,k}$.

It has to be mentioned that additional computation complexity is required within the forward iteration to determine the M best states. This can for instance been done using a simple search with $MQ - \sum_{j=1}^{M} j = MQ - \frac{1}{2}(M^2 + M)$ comparisons (states that have already been chosen do not need to be compared anymore). Note that there might be more efficient ways to select the M best values, like partial sorting algorithms with worst case complexity $O(Q + M \log Q)$ [Jos99] or asymptotic average complexity $O(Q + M \log M)$ [Mar04]. However, as Q and M tend to be relatively small, we do not consider these approaches in this work.

The computation of extrinsic information also has to be modified in the M-SDSD algorithm according to (exemplary for the AK1-INTRA case)

$$\mathsf{L}_{\mathrm{SD}}^{[\mathrm{ext}]}(b_{t,k,\mu}) = \ln \frac{\sum\limits_{\forall q \in \mathbb{M}_{t,k}} \left(1 - \bar{b}_{k,\mu}^{(q)}\right) \cdot \gamma_{t,k}^{[\mathrm{ext}]\setminus\mu}(q) \cdot \beta_{t,k}(q) \cdot A_{t,k}(q)}{\sum\limits_{\forall q \in \mathbb{M}_{t,k}} \bar{b}_{k,\mu}^{(q)} \cdot \gamma_{t,k}^{[\mathrm{ext}]\setminus\mu}(q) \cdot \beta_{t,k}(q) \cdot A_{t,k}(q)}. \tag{4.15}$$

with $A_{t,k}(q) \doteq \sum_{\forall \tilde{q} \in \mathbb{M}_{t,k-1}} \mathsf{Pr}\{I_{t,k} = q | I_{t,k-1} = \tilde{q}\} \alpha_{t,k-1}(\tilde{q})$ being an intermediate result from the forward recursion (4.13). Thus, the computation of extrinsic infor-

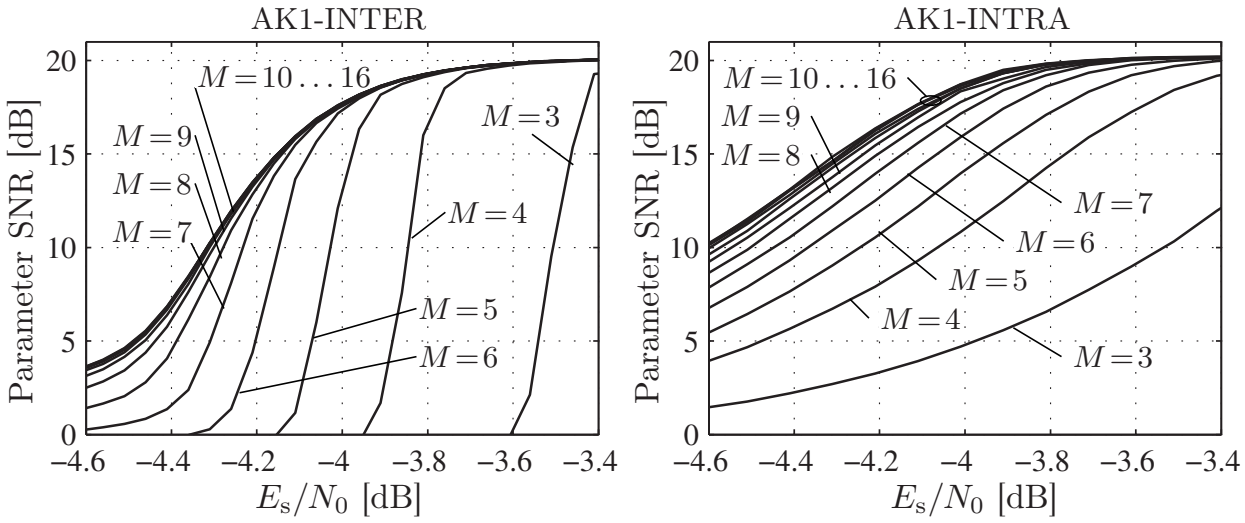

Figure 4.7: Comparison of different values of M in ISCD with M-SDSD for $\rho = 0.9$, $\delta = 0.9$, scalar LMQ, $N_I = 250$, $r_{\mathrm{BM}} = \frac{1}{2}$ repetition bit mapping, 8-state conv. code ($\mathbb{G}^{[\mathrm{CC}]} = \{\frac{10}{17}\}_8$), $\Omega = 25$ iterations, MMSE estimation.

mation uses also the transitions of the reduced trellis depicted in Fig. 4.6-b). This means that the complexity of the extrinsic information computation is also slightly reduced. A detailed complexity analysis of M-SDSD can be found in App. F.3.3.

Figure 4.7 shows the PSNR performance of M-SDSD for AK1-INTER and AK1-INTRA decoding and the system settings as presented in Sec. 3.1.4. In the AK1-INTER case, the performance of the original SDSD (i.e., $M = 16$) is nearly obtained for $M \geq 9$ while in the AK1-INTRA case M has to be larger than 10 in order to obtain the same performance as the original SDSD. The reason for this is that the decision of selecting M states is performed after the forward recursion, and therefore the backward recursion, which is only performed in AK1-INTRA decoding, is limited to the set of selected states and may thus not consider information from the non-visited states. If the PSNR target quality is high, e.g., PSNR $\geq 18\,\mathrm{dB}$ shall be achieved, then already with $M = 6$ sufficient results can be obtained in the AK1-INTER case in this example while $M = 10$ has to be selected in the AK1-INTRA case in order to achieve PSNR $\geq 18\,\mathrm{dB}$ in this example for roughly the same channel quality as with the original SDSD. An additional simulation example including a detailed analysis of the amount of necessary and saved operations by applying the complexity-reduced algorithms will be given in Sec. 4.4.

4.3 Combination of Conditional Quantization and M-SDSD

Combining conditional quantization with the M-SDSD algorithm as proposed in [SVA08] leads to a further complexity reduction of the source decoder at the expense of a transmitter modification. This combination leads to a further thinning of the corresponding trellis representation of the SDSD. We call the resulting algorithm

CQ-M-SDSD. At each step in the forward recursion, $\mathfrak{N}_{t,k}^{M}$ transitions are considered with

$$\mathfrak{N}_{t,k}^{M} = \sum_{\forall q \in \mathbb{M}_{t,k-1}} |\mathbb{V}_{\mathrm{red},q}^{[\mathrm{pos}]}| \tag{4.16}$$

for the example of AK1-INTRA decoding. Note that $\mathfrak{N}_{t,k}^{M}$ is not constant as $\mathbb{M}_{t,k-1}$ varies over time t and position k. As in the CQ case, the number of state transitions depends on the previous state and is not constant (as $|\mathbb{V}_{\mathrm{red},q}^{[\mathrm{pos}]}| \lessgtr |\mathbb{V}_{\mathrm{red},j}^{[\mathrm{pos}]}|$, $\forall q, j \in \mathbb{I}, q \neq j$). Therefore, the complexity of the CQ-M-SDSD algorithm cannot be directly given, as depending on the M selected states, the number of transitions may vary from stage to stage. Therefore, only a (tight) upper bound of the complexity can be given, which takes into account the worst case, i.e., the maximum number of considered transitions. Therefore we define $\mathfrak{N}_{\max}^{M,\alpha}$ to be the maximum number of transitions emerging from M out of Q states with

$$\mathfrak{N}_{\max}^{M,\alpha} \doteq \max_{\forall \boldsymbol{\chi} \in C_M^Q} \sum_{j=1}^{Q} \chi_j |\mathbb{V}_{\mathrm{red},j}^{[\mathrm{pos}]}| \tag{4.17}$$

by taking the maximum over all $\binom{Q}{M}$ combinations of states, stored in the combination set C_M^Q (see Sec. 4.2 for the definition of C_M^Q). As already mentioned above, the backward recursion exploits a smaller number of state transitions. This maximum number of states in the backward recursion $\mathfrak{N}_{\max}^{M,\beta}$ is given by

$$\mathfrak{N}_{\max}^{M,\beta} \doteq \max_{\forall \boldsymbol{\chi}_1, \boldsymbol{\chi}_2 \in C_M^Q} \sum_{j=1}^{Q} \chi_{1,j} \sum_{\forall q \in \mathbb{I}_{\mathrm{red},j}^{[\mathrm{pos}]}} \chi_{2,q}\,, \tag{4.18}$$

by considering all possible transitions between combinations of M states out of Q. The factors $\mathfrak{N}_{\max}^{M,\alpha}$ and $\mathfrak{N}_{\max}^{M,\beta}$ give the worst case of state transitions used either in the forward or backward recursions. Using these values, a hardware guaranteeing a certain throughput can be designed. The detailed complexity figures are given in App. F.3.4. A simulation example including a detailed listing of the amount of required operations will be given in Sec. 4.4.

Figure 4.8 shows the different stages of SDSD forward recursion trellis thinning by means of an example. Figure 4.8-a) shows the fully developed trellis utilized in the original SDSD algorithm for $Q = 16$, with a total number of $Q^2 = 256$ transitions. If CQ, as introduced in Sec. 4.1, is applied, only the most probable transitions given a certain state need to be considered. This reduction can be achieved by modifying the quantizer such that the utilized quantizer code book depends on the previously quantized value. If a CQ threshold of $\mathfrak{T} = 10^{-2}$ is utilized, the number of transitions is reduced from 256 to $\mathfrak{N} = 112$ for a source correlation of $\rho = 0.9$ (or $\delta = 0.9$, respectively). In this case, the quantizer can still achieve a maximum PSNR of about 19.84 dB. The maximum PSNR achievable with the original quantizer is 20.22 dB. The resulting snapshot trellis of M-SDSD utilized in the forward recursion with $M = 6$ and

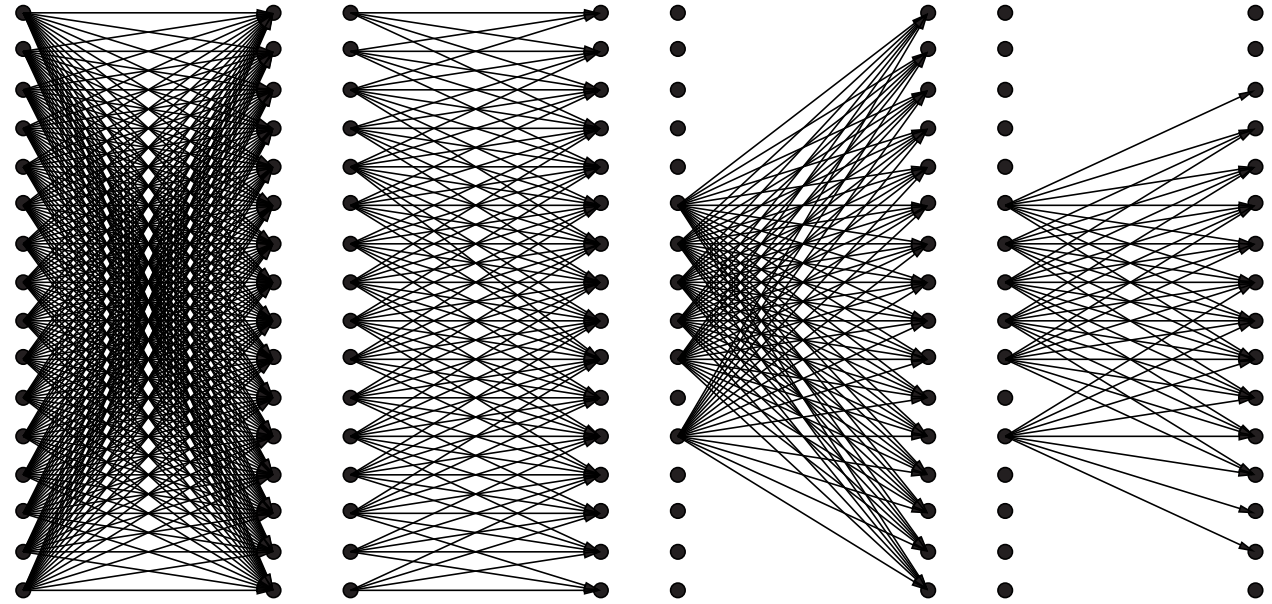

Figure 4.8: Comparison of different approaches for SDSD complexity reduction for $Q = 16$
a) full trellis representation of the SDSD with $Q^2 = 256$ state transitions
b) condition quantization with $\mathfrak{T} = 10^{-2}$ and $\mathfrak{N} = 112$ state transitions
c) trellis snapshot of M-SDSD ($M = 6$) with $Q \cdot M = 96$ state transitions
d) combined CQ and M-SDSD trellis snapshot with $\mathfrak{N}^M = 50$.

$\mathbb{M}_{t-1,k} = \{6, 7, 8, 9, 10, 12\}$ is depicted in Fig. 4.8-c). This trellis contains $MQ = 96$ transitions. Note that at the end of this transition a new set $\mathbb{M}_{t,k}$ has to selected by choosing the M best states. Further note that the backward recursion uses an even more reduced trellis (see also Fig. 4.6) with M^2 transitions. However, this is not depicted in the figure which only considers the forward recursion. Finally, Fig. 4.8-d) shows the forward recursion trellis of the combination of conditional quantization and M-SDSD. In this case, the number of transitions is further reduced to $\mathfrak{N} = 50$. Again, the backward recursion exploits a trellis containing even fewer transitions.

4.4 Comparison of Complexity Reduction Approaches

The complexity reduction achieved by employing the aforementioned algorithms can be used to increase the overall number of iterations in a system which can afford a certain given complexity. Let us consider the example introduced in Sec. 3.1.4 with a source ($N_U = 250$) according to Sec. 3.1.1, i.e., $\rho = 0.9$, $\delta = 0.9$. Quantization is performed using a $Q = 16$ level LMQ (i.e., $N_I = 250$) together with the repetition coded redundant bit mapping of rate $r_{\mathrm{BM}} = \frac{1}{2}$, i.e., $B_k = B = 8$. Channel coding is performed using the memory $J = 3$ convolutional code with $\mathbb{G}^{[\mathrm{CC}]} = \{\frac{10}{17}\}_8$. For the example, we consider conditional quantization with $\mathfrak{T} = 10^{-2}$ and M-SDSD with $M = 10$. For these given parameters we get $\mathfrak{N} = 112$ (CQ only) and $\mathfrak{N}_{\max}^{M,\alpha} = 80$, as well as $\mathfrak{N}_{\max}^{M,\beta} = 70$ (combined CQ-M-SDSD case). In order

to evaluate the overall receiver complexity, the operations to be performed by the *Maximum A Posteriori* (MAP) channel decoder also need to be taken into account. According to [RVH95], a trellis step requires $(5\cdot 2^J-2)$ $\max^\star$ operations and $10\cdot 2^J+11$ additions, with $\max^\star(\delta_1,\delta_2) \doteq \ln(\mathrm{e}^{\delta_1}+\mathrm{e}^{\delta_2}) = \max(\delta_1,\delta_2)+\ln(1+\mathrm{e}^{-|\delta_1-\delta_2|})$ [RVH95]. A detailed description of the $\max^\star$ operation along with some of its properties is given in App. F.2. If we assume that a $\max^\star$ operation requires a maximization, an addition and a (two-dimensional) table look-up, and if we assume that all operations (max, addition, look-up, multiplication) have the same complexity, then an overall number of $N_I B \cdot (25 \cdot 2^J + 5) = 410000$ operations are required for MAP channel decoding of one frame.

If AK1-INTRA SDSD is performed, the required complexity (see Table. F.3 with the complexity of a $\max^\star$ operation amounting to 3 operations as aforementioned) sums up to $N_I(8Q^2 + 6QB + 2Q + 2B) = 716000$ operations. This means that the total number of operations (channel decoding plus SDSD) amounts to $1.126 \cdot 10^6$ operations per iteration. Note that the complexity of (de-)interleaving is neglected in this example. If CQ-M-SDSD with the aforementioned parameters is employed, then (see Tab. F.9) then the complexity is upper bounded by $N_I(4\mathfrak{N}_{\max}^{M,\alpha} + 4\mathfrak{N}_{\max}^{M,\beta} + 3MB + (Q+M)(B+1) + 2B + M(Q-\frac{1}{2}(M+1))) = 298750$. The complexity of the SDSD is thus reduced by a factor of ≈ 2.4 if CQ-M-SDSD is employed. In this case, the overall complexity (source and channel decoding) amounts to $0.709 \cdot 10^6$ operations. Note that this is only an upper bound and that the actual complexity may be lower. Compared to the non-optimized case, the complexity per iteration is thus reduced by a factor of ≈ 1.59 which means that the number of iterations can be increased by a factor of 1.59 if CQ-M-SDSD is employed and if a certain overall complexity is available.

If the transmitter cannot be modified (i.e., CQ cannot be employed), then the decoding complexity reduction can be achieved by M-SDSD. In the given example, the source decoding complexity then amounts to $N_I(5QM+QB+Q+4M^2+4MB+M+2B-\frac{1}{2}M(M+1)) = 408750$ leading to a total complexity of $0.819 \cdot 10^6$ operations. Thus the complexity per iteration is reduced by a factor of 1.37 by only employing M-SDSD.

For the AK1-INTER case and $M = 6$, 424000 operations are required for the non complexity-reduced SDSD, 202750 for M-SDSD and less than 156750 for CQ-M-SDSD (as $\mathfrak{N}_{\max}^{M,\alpha} = 50$). This leads to complexity reduction factors of 1.36 for M-SDSD and 1.47 for CQ-M-SDSD if the overall receiver (channel decoder and source decoder) is considered. The source decoding complexities for both cases (AK1-INTER and AK1-INTRA) are summarized in Tab. 4.1.

Let us exemplarily assume that the given receiver setup allows us to utilize $7 \cdot 10^6$ operations per received frame. With AK1-INTER SDSD, a total number of $\Omega = 8$ iterations can be carried out while the application of M-SDSD allows us to utilize $\Omega = 11$ iterations and CQ-M-SDSD even allows $\Omega = 12$ iterations. With AK1-INTRA decoding, only $\Omega = 6$ conventional ISCD iterations can be carried out, while the application of M-SDSD allows to exploit up to $\Omega = 8$ iterations. If CQ-M-SDSD can be utilized, up to $\Omega = 9$ (almost 10) iterations can be carried out.

Variant	AK1-INTER	AK1-INTRA
Standard SDSD	424000	716000
M-SDSD	202750	408750
CQ-M-SDSD	< 156750	< 298750

Table 4.1: Source decoding operations per frame and iteration for the decoders used in the example of Fig. 4.9, $N_I = 250$, $Q = 16$, $B = 8$, $M = 6$ (AK1-INTER) or $M = 10$ (AK1-INTRA), $\mathfrak{N}_{\max}^{M,\alpha} = 50$ (AK1-INTER, $M = 6$), or $\mathfrak{N}_{\max}^{M,\alpha} = 80$ and $\mathfrak{N}_{\max}^{M,\beta} = 70$ (AK1-INTRA, $M = 10$).

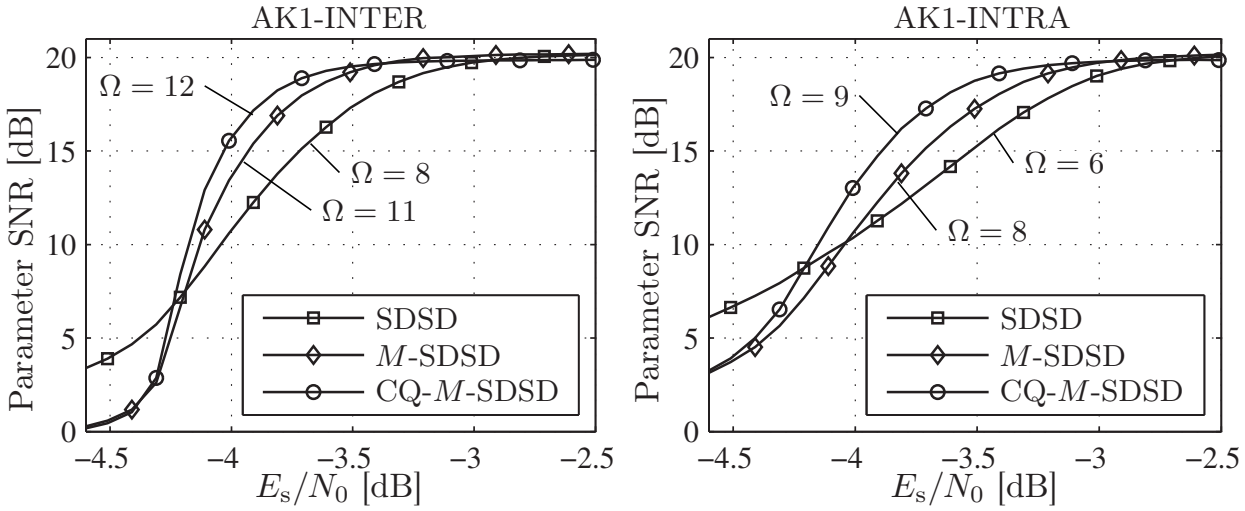

Figure 4.9: Comparison of different SDSD complexity reduction in ISCD with $\rho = 0.9$, $\delta = 0.9$, $Q = 16$ scalar LMQ, $N_I = 250$, $r_{\mathrm{BM}} = \frac{1}{2}$ repetition bit mapping, 8-state conv. code ($\mathbb{G}^{[\mathrm{CC}]} = \{\frac{10}{17}\}_8$), MMSE estimation and a total allowed amount of $7 \cdot 10^6$ operations per frame.

Figure 4.9 shows the PSNR of the proposed system if the receiver complexity is exemplarily limited to $7 \cdot 10^6$ operations per frame. In this case, the number of iterations that can be carried out with ISCD is limited to the previously computed values. It can be seen that the CQ-M-SDSD and M-SDSD algorithms outperform the pure SDSD in the most relevant range of channel conditions, as a higher number of iterations can be carried out. Note that for the given source and the complexity limitation at the receiver, it is beneficial to carry out AK1-INTER decoding at the receiver as more iterations can be carried out and the iterative receiver has not yet converged.

Note that the complexity can be further reduced by also employing a complexity-reduced channel decoder, such as the M-BCJR or T-BCJR algorithms proposed in [FA98]. However, as the focus of the present chapter is on the complexity reduction of source decoder, these approaches are not considered here.

4.5 Further Complexity Reduction Approaches

In this section, additional complexity reduction approaches are highlighted. These approaches are not explained in detail as the achievable reduction is only marginal or as they have already been sufficiently examined in the literature.

A first approach to further reduce the complexity is to replace the $\max^\star$ operation [RVH95] (see also App. F.2) in the logarithmic implementation by a simple max. This reduces the complexity of the $\max^\star$ call by a factor 3 by saving an addition and a table look-up. This approach is well known from channel decoding where it is successfully employed in the so-called *Max-Log-MAP* algorithm [RVH95, HOP96, CF02]. Besides reduced complexity, another advantage of Max-Log-MAP decoding is that the decoder is independent of the scaling of the L-values at its input, i.e., it does not require perfectly known *Channel State Information* (CSI) [RVH95, CF02]. This means that if all components of the receiver chain are realized with the Max-Log implementation, no CSI is necessary at the receiver. This fact has been exploited in [SVCS08, SVC08] to realize CSI independent ISCD. However, the decoding performance is also affected and a loss (in terms of channel quality E_s/N_0) of $\approx 0.4-0.6\,\mathrm{dB}$ in the waterfall region has to be tolerated. However, using a heuristic normalization technique [CF02, SVCS08], this loss can be somewhat reduced.

In order to reduce the complexity of the computation of $\gamma_{t,k}(q)$ (or $\tilde{\gamma}_{t,k}(q)$) and $\gamma_{t,k}^{[\mathrm{ext}]\setminus m}(q)$ (or $\tilde{\gamma}_{t,k}^{[\mathrm{ext}]\setminus m}(q)$) according to (F.2), (F.4), (F.43), (F.45), several multiplications (or additions in the logarithmic domain) can be saved by re-utilizing intermediate results. This can be interpreted by representing the set of bit mapping codewords $\mathbb{B}_k$ using a Balakirsky trellis [Bal97, BH00, Tho07c], frequently used in source decoders for ISCD with *Variable Length Codes* (VLCs). Each transition in this trellis corresponds to an operation. With the application of this trellis, the evaluation of (F.43) requires $\sum_{j=1}^{B^{[\mathrm{NB}]}} 2^j + (B_k - B^{[\mathrm{NB}]})Q$ additions instead of $B_k Q$. However, as the complexity reduction is rather small compared to the reduction potential of CQ or M-SDSD, this approach is not considered here. Moreover, the hardware implementation of the Balakirsky trellis would require additional control logic.

A MAP decoding approach for *Fixed Length Codes* (FLCs) and VLCs which reduces the SDSD complexity from $O(Q^2 N_I)$ to $O(QN_I)$ has been presented in [WDW04]. This approach is based on a fast matrix search algorithm. It is however limited to sources which have to fulfill certain monotonicity requirements and is therefore not considered here. However, the combination of this approach and the techniques introduced in this chapter permits to further reduce the complexity if the source fulfills the monotonicity requirements (which is the case for a Gauss-Markov source).

An elegant approach to reduce the complexity of the SDSD, which is especially favorable for large values of Q, is to utilize a *Soft Input Soft Output* (SISO) sequential decoder [LCC00] or variants thereof [HK07]. A sequential decoder performs a depth-first search instead of a breadth-first search [AM84], as it is performed by the SDSD based on the BCJR algorithm. The advantage of such a sequential algorithm is a very low complexity in good channel conditions with a small number of errors. However,

as soon as the channel quality degrades, the complexity of the decoder considerably increases and a breadth-first decoding behavior is approached. The complexity can be limited by an upper bound on the number of operations, however also limiting the performance in terms of reconstruction PSNR. As this non-constant amount of required operations complicates an actual implementation, a sequential decoding approach is not considered in this thesis.

4.6 Conclusions

In this chapter, several computational complexity reduction approaches of the SDSD have been discussed. The first complexity reduction approach is a transmitter-based modification of the quantizer, achieving a trade-off between quantizer distortion and receiver complexity. Depending on the source correlation, the complexity can be reduced by a certain factor if a reconstruction quality loss can be tolerated. This factor grows with the correlation of the source. Besides increasing the entropy and conditional entropy of the quantizer indices, the novel quantizer furthermore decreases the source coding related rate r_{SC}.

The computation complexity can be further reduced if known complexity reduction methods from channel decoding are applied to the SDSD. One such method is the M-algorithm, which leads to the M-SDSD if applied to the SDSD. Within the M-SDSD, the most unreliable state transitions are pruned without noticeably affecting the ISCD convergence behavior as well as the parameter reconstruction quality.

The combination of the M-SDSD with the concept of conditional quantization leads to the CQ-M-SDSD, which shows the lowest overall complexity. If the available computational resources at the receiver are constrained, these complexity-reduced versions of ISCD can lead to significant gains by increasing the number of exploitable decoding iterations. This can lead to a higher reconstruction parameter SNR over a wide range of channel conditions. Using the detailed complexity figures given in App. F.3 for all proposed SDSD variants, the exact savings and thus the additional allowable iterations can be computed.

5

Near-Lossless Source Coding Based on Iterative Source-Channel Decoding

In [MB02] and [GZ02], it has been highlighted that Turbo codes can also be used efficiently as source encoders. The compression can be near-lossless,[1] as in [MB02] and [GZ02], but there also exist approaches which modify the transmitter such that lossless compression is achieved [Düt06, DGGH06], at the expense of higher computational costs. Conventional (lossless) entropy source encoders such as Huffman codes or arithmetic codes are very sensitive to transmission errors while the Turbo source coding approach automatically incorporates error protection and can adapt to varying channel conditions by increasing or decreasing the amount of artificial redundancy introduced by the channel code. Instead of Turbo codes, *Low-Density Parity-Check* (LDPC) codes have been used as joint source-channel coding scheme in, e.g., [CSV03, FPPV10]. It will be shown in this chapter how the transmission system of Sec. 3.1 can be used for realizing a novel Turbo-like compression scheme for source codec parameters. Unlike conventional Turbo source compression [MB02, GZ02], the novel scheme performs compression on parameter level and not on bit level.

The novel source coding approach based on *Iterative Source-Channel Decoding* (ISCD) is particularly well-suited to realize a joint source-channel coding approach for state-of-the-art transform-based source codecs, such as, e.g., the *FlexCode* speech and audio codec [BGK+08b, SVC08, SSV08, SSV10] described in App. A or the JPEG2000 image codec [TM01, FC06, FC10]. These codecs all employ *Constrained Entropy Scalar Quantization* (CESQ), i.e., after applying a linear transform to the source samples, scalar uniform quantization followed by entropy coding of the quantizer indices is used. Such a source encoder achieves the rate-distortion function of a stationary and ergodic source within a bounded rate penalty [GP68, Ziv85, FC10]. However, the entropy coders used in such a scheme are frequently extremely sensitive to transmission errors. For example, the widely employed arithmetic coder [BCW90, BCK07] is unable to recover the bigger part of a frame if a single bit error occurs. In such a setup, the entropy coder can be replaced by the approach proposed in this section in order to realize an error-resilient joint-source channel coding scheme.

[1] Near-lossless means that the perfect reconstruction is not guaranteed, however, most of the symbols can be recovered with high probability.

5.1 Compression of Non-Binary Sources Using Irregular Component Codes

In this chapter, three variants of a novel concept for near-lossless compression of scalar-quantized source codec parameters are described. This concept uses a joint source-channel coding approach with ISCD at the receiver, similar to the Turbo source coding principle. The inner (channel) code of the transmitter is of rate $r_{\mathrm{CC}} \geq 1$, according to the design guidelines given in [AKtB04], [Tho07a]. If this inner (channel) code is fixed, the outer code, i.e., the redundant bit mappings of the different quantizer indices, can be matched quite well to the inner code using the principles of *Irregular Bit Mappings* (IBMs) (see Section 3.3 and [SVCS08]). This variant is described in Section 5.1.1. It is furthermore shown in Section 5.1.2 how the optimization can be modified such that the redundant bit mapping is fixed and the (inner) channel code is optimized with respect to a minimal number of encoded bits. Two competing methods for jointly optimized bit mappings and channel codes are given in Sec. 5.1.3.

All the variants presented in this section are based on the *EXtrinsic Information Transfer* (EXIT) chart technique [tB99b, tB01a, tB01c]. For this reason, the EXIT charts need to be known at the transmitter in order to adapt the system. This implies that the source statistics have to be known at the transmitter. However, as most entropy encoders, such as, e.g., the arithmetic encoder, also require the source statistics, this is usually not a problem. The *FlexCode* source encoder (see App. A) for instance models the source statistics using an *Auto Regressive* (AR) process whose parameters are transmitted over a side-channel.

Finally note that the presented approach is optimized only for sources which are either uncorrelated or which can be modeled by a Markov process of first order. Higher model orders lead to a considerably increased *Soft Decision Source Decoding* (SDSD) complexity [Fin98, FV01, Fin08].

5.1.1 Variant 1: Irregular Redundant Bit Mappings

In this section, the guideline of irregular bit mappings as introduced in Sec. 3.3 is modified such that the number of transmitted bits is minimized, leading to an efficient, flexible compression system which can easily adapt to varying channel conditions [SV09].

The task of the source encoder is to find bit mappings $\mathcal{B}_k$ that minimize the number of transmitted bits and that allow near-lossless decoding of the quantizer indices at the receiver/decoder. The approach presented here is based on the concept of *Irregular Bit Mappings* (IBMs), which extend the concept of irregular codes to the source encoder. The baseband model of the transmitter with irregular bit mappings, introduced in Sec. 3.3 is reproduced in Fig. 5.1.

The vector of quantizer indices $\mathbf{i}_t$ is partitioned into $M_{\mathcal{B}}$ sub-vectors $\mathbf{i}_t^{(j)}$, $j \in \{1, \ldots, M_{\mathcal{B}}\}$ according to $\mathbf{i}_t = (\mathbf{i}_t^{(1)}, \mathbf{i}_t^{(2)}, \ldots, \mathbf{i}_t^{(M_{\mathcal{B}})})$. Using the bit mapping $\mathcal{B}^{(j)}$,

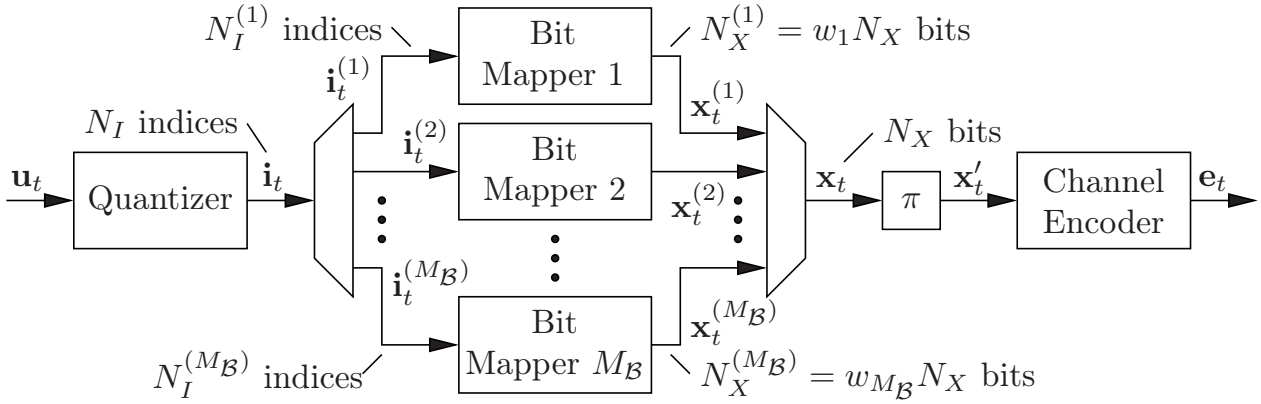

Figure 5.1: Baseband model for the transmitter of the variant with irregular bit mappings.

taken out of the set $\{\mathcal{B}^{(1)}, \ldots, \mathcal{B}^{(M_\mathcal{B})}\}$, the sub-vector $\mathbf{i}_t^{(j)}$, containing $N_I^{(j)}$ quantizer indices, is encoded to the bit vector $\mathbf{x}_t^{(j)}$ of length $N_X^{(j)}$. The overall bit vector $\mathbf{x}_t$ of size N_X is obtained according to $\mathbf{x}_t = (\mathbf{x}_t^{(1)}, \mathbf{x}_t^{(2)}, \ldots, \mathbf{x}_t^{(M_\mathcal{B})})$. We furthermore define $N_X^{(j)} = w_j N_X$, with $w_j \in [0; 1]$. As channel code, a convolutional code of rate $r_{\mathrm{CC}} > 1$ and constraint length $J + 1$, obtained by puncturing a mother code of rate $r_{\mathrm{CC,mother}} \leq 1$, is employed. The irregular bit mapping has to be optimized such that a minimum number of transmitted bits $N_E = (N_X + J)/r_{\mathrm{CC}}$ results.

Thus, the optimization goal is to find bit mappings $\mathcal{B}_k$ that minimize the number of transmitted bits N_E and thus also $N_X = N_I \cdot \bar{B}$ [SV09]. In order to perform source coding, the optimization goal is a different one than for the classical irregular bit mappings introduced in Sec. 3.3. The bit mappings which have a high rate (and thus result in a small number of output bits) shall be preferably used. The optimization goal is to find an EXIT characteristic which results in the smallest number of transmitted bits N_E with the constraint that an open decoding tunnel exists. Therefore, the weighting factors $\mathbf{w} = (w_1, w_2, \ldots w_{M_\mathcal{B}})^T$, corresponding to the $M_\mathcal{B}$ different bit mappings out of the set $\{\mathcal{B}^{(1)}, \ldots, \mathcal{B}^{(M_\mathcal{B})}\}$, have to be chosen such that the weights corresponding to high-rate bit mappings are preferred.

The number of resulting output bits after encoding a portion of $N_I^{(j)}$ indices with the bit mapping of rate $r_{\mathrm{BM}}^{(j)}$ amounts to

$$N_X^{(j)} = N_I^{(j)} \frac{B^{[\mathrm{NB}]}}{r_{\mathrm{BM}}^{(j)}} = w_j N_X \,. \tag{5.1}$$

Furthermore, the condition $\sum_{j=1}^{M_\mathcal{B}} N_I^{(j)} \stackrel{!}{=} N_I$ has to be fulfilled. Rewriting (5.1) to

$$N_X w_j r_{\mathrm{BM}}^{(j)} = B^{[\mathrm{NB}]} N_I^{(j)} \tag{5.2}$$

and summing up over all $M_\mathcal{B}$ different bit mappings leads to

$$N_X \sum_{j=1}^{M_\mathcal{B}} r_{\mathrm{BM}}^{(j)} w_j = B^{[\mathrm{NB}]} \sum_{j=1}^{M_\mathcal{B}} N_I^{(j)} \,, \tag{5.3}$$

which can be rewritten as

$$N_X \mathbf{r}_{\mathrm{BM}}^T \mathbf{w} = B^{[\mathrm{NB}]} N_I \qquad \Rightarrow \qquad N_X = \frac{B^{[\mathrm{NB}]} N_I}{\mathbf{r}_{\mathrm{BM}}^T \mathbf{w}}\,, \tag{5.4}$$

with $\mathbf{r}_{\mathrm{BM}} = (r_{\mathrm{BM}}^{(1)}, r_{\mathrm{BM}}^{(2)}, \ldots, r_{\mathrm{BM}}^{(M_{\mathcal{B}})})^T$. As N_I and $B^{[\mathrm{NB}]}$ are constant, minimizing the number of total bits N_X corresponds to maximizing $\mathbf{r}_{\mathrm{BM}}^T \mathbf{w}$. Thus, the task of optimizing the IBM such that the number of output bits N_X is minimized and decoding is still possible can be formulated as a linear programming problem with

$$\mathbf{w}_{\mathrm{opt}} = \arg\max_{\mathbf{w}} \mathbf{r}_{\mathrm{BM}}^T \mathbf{w} \tag{5.5}$$

subject to

$$\mathbf{C}_{\mathrm{SD}} \cdot \mathbf{w} > \mathbf{c}_{\mathrm{CD,inv}} + \mathbf{o}\,, \tag{5.6}$$

$$\sum_{j=1}^{M_{\mathcal{B}}} w_j = 1\,, \tag{5.7}$$

$$0 \le w_j \le 1 \qquad \forall j \in \{1, \ldots, M_{\mathcal{B}}\}\,, \tag{5.8}$$

with $\mathbf{C}_{\mathrm{SD}} = (\mathbf{c}_{\mathrm{SD}}^{(1)} \cdots \mathbf{c}_{\mathrm{SD}}^{(M_{\mathcal{B}})})$ ($\dim \mathbf{C}_{\mathrm{SD}} = \Xi \times M_{\mathcal{B}}$) being composed of sampled EXIT characteristics of each of the $M_{\mathcal{B}}$ bit mappings (Ξ sample points). The vector $\mathbf{c}_{\mathrm{CD,inv}}$ consists of Ξ sample points of the inverse channel decoder EXIT characteristic $\mathsf{C}_{\mathrm{CD}}^{-1}$, measured at the channel quality for which the optimization is carried out. The constraint (5.6) ensures that an open decoding tunnel is present. In (5.6), the vector $\mathbf{o}$ denotes an offset vector which can be chosen such that a larger open decoding tunnel is present, leading to faster convergence (and thus smaller complexity) of the receiver. In fact, the constraint $\mathbf{C}_{\mathrm{SD}} \cdot \mathbf{w} > \mathbf{c}_{\mathrm{CD,inv}}$ only guarantees an infinitely small decoding tunnel, which could only be exploited with an infinite block size ($N_I \to \infty$) and an infinite number of iterations ($\Omega \to \infty$). By an adequately chosen $\mathbf{o}$, the convergence and the decoding complexity (which linearly scales with the number of iterations) can be controlled. However, a penalty in the compression performance has to be tolerated if the decoding tunnel becomes wider, as the optimization tends to select mappings with lower rates in order to fulfill the constraint. The constraints (5.7) and (5.8) ensure that $\mathbf{w}$ contains valid weighting factors. The solution to this linear programming optimization problem can easily be found using numerical methods (see, e.g., [GMW81, GMW91, AL07a]).

After the solution of the optimization (5.5), the value N_X can be found by inserting $\mathbf{w}_{\mathrm{opt}}$ into (5.4). Using $\mathbf{w}_{\mathrm{opt}}$, the amount of indices $N_I^{(j)}$ which have to be encoded with the bit mapping $\mathcal{B}^{(j)}$ of rate $r_{\mathrm{BM}}^{(j)}$ can be determined by combining (5.1) and (5.4), leading to (with the rounding operation rnd such that $\sum_{j=1}^{M_{\mathcal{B}}} N_I^{(j)} = N_I$)

$$N_I^{(j)} = \mathrm{rnd}\left[w_{\mathrm{opt},j} \cdot r_{\mathrm{BM}}^{(j)} \cdot \frac{N_X}{B^{[\mathrm{NB}]}} \right] = \mathrm{rnd}\left[N_I \cdot \frac{w_{\mathrm{opt},j} \cdot r_{\mathrm{BM}}^{(j)}}{\mathbf{r}_{\mathrm{BM}}^T \mathbf{w}_{\mathrm{opt}}} \right]. \tag{5.9}$$

5.1.2 Variant 2: Irregular Inner Codes

In [TSV08], the concept of irregular codes has been applied to the inner channel code while utilizing a constant redundant bit mapping: This allows us to optimize the inner code to varying channel conditions and transmission scenarios. In this section, the system of [TSV08] is modified such that the number of channel encoded bits N_E is minimized while guaranteeing near-lossless reconstruction of the quantizer indices at the receiver [SV10a]. The advantage of this variant is that the optimization can easily cope with varying source properties.

As proposed in [TSV08], an irregular convolutional code of rate $r_{\mathrm{CC}} \geq 1$ is used for channel encoding of an interleaved frame $\mathbf{x}'_t$. The baseband model of the transmitter using irregular inner codes is depicted in Fig. 5.2. The interleaved bit vector $\mathbf{x}'_t$ of size N_X is partitioned into $M_{\mathcal{E}}$ different sub-frames $\mathbf{x}_t'^{(\chi)}$ according to $\mathbf{x}'_t = (\mathbf{x}_t'^{(1)}, \mathbf{x}_t'^{(2)}, \ldots, \mathbf{x}_t'^{(M_{\mathcal{E}})})$. Each sub-frame $\mathbf{x}_t'^{(\chi)}$ consisting of $N_X^{(\chi)} \doteq w_\chi N_X$ bits ($\chi \in \{1, \ldots, M_{\mathcal{E}}\}$) is individually encoded by one of the $M_{\mathcal{E}}$ dedicated channel encoders of rate $r_{\mathrm{CC}}^{(\chi)}$. Note that any channel code could be used as long as the respective decoder can generate the extrinsic information required within the ISCD loop. In this chapter, we restrict our considerations to convolutional codes. All of the convolutional codes are assumed to be zero terminated, i.e., $J^{(\chi)}$ tail bits are appended to the bit stream of each sub-frame. In this case, as the influence of eventual puncturing is not known, the length of the encoded frame approximately amounts to

$$N_E = \sum_{\chi=1}^{M_{\mathcal{E}}} N_E^{(\chi)} \approx \sum_{\chi=1}^{M_{\mathcal{E}}} \frac{N_X^{(\chi)} + J^{(\chi)}}{r_{\mathrm{CC}}^{(\chi)}} = \sum_{\chi=1}^{M_{\mathcal{E}}} \frac{w_\chi N_X + J^{(\chi)}}{r_{\mathrm{CC}}^{(\chi)}} \,. \tag{5.10}$$

The total rate of the inner irregular encoder amounts to $r_{\mathrm{CC}} = N_X/N_E = N_I \bar{B}/N_E$.

The EXIT characteristics $\mathsf{C}_{\mathrm{CD}}^{(\chi)}$ of the $M_{\mathcal{E}}$ different codes are measured for the design channel quality and sampled using Ξ sample points. The sample points are stored in the vector $\mathbf{c}_{\mathrm{CD}}^{(\chi)}$. The $M_{\mathcal{E}}$ different $\mathbf{c}_{\mathrm{CD}}^{(\chi)}$, $\chi \in \{1, \ldots, M_{\mathcal{E}}\}$ are grouped in the matrix $\mathbf{C}_{\mathrm{CD}} = \left(\mathbf{c}_{\mathrm{CD}}^{(1)} \cdots \mathbf{c}_{\mathrm{CD}}^{(M_{\mathcal{E}})}\right)$ with $\dim \mathbf{C}_{\mathrm{CD}} = \Xi \times M_{\mathcal{E}}$. Furthermore, the EXIT

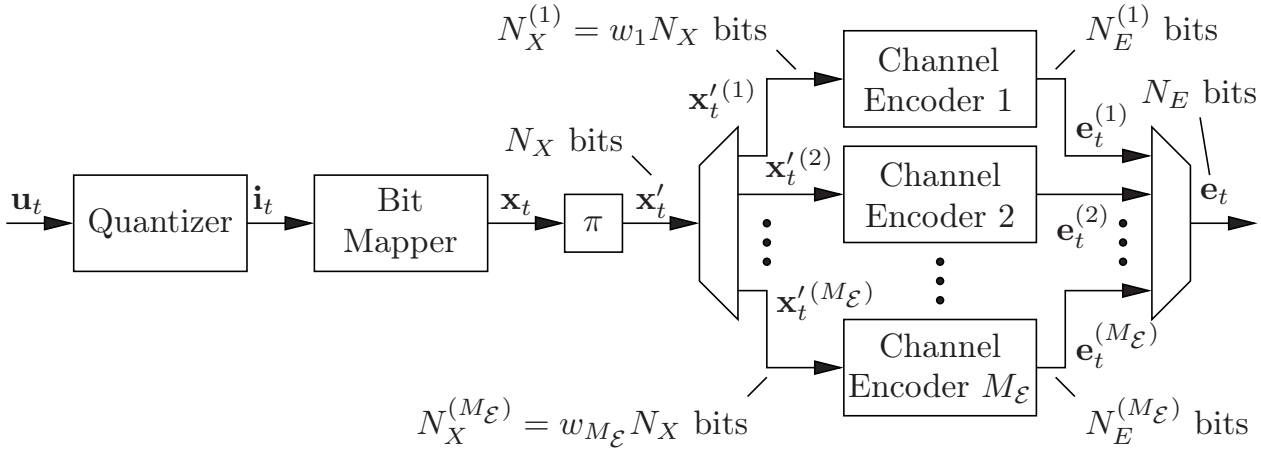

Figure 5.2: Baseband model for the transmitter of the variant with an irregular inner channel code.

characteristic C_{SD} of the SDSD is measured and Ξ sample points of its inverse $\mathsf{C}_{\mathrm{SD}}^{-1}$ are stored in the column vector $\mathbf{c}_{\mathrm{SD,inv}}$.

The optimization of the irregular inner code should deliver weights $\mathbf{w}_{\mathrm{opt}}$ which determine the amount of bits to be encoded by the $M_{\mathcal{E}}$ sub-codes. The goal of the optimization is to minimize the number of bits N_E under the constraint that the data can be recovered at the receiver (i.e., an open EXIT decoding tunnel is present). The number of bits N_E can be expressed as

$$N_E \approx \sum_{\chi=1}^{M_{\mathcal{E}}} \frac{w_\chi N_X + J^{(\chi)}}{r_{\mathrm{CC}}^{(\chi)}} = \sum_{\chi=1}^{M_{\mathcal{E}}} \frac{w_\chi N_X}{r_{\mathrm{CC}}^{(\chi)}} + \sum_{\chi=1}^{M_{\mathcal{E}}} \frac{J^{(\chi)}}{r_{\mathrm{CC}}^{(\chi)}} = N_X \cdot \tilde{\mathbf{r}}_{\mathrm{CC}}^T \mathbf{w} + \mathrm{K}_{\mathrm{term}} \tag{5.11}$$

with

$$\tilde{\mathbf{r}}_{\mathrm{CC}} \doteq \left(\frac{1}{r_{\mathrm{CC}}^{(1)}}, \quad \frac{1}{r_{\mathrm{CC}}^{(2)}}, \quad \ldots, \quad \frac{1}{r_{\mathrm{CC}}^{(M_{\mathcal{E}})}} \right)^T .$$

The constant offset $\mathrm{K}_{\mathrm{term}} = \tilde{\mathbf{r}}_{\mathrm{CC}}^T \cdot \left(J^{(1)}, J^{(2)}, \ldots, J^{(M_{\mathcal{E}})} \right)^T$ is due to the termination of the different sub-codes. Note that for performance and complexity considerations, we do not consider non-terminated and tail-biting codes [Wei01]. Minimizing N_E thus leads to the linear program

$$\mathbf{w}_{\mathrm{opt}} = \arg\min_{\mathbf{w}} \tilde{\mathbf{r}}_{\mathrm{CC}}^T \mathbf{w} \tag{5.12}$$

subject to

$$\mathbf{C}_{\mathrm{CD}} \cdot \mathbf{w} > \mathbf{c}_{\mathrm{SD,inv}} + \mathbf{o}\,, \tag{5.13}$$

$$\sum_{\chi=1}^{M_{\mathcal{E}}} w_\chi = 1\,, \tag{5.14}$$

$$0 \le w_\chi \le 1 \qquad \forall \chi \in \{1, \ldots, M_{\mathcal{E}}\}\,. \tag{5.15}$$

The solution to this linear programming optimization problem can be easily found using numerical methods (see, e.g., [GMW81, GMW91, AL07a]). The constraint (5.13) guarantees an open decoding tunnel in the EXIT chart. The vector $\mathbf{o}$ in (5.13) denotes an offset vector which can be chosen such that a larger open decoding tunnel is present. The remaining constraints ensure that $\mathbf{w}$ contains valid weighting factors.

In the case of large block lengths, $N_X \cdot \tilde{\mathbf{r}}_{\mathrm{CC}}^T \mathbf{w} \gg \mathrm{K}_{\mathrm{term}}$, and thus the effect of the termination can be neglected. However, as soon as N_X becomes smaller, the length of the compressed bit stream considerably increases with the number of utilized codes, as the constant additive term $\mathrm{K}_{\mathrm{term}} = \tilde{\mathbf{r}}_{\mathrm{CC}}^T \cdot \left(J^{(1)}, J^{(2)}, \ldots, J^{(M_{\mathcal{E}})} \right)^T$ grows with $M_{\mathcal{E}}$. Therefore, the number of bits N_E after compression can be further reduced by searching for a sparse solution of (5.12). Starting with a pool of $M_{\mathcal{E},\mathrm{total}}$ codes, all the combinations of $1 \le M_{\mathcal{E}} \le M_{\mathcal{E},\mathrm{total}}$ codes can be tried, i.e., one of the $\binom{M_{\mathcal{E},\mathrm{total}}}{M_{\mathcal{E}}}$ subsets of $M_{\mathcal{E}}$ codes is selected. The optimization is performed using this limited space of

all possible code patterns. The subset which results in the smallest N_E (if the linear program can be solved) is kept for building the actual inner code. This means that a total number of

$$\sum_{M_{\mathcal{E}}=1}^{M_{\mathcal{E},\text{total}}} \binom{M_{\mathcal{E},\text{total}}}{M_{\mathcal{E}}} = 2^{M_{\mathcal{E},\text{total}}} - 1 \tag{5.16}$$

linear programs have to be solved (full search). The expression (5.16) results from the binomial theorem $(x+y)^n = \sum_{j=0}^{n} \binom{n}{j} x^j y^{n-j}$ by setting $x = y = 1$ and $n = M_{\mathcal{E},\text{total}}$. Due to the complexity increase by the factor $2^{M_{\mathcal{E},\text{total}}} - 1$, this approach is only practical if the number $M_{\mathcal{E},\text{total}}$ is relatively small.

A different approach for finding a sparse solution without performing a full search over all sparsity patterns is to add the constraint $\|\mathbf{w}\|_0 \leq M_{\mathcal{E}}$ (with $\|\cdot\|_0$ denoting the zero norm, i.e., the number of non-zero elements of $\mathbf{w}$) to the optimization problem, to perform the optimization for each $M_{\mathcal{E}} \in \{1, \ldots, M_{\mathcal{E},\text{total}}\}$, and to retain the best overall solution. However, this constraint renders the optimization problem non-linear and non-convex and thus complicates the numerical optimization. In the following, we neglect the influence of the termination, as the proposed system with iterative decoding is known to perform best for large block lengths.

5.1.3 Variant 3: Inner and Outer Irregular Codes

Due to the shapes of the different characteristics, it can easily happen that the curve fitting is not able to generate perfectly fitting results, see for example Fig. 3.17 in Section 3.3.1. One remedy to overcome this problem is the utilization of different component codes. A different remedy is the application of inner *and* outer irregular codes, as proposed in [MH09a] for channel codes and in [MH09b] for ISCD using *Variable Length Codes* (VLCs).

Figure 5.3 depicts the relevant part of the transmitter using irregular bit mappings and an irregular channel code. This transmitter combines the irregular parts of the baseband block diagrams given in Figs. 5.1 and 5.2. The goal of the optimization is to find on the one hand the values $N_I^{(j)}$ controlling the partitioning $\mathbf{i}_t = (\mathbf{i}_t^{(1)}, \mathbf{i}_t^{(2)}, \ldots, \mathbf{i}_t^{(M_{\mathcal{B}})})$, and on the other hand the values $N_X^{(\chi)}$ controlling the partitioning $\mathbf{x}'_t = (\mathbf{x}'^{(1)}_t, \mathbf{x}'^{(2)}_t, \ldots, \mathbf{x}'^{(M_{\mathcal{E}})}_t)$, such that N_E is minimized.

Successive Matching

Maunder *et al.* propose in [MH09b] to use an iterative matching approach. First the outer component is fixed and the inner is optimized. This optimized inner component is then fixed while trying to match the outer component. This procedure is iteratively repeated several times until convergence is observed. The approach in [MH09b] uses the least squares approach of [TH02, Tüc04, SVCS08, TSV08] to optimize the EXIT chart decoding tunnel width. Furthermore, fixed rates (unity rate inner codes and

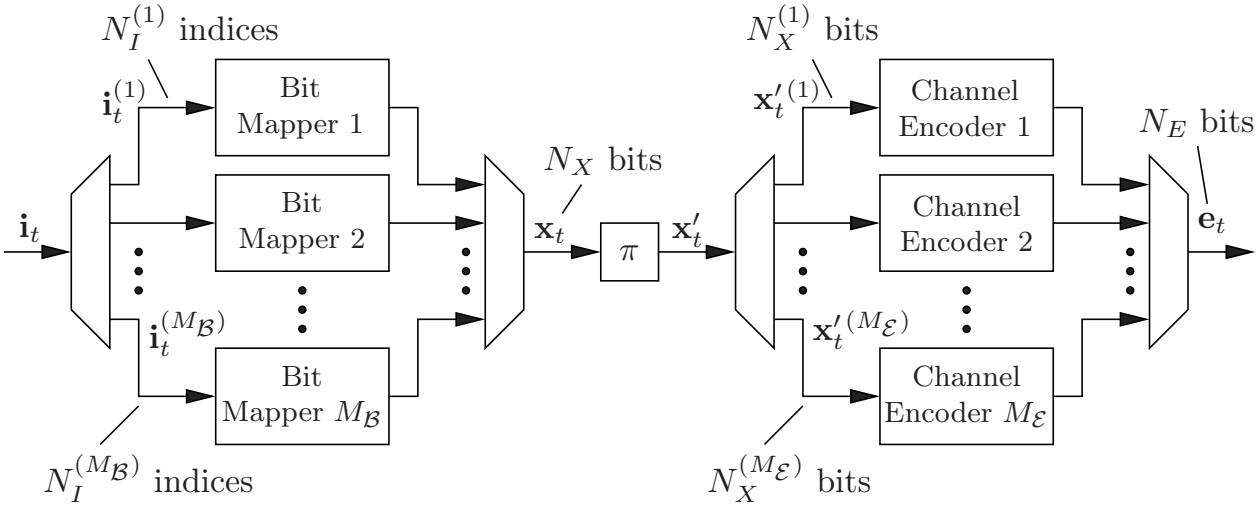

Figure 5.3: Baseband model for the transmitter of the variant with irregular bit mappings and an irregular inner channel code.

rate < 1 outer codes) are employed. This successive optimization approach can also be applied to the source coding problem by combining the algorithms of Sections 5.1.1 and 5.1.2 [SVCA10]. First, an outer irregular bit mapping is optimized according to (5.5), with $\mathbf{c}_{\mathrm{CD,inv}}$ containing Ξ sample points of the inverse of a starting inner code. Using the resulting optimized weights $\mathbf{w}_{\mathrm{BM,opt}}$, the outer EXIT characteristic is computed according to $\mathbf{C}_{\mathrm{SD}}\mathbf{w}_{\mathrm{BM,opt}}$, its inverse is interpolated and Ξ sample points of the inverse are stored in $\mathbf{c}_{\mathrm{SD,inv}}$. Using this $\mathbf{c}_{\mathrm{SD,inv}}$, the inner component is optimized according to (5.12). The resulting weights $\mathbf{w}_{\mathrm{CC,opt}}$ are used to compute the optimized inner characteristic according to $\mathbf{C}_{\mathrm{CD}}\mathbf{w}_{\mathrm{CC,opt}}$. The inverse of this new inner characteristic is interpolated and Ξ sample points are stored in $\mathbf{c}_{\mathrm{CD,inv}}$. This process is repeated until convergence is observed, i.e., if the required number of bits N_E, calculated according to (5.17) does not change significantly from one iteration to the other.

Joint Optimization of Both Components

If irregular inner and outer codes shall be used for source compression, a joint optimization, which allows to find a good matching solution in a single step, can be formulated [SVCA10]. The joint optimization of the inner and the outer component immediately follows by combining the results of Sections 5.1.1 and 5.1.2. The number of transmitted bits N_E amounts to

$$N_E \approx N_X \cdot \tilde{\mathbf{r}}_{\mathrm{CC}}^T \mathbf{w}_{\mathrm{CC}} + \mathrm{K}_{\mathrm{term}} = B^{[\mathrm{NB}]} N_I \cdot \frac{\tilde{\mathbf{r}}_{\mathrm{CC}}^T \mathbf{w}_{\mathrm{CC}}}{\mathbf{r}_{\mathrm{BM}}^T \mathbf{w}_{\mathrm{BM}}} + \mathrm{K}_{\mathrm{term}} \tag{5.17}$$

by combining (5.4) and (5.11). Minimizing (5.17) thus leads to the following constrained non-linear optimization problem

$$\mathbf{w}_{\mathrm{opt}} = \left(\mathbf{w}_{\mathrm{BM,opt}}^T \quad \mathbf{w}_{\mathrm{CC,opt}}^T\right)^T = \arg \min_{\mathbf{w}_{\mathrm{BM}}, \mathbf{w}_{\mathrm{CC}}} \frac{\tilde{\mathbf{r}}_{\mathrm{CC}}^T \mathbf{w}_{\mathrm{CC}}}{\mathbf{r}_{\mathrm{BM}}^T \mathbf{w}_{\mathrm{BM}}} \tag{5.18}$$

subject to

$$\underline{\mathcal{F}}_{\text{inv}}(\mathbf{C}_{\text{SD}} \cdot \mathbf{w}_{\text{BM}}) + \mathbf{o} < \mathbf{C}_{\text{CD}} \cdot \mathbf{w}_{\text{CC}} \tag{5.19}$$

$$0 \leq w_{\text{BM},j} \leq 1, \qquad \forall j \in \{1, \ldots, M_{\mathcal{B}}\} \tag{5.20}$$

$$0 \leq w_{\text{CC},\chi} \leq 1, \qquad \forall \chi \in \{1, \ldots, M_{\mathcal{E}}\} \tag{5.21}$$

$$\sum_{j=1}^{M_{\mathcal{B}}} w_{\text{BM},j} = 1 \quad \text{and} \quad \sum_{\chi=1}^{M_{\mathcal{E}}} w_{\text{CC},\chi} = 1\,. \tag{5.22}$$

Using the weights $\mathbf{w}_{\text{BM,opt}}$, the number of indices $N_I^{(j)}$ to be encoded with bit mapping $\mathcal{B}^{(j)}$ can be determined with (5.9). The fractions of bits (after redundant bit mapping) to be encoded by the χth channel code is immediately given by $N_X^{(\chi)} = w_{\text{CC,opt},\chi} \cdot N_X$, with N_X according to (5.4). Unfortunately, (5.18) is a non-linear problem. Furthermore, the optimization function is not necessarily convex in the general case. Additionally, the constraint (5.19) is non-linear due to the function $\underline{\mathcal{F}}_{\text{inv}}(\cdot)$. This function is necessary to determine the EXIT chart decoding tunnel. During the irregular EXIT chart optimization, the characteristics are evaluated at Ξ distinct sample points. In the approaches (5.5) and (5.12), where only one component is optimized, the sample points of the inverse characteristic $\mathsf{C}_{\text{CD/SD}}^{-1}$ (at the same positions as for the respective other component) are interpolated prior to the optimization. The results are stored in the vector $\mathbf{c}_{\text{CD/SD,inv}}$. In the joint optimization case, however, precomputing the interpolated characteristic is not possible as both components are jointly optimized. This leads to the modified non-linear constraint (5.19), where the function $\underline{\mathcal{F}}_{\text{inv}}$ computes the Ξ sample points of the inverse characteristic at the specific distinct locations by interpolation. Note that the inverse always exists, as EXIT characteristics are monotonically increasing continuous functions [tB01c, AKtB04].

The numerical solution of the problem (5.18)-(5.22) can be found for example using an active-set *Sequential Quadratic Programming* (SQP) algorithm [Mur88, CPS92], which uses a quasi Newton approximation to the Hessian of the Lagrangian [NW06, AL07a]. Solvers for such optimization problems can be found in a variety of commercial and non-commercial software packages for numerical optimization.

5.2 Simulation Examples

The capabilities of the proposed techniques shall be illustrated by means of simulation examples. For reasons of reproducibility, we utilize the source model given in Sec. 3.1.1 with $\rho = 0$ and $\delta = 0.9$. The transmitter uses a $Q = 16$ level scalar *Lloyd-Max Quantizer* (LMQ) [Max60, Llo82]. The irregular bit mappings are based on the mother generator matrix already utilized in [SVCS08, SVCA10], with

$$\mathbf{G}_{\text{mother},4}^{[\text{BM}]} = \begin{pmatrix} 1\,0\,0\,0\,1\,1\,1\,1\,0\,1\,1\,1\,0\,0\,0 \\ 0\,1\,0\,0\,1\,1\,1\,0\,1\,0\,0\,1\,1\,1\,0 \\ 0\,0\,1\,0\,1\,1\,0\,1\,1\,0\,1\,0\,1\,0\,1 \\ 0\,0\,0\,1\,1\,0\,1\,1\,1\,1\,0\,0\,0\,1\,1 \end{pmatrix}. \tag{5.23}$$

χ	$r_{\mathrm{CC}}^{(\chi)}$	Doping ratio	Puncturing matrix $\mathbf{G}_{\mathrm{punc}}$
1	1.25	1 : 40 or 1 : 25	(1 1 1 1 0)
2	1.5	1 : 40 or 1 : 25	(1 1 0)
3	1.75	1 : 40 or 1 : 25	(1 1 0 1 0 1 0)
4	2	1 : 40 or 1 : 25	(1 0 1 0)
5	2.5	1 : 40 or 1 : 25	(1 0 1 0 0)
6	3	1 : 40 or 1 : 25	(1 0 0)
7	3.5	1 : 40 or 1 : 25	(1 0 0 1 0 0 0)
8	4	1 : 40 or 1 : 25	(1 0 0 0 0 0 1 0)
9	5	1 : 40 or 1 : 25	(1 0 0 0 0)
10	6	1 : 40 or 1 : 25	(1 0 0 0 0 0)
11	8	1 : 40 or 1 : 25	(1 0 0 0 0 0 1 0 0 0 0 0 0 0 0 0)
12	10	1 : 40 or 1 : 25	(1 0 0 0 0 0 0 0 0 0)

Table 5.1: Rates and puncturing matrices $\mathbf{G}_{\mathrm{punc}}$ of the utilized convolutional codes based on an RNSC mother code of memory $J = 3$, rate $r_{\mathrm{CC}} = 1$, and octal generator $\mathbb{G}^{[\mathrm{CC}]} = \left\{\frac{10}{17}\right\}_8$.

The matrix $\mathbf{G}_{\mathrm{mother},4}^{[\mathrm{BM}]}$ with $\dim \mathbf{G}_{\mathrm{mother},4}^{[\mathrm{BM}]} = 4 \times 15$ is able to generate $M_{\mathcal{B}} = 11$ different bit mappings $\mathcal{B}^{(j)}$ of rates $r_{\mathrm{BM}}^{(j)} = 4/(4+j)$, $\forall j \in \{1, \ldots, M_{\mathcal{B}} = 11\}$. The different mappings $\mathcal{B}^{(j)}$ are generated by using the first $j+4$ columns of $\mathbf{G}_{\mathrm{mother},4}^{[\mathrm{BM}]}$.

Example: The quantizer index $i = 13$ shall be encoded by the bit mapping $\mathcal{B}^{(5)}$ of rate $r_{\mathrm{BM}}^{(5)} = \frac{4}{4+5} = \frac{4}{9}$, generated using $\mathbf{G}_{\mathrm{mother}}^{[\mathrm{BM}]}$. The generator matrix $\mathbf{G}^{[\mathrm{BM}](5)}$ is obtained by using the first $5+4=9$ columns of $\mathbf{G}_{\mathrm{mother}}^{[\mathrm{BM}]}$, i.e.,

$$\mathbf{G}^{[\mathrm{BM}](5)} = \begin{pmatrix} 1\,0\,0\,0\,1\,1\,1\,1\,0 \\ 0\,1\,0\,0\,1\,1\,1\,0\,1 \\ 0\,0\,1\,0\,1\,1\,0\,1\,1 \\ 0\,0\,0\,1\,1\,0\,1\,1\,1 \end{pmatrix}. \tag{5.24}$$

The natural binary representation of $i = 13$ (with $B^{[\mathrm{NB}]} = 4$) corresponds to $\mathbf{b}^{[\mathrm{NB}]} = (1\ 1\ 0\ 1)$, leading to $\mathbf{b} = \mathbf{b}^{[\mathrm{NB}]} \cdot \mathbf{G}^{[\mathrm{BM}](3)} = (1\ 1\ 0\ 1\ 1\ 0\ 1\ 0\ 0)$.

As due to varying source conditions the amount of bits N_X after source coding may vary, an interleaver which can cope with varying block lengths is required. In this work, we employ *prunable* S-random interleavers according to [FSB02] (see also [SVC08] for a detailed description of this interleaver class). Other prunable interleavers are given in [EH99, TDB07, DB05a, DB05b]. The inner irregular channel code is based on $M_{\mathcal{E},\mathrm{total}} = 12$ codes derived from the mother code with octal generator $\mathbb{G}^{[\mathrm{CC}]} = \left\{\frac{10}{17}\right\}_8$ ($J = 3$), already used in Sec 3.1. The utilized puncturing matrices (selected such that $\mathsf{I}_{\mathrm{CD}}^{[\mathrm{ext}]} = 1$ for $\mathsf{I}_{\mathrm{CD}}^{[\mathrm{apr}]} = 1$) are summarized in Tab. 5.1. As these punctured codes cannot directly be used for iterative decoding (as for $\mathsf{I}_{\mathrm{CD}}^{[\mathrm{apr}]} = 0$, $\mathsf{I}_{\mathrm{CD}}^{[\mathrm{ext}]} = 0$ results for rates $r_{\mathrm{CC}}^{(\chi)} > 1$, which signifies that the iterative decoding process cannot be triggered), the technique of *code doping* [tB00a, tB01b] is utilized. The doping ratio is selected to be either 1 : 40 or 1 : 25, which means that every 40th (or 25th) parity bit is replaced by a systematic bit.

Evaluation of the EXIT Chart Matching Performance

Figure 5.4 contains EXIT chart examples of the outer and inner optimizations introduced in Secs. 5.1.1 and 5.1.2 for the given source setup. The channel is assumed to be perfect, i.e., $E_s/N_0 \to \infty$, simulating a pure storage (no error) scenario. In Fig. 5.4-a), the optimization using irregular bit mappings (and a regular channel code) is shown. The utilized convolutional code is the rate $r_{\mathrm{CC}}^{(4)} = 2$ code given by Tab. 5.1. Additionally, the $M_{\mathcal{B}} = 11$ distinct characteristics of the bit mappings (with rates ranging from $r_{\mathrm{BM}}^{(1)} = \frac{4}{5}$ to $r_{\mathrm{BM}}^{(M_{\mathcal{B}})} = \frac{4}{15}$) are depicted. The optimization is carried out by solving the linear program derived in Sec. 5.1.1. The outcome of the optimization is summarized in Tab. 5.2. Besides the weights w_j, the normalized values $N_I^{(j)}/N_I$, with $N_I^{(j)}$ computed according to (5.9), are given, which are required for setting up the transmitter. If for example $N_I = 5000$, then $N_I^{(1)} = 3401$, $N_I^{(2)} = 1594$, and $N_I^{(11)} = 5$ by appropriate rounding. It can be seen that the optimization leads to a well matching characteristic $\mathsf{C}_{\mathrm{SD,irr}}$, requiring (theoretically) $N_E/N_I = 2.6642$ bit per quantizer index while the conditional quantizer index entropy (which describes the theoretical limit) amounts to $\mathsf{H}(I_t|I_{t-1}) = 2.6200$ bit. Note however that near-lossless compression with $\mathsf{H}(I_t|I_{t-1})$ bit per index can only be achieved asymptotically for infinite block lengths and an infinite number of iterations.

Figure 5.4-b) depicts the $M_{\mathcal{E}} = 12$ different characteristics of the considered $r_{\mathrm{CC}} > 1$ convolutional codes as well as the SDSD characteristic $\mathsf{C}_{\mathrm{SD}}^{(1)}$ of the rate $r_{\mathrm{BM}}^{(1)} = 4/5$ bit mapping (generated using the 5 first columns of $\mathbf{G}_{\mathrm{mother},4}^{[\mathrm{BM}]}$). The outcome of the

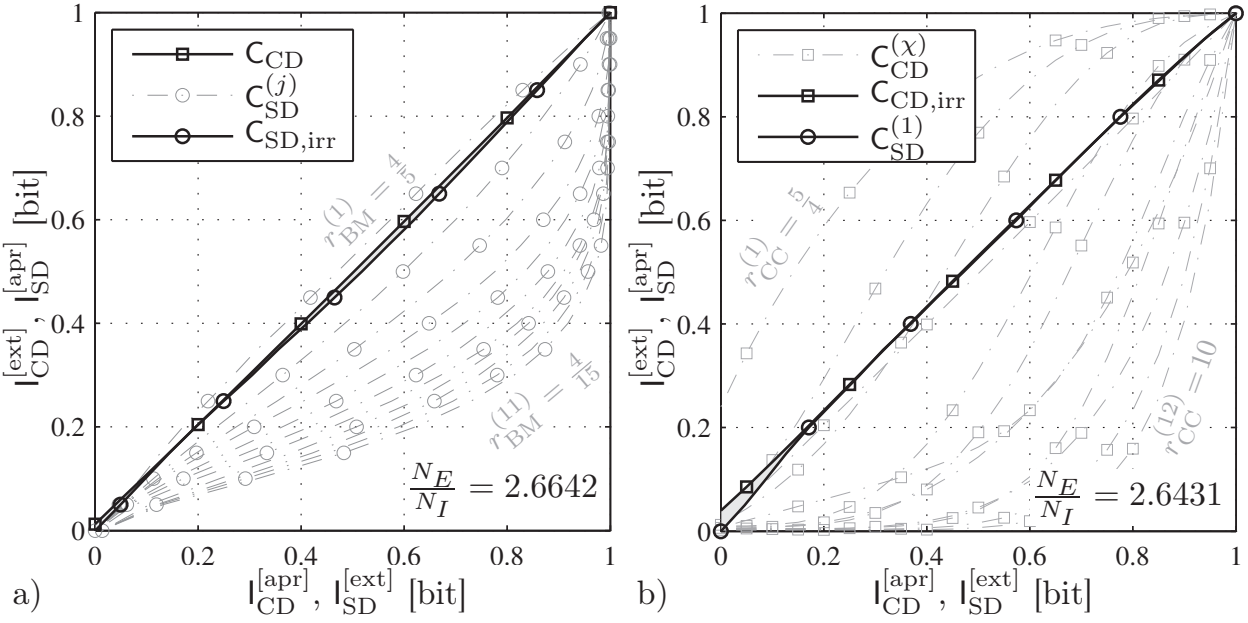

Figure 5.4: EXIT chart example for irregular bit mappings built using (5.23) and irregular inner convolutional codes according to Tab. 5.1, $\rho = 0$, $\delta = 0.9$, $Q = 16$-LMQ, AK1-INTRA decoding, no transmission errors, i.e., $E_s/N_0 \to \infty$.
a) Irregular bit mapping, regular channel code, according to Tab. 5.2.
b) Reggular bit mapping, irregular channel code according to Tab. 5.3.

j	1	2	11
$r_{\mathrm{BM}}^{(j)}$	$\frac{4}{5}$	$\frac{4}{6}$	$\frac{4}{15}$
w_j	0.6384	0.3589	0.0027
$N_I^{(j)}/N_I$	0.6803	0.3187	0.0010

Table 5.2: Irregular bit mapping built using (5.23) for $\rho = 0$, $\delta = 0.9$, $Q = 16$-LMQ, AK1-INTRA decoding, convolutional code of rate $r_{\mathrm{CC}}^{(4)} = 2$ given by Tab. 5.1, no transmission errors ($E_{\mathrm{s}}/N_0 \to \infty$). Only the non-zero w_j are given for clarity.

χ	1	2	4	6	9
$r_{\mathrm{CC}}^{(\chi)}$	1.25	1.5	2	3	5
w_χ	0.1063	0.1708	0.5800	0.0836	0.0593

Table 5.3: Irregular inner convolutional code built using the codes of Tab. 5.1 for $\rho = 0$, $\delta = 0.9$, $Q = 16$ LMQ, single parity check BM of rate $r_{\mathrm{BM}}^{(1)} = \frac{4}{5}$, no transmission errors ($E_{\mathrm{s}}/N_0 \to \infty$), AK1-INTRA. Only the non-zero w_χ are given for clarity.

Irregular bit mapping

j	1	2	7	11
$r_{\mathrm{BM}}^{(j)}$	$\frac{4}{5}$	$\frac{4}{6}$	$\frac{4}{11}$	$\frac{4}{15}$
$w_{\mathrm{BM},j}$	0.5614	0.1735	0.1113	0.1538
$N_I^{(j)}/N_I$	0.6960	0.1800	0.0600	0.0640

Irregular convolutional code

χ	4	5	6	8	9
$r_{\mathrm{CC}}^{(\chi)}$	2	2.5	3	4	5
$w_{\mathrm{CC},\chi}$	0.6634	0.0649	0.0630	0.0353	0.1734

Table 5.4: Jointly optimized irregular bit mapping built using (5.23) and irregular convolutional code using the component codes of Tab. 5.1 for $\rho = 0$, $\delta = 0.9$, $Q = 16$ LMQ, AK1-INTRA, no transmission errors ($E_{\mathrm{s}}/N_0 \to \infty$), zero offset vector $\mathbf{o} = \mathbf{0}_{\Xi\times 1}$. Only the non-zero $w_{\mathrm{BM},j}$ and $w_{\mathrm{CC},\chi}$ are given for clarity.

optimization obtained by solving the linear program derived in Sec. 5.1.2 is given in Tab. 5.3. Using the weights w_χ, the portions the number of bits $N_X^{(\chi)}$ to be encoded by the χth convolutional code are given by $N_X^{(\chi)} = w_\chi N_X = w_\chi N_I B = 5 \cdot w_\chi N_I$. The resulting matched characteristic $\mathsf{C}_{\mathrm{CD,irr}}$ is also shown in Fig. 5.4-b). It can be seen that both characteristics match reasonably well, leaving only a small decoding tunnel. The resulting system leads to $N_E/N_I = 2.6431\,\mathrm{bit/index}$, i.e., the system employing irregular bit mappings is slightly outperformed.

Figure 5.5 depicts an exemplary EXIT chart showing both the characteristics of the $M_{\mathcal{B}} = 11$ different constituent bit mappings and of the $M_{\mathcal{E}} = 12$ different convolutional codes summarized in Tab. 5.1. Additionally, the resulting irregular inner and outer characteristics obtained by the joint optimization introduced in Sec. 5.1.3 are given. Figure 5.5-a) shows the result using a zero offset vector $\mathbf{o} = \mathbf{0}_{\Xi\times 1}$. The components of $\mathbf{w}_{\mathrm{CC}}$ and $\mathbf{w}_{\mathrm{BM}}$, as well as the values $N_I^{(j)}$, necessary for setting up the transmitter, are summarized in Tab. 5.4. It can be seen that both irregular EXIT curves match quite well and an extremely narrow decoding tunnel is present resulting

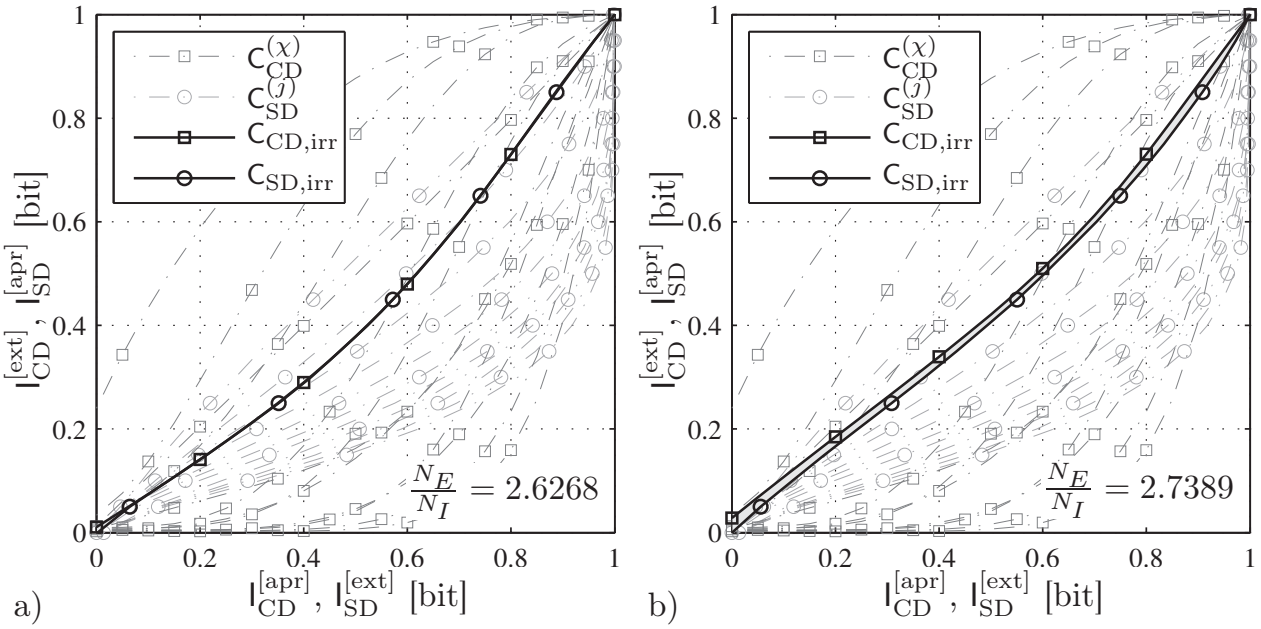

Figure 5.5: EXIT chart example for irregular bit mappings built using (5.23) and irregular inner convolutional codes according to Tab. 5.1, $\rho = 0$, $\delta = 0.9$, $Q = 16$ LMQ, AK1-INTRA decoding, no transmission errors, i.e., $E_s/N_0 \to \infty$. Joint optimization according to Sec. 5.1.3.
a) Zero offset vector $\mathbf{o} = \mathbf{0}_{\Xi \times 1}$ (Tab. 5.4)
b) Decoding tunnel control with a non-zero offset vector $\mathbf{o}$ (Tab. 5.5)

Irregular bit mapping			
j	1	2	11
$r_{\mathrm{BM}}^{(j)}$	$\frac{4}{5}$	$\frac{4}{6}$	$\frac{4}{15}$
$w_{\mathrm{BM},j}$	0.0165	0.9615	0.0220
$N_I^{(j)}/N_I$	0.0200	0.9720	0.0080

Irregular convolutional code				
χ	1	4	8	9
$r_{\mathrm{CC}}^{(\chi)}$	1.25	2	4	5
$w_{\mathrm{CC},\chi}$	0.0773	0.6697	0.0933	0.1597

Table 5.5: Jointly optimized irregular bit mapping built using (5.23) and irregular convolutional code using the component codes of Tab. 5.1 for $\rho = 0$, $\delta = 0.9$, $Q = 16$ LMQ, AK1-INTRA, no transmission errors ($E_s/N_0 \to \infty$), non-zero offset vector $\mathbf{o}$. Only the non-zero $w_{\mathrm{BM},j}$ and $w_{\mathrm{CC},\chi}$ are given for clarity.

in an almost perfect (ideal) compression. In fact, this example setup would result in a total number of $N_E/N_I = 2.6268\,\mathrm{bit/index}$ (computed using (5.17)), thus outperforming the systems with a single irregular component. Figure 5.5-b) depicts the outcome of the optimization with a non-zero offset vector $\mathbf{o}$, selected such that the width of the decoding tunnel (in vertical direction) should be 0.02. Again, the components of $\mathbf{w}_{\mathrm{CC}}$ and $\mathbf{w}_{\mathrm{BM}}$, as well as the values $N_I^{(j)}$, are summarized in Tab. 5.5. The selection of a non-zero offset vector sacrifices the overall performance such that now $N_E/N_I = 2.7389\,\mathrm{bit/index}$ are used. If perfect interleaving is assumed, i.e., if the decoding trajectory can fully exploit the decoding tunnel, then $\Omega \approx 60$ iterations are required in this case to reach the $(1, 1)$ point in the EXIT chart.

E_s/N_0	theoretical optimum (BPSK)	irregular BM only	irregular CC only	jointly opt. irregular BM and CC	successive irregular BM and CC
$\to \infty$	2.6200	2.6642	2.6431	2.6268	**2.6221**
7 dB	2.6284	2.6740	2.6525	**2.6362**	2.6397
5 dB	2.6835	2.7317	2.7093	**2.6902**	2.6940
3 dB	2.8721	2.9002	2.9064	**2.8767**	2.8818
2 dB	3.0477	3.0634	3.0978	**3.0502**	3.0553
1 dB	3.2931	3.3032	3.3536	**3.2968**	3.3027
0 dB	3.6310	3.6421	3.7057	**3.6326**	3.6363

Table 5.6: Bits/index ($Q = 16$ LMQ, $\rho = 0$, $\delta = 0.9$) required for an open decoding tunnel (decoding threshold) at different channel conditions E_s/N_0.
$\mathsf{H}(I_t|I_{t-1}) = 2.62$ (reference for $E_s/N_0 \to \infty$)

Table 5.6 shows the necessary number of bits/index at the decoding threshold for the three previously introduced systems at different channel qualities E_s/N_0. The theoretical optimum is obtained by dividing the conditional entropy $\mathsf{H}(I_t|I_{t-1})$ by the capacity $\mathsf{I}_\mathcal{C} \in [0; 1]$ of the *Binary Phase Shift Keying* (BPSK) channel [Sha48, LC04, Moo05], i.e., $\mathsf{H}(I_t|I_{t-1})/\mathsf{I}_\mathcal{C}$. This can be explained as follows: $\mathsf{H}(I_t|I_{t-1})$ data bits are required to transmit a quantizer index, however, the channel can only effectively transmit $\mathsf{I}_\mathcal{C}$ bits per channel use, i.e., $\mathsf{H}(I_t|I_{t-1})/\mathsf{I}_\mathcal{C}$ channel uses are required. In the BPSK case, a channel use corresponds to a channel encoded bit.

If both irregular inner and outer codes are employed, the estimated number of bits required for coding is always the lowest. The joint optimization of Sec. 5.1.3 also always outperforms the successive optimization approach presented in Sec. 5.1.3, except for $E_s/N_0 \to \infty$. The results in Tab. 5.6 confirm that employing irregular bit mappings and inner channel codes leads to the best compression for the given setup. Note that the optimization has been performed with $\mathbf{o} = (0, \ldots, 0)^T$ for obtaining the numbers in Tab. 5.6, resulting (theoretically) in an infinitesimally small EXIT tunnel. In this case, convergence can only be achieved for $N_I \to \infty$ and for $\Omega \to \infty$. For practical systems, an offset vector has to be chosen, such that a wider tunnel is obtained. It has also been found that the successive optimization is quite sensitive to the starting point (i.e., the initial $\mathbf{c}_{\mathrm{CD,inv}}$), which means that the optimization should be performed using different starting values to overcome this influence.

In [SV10a] and [SVCA10], additional examples employing *Randomly Punctured Recursive Systematic Convolutional* (RPRSC) codes have been presented, showing similar results. RPRSC codes have been introduced in [Tho07a, Tho07c, TSV08] and consist of a rate < 1 *Recursive Systematic Convolutional* (RSC) code punctured with a (pseudo) random puncturing matrix to a resulting rate $r_{\mathrm{CC}}^{(\chi)}$. Besides their final rate, they are also characterized by the fraction $\mathsf{P}_{\mathrm{sys}}^{(\chi)}$ of punctured systematic bits. Using $\mathsf{P}_{\mathrm{sys}}^{(\chi)}$ and $r_{\mathrm{CC}}^{(\chi)}$, the fraction of punctured non-systematic bits can be computed and the puncturing can be performed using a Bernoulli pseudo-random number generator [Tho07a]. One advantage of RPRSC codes is that their EXIT characteristic can

easily be computed from the characteristic of the mother code [Tho07b]. In [SVCA10], an additional example with modified system settings ($Q = 32$ LMQ, i.e., $B^{[\mathrm{NB}]} = 5$, together with a non-correlated source, i.e., $\rho = 0$, $\delta = 0$) shows the applicability of the proposed variants to different source settings.

Finally, it has to be noticed that the first two variants presented in Secs. 5.1.1 and 5.1.2 (i.e., the systems with only a single irregular component) can also lead to results comparable with those of the joint optimization. However, great care has to be taken for the selection of the regular component, such that the matching algorithms can find a reasonable result. In the third variant with two irregular components, finding good matching characteristics is easier, as the search space is increased by the larger set of possible codes. For finite E_s/N_0, the proposed concept does not only perform compression, but minimizes the number of bits necessary for successful transmission.

Residual Symbol Error Rate for Compression

In the first simulation example, the compression performance shall be compared with existing schemes. The source according to Sec. 3.1.1 emits samples with intra-frame correlation ($\rho = 0$, $\delta = 0.9$) which are quantized by a $Q = 16$ LMQ. According to Tab. 5.6, theoretically 2.6200 bit per quantizer index can be reached by the compression. As it has been found in the previous section and in [SVCA10] that the system with jointly optimized inner and outer component yields the best compression performance, only that system is considered and adapted by choosing different offset vectors $\mathbf{o}$, such that the number of bits per index N_E/N_I varies. The resulting parameters for setting up the transmitter (and the receiver) are given in App. H.

The *Symbol Error Rate* (SER) results of the different setups with $N_I \in \{1000, 5000, 10000\}$ and $\Omega \in \{10, 25, 75\}$ are given in Fig. 5.6. As comparison serve different state-of-the-art lossless entropy coding schemes. The first comparison scheme uses a Huffman code [Huf52] grouping $m = 2$ consecutive quantizer indices, thus resulting in an alphabet size of 256 and in $N_E/N_I = 3.2113$. Besides Huffman codes, arithmetic codes [BCW90, BCK07], which are known to outperform Huffman codes, are utilized. In order to exploit the intra-frame correlation, $m \in \{2, 3, 4\}$ consecutive quantizer indices are grouped, leading to alphabet sizes of 256, 4096, or 65536, respectively. The required number of bits per quantizer index amounts to $N_E/N_I = 3.1945$ ($m = 2$), $N_E/N_I = 3.0092$ ($m = 3$), or $N_E/N_I = 2.9396$ ($m = 4$) in that case. Finally, the *gzip* [GA03] and the *bzip2* [Sew08, SM09] compression programs have been used for comparison. The *gzip* algorithm essentially utilizes the *Lempel-Ziv* scheme [ZL77] and leads to $N_E/N_I = 3.18079$, while the *bzip2* algorithm combines a *Burrows-Wheeler transform* [BW94], a *move-to-front transform* [BSTW86], and Huffman coding [Huf52]. A total number of $N_E/N_I = 2.85493$ bits per quantizer index are required in the case of *bzip2* compression.

The simulation results indicate that for the given setup, the proposed approach is able to outperform arithmetic coding with $m = 4$ for $N_I \geq 5000$ and $\Omega > 25$ iterations. For $\Omega = 75$ iterations, even the *bzip2* algorithm is outperformed with a sufficiently large block length $N_I \geq 5000$, if a target SER of 10^{-5} is allowed. If the required target SER

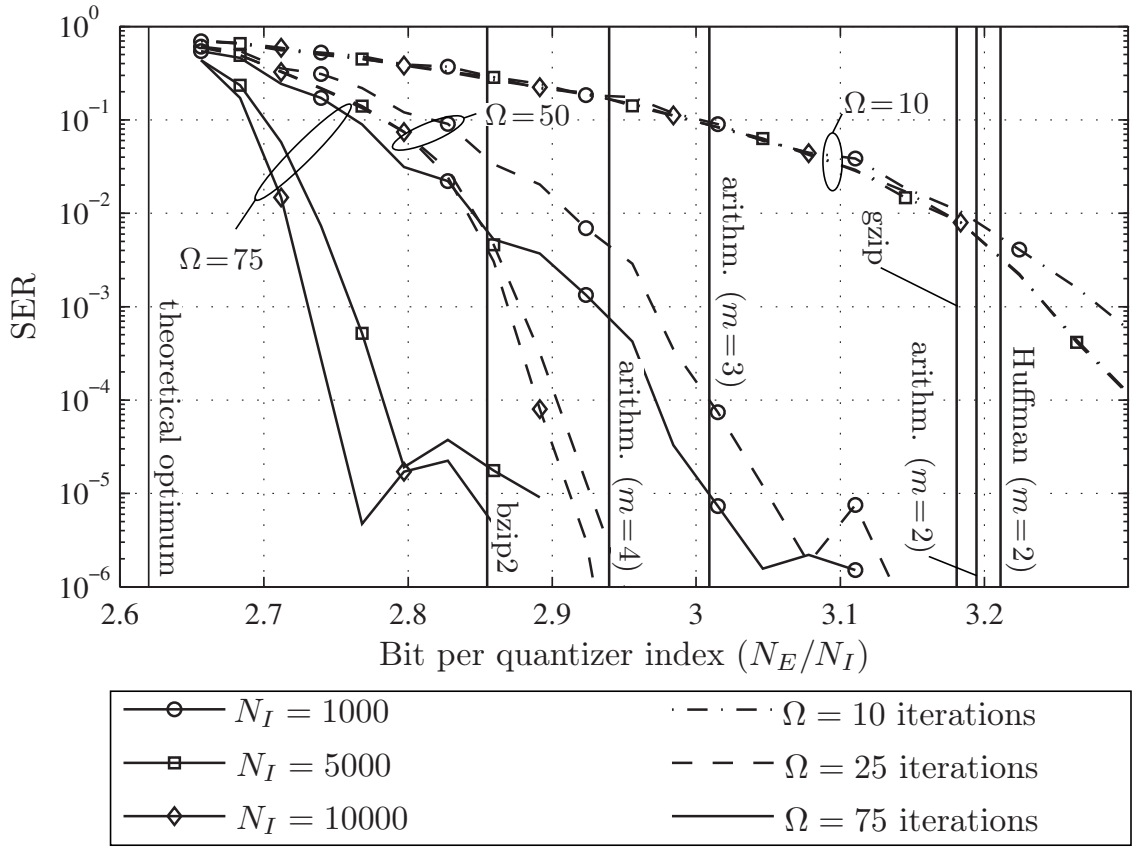

Figure 5.6: SER performance of the jointly optimized inner irregular and outer irregular scheme in a compression scenario ($E_s/N_0 \to \infty$) for $N_I \in \{1000, 5000, 10000\}$ and $\Omega \in \{10, 25, 75\}$ for a source with $\rho = 0$, $\delta = 0.9$, $Q = 16$ LMQ, AK1-INTRA decoding, as a function of the number of bits per quantizer index (resulting from varying offset vectors $\mathbf{o}$).

is larger (as is usually the case in multimedia transmission, like speech and audio), even a better performance can be achieved. In the case of small frame sizes, such as $N_I = 1000$, there is already a considerable loss compared to $N_I \in \{5000, 10000\}$. For example, a loss of ≈ 0.2 bit per index has to be tolerated for $\Omega = 75$ iterations at a target SER of 10^{-4}. The reason for the non-monotonic behavior of the results is that for different $\mathbf{o}$, the optimizer selects a different set of bit mappings and channel codes. As seen in Sec. 3.4, the error floor behavior is strongly dependent on the selected codes. Thus, a different offset vector $\mathbf{o}$ leads to a different setup and thus to a different error floor behavior.

Finally note that if inter-frame correlation is available and the AK1-INTER or the AK1-NOPT algorithm can be used, the convergence will be faster due to the overshooting effect discussed in Sec. 3.1.6, however, the overall performance (in terms of achievable bits per index) will be worse due to the suboptimality of the decoder.

Joint Compression-Protection Performance

In order to evaluate the performance of the different optimization variants presented in Sec. 5.1 in the presence of channel noise, the following scenario is considered. The

	bit mapping parameters				channel code parameters		
	irr. BM $N_I^{(j)}$	irr. CC $N_I^{(j)}$	joint opt. $N_I^{(j)}$		irr. BM $N_X^{(\chi)}$	irr. CC $N_X^{(\chi)}$	joint opt. $N_X^{(\chi)}$
$r_{\mathrm{BM}}^{(j)} = \frac{4}{5}$		1000		$r_{\mathrm{CC}}^{(\chi)} = 1.25$		2100	2966
$r_{\mathrm{BM}}^{(j)} = \frac{4}{6}$	293		658	$r_{\mathrm{CC}}^{(\chi)} = 1.5$		2761	
$r_{\mathrm{BM}}^{(j)} = \frac{4}{7}$	646		342	$r_{\mathrm{CC}}^{(\chi)} = 1.75$		139	
$r_{\mathrm{BM}}^{(j)} = \frac{4}{15}$	61			$r_{\mathrm{CC}}^{(\chi)} = 2$	7195		1127
				$r_{\mathrm{CC}}^{(\chi)} = 3$			445
				$r_{\mathrm{CC}}^{(\chi)} = 3.5$			1804

Table 5.7: Setup ($N_I^{(j)}$ and $N_X^{(\chi)}$) of the three irregular systems (irregular bit mapping only (irr. BM), irregular channel code only (irr. CC), jointly optimized irregular bit mapping and channel code (joint opt.)) used in the simulation results of Fig. 5.7 for $N_I = 1000$. Optimization performed for $E_\mathrm{s}/N_0 = 1\,\mathrm{dB}$.

source setting introduced in the previous paragraph is used ($\rho = 0$, $\delta = 0.9$, $Q = 16$ LMQ). The quantizer indices shall be compressed while tolerating channel noise with $E_\mathrm{s}/N_0 > 1\,\mathrm{dB}$. According to Tab. 5.6, theoretically 3.2931 bits per quantizer index have to be used. In order to get a decoding tunnel which is not infinitely narrow, the offset vector $\mathbf{o}$ in all three different optimizations[2] is selected such that $N_E/N_I \approx 3.6\,\mathrm{bit}$ results. The doping ratio has been selected to $1:25$ (instead of $1:40$) for an easier triggering of the iterative decoding process.

The results of the optimization performed according to Secs. 5.1.1, 5.1.2, and 5.1.3 are given in Tab. 5.7. The number of indices $N_I^{(j)}$ to be encoded with the jth bit mapping (obtained using (5.9)) as well as the number of bits $N_X^{(\chi)}$ to be encoded by the χth convolutional encoder (obtained according to $N_X^{(\chi)} = w_{\mathrm{CC,opt},\chi} N_X$) are given for $N_I = 1000$. Note that the codes not indicated in Tab. 5.7 have not been selected by the optimizer.

SER results for the given setup are depicted in Fig. 5.7 for $N_I \in \{1000, 10000\}$ and for $\Omega \in \{10, 75\}$ iterations. The target E_s/N_0 of 1 dB, below which a successful transmission is not guaranteed, is indicated by the vertical line. It can be seen that for $N_I = 1000$ (left sub-plot of Fig. 5.7), a residual SER of ≈ 0.03 results at $E_\mathrm{s}/N_0 = 1\,\mathrm{dB}$. The error floor is reached for $E_\mathrm{s}/N_0 > 1.6\,\mathrm{dB}$, if the jointly optimized variant with irregular inner and outer codes is considered. The other variants with a single irregular component perform even worse.

For $N_I = 10000$, an SER of $\approx 4 \cdot 10^{-6}$ can be achieved by the jointly optimized variant at $E_\mathrm{s}/N_0 = 1\,\mathrm{dB}$, such that near-lossless compression and protection can be achieved. The designed system can even lead to low SERs at channel qualities $E_\mathrm{s}/N_0 < 1\,\mathrm{dB}$. However, an error floor with a slowly decreasing slope is observed. As expected, the error floor is about a decade below the one of the left sub-plot (for $N_I = 1000$) which is due to the longer interleaver [BDMP98a, Tüc04]. The systems with a single

[2] The successive joint approximation is not considered anymore in this example.

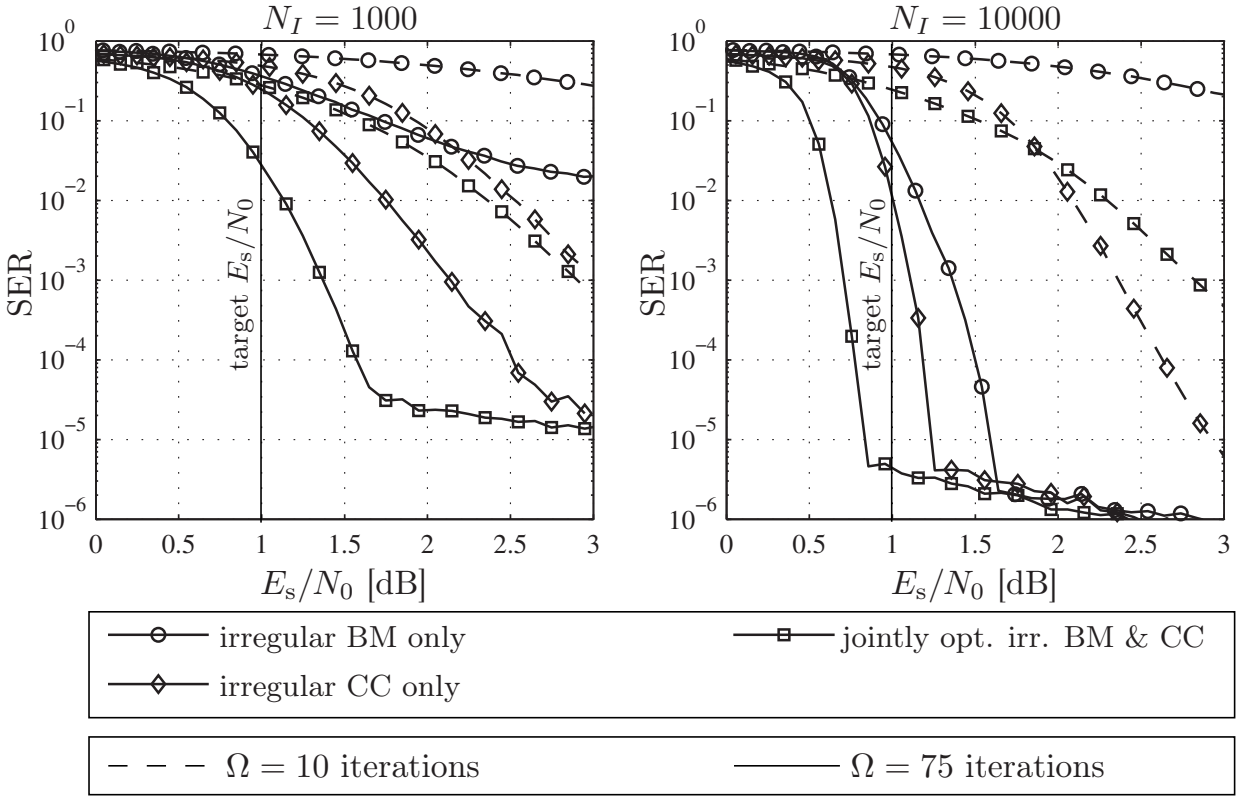

Figure 5.7: Comparison of the variants of Secs. 5.1.1 (irregular bit mapping), 5.1.2 (irregular channel code), and 5.1.3 (jointly opt. irregular bit mapping and irregular channel code) for $\rho = 0$, $\delta = 0.9$, $Q = 16$ LMQ, optimized such that $N_E/N_I \approx 3.6$, AK1-INTRA decoding.

irregular component also show a steep waterfall behavior, however, towards higher values of E_s/N_0. In all cases, it is observed that $\Omega = 10$ iterations are not sufficient for achieving considerably low SERs. In order to further reduce the error floor, all the approaches presented in Sec. 3.4 can be applied, e.g., a distance optimized bit mapping or *Multi-Dimensional Bit Mappings* (MDBMs). Note that the configuration parameters of Tab. 5.7 can also be used for $N_I = 10000$ by appropriate scaling.

Besides the simulation examples presented in this section, another comparison of the schemes with only a single irregular component using different component codes can be found in [SV10a].

5.3 Conclusions

In this chapter, the realization of ISCD-based error-resilient compression schemes for source codec parameters has been introduced. It has been demonstrated that by carefully setting up the transmitter, the number of transmitted bits can be minimized while guaranteeing decodability at the receiver. Again, the concept of irregular transmitter (and receiver) components has proved to be a powerful and versatile tool for realizing the envisaged goals. Three novel variants for setting up the transmitter and receiver have been studied: The first variant uses irregular bit mappings, while the

second variant uses irregular channel codes. The third variant utilizes irregular bit mappings as well as irregular channel codes. In the case of the first two variants, the optimum transmitter setup can be found by solving a constrained linear programming optimization problem. In the case of the latter variant, i.e., if the bit mapping as well as the channel coding stage are irregular, the transmitter setup can be found by numerically solving a non-convex, nonlinear constrained optimization problem. This latter variant has been found to be the most versatile, leading to good compression ratios and system designs offering good convergence properties.

All variants of the newly proposed concept have been compared and it has been found that the jointly optimized third variant leads to the (theoretically) best compression performance. These findings have been confirmed by a simulation example, where the novel concept has outperformed classical entropy coding schemes like Huffman codes or arithmetic codes if large block lengths are employed and only near-lossless reconstruction is required. The outstanding performance in the case of channel noise has been demonstrated in a second example.

6

Iterative Source-Channel Decoding of Multiple Descriptions

A popular method to deliver multimedia content over a heterogeneous network prone to packet losses is *Multiple Description Coding* (MDC) [Vai93, Goy01]. MDC can either be used for error concealment or for a more general kind of hierarchical coding [Erd05]: It is possible to reconstruct the signal if parts of the signal (descriptions) are missing. Missing signal portions can have two reasons: On the one hand, parts of the packetized signal can be rejected by an error detection mechanism due to channel noise. On the other hand, parts of the packets may need to be rejected due to bottlenecks in the network in order to fulfill delay or rate constraints. MDC provides a joint source-channel coding approach for erasure channels by its nature [PPR04]. One example of a speech and audio codec designed according to the MDC principle is the *FlexCode* source codec [BGK$^+$08b, BGK$^+$08c, KLK10] (see also App. A).

This chapter does not aim at providing new design guidelines for multiple description quantization, but the goals are to analyze and improve the behavior of systems employing MDC if bit errors (caused by *Additive White Gaussian Noise* (AWGN)) and/or packet losses are present. Bit errors can occur beside packet losses if the transmission takes place in a heterogeneous network, where parts of the packet-switched network are realized, e.g., by a wireless transmission. This is for example the case if a *Voice over IP* (VoIP) call is realized using the upcoming *Long Term Evolution* (LTE) network on the one side and the Internet on the other side.

Approaches to utilize soft information within the decoding of multiple descriptions can be found in, e.g., [Sri99, BHG02, GGF02, Cui08, SV10b]. The concept presented in [BHG02] utilizes the inherent redundancy contained in multiple descriptions to improve the decoding performance and is extended to realize a Turbo-like transceiver with iterative decoding. In [SVC08, Cui08, SV10b], *Soft Decision Source Decoding* (SDSD) with *Minimum Mean Square Error* (MMSE) estimation has been successfully applied to MDC. Similar MMSE and *Maximum A Posteriori* (MAP) estimators are given in [WW06, WWW09], however, these approaches do not incorporate channel coding, consider *Errors-and-Erasure Channels* (EECs) only and do not jointly exploit inter- and intra-frame correlation. With SDSD, the residual redundancy of the quantized parameters as well as the artificial MDC redundancy can

inherently be exploited. Besides improving the quality in the case without packet losses (AWGN only), it is shown in Sec. 6.2 that the quality in the packet loss only case can also be improved by exploiting the correlation of the different quantizer indices. This latter case is especially important if MDC is considered in a "traditional" scenario, i.e., in a network with no bit errors but with packet losses [Goy01].

Furthermore, the SDSD can be combined with a possibly present channel code to realize an *Iterative Source-Channel Decoding* (ISCD) receiver in Sec. 6.3, which allows to further boost the system performance if the source parameters are correlated. This approach presents a generalization of the cross decoding algorithm given in [BHG02]. The non-iterative concatenation of multiple descriptions and a channel code has been studied in [SY05, YS05]. Moreover, the performance gain is visualized by means of a simulation example. It will be shown in Sec. 6.4 how the *EXtrinsic Information Transfer* (EXIT) charts can be utilized to understand the convergence of the MDC-ISCD receiver and to easily optimize the system settings. Based on the EXIT chart analysis, an application layer coding approach, which does not explicitly add bits to each description but performs an overall rate 1 encoding of the descriptions, is presented in Sec. 6.4.2. If bit errors (or even soft information in terms of L-values, for example) reach the application layer at the receiver side, the decoding performance can be improved by several dB as long as the source parameters show residual redundancy in terms of correlation.

Finally, in Sec. 6.5, an alternative multiple description approach for highly correlated source parameters is introduced. This approach, denoted *Multiple Descriptions by Channel Coding* (MDCC), is based on the conventional ISCD system introduced in Sec. 3.1 and demultiplexes the convolutional code output to generate the single descriptions. This scheme can further improve the reconstruction quality if some descriptions are erased but also in the presence of channel noise.

6.1 Multiple Description Coding

In general, MDC can generate an arbitrary number of descriptions. However, it has been found that in the context of audio and speech transmission, two descriptions are generally sufficient in the most interesting range of conditions [BGK+08b, KK09]. For this reason, only systems generating two descriptions for each frame are considered in this thesis. Figure 6.1 depicts the baseband transmitter block diagram of the MDC scheme considered in this thesis. The system differs from the transmitter introduced

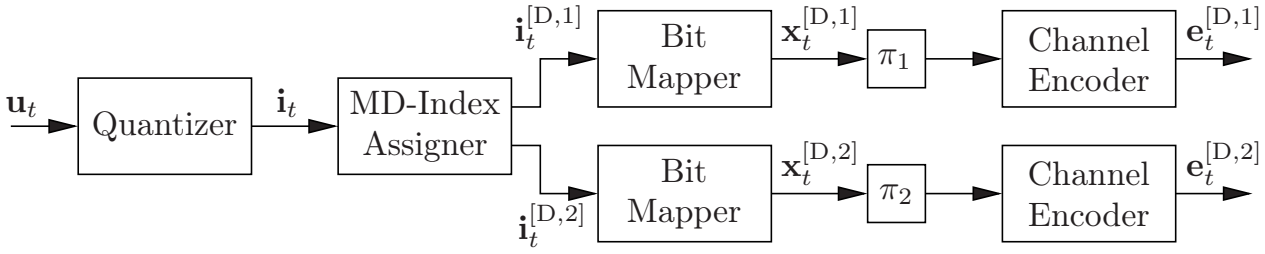

Figure 6.1: Baseband model for the multiple description transmitter of a scheme prepared for ISCD.

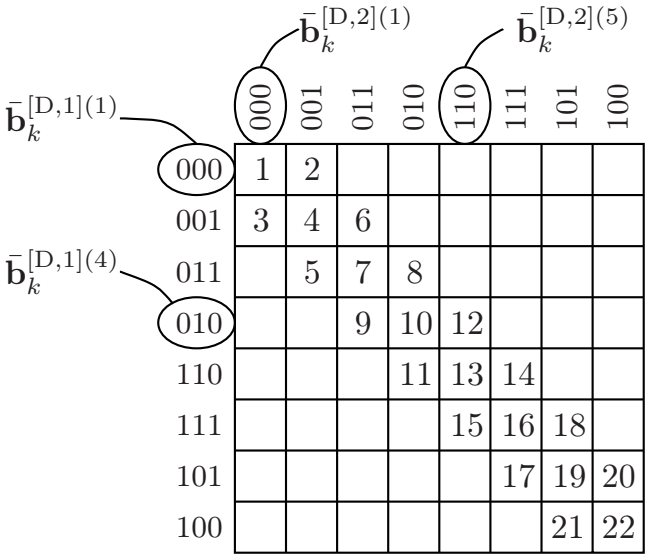

Figure 6.2: Nested *Multiple Description Index Assignment* (MDIA) with 3 filled diagonals optimized for a packet loss rate of $\epsilon = 0.05$ according to [KKK08], $Q = 22$, $Q^{[\mathrm{D},1]} = Q^{[\mathrm{D},2]} = 8$, and non-redundant Gray bit mapping $\mathcal{B}_k^{[\mathrm{D},\nu]}$ (i.e., $B_k^{[\mathrm{D},\nu]} = 3$, $\nu \in \{1, 2\}$).

in Chapter 3 (see Fig. 3.2) by an additional unit placed after the quantizer. This additional unit, which is denoted *Multiple Description Index Assignment* (MDIA), generates the two descriptions from the quantizer index $i_{t,k}$. Before giving the formal description of the MDIA, we first give an introductory example using the MDIA illustrated in Fig. 6.2. The $Q = 22$ quantizer indices are arranged in a matrix according to a certain structure. If the quantizer selects for instance the index $i = 12$, the MDIA then outputs $i^{[\mathrm{D},1]} = 4$ (corresponding to the fourth row) and $i^{[\mathrm{D},2]} = 5$ (corresponding to the fifth column). This leads to the bit patterns $\bar{\mathbf{b}}^{[\mathrm{D},1](4)} = (010)$ for the first description and $\bar{\mathbf{b}}^{[\mathrm{D},2](5)} = (110)$ for the second description.

The MDIA can be formally described by the function

$$\begin{aligned} &\mathcal{D} : \mathbb{I} \to \mathbb{I}^{[\mathrm{D},1]} \times \mathbb{I}^{[\mathrm{D},2]} \\ &\quad i_{t,k} \mapsto \mathcal{D}(i_{t,k}) = \left(i_{t,k}^{[\mathrm{D},1]}, i_{t,k}^{[\mathrm{D},2]}\right) = \left(\mathcal{D}_1(i_{t,k}), \mathcal{D}_2(i_{t,k})\right) . \end{aligned} \tag{6.1}$$

The indices $i_{t,k}^{[\mathrm{D},\nu]} \in \mathbb{I}^{[\mathrm{D},\nu]} \subset \mathbb{N}_1$, $\nu \in \{1, 2\}$, can be considered as indices of so-called *side quantizers* (utilizing potentially smaller code books) and are commonly denoted *side indices*. The side quantizers can be considered as quantizers with $Q^{[\mathrm{D},\nu]}$ code book entries. The quantizer in Fig. 6.1 is often called *central quantizer*. Individual bit mapping (as defined in Sec. 3.1.2 on page 30) is performed for each of the descriptions using a bit mapping function $\mathcal{B}_k^{[\mathrm{D},\nu]}$, $\nu \in \{1, 2\}$. The bit mapping functions map a bit pattern out of the set $\mathbb{B}_k^{[\mathrm{D},\nu]} = \{\bar{\mathbf{b}}_k^{[\mathrm{D},\nu](1)}, \ldots, \bar{\mathbf{b}}_k^{[\mathrm{D},\nu](Q^{[\mathrm{D},\nu]})}\}$ to the index $i_{t,k}^{[\mathrm{D},\nu]}$ according to

$$\mathbf{b}_{t,k}^{[\mathrm{D},\nu]} = \mathcal{B}_k^{[\mathrm{D},\nu]}\left(i_{t,k}^{[\mathrm{D},\nu]}\right) = \bar{\mathbf{b}}_k^{[\mathrm{D},\nu](i_{t,k}^{[\mathrm{D},\nu]})} .$$

a)

	000	001	011	010	110	111	101	100
000	1							
001		2						
011			3					
010				4				
110					5			
111						6		
101							7	
100								8

b)

	000	001	011	010	110	111	101	100
000	1	2						
001	3	4	6					
011		5	7	8				
010			9	10	12			
110				11	13	14		
111					15	16	18	
101						17	19	20
100							21	22

c)

	000	001	011	010	110	111	101	100
000	1	2	4	6	8	10	12	14
001	3	16	17	19	21	23	25	27
011	5	18	29	30	32	34	36	38
010	7	20	31	40	41	43	45	47
110	9	22	33	42	49	50	52	54
111	11	24	35	44	51	56	57	59
101	13	26	37	46	53	58	61	62
100	15	28	39	48	55	60	63	64

Figure 6.3: Nested MDIA with $Q^{[\mathrm{D},1]} = Q^{[\mathrm{D},2]} = 8$, and non-redundant Gray bit mapping.
a) $Q = 8$, optimized for high packet loss probabilities.
b) $Q = 22$, optimized for $\epsilon = 0.05$.
c) $Q = 64$, optimized for low packet loss probabilities ($\epsilon \to 0$).

The bit patterns of the individual descriptions $\mathbf{b}_{t,k}^{[\mathrm{D},\nu]}$, consisting of $B_k^{[\mathrm{D},\nu]}$ bits, are grouped to a bit vector $\mathbf{x}_t^{[\mathrm{D},\nu]}$, interleaved and optionally channel encoded (if bit errors are expected on the transmission link). Each of the channel encoded vectors $\mathbf{e}_t^{[\mathrm{D},\nu]}$ contains $N_E^{[\mathrm{D},\nu]}$ entries.

The MDIA for two descriptions is commonly defined by means of a matrix. An exemplary MDIA (denoted *nested index assignment* in [Vai93]) is given in Fig. 6.2 for $Q = 22$ central quantizer code book entries and $Q^{[\mathrm{D},1]} = Q^{[\mathrm{D},2]} = 8$ side code book entries. The code book and the index assignment have been generated according to the guidelines in [KKK08]. The bit mapping for both descriptions is a non-redundant *Gray* mapping. The single quantizer indices are arranged in the two-dimensional grid according to the nested algorithm and point to certain side bit patterns. A trade-off between the reconstruction quality in the case where a description is lost and the case where all descriptions are available can be achieved by adjusting the number of filled diagonals in the MDIA. If very high packet loss probabilities are expected on the transmission link, only the main diagonal is filled and the information can be perfectly reconstructed if one description is lost. This case is depicted in Fig. 6.3-a). However, the overall reconstruction quality (if both descriptions are available) is low, as only $Q = 8$ central quantizer levels are used (instead of $Q = 22$ in Fig. 6.2). Figure 6.3-b) reproduces the MDIA of Fig. 6.2, which has been optimized for an expected packet loss rate of $\epsilon = 0.05$. If no packet losses are expected, an optimal solution (in terms of reconstruction quality) would be the use of a central code book with $Q = Q^{[\mathrm{D},1]}Q^{[\mathrm{D},2]} = 64$. This case is depicted in Fig. 6.3-c) for a nested index assignment. Due to $Q = 64$, a high reconstruction quality is achieved if both descriptions are available at the receiver. If one description is however lost, large distortions result. We can finally conclude that depending on the expected packet loss rate, the MDIA can be set up accordingly [Vai93, KKK08, ZKK09, BGK+08b].

Figure 6.4 depicts the proposed ISCD receiver for MDC [SV10b]. Contrary to most receivers utilizing a central decoder (for the case that both descriptions are received) and side decoders (if only a single description is received), we propose a receiver similar

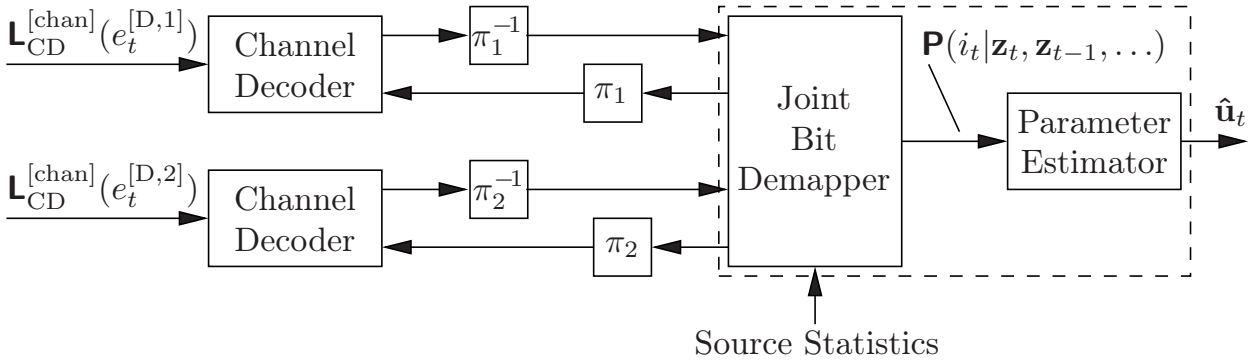

Figure 6.4: Baseband model for the proposed receiver of a multiple description coding scheme (2 descriptions) with ISCD

to the ones given in Secs. 3.2 and 3.6. The receiver consists of individual channel decoders for each description, individual (de-)interleaving blocks and an SDSD which performs joint decoding of both descriptions (if available).

As it is assumed that each description is individually transmitted over independent channels, a channel-related factor $\gamma_{t,k}^{[\mathrm{D},\nu]}(q)$, $\forall q \in \mathbb{I}^{[\mathrm{D},\nu]}$, which is required for SDSD, can be computed by taking into account the bit mapping of each description according to [WWW09, SV10b] (see also App. F.1)

$$\begin{aligned}\gamma_{t,k}^{[\mathrm{D},\nu]}(q) &\doteq \prod_{\mu=1}^{B_k^{[\mathrm{D},\nu]}} \mathsf{P}_{\mathrm{CD}}^{[\mathrm{ext}]}\left(b_{t,k,\mu}^{[\mathrm{D},\nu]} = \bar{b}_{k,\mu}^{[\mathrm{D},\nu](q)}\right) \\ &= \prod_{\mu=1}^{B_k^{[\mathrm{D},\nu]}} \left(1 + \exp\left(-\left(1 - 2\cdot\bar{b}_{k,\mu}^{[\mathrm{D},\nu](q)}\right)\cdot \mathsf{L}_{\mathrm{CD}}^{[\mathrm{ext}]}(b_{t,k,\mu}^{[\mathrm{D},\nu]})\right)\right)^{-1}. \end{aligned} \tag{6.2}$$

If a description is not received, for instance due to a packet loss, then $\mathsf{L}_{\mathrm{CD}}^{[\mathrm{ext}]}(b_{t,k,\mu}^{[\mathrm{D},\nu]}) = 0$, or $\mathsf{P}_{\mathrm{CD}}^{[\mathrm{ext}]}(b_{t,k,\mu}^{[\mathrm{D},\nu]} = \bar{b}_{k,\mu}^{[\mathrm{D},\nu](q)}) = \frac{1}{2}$, respectively. In that case, equiprobable factors $\gamma_{t,k}^{[\mathrm{D},\nu]}(q)$ result with

$$\gamma_{t,k}^{[\mathrm{D},\nu]}(q)\Big|_{\substack{\mathrm{desc.}\\ \mathrm{lost}}} = \frac{1}{Q^{[\mathrm{D},\nu]}} = \frac{1}{|\mathbb{I}^{[\mathrm{D},\nu]}|} = \frac{1}{|\mathbb{B}_k^{[\mathrm{D},\nu]}|}, \qquad \forall q \in \mathbb{I}^{[\mathrm{D},\nu]}. \tag{6.3}$$

Using the MDIA function $\mathcal{D}(q) = (\mathcal{D}_1(q), \mathcal{D}_2(q))$ and the fact that both descriptions are transmitted independently, the factor $\gamma_{t,k}(q)$ for all central quantizer code book entries (i.e., $\forall q \in \mathbb{I}$) can be written as [SV10b]

$$\gamma_{t,k}(q) = \gamma_{t,k}^{[\mathrm{D},1]}(\mathcal{D}_1(q)) \cdot \gamma_{t,k}^{[\mathrm{D},2]}(\mathcal{D}_2(q)). \tag{6.4}$$

With $\gamma_{t,k}(q)$, the SDSD equations given in App. F can be utilized and *a posteriori* probabilities can be estimated for the central code book entries. These *a posteriori* probabilities can then be used to compute an estimate based on the central code book (with Q entries) according to the MMSE or MAP criterion (see also

Sec. 3.1.3). The equations for computing the *a posteriori* probabilities are summarized in App. G for the four considered SDSD algorithms (AK0, AK1-INTER, AK1-INTRA, AK1-NOPT). A conventional hard decision decoder reconstructs the code book entry using a table look-up. If only a single description is available, an averaging over all possible code book entries corresponding to the received description is performed, or appropriately precomputed side code books [Vai93] can be used.

In the iterative case, extrinsic information $\mathsf{L}_{\mathrm{SD}}^{[\mathrm{ext}]}(x_t)$ for the use within channel decoding of subsequent iterations has to be generated. This generation of extrinsic information will be described in Sec. 6.3. In the following Section 6.2, the non-iterative case will be studied by means of simulation examples and it will be shown what gains can be expected by employing SDSD to multiple descriptions if AWGN and/or packet losses are expected on the transmission link.

6.2 Non-Iterative Source-Channel Decoding of Multiple Descriptions

First, a non-iterative receiver is assumed and the possible gains by employing SDSD to multiple descriptions are highlighted and compared with conventional approaches. We use the following system setup according to [SV10b] for the examples: A source emits $N_U = 10$ Gaussian i.i.d. source parameters with temporal correlation coefficient $\rho = 0.9$ (i.e., $\delta = 0$) according to Sec. 3.1.1. The parameters are quantized using a $Q = 22$ level scalar quantizer. The MDIA is based on a 8×8 matrix with the nested 3-diagonal index assignment according to Fig. 6.2, resulting in 6 bits per parameter (3 bits per description). The central and side code books are generated according to [KKK08]. No interleaving and channel coding is used in this first example.

Figure 6.5 shows the parameter *Signal-to-Noise Ratio* (SNR) between the original parameters u and the reconstructed parameters $\hat{u}$ for packet loss probabilities of $\epsilon \in \{0, 0.05\}$. It can be seen that the cross decoding method presented in [BHG02] already improves the conventional hard decision table look-up decoding considerably. The cross decoding method computes extrinsic *cross probabilities* for each description by exploiting the inherent code redundancy of the MDIA. These extrinsic cross probabilities are added to the respective channel output together with *a priori* knowledge on bit level to compute *a posteriori* L-values on bit level, which are used to perform conventional hard decision decoding.

The proposed SDSD-based estimation method exploiting either no *a priori* knowledge (NAK), zeroth order *a priori* knowledge (AK0) or first order *a priori* knowledge (AK1-INTER) leads to significant parameter SNR improvements [SVC08, Cui08, WWW09, SV10b]. In the case of a packet loss probability of $\epsilon = 0.05$, it can be seen that the application of the AK1-INTER MMSE estimator can improve the overall signal quality in the noiseless case (for $E_{\mathrm{s}}/N_0 \to \infty$) by $\approx 1.5\,\mathrm{dB}$. This effect is due to the inter-frame correlation of the parameters, which is exploited by the AK1-INTER MMSE estimator [SVC08, Cui08, WWW09, SV10b].

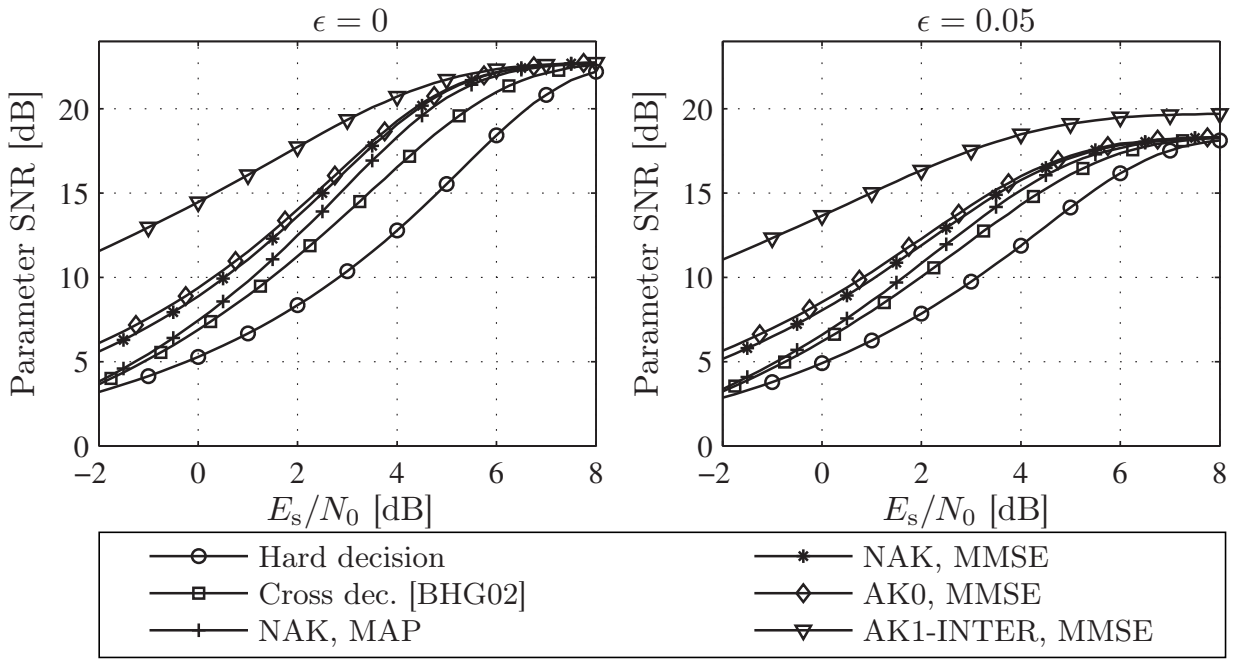

Figure 6.5: Comparison of the different MDC decoding algorithms for a source with $\rho = 0.9$ and $\delta = 0$ for $\epsilon = 0$ (left sub-plot) and for $\epsilon = 0.05$ (right sub-plot), no channel coding, MDIA as given in Fig. 6.2, $N_U = N_I = 10$.

In a second experiment, the gains by AK1-INTER MMSE estimation in a pure packet loss scenario (i.e. no AWGN or $E_s/N_0 \to \infty$, respectively) are quantified. These gains have been observed in Fig. 6.5 for $\epsilon > 0$. In the pure packet loss case, the AK1 MMSE estimator can improve the overall reconstruction quality by exploiting the frame correlation of the source codec parameters. Again, a block consists of $N_I = 10$ i.i.d parameters which possess inter- (or intra-)frame correlation. The left sub-plot of Fig. 6.6 depicts the achievable gain in terms of parameter SNR by employing AK1-INTER MMSE decoding instead of conventional hard bit decoding (or any other MMSE estimator not exploiting the inter-frame correlation) for a source with $\delta = 0$ and varying ρ. High gains are observed with increasing packet loss probabilities. However, it has to be kept in mind that the nested MDIA of Fig. 6.2 is not optimized for high packet loss probabilities. For $\epsilon > 0.2$, an MDIA with less diagonals is beneficial.

The right sub-plot of Fig. 6.6 shows the situation for AK1-INTRA decoding. In this case, the source is set up with $\rho = 0$ and δ is varied. Again, the exploitation of correlation permits to improve the overall signal quality even if no channel noise is present. The gains are, however, smaller than in the inter-frame case (note the different y-axis scaling) and a maximum gain is obtained for $\epsilon \approx 0.1$. The reason for this is that if both descriptions are lost, no estimate can be given in this case and no information from past frames can be used to give an estimate. The mean of the central code book gives the optimal estimate in the MMSE sense. If ϵ increases, these situations occur more often (with their probability of occurrence being ϵ^2). If only one of both descriptions is lost (occurring with probability $2\epsilon(1-\epsilon)$), the intra-frame correlation can be used to enhance the estimation of the central quantizer indices.

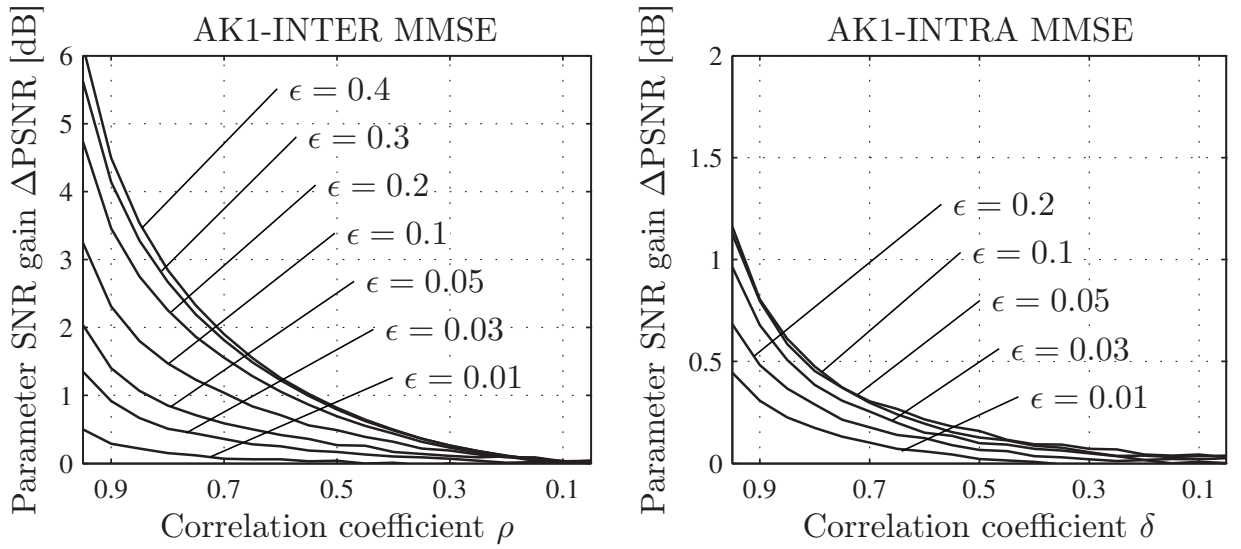

Figure 6.6: Parameter SNR gain of AK1-INTER (left) and AK1-INTRA (right) MMSE estimation compared to conventional hard bit decoding if no AWGN is present on the channel (no bit errors) and for different packet loss probabilities ϵ, $N_I = 10$, nested MDIA according to Fig. 6.2.

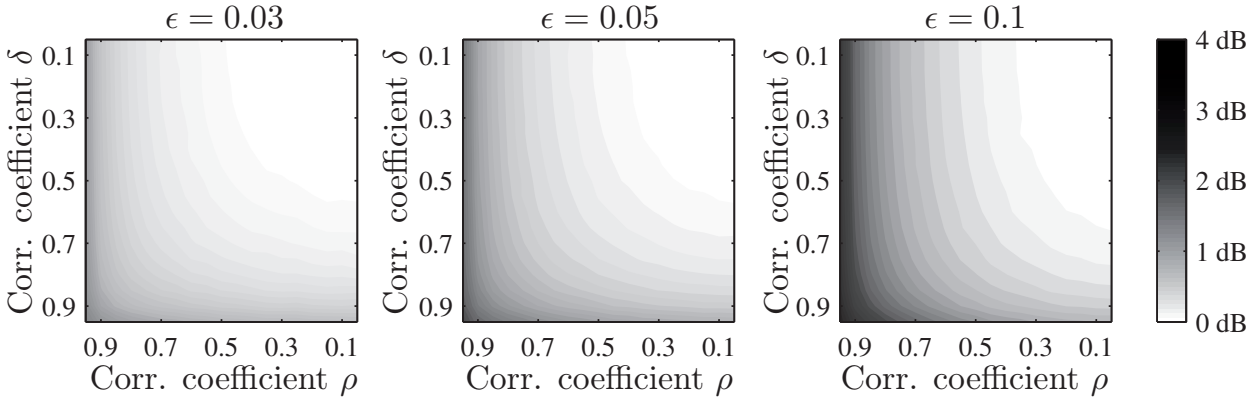

Figure 6.7: Parameter SNR gain ΔPSNR (in dB) of AK1-NOPT MMSE estimation compared to conventional hard bit decoding if no AWGN is present on the channel (no bit errors) and $\epsilon \in \{0.03, 0.05, 0.1\}$, nested MDIA according to Fig. 6.2.

Similar results are achieved for the AK1-NOPT case. Figure 6.7 visualizes the relative parameter SNR gains in the AK1-NOPT case for varying correlation coefficients and for $\epsilon \in \{0.03, 0.05, 0.1\}$. It can be seen that the exploitation of both types of correlation leads to further improvements of the parameter SNR gain. For instance, if $\rho = 0.95$ and $\delta = 0.95$, the gain amounts to $\Delta\text{PSNR} \approx 3.8\,\text{dB}$ compared to $3.15\,\text{dB}$ in the AK1-INTER case and $1.15\,\text{dB}$ in the AK1-INTRA case (for the given correlation coefficients). Therefore, the utilization of the AK1-NOPT algorithm also leads to considerable performance improvements in this case, at the expense of slightly increased computational demands.

It can be seen that the improvement of the parameter SNR increases with the correlation coefficient, as expected. Furthermore, the gain is larger for higher packet loss rates. If no packet losses occur, the decoding result of the AK1-INTER/AK1-INTRA

MMSE algorithms is identical to the result of the hard bit decoding algorithm (for the non-AWGN case). If only a small number of packet losses occur, there are only some parameters where the quality can be improved by AK1-MMSE decoding. Thus, a higher number of packet losses increases the occurrence of those situations where an improvement is obtained.

It can be concluded that once there is exploitable frame correlation in the source parameters, the application of the AK1 SDSD algorithms for multiple descriptions is beneficial, even if no channel noise is expected (packet losses only). In this latter case, the complexity of the decoding algorithm is considerably reduced, as $\gamma_{t,k}^{[\mathrm{D},\nu]}(q) = 1$ if the qth bit pattern has been received and zero otherwise. Thus, the sums for computing the *a posteriori* probabilities can be considerably simplified as most summands are zero [WWW09, SV10b]. The joint exploitation of inter- and intra-frame correlation marks the main advancement compared with the generalized approach of [WWW09], which only considers either inter- or intra-frame correlation and a special channel model. The non-iterative system given here is the basis for the MDC based ISCD receiver, which is presented in the following section and further improves the reconstruction quality in the presence of AWGN.

6.3 Iterative Source-Channel Decoding of Multiple Descriptions

The iterative decoder requires extrinsic information from the SDSD, which is fed back to the channel decoder during the first $\Omega - 1$ iterations. In the final iteration, *a posteriori* probabilities are computed as postulated in the previous section and used for estimating the reconstructed source values $\hat{u}$ (using either MMSE or MAP estimation). Analog to the non-MDC case, we define extrinsic channel-related reliabilities for the different bit positions χ of the bit patterns of both descriptions ($\nu \in \{1, 2\}$) according to

$$\gamma_{t,k}^{[\mathrm{D},\nu,\mathrm{ext}]\setminus\chi}(q) \doteq \prod_{\substack{\mu=1 \\ \mu\neq\chi}}^{B_k^{[\mathrm{D},\nu]}} \mathsf{P}_{\mathrm{CD}}^{[\mathrm{ext}]}\left(b_{t,k,\mu}^{[\mathrm{D},\nu]} = \bar{b}_{k,\mu}^{[\mathrm{D},\nu](q)}\right) \tag{6.5}$$

$$= \prod_{\substack{\mu=1 \\ \mu\neq\chi}}^{B_k^{[\mathrm{D},\nu]}} \left(1 + \exp\left(-\left(1 - 2 \cdot \bar{b}_{k,\mu}^{[\mathrm{D},\nu](q)}\right) \cdot \mathsf{L}_{\mathrm{CD}}^{[\mathrm{ext}]}(b_{t,k,\mu}^{[\mathrm{D},\nu]})\right)\right)^{-1} . \tag{6.6}$$

In order to simplify the expressions for the MDC SDSD, we define the support sets of the MDIA as

$$\mathbb{D}_{\chi}^{[\mathrm{D},1]} \doteq \{j : \mathcal{D}(q) = (\chi, j), \forall q \in \mathbb{I}\} \text{ and } \mathbb{D}_{\chi}^{[\mathrm{D},2]} \doteq \{j : \mathcal{D}(q) = (j, \chi), \forall q \in \mathbb{I}\} . \tag{6.7}$$

The set $\mathbb{D}_{\chi}^{[\mathrm{D},1]}$ contains all possible indices $i^{[\mathrm{D},2]}$ of description 2 if the index of the first description is encoded to $i^{[\mathrm{D},1]} = \chi$. The set $\mathbb{D}_{\chi}^{[\mathrm{D},2]}$ is defined in an analog manner.

With the definition of the support sets in (6.7), the extrinsic information for use within the ISCD system can be computed by taking into account different kinds of *a priori* knowledge. In the following, we give the SDSD expressions for computing the extrinsic information in the AK0 case only. The expressions for the AK1-INTER, AK1-INTRA and AK1-NOPT cases are given in App. G and immediately result from the AK0 case and the equations for the non-MDC case given in App. F. The equations in the logarithmic domain, required for a numerically convenient implementation are also given in App. G.

AK0 Case

With the definition $\bar{\nu} \doteq 3 - \nu$ (i.e., if $\nu = 1$, then $\bar{\nu} = 2$ and vice versa) the extrinsic information in the AK0 case can be computed by

$$\mathsf{L}_{\mathrm{SD}}^{[\mathrm{ext}]}(b_{t,k,\mu}^{[\mathrm{D},\nu]}) = \tag{6.8}$$

$$\ln \frac{\sum_{q_\nu=1}^{Q^{[\mathrm{D},\nu]}} \left(1 - \bar{b}_{k,\mu}^{[\mathrm{D},\nu](q_\nu)}\right) \gamma_{t,k}^{[\mathrm{D},\nu,\mathrm{ext}]\setminus\mu}(q_\nu) \sum_{\forall q_{\bar{\nu}} \in \mathbb{D}_{q_\nu}^{[\mathrm{D},\nu]}} \gamma_{t,k}^{[\mathrm{D},\bar{\nu}]}(q_{\bar{\nu}}) \mathsf{Pr}\{I_{t,k} = \mathcal{D}^{-1}(q_1, q_2)\}}{\sum_{q_\nu=1}^{Q^{[\mathrm{D},\nu]}} \bar{b}_{k,\mu}^{[\mathrm{D},\nu](q_\nu)} \gamma_{t,k}^{[\mathrm{D},\nu,\mathrm{ext}]\setminus\mu}(q_\nu) \sum_{\forall q_{\bar{\nu}} \in \mathbb{D}_{q_\nu}^{[\mathrm{D},\nu]}} \gamma_{t,k}^{[\mathrm{D},\bar{\nu}]}(q_{\bar{\nu}}) \mathsf{Pr}\{I_{t,k} = \mathcal{D}^{-1}(q_1, q_2)\}}.$$

The main difference compared to the non-MDC case (see App. F.1) is the additional summation over the support set $\mathbb{D}^{[\mathrm{D},\nu]}$ which takes into account the information from the bit patterns of the according other description $\bar{\nu}$. For example, if the extrinsic information for the first bit of the first description (i.e., $b_{t,k,1}^{[\mathrm{D},1]}$) is seeked, then all the combinations of the second and third bit need to be considered (with $b_{t,k,1}^{[\mathrm{D},1]}$ being either "1" (numerator) or "0" (denominator)). This is the first summation in (6.8). For each of the bit patterns of the first description, all the bit patterns of the second description that can occur for this description need to be accounted for. Thus, the second summation in (6.8) is being performed over the support set of the first description in the example. Using the inverse MDIA, the central code book index is given by both descriptions.

If the quantizer indices $I_{t,k}$ are assumed to be equiprobable, i.e., $\mathsf{Pr}\{I_{t,k} = j\} = 1/Q$, $\forall j \in \mathbb{I}$, then (6.8) reduces to the expression given in [BHG02] with the second sum in the numerator and denominator being the *cross probabilities* (as denoted in [BHG02]). Thus, our proposed approach generalizes the concept of [BHG02] and improves its decoding performance if the parameters are non-uniformly distributed and/or correlated. Besides not exploiting any *a priori* knowledge, [BHG02] does not utilize any techniques known to improve the performance of ISCD, like, e.g., redundant bit mappings [AVC05, CVA06b, CAV06, PYH07, CSVA08a, PYOH08, NEO+08, NH08, NH09a, NH09b].

6.3.1 Simulation Example

The capabilities of iterative source-channel decoding of multiple descriptions are demonstrated using a simulation example. The source according to Sec. 3.1.1 is configured as follows: In each frame, $N_U = 250$ parameters are generated with inter-frame correlation coefficient $\rho = 0.9$ and no intra-frame correlation ($\delta = 0$). These parameters are quantized by a $Q = 22$ level scalar quantizer ($N_I = N_U$). For the simulation example, we consider two different configurations of the MDC transmitter depicted in Fig. 6.1.

Configuration A: The MDIA and the rate $r_{\mathrm{BM}} = 1$ Gray bit mapping given in Fig. 6.2 are utilized leading to bit patterns of $B_k^{[\mathrm{D},\nu]} = 3\,\mathrm{bit}$ per index and description. The interleavers of each description are S-random interleavers [DP95a, DP95b, VY00] with $\mathsf{S} = 15$ of size $N_X^{[\mathrm{D},\nu]} = N_I B^{[\mathrm{D},\nu]} = 750$, $\forall \nu \in \{1, 2\}$. In the first example, the $r_{\mathrm{CC}} = \frac{1}{2}$ feed forward convolutional code depicted in Fig. 2.1 is utilized ($J = 6$, $\mathbb{G}^{[\mathrm{CC}]} = \{133, 171\}_8$) leading to $N_E^{[\mathrm{D},\nu]} \approx 1500$, $\forall \nu \in \{1, 2\}$. Although a feed forward inner code is used, gains by iterative processing can be expected. Details on the convergence properties of feed forward convolutional codes can be found in [SVAC07] and in App. E. The overall coding rate of this configuration amounts to $r_{\mathrm{BM}} \cdot r_{\mathrm{CC}} = \frac{1}{2}$.

Configuration B: In a second system setup, the optimized settings of the ISCD system of Sec. 3.1.4, used for the simulation results in Fig. 3.4 on page 36, are employed: A rate $r_{\mathrm{BM}} = \frac{1}{2}$ repetition coded bit mapping with $\mathbf{G}_k^{[\mathrm{D},\nu]} = (\mathbf{I}_3\ \mathbf{I}_3)$ is utilized leading to (S-random) interleavers of size $N_X^{[\mathrm{D},\nu]} = N_I B^{[\mathrm{D},\nu]} = 1500$, $\forall \nu \in \{1, 2\}$ with $\mathsf{S} = 15$. The convolutional code is the rate $r_{\mathrm{CC}} = 1$ *Recursive Non-Systematic Convolutional* (RNSC) code with $J = 3$, $\mathbb{G}^{[\mathrm{CC}]} = \{\frac{10}{17}\}_8$, leading to $N_E^{[\mathrm{D},\nu]} \approx 1500$, $\forall \nu \in \{1, 2\}$. The overall coding rate of this second configuration also amounts to $r_{\mathrm{BM}} \cdot r_{\mathrm{CC}} = \frac{1}{2}$.

Figure 6.8 shows simulation results for both system configurations and two packet loss rates $\epsilon \in \{0, 0.05\}$. As expected, the application of ISCD leads to large gains compared to the non-iterative scheme (results in Fig. 6.8). The direct application of ISCD to the system with a feed forward rate $r_{\mathrm{CC}} = \frac{1}{2}$ channel code and Gray coded bit mapping (Configuration A) leads to an improvement of $\approx 2.5\,\mathrm{dB}$ after $\Omega = 5$ iterations. Further iterations do not lead to noteworthy improvements. Additionally, the hard decision decoding results of this system are shown as reference. The gain obtained by applying ISCD to the MDC system is larger than the gain obtained by applying ISCD to a comparable non-MDC system (with Gray coded bit mapping, and the $J = 6$ feed forward convolutional code) [AVS01, Adr03, AV05]. The reason for this is that besides the residual source redundancy, the MDIA introduces additional artificial redundancy. In the case of the utilized MDIA given in Fig. 6.2, $B^{[\mathrm{D},1]} + B^{[\mathrm{D},2]} = 6\,\mathrm{bit}$ are used to represent $Q = 22$ quantizer reproduction levels. In fact the MDIA alone can be seen as a special kind of channel code [PPR04].

As expected, the second system setup according to Configuration B with rate $r_{\mathrm{BM}} = \frac{1}{2}$ repetition coded bit mapping and a rate $r_{\mathrm{CC}} = 1$ channel code outperforms the system according to Configuration A in the most interesting range of channel conditions

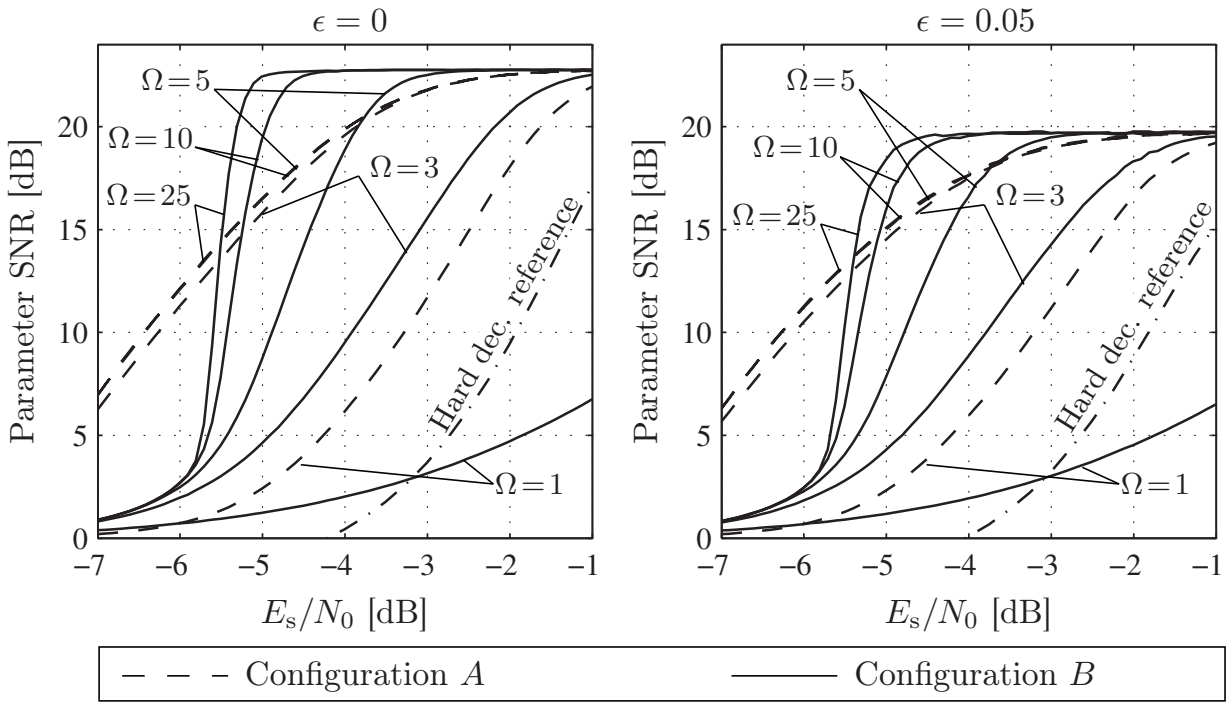

Figure 6.8: ISCD for MDC, source with $\rho = 0.9$ and $\delta = 0$, $N_I = 250$, MDIA as given in Fig. 6.2, $\epsilon = 0$ (left sub-plot) and $\epsilon = 0.05$ (right sub-plot).
Config. A: $r_{\mathrm{BM}} = 1$ Gray bit mapping, convolutional code with $r_{\mathrm{CC}} = \frac{1}{2}$, $J = 6$, $\mathbb{G}^{[\mathrm{CC}]} = \{133, 171\}$ (dashed lines – – –).
Config. B: $r_{\mathrm{BM}} = \frac{1}{2}$ repetition coded redundant bit mapping, convolutional code with $r_{\mathrm{CC}} = 1$, $J = 3$, $\mathbb{G}^{[\mathrm{CC}]} = \{\frac{10}{17}\}$ (solid lines ——).

($E_s/N_0 \gtrapprox -5.5\,\mathrm{dB}$) and is able to maintain a high parameter SNR for a broader range of channel conditions. Furthermore, more iterations can be exploited due to the more careful system design. In the first setup, no notable performance improvements are observed for more than $\Omega = 5$ iterations, while in the second setup, more than $\Omega = 10$ iterations can lead to improvements.

6.4 Convergence Analysis and System Optimization

In this section, the EXIT chart analysis is applied to the MDC-based ISCD scheme introduced in Sec. 6.3 in order to analyze the convergence properties of the presented approaches. Furthermore, the EXIT chart analysis is used to design a further system (denoted *Configuration C*) which does not transmit any additional channel coding bits but outperforms the SDSD only scheme (which uses no channel coding) of Sec. 6.2.

6.4.1 Convergence Analysis Using EXIT Charts

As for all iterative decoding schemes, such as the proposed MDC-based ISCD setup, EXIT charts are a valuable tool for convergence analysis and for system design. The

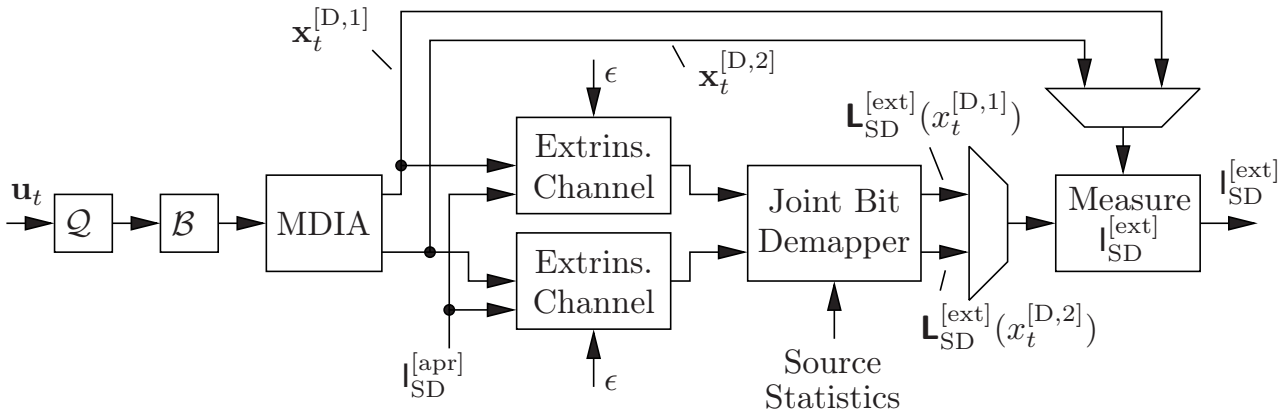

Figure 6.9: Block diagram for measuring the EXIT characteristics of MDC-SDSD.

EXIT characteristic measurement is complicated by the fact that the MDC-ISCD receiver, as depicted in Fig. 6.4, does not correspond to a conventional receiver of a serially concatenated system. In fact, two channel decoders and two interleavers are present, while the SDSD has two inputs for receiving information from both channel decoders (corresponding to one description each). In order to perform an EXIT chart analysis using conventional two-dimensional EXIT charts, the following simplifications are applied.

First, as it has been assumed that both channel codes in Fig. 6.1 are identical, the characteristic C_{CD} of the channel decoder can directly be used if no packets have been lost (which occurs with probability $(1-\epsilon)^2$). This works under the assumption that both channel decoders can be considered as decoders of a single code, which can easily be done in the case of a convolutional code (which can be partitioned into blocks of about five times the constraint length with only a slight performance sacrifice [Fri96, JZ99]).

If description ν is erased, however, the channel decoder of description ν has no exploitable channel-related information available at its input, i.e., $\mathsf{L}_{\mathrm{CD}}^{[\mathrm{chan}]}(e_t^{[\mathrm{D},\nu]}) = \mathbf{0}$. In this case, we can measure the EXIT characteristic $\mathsf{C}'_{\mathrm{CD}} \doteq \mathsf{C}_{\mathrm{CD}}(\mathsf{L}_{\mathrm{CD}}^{[\mathrm{chan}]}(e_t^{[\mathrm{D},\nu]}) = \mathbf{0})$. Note that in most considered cases $\mathsf{C}'_{\mathrm{CD}} = 0$ as the decoder is unable to generate extrinsic information if no channel-related knowledge is available. If the other description $\bar{\nu} = 3-\nu$ is available, then the effective characteristic amounts to $(\mathsf{C}_{\mathrm{CD}}+\mathsf{C}'_{\mathrm{CD}})/2$. This case occurs with probability $2\cdot\epsilon\cdot(1-\epsilon)$. If both descriptions are lost, both decoders do not have access to reliable channel-related information. The total channel decoder characteristic $\mathsf{C}_{\mathrm{CD,MDC}}$ can thus be described by

$$\begin{aligned}\mathsf{C}_{\mathrm{CD,MDC}}(\epsilon) &= (1-\epsilon)^2\mathsf{C}_{\mathrm{CD}} + \epsilon(1-\epsilon)(\mathsf{C}_{\mathrm{CD}} + \mathsf{C}'_{\mathrm{CD}}) + \epsilon^2\mathsf{C}'_{\mathrm{CD}} && (6.9)\\ &= (1-\epsilon)\mathsf{C}_{\mathrm{CD}} + \epsilon\mathsf{C}'_{\mathrm{CD}} && (6.10)\\ &= (1-\epsilon)\mathsf{C}_{\mathrm{CD}}\,, \qquad \text{if } \mathsf{C}'_{\mathrm{CD}} = 0\,. && (6.11)\end{aligned}$$

As the MDC-SDSD utilized in this work possesses two *a priori* inputs and two extrinsic outputs, the measurement block diagram has to be modified in order to account for these additional inputs and outputs. This modified block diagram is given in

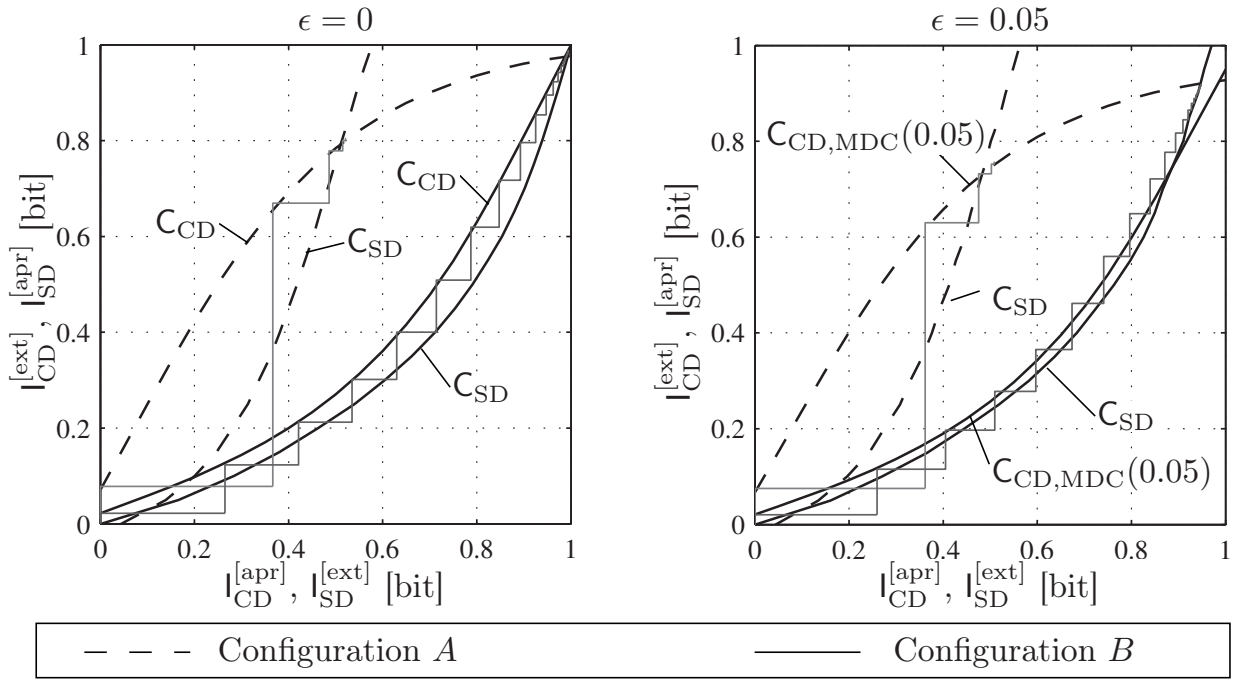

Figure 6.10: EXIT chart analysis of both systems considered in Fig. 6.8 for $E_s/N_0 = -5\,\mathrm{dB}$ and $\epsilon = 0$ (left sub-plot) or $\epsilon = 0.05$ (right sub-plot).

Fig. 6.9 and uses two extrinsic channels to model the *a priori* information at both inputs of the MDC-SDSD. If one of the descriptions is lost, the according extrinsic channel shall output zeros. This is indicated by the erasure probability ϵ at the input of both extrinsic channels.

Figure 6.10 depicts the EXIT charts of the systems considered in Fig. 6.8 for $E_s/N_0 = -5\,\mathrm{dB}$. The left sub-plot shows the case of a packet loss probability of $\epsilon = 0$ while the right sub-plot shows the case of $\epsilon = 0.05$. Configuration A and configuration B are shown. The EXIT chart permits to precisely predict the convergence behavior of both systems. Again, an overshooting effect as already described in Sec. 3.1.6 is observed. In this case, the decoding trajectory can also be precisely predicted by employing the *EXIT Trajectory Bound* (ETB), however, for clarity, it is not shown in Fig. 6.10. Notice that for the characteristic of the feed forward code (dashed line – – –) it is not possible to reach the $(1, 1)$ point in the chart [SVAC07], as derived in App. E.

If packet losses occur, the characteristics still can predict the convergence, however, the precision is more inaccurate than in the case without packet losses. The reason for this is that the underlying assumptions do not correctly match the real system, especially if inter-frame correlation is exploited. If description ν is erased, the MDC-SDSD can generate extrinsic information for this description, however, this information can not be exploited by the channel decoder due to the absence of channel-related knowledge. Furthermore, the smaller effective interleaver also leads to a trajectory which overshoots the channel decoder characteristic. Thus, it can be concluded that the proposed EXIT chart analysis presents a valuable tool for the case with AWGN only (i.e., no packet losses), but shows some inaccuracies in the packet loss case.

6.4.2 Multiple Description Coding with Turbo Error Concealment

Systems employing MDC are often designed considering only the application layer [OSI96], signifying that during the design process only packet losses and no bit errors are expected. As an exception, the *FlexCode* source encoder [BGK+08a, BGK+08b, BGK+08c, KLK10] uses MDC and has been developed for heterogeneous networks where packet losses and bit errors can occur. In order to fully exploit the knowledge about bit errors and packet losses, source and channel coding can be jointly designed. However, in systems where the design shall take place on the application layer only, and which shall be used with arbitrary channel codes, no additional data rate can usually be spent for error protection.

For this reason, we introduce a scheme which uses no additional data rate for dedicated channel coding like the systems analyzed in Sec. 6.3. This scheme, built using the transmitter given in Fig. 6.1, is denoted *Configuration C* in what follows. As in the previous configurations, the exemplary MDIA of Fig. 6.2 is used. However, instead of the Gray coded bit mapping, a rate $r_{\mathrm{BM}} = \frac{3}{4}$ single parity check bit mapping with $\mathbf{G}^{[\mathrm{D},\nu]} = (\mathbf{I}_3 \ \mathbf{1}_{3\times 1})$ is employed. After interleaving, a doped and punctured convolutional code [tB01b] with $J = 3$, $\mathbb{G}^{[\mathrm{CC}]} = \{\frac{10}{17}\}_8$, puncturing matrix $\mathbf{G}_{\mathrm{punc}} = (1\ 1\ 1\ 0)$ and doping ratio of $1 : 25$ is used. The rate of this code is $r_{\mathrm{CC}} = \frac{4}{3}$. The total coding rate of this scheme thus amounts to $r_{\mathrm{BM}} \cdot r_{\mathrm{CC}} = 1$ such that in total only 3 bit per description and quantizer index are transmitted, as in the case without channel coding. A detailed description of doped and punctured convolutional codes is given in Sec. 5.2.

Configuration C is similar to the *Turbo error concealment* approaches for the single description case [AV04a, AV04b, Cle06] and the system given in [Tho07a, TSV08]. The Turbo error concealment schemes [AV04a, AV04b], however, utilize non-redundant bit mappings and $r_{\mathrm{CC}} = 1$ codes. In this setup, $r_{\mathrm{CC}} > 1$ codes together with redundant bit mappings have been chosen due to their property to be able to reach the $(1, 1)$ point in the EXIT chart. The drawback of this latter approach is that decoding is slightly complicated in the error-free case, as several iterations have to be performed.

Figure 6.11 shows simulation results for configuration C with identical source settings as in Fig. 6.8, i.e., $N_U = N_I = 250$, $\rho = 0.9$, and $\delta = 0$. As comparison serve the results for MDC hard decision decoding and AK1-INTER SDSD with MMSE estimation, as given in Fig. 6.5 (however, for $N_I = 250$). Note that no channel coding is employed in the reference system. In all cases, the number of bits per description amounts to $N_E^{[\mathrm{D},\nu]} = 750$, $\nu \in \{1, 2\}$ (plus some termination bits), which signifies that the number of bits transmitted on the channel is identical for configuration C and the references. As expected, the proposed ISCD system outperforms even the AK1-INTER non-iterative scheme by several dB (if a target parameter SNR of $> 20\,\mathrm{dB}$ is considered) after only $\Omega = 5$ iterations. If $\Omega = 25$ iterations are carried out, the achieved gains are even larger. The results are similar if a packet loss rate of $\epsilon = 0.05$ is expected on the transmission link. The convergence behavior of the proposed system has been confirmed by an EXIT chart analysis (not shown here).

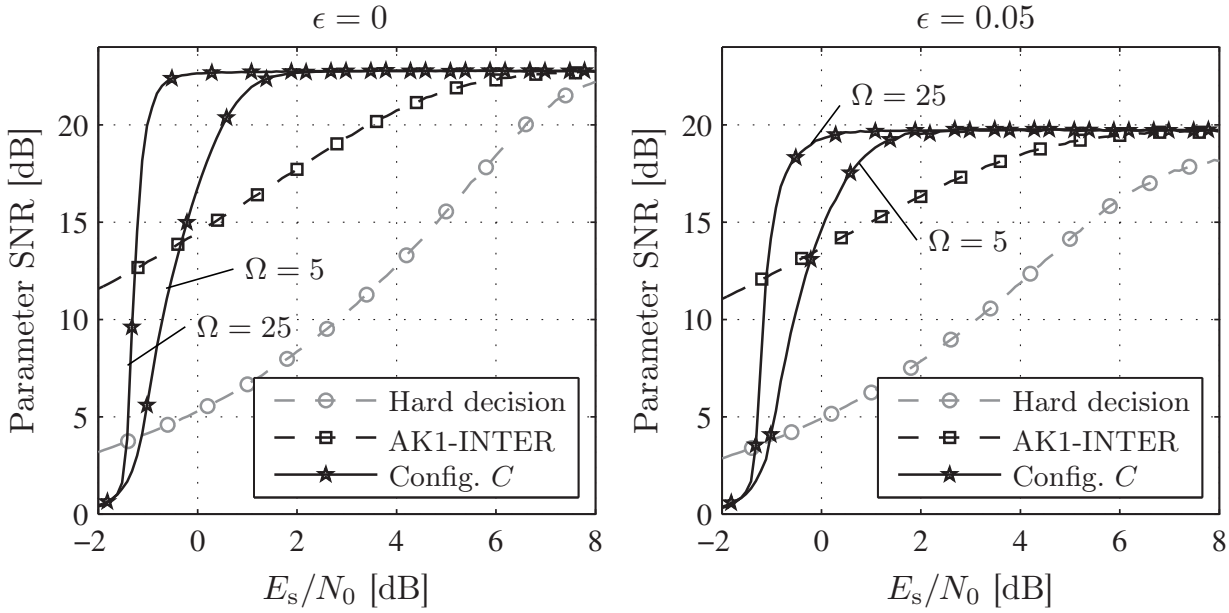

Figure 6.11: Comparison of non-iterative MDC decoding algorithms (Hard decision and AK1-INTER SDSD with MMSE estimation) with the proposed iteratively decodable configuration C with AK1-INTER SDSD and MMSE estimation for a source with $\rho = 0.9$ and $\delta = 0$, for $\epsilon = 0$ (left sub-plot) and $\epsilon = 0.05$ (right sub-plot). The MDIA is chosen as in Fig. 6.2, $N_U = N_I = 250$, $N_E^{[\mathrm{D},\nu]} \approx 750$ in all cases.

The Turbo error concealment concept presented here can also be extended such that $r_{\mathrm{CC}} = 1$ codes can be used [Tsc11]. In this case, no artificial redundancy (e.g., by using a linear block code) can be added to the bit mapping (i.e., $r_{\mathrm{BM}} = 1$) in order to fulfill the rate constraints. However, due to the special properties of the MDIA which already includes inherent redundancy, a bit mapping which allows perfect reconstruction in the extrinsic error-free feedback case (i.e., if all but one of the bits are perfectly reliable) can be found in some cases, if both descriptions are available. Such a bit mapping is unfortunately not possible for the nested index assignment depicted in Fig. 6.2. A thorough analysis of such bit mappings and a detailed assessment of the applicability to a given index assignment are given in [Tsc11]. A variety of other system optimizations for MDC-based ISCD including the study of different redundant bit mappings, cascades of two-dimensional MDIAs for realizing more than two descriptions, as well as a heuristic stopping criterion can be found in [Cui08].

6.5 Multiple Descriptions by Channel Coding

In this section, an alternative approach [Tsc11] to MDC is studied. This approach, denoted *Multiple Descriptions by Channel Coding* (MDCC), shall mainly be designed for error-free channel conditions (packet losses only), but its performance will also be studied in an AWGN environment. The transmitter of the proposed approach is depicted in Fig. 6.12. The main difference compared to the transmitter given in Fig. 6.1 is that no MDIA exists but the single descriptions are generated after

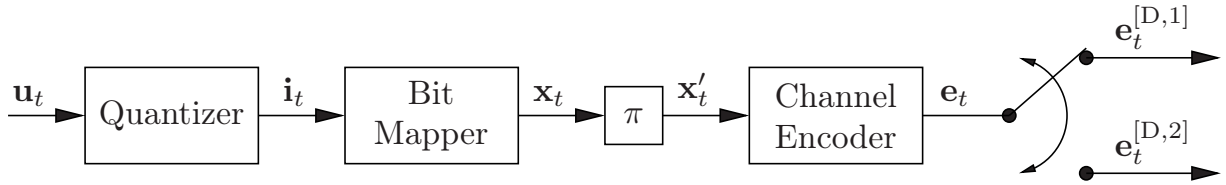

Figure 6.12: Baseband model for the transmitter of an MDCC scheme.

channel coding by splitting the vector $\mathbf{e}_t$ into two descriptions $\mathbf{e}^{[\mathrm{D},1]}$ and $\mathbf{e}^{[\mathrm{D},2]}$, which are independently transmitted. In this section, the descriptions are generated by alternatingly assigning the output bits to both descriptions, i.e.,

$$\mathbf{e}_t^{[\mathrm{D},1]} = (e_{t,1},\ e_{t,3},\ e_{t,5},\ \ldots) \tag{6.12}$$

$$\mathbf{e}_t^{[\mathrm{D},2]} = (e_{t,2},\ e_{t,4}, e_{t,6},\ \ldots)\ . \tag{6.13}$$

The MDCC approach follows the proposal of [PR99, SMB+09], where the generation of multiple descriptions using a channel code has been attempted. Another alternative multiple description approach for correlated sources, based on the modification of the quantizer, is proposed in [PE10].

At the receiver, both descriptions are multiplexed and the ISCD receiver given in Fig. 3.3 on page 33 can be used. If description ν is lost, the received L-values $\mathsf{L}_{\mathrm{CD}}^{[\mathrm{chan}]}(e_{t,\eta})$ of the channel decoder input corresponding to the bits of description ν are set to zero (no available information), i.e., $\mathsf{L}_{\mathrm{CD}}^{[\mathrm{chan}]}(e_{t,\eta}^{[\mathrm{D},\nu]}) = 0$. If both descriptions are lost, channel decoding is useless and the SDSD has to perform the estimation without input reliabilities. In the case of inter-frame correlation, information from previous frames can be exploited, however, in the case of intra-frame correlation, the SDSD has to output the mean of the central quantizer code book which is optimal in the MMSE sense [JN84, Vai93]. The goal of the proposed alternative approach is to fully reconstruct the original data even if one description is lost. This is, however, only possible if the system setup fulfills certain conditions. The analysis of these conditions is subject of the forthcoming paragraphs.

If a description is lost, this means that the output of the channel encoder is punctured such that its rate is doubled. If, for instance, a rate $r_{\mathrm{CC}} = 1$ channel code is used, the effective rate of the channel code thus becomes $r_{\mathrm{CC,eff}} = 2$ in the case of a packet loss. From Sec. 3.1.6 it is known that the area underneath the channel decoder EXIT characteristic amounts to $\mathcal{A}(\mathsf{C}_{\mathrm{CD}}) = \mathsf{I}_{\mathcal{C}}/r_{\mathrm{CC,eff}}$ if $r_{\mathrm{CC,eff}} \geq 1$. In the given example, $\mathsf{I}_{\mathcal{C}} = 1$ as no AWGN noise is present for the received description and $r_{\mathrm{CC,eff}} = 2$, leading to $\mathcal{A}(\mathsf{C}_{\mathrm{CD}}) = 1/2$. Thus, a necessary (but not sufficient) condition for reconstructing the frame if description ν is erased is $1 - \mathcal{A}(\mathsf{C}_{\mathrm{SD}}) < \mathcal{A}(\mathsf{C}_{\mathrm{CD}}) = 0.5$, leading to $\mathcal{A}(\mathsf{C}_{\mathrm{SD}}) > 0.5$.

In order to compare the novel MDCC approach with the original MDC scheme of Fig. 6.1, the following setup is utilized: A $Q = 22$ scalar *Lloyd-Max Quantizer* (LMQ) is followed by a redundant single parity check bit mapping. The bit mapping is realized using a single parity check bit in order to guarantee $d_{\min} = 2$. As already mentioned, a rate $r_{\mathrm{CC}} = 1$ inner code is employed. This setup leads to the same

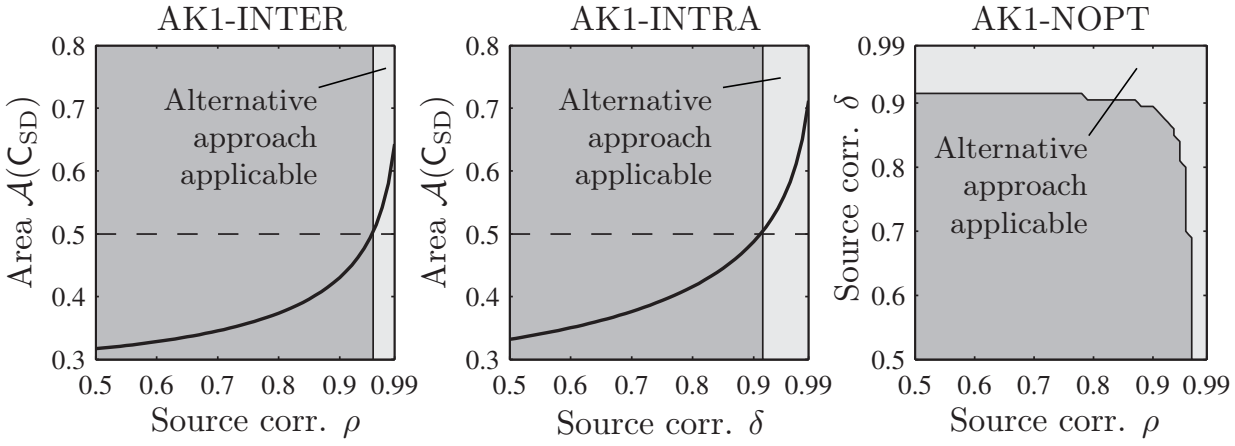

Figure 6.13: Residual source correlation required for applying the MDCC approach (2 descriptions) for $Q = 22$ scalar LMQ, single parity check bit mapping with $B_k = 6$ bits.

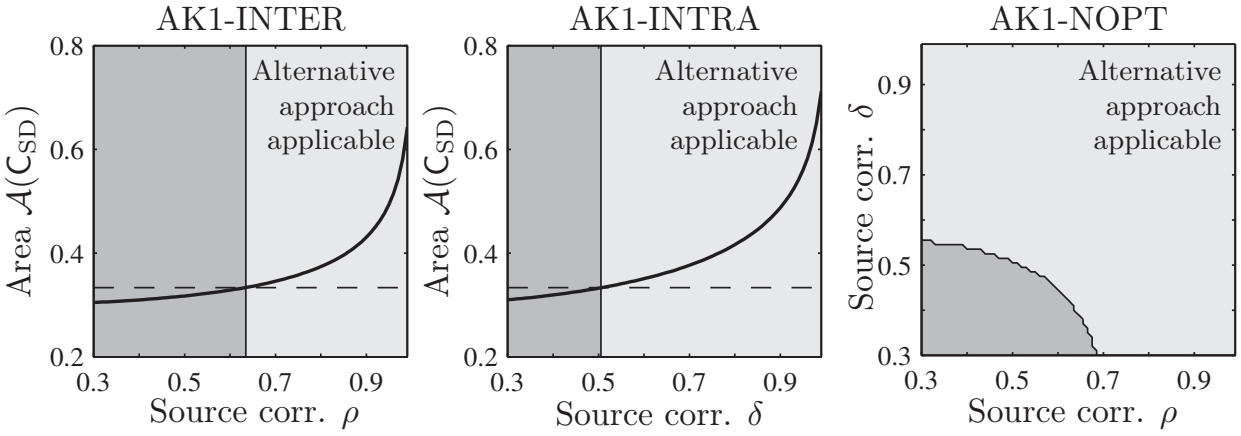

Figure 6.14: Residual source correlation required for applying the MDCC approach (3 descriptions) for $Q = 22$ scalar LMQ, single parity check bit mapping with $B_k = 6$ bits, allowing reconstruction if two out of three descriptions are available.

dimensioning as with the MDIA of Fig. 6.2, resulting in $B_k = 6$ bit per (central) quantizer index $i_{t,k}$. Figure 6.13 shows the required residual source correlation for guaranteeing $\mathcal{A}(\mathsf{C}_{\mathrm{SD}}) > 0.5$ for AK1-INTER, AK1-INTRA, and AK1-NOPT decoding, indicated by the light-gray regions. It can be seen that quite a high amount of correlation is necessary for guaranteeing decoding if a single description is lost. An in-depth analysis of this alternative approach and its applicability is given in [Tsc11].

The proposed approach is not limited to the generation of two descriptions, as depicted in Fig. 6.12. An arbitrary number of descriptions can be generated by appropriate demultiplexing. If we consider for instance the generation of three descriptions, we can for example set up the following constraint: The signal shall be reconstructed perfectly if two out of the three descriptions are received. In this case, the effect code rate of the original $r_{\mathrm{CC}} = 1$ inner code amounts to $r_{\mathrm{CC,eff}} = \frac{3}{2}$, as one third of the code bits are punctured by the packet loss. As already mentioned, a necessary (but not sufficient) condition for reconstructing the frame if one description is erased is $1 - \mathcal{A}(\mathsf{C}_{\mathrm{SD}}) < \mathcal{A}(\mathsf{C}_{\mathrm{CD}}) = \mathsf{I}_{\mathcal{C}}/r_{\mathrm{CC,eff}}$. Under the assumption that no AWGN noise

is present, we have $\mathsf{I}_{\mathcal{C}} = 1$, resulting in $\mathcal{A}(\mathsf{C}_{\mathrm{CD}}) = \frac{2}{3}$. Thus, we get the necessary condition $\mathcal{A}(\mathsf{C}_{\mathrm{SD}}) > \frac{1}{3}$ for this case. Figure 6.14 shows the necessary residual source correlation in this case for three decoding algorithms, marked by the light-gray regions. It can be seen that the amount of required correlation is significantly lower than in Fig. 6.13, however, one has to keep in mind that no reconstruction is possible in this case if only one description is received. In what follows we only focus on the former case with two descriptions, as this system allows for a better comparison with conventional MDC systems.

Simulation Example

The capabilities of the proposed approach shall be demonstrated by means of a simulation example. Two different source setups using the model of Fig. 3.1 are studied in this example. The first setup uses the correlation settings $\rho = 0$ and $\delta = 0.98$, such that intra-frame decoding is possible. The second setup is based on the correlation settings $\rho = 0.98$ and $\delta = 0$, allowing inter-frame decoding. Such high correlation values can be observed for instance for the gain factors of the *FlexCode* source codec (see also App. A and Fig. 2.10 on page 23). A $Q = 22$ scalar LMQ is used with a single parity check bit mapping leading to $B_k = 6$, $\forall k \in \{1, \ldots, N_I\}$. According to Fig. 6.13, the novel MDC approach is applicable for the given source settings.

The channel code for generating the descriptions is the $r_{\mathrm{CC}} = 1$, $J = 3$, $\mathbb{G}^{[\mathrm{CC}]} = \{\frac{10}{17}\}_8$ RNSC code, doped [tB01b] with a doping ratio of 1 : 25. Doping is necessary to trigger the decoding process for the given code [tB00a, tB01b] in the case of a packet loss, i.e., if only half of the bits are received ($r_{\mathrm{CC,eff}} = 2$). In this case, $\mathsf{I}_{\mathrm{CD}}^{[\mathrm{ext}]}(\mathsf{I}_{\mathrm{CD}}^{[\mathrm{apr}]} = 0) = 0$ for the given mother code. Doping leads to $\mathsf{I}_{\mathrm{CD}}^{[\mathrm{ext}]}(\mathsf{I}_{\mathrm{CD}}^{[\mathrm{apr}]} = 0) > 0$. Note that the doping ratio needs to be selected such that the doped positions (i.e., the positions where the output bit is replaced by a systematic bit) are equally assigned to $\mathbf{e}_t^{[\mathrm{D},1]}$ and $\mathbf{e}_t^{[\mathrm{D},2]}$. For the demultiplexing strategy given by (6.12) and (6.13), this means that the doping ratio has to be based on an odd number. The selection of this convolutional code with the given demultiplexing strategy has been confirmed by an EXIT chart analysis [Tsc11].

Figure 6.15 shows the behavior of the proposed approach for $N_I = 250$, $Q = 22$ scalar LMQ, and varying packet loss probabilities ϵ if no channel noise is present ($E_{\mathrm{s}}/N_0 \to \infty$). If both packets are received, the frame can immediately be reconstructed by performing only a single iteration (as for $E_{\mathrm{s}}/N_0 \to \infty$, the utilized $r_{\mathrm{CC}} = 1$ code delivers perfectly reliable extrinsic information, regardless of $\mathsf{I}_{\mathrm{CD}}^{[\mathrm{apr}]}$). In the case of a packet loss, $\Omega = 25$ iterations have been carried out. As a reference serves the non-iterative system setup without channel coding according to Sec. 6.2, employing either conventional hard decision decoding or AK1-INTRA/AK1-INTER decoding with MMSE estimation.

It can be seen that the proposed scheme outperforms the reference setups in all cases. In the case of the source with intra-frame correlation, the following upper limit can be computed, if we assume that the packet can be reconstructed completely as long as

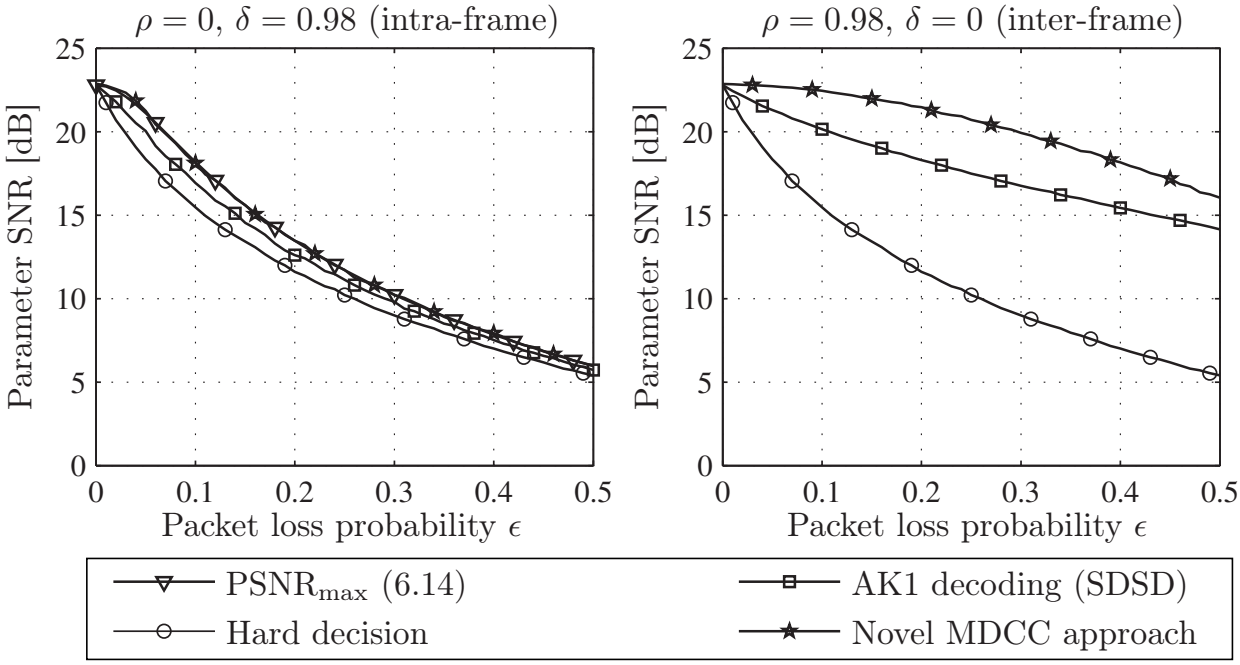

Figure 6.15: Achievable parameter SNR for the novel MDCC setup and conventional MDC of Fig. 6.1 with the MDIA of Fig. 6.2 and without channel coding (Hard decision and AK1 SDSD with MMSE estimation). $N_I = 250$, $Q = 22$ scalar LMQ. MDCC with single parity check bit mapping, doped $r_{\mathrm{CC}} = 1$ channel code with $J = 3$, $\mathbb{G}^{[\mathrm{CC}]} = \{\frac{10}{17}\}_8$, doping ratio 1 : 25, $\Omega = 25$. Identical number of transmitted bits $N_E^{[\mathrm{D},1]} = N_E^{[\mathrm{D},2]} = 750$ in all cases. Two source setups: $\rho = 0$, $\delta = 0.98$ (intra-frame correlation) and $\rho = 0.98$, $\delta = 0$ (inter-frame correlation). No channel noise, i.e., $E_{\mathrm{s}}/N_0 \to \infty$ (packet losses only).

one description is available, and that $\hat{u}_{t,\kappa} = 0$ if both descriptions are lost (as in this case the parameter SNR is maximized [JN84, Vai93] if the code book is symmetric around zero). This latter case occurs with probability ϵ^2 while the former case occurs with probability $2\epsilon(1-\epsilon)$. The maximum achievable parameter SNR for the intra-frame correlation case can then be written as

$$\mathrm{PSNR}_{\max}(\epsilon) = \frac{S}{(1-\epsilon)^2 N_{\mathrm{LMQ}} + 2\epsilon(1-\epsilon)N_{\mathrm{LMQ}} + \epsilon^2 S} = \frac{\frac{S}{N_{\mathrm{LMQ}}}}{1-\epsilon^2+\epsilon^2\frac{S}{N_{\mathrm{LMQ}}}}, \quad (6.14)$$

with $S = \mathsf{E}\{U^2\}$ denoting the power of the source symbols and N_{LMQ} the quantization noise power due to LMQ. If both descriptions are lost, the noise is assumed to be S as $\hat{u}_{t,\kappa} = 0$ and thus $u_{t,\kappa} - \hat{u}_{t,\kappa} = u_{t,\kappa}$. It can be seen in the left part of Fig. 6.15 that the proposed approach is able to closely reach this limit.

On the other hand, if inter-frame correlation can be exploited by the AK1-INTER SDSD (right sub-plot of Fig. 6.15), the gains are tremendously higher compared with the hard decision case. This is due to the high inter-frame correlation of $\rho = 0.98$ which is used to extrapolate the quantizer indices, even if both descriptions are lost. Also in this case, the novel MDCC approach leads to significant gains compared to the AK1 decoder, which is due to its ability to perfectly reconstruct the quantizer indices even if one description is missing.

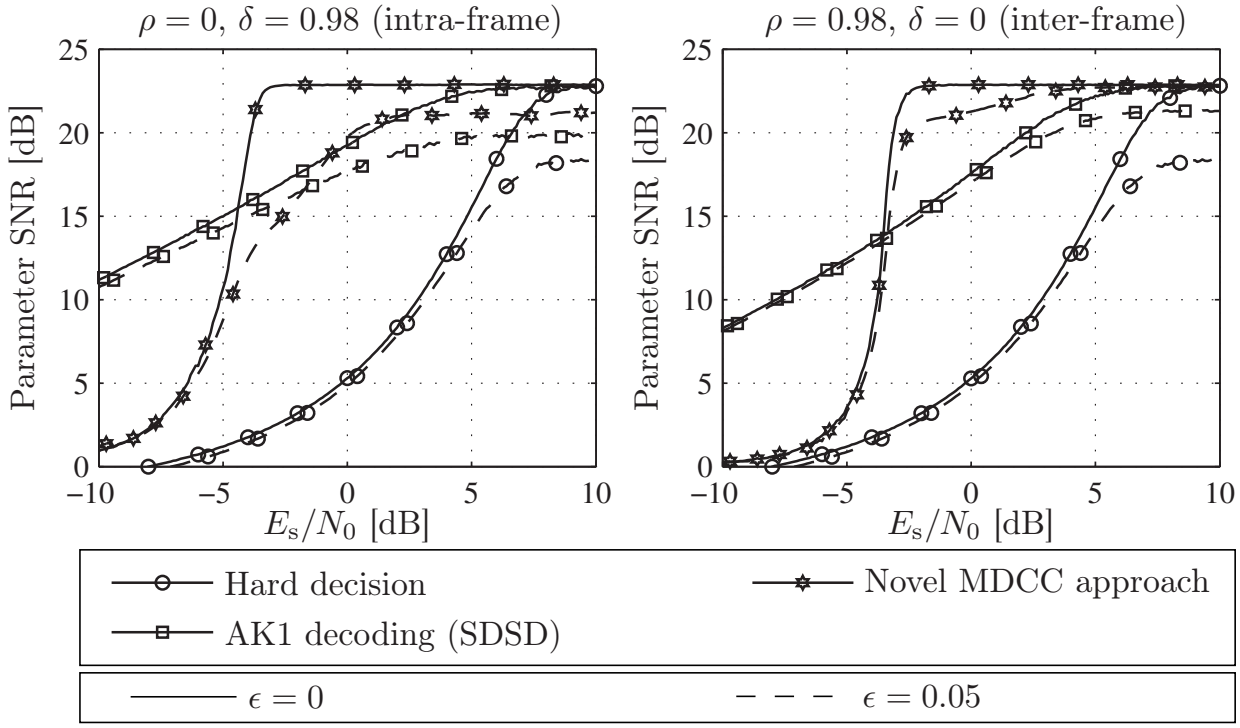

Figure 6.16: Performance of the novel MDCC scheme in the presence of AWGN channel noise compared to conventional MDC according to Fig. 6.1 with the MDIA of Fig. 6.2 and no channel coding. $N_I = 250$, $Q = 22$ scalar LMQ, MDCC with single parity check bit mapping, doped $r_{\mathrm{CC}} = 1$ channel code with $J = 3$, $\mathbb{G}^{[\mathrm{CC}]} = \{\frac{10}{17}\}_8$, doping ratio 1 : 25, $\Omega = 25$. $N_E^{[\mathrm{D},1]} = N_E^{[\mathrm{D},2]} = 750$ in all cases.

Finally, Fig. 6.16 shows the behavior of the novel approach if AWGN channel noise is present. Simulation results are given for $\epsilon = 0$ (solid lines ——) and $\epsilon = 0.05$ (dashed lines – – –). Again, the hard decision approach is significantly outperformed by the AK1-INTER decoder (or the AK1-INTRA decoder, respectively). As already observed in Fig. 6.15, the novel MDCC approach outperforms the conventional MDC scheme according to Fig. 6.1 with the MDIA of Fig. 6.2 and without channel coding in very good channel conditions. The right sub-plot of Fig. 6.16 confirms that the novel approach also outperforms the conventional MDC system for $E_{\mathrm{s}}/N_0 \gtrapprox -4\,\mathrm{dB}$ in the inter-frame correlation case. For $\epsilon = 0.05$, almost the same reconstruction quality as for $\epsilon = 0$ is observed for $E_{\mathrm{s}}/N_0 \gtrapprox 5\,\mathrm{dB}$.

In the intra-frame correlation case (left sub-plot of Fig. 6.16), the situation is similar, however, the gains in the case of packet losses are smaller than in the inter-frame case. The waterfall behavior is not as steep as in the inter-frame case for $\epsilon = 0.05$. This is due to the fact that the convergence speed is reduced in the intra-frame case (see Sec. 3.1.6). Thus the limited amount of iterations ($\Omega = 25$) and the relatively small interleaver size of $N_X^{[\mathrm{D},\nu]} = 750$ do not allow to reach the $(1, 1)$ point in the EXIT chart. Note that the area under C_{CD} is halved if a packet is lost (as $\mathcal{A}(\mathsf{C}_{\mathrm{CD}}) = \mathsf{I}_{\mathcal{C}}/r_{\mathrm{CC}}$) and $r_{\mathrm{CC,eff}} = 2$ if one description is lost, in contrast to $r_{\mathrm{CC,eff}} = 1$ if both descriptions are available.

Note that no additional data rate is spent explicitly for dedicated channel coding, i.e., the number of transmitted bits per description amounts to $N_E^{[\mathrm{D},\nu]} = N_I B^{[\mathrm{D},\nu]} = 750$ (plus some terminating bits) in all cases. If the system design allows for channel coding, more redundancy bits can be used for bit mapping (i.e., $B^{[\mathrm{D},\nu]}$ can be increased). In this case, the system is still capacity-achieving as $r_{\mathrm{CC}} \geq 1$ [AKtB04]. Finally note that all the techniques for realizing a joint compression-protection scheme introduced in Chapter 5 can also be used in the context of MDC.

6.6 Conclusions

In this chapter, the applicability of SDSD and ISCD to *Multiple Description Coding* (MDC) has been studied. The MDC concept is especially important for the transmission of audio-visual content over heterogeneous networks, where bit errors can occur alongside packet losses. The application of SDSD to MDC even leads to gains if only packet losses occur without bit errors. This signifies that the application of SDSD is always beneficial if packet losses are expected in the network. Already a small amount of residual source correlation can lead to significant gains in terms of reconstruction quality.

If a channel coding component is available, the MDC-based ISCD scheme allows to reconstruct the quantizer indices even in bad channel noise conditions. Optimized system settings for single-description ISCD can also be applied to MDC-based ISCD, showing good performance and convergence properties. The convergence of MDC-based ISCD schemes can be analyzed using a modified EXIT chart technique to account for the novel receiver topology. Based on this novel EXIT charts, we have suggested a system design which does not explicitly increase the bit rate using a dedicated channel code. This system yields superior reconstruction performance over a wide range of channel conditions compared to conventional MDC approaches.

In the final part of this chapter, an innovative MDC concept, where the single descriptions are generated by a convolutional code prior to symbol mapping, is introduced. This novel alternative approach, denoted MDCC, has been developed with the goal to exploit the residual source correlation such that the signal can be completely reconstructed if only one description is available at the receiver. The resulting system shows a superior reconstruction quality over a wide range of packet loss conditions, compared to a conventional MDIA-based MDC scheme. Even in the presence of additive channel noise, an excellent reconstruction quality can be guaranteed over a wide range of channel conditions.

7

Summary

With the discovery of Turbo codes, channel coding close to the theoretical limits postulated by Shannon became possible with moderate computational complexity and delay. Today, Turbo codes are included in the most important wireless communication standards, e.g., UMTS, LTE, or WiMAX. The Turbo principle of exchanging *extrinsic* information, which is the key for the success of Turbo codes, has been applied to other components of the receiver chain, too. A prominent example of such Turbo-like processing is *Iterative Source-Channel Decoding* (ISCD), which evaluates the residual redundancy of the source codec parameters as well as the eventual dedicated bit mapping redundancy in conjunction with the channel coding redundancy in an iterative loop.

ISCD is a well known concept which can be applied to existing transmission systems. However, it has been shown in previous publications on ISCD that it is not possible to fully exploit the available redundancy in purely receiver-based ISCD. The reason is that conventional systems are not optimized for ISCD and thus do not fully utilize the possibilities of a dedicated system design. The best performance can be achieved if the transmitter can be modified. The European Union funded *FlexCode* project tried to overcome these restrictions by designing a source-channel coding scheme that has the inherent capabilities to incorporate ISCD with optimized system settings. Most of the innovations presented in this thesis therefore had its seeds within the work in the *FlexCode* project. It has been shown that ISCD is not only able to improve the quality of existing systems, but that completely new system design guidelines may be beneficial if a receiver with iterative processing is envisaged.

In this thesis, we have considerably extended the ISCD system and introduced new design guidelines, improved receivers, as well as novel *Multi-Dimensional Bit Mappings* (MDBMs) which allow to lower the error floor. We have highlighted the applicability of ISCD to transmission systems with incremental redundancy and to *Multiple Description Coding* (MDC), which is important in packet-based networks prone to packet losses. We have furthermore derived that by a slight modification of the design guidelines, the ISCD transceiver becomes a powerful source compression scheme which has inherent error correction capabilities. Finally, a large part of this thesis deals with the reduction of the receiver complexity, either by limiting the

amount of executed iterations to the necessary minimum required for convergence, or by a novel system design that permits low-complexity receivers.

Iterative Source-Channel Decoding

After a thorough description of the transmitter and the receiver of the employed ISCD scheme, we have demonstrated its performance for different kinds of residual source redundancies. A figurative examples has been employed to clarify the interaction of the different algorithms. Additionally, the applicability of ISCD to the *FlexCode* source encoder has been proved by the aid of a simulation example.

EXtrinsic Information Transfer (EXIT) charts have been used to design most of the best performing ISCD systems so far. However, if inter-frame correlation is exploited, a precise prediction of the convergence is not possible. This inaccuracy is mainly due to a suboptimal receiver resulting from delay constraints. As a remedy, the new *EXIT Trajectory Bound* (ETB) has been proposed in this thesis. The ETB permits to precisely analyze the number of required decoding iterations. Moreover, we have given directions on how to utilize the EXIT chart to precisely predict the *Symbol Error Rate* (SER) behavior of ISCD.

In order to overcome the suboptimal performance of ISCD if correlation between consecutive frames is exploited and delay constraints exist, we have proposed a novel receiver concept which partly overcomes this suboptimality. This receiver better exploits the interrelations between consecutive frames in the iterative loop without imposing any additional delay limitations. The achievable gains by this novel receiver have been confirmed in a simulation example.

The key design aspect of ISCD is the mapping between the quantizer indices and their respective bit patterns. As it has been found in previous publications on ISCD that redundant bit mappings, i.e., bit mappings adding dedicated redundancy, lead to the best performing ISCD systems, this thesis focuses mainly on this kind of bit mappings. A powerful ISCD scheme based on the novel *Irregular Bit Mappings* (IBMs) has been proposed in this thesis. In this context, irregular means that different bit mappings can be specified for each parameter in a frame. Irregular bit mappings allow a system optimization based on the EXIT chart technique and lead to capacity-achieving ISCD systems. In fact, the concept of irregularity is the key technique used for most of the innovations presented in this thesis. We have further revealed that irregular bit mappings offer inherent *Unequal Error Protection* (UEP) capabilities on parameter level. Based on this observation, we have reformulated the optimization problem such that UEP can be taken into account. The use of UEP is especially beneficial in applications where some of the source codec parameters have a higher impact on the signal reconstruction quality than others.

A drawback of several known ISCD systems showing good waterfall performance is the error floor in good channel conditions. This error floor is mainly influenced by the distance properties of the bit mapping. We have demonstrated that the error floor can be substantially lowered by a careful selection of the bit mapping. As the resulting bit mappings often lead to a somewhat degraded waterfall performance,

we have proposed a specific low-complexity inner irregular convolutional code that overcomes this loss. We have furthermore shown how this code can efficiently be employed in the *FlexCode* source-channel encoder for the robust transmission of the transform coefficients, using a simple frame-by-frame adaptation algorithm.

The error floor problem occurs especially in the case of small quantizer code books. We have proposed an innovative novel transmitter and receiver concept to overcome this problem. In the case of small code books, bit mappings with good distance properties do not exist. The proposed remedy, denoted *Multi-Dimensional Bit Mapping* (MDBM), thus groups several consecutive quantizer indices to multi-dimensional super indices, allowing the use of bit mappings with better properties. In addition to a thorough description of the novel transmitter, we have given decoding algorithms for different kinds of *a priori* information. The improved error floor performance of ISCD with MDBMs has been confirmed by simulation examples.

As the convergence of the ISCD receiver is influenced by the channel quality on the one hand and the system setup on the other hand, it is beneficial to have an automatic control of the number of executed iterations. For this reason, we have compared several stopping criteria which detect convergence and only execute as many receiver iterations as necessary. Simulations have revealed that our proposed scheme, which is based on the parity check matrix of the redundant bit mapping, performs close to the optimum given by a genie bound. The proposed scheme outperforms most of the compared heuristic stopping criteria and performs very close to the known cross-entropy stopping scheme, which is however computationally more demanding.

Finally, the stopping criterion has been used to realize two novel ISCD-based *Hybrid Automatic Repeat reQuest* (HARQ) schemes. If the receiver is unable to correctly decode the current frame, a *Not-Acknowledge* (NACK) signal is sent back to the transmitter via a feedback channel. In this case, the transmitter does not repeat the frame, but incrementally transmits packets containing additional parity symbols that help decoding the current frame. The performance of two different realizations of such HARQ systems, which permit to effectively increase the user throughput, has been evaluated by means of an example.

Complexity Reduction of the Soft Decision Source Decoder

In the *second part* of this thesis, we have discussed several approaches for reducing the complexity of the main building block of ISCD – *Soft Decision Source Decoding* (SDSD). These can be combined with known complexity reduction techniques for channel decoding. The first approach is a transmitter-based modification of the quantizer such that a trade-off between quantizer distortion and receiver complexity can be adjusted. The proposed novel *conditional quantizer* has been thoroughly analyzed and it has been highlighted to what extend the complexity can be reduced if a certain reconstruction quality loss can be tolerated. We have furthermore analytically derived that the proposed quantizer decreases the entropy and the conditional entropy of the quantizer indices. Measurements have confirmed that the source coding related rate decreases.

The second complexity reduction approach is based on a methodology known from channel decoding: The most unreliable transitions in the SDSD are pruned as they only have a negligible influence on the final decoding result. We have shown by means of an example that many transitions can be pruned without noticeably affecting the convergence behavior and the reconstruction quality.

Finally, in a third step, both methods have been combined in order to realize a transmission system with the lowest overall complexity. We have found that the complexity-reduced versions of ISCD can lead to significant gains if the available computational resources are constrained. In this case, the number of iterations can even be increased by employing the novel combined algorithm, leading to higher reconstruction parameter SNRs over a wide range of channel conditions. In addition, we have given detailed complexity figures for all realizations of the SDSD in different domains.

Near-Lossless Turbo Source Compression

The *third part* of the thesis at hand deals with the realization of ISCD-based error-resilient source compression schemes for source codec parameters. The compression is achieved by configuring the transmitter in such a way that the number of transmitted bits is minimized while guaranteeing decodability at the receiver for a given channel quality. Again, the concept of irregularity has proved to be a powerful and versatile tool. We have derived that the optimum setup of the irregular bit mapping or of the irregular channel code can be found by solving a constrained linear optimization problem. We have additionally demonstrated how both components, i.e., bit mapping and channel code, can be jointly optimized and configured. This latter variant is the most versatile, leading to good compression ratios and system designs offering good convergence properties. All newly proposed designs have been compared with each other and it has been found that the jointly optimized system leads to the (theoretically) best compression performance. These findings have been confirmed by a simulation example, demonstrating that the novel ISCD-based approach is able to outperform classical entropy coding schemes like Huffman codes or arithmetic codes. Even widely available Unix compression tools can be outperformed.

Iterative Source-Channel Decoding of Multiple Descriptions

In the *final part* of this thesis, we have studied the applicability of ISCD to *Multiple Description Coding* (MDC). The MDC concept becomes increasingly important in heterogeneous networks where bit errors can occur alongside packet losses. We have shown that (non-iterative) SDSD can be applied to MDC and that gains are even possible if only packet losses occur without bit errors. This signifies that the application of SDSD is always beneficial if packet losses are expected in the network. A detailed analysis of the expected gains has been given for different kinds of exploitable *a priori* knowledge. We have found that even a small amount of residual source correlation can lead to significant gains in terms of reconstruction quality.

We have additionally generalized a known iterative MDC decoding concept to incorporate *a priori* knowledge, i.e., the unequal distribution and/or the correlation of quantizer indices. The resulting MDC-based ISCD scheme allows to reconstruct the quantizer indices even in bad channel noise conditions. We have modified the EXIT chart technique to account for the novel receiver topology. The resulting novel EXIT charts present a valuable tool for the convergence evaluation and analysis and permit to design capacity-approaching MDC systems. Based on the EXIT chart, we have suggested an innovative system design which does not explicitly add bit rate resulting from a dedicated channel code. Compared to conventional MDC approaches, our proposed system yields superior reconstruction performance over a wide range of channel conditions.

Finally, we have presented a new, second MDC concept, denoted *Multiple Descriptions by Channel Coding* (MDCC), where the single descriptions are not generated by a *Multiple Description Index Assignment* (MDIA) immediately after quantization, but by a convolutional code. This alternative code-generated MDC approach has been developed with the goal to exploit the residual source correlation such that the signal can be completely reconstructed, even if one out of two descriptions is missing. We have measured the necessary amount of required residual source redundancy for achieving this target. The resulting system yields superior performance over a wide range of packet loss conditions compared to a conventional MDIA-based MDC scheme. Even in the presence of additive channel noise, an excellent reconstruction quality can be observed and the proposed approach presents a promising alternative to conventional multiple description coding.

A

The *FlexCode* Source and Channel Coding Approach

The increasing heterogeneity of communication networks and the variability in user requirements form a challenge for source and channel coding algorithms. To address this challenge, the aim of the *FlexCode* project, financed by the European Union, was to create a speech and audio coder that can adapt instantaneously to network and user requirements. The channel encoder can flexibly select the required coding rate depending on the current network conditions, the available data rate and the computational power available at the terminal or base station. Thus the source coder can be set up according to the required *Quality of Service* (QoS).

A joint source-channel coding approach with iterative decoding has been selected for the *FlexCode* concept. However, several major modifications were needed to adapt the channel coder to the specific source coder and to realize a flexible adaptive scheme [SVC08, Sch08, SSJ+08, SSV08, SSV10].

The design goal of the *FlexCode* source and channel coding platform was to realize a system that is flexible in rate and that can instantly adapt to varying channel and network conditions. Therefore, a flexible source encoder has been designed without utilizing fixed code books. In contrast to, e.g., the *Adaptive Multi-Rate Wideband* (AMR-WB) codec [3GP01], which uses nine different operating modes to select between nine possibly available rates, the *FlexCode* system offers ultimate flexibility: any rate larger than a minimum rate can be selected on a quasi continuous scale. The rate adaptation in the *FlexCode* system works as follows: a certain gross rate is given by the network; using the knowledge of the channel quality, the *FlexCode* rate adaptation mechanism automatically allocates the source and channel coding rate such that possible transmission errors are minimized while maintaining a maximum speech quality.

A.1 The *FlexCode* Source Coding Concept

The baseline *FlexCode* source coding concept is described in [KO07, BGK+08a, BGK+08c, BGK+08b, KLK10]. A simplified block diagram is given in Fig. A.1.

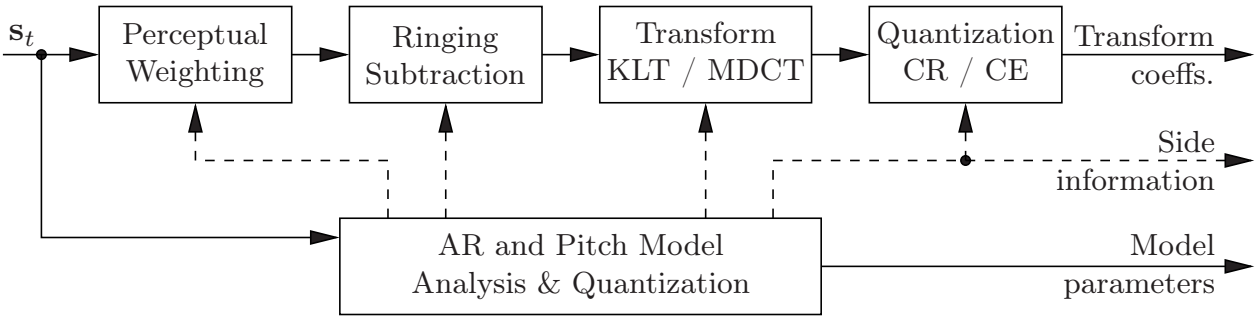

Figure A.1: The *FlexCode* source coding approach, simplified high-level block diagram.

In fact, the *FlexCode* source encoder is a transform-based speech and audio codec. For each frame, the source encoder provides a set of parameters that can be grouped into two main parts: model parameters and transform coefficients. The model parameters include the *Linear Prediction* (LP) coefficients describing the spectral envelope of the signal, gain factors, and parameters describing the pitch. Based on the model parameters, the transform coefficients can be derived using a *Karhunen-Loève Transform* (KLT). The model parameters are quantized with a fixed rate. It has been shown in [KO07] that for the model parameters, a minimum constant bit rate, which is independent of the total overall rate, is required and that the remainder of the bit rate shall be distributed to the transform coefficients. As an alternative to the KLT, an *Modified Discrete Cosine Transform* (MDCT) can be employed to realize a system with reduced complexity (but with somewhat lower overall performance in terms of audio quality).

Using the model parameters, the source encoder determines the quantizer setup for the transform coefficients which are quantized using either *Constrained Entropy Scalar Quantization* (CESQ) [LK07, ZSN08] or *Constrained Resolution Scalar Quantization* (CRSQ) [Ger79, GN98]. In the case of CRSQ, resulting in a bit stream of fixed rate, the source encoder determines the bit allocation of the transform coefficients, i.e., the number of quantization levels to be used for the considered parameter resulting in a fixed bit rate. In the case of CESQ, resulting in a bit stream of variable rate, the source encoder implicitly uses the model parameters to determine the distribution of the transform coefficients and the step size of the uniform quantizer. Using this information, an entropy coder (for example an arithmetic coder [BCW90, BCK07] or the ISCD based source compression presented in Sec. 5) can efficiently generate a compressed bit stream of variable bit rate, with a fixed mean rate however. The main characteristics of the *FlexCode* source coding setup are summarized in Table A.1 for both possible transform versions.

As already highlighted in Fig. A.1, the *FlexCode* source encoder generates model parameters and transform coefficients. The different model parameters in the KLT setup are summarized in Tab. A.2. The first parameter is the *Gaussian Mixture Model* (GMM) index, which selects the quantizers used for encoding the *Line Spectral Frequency* (LSF) representation of the spectral envelope [Sam04, BGK$^+$08a, BGK$^+$08b, ZSN08]. The LSFs are encoded using the GMM based quantizer, which means that the number of bits spent for quantizing a single LSF is not fixed. Only

	KLT	MDCT
Sampling rate	12.8 kHz	16 kHz
Frame length	20 ms (256 samples)	16 ms (256 samples)
Sub-frames	4	2
LP model order	16	16
Transform size	64	128
Bit rate for model	5.4 kbps (constant)	≈ 3.6 kbps (constant)
Source coding	10 kbps – 64 kbps	10 kbps – 64 kbps

Table A.1: Details of the possible *FlexCode* source coding setups.

Parameter	Sub-frame 1	Sub-frame 2	Sub-frame 3	Sub-frame 4	Bits per frame (20 ms)
GMM index					4
16 LSFs					34
Gain factor	6	6	6	6	24
Pitch					14
Pitch refine	4	4	4	4	16
Pitch decay	4	4	4	4	16
				Total:	108

Table A.2: Model parameters of the *FlexCode* source encoder in the KLT configuration.

the total number of 34 bits for all 16 LSFs is fixed. The remainder of the model parameters are gain factors for each sub-frame, a pitch period as well as pitch refine and decay parameters for each sub-frame. The total number of bits per frame amounts to 108, leading to the constant model bit rate of 5.4 kbps. More details on the model parameters and the bit allocation in the MDCT case can be found in [BGK+08b, SSV08].

A.2 The *FlexCode* Transmission Concept

The *FlexCode* channel coding concept has been adapted to the basic structure of the source encoder. As the quantization of the transform coefficients is controlled by the *Auto Regressive* (AR) and pitch model parameters, these need to be known prior to setting up the quantizers. Thus in order to apply *Iterative Source-Channel Decoding* (ISCD) to the transform coefficients, the source-channel decoder requires knowledge about the model in order to determine the encoding parameters of the transform coefficients like bit allocation and step sizes. Therefore, model parameters and the transform coefficients are separately encoded as shown in Fig. A.2 [SSJ+08, SSV10], which depicts a high-level representation of the complete *FlexCode* source-channel coding system in the single description case.

The *FlexCode* source encoder outputs the quantizer indices of the model parameters $\mathbf{i}_t^{[\text{Model}]}$ and of the transform coefficients $\mathbf{i}_t^{[\text{TC}]}$ which are applied to independent bit

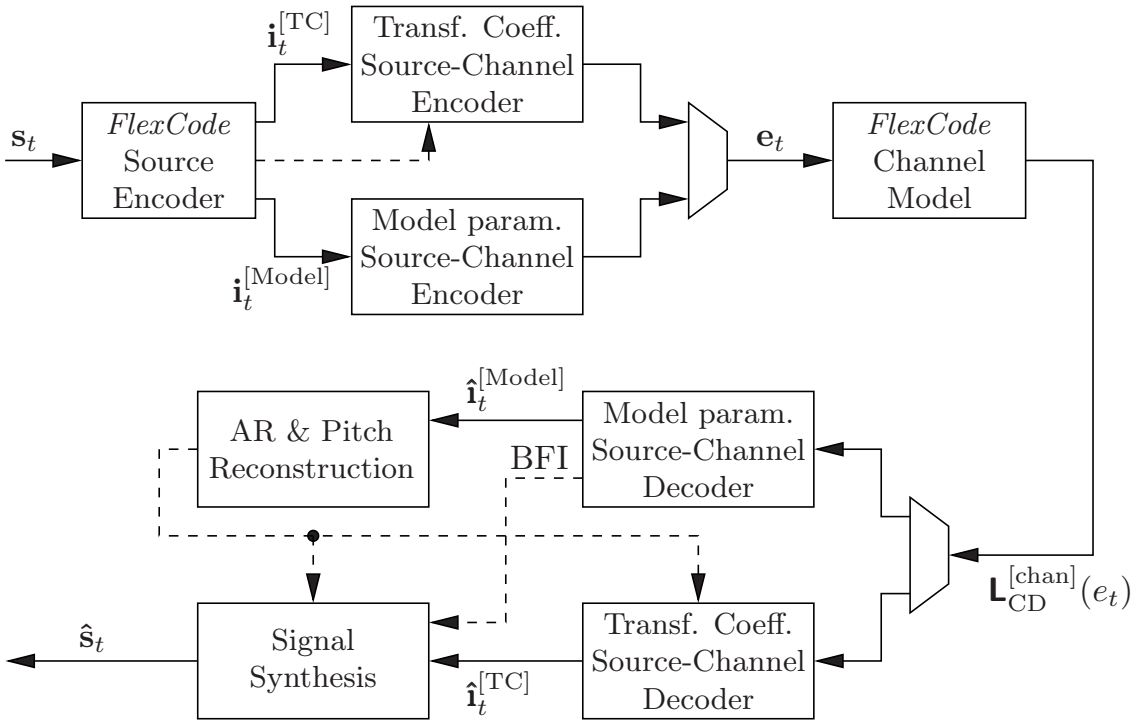

Figure A.2: The *FlexCode* source-channel coding approach for the single description case, simplified high-level block diagram.

mappers, interleavers and channel encoders in two branches. In order to encode the transform coefficients, side information (which depends on the utilized quantization mode) resulting from the model parameters is required. The *FlexCode* model parameters are always quantized using CRSQ. In this case, bit mapping, interleaving, and channel encoding can directly be applied as proposed in Sec. 3.1.2 and the ISCD system of Sec. 3.1.3 can be used at the receiver. A simulation example, given in Sec. 3.1.4, shows that ISCD can be efficiently utilized to improve the reconstruction of the model parameters.

The transform coefficients can however be quantized using either CESQ or CRSQ. In the case of CRSQ, the source encoder outputs the vector of quantizer indices $\mathbf{i}_t^{[TC]}$ consisting of $N_I = 256$ transform coefficients (four sub-frames, KLT of size 64) and as side information the number $Q_{t,k}$ of quantizer levels used to quantize each coefficient. Note that in contrast to the simplified system model of Sec. 3.1.2, the number of quantization levels is not fixed for all the parameters of a frame. Using this side information, the bit mapping can easily be performed in order to generate a bit stream. In the MDCT setup, a frame can also consist of less than 256 transform coefficients, quantized with higher resolution. Specifically, $N_I \in \{64, 128, 192, 256\}$. The non-transmitted coefficients are estimated at the receiver using the spectral envelope and artificial *BandWidth Extension* (BWE) techniques.

On the other hand, if CESQ is employed, the source encoder also outputs quantizer indices $\mathbf{i}_t^{[TC]}$ resulting from a uniform scalar quantization of the transform coefficients. The side information is in this case the variance of the estimated Gaussian distribution of each transform coefficient as well as the quantizer step size. Using

this side information, the probabilities of occurrence of each quantizer index can be computed and used as input to an entropy coding scheme, such as, e.g., an arithmetic encoder [BCW90, BCK07]. On the other hand, one of the ISCD based source compression schemes presented in Chapter 5 can be used. Especially the optimization using only inner irregular codes is beneficial as only a linear programming optimization needs to be solved each frame. No side information concerning the setup of the irregular code needs to be transmitted as transmitter and receiver have access to the same side information (computed from the model parameters). The concept of Chap. 5 has the advantage of inherent channel coding if bit errors occur on the channel. In the classical entropy coding case, bit errors can cause synchronization loss resulting in insertions or deletions and thus requiring an additional channel coding stage. A summary of compression and protection approaches in the CESQ case along with quality improvement techniques are given in [SVC08, Sch08, SSV08, SSV10].

After separate encoding of both model parameters and transform coefficients, the resulting multiplexed bit stream $\mathbf{e}_t$ is transmitted over the *FlexCode* channel model [Rei06, SV07] which outputs channel-related L-values $\mathsf{L}_{\mathrm{CD}}^{[\mathrm{chan}]}(e_t)$. At the receiver, the received L-values are demultiplexed and first of all, the model parameters are decoded. It has been found by measurements that there is still exploitable redundancy contained within the model parameters. Examples of two parameters are given in Fig. 2.10 in Sec. 2.4 on page 23. The model parameter source-channel decoder can exploit this residual redundancy. The model source-channel decoder generates, besides the estimated model quantizer indices $\hat{\mathbf{i}}_t^{[\mathrm{Model}]}$, a *Bad Frame Indicator* (BFI) by means of error detection. Such a BFI can be used for instance at the signal synthesis stage to perform *frame erasure concealment*. Using the estimated model parameters, the source decoder reconstructs the AR and pitch model, as well as the signal gains, which are then used to compute the side information required by the transform coefficient source-channel decoder. Without this side information, it is not possible to reconstruct the transform coefficients as the quantizers are not known. Therefore, the BFI is computed from the model parameters as an erroneously decoded model would result in a complete decoding failure of the remainder of the packet. If the transform coefficients cannot be recovered, a signal with acceptable quality can be reconstructed as the spectral envelope and the gains are available in the model and can be used to approximate the signal. With fully recovered side information, the estimated transform coefficients $\hat{\mathbf{i}}_t^{[\mathrm{TC}]}$ can be reconstructed and the source decoder can resynthesize the audio signal $\hat{\mathbf{s}}_t$.

If packet losses are expected on the transmission link, the *FlexCode* source-channel coding platform can instantly switch from single description mode to multiple description mode [BGK+08b]. The block diagram of the resulting system is depicted in Fig. A.3. The multiple descriptions are generated by the transform coefficient quantizers, which employ an adaptive *Multiple Description Index Assignment* (MDIA) according to [KKK08, BGK+08b]. The model is generated as in the single description case, however, it is included in both packets. In this case, the model can be fully reconstructed, even if one of the packets has been lost on the transmission link. This diversity transmission of the model parameters can be exploited at the receiver by

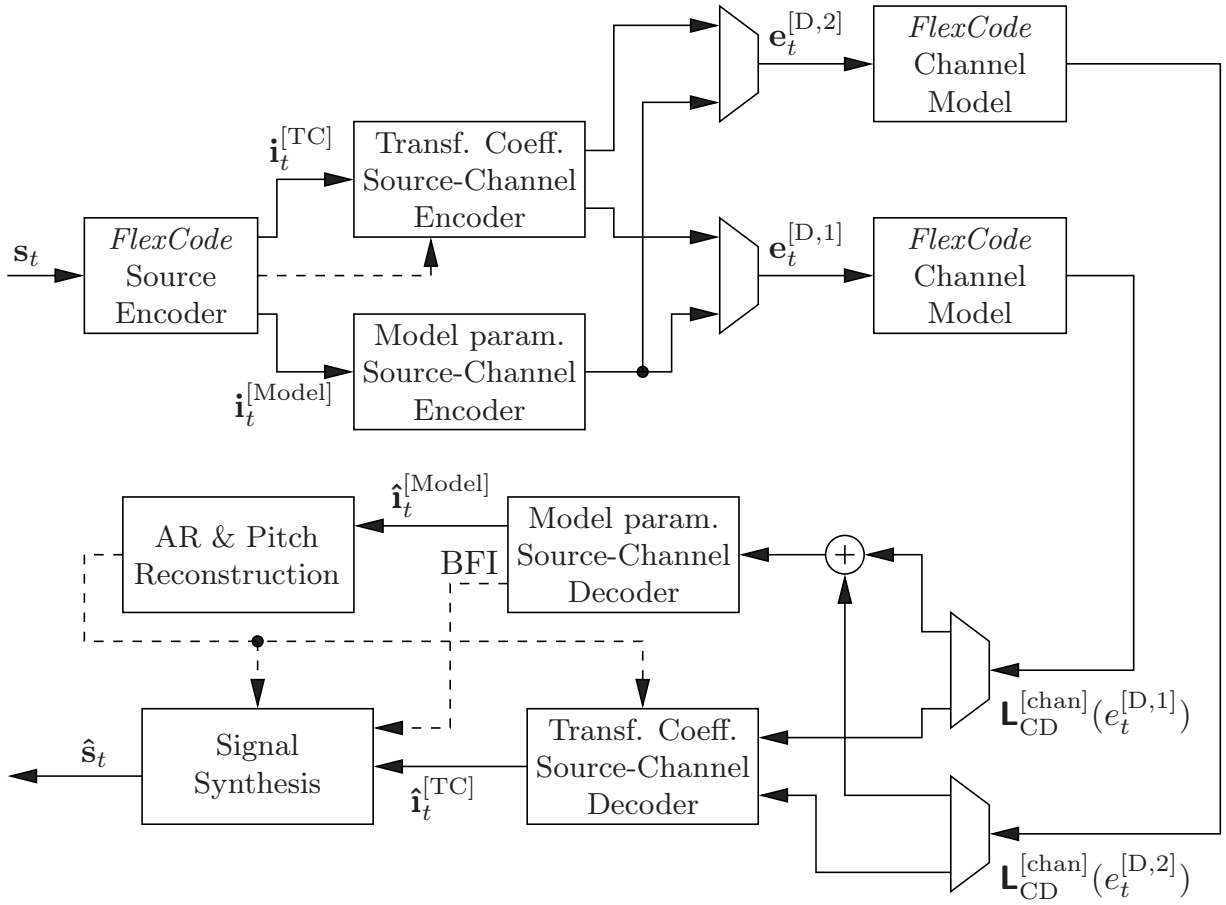

Figure A.3: The *FlexCode* source-channel coding approach for the multiple description case, simplified high-level block diagram.

summing up the L-values of the model parameter bits of both descriptions [LHHH05]. Using the model, the side information necessary for reconstructing the transform coefficients is generated as in the single description case. The transform coefficients can be reconstructed using the knowledge of the respective MDIA, known from the side information. All the algorithms and approaches given in Chapter 6 can be applied.

B

Derivation of Source Code Rates

B.1 Source Code Rate for Temporal Correlation

Theorem B.1. The rate $r_{\mathrm{SC}}^{[\mathrm{Markov,INTER}]}$ of a source which is temporally correlated (see Fig. 3.1) and quantized using quantizer $\mathcal{Q}$ amounts to

$$r_{\mathrm{SC}}^{[\mathrm{Markov,INTER}]}(t) = \frac{(t-1)\mathsf{H}(I_{t,k}|I_{t-1,k}) + \mathsf{H}(I_{t,k})}{t \cdot \mathsf{H}(I_{t,k})}$$

with $I_{t,k}$ denoting the random process describing the quantized indices at time t and at position k (within a frame).

Proof. The proof follows directly from the proof given in [Tho07c] for the case of intra-frame correlation by exchanging t and N_I. The rate $r_{\mathrm{SC}}^{[\mathrm{Markov,INTER}]}(t)$ can be written as

$$r_{\mathrm{SC}}^{[\mathrm{Markov,INTER}]}(t) = \frac{\mathsf{H}(I_{1,1},\ldots,I_{1,N_I},I_{2,1},\ldots,I_{2,N_I},\ldots,I_{t,1},\ldots,I_{t,N_I})}{t \cdot N_I \cdot \mathsf{H}(I_{t,k})}\,. \tag{B.1}$$

The joint entropy in the numerator of (B.1) can be rewritten using the chain rule of entropy [CT06] and the first order temporal Markov property of the source (the quantizer index $I_{t,k}$ is only dependent on $I_{t-1,k}$) and the assumption of the independence of the single indices in a frame, to

$$\begin{aligned}
&\mathsf{H}(I_{1,1},\ldots,I_{1,N_I},I_{2,1},\ldots,I_{2,N_I},\ldots,I_{t,1},\ldots,I_{t,N_I}) = \\
&\quad \mathsf{H}(I_{t,N_I}|I_{t-1,N_I}) + \mathsf{H}(I_{t-1,N_I}|I_{t-2,N_I}) + \ldots + \mathsf{H}(I_{2,N_I}|I_{1,N_I}) + \mathsf{H}(I_{1,N_I}) \\
&\qquad + \mathsf{H}(I_{t,N_I-1}|I_{t-1,N_I-1}) + \ldots + \mathsf{H}(I_{2,N_I-1}|I_{1,N_I-1}) + \mathsf{H}(I_{1,N_I-1}) \\
&\qquad\quad + \mathsf{H}(I_{t,1}|I_{t-1,1}) + \mathsf{H}(I_{t-1,1}|I_{t-2,1}) + \ldots + \mathsf{H}(I_{2,1}|I_{1,1}) + \mathsf{H}(I_{1,1})\,.
\end{aligned} \tag{B.2}$$

Note that the transmission is assumed to start at $t = 1$ (see also Sec. 3.1).

Under the assumption that the source is stationary and ergodic, i.e., $\mathsf{H}(I_{t,k}|I_{t-1,k})$ is independent of the values t and k (the same holds for $\mathsf{H}(I_{t,k})$), the expression in (B.2) can be simplified to ($\forall k \in \{1,\ldots,N_I\}$)

$$\begin{aligned}\mathsf{H}(I_{1,1},\ldots,I_{1,N_I},\ldots,I_{2,1},\ldots,I_{2,N_I},\ldots,I_{t,1},\ldots,I_{t,N_I}) = \\ N_I\left(\mathsf{H}(I_{t,k}|I_{t-1,k}) + \mathsf{H}(I_{t-1,k}|I_{t-2,k}) + \ldots + \mathsf{H}(I_{2,k}|I_{1,k}) + \mathsf{H}(I_{1,k})\right) = \\ N_I \cdot (t-1) \cdot \mathsf{H}(I_{t,k}|I_{t-1,k}) + N_I \cdot \mathsf{H}(I_{1,k}) \end{aligned} \tag{B.3}$$

Inserting (B.3) into (B.1) proves the theorem. □

B.2 Source Code Rate for Spatial and Temporal Correlation

Theorem B.2. The rate $r_{\mathrm{SC}}^{[\mathrm{Markov,OPT}]}$ of a source which is spatially and temporally correlated (see Fig. 3.1) and quantized using quantizer $\mathcal{Q}$ amounts to

$$\begin{aligned} r_{\mathrm{SC}}^{[\mathrm{Markov,OPT}]}(t) = \frac{(N_I-1)(t-1)\mathsf{H}(I_{t,k}|I_{t-1,k},I_{t,k-1}) + (t-1)\mathsf{H}(I_{t,k}|I_{t-1,k})}{t \cdot N_I \cdot \mathsf{H}(I_{t,k})} \\ + \frac{(N_I-1)\mathsf{H}(I_{t,k}|I_{t,k-1}) + \mathsf{H}(I_{t,k})}{t \cdot N_I \cdot \mathsf{H}(I_{t,k})} \end{aligned}$$

with $I_{t,k}$ denoting the random process describing the quantized indices at time t and at position k (within a frame).

Proof. The proof uses the same approach as described in [Tho07c] for the case of intra-frame correlation. The rate $r_{\mathrm{SC}}^{[\mathrm{Markov,OPT}]}$ can be written as

$$r_{\mathrm{SC}}^{[\mathrm{Markov,OPT}]}(t) = \frac{\mathsf{H}(I_{1,1},\ldots,I_{1,N_I},I_{2,1},\ldots,I_{2,N_I},\ldots,I_{t,1},\ldots,I_{t,N_I})}{t \cdot N_I \cdot \mathsf{H}(I_{t,k})}\,. \tag{B.4}$$

The joint entropy in the numerator of (B.4) can be rewritten using the chain rule of entropy [CT06] and the first order Markov properties of the source (the quantizer index $I_{t,k}$ is only dependent on $I_{t-1,k}$ and $I_{t,k-1}$) to

$$\begin{aligned} &\mathsf{H}(I_{1,1},\ldots,I_{1,N_I},I_{2,1},\ldots,I_{2,N_I},\ldots,I_{t,1},\ldots,I_{t,N_I}) = \mathsf{H}(I_{t,N_I}|I_{t-1,N_I},I_{t,N_I-1}) \\ &+ \mathsf{H}(I_{t,N_I-1}|I_{t-1,N_I-1},I_{t,N_I-2}) + \ldots + \mathsf{H}(I_{t,2}|I_{t-1,2},I_{t,1}) + \mathsf{H}(I_{t,1}|I_{t-1,1}) \\ &+ \mathsf{H}(I_{t-1,N_I}|I_{t-2,N_I},I_{t-1,N_I-1}) + \ldots + \mathsf{H}(I_{t-1,2}|I_{t-2,2},I_{t-1,1}) + \mathsf{H}(I_{t-1,1}|I_{t-2,1}) \\ &+ \mathsf{H}(I_{2,N_I}|I_{1,N_I},I_{2,N_I-1}) + \ldots + \mathsf{H}(I_{2,2}|I_{1,2},I_{2,1}) + \mathsf{H}(I_{2,1}|I_{1,1}) \\ &\quad + \mathsf{H}(I_{1,N_I}|I_{1,N_I-1}) + \mathsf{H}(I_{1,N_I-1}|I_{1,N_I-2}) + \mathsf{H}(I_{1,2}|I_{1,1}) + \mathsf{H}(I_{1,1})\,. \end{aligned} \tag{B.5}$$

Note that the transmission is assumed to start at $t = 1$ (see also Sec. 3.1).

Under the assumption that the source is stationary (with respect to time t and position k) and ergodic, i.e., $\mathsf{H}(I_{t,k}|I_{t-1,k}, I_{t,k-1})$ is independent of the values t and k (the same holds for $\mathsf{H}(I_{t,k}|I_{t-1,k})$, $\mathsf{H}(I_{t,k}|I_{t,k-1})$, and $\mathsf{H}(I_{t,k})$), the expression in (B.5) can be simplified to

$$\begin{aligned}\mathsf{H}(I_{1,1}, \ldots, I_{1,N_I}, \ldots, I_{2,1}, \ldots, I_{2,N_I}, \ldots, I_{t,1}, \ldots, I_{t,N_I}) = \\ (t-1) \cdot (N_I - 1) \cdot \mathsf{H}(I_{t,k}|I_{t-1,k}, I_{t,k-1}) + (t-1) \cdot \mathsf{H}(I_{t,k}|I_{t-1,k}) \\ + (N_I - 1) \cdot \mathsf{H}(I_{t,k}|I_{t,k-1}) + \mathsf{H}(I_{t,k}) \quad \text{(B.6)}\end{aligned}$$

Inserting (B.6) into (B.4) proves the theorem. □

C

A Priori Probabilities for AK1-INTRA Multi-Dimensional SDSD

Theorem C.1. If *Multi-Dimensional Bit Mappings* (MDBMs), as introduced in Sec. 3.4.2, are utilized with AK1-INTRA decoding, the *a priori* probabilities on super index level are given by

$$\begin{aligned}&\mathsf{Pr}\{I^{\star}_{t,k'} = q^{\star} | I^{\star}_{t,k'-1} = \tilde{q}^{\star}\} = \\ &\mathsf{Pr}\{I_{t,\Psi(k'-1)+1} = q_1 | I_{t,\Psi(k'-2)+\Psi} = \tilde{q}_{\Psi}\} \prod_{j=2}^{\Psi} \mathsf{Pr}\{I_{t,\Psi(k'-1)+j} = q_j | I_{t,\Psi(k'-1)+j-1} = q_{j-1}\}\end{aligned} \tag{C.1}$$

with

$$i^{\star}_{t,k'} = 1 + \sum_{j=1}^{\Psi} \left(i_{t,(k'-1)\Psi+j} - 1 \right) Q^{\Psi-j}$$

and thus $q^{\star} = 1 + \sum_{j=1}^{\Psi} (q_j - 1) Q^{\Psi-j}$ and $\tilde{q}^{\star} = 1 + \sum_{j=1}^{\Psi} (\tilde{q}_j - 1) Q^{\Psi-j}$.

Proof. The probability $\mathsf{Pr}\{I^{\star}_{t,k'} = q^{\star} | I^{\star}_{t,k'-1} = \tilde{q}^{\star}\}$ is decomposed using Bayes' theorem and by exploiting the first order Markov property of the single indices, leading to (in simplified probability notation)

$$\begin{aligned}\mathsf{P}(i^{\star}_{t,k'} | i^{\star}_{t,k'-1}) &= \mathsf{P}(i_{t,\Psi(k'-1)+1}, \ldots, i_{t,\Psi(k'-1)+\Psi} | i_{t,\Psi(k'-2)+1}, \ldots, i_{t,\Psi(k'-2)+\Psi}) \\ &= \frac{\mathsf{P}(i_{t,\Psi(k'-1)+1}, \ldots, i_{t,\Psi(k'-1)+\Psi}, i_{t,\Psi(k'-2)+1}, \ldots, i_{t,\Psi(k'-2)+\Psi})}{\mathsf{P}(i_{t,\Psi(k'-2)+1}, \ldots, i_{t,\Psi(k'-2)+\Psi})} \\ &= \frac{\mathsf{P}(i_{t,\mathfrak{k}}, \ldots, i_{t,\mathfrak{k}-\Psi+1}, i_{t,\mathfrak{k}-\Psi}, \ldots, i_{t,\mathfrak{k}-2\Psi+1})}{\mathsf{P}(i_{t,\mathfrak{k}-\Psi}, \ldots, i_{t,\mathfrak{k}-2\Psi+1})}\end{aligned}$$

with the index substitution $\mathfrak{k} = \Psi(k'-1)+\Psi$. By applying the chain rule of probability [PU02] and by exploiting the Markov property of neighboring indices, we get

$$\begin{aligned}
\mathsf{P}(i^{\star}_{t,k'}|i^{\star}_{t,k'-1}) &= \mathsf{P}(i_{t,\mathfrak{k}}|i_{t,\mathfrak{k}-1}) \cdot \mathsf{P}(i_{t,\mathfrak{k}-1}|i_{t,\mathfrak{k}-2}) \cdots \mathsf{P}(i_{t,\mathfrak{k}-\Psi+1}|i_{t,\mathfrak{k}-\Psi}) \\
&\qquad \times \frac{\mathsf{P}(i_{t,\mathfrak{k}-\Psi}|i_{t,\mathfrak{k}-\Psi-1}) \cdots \mathsf{P}(i_{t,\mathfrak{k}-2\Psi+2}|i_{t,\mathfrak{k}-2\Psi+1}) \cdot \mathsf{P}(i_{t,\mathfrak{k}-2\Psi+1})}{\mathsf{P}(i_{t,\mathfrak{k}-\Psi}|i_{t,\mathfrak{k}-\Psi-1}) \cdots \mathsf{P}(i_{t,\mathfrak{k}-2\Psi+2}|i_{t,\mathfrak{k}-2\Psi+1}) \cdot \mathsf{P}(i_{t,\mathfrak{k}-2\Psi+1})} \\
&= \mathsf{P}(i_{t,\mathfrak{k}}|i_{t,\mathfrak{k}-1}) \cdot \mathsf{P}(i_{t,\mathfrak{k}-1}|i_{t,\mathfrak{k}-2}) \cdots \mathsf{P}(i_{t,\mathfrak{k}-\Psi+1}|i_{t,\mathfrak{k}-\Psi}) \\
&= \mathsf{P}(i_{t,\Psi(k'-1)+\Psi}|i_{t,\Psi(k'-1)+\Psi-1}) \cdots \mathsf{P}(i_{t,\Psi(k'-1)+1}|i_{t,\Psi(k'-1)}) \\
&= \mathsf{P}(i_{t,\Psi(k'-1)+\Psi}|i_{t,\Psi(k'-1)+\Psi-1}) \cdots \mathsf{P}(i_{t,\Psi(k'-1)+1}|i_{t,\Psi(k'-2)+\Psi}) \,.
\end{aligned}$$

This means that the product of the $\Psi-1$ crossover probabilities between each of the Ψ indices contained in one super index has to be multiplied by the crossover probability between the last index of super index $i^{\star}_{t,k'-1}$ $(i_{t,\Psi(k'-2)+\Psi})$ and the first index of $i^{\star}_{t,k'}$ $(i_{t,\Psi(k'-1)+1})$. Rewriting this fact using the product notation and by distinguishing two neighboring super indices directly leads to (C.1). □

D

Quantizer Index Conditional Entropy after Conditional Quantization

Theorem D.1. The entropy $\mathsf{H}(I_{t,k}^{[\mathrm{CQ}]})$ of conditional quantization is less than or equal to the entropy $\mathsf{H}(I_{t,k})$ of the original quantizer indices if identical system settings are applied.

Proof. The proof is conducted for the inter-frame CQ case, i.e., conditional quantization based on the previous index $i_{t-1,k}$. The proof can easily be applied to intra-frame CQ by exchanging time and position indices.

In order to simplify notation, we introduce the time and position-dependent set $\mathbb{I}_{t,k}^{[\mathrm{CQ}]}$ which corresponds to the index set which is currently employed at position t, k, i.e., if the previous quantizer index has been $i_{t-1,k}^{[\mathrm{CQ}]} = q$, then $\mathbb{I}_{t,k}^{[\mathrm{CQ}]} = \mathbb{I}_{\mathrm{red},i_{t-1,k}^{[\mathrm{CQ}]}}^{[\mathrm{tim}]} = \mathbb{I}_{\mathrm{red},q}^{[\mathrm{tim}]}$.

As already mentioned in Sec. 4.1.3, the conditional quantizer function $\mathcal{Q}_{\mathrm{CQ}}$ can be decomposed into $\mathcal{I}_{t,k}^{[\mathrm{CQ}]} \circ \mathcal{Q}$ with $\mathcal{Q}$ being the original quantizer function and $\mathcal{I}_{t,k}^{[\mathrm{CQ}]}$ being a surjective function with time and position-dependent codomain $\mathbb{I}_{t,k}^{[\mathrm{CQ}]} \subseteq \mathbb{I}$ and $\mathcal{I}_{t,k}^{[\mathrm{CQ}]}(i_{t,k}) = i_{t,k}^{[\mathrm{CQ}]}$. We have under the assumption that $i_{t-1,k}^{[\mathrm{CQ}]} = q$ is given (see also [CT06] for a similar conduct of proof)

$$\mathsf{P}(i_{t,k}^{[\mathrm{CQ}]}) = \sum_{\forall i \in \mathbb{I}, i_{t,k}^{[\mathrm{CQ}]} = \mathcal{I}_{t,k}^{[\mathrm{CQ}]}(i)} \mathsf{P}(i)\,, \tag{D.1}$$

with $\mathsf{P}(i_{t,k}^{[\mathrm{CQ}]}) \geq \mathsf{P}(i)$ (for $i_{t,k}^{[\mathrm{CQ}]} = \mathcal{I}_{t,k}^{[\mathrm{CQ}]}(i)$) as a direct consequence. For any given $i_{t,k}^{[\mathrm{CQ}]}$, we therefore have

$$\begin{aligned} \sum_{\forall i \in \mathbb{I}, i_{t,k}^{[\mathrm{CQ}]} = \mathcal{I}_{t,k}^{[\mathrm{CQ}]}(i)} \mathsf{P}(i) \operatorname{ld} \mathsf{P}(i) &\leq \sum_{\forall i \in \mathbb{I}, i_{t,k}^{[\mathrm{CQ}]} = \mathcal{I}_{t,k}^{[\mathrm{CQ}]}(i)} \mathsf{P}(i) \operatorname{ld} \mathsf{P}(i_{t,k}^{[\mathrm{CQ}]}) \\ &= \mathsf{P}(i_{t,k}^{[\mathrm{CQ}]}) \operatorname{ld} \mathsf{P}(i_{t,k}^{[\mathrm{CQ}]}) \end{aligned} \tag{D.2}$$

due to the monotonicity of the ld function and the aforementioned inequality. Thus, the entropy $\mathsf{H}(I_{t,k})$ can be written as (with the assumption of temporal and spatial stationarity of the original quantizer indices I)

$$\begin{aligned}\mathsf{H}(I_{t,k}) = \mathsf{H}(I) &= -\sum_{\forall i \in \mathbb{I}} \mathsf{P}(i) \operatorname{ld} \mathsf{P}(i) \\ &= -\sum_{\forall i_{t,k}^{[\mathrm{CQ}]} \in \mathbb{I}_{t,k}^{[\mathrm{CQ}]}} \sum_{\forall i \in \mathbb{I}, i_{t,k}^{[\mathrm{CQ}]} = \mathcal{I}_{t,k}^{[\mathrm{CQ}]}(i)} \mathsf{P}(i) \operatorname{ld} \mathsf{P}(i) \\ &\geq -\sum_{\forall i_{t,k}^{[\mathrm{CQ}]} \in \mathbb{I}_{t,k}^{[\mathrm{CQ}]}} \mathsf{P}(i_{t,k}^{[\mathrm{CQ}]}) \operatorname{ld} \mathsf{P}(i_{t,k}^{[\mathrm{CQ}]}) \\ &= \mathsf{H}(I_{t,k}^{[\mathrm{CQ}]}) \,. \end{aligned} \tag{D.3}$$

Thus, for any given $i_{t-1,k}^{[\mathrm{CQ}]}$, $\mathsf{H}(I_{t,k}) \geq \mathsf{H}(I_{t,k}^{[\mathrm{CQ}]})$, which then also holds in the general case. □

Theorem D.2. The conditional entropy $\mathsf{H}(I_{t,k}^{[\mathrm{CQ}]}|I_{t-1,k}^{[\mathrm{CQ}]})$ of conditional quantization is less than or equal to the conditional entropy $\mathsf{H}(I_{t,k}|I_{t-1,k})$ of the original quantizer if identical system settings are applied.

Proof. The proof can be built by extending the previous proof. Again, we get

$$\mathsf{P}(i_{t,k}^{[\mathrm{CQ}]}|i_{t-1,k}) = \sum_{\forall i_{t,k} \in \mathbb{I}, i_{t,k}^{[\mathrm{CQ}]} = \mathcal{I}_{t,k}^{[\mathrm{CQ}]}(i_{t,k})} \mathsf{P}(i_{t,k}|i_{t-1,k}) \,, \tag{D.4}$$

thus $\mathsf{P}(i_{t,k}^{[\mathrm{CQ}]}|i_{t-1,k}) \geq \mathsf{P}(i_{t,k}|i_{t-1,k})$ for $i_{t,k}^{[\mathrm{CQ}]} = \mathcal{I}_{t,k}^{[\mathrm{CQ}]}(i_{t,k})$. Following the same approach as in (D.2) leads to

$$\sum_{\forall i_{t,k} \in \mathbb{I}, i_{t,k}^{[\mathrm{CQ}]} = \mathcal{I}_{t,k}^{[\mathrm{CQ}]}(i_{t,k})} \mathsf{P}(i_{t,k}, i_{t-1,k}) \operatorname{ld} \mathsf{P}(i_{t,k}|i_{t-1,k}) \leq \sum_{\forall i_{t,k} \in \mathbb{I}, i_{t,k}^{[\mathrm{CQ}]} = \mathcal{I}_{t,k}^{[\mathrm{CQ}]}(i_{t,k})} \mathsf{P}(i_{t,k}, i_{t-1,k}) \operatorname{ld} \mathsf{P}(i_{t,k}^{[\mathrm{CQ}]}|i_{t,k}) \tag{D.5}$$

$$= \mathsf{P}(i_{t,k}^{[\mathrm{CQ}]}, i_{t-1,k}) \operatorname{ld} \mathsf{P}(i_{t,k}^{[\mathrm{CQ}]}|i_{t-1,k}) \,. \tag{D.6}$$

Furthermore note that $\mathsf{P}(i_{t,k}^{[\mathrm{CQ}]}|i_{t-1,k}) \leq \mathsf{P}(i_{t,k}^{[\mathrm{CQ}]}|i_{t-1,k}^{[\mathrm{CQ}]})$, as

$$\mathsf{P}(i_{t,k}^{[\mathrm{CQ}]}|i_{t-1,k}) = \begin{cases} \mathsf{P}(i_{t,k}^{[\mathrm{CQ}]}|i_{t-1,k}^{[\mathrm{CQ}]}) & \text{if } i_{t,k}^{[\mathrm{CQ}]} \in \mathbb{I}_{\mathrm{red},i_{t-1,k}}^{[\mathrm{tim}]} \\ 0 & \text{if } i_{t,k}^{[\mathrm{CQ}]} \notin \mathbb{I}_{\mathrm{red},i_{t-1,k}}^{[\mathrm{tim}]} \,. \end{cases} \tag{D.7}$$

Thus, the conditional entropy $\mathsf{H}(I_{t,k}|I_{t-1,k})$ can be written as

$$\mathsf{H}(I_{t,k}|I_{t-1,k}) = -\sum_{\forall i_{t-1,k} \in \mathbb{I}} \sum_{\forall i_{t,k} \in \mathbb{I}} \mathsf{P}(i_{t,k}, i_{t-1,k}) \operatorname{ld} \mathsf{P}(i_{t,k}|i_{t-1,k})$$

$$
\begin{aligned}
&= -\sum_{\forall i_{t-1,k} \in \mathbb{I}} \sum_{\forall i_{t,k}^{[\mathrm{CQ}]} \in \mathbb{I}_{t,k}^{[\mathrm{CQ}]}} \sum_{\forall i_{t,k} \in \mathbb{I}, i_{t,k}^{[\mathrm{CQ}]} = \mathcal{I}_{t,k}^{[\mathrm{CQ}]}(i_{t,k})} \mathsf{P}(i_{t,k}, i_{t-1,k}) \operatorname{ld} \mathsf{P}(i_{t,k} | i_{t-1,k}) \\
&\geq -\sum_{\forall i_{t-1,k} \in \mathbb{I}} \sum_{\forall i_{t,k}^{[\mathrm{CQ}]} \in \mathbb{I}_{t,k}^{[\mathrm{CQ}]}} \mathsf{P}(i_{t,k}^{[\mathrm{CQ}]}, i_{t-1,k}) \operatorname{ld} \mathsf{P}(i_{t,k}^{[\mathrm{CQ}]} | i_{t-1,k}) \\
&\geq -\sum_{\forall i_{t-1,k}^{[\mathrm{CQ}]} \in \mathbb{I}_{t-1,k}^{[\mathrm{CQ}]}} \sum_{\substack{\forall i_{t-1,k} \in \mathbb{I} \\ i_{t-1,k}^{[\mathrm{CQ}]} = \mathcal{I}_{t-1,k}^{[\mathrm{CQ}]}(i_{t-1,k})}} \sum_{\forall i_{t,k}^{[\mathrm{CQ}]} \in \mathbb{I}_{t,k}^{[\mathrm{CQ}]}} \mathsf{P}(i_{t,k}^{[\mathrm{CQ}]}, i_{t-1,k}) \operatorname{ld} \mathsf{P}(i_{t,k}^{[\mathrm{CQ}]} | i_{t-1,k}^{[\mathrm{CQ}]}) \\
&= -\sum_{\forall i_{t-1,k}^{[\mathrm{CQ}]} \in \mathbb{I}_{t-1,k}^{[\mathrm{CQ}]}} \sum_{\forall i_{t,k}^{[\mathrm{CQ}]} \in \mathbb{I}_{t,k}^{[\mathrm{CQ}]}} \mathsf{P}(i_{t,k}^{[\mathrm{CQ}]}, i_{t-1,k}^{[\mathrm{CQ}]}) \operatorname{ld} \mathsf{P}(i_{t,k}^{[\mathrm{CQ}]} | i_{t-1,k}^{[\mathrm{CQ}]}) \\
&= \mathsf{H}(I_{t,k}^{[\mathrm{CQ}]} | I_{t-1,k}^{[\mathrm{CQ}]}) \qquad \text{(D.8)}
\end{aligned}
$$

□

E

EXIT-Chart Properties of Inner Feed-Forward Convolutional Codes

In this appendix, several properties of feed-forward convolutional codes, used as inner codes in a *serially concatenated convolutional code* (SCCC) setup, are discussed. Those properties have been given in [SVAC07] and are reproduced here. The properties, dealing with the extrinsic information if perfect *a priori* information is available, are especially important if *Iterative Source-Channel Decoding* (ISCD) shall be applied to transmission systems employing feed-forward convolutional codes, such as, e.g., the *Global System for Mobile Communications* (GSM).

Figure E.1 shows the block diagram of an EXIT chart measurement circuit [AKtB04] for a feed forward convolutional code employed in a parallel concatenated iterative decoding scheme or as an inner component in a serially concatenated iterative decoding scheme. A binary source generates a vector $\mathbf{x}$ of N_X binary data bits x_ξ, $\xi \in \{1, \ldots, N_X\}$. The vector $\mathbf{x}$ is encoded to vector $\mathbf{e}$ of length N_E using a convolutional encoder. Note that for clarity, we omit the time index t in this chapter as all operations are on a frame-by-frame basis and do not exploit inter-frame dependencies.

After transmission over a communication channel, the channel decoder receives channel-related L-values $\mathsf{L}_{\mathrm{CD}}^{[\mathrm{chan}]}(e) = (\mathsf{L}_{\mathrm{CD}}^{[\mathrm{chan}]}(e_1), \ldots, \mathsf{L}_{\mathrm{CD}}^{[\mathrm{chan}]}(e_{N_E}))$. Here, we assume that the communication channel consists of *Binary Phase Shift Keying* (BPSK) modulation with symbol energy $E_\mathrm{s} = 1$, *Additive White Gaussian Noise* (AWGN) with

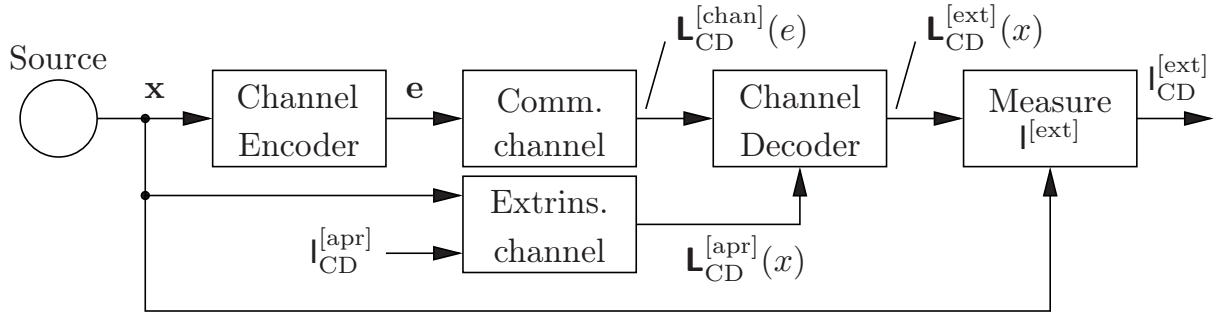

Figure E.1: Block diagram showing the measurement of the EXIT chart of a MAP SISO convolutional decoder [AKtB04]

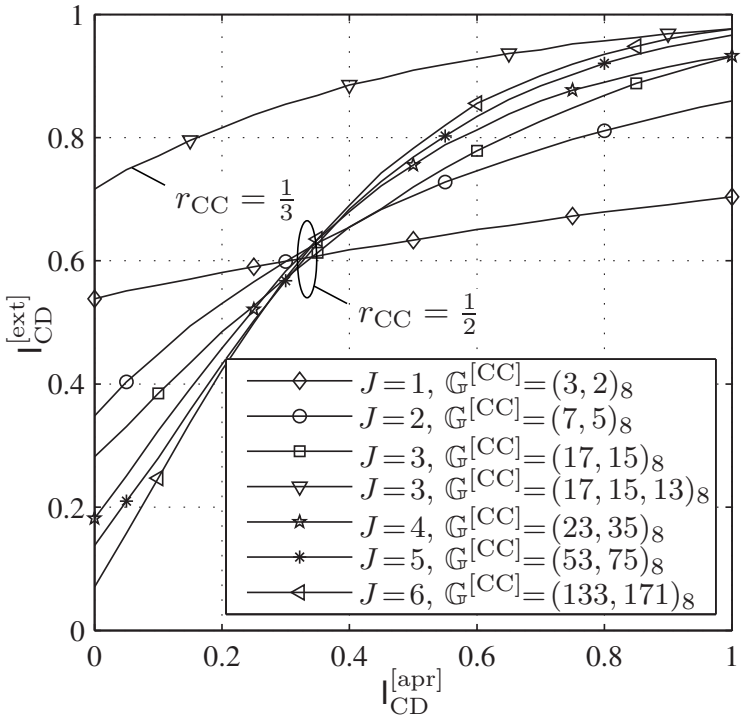

Figure E.2: EXIT characteristics of different feed forward convolutional codes for $E_{\mathrm{s}}/N_0 = 1/(2\sigma_n^2) = -5\,\mathrm{dB}$

noise variance $\sigma_n^2 = N_0/2$, BPSK demodulation, and conversion to L-values according to [HOP96]. The channel decoder, realized as *Maximum A Posteriori* (MAP) *Soft Input Soft Output* (SISO) decoder [BDMP97] receives additional *a priori* information on the data bits $\mathbf{x}$ from the extrinsic output of the (notional) second constituent decoder of the iterative decoding scheme. This information is modeled by the *extrinsic channel* which adds Gaussian noise with defined mean and variance [tB01c], [AKtB04] to the bipolar representation of those bits. Note that the input and the output values of the channel decoder are represented as L-values. The channel decoder computes extrinsic information on the data bits $\mathsf{L}_{\mathrm{CD}}^{[\mathrm{ext}]}(x)$ and extrinsic information on the encoded bits $\mathsf{L}_{\mathrm{CD}}^{[\mathrm{ext}]}(e)$. However, in our case, as we want to compute the *EXtrinsic Information Transfer* (EXIT) characteristics of the inner component code, the information of interest is $\mathsf{L}_{\mathrm{CD}}^{[\mathrm{ext}]}(x)$.

The mutual information necessary to compute the EXIT charts of the inner component is the *a priori* mutual information $\mathsf{I}_{\mathrm{CD}}^{[\mathrm{apr}]} = \mathsf{I}(X; \mathsf{L}_{\mathrm{CD}}^{[\mathrm{apr}]}(X))$ and the extrinsic mutual information $\mathsf{I}_{\mathrm{CD}}^{[\mathrm{ext}]} = \mathsf{I}(X; \mathsf{L}_{\mathrm{CD}}^{[\mathrm{ext}]}(X))$ with X denoting the random process describing the data bits of $\mathbf{x}$ and $\mathsf{L}_{\mathrm{CD}}^{[\mathrm{apr}]}(X)$ (or $\mathsf{L}_{\mathrm{CD}}^{[\mathrm{ext}]}(X)$, respectively) denoting the random process describing the *a priori* (extrinsic) L-values at the channel decoder input (or output, respectively).

Figure E.2 shows the EXIT characteristics of different rate $r_{\mathrm{CC}} = 1/2$ and one rate $r_{\mathrm{CC}} = 1/3$ feed forward convolutional codes acting in a parallel concatenated system or as an inner code in a serially concatenated system, i.e., the input to the decoder consists of the *a priori* knowledge on the data bits and of the received channel-related

Generator polynomials	$\mathsf{I}_{\mathrm{CD}}^{[\mathrm{ext}]}\Big\vert_{\mathsf{I}_{\mathrm{CD}}^{[\mathrm{apr}]}=1}$
$\mathbb{G}^{[\mathrm{CC}]} = (3,2)_8$	0.7038
$\mathbb{G}^{[\mathrm{CC}]} = (7,5)_8$	0.8595
$\mathbb{G}^{[\mathrm{CC}]} = (17,15)_8$	0.9316
$\mathbb{G}^{[\mathrm{CC}]} = (17,15,13)_8$	0.9764
$\mathbb{G}^{[\mathrm{CC}]} = (23,35)_8$	0.9324
$\mathbb{G}^{[\mathrm{CC}]} = (53,75)_8$	0.9665
$\mathbb{G}^{[\mathrm{CC}]} = (133,171)_8$	0.9762

Table E.1: Measured maximum mutual information for the codes utilized in Fig. E.2 and $E_{\mathrm{s}}/N_0 = 1/(2\sigma_n^2) = -5\,\mathrm{dB}$

values of the encoded bits; the decoder generates extrinsic information $\mathsf{L}_{\mathrm{CD}}^{[\mathrm{ext}]}(x)$ for the data bits $\mathbf{x}$. As visible in Fig. E.2, the characteristics do not reach the point $(\mathsf{I}_{\mathrm{CD}}^{[\mathrm{apr}]} = 1\,\mathrm{bit}\ , \mathsf{I}_{\mathrm{CD}}^{[\mathrm{ext}]} = 1\,\mathrm{bit})$ which is needed for perfect decoding. Table E.1 lists the maximum mutual information for perfect *a priori* knowledge (i.e., $\mathsf{I}_{\mathrm{CD}}^{[\mathrm{apr}]} = 1\,\mathrm{bit}$) for the codes used in Fig. E.2. An easy to understand explanation of this behavior and an expression to analytically compute the mutual information $\mathsf{I}_{\mathrm{CD}}^{[\mathrm{ext}]}$ for $\mathsf{I}_{\mathrm{CD}}^{[\mathrm{apr}]} = 1\,\mathrm{bit}$ is given in what follows.

E.1 Maximum Attainable Mutual Information

It has already been observed in [tB01d] that the EXIT characteristics of feed forward convolutional codes do not reach $\mathsf{I}_{\mathrm{CD}}^{[\mathrm{ext}]} = 1\,\mathrm{bit}$ for $\mathsf{I}_{\mathrm{CD}}^{[\mathrm{apr}]} = 1\,\mathrm{bit}$. The explanation given is based on the fact that the coupling of the bits is limited by the constraint length of the code. A more detailed explanation of this behavior using the trellis representation of the convolutional code is given here. In Section E.1.2, the problem is considered theoretically and an analytical solution for the maximum attainable mutual information is provided.

E.1.1 Illustrative Explanation

The behavior of imperfect mutual information if perfect *a priori* knowledge is available can best be visualized using the trellis representation of the convolutional code. Figure E.3 depicts parts of the trellis diagram of a memory $J = 2$ feed forward convolutional code. Without loss of generality (due of the linearity of the code), it can be assumed that the all-zero path has been encoded and transmitted, i.e, $\mathbf{x} = (0, 0, \ldots, 0)$. Determining the extrinsic information for x_ξ at bit position ξ means determining the probability that the estimated data bit $\hat{x}_\xi$ at bit position ξ is either 0 or 1 if *a priori*

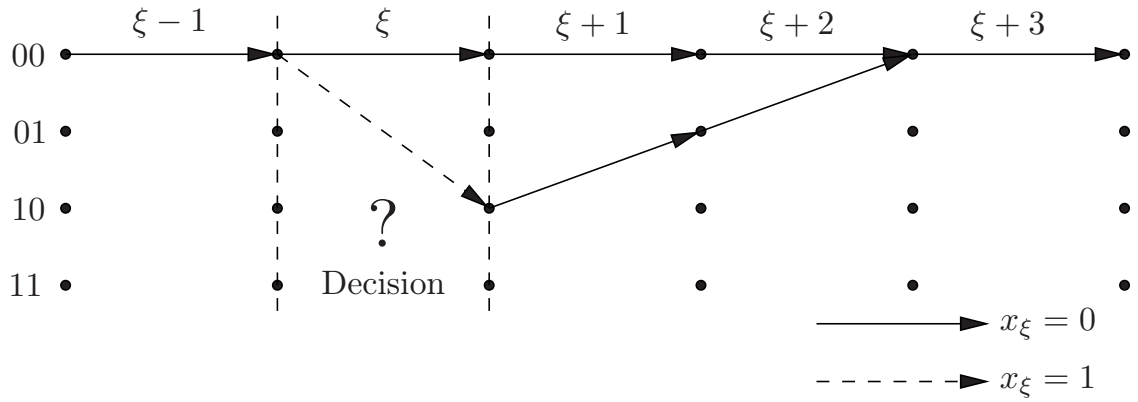

Figure E.3: Extrinsic decision if perfect *a priori* knowledge is available in the case of a memory $J = 2$ feed forward convolutional code

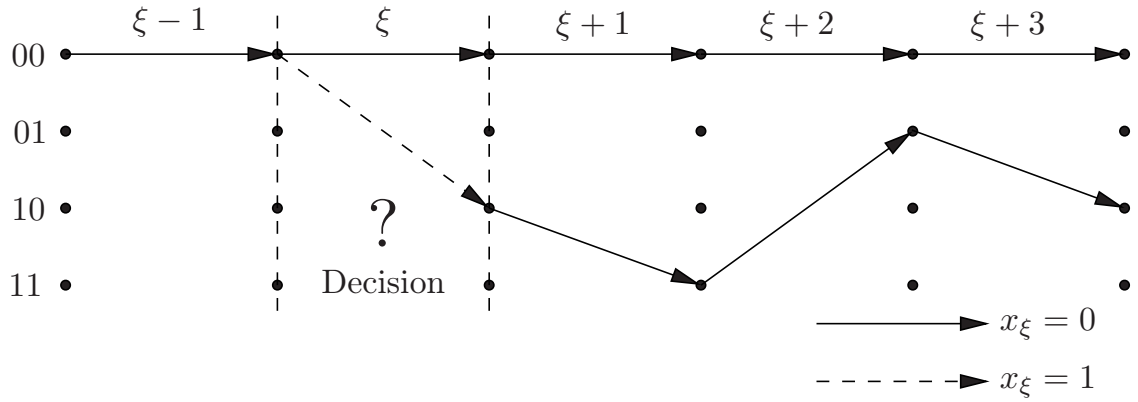

Figure E.4: Extrinsic decision if perfect *a priori* knowledge is available in the case of a memory $J = 2$ recursive convolutional code

information on the data bits $\mathbf{x}$ is available at all bit positions except for ξ. If we take a look at Fig. E.3, we see immediately that, if it is perfectly known that the all-zero data sequence has been sent ($\mathsf{I}_{\mathrm{CD}}^{[\mathrm{apr}]} = 1\,\mathrm{bit}$), the decision at bit position ξ cannot be determined by purely considering the *a priori* knowledge at all bit positions except ξ. However, in order to compute the extrinsic output at bit position ξ, the decision on $\hat{x}_\xi$ has to be made using the channel output only. This decision is not influenced by the *a priori* knowledge as the (perfectly known) inputs at bit positions $\xi+1, \xi+2, \ldots$ lead to the same inner state of the convolutional encoder after J inputs (due to the non-recursive structure of the code).

In the case of recursive convolutional codes, however, a different data input x_ξ at bit position ξ and identical, perfectly known inputs at subsequent bit positions do not lead to the same state after J inputs, resulting from the recursiveness of the encoder as shown in Fig. E.4. A different decision at bit position ξ, followed by perfectly known data bits leads to a different trellis path which does not end in the same state. Thus, if the encoder is terminated (i.e., the encoding stops in a defined state) and the input vector $\mathbf{x}$ is of finite length, perfect *a priori* knowledge leads to a non-ambiguous decision on the extrinsic output at bit position ξ. If the recursive code is not terminated, similar effects as in the case of feed forward codes are observed, i.e., no perfect extrinsic information can be generated even if perfect *a priori* knowledge

is available. Nevertheless, the remainder of this appendix will only focus on feed forward convolutional codes.

E.1.2 Theoretical Results

Definition E.1. Let $\mathcal{E}$ be a rate $r_{\mathrm{CC}} = 1/\tilde{r}_{\mathrm{CC}}$ (i.e., $\tilde{r}_{\mathrm{CC}} \doteq 1/r_{\mathrm{CC}}$) feed forward convolutional encoder which is described by the time-domain generator matrix $\mathbf{G}^{[\mathrm{CC}]}$. Let $\mathbf{x}^{(1)} = (1, 0, \ldots, 0)$ be a weight one input vector of length $J+1$. The vector $\mathbf{x}^{(1)}$ is encoded by $\mathcal{E}$ to the code vector $\mathbf{e}^{(1)} = \mathbf{x}^{(1)} \cdot \mathbf{G}^{[\mathrm{CC}]} = \left(e_1^{(1)}, e_2^{(1)}, \ldots\right)$ of length $\tilde{r}_{\mathrm{CC}}(J+1)$ with $e_\eta^{(1)} \in \mathbb{F}_2$ (and thus $\mathbf{e}^{(1)} \in \mathbb{F}_2^{\tilde{r}_{\mathrm{CC}}(J+1)}$). The vector $\mathbf{e}^{(1)}$ is also denoted as the impulse response of the convolutional code. The Hamming weight of the impulse response vector $\mathbf{e}^{(1)}$ is defined as $d_{\mathcal{E}}^{(1)}$ and it holds

$$d_{\mathcal{E}}^{(1)} = \sum_{\eta=1}^{\tilde{r}_{\mathrm{CC}}(J+1)} e_\eta^{(1)}\,, \tag{E.1}$$

with the sum being performed over the natural numbers $\mathbb{N}_0$, i.e., $d_{\mathcal{E}}^{(1)} \in \mathbb{N}_0$.

Theorem E.2. Given a rate $r_{\mathrm{CC}} = 1/\tilde{r}_{\mathrm{CC}}$ feed forward convolutional code $\mathcal{E}$ with memory J and transmission over an AWGN channel with noise variance σ_n^2, the L-values of the extrinsic MAP SISO decoder output $\mathsf{L}_{\mathrm{CD}}^{[\mathrm{ext}]}(x)$ are Gaussian distributed with mean $\mu_e = 2d_{\mathcal{E}}^{(1)}/\sigma_n^2$ and variance $\sigma_e^2 = 2\mu_e = 4d_{\mathcal{E}}^{(1)}/\sigma_n^2$ if perfect *a priori* knowledge on the equiprobable data bits X is available (i.e., $\mathsf{I}_{\mathrm{CD}}^{[\mathrm{apr}]} = 1\,\mathrm{bit}$).

Proof. (*This proof uses intermediate results from [KHC06]*)
Let $\mathbf{x}^{(0)} = (x_1^{(0)}, \ldots, x_{J+1}^{(0)}) = (0, \ldots, 0)$ be the all zero vector and $\mathbf{x}^{(1)} = (x_1^{(1)}, x_2^{(1)} \ldots, x_{J+1}^{(1)}) = (1, 0, \ldots, 0)$ a weight one input vector. The length of the input vectors can be restricted to $J+1$, as after J identical (zero) inputs, the feed forward convolutional encoder will have the same inner state independent of the initial state. Let $\mathbf{G}^{[\mathrm{CC}]}$ be the time domain generator matrix of the feed forward convolutional code $\mathcal{E}$. Encoding both vectors $\mathbf{x}^{(0)}$ and $\mathbf{x}^{(1)}$ with $\mathcal{E}$ produces the outputs

$$\mathbf{e}^{(0)} = \mathbf{x}^{(0)} \cdot \mathbf{G}^{[\mathrm{CC}]} = \left(e_1^{(0)}, \ldots, e_{\tilde{r}_{\mathrm{CC}}(J+1)}^{(0)}\right) = (0, 0, \ldots, 0)$$
$$\mathbf{e}^{(1)} = \mathbf{x}^{(1)} \cdot \mathbf{G}^{[\mathrm{CC}]} = \left(e_1^{(1)}, \ldots, e_{\tilde{r}_{\mathrm{CC}}(J+1)}^{(1)}\right).$$

Let $\mathbf{x}_{\setminus 1}^{(j)} \doteq \left(x_2^{(j)}, \ldots, x_{J+1}^{(j)}\right) = (0, 0, \ldots, 0)$, $j \in \{0, 1\}$, denote the vector of length J which does not contain the first element of either $\mathbf{x}^{(0)}$ or $\mathbf{x}^{(1)}$. Due to the linearity of the convolutional code, it is sufficient to perform the proof for the all-zero vector only. The encoded vector $\mathbf{e}^{(0)}$ of length $\tilde{r}_{\mathrm{CC}}(J+1)$ is BPSK modulated onto the vector $\mathbf{y}^{(0)}$ with elements $y_\eta^{(0)} = 1 - 2e_\eta^{(0)} = +1$, $\eta = 1, 2, \ldots, \tilde{r}_{\mathrm{CC}}(J+1)$ and $\mathbf{e}^{(1)}$ is modulated onto $\mathbf{y}^{(1)}$. After transmission of $\mathbf{y}^{(0)}$ over a channel with additive white

Gaussian noise of zero mean and variance $\sigma_n^2 = N_0/2$, the vector $\mathbf{z}^{(0)}$ is received with $\mathbf{z}^{(0)} = \mathbf{y}^{(0)} + \mathbf{n}$, and $\mathbf{n} = \left(n_1, \ldots, n_{\tilde{r}_{\mathrm{CC}}(J+1)}\right)$ denoting the noise vector. The extrinsic outputs of the MAP SISO decoder are the probabilities that the decoded data bit $\hat{x}_\xi$ is either 0 or 1 under the condition that *a priori* knowledge on all data bits except the one at position ξ and the entire received sequence $\mathbf{z}^{(0)}$ are available. Without loss of generality, it is sufficient to consider only the first bit position of the vectors, as a consequence of the linearity of convolutional codes. Using the Bayes theorem and the assumption that the data bits x_ξ are equiprobable, the extrinsic probabilities can be expressed as (with $j \in \mathbb{F}_2$) [KHC06]

$$\mathsf{Pr}\left\{X_1 = j|\mathbf{z}^{(0)}, \mathbf{x}_{\setminus 1}^{(0)}\right\} = \frac{\mathsf{p}\left(\mathbf{z}^{(0)}|\mathbf{x}^{(j)}\right)}{\mathsf{p}\left(\mathbf{z}^{(0)}|\mathbf{x}^{(0)}\right) + \mathsf{p}\left(\mathbf{z}^{(0)}|\mathbf{x}^{(1)}\right)}$$

with

$$\mathsf{p}\left(\mathbf{z}^{(0)}|\mathbf{x}^{(0)}\right) = \left(\frac{1}{\sqrt{2\pi}\sigma_n}\right)^{\tilde{r}_{\mathrm{CC}}(J+1)} \cdot \prod_{\eta=1}^{\tilde{r}_{\mathrm{CC}}(J+1)} \exp\left(-\frac{n_\eta^2}{2\sigma_n^2}\right)$$

$$\mathsf{p}\left(\mathbf{z}^{(0)}|\mathbf{x}^{(1)}\right) = \left(\frac{1}{\sqrt{2\pi}\sigma_n}\right)^{\tilde{r}_{\mathrm{CC}}(J+1)} \cdot \prod_{\eta=1}^{\tilde{r}_{\mathrm{CC}}(J+1)} \exp\left(-\frac{(n_\eta + d_\eta)^2}{2\sigma_n^2}\right)$$

and d_η elements of the vector $\mathbf{d} \doteq \mathbf{y}^{(0)} - \mathbf{y}^{(1)}$, i.e., $d_\eta \in \{0, +2\}$. Using vector notation, the extrinsic probabilities can be expressed as

$$\mathsf{Pr}\left\{X_1 = 0|\mathbf{z}^{(0)}, \mathbf{x}_{\setminus 1}^{(0)}\right\} = \frac{\exp\left(\frac{|\mathbf{n}+\mathbf{d}|^2 - |\mathbf{n}|^2}{2\sigma_n^2}\right)}{1 + \exp\left(\frac{|\mathbf{n}+\mathbf{d}|^2 - |\mathbf{n}|^2}{2\sigma_n^2}\right)} \tag{E.2}$$

$$\mathsf{Pr}\left\{X_1 = 1|\mathbf{z}^{(0)}, \mathbf{x}_{\setminus 1}^{(0)}\right\} = \frac{1}{1 + \exp\left(\frac{|\mathbf{n}+\mathbf{d}|^2 - |\mathbf{n}|^2}{2\sigma_n^2}\right)} \tag{E.3}$$

with $|\mathbf{n}|^2 = \sum_{\eta=1}^{\tilde{r}_{\mathrm{CC}}(J+1)} n_\eta^2$ and $|\mathbf{n} + \mathbf{d}|^2$ defined similarly. By using (E.2) and (E.3) the extrinsic L-values of $\mathsf{L}_{\mathrm{CD}}^{[\mathrm{ext}]}(X)$ can be determined as

$$\begin{aligned}
\mathsf{L}_{\mathrm{CD}}^{[\mathrm{ext}]}(X_1) &= \mathsf{L}(X_1|\mathbf{z}^{(0)}, \mathbf{x}_{\setminus 1}^{(0)}) \\
&= \ln\left(\frac{\mathsf{Pr}\left\{X_1 = 0|\mathbf{z}^{(0)}, \mathbf{x}_{\setminus 1}^{(0)}\right\}}{\mathsf{Pr}\left\{X_1 = 1|\mathbf{z}^{(0)}, \mathbf{x}_{\setminus 1}^{(0)}\right\}}\right) \\
&= \frac{|\mathbf{n} + \mathbf{d}|^2 - |\mathbf{n}|^2}{2\sigma_n^2}\,.
\end{aligned}$$

The factor $|\mathbf{n}+\mathbf{d}|^2 - |\mathbf{n}|^2$ can be further simplified

$$\begin{aligned}|\mathbf{n}+\mathbf{d}|^2 - |\mathbf{n}|^2 &= \sum_{\eta=1}^{\tilde{r}_{\mathrm{CC}}(J+1)} (n_\eta + d_\eta)^2 - \sum_{\eta=1}^{\tilde{r}_{\mathrm{CC}}(J+1)} n_\eta^2 \\ &= 2 \sum_{\eta=1}^{\tilde{r}_{\mathrm{CC}}(J+1)} n_\eta d_\eta + \sum_{\eta=1}^{\tilde{r}_{\mathrm{CC}}(J+1)} d_\eta^2 \\ &= 2 \sum_{\eta=1}^{\tilde{r}_{\mathrm{CC}}(J+1)} n_\eta d_\eta + 4 d_{\mathcal{E}}^{(1)} ,\end{aligned}$$

using the fact that $\sum_{\eta=1}^{\tilde{r}_{\mathrm{CC}}(J+1)} d_\eta^2 = 4 d_{\mathcal{E}}^{(1)}$ (see definition of $d_{\mathcal{E}}^{(1)}$ in (E.1)). Therefore, we obtain

$$\mathsf{L}_{\mathrm{CD}}^{[\mathrm{ext}]}(X_1) = \mathsf{L}(X_1|\mathbf{z}^{(0)}, \mathbf{x}_{\setminus 1}^{(0)}) = 2\frac{d_{\mathcal{E}}^{(1)}}{\sigma_n^2} + \sum_{\eta=1}^{\tilde{r}_{\mathrm{CC}}(J+1)} \frac{d_\eta}{\sigma_n^2} n_\eta \,. \tag{E.4}$$

Equation (E.4) states that the L-values of the extrinsic output are composed by the sum of weighted Gaussian distributed noise values and an offset $2d_{\mathcal{E}}^{(1)}/\sigma_n^2$. A random process composed by sum of Gaussian distributed processes is again a Gaussian process [PU02]. The mean of the resulting process is the sum of the means of the sub-processes and the resulting variance is the sum of the sub-processes' variances. As the noise samples n_η have zero mean, the process resulting from the sum of all noise samples has zero mean. As a consequence, the mean of the L-values is only determined by the offset in (E.4). Thus, the mean μ_e of the L-value distribution amounts to

$$\mu_e = 2 \cdot \frac{d_{\mathcal{E}}^{(1)}}{\sigma_n^2} \,.$$

The variance of the noise samples n_η is σ_n^2, but as the noise samples n_η are scaled by d_η/σ_n^2, the variances of the scaled samples in the sum (E.4) amount to $\sigma_n^2 \cdot \frac{d_\eta^2}{\sigma_n^4} = d_\eta^2/\sigma_n^2$. Therefore, the total variance σ_e^2 of the L-value distribution is

$$\sigma_e^2 = \sum_{\eta=1}^{\tilde{r}_{\mathrm{CC}}(J+1)} \frac{d_\eta^2}{\sigma_n^2} = \frac{1}{\sigma_n^2} \sum_{\eta=1}^{\tilde{r}_{\mathrm{CC}}(J+1)} d_\eta^2 = 4\frac{d_{\mathcal{E}}^{(1)}}{\sigma_n^2} = 2\mu_e \,. \qquad \square$$

Corollary E.3. Given a feed forward convolutional code $\mathcal{E}$, the hard decision bit error probability of the extrinsic output after transmission over an AWGN channel with noise variance σ_n^2 and after MAP SISO decoding is given by

$$\mathsf{P}_{\mathrm{b}}^{[\mathrm{ext}]}\big|_{\mathsf{I}_{\mathrm{CD}}^{[\mathrm{apr}]}=1} = \frac{1}{2}\,\mathrm{erfc}\left(\frac{\sqrt{d_{\mathcal{E}}^{(1)}}}{\sqrt{2}\sigma_n}\right) \tag{E.5}$$

under the condition that perfect *a priori* knowledge on the data bits $\mathbf{x}$ is available ($\mathsf{I}_{\mathrm{CD}}^{[\mathrm{apr}]} = 1\,\mathrm{bit}$).

Proof. Due to the linearity of the convolutional code $\mathcal{E}$, it can be assumed, without loss of generality, that the all-zero codeword has been sent. It is known from Theorem E.2 that the pdf of the extrinsic information, given that the all-zero codeword $\mathbf{x}^{(0)} = (0, 0, \ldots, 0)$ has been encoded resulting in the transmitted BPSK modulated vector $\mathbf{y}^{(0)} = (+1, +1, \ldots, +1)$, is Gaussian distributed with mean $\mu_e = 2d_{\mathcal{E}}^{(1)}/\sigma_n^2$ and variance $\sigma_e^2 = 4d_{\mathcal{E}}^{(1)}/\sigma_n^2$. Thus, the bit error probability of the extrinsic output can be determined as

$$\mathsf{P}_{\mathrm{b}}^{[\mathrm{ext}]}\Big|_{\mathsf{I}_{\mathrm{CD}}^{[\mathrm{apr}]}=1} = \frac{1}{\sqrt{2\pi}\sigma_e} \int_{-\infty}^{0} \exp\left(-\frac{(j-\mu_e)^2}{2\sigma_e^2}\right) \mathrm{d}j \tag{E.6}$$

$$= \frac{1}{2}\operatorname{erfc}\left(\frac{\mu_e}{\sqrt{2}\sigma_e}\right) = \frac{1}{2}\operatorname{erfc}\left(\frac{\sqrt{d_{\mathcal{E}}^{(1)}}}{\sqrt{2}\sigma_n}\right) . \tag{E.7}$$

□

Corollary E.4. The mutual information $\mathsf{I}_{\mathrm{CD}}^{[\mathrm{ext}]}$ between the data bits X and the extrinsic L-value output $\mathbf{L}_{\mathrm{CD}}^{[\mathrm{ext}]}(X)$ of a MAP SISO decoder for a feed forward convolutional code $\mathcal{E}$, given the conditions that perfect *a priori* knowledge on the data bits X is available ($\mathsf{I}_{\mathrm{CD}}^{[\mathrm{apr}]} = 1\,\mathrm{bit}$), that the data bits X are equiprobable, and that the transmission is performed on an AWGN channel, depends solely on the noise variance σ_n^2 and on the Hamming weight $d_{\mathcal{E}}^{(1)}$ of the impulse response. This mutual information can be expressed as

$$\mathsf{I}_{\mathrm{CD}}^{[\mathrm{ext}]}\Big|_{\mathsf{I}_{\mathrm{CD}}^{[\mathrm{apr}]}=1} = \mathcal{J}\left(\frac{2\sqrt{d_{\mathcal{E}}^{(1)}}}{\sigma_n}\right) \tag{E.8}$$

$$= 1 - \frac{\sigma_n}{\sqrt{8\pi d_{\mathcal{E}}^{(1)}}} \int_{-\infty}^{+\infty} \exp\left(-\frac{\left(j\sigma_n^2 - 2d_{\mathcal{E}}^{(1)}\right)^2}{8d_{\mathcal{E}}^{(1)}\sigma_n^2}\right) \operatorname{ld}\left(1 + \mathrm{e}^{-j}\right) \mathrm{d}j\,. \tag{E.9}$$

Proof. Due to the linearity of convolutional codes, we can assume, without loss of generality, that the all zero sequence has been encoded and thus the $(+1, +1 \ldots, +1)$ sequence has been transmitted. Therefore, according to Theorem E.2, the L-values of the extrinsic decoder output show a Gaussian distribution with mean $\mu_e = 2d_{\mathcal{E}}^{(1)}/\sigma_n^2$ and variance $\sigma_e^2 = 4d_{\mathcal{E}}^{(1)}/\sigma_n^2$. According to [tB01c], the mutual information $\mathsf{I}_{\mathrm{CD}}^{[\mathrm{ext}]}$ can then be expressed as

$$\mathsf{I}_{\mathrm{CD}}^{[\mathrm{ext}]}(\sigma_e) = 1 - \int_{-\infty}^{+\infty} \frac{\exp\left(-((j-\mu_e)^2/(2\sigma_e^2))\right)}{\sqrt{2\pi}\sigma_e} \operatorname{ld}\left(1 + \mathrm{e}^{-j}\right) \mathrm{d}j\,, \tag{E.10}$$

see also Sec. 2.3. Substituting $\mu_e = 2d_{\mathcal{E}}^{(1)}/\sigma_n^2$ and $\sigma_e^2 = 4d_{\mathcal{E}}^{(1)}/\sigma_n^2$ into (E.10) proves the corollary. □

E.2 Evaluation

Figure E.5 shows the result of Corollary E.4, i.e., the mutual information of the extrinsic output of a MAP SISO decoder of a feed forward convolutional code $\mathcal{E}$ if perfect *a priori* knowledge is available. It can easily be seen that the upper right point of the EXIT characteristic (i.e., $\mathsf{I}_{\mathrm{CD}}^{[\mathrm{ext}]} = 1\,\mathrm{bit}$, given $\mathsf{I}_{\mathrm{CD}}^{[\mathrm{apr}]} = 1\,\mathrm{bit}$) can closely be reached only for large $d_{\mathcal{E}}^{(1)}$ and in good channel conditions. For terminated (or tailbiting) recursive convolutional codes, this plot would be a flat surface, as $d_{\mathcal{E}}^{(1)}$ tends to infinity in the case of such recursive codes [KHC06].

Figure E.6 shows the hard decision bit error probability of the extrinsic output of the MAP SISO decoder if perfect *a priori* knowledge is available ($\mathsf{I}_{\mathrm{CD}}^{[\mathrm{apr}]} = 1\,\mathrm{bit}$). The maximum mutual information of the EXIT characteristics in Fig. E.2 (see also Table E.1) can be read off in Fig. E.5 using the information in Table E.2. Table E.2 also contains the calculated values of $\mathsf{P}_{\mathrm{b}}^{[\mathrm{ext}]}\big|_{\mathsf{I}_{\mathrm{CD}}^{[\mathrm{apr}]}=1}$ (using (E.7)) and $\mathsf{I}_{\mathrm{CD}}^{[\mathrm{ext}]}\big|_{\mathsf{I}_{\mathrm{CD}}^{[\mathrm{apr}]}=1}$ (using (E.9)) for a channel quality of $E_{\mathrm{s}}/N_0 = -5\,\mathrm{dB}$. It can be seen that the calculated maximum mutual information almost perfectly matches the measured values of Table E.1. The differences can be explained by numerical inaccuracies during the measurement and/or by the finite histogram resolution.

In this appendix the behavior of the EXIT characteristics of feed forward convolutional codes [SVAC07] has been analyzed. Simulations have shown that the mutual information at the extrinsic output of a MAP SISO decoder for feed forward and

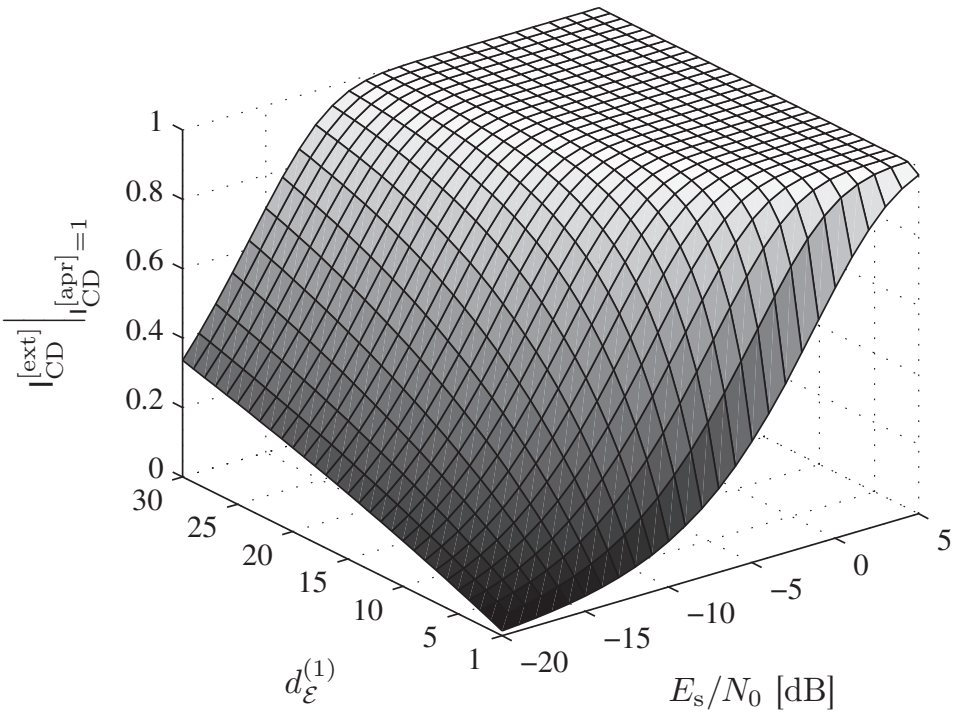

Figure E.5: Mutual information of the extrinsic output as a function of channel quality (E_{s}/N_0) and $d_{\mathcal{E}}^{(1)}$

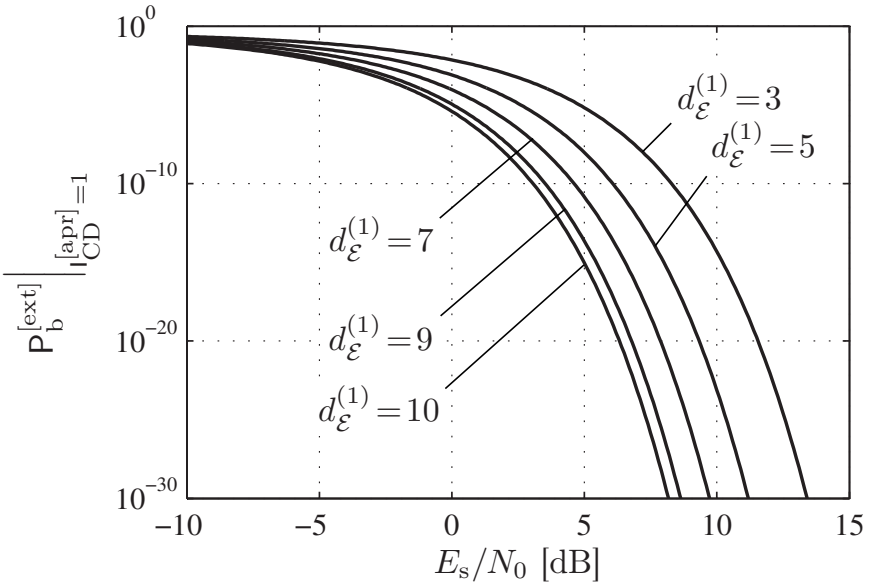

Figure E.6: Hard decision bit error probability of the extrinsic output for $\mathsf{I}_{\mathrm{CD}}^{[\mathrm{apr}]} = 1\,\mathrm{bit}$ ($d_{\mathcal{E}}^{(1)} \in \{3, 5, 7, 9, 10\}$)

Generator polynomials	memory J	$d_{\mathcal{E}}^{(1)}$	$\mathsf{P}_{\mathrm{b}}^{[\mathrm{ext}]}\big\vert_{\mathsf{I}_{\mathrm{CD}}^{[\mathrm{apr}]}=1}$	$\mathsf{I}_{\mathrm{CD}}^{[\mathrm{ext}]}\big\vert_{\mathsf{I}_{\mathrm{CD}}^{[\mathrm{apr}]}=1}$
$\mathbb{G}^{[\mathrm{CC}]} = (3, 2)_8$	1	3	0.0842	0.7038
$\mathbb{G}^{[\mathrm{CC}]} = (7, 5)_8$	2	5	0.0377	0.8592
$\mathbb{G}^{[\mathrm{CC}]} = (17, 15)_8$	3	7	0.0177	0.9315
$\mathbb{G}^{[\mathrm{CC}]} = (17, 15, 13)_8$	3	10	0.0060	0.9762
$\mathbb{G}^{[\mathrm{CC}]} = (23, 35)_8$	4	7	0.0177	0.9315
$\mathbb{G}^{[\mathrm{CC}]} = (53, 75)_8$	5	9	0.0085	0.9662
$\mathbb{G}^{[\mathrm{CC}]} = (133, 171)_8$	6	10	0.0060	0.9762

Table E.2: Impulse response Hamming weights for some selected convolutional codes and numerical results for $E_{\mathrm{s}}/N_0 = 1/(2\sigma_n^2) = -5\,\mathrm{dB}$

non-terminated recursive convolutional codes does not reach $\mathsf{I}_{\mathrm{CD}}^{[\mathrm{ext}]} = 1\,\mathrm{bit}$ if perfect *a priori* information is available – a fact that has already been noted in the literature, e.g., [tB01d]. This maximum attainable mutual information solely depends on the channel noise variance and the Hamming weight of the code impulse response. An easy explanation of this property has been given using the trellis representation of the convolutional code. Furthermore, it has been shown that the extrinsic output of a MAP SISO decoder is Gaussian distributed if the channel noise is Gaussian, the data bits are equiprobable, and the *a priori* information on the data bits is considered to be perfect. Additionally, analytical expressions of the attainable mutual information if perfect *a priori* knowledge is available and the hard decision bit error rate of the extrinsic output have been derived. Finally, an evaluation of different codes and the verification of the theoretical results has been presented.

F

Soft Decision Source Decoding

In this appendix, the equations for the *Bit Demapper* (depicted in Fig. F.1) are given. Besides the parameter estimation, the bit demapper is the main part of *Soft Decision Source Decoding* (SDSD). The equations are given in two different domains:

- The probability domain which follows directly from the derivation of the equations;
- The logarithmic domain which offers several advantages with regard to the implementation. For instance, the well known LogMAP and MaxLogMAP algorithms [RVH95], known from channel decoding, operate in the logarithmic domain.

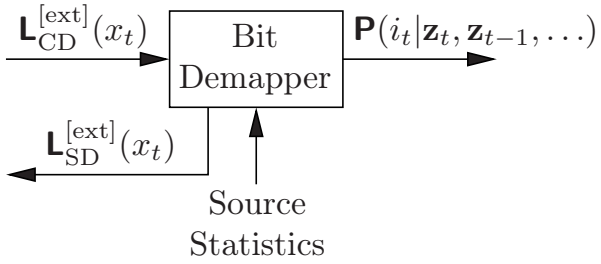

Figure F.1: Bit demapper part of Soft Decision Source Decoding

The SDSD features two inputs: L-values $\mathsf{L}_{\mathrm{CD}}^{[\mathrm{ext}]}(x_t)$ originating from the channel decoder and the source statistics. The source statistics that the SDSD requires may differ, depending on the utilized SDSD algorithm. The required source statistics are summarized in Tab. F.1 for the four considered SDSD algorithms. The aim of the SDSD is on the one hand the computation of *a posteriori* probabilities that are utilized for reconstructing the quantizer indices in the block *Parameter Estimation* [Fin98, FV01, Fin08] (see also Fig. 3.3) and on the other hand the generation of extrinsic information which is used in the iterative Turbo loop and fed back to the channel decoder. The extrinsic information is usually represented as (a vector of) L-values $\mathsf{L}_{\mathrm{SD}}^{[\mathrm{ext}]}(x_t)$.

In what follows the SDSD equations are first given in the probability domain in Sec. F.1 and then transformed into the logarithmic domain in view of a numerically more stable implementation in Sec. F.2.

Algorithm	Necessary Source Statistics
AK0	$\mathsf{P}(i_{t,k})$
AK1-INTER	$\mathsf{P}(i_{t,k}\|i_{t-1,k})$
AK1-INTRA	$\mathsf{P}(i_{t,k}\|i_{t,k-1})$
AK1-NOPT	$\mathsf{P}(i_{t,k}\|i_{t-1,k})$ and $\mathsf{P}(i_{t,k}\|i_{t,k-1})$

Table F.1: Necessary source statistics used within SDSD

F.1 SDSD Equations in the Probability Domain

For a derivation of the SDSD equations in the probability domain, we refer to the literate, e.g., [Gör00, AVS01, Gör01a, Gör01b, Adr03, AV05, ACS08].

The first steps are common for all four SDSD algorithms. First, the L-values for all the N_I bit patterns of a block, i.e., $\mathbf{L}_{\mathrm{CD}}^{[\mathrm{ext}]}(\mathbf{b}_{t,k}) = (\mathsf{L}_{\mathrm{CD}}^{[\mathrm{ext}]}(b_{t,k,1}), \ldots, \mathsf{L}_{\mathrm{CD}}^{[\mathrm{ext}]}(b_{t,k,B_k}))$ are extracted from the input vector for $k \in \{1, \ldots, N_I\}$. This corresponds to a serial-to-parallel conversion of the L-values. Under the assumption of a memoryless channel, a set of reliabilities[1]

$$\gamma_{t,k}(q) \doteq \prod_{\mu=1}^{B_k} \mathsf{P}_{\mathrm{CD}}^{[\mathrm{ext}]}\left(b_{t,k,\mu} = \bar{b}_{k,\mu}^{(q)}\right) \tag{F.1}$$

$$= \prod_{\mu=1}^{B_k} \left(1 + \exp\left(-\left(1 - 2 \cdot \bar{b}_{k,\mu}^{(q)}\right) \cdot \mathsf{L}_{\mathrm{CD}}^{[\mathrm{ext}]}(b_{t,k,\mu})\right)\right)^{-1} \tag{F.2}$$

is determined (see [HOP96] for details on the relation between probabilities and L-values) for each different quantization index $q \in \mathbb{I}$ at each position k within a frame, resulting in a total number of $N_I Q$ different expressions for each frame at time instant t. Note that $\bar{b}_{k,\mu}^{(q)}$ denotes the μth entry of the bit vector $\bar{\mathbf{b}}_k^{(q)}$, i.e., the μth bit of the pattern. We further define the extrinsic channel-related reliabilities considering all bits of a bit pattern with the exception of the χth bit

$$\gamma_{t,k}^{[\mathrm{ext}]\setminus\chi}(q) \doteq \prod_{\substack{\mu=1 \\ \mu\neq\chi}}^{B_k} \mathsf{P}_{\mathrm{CD}}^{[\mathrm{ext}]}\left(b_{t,k,\mu} = \bar{b}_{k,\mu}^{(q)}\right) \tag{F.3}$$

$$= \prod_{\substack{\mu=1 \\ \mu\neq\chi}}^{B_k} \left(1 + \exp\left(-\left(1 - 2 \cdot \bar{b}_{k,\mu}^{(q)}\right) \cdot \mathsf{L}_{\mathrm{CD}}^{[\mathrm{ext}]}(b_{t,k,\mu})\right)\right)^{-1}. \tag{F.4}$$

Using the expressions in (F.2) and (F.4), the *a posteriori* probabilities and the extrinsic output of the SDSD can be computed, depending on the available source statistics.

[1] Note that the reliability $\gamma_{t,k}(q)$ does not correspond directly to the factor γ used in the *Bahl, Cocke, Jelinek, Raviv* (BCJR) algorithm [BCJR74] and in the original description of the *Soft Decision Source Decoding* (SDSD) [AVS01, Adr03, ACS08]. In this thesis, $\gamma_{t,k}(q)$ denote the SDSD input reliabilities only, excluding any *a priori* information on the source statistics. In [AV05] for instance, these input reliabilities have been denoted $\theta_{t,k}(q)$.

AK0

If only *a priori* information of zeroth order, i.e., the probabilities $\mathsf{P}(i_{t,k}) = \mathsf{Pr}\{I_{t,k} = i_{t,k}\}$, is available, the *a posteriori* probabilities can be computed by [Fin98]

$$\begin{aligned}\mathsf{Pr}\{I_{t,k} = q|\mathbf{z}_t, \mathbf{z}_{t-1}, \ldots\} &= \mathsf{Pr}\{I_{t,k} = q|\mathbf{z}_t\} \\ &= \frac{1}{\mathrm{K}} \cdot \gamma_{t,k}(q) \cdot \mathsf{Pr}\{I_{t,k} = q\} \qquad \forall q \in \mathbb{I}\,, \end{aligned} \tag{F.5}$$

with K being a normalization constant ensuring $\sum_{q=1}^{Q} \mathsf{Pr}\{I_{t,k} = q|\mathbf{z}_t, \mathbf{z}_{t-1}, \ldots\} = 1$. Note that the probabilities $\mathsf{Pr}\{I_{t,k} = q\}$ may vary from parameter to parameter and from frame to frame. The process $I_{t,k}$ does not need to be stationary in this case. However, the probabilities of occurrence have to be known at the receiver, either as side information or by means of estimation [SVC07].

The extrinsic information is computed for all bits of the different bit patterns, i.e., $\mathsf{L}_{\mathrm{SD}}^{[\mathrm{ext}]}(b_{t,k,\mu})$ with $\mu \in \{1, \ldots, B_k\}$ is determined according to

$$\mathsf{L}_{\mathrm{SD}}^{[\mathrm{ext}]}(b_{t,k,\mu}) = \ln \frac{\sum\limits_{q=1}^{Q} \left(1 - \bar{b}_{k,\mu}^{(q)}\right) \gamma_{t,k}^{[\mathrm{ext}]\setminus\mu}(q) \cdot \mathsf{Pr}\{I_{t,k} = q\}}{\sum\limits_{q=1}^{Q} \bar{b}_{k,\mu}^{(q)} \gamma_{t,k}^{[\mathrm{ext}]\setminus\mu}(q) \cdot \mathsf{Pr}\{I_{t,k} = q\}}\,. \tag{F.6}$$

The multiplication with $1 - \bar{b}_{k,\mu}^{(q)}$ and $\bar{b}_{k,\mu}^{(q)}$ in the numerator and denominator of (F.6) ensures that only those patterns $\bar{\mathbf{b}}_k^{(q)}$, where the bit at position μ is zero or one, are considered in the summation. Note that we assume throughout this work that the bit mappings are designed such that $0 < \sum_{q=1}^{Q} \bar{b}_{k,\mu}^{(q)} < Q$, $\forall k \in \{1, \ldots, N_I\}, \forall \mu \in \{1, \ldots, B_k\}$. This means that no bit position can be always zero (or always one) for all Q distinct entries, leading to a zero denominator or numerator in (F.6).

After the computation of $\mathsf{L}_{\mathrm{SD}}^{[\mathrm{ext}]}(b_{t,k,\mu})$ for all N_I bit patterns, the output vector $\mathbf{L}_{\mathrm{SD}}^{[\mathrm{ext}]}(x_t)$ is formed according to

$$\begin{aligned}&\mathbf{L}_{\mathrm{SD}}^{[\mathrm{ext}]}(x_t) = \\ &\left(\mathsf{L}_{\mathrm{SD}}^{[\mathrm{ext}]}(b_{t,1,1}), \ldots, \mathsf{L}_{\mathrm{SD}}^{[\mathrm{ext}]}(b_{t,1,B_1}), \ldots, \mathsf{L}_{\mathrm{SD}}^{[\mathrm{ext}]}(b_{t,N_I,1}), \ldots, \mathsf{L}_{\mathrm{SD}}^{[\mathrm{ext}]}(b_{t,N_I,B_{N_I}})\right)\,. \end{aligned} \tag{F.7}$$

AK1-INTER

If *a priori* information describing the dependency of quantization indices between consecutive frames is available, the temporal correlation ρ is exploited. In this case, the N_I indices are modeled by N_I stationary Markov processes $I_{t,k}$ of first order, i.e.,

$$\mathsf{P}(i_{t,k}|i_{t-1,k}, i_{t-2,k}, i_{t-3,k}, \ldots) = \mathsf{P}(i_{t,k}|i_{t-1,k}) \qquad \forall k \in \{1, \ldots, N_I\} \tag{F.8}$$

$$\mathsf{P}(i_{t,k}|i_{t-1,k}) = \mathsf{P}(i_{t+\tilde{t},k}|i_{t+\tilde{t}-1,k}) \qquad \forall k \in \{1, \ldots, N_I\}, \forall \tilde{t} \in \mathbb{Z}\,. \tag{F.9}$$

The *a posteriori* probabilities amount to [Fin98]

$$\mathsf{Pr}\{I_{t,k} = q|\mathbf{z}_t, \mathbf{z}_{t-1}, \ldots\} = \alpha_{t,k}(q) \qquad \forall q \in \mathbb{I}\,, \tag{F.10}$$

with $\alpha_{t,k}(q)$ being evaluated in the inter-frame forward recursion

$$\alpha_{t,k}(q) = \frac{1}{\mathrm{K}} \cdot \gamma_{t,k}(q) \cdot \sum_{\tilde{q}=1}^{Q} \mathsf{Pr}\{I_{t,k}=q|I_{t-1,k}=\tilde{q}\} \cdot \alpha_{t-1,k}(\tilde{q}) \tag{F.11}$$

$$\doteq \frac{1}{\mathrm{K}} \cdot \gamma_{t,k}(q) \cdot A_{t,k}(q)\,, \tag{F.12}$$

with K being a normalization constant ensuring that $\sum_{q=1}^{Q} \alpha_{t,k}(q) = 1$, required for numerical stability reasons in a practical implementation. The values $\alpha_{0,k}$ (the transmission is assumed to start at time instant $t = 1$) are initialized by

$$\alpha_{0,k}(q) = \mathsf{Pr}\{I_{1,k} = q\} \qquad \forall q \in \mathbb{I}\,. \tag{F.13}$$

Note that the processes $I_{t,k}$ are assumed to be stationary temporal first order Markov processes, i.e., $\mathsf{Pr}\{I_{1,k} = q\} = \mathsf{Pr}\{I_{t,k} = q\}$, $\forall t \in \mathbb{N}_1$. As the values $\alpha_{t,k}(q)$ are reused in the subsequent frame, they need to be stored, resulting in memory requirements of $N_I \cdot Q$ values.

The extrinsic information is given by [AVS01, Adr03]

$$\begin{aligned}
\mathsf{L}_{\mathrm{SD}}^{[\mathrm{ext}]}(b_{t,k,\mu}) &= \ln \frac{\sum_{q=1}^{Q} \left(1-\bar{b}_{k,\mu}^{(q)}\right) \gamma_{t,k}^{[\mathrm{ext}]\setminus\mu}(q) \sum_{\tilde{q}=1}^{Q} \mathsf{Pr}\{I_{t,k}=q|I_{t-1,k}=\tilde{q}\}\alpha_{t-1,k}(\tilde{q})}{\sum_{q=1}^{Q} \bar{b}_{k,\mu}^{(q)} \gamma_{t,k}^{[\mathrm{ext}]\setminus\mu}(q) \sum_{\tilde{q}=1}^{Q} \mathsf{Pr}\{I_{t,k}=q|I_{t-1,k}=\tilde{q}\}\alpha_{t-1,k}(\tilde{q})} \\
&= \ln \frac{\sum_{q=1}^{Q} \left(1-\bar{b}_{k,\mu}^{(q)}\right) \cdot \gamma_{t,k}^{[\mathrm{ext}]\setminus\mu}(q) \cdot A_{t,k}(q)}{\sum_{q=1}^{Q} \bar{b}_{k,\mu}^{(q)} \cdot \gamma_{t,k}^{[\mathrm{ext}]\setminus\mu}(q) \cdot A_{t,k}(q)}\,,
\end{aligned} \tag{F.14}$$

with $A_{t,k}(q) = \sum_{\tilde{q}=1}^{Q} \mathsf{Pr}\{I_{t,k}=q|I_{t,k-1}=\tilde{q}\}\alpha_{t,k-1}(\tilde{q})$. Note that in the computation of (F.10) and (F.11), which only have to be performed once per frame, different intermediate calculations from (F.14) can be reused. Finally, the terms $\mathsf{L}_{\mathrm{SD}}^{[\mathrm{ext}]}(b_{t,k,\mu})$ are grouped to the vector $\boldsymbol{\mathsf{L}}_{\mathrm{SD}}^{[\mathrm{ext}]}(x_t)$ as described in the AK0 case.

Note that in this work, we do not allow any additional delay and therefore only consider a single frame during decoding. However, it can be shown that the decoding performance can be improved if Λ consecutive frames are grouped together. This results in an additional delay of $\Lambda - 1$ time instants but the decoder can take advantage of information not only from previous time instants but also from future time instants. In that case, (F.10) and (F.14) have to be modified such that an additional backward recursion factor (taking into account the information from future time instants) is included. The modified equations are not given here, they can be found in the literature, e.g., [Adr03, AV05, ACS08].

AK1-INTRA

If *a priori* information describing the relation between quantization indices within one frame are available, the intra-frame correlation δ is exploited. In that case, the N_I indices in a frame emerge from a stationary Markov process of first order. There is no relation between the coefficients of consecutive frames such that the processing can be performed on a true frame-by-frame basis. Due to the first order Markov property and the stationarity, we have

$$\mathsf{P}(i_{t,k}|i_{t,k-1}, i_{t,k-2}, i_{t,k-3}, \ldots) = \mathsf{P}(i_{t,k}|i_{t,k-1}) \qquad \forall t \in \mathbb{N}_1 \tag{F.15}$$

$$\mathsf{P}(i_{t,k}|i_{t,k-1}) = \mathsf{P}(i_{t,k+\tilde{k}}|i_{t,k+\tilde{k}-1}) \qquad \forall t \in \mathbb{N}_1, \forall \tilde{k} \in \mathbb{Z}\,. \tag{F.16}$$

Unlike in the AK1-INTER case, the decoding algorithm can now exploit information from all neighboring positions, i.e., past and future positions $k-1$ and $k+1$, as a complete frame is processed in one pass of the SDSD. The equations for determining *a posteriori* probabilities and extrinsic information follow directly from the AK1-INTER case with grouping of $\Lambda > 1$ frames by exchanging position and time indices [Adr03, AV05].

The *a posteriori* probabilities $\mathsf{Pr}\{I_{t,k} = q|\mathbf{z}_t, \mathbf{z}_{t-1}, \ldots\} = \mathsf{Pr}\{I_{t,k} = q|\mathbf{z}_t\}$ (no inter-frame relations present) amount to

$$\mathsf{Pr}\{I_{t,k} = q|\mathbf{z}_t\} = \frac{1}{\mathrm{K}_1} \cdot \alpha_{t,k}(q) \cdot \beta_{t,k}(q) \qquad \forall q \in \mathbb{I}\,, \tag{F.17}$$

with K_1 being a normlization constant ensuring $\sum_{q=1}^{Q} \mathsf{Pr}\{I_{t,k} = q|\mathbf{z}_t\} = 1$ and $\alpha_{t,k}(q)$ and $\beta_{t,k}(q)$ being evaluated in the forward and backward recursions

$$\alpha_{t,k}(q) = \frac{\gamma_{t,k}(q)}{\mathrm{K}_2} \sum_{\tilde{q}=1}^{Q} \mathsf{Pr}\{I_{t,k}=q|I_{t,k-1}=\tilde{q}\}\alpha_{t,k-1}(\tilde{q})\,,\ k \in \{1, \ldots, N_I\} \tag{F.18}$$

$$\doteq \frac{\gamma_{t,k}(q)}{\mathrm{K}_2} \cdot A'_{t,k}(q) \tag{F.19}$$

$$\beta_{t,k-1}(q) = \frac{1}{\mathrm{K}_3} \sum_{\tilde{q}=1}^{Q} \gamma_{t,k}(\tilde{q})\mathsf{Pr}\{I_{t,k}=\tilde{q}|I_{t,k-1}=q\}\beta_{t,k}(\tilde{q})\,,\ k \in \{2, \ldots, N_I\} \tag{F.20}$$

with the initialization

$$\alpha_{t,0}(q) = \mathsf{Pr}\{I_{t,1} = q\} \qquad \forall q \in \mathbb{I} \tag{F.21}$$

$$\beta_{t,N_I}(q) = \frac{1}{Q} \qquad \forall q \in \mathbb{I}\,. \tag{F.22}$$

The factors K_2 and K_3 in (F.18) and (F.20) are used to ensure that $\sum_{q=1}^{Q} \alpha_{t,k}(q) = 1$ and $\sum_{q=1}^{Q} \beta_{t,k}(q) = 1$, $\forall k \in \{1, \ldots, N_I\}$, and are mainly required for stability reasons.

The extrinsic information is given by

$$\mathsf{L}_{\mathrm{SD}}^{[\mathrm{ext}]}(b_{t,k,\mu}) = \ln \frac{\sum_{q=1}^{Q} \left(1-\bar{b}_{k,\mu}^{(q)}\right) \cdot \gamma_{t,k}^{[\mathrm{ext}]\setminus\mu}(q) \cdot \beta_{t,k}(q) \cdot A'_{t,k}(q)}{\sum_{q=1}^{Q} \bar{b}_{k,\mu}^{(q)} \cdot \gamma_{t,k}^{[\mathrm{ext}]\setminus\mu}(q) \cdot \beta_{t,k}(q) \cdot A'_{t,k}(q)}. \tag{F.23}$$

The factor $A'_{t,k}(q) = \sum_{\tilde{q}=1}^{Q} \mathsf{Pr}\{I_{t,k}=q|I_{t,k-1}=\tilde{q}\}\alpha_{t,k-1}(\tilde{q})$ is required both in (F.18) and (F.23) and can therefore be computed only once and then reused. After evaluating (F.23) for all B_k of all N_I bit patterns in the current frame, the terms $\mathsf{L}_{\mathrm{SD}}^{[\mathrm{ext}]}(b_{t,k,\mu})$ are grouped to the vector $\mathbf{L}_{\mathrm{SD}}^{[\mathrm{ext}]}(x_t)$ as described in the AK0 and AK1-INTER cases.

AK1-NOPT

If *a priori* information describing relations between quantization indices within one frame as well as *a priori* information describing relations between quantization indices of successive frames are available, an algorithm exploiting both the inter-frame correlation ρ as well as the intra-frame correlation δ is required. An SDSD algorithm which optimally exploits both types of correlation via the conditional probabilities $\mathsf{P}(i_{t,k}|i_{t-1,k}, i_{t,k-1})$ has been introduced in [Hei01a, Hei01b]. This approach however is of complexity order $O(N_I^3)$. Several solutions for near-optimal *Minimum Mean Square Error* (MMSE) estimators which exploit the temporal and spatial Markov property independently, i.e., make use of the probabilities $\mathsf{P}(i_{t,k}|i_{t-1,k})$ and $\mathsf{P}(i_{t,k}|i_{t,k-1})$ have been proposed [ASHV00, KG01, LK01, Hin01, FHCS02, Adr03, APV04, KG05, HA08]. In this work, we restrict ourselves to the algorithm introduced in [Hin01, FHCS02] and analyzed in detail in [Adr03, APV04, HA08]. This algorithm is denoted by AK1-NOPT in what follows. For the utilization of the simplified estimator presented in [KG01] in the context of *Iterative Source-Channel Decoding* (ISCD), we refer to [KG02].

In this section, we show how extrinsic information required for ISCD can be generated within the AK1-NOPT algorithm. In this work, no additional delay is allowed by considering Λ consecutive frames at the receiver. Therefore, only the simplified equations not considering information from future frames are given here ($\Lambda = 1$). For the full equations, we refer to [Adr03, APV04, HA08] where the estimators are derived and expressions for the *a posteriori* probabilities are given. The computation of extrinsic information using the full equations is straightforward by using the same approach as given below.

In the AK1-NOPT algorithm, the quantization indices are assumed to be temporally (inter-frame) and spatially (intra-frame) stationary. Furthermore, they can be modeled by a two Markov processes of first order. Due to the Markov properties and the stationarity, we have

$$\mathsf{P}(i_{t,k}|i_{t-1,k}, i_{t-2,k}, i_{t-3,k}, \ldots) = \mathsf{P}(i_{t,k}|i_{t-1,k}) \qquad \forall k \in \{1, \ldots, N_I\} \tag{F.24}$$

$$\mathsf{P}(i_{t,k}|i_{t-1,k}) = \mathsf{P}(i_{t+\tilde{t},k}|i_{t+\tilde{t}-1,k}) \quad \forall k \in \{1,\ldots,N_I\}, \forall \tilde{t} \in \mathbb{Z} \tag{F.25}$$

$$\mathsf{P}(i_{t,k}|i_{t,k-1}, i_{t,k-2}, i_{t,k-3}, \ldots) = \mathsf{P}(i_{t,k}|i_{t,k-1}) \qquad \forall t \in \mathbb{N}_1 \tag{F.26}$$

$$\mathsf{P}(i_{t,k}|i_{t,k-1}) = \mathsf{P}(i_{t,k+\tilde{k}}|i_{t,k+\tilde{k}-1}) \qquad \forall t \in \mathbb{N}_1, \forall \tilde{k} \in \mathbb{Z}\,. \tag{F.27}$$

The *a posteriori* probabilities are given by [HA08]

$$\mathsf{Pr}\{I_{t,k} = q|\mathbf{z}_t, \mathbf{z}_{t-1}, \ldots\} = \frac{1}{\mathrm{K}_1} \cdot \alpha_{t,k}^{[\mathrm{pos}]}(q) \cdot \beta_{t,k}^{[\mathrm{pos}]}(q) \cdot \gamma_{t,k}(q) \cdot A_{t,k}(q) \qquad \forall q \in \mathbb{I}\,, \tag{F.28}$$

with the normalization constant K_1 such that $\sum_{q=1}^{Q} \mathsf{Pr}\{I_{t,k} = q|\mathbf{z}_t, \mathbf{z}_{t-1}, \ldots\} = 1$. The first two terms in (F.28) are given by the spatial forward/backward recursions $\forall q \in \mathbb{I}$

$$\alpha_{t,k}^{[\mathrm{pos}]}(q) \doteq \frac{1}{\mathrm{K}_2} \sum_{\tilde{q}=1}^{Q} \alpha_{t,k-1}^{[\mathrm{pos}]}(\tilde{q}) \gamma_{t,k-1}(\tilde{q}) \mathsf{Pr}\{I_{t,k} = q|I_{t,k-1} = \tilde{q}\},\ \forall k \in \{2,\ldots,N_I\} \tag{F.29}$$

$$\beta_{t,k-1}^{[\mathrm{pos}]}(q) \doteq \frac{1}{\mathrm{K}_3} \sum_{\tilde{q}=1}^{Q} \beta_{t,k}^{[\mathrm{pos}]}(\tilde{q}) \gamma_{t,k}(\tilde{q}) \mathsf{Pr}\{I_{t,k} = \tilde{q}|I_{t,k-1} = q\},\ \forall k \in \{2,\ldots,N_I\} \tag{F.30}$$

and are initialized by

$$\alpha_{t,1}^{[\mathrm{pos}]}(q) = \beta_{t,N_I}^{[\mathrm{pos}]}(q) = 1 \qquad \forall q \in \mathbb{I}\,. \tag{F.31}$$

The term $A_{t,k}(q)$ in (F.28) is given by

$$A_{t,k}(q) = \sum_{\tilde{q}=1}^{Q} \mathsf{Pr}\{I_{t,k} = q|I_{t-1,k} = \tilde{q}\} \cdot \alpha_{t-1,k}^{[\mathrm{tim}]}(\tilde{q}) \tag{F.32}$$

with $\alpha_{t,k}^{[\mathrm{tim}]}$ being updated (and stored for use in the subsequent frame) in the temporal forward recursion

$$\alpha_{t,k}^{[\mathrm{tim}]}(q) = \frac{1}{\mathrm{K}_4} \cdot \alpha_{t,k}^{[\mathrm{pos}]}(q) \cdot \beta_{t,k}^{[\mathrm{pos}]}(q) \cdot \gamma_{t,k}(q) \cdot \sum_{\tilde{q}=1}^{Q} \mathsf{Pr}\{I_{t,k} = q|I_{t-1,k} = \tilde{q}\} \cdot \alpha_{t-1,k}^{[\mathrm{tim}]}(\tilde{q}) \tag{F.33}$$

$$= \frac{1}{\mathrm{K}_4} \cdot \alpha_{t,k}^{[\mathrm{pos}]}(q) \cdot \beta_{t,k}^{[\mathrm{pos}]}(q) \cdot \gamma_{t,k}(q) \cdot A_{t,k}(q)\,. \tag{F.34}$$

Similar to the AK1-INTER case, $\alpha_{0,k}^{[\mathrm{tim}]}$ is initialized by (note that the transmission starts at $t = 1$)

$$\alpha_{0,k}^{[\mathrm{tim}]}(q) = \mathsf{Pr}\{I_{1,k} = q\} \qquad \forall q \in \mathbb{I}\,. \tag{F.35}$$

Note that $\mathsf{Pr}\{I_{t,k} = q|\mathbf{z}_t, \mathbf{z}_{t-1}, \ldots\} = \alpha_{t,k}^{[\mathrm{tim}]}(q)$. The normalization constants K_2, K_3, and K_4 are mainly required for stability reasons in a practical implementation.

Finally, the extrinsic information is given by

$$\mathsf{L}_{\mathrm{SD}}^{[\mathrm{ext}]}(b_{t,k,\mu}) = \ln \frac{\sum_{q=1}^{Q} \left(1-\bar{b}_{k,\mu}^{(q)}\right) \cdot \gamma_{t,k}^{[\mathrm{ext}]\setminus\mu}(q) \cdot \alpha_{t,k}^{[\mathrm{pos}]}(q) \cdot \beta_{t,k}^{[\mathrm{pos}]}(q) \cdot A_{t,k}(q)}{\sum_{q=1}^{Q} \bar{b}_{k,\mu}^{(q)} \cdot \gamma_{t,k}^{[\mathrm{ext}]\setminus\mu}(q) \cdot \alpha_{t,k}^{[\mathrm{pos}]}(q) \cdot \beta_{t,k}^{[\mathrm{pos}]}(q) \cdot A_{t,k}(q)}\,, \tag{F.36}$$

with $A_{t,k}(q)$ according to (F.32). Note that in the original approach no equations for computing extrinsic reliabilities were given, however, the derivation is straightforward using the same reasoning as in the cases AK0, AK1-INTER, and AK1-INTRA. After evaluating (F.36) for all B_k of all N_I bit patterns in the current frame, the terms $\mathsf{L}_{\mathrm{SD}}^{[\mathrm{ext}]}(b_{t,k,\mu})$ are grouped to the vector $\mathbf{L}_{\mathrm{SD}}^{[\mathrm{ext}]}(x_t)$ as described in all previous cases.

F.2 SDSD Equations in the Logarithmic Domain

In a practical implementation, the translation of BCJR-like algorithms [BCJR74] to the logarithmic domain offers several advantages such as, e.g., better numerical stability [RVH95]. In the following, we modify the SDSD equations given in Sec. F.1 towards an implementation in the logarithmic domain. Expressions for the AK1-INTER and AK1-INTRA have already been given in [SVAC08, SVA08]. They are reproduced here and extended to the AK0 and AK1-NOPT cases. The basic guideline is identical in all cases: instead of using α and β, the algorithms in the logarithmic domain use $\ln(\alpha)$ and $\ln(\beta)$. Extremely important during the implementation of the algorithms in the logarithmic domain is the so-called *Jacobian logarithm* [RVH95]

$$\ln(\mathrm{e}^{\delta_1} + \mathrm{e}^{\delta_2}) = \max(\delta_1, \delta_2) + \ln(1 + \mathrm{e}^{-|\delta_1 - \delta_2|}) \doteq \max^{\star}(\delta_1, \delta_2)\,,\ \forall \delta_1, \delta_2 \in \mathbb{R}. \tag{F.37}$$

The correction term $\ln(1 + \mathrm{e}^{-|\delta_1-\delta_2|})$ in (F.37) can be precomputed and stored in a *Look-Up Table* (LUT). Furthermore, the $\max^{\star}$ function can be approximated by $\max^{\star}(\delta_1, \delta_2) \approx \max(\delta_1, \delta_2)$. This approximation is for example applied in the famous MaxLogMAP implementation of the BCJR algorithm [RVH95].

The $\max^{\star}$ function has the following properties

$$\max^{\star}(\delta_1, \delta_2) = \max^{\star}(\delta_2, \delta_1) \qquad \forall \delta_1, \delta_2 \in \mathbb{R} \tag{F.38}$$

$$\lim_{\delta_2 \to -\infty} \max^{\star}(\delta_1, \delta_2) = \delta_1 \qquad \forall \delta_1 \in \mathbb{R} \tag{F.39}$$

$$\begin{aligned} \max^{\star}(\delta_1, \delta_2, \delta_3) &= \ln(\mathrm{e}^{\delta_1} + \mathrm{e}^{\delta_2} + \mathrm{e}^{\delta_3}) \\ &= \max^{\star}(\delta_1, \max^{\star}(\delta_2, \delta_3)) \qquad \forall \delta_1, \delta_2, \delta_3 \in \mathbb{R} \end{aligned} \tag{F.40}$$

$$\begin{aligned} \max^{\star}(j + \delta_1, j + \delta_2) &= \ln(\mathrm{e}^{j+\delta_1} + \mathrm{e}^{j+\delta_2}) \\ &= \ln(\mathrm{e}^{j}(\mathrm{e}^{\delta_1} + \mathrm{e}^{\delta_2})) \\ &= j + \max^{\star}(\delta_1, \delta_2) \qquad \forall \delta_1, \delta_2, j \in \mathbb{R}\,. \end{aligned} \tag{F.41}$$

We furthermore define

$$\max_{j=1}^{\chi\star} \delta_j = \max^\star(\delta_1, \delta_2, \ldots, \delta_\chi) \qquad \text{and} \qquad \max_{j=1}^{1\star} \delta_j = \delta_1 \,. \tag{F.42}$$

The first decoding step is again identical for all four SDSD algorithms. First, the L-values for all the N_I bit patterns of a block, i.e., $\mathsf{L}_{\mathrm{CD}}^{[\mathrm{ext}]}(\mathbf{b}_{t,k}) = (\mathsf{L}_{\mathrm{CD}}^{[\mathrm{ext}]}(b_{t,k,1}), \ldots, \mathsf{L}_{\mathrm{CD}}^{[\mathrm{ext}]}(b_{t,k,B_k}))$ are extracted from the input vector. This corresponds to a serial-to-parallel conversion of the L-values. Instead of computing $\gamma_{t,k}(q)$, the first step of all four SDSD algorithms in the logarithmic domain consists in computing

$$\tilde{\gamma}_{t,k}(q) \doteq \frac{1}{2} \sum_{\mu=1}^{B_k} \left(1 - 2 \cdot \bar{b}_{k,\mu}^{(q)}\right) \mathsf{L}_{\mathrm{CD}}^{[\mathrm{ext}]}(b_{t,k,\mu}) \,. \tag{F.43}$$

It can be easily shown that

$$\ln \gamma_{t,k}(q) = \tilde{\gamma}_{t,k}(q) - \sum_{\mu=1}^{B_k} \ln\left(2\cosh\left(\frac{1}{2}\mathsf{L}_{\mathrm{CD}}^{[\mathrm{ext}]}(b_{t,k,\mu})\right)\right) \doteq \tilde{\gamma}_{t,k}(q) + \tilde{\mathrm{K}}_{t,k} \,. \tag{F.44}$$

This means that instead of using $\ln \gamma_{t,k}(q)$, usually $\tilde{\gamma}_{t,k}(q)$ defined by (F.43) can be used in the computation of the extrinsic information and the *a posteriori* probabilities as $\tilde{\mathrm{K}}_{t,k}$ is independent of the bit position μ. It will be shown in the AK0 case how this simplification is used in the computation of the *a posteriori* probabilities. We furthermore define

$$\tilde{\gamma}_{t,k}^{[\mathrm{ext}]\setminus\chi}(q) \doteq \frac{1}{2} \sum_{\substack{\mu=1 \\ \mu\neq\chi}}^{B_k} \left(1 - 2 \cdot \bar{b}_{k,\mu}^{(q)}\right) \mathsf{L}_{\mathrm{CD}}^{[\mathrm{ext}]}(b_{t,k,\mu}) \tag{F.45}$$

$$= \tilde{\gamma}_{t,k}(q) - \frac{1}{2}\left(1 - 2 \cdot \bar{b}_{k,\chi}^{(q)}\right) \mathsf{L}_{\mathrm{CD}}^{[\mathrm{ext}]}(b_{t,k,\chi}) \,. \tag{F.46}$$

According to (F.44) we have

$$\ln \gamma_{t,k}^{[\mathrm{ext}]\setminus\chi}(q) = \frac{1}{2} \sum_{\substack{\mu=1 \\ \mu\neq\chi}}^{B_k} \left(1 - 2\bar{b}_{k,\mu}^{(q)}\right) \mathsf{L}_{\mathrm{CD}}^{[\mathrm{ext}]}(b_{t,k,\mu}) - \sum_{\substack{\mu=1 \\ \mu\neq\chi}}^{B_k} \ln\left(2\cosh\left(\frac{1}{2}\mathsf{L}_{\mathrm{CD}}^{[\mathrm{ext}]}(b_{t,k,\mu})\right)\right)$$

$$\doteq \tilde{\gamma}_{t,k}^{[\mathrm{ext}]\setminus\chi}(q) + \tilde{\mathrm{K}}_{t,k}^{[\mathrm{ext}]\setminus\chi} \tag{F.47}$$

$$= \tilde{\gamma}_{t,k}(q) - \frac{1}{2}\left(1 - 2 \cdot \bar{b}_{k,\chi}^{(q)}\right) \mathsf{L}_{\mathrm{CD}}^{[\mathrm{ext}]}(b_{t,k,\chi}) + \tilde{\mathrm{K}}_{t,k}^{[\mathrm{ext}]\setminus\chi} \tag{F.48}$$

In the AK0 case below it is shown that $\tilde{\gamma}_{t,k}^{[\mathrm{ext}]\setminus\chi}(q)$ from (F.45) can be used instead of $\ln \gamma_{t,k}^{[\mathrm{ext}]\setminus\chi}(q)$, a fact which is then subsequently used in the extrinsic information computation of the three other cases. Using these expressions, the equations of the four different algorithms can be given. For a detailed explanation of the annotation, the different factors used, the preliminaries, as well as the partitioning of the input and output L-value stream, we refer to Sec. F.1.

AK0

In the AK0 case, the extrinsic information amounts to

$$\mathsf{L}_{\mathrm{SD}}^{[\mathrm{ext}]}(b_{t,k,\mu}) = \ln \frac{\sum_{q=1}^{Q} \left(1 - \bar{b}_{k,\mu}^{(q)}\right) \gamma_{t,k}^{[\mathrm{ext}]\setminus\mu}(q) \cdot \mathsf{Pr}\{I_{t,k} = q\}}{\sum_{q=1}^{Q} \bar{b}_{k,\mu}^{(q)} \gamma_{t,k}^{[\mathrm{ext}]\setminus\mu}(q) \cdot \mathsf{Pr}\{I_{t,k} = q\}} \tag{F.49}$$

$$= \ln \frac{\sum_{q=1}^{Q} \left(1 - \bar{b}_{k,\mu}^{(q)}\right) \mathrm{e}^{\ln \gamma_{t,k}^{[\mathrm{ext}]\setminus\mu}(q)} \cdot \mathrm{e}^{\ln \mathsf{Pr}\{I_{t,k}=q\}}}{\sum_{q=1}^{Q} \bar{b}_{k,\mu}^{(q)} \mathrm{e}^{\ln \gamma_{t,k}^{[\mathrm{ext}]\setminus\mu}(q)} \cdot \mathrm{e}^{\ln \mathsf{Pr}\{I_{t,k}=q\}}} \tag{F.50}$$

$$= \ln \frac{\mathrm{e}^{\tilde{\mathrm{K}}_{t,k}^{[\mathrm{ext}]\setminus\mu}} \sum_{q=1}^{Q} \left(1 - \bar{b}_{k,\mu}^{(q)}\right) \mathrm{e}^{\tilde{\gamma}_{t,k}^{[\mathrm{ext}]\setminus\mu}(q)} \cdot \mathrm{e}^{\ln \mathsf{Pr}\{I_{t,k}=q\}}}{\mathrm{e}^{\tilde{\mathrm{K}}_{t,k}^{[\mathrm{ext}]\setminus\mu}} \sum_{q=1}^{Q} \bar{b}_{k,\mu}^{(q)} \mathrm{e}^{\tilde{\gamma}_{t,k}^{[\mathrm{ext}]\setminus\mu}(q)} \cdot \mathrm{e}^{\ln \mathsf{Pr}\{I_{t,k}=q\}}} \tag{F.51}$$

$$= \ln \left(\sum_{\substack{q=1 \\ \bar{b}_{k,\mu}^{(q)}=0}}^{Q} \mathrm{e}^{\tilde{\gamma}_{t,k}^{[\mathrm{ext}]\setminus\mu}(q) + \ln \mathsf{Pr}\{I_{t,k}=q\}} \right) - \ln \left(\sum_{\substack{q=1 \\ \bar{b}_{k,\mu}^{(q)}=1}}^{Q} \mathrm{e}^{\tilde{\gamma}_{t,k}^{[\mathrm{ext}]\setminus\mu}(q) + \ln \mathsf{Pr}\{I_{t,k}=q\}} \right) \tag{F.52}$$

$$= \max_{\substack{q=1 \\ \bar{b}_{k,\mu}^{(q)}=0}}^{Q\,\star} \left(\tilde{\gamma}_{t,k}^{[\mathrm{ext}]\setminus\mu}(q) + \widetilde{\mathsf{Pr}}\{I_{t,k}=q\} \right) - \max_{\substack{q=1 \\ \bar{b}_{k,\mu}^{(q)}=1}}^{Q\,\star} \left(\tilde{\gamma}_{t,k}^{[\mathrm{ext}]\setminus\mu}(q) + \widetilde{\mathsf{Pr}}\{I_{t,k}=q\} \right) \tag{F.53}$$

with $\widetilde{\mathsf{Pr}}\{I_{t,k} = q\} \doteq \ln \mathsf{Pr}\{I_{t,k} = q\}$. Note that the logarithm of the *a priori* information $\mathsf{Pr}\{I_{t,k} = q\}$ can be precomputed and stored.

The *a posteriori* probabilities amount to

$$\mathsf{Pr}\{I_{t,k} = q|\mathbf{z}_t\} = \frac{1}{\mathrm{K}_1} \mathrm{e}^{\ln \gamma_{t,k}(q)} \cdot \mathrm{e}^{\ln \mathsf{Pr}\{I_{t,k}=q\}} \tag{F.54}$$

$$= \frac{1}{\mathrm{K}_1} \exp\left(\tilde{\gamma}_{t,k}(q) + \tilde{\mathrm{K}}_{t,k} + \widetilde{\mathsf{Pr}}\{I_{t,k} = q\} \right) \tag{F.55}$$

$$= \frac{1}{\mathrm{K}_2} \cdot \exp\left(\tilde{\gamma}_{t,k}(q) + \widetilde{\mathsf{Pr}}\{I_{t,k} = q\} \right) \qquad \forall q \in \mathbb{I}\,, \tag{F.56}$$

with K_1 and K_2 ensuring $\sum_{q=1}^{Q} \mathsf{Pr}\{I_{t,k}=q|\mathbf{z}_t\}=1$. By defining $\tilde{\alpha}_{t,k}(q) \doteq \tilde{\gamma}_{t,k}(q) + \widetilde{\mathsf{Pr}}\{I_{t,k}=q\}$, the expressions can be simplified to

$$\mathsf{Pr}\{I_{t,k}=q|\mathbf{z}_t\} = \frac{1}{\mathrm{K}_2} \cdot \exp\left(\tilde{\alpha}_{t,k}(q)\right) \qquad \forall q \in \mathbb{I} \tag{F.57}$$

$$\mathsf{L}_{\mathrm{SD}}^{[\mathrm{ext}]}(b_{t,k,\mu}) = \max_{\substack{q=1 \\ \bar{b}_{k,\mu}^{(q)}=0}}^{Q\,\star} \left(\tilde{\alpha}_{t,k}(q) - \frac{1}{2}\mathsf{L}_{\mathrm{CD}}^{[\mathrm{ext}]}(b_{t,k,\mu})\right) - \max_{\substack{q=1 \\ \bar{b}_{k,\mu}^{(q)}=1}}^{Q\,\star} \left(\tilde{\alpha}_{t,k}(q) + \frac{1}{2}\mathsf{L}_{\mathrm{CD}}^{[\mathrm{ext}]}(b_{t,k,\mu})\right) \tag{F.58}$$

by exploiting (F.46). Note that if *Maximum A Posteriori* (MAP) estimation is utilized instead of MMSE estimation (see Sec. 3.1.3), the $\tilde{\alpha}_{t,k}(q)$ can be used directly in (F.57) without evaluating the exponential function, which is a monotonically increasing function and thus does not influence the maximization.

AK1-INTER

First, we define (with $\alpha_{t,k}(q)$ similar to (F.11) without considering the normalization factor) for all $q \in \{1,\ldots,N_I\}$

$$\tilde{\alpha}_{t,k}(q) \doteq \ln \alpha_{t,k}(q) = \ln\left(\gamma_{t,k}(q) \sum_{\tilde{q}=1}^{Q} \mathsf{Pr}\{I_{t,k}=q|I_{t-1,k}=\tilde{q}\} \cdot \alpha_{t-1,k}(\tilde{q})\right) \tag{F.59}$$

$$= \ln \gamma_{t,k}(q) + \ln\left(\sum_{\tilde{q}=1}^{Q} \mathrm{e}^{\ln \mathsf{Pr}\{I_{t,k}=q|I_{t-1,k}=\tilde{q}\}} \cdot \mathrm{e}^{\ln \alpha_{t-1,k}(\tilde{q})}\right) \tag{F.60}$$

$$= \tilde{\gamma}_{t,k}(q) + \ln\left(\sum_{\tilde{q}=1}^{Q} \mathrm{e}^{\widetilde{\mathsf{Pr}}\{I_{t,k}=q|I_{t-1,k}=\tilde{q}\}+\tilde{\alpha}_{t-1,k}(\tilde{q})}\right) \tag{F.61}$$

$$= \tilde{\gamma}_{t,k}(q) + \max_{\tilde{q}=1}^{Q\,\star} \left(\widetilde{\mathsf{Pr}}\{I_{t,k}=q|I_{t-1,k}=\tilde{q}\} + \tilde{\alpha}_{t-1,k}(\tilde{q})\right) \tag{F.62}$$

and get a forward recursion similar to (F.11). Note that $\ln \gamma_{t,k}(q)$ has been replaced by $\tilde{\gamma}_{t,k}(q)$ and the additive constant $\tilde{\mathrm{K}}_{t,k}$ has been omitted. $\tilde{\mathrm{K}}_{t,k}$ can be omitted as it is either canceled within the determination of the extrinsic information (see also the AK0 case) or it results in a constant multiplicative factor in the determination of the *a posteriori* information. As this simplification can be performed in all of the subsequent cases, it will not be explicitely mentioned anymore.

Again, $\widetilde{\mathsf{Pr}}\{I_{t,k}=q|I_{t-1,k}=\tilde{q}\} \doteq \ln \mathsf{Pr}\{I_{t,k}=q|I_{t-1,k}=\tilde{q}\}$. At the beginning of the transmission, the $\tilde{\alpha}_{t,k}(q)$ are initialized with $\tilde{\alpha}_{0,k}(q) = \ln \mathsf{Pr}\{I_{1,k}=q\}$, $\forall q \in \mathbb{I}$ (note that $I_{t,k}$ is assumed to be stationary over time t). Using $\tilde{\alpha}_{t,k}(q)$, the *a posteriori* probabilities are given by

$$\mathsf{Pr}\{I_{t,k}=q|\mathbf{z}_t,\mathbf{z}_{t-1},\ldots\} = \frac{1}{\mathrm{K}} \cdot \exp\left(\tilde{\alpha}_{t,k}(q)\right) \qquad \forall q \in \mathbb{I}\,, \tag{F.63}$$

with K ensuring that $\sum_{q=1}^{Q} \mathsf{Pr}\{I_{t,k} = q|\mathbf{z}_t, \mathbf{z}_{t-1}, \ldots\} = 1$. Again, if MAP estimation is utilized instead of MMSE estimation (see Sec. 3.1.3), the $\tilde{\alpha}_{t,k}(q)$ can be used directly without evaluating the monotonically increasing exponential function. The extrinsic information is given by

$$\begin{aligned}
\mathsf{L}_{\mathrm{SD}}^{[\mathrm{ext}]}(b_{t,k,\mu}) &= \ln \frac{\sum_{q=1}^{Q} \left(1-\bar{b}_{k,\mu}^{(q)}\right) \gamma_{t,k}^{[\mathrm{ext}]\setminus\mu}(q) \sum_{\tilde{q}=1}^{Q} \mathsf{Pr}\{I_{t,k}=q|I_{t-1,k}=\tilde{q}\}\alpha_{t-1,k}(\tilde{q})}{\sum_{q=1}^{Q} \bar{b}_{k,\mu}^{(q)} \gamma_{t,k}^{[\mathrm{ext}]\setminus\mu}(q) \sum_{\tilde{q}=1}^{Q} \mathsf{Pr}\{I_{t,k}=q|I_{t-1,k}=\tilde{q}\}\alpha_{t-1,k}(\tilde{q})} \\
&= \ln \left(\sum_{\substack{q=1 \\ \bar{b}_{k,\mu}^{(q)}=0}}^{Q} \mathrm{e}^{\tilde{\gamma}_{t,k}^{[\mathrm{ext}]\setminus\mu}(q)} \mathrm{e}^{\ln \sum_{\tilde{q}=1}^{Q} \mathsf{Pr}\{I_{t,k}=q|I_{t-1,k}=\tilde{q}\}\alpha_{t-1,k}(\tilde{q})} \right) \\
&\quad - \ln \left(\sum_{\substack{q=1 \\ \bar{b}_{k,\mu}^{(q)}=1}}^{Q} \mathrm{e}^{\tilde{\gamma}_{t,k}^{[\mathrm{ext}]\setminus\mu}(q)} \mathrm{e}^{\ln \sum_{\tilde{q}=1}^{Q} \mathsf{Pr}\{I_{t,k}=q|I_{t-1,k}=\tilde{q}\}\alpha_{t-1,k}(\tilde{q})} \right) \\
&= \max_{\substack{q=1 \\ \bar{b}_{k,\mu}^{(q)}=0}}^{Q\star} \left(\tilde{\gamma}_{t,k}^{[\mathrm{ext}]\setminus\mu}(q) + \max_{\tilde{q}=1}^{Q\star} \left(\widetilde{\mathsf{Pr}}\{I_{t,k}=q|I_{t-1,k}=\tilde{q}\} + \tilde{\alpha}_{t-1,k}(\tilde{q}) \right) \right) \\
&\quad - \max_{\substack{q=1 \\ \bar{b}_{k,\mu}^{(q)}=1}}^{Q\star} \left(\tilde{\gamma}_{t,k}^{[\mathrm{ext}]\setminus\mu}(q) + \max_{\tilde{q}=1}^{Q\star} \left(\widetilde{\mathsf{Pr}}\{I_{t,k}=q|I_{t-1,k}=\tilde{q}\} + \tilde{\alpha}_{t-1,k}(\tilde{q}) \right) \right)
\end{aligned} \tag{F.64}$$

which is further simplified by combining (F.62) with (F.46) in (F.64) to

$$\mathsf{L}_{\mathrm{SD}}^{[\mathrm{ext}]}(b_{t,k,\mu}) = \max_{\substack{q=1 \\ \bar{b}_{k,\mu}^{(q)}=0}}^{Q\star} \left(\tilde{\alpha}_{t,k}(q) - \frac{1}{2}\mathsf{L}_{\mathrm{CD}}^{[\mathrm{ext}]}(b_{t,k,\mu}) \right) - \max_{\substack{q=1 \\ \bar{b}_{k,\mu}^{(q)}=1}}^{Q\star} \left(\tilde{\alpha}_{t,k}(q) + \frac{1}{2}\mathsf{L}_{\mathrm{CD}}^{[\mathrm{ext}]}(b_{t,k,\mu}) \right). \tag{F.65}$$

AK1-INTRA

The AK1-INTRA case is similar to the AK1-INTER case. Using the same approach as in (F.59)-(F.62), expressions for a forward and backward recursion can be established

$$\tilde{\alpha}_{t,k}(q) \doteq \tilde{\gamma}_{t,k}(q) + \max_{\tilde{q}=1}^{Q\star} \left(\widetilde{\mathsf{Pr}}\{I_{t,k}=q|I_{t,k-1}=\tilde{q}\} + \tilde{\alpha}_{t,k-1}(\tilde{q}) \right), \; k \in \{1, \ldots, N_I\} \tag{F.66}$$

$$\tilde{\beta}_{t,k-1}(q) = \max_{\tilde{q}=1}^{Q\star} \left(\tilde{\gamma}_{t,k}(\tilde{q}) + \widetilde{\mathsf{Pr}}\{I_{t,k} = \tilde{q} | I_{t,k-1} = q\} + \tilde{\beta}_{t,k}(\tilde{q}) \right), \; k \in \{2, \ldots, N_I\} \tag{F.67}$$

with the initialization

$$\tilde{\alpha}_{t,0}(q) = \widetilde{\mathsf{Pr}}\{I_{t,1} = q\} \qquad \forall q \in \mathbb{I} \tag{F.68}$$

$$\tilde{\beta}_{t,N_I}(q) = 0 \qquad \forall q \in \mathbb{I} \tag{F.69}$$

and $\widetilde{\mathsf{Pr}}\{I_{t,k} = q | I_{t,k-1} = \tilde{q}\} \doteq \ln \mathsf{Pr}\{I_{t,k} = q | I_{t,k-1} = \tilde{q}\}$. The extrinsic information is given by

$$\begin{aligned} \mathsf{L}_{\mathrm{SD}}^{[\mathrm{ext}]}(b_{t,k,\mu}) = & \max_{\substack{q=1 \\ \bar{b}_{k,\mu}^{(q)}=0}}^{Q\star} \left(\tilde{\gamma}_{t,k}^{[\mathrm{ext}]\setminus\mu}(q) + \tilde{\beta}_{t,k}(q) + \max_{\tilde{q}=1}^{Q\star} \left(\widetilde{\mathsf{Pr}}\{I_{t,k} = q | I_{t-1,k} = \tilde{q}\} + \tilde{\alpha}_{t-1,k}(\tilde{q}) \right) \right) \\ & - \max_{\substack{q=1 \\ \bar{b}_{k,\mu}^{(q)}=1}}^{Q\star} \left(\tilde{\gamma}_{t,k}^{[\mathrm{ext}]\setminus\mu}(q) + \tilde{\beta}_{t,k}(q) + \max_{\tilde{q}=1}^{Q\star} \left(\widetilde{\mathsf{Pr}}\{I_{t,k} = q | I_{t-1,k} = \tilde{q}\} + \tilde{\alpha}_{t-1,k}(\tilde{q}) \right) \right) \end{aligned} \tag{F.70}$$

which can be simplified to

$$\begin{aligned} \mathsf{L}_{\mathrm{SD}}^{[\mathrm{ext}]}(b_{t,k,\mu}) = & \max_{\substack{q=1 \\ \bar{b}_{k,\mu}^{(q)}=0}}^{Q\star} \left(\tilde{\alpha}_{t,k}(q) + \tilde{\beta}_{t,k}(q) - \frac{1}{2} \mathsf{L}_{\mathrm{CD}}^{[\mathrm{ext}]}(b_{t,k,\mu}) \right) \\ & - \max_{\substack{q=1 \\ \bar{b}_{k,\mu}^{(q)}=1}}^{Q\star} \left(\tilde{\alpha}_{t,k}(q) + \tilde{\beta}_{t,k}(q) + \frac{1}{2} \mathsf{L}_{\mathrm{CD}}^{[\mathrm{ext}]}(b_{t,k,\mu}) \right). \end{aligned} \tag{F.71}$$

The *a posteriori* probabilities amount to

$$\mathsf{Pr}\{I_{t,k} = q | \mathbf{z}_t\} = \frac{1}{\mathrm{K}} \cdot \exp\left(\tilde{\alpha}_{t,k}(q) + \tilde{\beta}_{t,k}(q) \right) \qquad \forall q \in \mathbb{I}. \tag{F.72}$$

Again, if MAP estimation is utilized instead of MMSE estimation, $\tilde{\alpha}_{t,k}(q) + \tilde{\beta}_{t,k}(q)$ can be used directly without evaluating the monotonically increasing exponential function.

AK1-NOPT

The equations for the AK1-NOPT can almost immediately be given by combining the equations derived for AK1-INTER and AK1-INTRA cases. Therefore, we do not give a detailed explanation and derivation of the expressions here as the approaches

used are identical to the previous cases. The spatial forward and backward recursions are given by

$$\tilde{\alpha}_{t,k}^{[\mathrm{pos}]}(q) \doteq \max_{\tilde{q}=1}^{Q\star}\Big(\tilde{\alpha}_{t,k-1}^{[\mathrm{pos}]}(\tilde{q}) + \tilde{\gamma}_{t,k-1}(\tilde{q}) + \widetilde{\mathsf{Pr}}\{I_{t,k}=q|I_{t,k-1}=\tilde{q}\}\Big),\ \forall k \in \{2,\ldots,N_I\}$$

$$\tilde{\beta}_{t,k-1}^{[\mathrm{pos}]}(q) \doteq \max_{\tilde{q}=1}^{Q\star}\Big(\tilde{\beta}_{t,k}^{[\mathrm{pos}]}(\tilde{q}) + \tilde{\gamma}_{t,k}(\tilde{q}) + \widetilde{\mathsf{Pr}}\{I_{t,k}=\tilde{q}|I_{t,k-1}=q\}\Big)\,,\ \forall k \in \{2,\ldots,N_I\}$$

with the initialization [ASHV00, HA08]

$$\tilde{\alpha}_{t,1}^{[\mathrm{pos}]}(q) = \tilde{\beta}_{t,N_I}^{[\mathrm{pos}]}(q) = 0 \qquad \forall q \in \mathbb{I} \tag{F.73}$$

The temporal forward recursion $\forall q \in \mathbb{I}$ is given by

$$\tilde{\alpha}_{t,k}^{[\mathrm{tim}]}(q) = \tilde{\gamma}_{t,k}(q) + \tilde{\alpha}_{t,k}^{[\mathrm{pos}]}(q) + \tilde{\beta}_{t,k}^{[\mathrm{pos}]}(q) + \max_{\tilde{q}=1}^{Q\star}\Big(\widetilde{\mathsf{Pr}}\{I_{t,k}=q|I_{t-1,k}=\tilde{q}\} + \tilde{\alpha}_{t-1,k}^{[\mathrm{tim}]}(\tilde{q})\Big) \tag{F.74}$$

with (note that the transmission starts at $t = 1$)

$$\tilde{\alpha}_{0,k}^{[\mathrm{tim}]}(q) = \widetilde{\mathsf{Pr}}\{I_{1,k} = q\} \qquad \forall q \in \mathbb{I}\,. \tag{F.75}$$

The extrinsic information is given by

$$\mathsf{L}_{\mathrm{SD}}^{[\mathrm{ext}]}(b_{t,k,\mu}) = \max_{\substack{q=1 \\ \bar{b}_{k,\mu}^{(q)}=0}}^{Q\star}\left(\tilde{\alpha}_{t,k}^{[\mathrm{tim}]}(q) - \frac{1}{2}\mathsf{L}_{\mathrm{CD}}^{[\mathrm{ext}]}(b_{t,k,\mu})\right) - \max_{\substack{q=1 \\ \bar{b}_{k,\mu}^{(q)}=1}}^{Q\star}\left(\tilde{\alpha}_{t,k}^{[\mathrm{tim}]}(q) + \frac{1}{2}\mathsf{L}_{\mathrm{CD}}^{[\mathrm{ext}]}(b_{t,k,\mu})\right). \tag{F.76}$$

Finally, the *a posteriori* probabilities are given by ($\forall q \in \mathbb{I}$)

$$\mathsf{Pr}\{I_{t,k} = q|\mathbf{z}_t, \mathbf{z}_{t-1}, \ldots\} = \frac{1}{\mathrm{K}} \cdot \exp\left(\tilde{\alpha}_{t,k}^{[\mathrm{pos}]}(q) + \tilde{\beta}_{t,k}^{[\mathrm{pos}]}(q) + \tilde{\alpha}_{t,k}^{[\mathrm{tim}]}(q)\right). \tag{F.77}$$

where the exp function does not need to be evaluated if MAP estimation is performed at the receiver (see above).

F.3 Complexity Evaluation

In Sec. F.3.1, some basic complexity figures for the algorithms described in Secs. F.1 and F.2 are given first, starting with the required number of operations for the algorithms operating in the probability domain. Afterwards, the required operations for the practically more relevant implementation in the logarithmic domain are presented.

The operations that are given below are the operations that are required to compute the extrinsic information of all the bits within a single bit pattern $\mathbf{b}_{t,k}$ (corresponding to the quantizer index $i_{t,k}$), i.e., one position k within a frame. The total number of operations per frame is obtained by summing up over all N_I quantizer indices. We only consider the number of operations required for computing the extrinsic information as this computation is performed once per iteration whereas the *a posteriori* probabilities are only required once per frame. Furthermore, in Secs. F.3.2, F.3.3, and F.3.4, complexity figures for the *Conditional Quantization* (CQ) SDSD, the M-SDSD, as well as the combined CQ-M-SDSD are given.

The complexity analysis is not targeted for a specific system architecture. Instead, we count only operations such as *addition* (ADD), *multiplication* (MUL), *Multiply ACcumulate* (MAC), *division* (DIV), *exponential* (EXP), *logarithm* (LOG), *compare* (CMP), or the $\max^\star$ operation introduced earlier (see Sec. F.2). The cost of each of these operations strongly depends on the utilized hardware. For example, most *Digital Signal Processors* (DSPs) can perform a MAC operation within one cycle, while general purpose *Central Processing Units* (CPUs) need to divide the MAC operation in two independent operations (multiplication and addition). Furthermore, if an *Application Specific Integrated Circuit* (ASIC) or *Field Programmable Gate Array* (FPGA) is designed to perform logarithmic SDSD, the $\max^\star$ operation can be implemented to be executed in one cycle while on general purpose CPUs or DSPs, several cycles are necessary (maximization, addition, table look-up, etc.). Memory accesses are not taken into account in this section as they strongly depend on the realization and implementation of the algorithm on a specific target hardware. If a hardware with slow memory access is considered, a more thorough analysis has to be performed. An example of such an implementation, which has to aim at a careful memory usage, is the massively parallel *Compute Unified Device Architecture* (CUDA) implementation of the SDSD on *Graphical Processing Units* (GPUs) [Vol09].

F.3.1 Complexity of Standard SDSD

Complexity in the Probability Domain

The first step common to all SDSD algorithms in the probability domain is the computation of $\gamma_{t,k}(q)$ and $\gamma_{t,k}^{[\mathrm{ext}]\setminus\chi}(q)$. If (F.2) is directly evaluated, each $2B_k$ additions, exponentials, and divisions for computing the multiplicands (two cases: $\bar{b}_{k,\mu}^{(q)} = 0$ and $\bar{b}_{k,\mu}^{(q)} = 1$) as well as QB_k multiplications are required[2] (note that the multiplication

[2]Depending on the implementation, the number of multiplications may also be counted as $Q(B_k - 1)$, as B_k multiplicands require $B_k - 1$ multiplications. However, in this section, it is assumed that the variable containing the result is initialized with the neutral element of the operation ("1" for the multiplication), and B_k operations are carried out with storing the result in the aforementioned variable. This approach is utilized in the remainder of this section for all operations. This means that the given figures do not necessarily represent the lowest possible number of operations. However, the algorithms can be effectively compared as the operations are all counted in the same way.

with $1 - 2 \cdot \bar{b}_{k,\mu}^{(q)}$ corresponds to a sign change which is not counted as an operation here). The evaluation of (F.4) requires $QB_k(B_k - 1)$ additional multiplications (as $Q(B_k - 1)$ multiplications have to be carried out for each distinct $\chi \in \{1, \ldots, B_k\}$). Note that the multiplicands have already been computed. This leads to a total number of QB_k^2 multiplications for (F.2) and (F.4).

The evaluation of (F.6) in the AK0 case requires B_k times taking the logarithm, QB_k MAC operations for evaluating the numerator and denominator, as well as B_k divisions. Note that the multiplication by $(1 - \bar{b}_{k,\mu}^{(q)})$ or $\bar{b}_{k,\mu}^{(q)}$, respectively, with $\bar{b}_{k,\mu}^{(q)} \in \mathbb{F}_2$ signifies that parts of the sum are not evaluated and therefore no operations need to be counted for those terms of the sum. Only those bit patterns where the bit at position μ is zero (numerator) or one (denominator) are taken into account in the respective sums.

In the AK1-INTER case, Q^2 MAC operations (Q operations for each $\alpha_{t,k}(q)$ and an overall number of Q distinct $\alpha_{t,k}(q)$) are required for evaluating the Q distinct values $A_{t,k}(q)$ ($q \in \{1, \ldots, Q\}$) according to (F.11) and (F.12). In order to determine the $\alpha_{t,k}(q)$ according to (F.12), Q multiplications ($\gamma_{t,k}(q) \cdot A_{t,k}(q)$ for each $q \in \{1, \ldots, Q\}$) are necessary. In order to perform the normalization in (F.12), Q additions (sum over all $\alpha_{t,k}$), 1 division (building the reciprocal $\frac{1}{\mathrm{K}}$), and Q multiplications are required. Note that the update (F.12) is only necessary once per frame, as only $A_{t,k}(q)$ contributes to the computation of extrinsic knowledge. However, we nevertheless perform the update in each frame, as $\alpha_{t,k}(q)$ might be required for various reasons (stopping criteria, intermediate results, etc.). The same holds for the temporal update in the AK1-NOPT algorithm to be discussed below. Finally, the determination of the extrinsic information (F.14) is performed using B_k divisions, B_k logarithms, and B_kQ MAC operations, similarly as in the AK0 case.

The AK1-INTRA decoder requires additional computations for the factors $\beta_{t,k}(q)$ according to (F.20): Q multiplications for $\gamma_{t,k}(\tilde{q}) \cdot \beta_{t,k}(\tilde{q})$ which only need to be computed for each distinct $\tilde{q} \in \{1, \ldots, Q\}$ as well as Q^2 MAC operations. An additional normalization (requiring Q additions, 1 division, and Q multiplications) has to be performed and the evaluation of (F.23) requires B_kQ additional multiplications compared to the AK1-INTER case (multiplication with $\beta_{t,k}(q)$ in the numerator and denominator).

The AK1-NOPT case is similar to the AK1-INTRA case with one additional temporal recursion and an additional normalization. The temporal recursion however requires more operations as the term $A_{t,k}(q)$ has to be multiplied by the factors $\alpha_{t,k}^{[\mathrm{pos}]}(q)$ and $\beta_{t,k}^{[\mathrm{pos}]}(q)$ besides $\gamma_{t,k}(q)$, resulting in $3Q$ multiplications. However, the intermediate results $\alpha_{t,k}^{[\mathrm{pos}]}(q) \cdot \beta_{t,k}^{[\mathrm{pos}]}(q) \cdot A_{t,k}(q)$ can be reused within the determination of the extrinsic information according to (F.36), such that the evaluation of (F.36) only requires QB_k MAC operations as well as B_k divisions.

The required operations of all four considered algorithms are summarized in Tab. F.2.

	AK0	AK1-INTER	AK1-INTRA	AK1-NOPT
ADD	$2B_k$	$2B_k + Q$	$2B_k + 2Q$	$2B_k + 3Q$
MUL	QB_k^2	$Q(B_k^2 + 2)$	$Q(B_k^2 + 4 + B_k)$	$Q(B_k^2 + 8)$
MAC	B_kQ	$Q^2 + B_kQ$	$2Q^2 + B_kQ$	$3Q^2 + B_kQ$
DIV	$3B_k$	$3B_k + 1$	$3B_k + 2$	$3B_k + 3$
EXP	$2B_k$	$2B_k$	$2B_k$	$2B_k$
LOG	B_k	B_k	B_k	B_k

Table F.2: Operations required for computing the extrinsic information per quantizer index $i_{t,k}$ by the SDSD operating in the probability domain

Complexity in the Logarithmic Domain

In the logarithmic domain, mostly additions and max* operations are necessary. The max* operation internally performs a max operation, one addition and a (two-dimensional) table look-up[3] according to [RVH95].

First, the evaluation of (F.43), which is common for all four algorithms, requires a total number of QB_k additions per parameter as the $\tilde{\gamma}_{t,k}(q)$ have to be determined for each of the Q possible bit patterns. Instead of multiplying the result of the sum (as in (F.43)) by $\frac{1}{2}$ it is advantageous to precompute $\frac{1}{2}\mathsf{L}_{\mathrm{CD}}^{[\mathrm{ext}]}(b_{t,k,\mu})$ using B_k multiplications, as these factors are required in subsequent steps of the algorithm.

The evaluation of (F.58) in the AK0 flavor of the logarithmic SDSD requires Q additions for computing $\tilde{\alpha}_{t,k}(q)$ as well as $(Q+1)B_k$ additions and QB_k max* operations.

In the AK1-INTER case, $Q + Q^2$ additions and Q^2 max* operations are required for evaluating (F.62): Q additions are required for computing the elements of the max* operations, however, these elements have to be recomputed for each of the Q distinct $\tilde{\alpha}_{t,k}(q)$. The max* operation has to be carried out Q times for each of the Q values of q. Furthermore, Q additions are required for adding $\tilde{\gamma}_{t,k}(q)$ to the result of the max* operations. The computation of the extrinsic information according to (F.65) utilizes $B_k(Q + 1)$ additions and B_kQ max* operations.

The AK1-INTRA case has to determine an additional backward recursion (F.67) requiring $Q + Q^2$ additions (the factors $\tilde{\gamma}_{t,k}(\tilde{q}) + \tilde{\beta}_{t,k}(\tilde{q})$ only need to be computed for Q distinct values of $\tilde{q}$) and Q^2 max* operations. For the determination of the extrinsic information in (F.71), QB_k additional additions compared to (F.65) need to be performed.

The AK1-NOPT case basically combines two spatial recursions requiring each $Q^2 + Q$ additions and Q^2 max* operations and a temporal forward recursion with $Q^2 + 3Q$ additions and Q^2 max* operations. The determination of extrinsic information according to (F.76) performs $B_k(Q + 1)$ additions as well as B_kQ max* operations.

The number of operations required for the different SDSD flavors operating in the logarithmic domain are summarized in Table F.3.

[3]The two-dimension table look-up can be replaced by a one-dimensional table look-up at the expense of an additional addition and the computation of an absolute value.

	AK0	AK1-INTER
$\max^\star$	QB_k	$Q^2 + QB_k$
ADD	$Q(2B_k + 1) + B_k$	$Q^2 + Q(2B_k + 1) + B_k$
MUL	B_k	B_k

	AK1-INTRA	AK1-NOPT
$\max^\star$	$2Q^2 + QB_k$	$3Q^2 + QB_k$
ADD	$2Q^2 + Q(3B_k + 2) + B_k$	$3Q^2 + Q(2B_k + 5) + B_k$
MUL	B_k	B_k

Table F.3: Operations required for computing the extrinsic information per quantizer index $i_{t,k}$ by the SDSD operating in the logarithmic domain

F.3.2 Complexity for the Conditional Quantization Case

If conditional quantization (see Sec. 4.1) is employed, the complexity of the SDSD can be reduced by only considering the permitted transitions between either spatially or temporally adjacent frames (depending on how the conditional quantizer is set up). The number of transitions is reduced from Q^2 to $\mathfrak{N}$ with $\mathfrak{N}$ being a function of the design threshold $\mathfrak{T}$ of the conditional quantizer. This means that in the forward (or backward) recursion, the summations (or $\max^\star$ operations in the logarithmic domain) do not run over all Q parameters but only over those considered by the conditional quantizer. The sum of those considered summations corresponds to the number of transitions $\mathfrak{N}$ defined according to (4.4). The other computations, like, e.g., the determination of extrinsic information, are not affected by conditional quantization. As the AK1-INTER algorithm only uses a forward recursion while the AK1-INTRA algorithm utilizes forward and backward recursions, the complexity reduction in the latter is larger. Tables F.4 and F.5 summarize the number of operations required for the AK1-INTER and AK1-INTRA decoders for conditional quantization in the probability and the logarithmic domain. A detailed derivation of the complexity figures for both cases can be found in [SVAC08].

If both inter- and intra-frame correlation is available ($\rho > 0$ and $\delta > 0$) it is advantageous to employ the AK1-NOPT algorithm. However, the complexity is influenced

	CQ-AK1-INTER	CQ-AK1-INTRA	CQ-AK1-NOPT Inter-frame CQ	CQ-AK1-NOPT Intra-frame CQ
ADD	$2B_k + Q$	$2B_k + 2Q$	$2B_k + 3Q$	$2B_k + 3Q$
MUL	$Q(B_k^2 + 2)$	$Q(B_k^2 + 4 + B_k)$	$Q(B_k^2 + 8)$	$Q(B_k^2 + 8)$
MAC	$\mathfrak{N} + B_kQ$	$2\mathfrak{N} + B_kQ$	$2Q^2 + \mathfrak{N} + B_kQ$	$Q^2 + 2\mathfrak{N} + B_kQ$
DIV	$3B_k + 1$	$3B_k + 2$	$3B_k + 3$	$3B_k + 3$
EXP	$2B_k$	$2B_k$	$2B_k$	$2B_k$
LOG	B_k	B_k	B_k	B_k

Table F.4: Operations required for computing the extrinsic information per quantizer index $i_{t,k}$ by the conditional quantization SDSD operating in the probability domain

	CQ-AK1-INTER	CQ-AK1-INTRA
$\max^\star$	$\mathfrak{N} + QB_k$	$2\mathfrak{N} + QB_k$
ADD	$\mathfrak{N} + Q(2B_k + 1) + B_k$	$2\mathfrak{N} + Q(3B_k + 2) + B_k$
MUL	B_k	B_k

	CQ-AK1-NOPT Inter-frame CQ	CQ-AK1-NOPT Intra-frame CQ
$\max^\star$	$2Q^2 + \mathfrak{N} + QB_k$	$Q^2 + 2\mathfrak{N} + QB_k$
ADD	$2Q^2 + \mathfrak{N} + Q(2B_k + 5) + B_k$	$Q^2 + 2\mathfrak{N} + Q(2B_k + 5) + B_k$
MUL	B_k	B_k

Table F.5: Operations required for computing the extrinsic information per quantizer index $i_{t,k}$ by the conditional quantization SDSD operating in the logarithmic domain

by the direction of the conditional quantizer, i.e., depending on whether inter- or intra-frame conditional quantization is employed. In the case of inter-frame CQ, the complexity savings only apply to the single forward recursion while in the case of intra-frame CQ, both spatial forward and backward recursions can be simplified. The required number of operations per quantizer index is summarized in Tables F.4 (probability domain) and F.5 (logarithmic domain).

F.3.3 Complexity for the M-SDSD Case

Complexity in the Probability Domain

If the M-SDSD decoding algorithm (see Sec. 4.2) is utilized, the complexity of the SDSD is reduced by only considering the transitions that have been selected by the decoder. As already mentioned in Sec. 4.2, the number of transitions is reduced from Q^2 to MQ, with M being the parameter of the M-SDSD algorithm. In the AK1-INTER algorithm for example, the complexity for (F.11) is reduced from Q^2 to MQ MAC operations for computing $A_{t,k}(q)$. Additionally, Q multiplications for computing $\alpha_{t,k}(q)$ are still necessary. The complexity of the normalization of the $\alpha_{t,k}(q)$ requires only M additions and multiplications instead of Q. The number of MAC operations in the calculation of (F.14) is also reduced from B_kQ to B_kM. Furthermore, $MQ - \frac{1}{2}(M^2 + M)$ comparisons are necessary in each step to determine the M best $\alpha_{t,k}(q)$.

In the AK1-INTRA case, the situation is similar. However, the complexity of the backward recursion can be further reduced. In order to evaluate (F.20), M multiplications and M^2 MAC operations are necessary. An additional normalization has to be performed. Finally, the computation of the extrinsic information requires B_kM additional multiplications compared to the AK1-INTER case.

If M-SDSD is used in conjunction with the AK1-NOPT decoding algorithm, the complexity of the temporal forward recursion reduces from Q^2 to QM and the spatial recursions only need to take into account M^2 transitions. The overall values for the

	AK1-INTER	AK1-INTRA	AK1-NOPT
ADD	$2B_k + M$	$2B_k + 2M$	$2B_k + 3M$
MUL	$Q(B_k^2+1)+M$	$Q(B_k^2+1)+M(B_k+3)$	$Q(B_k^2+3)+5M$
MAC	$MQ + B_kM$	$MQ + M^2 + B_kM$	$MQ + 2M^2 + B_kM$
DIV	$3B_k + 1$	$3B_k + 2$	$3B_k + 3$
EXP	$2B_k$	$2B_k$	$2B_k$
LOG	B_k	B_k	B_k
CMP	$M(Q - \frac{1}{2}(M + 1))$	$M(Q - \frac{1}{2}(M + 1))$	$M(Q - \frac{1}{2}(M + 1))$

Table F.6: Operations required for computing the extrinsic information per quantizer index $i_{t,k}$ by the M-SDSD operating in the probability domain

complexity in the M-SDSD case are found in Table F.6. Note that the AK0 case is not listed in the table, as the application of M-SDSD does not save complexity in that case.

Complexity in the Logarithmic Domain

If the M-SDSD is applied in the logarithmic domain, the complexity of the different decoding algorithms is reduced accordingly. Similar to the descriptions of the algorithm in the probability domain, the amount of additions and $\max^\star$ operations in the forward and backward recursions only need to be carried out for the MQ (or M^2, respectively) considered transitions. The computation of the extrinsic information also only considers the retained transitions. The required complexity for the M-SDSD in the logarithmic domain is summarized in Table F.7. For additional details on the complexity in the logarithmic domain, see [SVA08].

	AK1-INTER	AK1-INTRA	AK1-NOPT
$\max^\star$	$M(Q + B_k)$	$M(Q + M + B_k)$	$M(Q + 2M + B_k)$
ADD	$(Q+B_k)(M+1)+QB_k$	$Q(M+B_k+1)+M(M+B_k+1)+B_k$	$Q(M+B_k+3)+M(2M+B_k+2)+B_k$
MUL	B_k	B_k	B_k
CMP	$M(Q - \frac{1}{2}(M + 1))$	$M(Q - \frac{1}{2}(M + 1))$	$M(Q - \frac{1}{2}(M + 1))$

Table F.7: Operations required for computing the extrinsic information per quantizer index $i_{t,k}$ by the M-SDSD operating in the logarithmic domain

F.3.4 Complexity for the CQ-M-SDSD Case

The complexity in the combined CQ-M-SDSD case is similar to the complexity in the M-SDSD case, however, only a (tight) upper bound can be given, as the actual complexity can vary. The upper bound is obtained by replacing the operations required

	AK1-INTER	AK1-INTRA
ADD	$2B_k + M$	$2B_k + 2M$
MUL	$Q(B_k^2 + 1) + M$	$Q(B_k^2 + 1) + M(B_k + 3)$
MAC	$\mathfrak{N}_{\max}^{M,\alpha} + B_k M$	$\mathfrak{N}_{\max}^{M,\alpha} + \mathfrak{N}_{\max}^{M,\beta} + B_k M$
DIV	$3B_k + 1$	$3B_k + 2$
EXP	$2B_k$	$2B_k$
LOG	B_k	B_k
CMP	$M(Q - \frac{1}{2}(M + 1))$	$M(Q - \frac{1}{2}(M + 1))$

	AK1-NOPT Inter-frame CQ	AK1-NOPT Intra-frame CQ
ADD	$2B_k + 3M$	$2B_k + 3M$
MUL	$Q(B_k^2 + 3) + 5M$	$Q(B_k^2 + 3) + 5M$
MAC	$\mathfrak{N}_{\max}^{M,\alpha} + 2M^2 + B_k M$	$MQ + 2\mathfrak{N}_{\max}^{M,\beta} + B_k M$
DIV	$3B_k + 3$	$3B_k + 3$
EXP	$2B_k$	$2B_k$
LOG	B_k	B_k
CMP	$M(Q - \frac{1}{2}(M + 1))$	$M(Q - \frac{1}{2}(M + 1))$

Table F.8: Operations required (upper bound) for computing the extrinsic information per quantizer index $i_{t,k}$ by the CQ-M-SDSD operating in the probability domain

for QM transitions in the forward recursions by the maximum number of transitions $\mathfrak{N}_{\max}^{M,\alpha}$ and by replacing the operations needed for the M^2 transitions in the backward recursion by $\mathfrak{N}_{\max}^{M,\beta}$. The expressions for $\mathfrak{N}_{\max}^{M,\alpha}$ and $\mathfrak{N}_{\max}^{M,\beta}$ are given in (4.17) and (4.18), respectively. In the AK1-NOPT case, the distinction between inter-frame CQ and intra-frame CQ has to be made as the quantization only affects a reduction of the possible transitions in one direction (either temporal or spatial). The resulting complexity figures (upper bounds) for an implementation in the probability domain are given in Tab. F.8. The according complexity upper bounds for an implementation in the logarithmic domain are given in Tab. F.9.

	AK1-INTER	AK1-INTRA
max*	$\mathfrak{N}_{\max}^{M,\alpha} + MB_k$	$\mathfrak{N}_{\max}^{M,\alpha} + \mathfrak{N}_{\max}^{M,\beta} + MB_k$
ADD	$\mathfrak{N}_{\max}^{M,\alpha} + Q + B_k(Q + M + 1)$	$\mathfrak{N}_{\max}^{M,\alpha} + \mathfrak{N}_{\max}^{M,\beta} + (Q + M)(B_k + 1) + B_k$
MUL	B_k	B_k
CMP	$M(Q - \frac{1}{2}(M + 1))$	$M(Q - \frac{1}{2}(M + 1))$

	AK1-NOPT Inter-frame CQ
max*	$\mathfrak{N}_{\max}^{M,\alpha} + M(M + B_k)$
ADD	$\mathfrak{N}_{\max}^{M,\alpha} + Q(B_k + 3) + M(2M + B_k + 2) + B_k$
MUL	B_k
CMP	$M(Q - \frac{1}{2}(M + 1))$

	AK1-NOPT Intra-frame CQ
max*	$\mathfrak{N}_{\max}^{M,\beta} + M(Q + B_k)$
ADD	$2\mathfrak{N}_{\max}^{M,\beta} + Q(M + B_k + 3) + M(B_k + 2) + B_k$
MUL	B_k
CMP	$M(Q - \frac{1}{2}(M + 1))$

Table F.9: Operations required (upper bound) for computing the extrinsic information per quantizer index $i_{t,k}$ by the CQ-M-SDSD operating in the logarithmic domain

G

Soft Decision Source Decoding of Multiple Descriptions

In this appendix, the *Soft Decision Source Decoding* (SDSD) equations for the joint bit demapper in the *Multiple Description Coding* (MDC) case (see Fig. 6.4) are given. The structure of this appendix follows the structure of App. F: First the equations are given in the probability domain, afterwards the equations are transformed into the logarithmic domain for an easier and numerically more stable implementation. Complexity figures are not given in the MDC case as no complexity reduction approaches for the MDC case are presented in this thesis. However, the complexity figures follow those of Sec. F.3 with Q^2 being the dominant term.

G.1 MDC-SDSD in the Probability Domain

The first step is common for all four distinct MDC-SDSD algorithms. First, the L-values for all N_I bit patterns of description ν ($\nu \in \{1, 2\}$) of a frame, i.e.,

$$\mathsf{L}_{\mathrm{CD}}^{[\mathrm{ext}]}(\mathbf{b}_{t,k}^{[\mathrm{D},\nu]}) = \left(\mathsf{L}_{\mathrm{CD}}^{[\mathrm{ext}]}\left(b_{t,k,1}^{[\mathrm{D},\nu]}\right), \ \ldots, \ \mathsf{L}_{\mathrm{CD}}^{[\mathrm{ext}]}\left(b_{t,k,B_k^{[\mathrm{D},\nu]}}^{[\mathrm{D},\nu]}\right) \right) ,$$

are extracted from the input vector. This corresponds to a serial-to-parallel conversion of the L-values. Under the assumption of a memoryless channel, the reliabilities

$$\begin{aligned} \gamma_{t,k}^{[\mathrm{D},\nu]}(q) &\doteq \prod_{\mu=1}^{B_k^{[\mathrm{D},\nu]}} \mathsf{P}_{\mathrm{CD}}^{[\mathrm{ext}]}\left(b_{t,k,\mu}^{[\mathrm{D},\nu]} = \bar{b}_{k,\mu}^{[\mathrm{D},\nu](q)}\right) \\ &= \prod_{\mu=1}^{B_k^{[\mathrm{D},\nu]}} \left(1 + \exp\left(-\left(1 - 2 \cdot \bar{b}_{k,\mu}^{[\mathrm{D},\nu](q)}\right) \cdot \mathsf{L}_{\mathrm{CD}}^{[\mathrm{ext}]}\left(b_{t,k,\mu}^{[\mathrm{D},\nu]}\right)\right)\right)^{-1} . \end{aligned} \tag{G.1}$$

are computed (see also Secs. 6.2 and F.1). Furthermore,

$$\gamma_{t,k}^{[\mathrm{D},\nu,\mathrm{ext}]\setminus\chi}(q) \doteq \prod_{\substack{\mu=1\\ \mu\neq\chi}}^{B_k^{[\mathrm{D},\nu]}} \mathsf{P}_{\mathrm{CD}}^{[\mathrm{ext}]}\left(b_{t,k,\mu}^{[\mathrm{D},\nu]} = \bar{b}_{k,\mu}^{[\mathrm{D},\nu](q)}\right) \tag{G.2}$$

$$= \prod_{\substack{\mu=1\\ \mu\neq\chi}}^{B_k^{[\mathrm{D},\nu]}} \left(1+\exp\left(-\left(1-2\cdot\bar{b}_{k,\mu}^{[\mathrm{D},\nu](q)}\right)\cdot \mathsf{L}_{\mathrm{CD}}^{[\mathrm{ext}]}(b_{t,k,\mu}^{[\mathrm{D},\nu]})\right)\right)^{-1}. \tag{G.3}$$

denote the extrinsic channel-related reliabilities which take into account information from all bits of a bit pattern of description ν except bit (position) χ.

In order to simplify the notation of the generation of extrinsic information, we define (as introduced in Sec. 6.3) the support sets

$$\mathbb{D}_{\chi}^{[\mathrm{D},1]} \doteq \{j : \mathcal{D}(q) = (\chi, j), \forall q \in \mathbb{I}\} \tag{G.4}$$

$$\mathbb{D}_{\chi}^{[\mathrm{D},2]} \doteq \{j : \mathcal{D}(q) = (j, \chi), \forall q \in \mathbb{I}\}\,. \tag{G.5}$$

for both descriptions. The set $\mathbb{D}_{\chi}^{[\mathrm{D},1]}$ contains all possible indices $i^{[\mathrm{D},2]}$ of description $\nu = 2$ if the index of the first description is encoded to $i^{[\mathrm{D},1]} = \chi$. The set $\mathbb{D}_{\chi}^{[\mathrm{D},2]}$ is defined in an analog manner.

AK0

With the definition $\bar{\nu} \doteq 3 - \nu$ (i.e., if $\nu = 1$, then $\bar{\nu} = 2$ and vice versa) the extrinsic information in the AK0 case can be computed by (as introduced in Sec. 6.3)

$$\mathsf{L}_{\mathrm{SD}}^{[\mathrm{ext}]}(b_{t,k,\mu}^{[\mathrm{D},\nu]}) = \ln \frac{\sum_{q_\nu=1}^{Q^{[\mathrm{D},\nu]}} \left(1-\bar{b}_{k,\mu}^{[\mathrm{D},\nu](q_\nu)}\right)\gamma_{t,k}^{[\mathrm{D},\nu,\mathrm{ext}]\setminus\mu}(q_\nu) \sum_{\forall q_{\bar{\nu}}\in\mathbb{D}_{q_\nu}^{[\mathrm{D},\nu]}} \gamma_{t,k}^{[\mathrm{D},\bar{\nu}]}(q_{\bar{\nu}})\mathsf{Pr}\{I_{t,k}=\mathcal{D}^{-1}(q_1,q_2)\}}{\sum_{q_\nu=1}^{Q^{[\mathrm{D},\nu]}} \bar{b}_{k,\mu}^{[\mathrm{D},\nu](q_\nu)}\gamma_{t,k}^{[\mathrm{D},\nu,\mathrm{ext}]\setminus\mu}(q_\nu) \sum_{\forall q_{\bar{\nu}}\in\mathbb{D}_{q_\nu}^{[\mathrm{D},\nu]}} \gamma_{t,k}^{[\mathrm{D},\bar{\nu}]}(q_{\bar{\nu}})\mathsf{Pr}\{I_{t,k}=\mathcal{D}^{-1}(q_1,q_2)\}}\,. \tag{G.6}$$

The main difference compared to the non-MDC case (see Sec. F.1) is the additional summation over the support set $\mathbb{D}^{[\mathrm{D},\nu]}$ which takes into account the information from the bit patterns of the according other description $\bar{\nu}$.

The *a posteriori* probabilities can be expressed as $\mathsf{Pr}\{I_{t,k} = q|\mathbf{z}_t, \mathbf{z}_{t-1}, \ldots\} = \mathsf{Pr}\{I_{t,k} = q|\mathbf{z}_t\}$ (no inter-frame relations present) and amount to

$$\mathsf{Pr}\{I_{t,k} = q|\mathbf{z}_t, \mathbf{z}_{t-1}, \ldots\} = \mathsf{Pr}\{I_{t,k} = q|\mathbf{z}_t\} \tag{G.7}$$

$$= \frac{1}{\mathrm{K}} \cdot \gamma_{t,k}^{[\mathrm{D},1]}\big(\mathcal{D}_1(q)\big)\gamma_{t,k}^{[\mathrm{D},2]}\big(\mathcal{D}_2(q)\big) \cdot \mathsf{Pr}\{I_{t,k} = q\} \qquad \forall q \in \mathbb{I}\,,$$

with K such that $\sum_{q=1}^{Q} \mathsf{Pr}\{I_{t,k} = q|\mathbf{z}_t, \mathbf{z}_{t-1}, \ldots\} = 1$.

AK1-INTER

If *a priori* knowledge of first order is available, temporal correlation shall be exploited, and no information from future frames is accessible due to delay constraints, the AK1-INTER algorithm can be utilized. Similarly to the non-MDC case, the extrinsic information can be computed by

$$\mathsf{L}_{\mathrm{SD}}^{[\mathrm{ext}]}(b_{t,k,\mu}^{[\mathrm{D},\nu]}) = \ln \frac{\sum_{q_\nu=1}^{Q^{[\mathrm{D},\nu]}} \left(1-\bar{b}_{k,\mu}^{[\mathrm{D},\nu](q_\nu)}\right) \gamma_{t,k}^{[\mathrm{D},\nu,\mathrm{ext}]\setminus\mu}(q_\nu) \sum_{\forall q_{\bar{\nu}} \in \mathbb{D}_{q_\nu}^{[\mathrm{D},\nu]}} \gamma_{t,k}^{[\mathrm{D},\bar{\nu}]}(q_{\bar{\nu}}) A_{t,k}\left(\mathcal{D}^{-1}(q_1,q_2)\right)}{\sum_{q_\nu=1}^{Q^{[\mathrm{D},\nu]}} \bar{b}_{k,\mu}^{[\mathrm{D},\nu](q_\nu)} \gamma_{t,k}^{[\mathrm{D},\nu,\mathrm{ext}]\setminus\mu}(q_\nu) \sum_{\forall q_{\bar{\nu}} \in \mathbb{D}_{q_\nu}^{[\mathrm{D},\nu]}} \gamma_{t,k}^{[\mathrm{D},\bar{\nu}]}(q_{\bar{\nu}}) A_{t,k}\left(\mathcal{D}^{-1}(q_1,q_2)\right)} . \quad \text{(G.8)}$$

with $A_{t,k}(q) = \sum_{\tilde{q}=1}^{Q} \mathsf{Pr}\{I_{t,k} = q | I_{t-1,k} = \tilde{q}\} \alpha_{t-1,k}(\tilde{q})$ as being defined in App. F.1. The factor $\alpha_{t,k}(q)$ is updated in the forward recursion

$$\begin{aligned} \alpha_{t,k}(q) &= \frac{1}{\mathrm{K}} \cdot \gamma_{t,k}^{[\mathrm{D},1]}\big(\mathcal{D}_1(q)\big) \gamma_{t,k}^{[\mathrm{D},2]}\big(\mathcal{D}_2(q)\big) \cdot A_{t,k}(q) \qquad \text{(G.9)} \\ &= \frac{1}{\mathrm{K}} \cdot \gamma_{t,k}^{[\mathrm{D},1]}\big(\mathcal{D}_1(q)\big) \gamma_{t,k}^{[\mathrm{D},2]}\big(\mathcal{D}_2(q)\big) \cdot \sum_{\tilde{q}=1}^{Q} \mathsf{Pr}\{I_{t,k} = q | I_{t-1,k} = \tilde{q}\} \alpha_{t-1,k}(\tilde{q}) \end{aligned}$$

which has to be carried out for each distinct $q \in \mathbb{I}$. K is a normalization constant ensuring that $\sum_{q=1}^{Q} \alpha_{t,k}(q) = 1$, required for numerical stability reasons in a practical implementation. The values $\alpha_{0,k}$ (the transmission is assumed to start at time instant $t = 1$) are initialized by

$$\alpha_{0,k}(q) = \mathsf{Pr}\{I_{1,k} = q\} \qquad \forall q \in \mathbb{I} . \qquad \text{(G.10)}$$

Further note that the processes $I_{t,k}$ are assumed to be stationary temporal Markov processes, i.e., $\mathsf{Pr}\{I_{1,k} = q\} = \mathsf{Pr}\{I_{t,k} = q\}$, $\forall t \in \mathbb{N}_1$. As the values $\alpha_{t,k}(q)$ are reused in the subsequent frame, they need to be stored (see also Sec. F.1).

The *a posteriori* probabilities are finally obtained by

$$\mathsf{Pr}\{I_{t,k} = q | \mathbf{z}_t, \mathbf{z}_{t-1}, \ldots\} = \alpha_{t,k}(q) \qquad \forall q \in \mathbb{I} . \qquad \text{(G.11)}$$

AK1-INTRA

In the AK1-INTRA case, a spatial forward recursion (as in the AK1-INTER case), as well as an additional spatial backward recursion have to be carried out. The extrinsic

information is given by

$$\mathsf{L}_{\mathrm{SD}}^{[\mathrm{ext}]}(b_{t,k,\mu}^{[\mathrm{D},\nu]}) = \tag{G.12}$$

$$\ln \frac{\sum_{q_\nu=1}^{Q^{[\mathrm{D},\nu]}} \Big(1-\bar{b}_{k,\mu}^{[\mathrm{D},\nu](q_\nu)}\Big)\gamma_{t,k}^{[\mathrm{D},\nu,\mathrm{ext}]\setminus\mu}(q_\nu) \sum_{\forall q_{\bar{\nu}}\in\mathbb{D}_{q_\nu}^{[\mathrm{D},\nu]}} \gamma_{t,k}^{[\mathrm{D},\bar{\nu}]}(q_{\bar{\nu}})\beta_{t,k}(\mathcal{D}^{-1}(q_1,q_2))A'_{t,k}(\mathcal{D}^{-1}(q_1,q_2))}{\sum_{q_\nu=1}^{Q^{[\mathrm{D},\nu]}} \bar{b}_{k,\mu}^{[\mathrm{D},\nu](q_\nu)}\gamma_{t,k}^{[\mathrm{D},\nu,\mathrm{ext}]\setminus\mu}(q_\nu) \sum_{\forall q_{\bar{\nu}}\in\mathbb{D}_{q_\nu}^{[\mathrm{D},\nu]}} \gamma_{t,k}^{[\mathrm{D},\bar{\nu}]}(q_{\bar{\nu}})\beta_{t,k}(\mathcal{D}^{-1}(q_1,q_2))A'_{t,k}(\mathcal{D}^{-1}(q_1,q_2))}$$

with $A'_{t,k}(q) \doteq \sum_{\tilde{q}=1}^{Q} \mathsf{Pr}\{I_{t,k}=q|I_{t,k-1}=\tilde{q}\}\alpha_{t,k-1}(\tilde{q})$. The factors $\alpha_{t,k}(q)$ and $\beta_{t,k}(q)$ are obtained in the forward-backward recursions

$$\alpha_{t,k}(q) = \frac{1}{\mathrm{K}_2}\cdot\gamma_{t,k}^{[\mathrm{D},1]}\big(\mathcal{D}_1(q)\big)\gamma_{t,k}^{[\mathrm{D},2]}\big(\mathcal{D}_2(q)\big)\cdot A'_{t,k}(q) \tag{G.13}$$

$$\beta_{t,k-1}(q) = \frac{1}{\mathrm{K}_3}\sum_{\tilde{q}=1}^{Q}\gamma_{t,k}^{[\mathrm{D},1]}\big(\mathcal{D}_1(\tilde{q})\big)\gamma_{t,k}^{[\mathrm{D},2]}\big(\mathcal{D}_2(\tilde{q})\big)\mathsf{Pr}\{I_{t,k}=\tilde{q}|I_{t,k-1}=q\}\beta_{t,k}(\tilde{q})\,. \tag{G.14}$$

Equation (G.13) has to be performed for each $k \in \{1,\ldots,N_I\}$ and (G.14) has to be performed for each $k \in \{2,\ldots,N_I\}$. As in the non-MDC case, the initialization is performed according to

$$\alpha_{t,0}(q) = \mathsf{Pr}\{I_{t,1}=q\} \qquad \forall q\in\mathbb{I} \tag{G.15}$$

$$\beta_{t,N_I}(q) = 1 \qquad \forall q\in\mathbb{I}\,. \tag{G.16}$$

The factors K_2 and K_3 in (G.13) and (G.14) are used to ensure that $\sum_{q=1}^{Q}\alpha_{t,k}(q)=1$ and $\sum_{q=1}^{Q}\beta_{t,k}(q)=1$, $\forall k\in\{1,\ldots,N_I\}$.

The *a posteriori* probabilities can be expressed as $\mathsf{Pr}\{I_{t,k}=q|\mathbf{z}_t,\mathbf{z}_{t-1},\ldots\} = \mathsf{Pr}\{I_{t,k}=q|\mathbf{z}_t\}$ (no inter-frame relations present) and amount to

$$\mathsf{Pr}\{I_{t,k}=q|\mathbf{z}_t\} = \frac{1}{\mathrm{K}_4}\cdot\alpha_{t,k}(q)\cdot\beta_{t,k}(q) \qquad \forall q\in\mathbb{I}\,, \tag{G.17}$$

with K_4 being a normalization constant ensuring that $\sum_{q=1}^{Q}\mathsf{Pr}\{I_{t,k}=q|\mathbf{z}_t\}=1$ and $\alpha_{t,k}(q)$ and $\beta_{t,k}(q)$ according to (G.13) and (G.14).

AK1-NOPT

In the AK1-NOPT case [ASHV00, Hei01b, HA08] adopted to MDC, a temporal forward recursion as well as spatial forward and backward recursion have to be carried

out. The extrinsic information is obtained by

$$\mathsf{L}_{\mathrm{SD}}^{[\mathrm{ext}]}(b_{t,k,\mu}^{[\mathrm{D},\nu]}) = \ln \frac{\sum_{q_\nu=1}^{Q^{[\mathrm{D},\nu]}} \left(1-\bar{b}_{k,\mu}^{[\mathrm{D},\nu](q_\nu)}\right) \gamma_{t,k}^{[\mathrm{D},\nu,\mathrm{ext}]\setminus\mu}(q_\nu) \sum_{\forall q_{\bar{\nu}} \in \mathbb{D}_{q_\nu}^{[\mathrm{D},\nu]}} \gamma_{t,k}^{[\mathrm{D},\bar{\nu}]}(q_{\bar{\nu}}) A''_{t,k}(\mathcal{D}^{-1}(q_1,q_2))}{\sum_{q_\nu=1}^{Q^{[\mathrm{D},\nu]}} \bar{b}_{k,\mu}^{[\mathrm{D},\nu](q_\nu)} \gamma_{t,k}^{[\mathrm{D},\nu,\mathrm{ext}]\setminus\mu}(q_\nu) \sum_{\forall q_{\bar{\nu}} \in \mathbb{D}_{q_\nu}^{[\mathrm{D},\nu]}} \gamma_{t,k}^{[\mathrm{D},\bar{\nu}]}(q_{\bar{\nu}}) A''_{t,k}(\mathcal{D}^{-1}(q_1,q_2))} . \quad \text{(G.18)}$$

with

$$A''_{t,k}(q) = \alpha_{t,k}^{[\mathrm{pos}]}(q)\beta_{t,k}^{[\mathrm{pos}]}(q) \sum_{\tilde{q}=1}^{Q} \mathsf{Pr}\{I_{t,k}=q | I_{t,k-1}=\tilde{q}\} \cdot \alpha_{t,k-1}^{[\mathrm{tim}]}(\tilde{q}) . \quad \text{(G.19)}$$

The factor $\alpha_{t,k}^{[\mathrm{tim}]}$ is updated (and stored for use in the subsequent frame) in the temporal forward recursion

$$\alpha_{t,k}^{[\mathrm{tim}]}(q) = \frac{1}{\mathrm{K}_5} \cdot \gamma_{t,k}^{[\mathrm{D},1]}(\mathcal{D}_1(q))\gamma_{t,k}^{[\mathrm{D},2]}(\mathcal{D}_2(q)) \cdot \alpha_{t,k}^{[\mathrm{pos}]}(q) \cdot \beta_{t,k}^{[\mathrm{pos}]}(q) \times \sum_{\tilde{q}=1}^{Q} \mathsf{Pr}\{I_{t,k}=q | I_{t-1,k}=\tilde{q}\} \cdot \alpha_{t-1,k}^{[\mathrm{tim}]}(\tilde{q}) , \quad \text{(G.20)}$$

with the normalization constant K_5 such that $\sum_{q=1}^{Q} \alpha_{t,k}^{[\mathrm{tim}]}(q) = 1$.

Similar to the AK1-INTER case, $\alpha_{0,k}^{[\mathrm{tim}]}$ is initialized by (note that the transmission starts at $t = 1$)

$$\alpha_{0,k}^{[\mathrm{tim}]}(q) = \mathsf{Pr}\{I_{1,k} = q\} \qquad \forall q \in \mathbb{I} . \quad \text{(G.21)}$$

The factors $\alpha_{t,k}^{[\mathrm{pos}]}(q)$ and $\beta_{t,k}^{[\mathrm{pos}]}(q)$ of the spatial forward and backward recursions are updated using

$$\alpha_{t,k}^{[\mathrm{pos}]}(q) \doteq \frac{1}{\mathrm{K}_6} \sum_{\tilde{q}=1}^{Q} \alpha_{t,k-1}^{[\mathrm{pos}]}(\tilde{q})\gamma_{t,k-1}^{[\mathrm{D},1]}(\mathcal{D}_1(\tilde{q}))\gamma_{t,k-1}^{[\mathrm{D},2]}(\mathcal{D}_2(\tilde{q}))\mathsf{Pr}\{I_{t,k}=q | I_{t,k-1}=\tilde{q}\} \quad \text{(G.22)}$$

$$\beta_{t,k-1}^{[\mathrm{pos}]}(q) \doteq \frac{1}{\mathrm{K}_7} \sum_{\tilde{q}=1}^{Q} \beta_{t,k}^{[\mathrm{pos}]}(\tilde{q})\gamma_{t,k}^{[\mathrm{D},1]}(\mathcal{D}_1(\tilde{q}))\gamma_{t,k}^{[\mathrm{D},2]}(\mathcal{D}_2(\tilde{q}))\mathsf{Pr}\{I_{t,k}=\tilde{q} | I_{t,k-1}=q\} \quad \text{(G.23)}$$

for all $k \in \{2, \ldots, N_I\}$ and are initialized by

$$\alpha_{t,1}^{[\mathrm{pos}]}(q) = \beta_{t,N_I}^{[\mathrm{pos}]}(q) = 1 \qquad \forall q \in \mathbb{I} . \quad \text{(G.24)}$$

The normalization constants K_6 and K_7 ensure that $\sum_{q=1}^{Q} \alpha_{t,k}^{[\mathrm{pos}]}(q) = \sum_{q=1}^{Q} \beta_{t,k-1}^{[\mathrm{pos}]}(q) = 1$.

The *a posteriori* probabilities are finally obtained by (see Sec. F.1 and [HA08])

$$\mathsf{Pr}\{I_{t,k} = q | \mathbf{z}_t, \mathbf{z}_{t-1}, \ldots\} = \alpha_{t,k}^{[\mathrm{tim}]}(q) \qquad \forall q \in \mathbb{I}\,. \tag{G.25}$$

G.2 MDC-SDSD in the Logarithmic Domain

Similarly to the non-MDC case, the SDSD equations can also be transformed into the logarithmic domain, leading to an easier implementation with better numerical properties [RVH95, HOP96]. The approach is identical to the one highlighted in Sec. F.2. First, we define the factors

$$\tilde{\gamma}_{t,k}^{[\mathrm{D},\nu]}(q_\nu) \doteq \frac{1}{2} \sum_{\mu=1}^{B_k^{[\mathrm{D},\nu]}} \left(1 - 2 \cdot \bar{b}_{k,\mu}^{[\mathrm{D},\nu](q_\nu)}\right) \mathsf{L}_{\mathrm{CD}}^{[\mathrm{ext}]}(b_{t,k,\mu}^{[\mathrm{D},\nu]}) \tag{G.26}$$

$$= \ln \gamma_{t,k}^{[\mathrm{D},\nu]}(q_\nu) + \tilde{\mathrm{K}}_{t,k} \tag{G.27}$$

and

$$\tilde{\gamma}_{t,k}^{[\mathrm{D},\nu,\mathrm{ext}]\setminus\chi}(q_\nu) \doteq \frac{1}{2} \sum_{\substack{\mu=1 \\ \mu\neq\chi}}^{B_k^{[\mathrm{D},\nu]}} \left(1 - 2 \cdot \bar{b}_{k,\mu}^{[\mathrm{D},\nu](q_\nu)}\right) \mathsf{L}_{\mathrm{CD}}^{[\mathrm{ext}]}(b_{t,k,\mu}^{[\mathrm{D},\nu]}) \tag{G.28}$$

$$= \tilde{\gamma}_{t,k}^{[\mathrm{D},\nu]}(q_\nu) - \frac{1}{2} \left(1 - 2 \cdot \bar{b}_{k,\chi}^{[\mathrm{D},\nu](q_\nu)}\right) \mathsf{L}_{\mathrm{CD}}^{[\mathrm{ext}]}(b_{t,k,\chi}^{[\mathrm{D},\nu]}) \tag{G.29}$$

$$= \ln \gamma_{t,k}^{[\mathrm{D},\nu,\mathrm{ext}]\setminus\chi}(q_\nu) + \tilde{\mathrm{K}}_{t,k}^{[\mathrm{ext}]\setminus\chi}\,, \tag{G.30}$$

for all distinct vales $q_\nu \in \mathbb{I}^{[\mathrm{D},\nu]}$. The constant offset terms $\tilde{\mathrm{K}}_{t,k}$ and $\tilde{\mathrm{K}}_{t,k}^{[\mathrm{ext}]\setminus\chi}$ are neglected in what follows, see App. F.2 for a detailed reasoning.

Following the same approach as in the non-MDC SDSD case (see App. F.2), the equations for determining the extrinsic information of all four considered algorithms in the logarithmic domain can be given.

AK0

In the logarithmic domain, the extrinsic information $\mathsf{L}_{\mathrm{SD}}^{[\mathrm{ext}]}(b_{t,k,\mu}^{[\mathrm{D},\nu]})$ for the μth bit of the bit pattern at position k is given by

$$\mathsf{L}_{\mathrm{SD}}^{[\mathrm{ext}]}(b_{t,k,\mu}^{[\mathrm{D},\nu]}) = \max_{\substack{q_\nu=1 \\ \bar{b}_{k,\mu}^{[\mathrm{D},\nu](q_\nu)}=0}}^{Q^{[\mathrm{D},\nu]\star}} \left(\tilde{\gamma}_{t,k}^{[\mathrm{D},\nu,\mathrm{ext}]\setminus\mu}(q_\nu) + \max_{\forall q_{\bar{\nu}} \in \mathbb{D}_{q_\nu}^{[\mathrm{D},\nu]}}{}^{\star} \left(\tilde{\gamma}_{t,k}^{[\mathrm{D},\bar{\nu}]}(q_{\bar{\nu}}) + \widetilde{\mathsf{Pr}}\{I_{t,k} = \mathcal{D}^{-1}(q_1, q_2)\} \right) \right)$$

$$- \max_{\substack{q_\nu=1 \\ \bar{b}_{k,\mu}^{[\mathrm{D},\nu](q_\nu)}=1}}^{Q^{[\mathrm{D},\nu]}} \left(\tilde{\gamma}_{t,k}^{[\mathrm{D},\nu,\mathrm{ext}]\setminus\mu}(q_\nu) + \max_{\forall q_{\bar{\nu}} \in \mathbb{D}_{q_\nu}^{[\mathrm{D},\nu]}}{}^{\star} \left(\tilde{\gamma}_{t,k}^{[\mathrm{D},\bar{\nu}]}(q_{\bar{\nu}}) + \widetilde{\mathsf{Pr}}\{I_{t,k} = \mathcal{D}^{-1}(q_1, q_2)\} \right) \right) . \tag{G.31}$$

with $\widetilde{\mathsf{Pr}}\{I_{t,k} = \mathcal{D}^{-1}(q_1, q_2)\} \doteq \ln \mathsf{Pr}\{I_{t,k} = \mathcal{D}^{-1}(q_1, q_2)\}$. Equation (G.31) is obtained by exploiting (G.27), (G.30), neglecting the offset constants (see App. F.2 for the complete reasoning), and by exploiting the fact that

$$\ln \sum_{\substack{q_\nu=1 \\ \bar{b}_{k,\mu}^{[\mathrm{D},\nu](q_\nu)}=0}}^{Q^{[\mathrm{D},\nu]}} \gamma_{t,k}^{[\mathrm{D},\nu,\mathrm{ext}]\setminus\mu}(q_\nu) \sum_{\forall q_{\bar{\nu}} \in \mathbb{D}_{q_\nu}^{[\mathrm{D},\nu]}} \gamma_{t,k}^{[\mathrm{D},\bar{\nu}]}(q_{\bar{\nu}}) \mathsf{Pr}\{I_{t,k} = \mathcal{D}^{-1}(q_1, q_2)\} =$$

$$\ln \sum_{\substack{q_\nu=1 \\ \bar{b}_{k,\mu}^{[\mathrm{D},\nu](q_\nu)}=0}}^{Q^{[\mathrm{D},\nu]}} \mathrm{e}^{\tilde{\gamma}_{t,k}^{[\mathrm{D},\nu,\mathrm{ext}]\setminus\mu}(q_\nu)} \sum_{\forall q_{\bar{\nu}} \in \mathbb{D}_{q_\nu}^{[\mathrm{D},\nu]}} \mathrm{e}^{\tilde{\gamma}_{t,k}^{[\mathrm{D},\bar{\nu}]}(q_{\bar{\nu}}) + \widetilde{\mathsf{Pr}}\{I_{t,k} = \mathcal{D}^{-1}(q_1, q_2)\}} =$$

$$\ln \sum_{\substack{q_\nu=1 \\ \bar{b}_{k,\mu}^{[\mathrm{D},\nu](q_\nu)}=0}}^{Q^{[\mathrm{D},\nu]}} \exp \left(\tilde{\gamma}_{t,k}^{[\mathrm{D},\nu,\mathrm{ext}]\setminus\mu}(q_\nu) + \ln \sum_{\forall q_{\bar{\nu}} \in \mathbb{D}_{q_\nu}^{[\mathrm{D},\nu]}} e^{\tilde{\gamma}_{t,k}^{[\mathrm{D},\bar{\nu}]}(q_{\bar{\nu}}) + \widetilde{\mathsf{Pr}}\{I_{t,k} = \mathcal{D}^{-1}(q_1, q_2)\}} \right) ,$$

followed by the application of the $\max^\star$ operation defined in (F.37). In order to further simplify (G.31), we define

$$\tilde{\alpha}_{t,k}(q) \doteq \tilde{\gamma}_{t,k}^{[\mathrm{D},1]}(\mathcal{D}_1(q)) + \tilde{\gamma}_{t,k}^{[\mathrm{D},2]}(\mathcal{D}_2(q)) + \widetilde{\mathsf{Pr}}\{I_{t,k} = q\} . \tag{G.32}$$

Using $\tilde{\alpha}_{t,k}(q)$, (G.31) can be further refined

$$\mathsf{L}_{\mathrm{SD}}^{[\mathrm{ext}]}(b_{t,k,\mu}^{[\mathrm{D},\nu]}) =$$

$$\max_{\substack{q_\nu=1 \\ \bar{b}_{k,\mu}^{[\mathrm{D},\nu](q_\nu)}=0}}^{Q^{[\mathrm{D},\nu]}} \left(\tilde{\gamma}_{t,k}^{[\mathrm{D},\nu,\mathrm{ext}]\setminus\mu}(q_\nu) + \max_{\forall q_{\bar{\nu}} \in \mathbb{D}_{q_\nu}^{[\mathrm{D},\nu]}}{}^{\star} \left(\tilde{\alpha}_{t,k}(\mathcal{D}^{-1}(q_1, q_2)) - \tilde{\gamma}_{t,k}^{[\mathrm{D},\nu]}(q_\nu) \right) \right)$$

$$- \max_{\substack{q_\nu=1 \\ \bar{b}_{k,\mu}^{[\mathrm{D},\nu](q_\nu)}=1}}^{Q^{[\mathrm{D},\nu]}} \left(\tilde{\gamma}_{t,k}^{[\mathrm{D},\nu,\mathrm{ext}]\setminus\mu}(q_\nu) + \max_{\forall q_{\bar{\nu}} \in \mathbb{D}_{q_\nu}^{[\mathrm{D},\nu]}}{}^{\star} \left(\tilde{\alpha}_{t,k}(\mathcal{D}^{-1}(q_1, q_2)) - \tilde{\gamma}_{t,k}^{[\mathrm{D},\nu]}(q_\nu) \right) \right) .$$

Applying property (F.41) of the $\max^\star$ function gives

$$\mathsf{L}_{\mathrm{SD}}^{[\mathrm{ext}]}(b_{t,k,\mu}^{[\mathrm{D},\nu]}) =$$

$$\max_{\substack{q_\nu=1 \\ \bar{b}_{k,\mu}^{[\mathrm{D},\nu](q_\nu)}=0}}^{Q^{[\mathrm{D},\nu]}} \left(\tilde{\gamma}_{t,k}^{[\mathrm{D},\nu,\mathrm{ext}]\setminus\mu}(q_\nu) - \tilde{\gamma}_{t,k}^{[\mathrm{D},\nu]}(q_\nu) + \max_{\forall q_{\bar{\nu}} \in \mathbb{D}_{q_\nu}^{[\mathrm{D},\nu]}}{}^{\star} \left(\tilde{\alpha}_{t,k}(\mathcal{D}^{-1}(q_1, q_2)) \right) \right)$$

$$- \max_{\substack{q_\nu=1 \\ \bar{b}_{k,\mu}^{[\mathrm{D},\nu]}(q_\nu)=1}}^{Q^{[\mathrm{D},\nu]}} \left(\tilde{\gamma}_{t,k}^{[\mathrm{D},\nu,\mathrm{ext}]\setminus\mu}(q_\nu) - \tilde{\gamma}_{t,k}^{[\mathrm{D},\nu]}(q_\nu) + \max_{\forall q_{\bar{\nu}} \in \mathbb{D}_{q_\nu}^{[\mathrm{D},\nu]}}{}^{\star} \left(\tilde{\alpha}_{t,k}(\mathcal{D}^{-1}(q_1,q_2)) \right) \right).$$

With (G.29), the previous expression can be further simplified to

$$\begin{aligned} &\mathsf{L}_{\mathrm{SD}}^{[\mathrm{ext}]}(b_{t,k,\mu}^{[\mathrm{D},\nu]}) = \\ &\quad \max_{\substack{q_\nu=1 \\ \bar{b}_{k,\mu}^{[\mathrm{D},\nu]}(q_\nu)=0}}^{Q^{[\mathrm{D},\nu]}} \left(\max_{\forall q_{\bar{\nu}} \in \mathbb{D}_{q_\nu}^{[\mathrm{D},\nu]}}{}^{\star} \left(\tilde{\alpha}_{t,k}(\mathcal{D}^{-1}(q_1,q_2)) \right) - \frac{1}{2}\mathsf{L}_{\mathrm{CD}}^{[\mathrm{ext}]}(b_{t,k,\mu}^{[\mathrm{D},\nu]}) \right) \\ &\qquad - \max_{\substack{q_\nu=1 \\ \bar{b}_{k,\mu}^{[\mathrm{D},\nu]}(q_\nu)=1}}^{Q^{[\mathrm{D},\nu]}} \left(\max_{\forall q_{\bar{\nu}} \in \mathbb{D}_{q_\nu}^{[\mathrm{D},\nu]}}{}^{\star} \left(\tilde{\alpha}_{t,k}(\mathcal{D}^{-1}(q_1,q_2)) \right) + \frac{1}{2}\mathsf{L}_{\mathrm{CD}}^{[\mathrm{ext}]}(b_{t,k,\mu}^{[\mathrm{D},\nu]}) \right). \end{aligned} \tag{G.33}$$

Using $\tilde{\alpha}_{t,k}(q)$, the *a posteriori* probabilities simply amount to

$$\mathsf{Pr}\{I_{t,k} = q | \mathbf{z}_t, \mathbf{z}_{t-1}, \ldots\} = \frac{1}{\mathrm{K}} \exp\left(\alpha_{t,k}(q)\right) \qquad \forall q \in \mathbb{I},$$

with K such that $\sum_{q=1}^{Q} \mathsf{Pr}\{I_{t,k} = q | \mathbf{z}_t, \mathbf{z}_{t-1}, \ldots\} = 1$.

AK1-INTER

Using the same reasoning as in the AK0 case, the equations in the logarithmic domain follow almost immediately. Besides the computation of the extrinsic information, a temporal update recursion step has to be performed. This forward recursion of the AK1-INTER algorithm is given by

$$\begin{aligned} \tilde{\alpha}_{t,k}(q) = \tilde{\gamma}_{t,k}^{[\mathrm{D},1]}\big(\mathcal{D}_1(q)\big) + \tilde{\gamma}_{t,k}^{[\mathrm{D},2]}\big(\mathcal{D}_2(q)\big) \\ + \max_{\tilde{q}=1}^{Q}{}^{\star} \left(\widetilde{\mathsf{Pr}}\{I_{t,k} = q | I_{t-1,k} = \tilde{q}\} + \tilde{\alpha}_{t-1,k}(\tilde{q}) \right), \end{aligned} \tag{G.34}$$

with $\tilde{\alpha}_{t,k}(q) = \ln \alpha_{t,k}(q)$. Using the results of the forward recursion, an expression for the extrinsic information can be obtained by

$$\begin{aligned} &\mathsf{L}_{\mathrm{SD}}^{[\mathrm{ext}]}(b_{t,k,\mu}^{[\mathrm{D},\nu]}) = \\ &\quad \max_{\substack{q_\nu=1 \\ \bar{b}_{k,\mu}^{[\mathrm{D},\nu]}(q_\nu)=0}}^{Q^{[\mathrm{D},\nu]}} \left(\tilde{\gamma}_{t,k}^{[\mathrm{D},\nu,\mathrm{ext}]\setminus\mu}(q_\nu) + \max_{\forall q_{\bar{\nu}} \in \mathbb{D}_{q_\nu}^{[\mathrm{D},\nu]}}{}^{\star} \left(\tilde{\gamma}_{t,k}^{[\mathrm{D},\bar{\nu}]}(q_{\bar{\nu}}) + \ln A_{t,k}(\mathcal{D}^{-1}(q_1,q_2)) \right) \right) \\ &\quad - \max_{\substack{q_\nu=1 \\ \bar{b}_{k,\mu}^{[\mathrm{D},\nu]}(q_\nu)=1}}^{Q^{[\mathrm{D},\nu]}} \left(\tilde{\gamma}_{t,k}^{[\mathrm{D},\nu,\mathrm{ext}]\setminus\mu}(q_\nu) + \max_{\forall q_{\bar{\nu}} \in \mathbb{D}_{q_\nu}^{[\mathrm{D},\nu]}}{}^{\star} \left(\tilde{\gamma}_{t,k}^{[\mathrm{D},\bar{\nu}]}(q_{\bar{\nu}}) + \ln A_{t,k}(\mathcal{D}^{-1}(q_1,q_2)) \right) \right), \end{aligned}$$

which can be simplified to (by considering the definition of $A_{t,k}(\cdot)$)

$$\begin{aligned}
&\mathsf{L}_{\mathrm{SD}}^{[\mathrm{ext}]}(b_{t,k,\mu}^{[\mathrm{D},\nu]}) = \\
&\quad \max_{\substack{q_\nu=1 \\ \bar{b}_{k,\mu}^{[\mathrm{D},\nu](q_\nu)}=0}}^{Q^{[\mathrm{D},\nu]}} \left(\max_{\forall q_{\bar{\nu}} \in \mathbb{D}_{q_\nu}^{[\mathrm{D},\nu]}}{}^{\star} \left(\tilde{\alpha}_{t,k}(\mathcal{D}^{-1}(q_1,q_2)) \right) - \frac{1}{2}\mathsf{L}_{\mathrm{CD}}^{[\mathrm{ext}]}(b_{t,k,\mu}^{[\mathrm{D},\nu]}) \right) \\
&\qquad - \max_{\substack{q_\nu=1 \\ \bar{b}_{k,\mu}^{[\mathrm{D},\nu](q_\nu)}=1}}^{Q^{[\mathrm{D},\nu]}} \left(\max_{\forall q_{\bar{\nu}} \in \mathbb{D}_{q_\nu}^{[\mathrm{D},\nu]}}{}^{\star} \left(\tilde{\alpha}_{t,k}(\mathcal{D}^{-1}(q_1,q_2)) \right) + \frac{1}{2}\mathsf{L}_{\mathrm{CD}}^{[\mathrm{ext}]}(b_{t,k,\mu}^{[\mathrm{D},\nu]}) \right), \quad \text{(G.35)}
\end{aligned}$$

by following the same reasoning as in the AK0 case. Note that in the AK1-INTER case, the value $\tilde{\alpha}_{t,k}(\cdot)$ is defined differently as in the AK0 case and needs to be updated using (G.34).

AK1-INTRA

The forward and backward recursions of the AK1-INTRA algorithm are given by

$$\begin{aligned}
\tilde{\alpha}_{t,k}(q) = \tilde{\gamma}_{t,k}^{[\mathrm{D},1]}(\mathcal{D}_1(q)) + \tilde{\gamma}_{t,k}^{[\mathrm{D},2]}(\mathcal{D}_2(q)) \\
+ \max_{\tilde{q}=1}^{Q}{}^{\star} \left(\widetilde{\mathsf{Pr}}\{I_{t,k}=q | I_{t,k-1}=\tilde{q}\} + \tilde{\alpha}_{t,k-1}(\tilde{q}) \right) \quad \text{(G.36)}
\end{aligned}$$

and

$$\begin{aligned}
\tilde{\beta}_{t,k-1}(q) = \max_{\tilde{q}=1}^{Q}{}^{\star} \Big(\tilde{\gamma}_{t,k}^{[\mathrm{D},1]}\big(\mathcal{D}_1(\tilde{q})\big) + \tilde{\gamma}_{t,k}^{[\mathrm{D},2]}\big(\mathcal{D}_2(\tilde{q})\big) \\
+ \widetilde{\mathsf{Pr}}\{I_{t,k}=\tilde{q} | I_{t,k-1}=q\} + \tilde{\beta}_{t,k}(\tilde{q}) \Big), \quad \text{(G.37)}
\end{aligned}$$

with $\tilde{\alpha}_{t,k}(q) = \ln \alpha_{t,k}(q)$ and $\tilde{\beta}_{t,k-1}(q) = \ln \beta_{t,k-1}(q)$. Following the same reasoning as in the AK1-INTER case, the extrinsic information is given by

$$\begin{aligned}
&\mathsf{L}_{\mathrm{SD}}^{[\mathrm{ext}]}(b_{t,k,\mu}^{[\mathrm{D},\nu]}) = \\
&\quad \max_{\substack{q_\nu=1 \\ \bar{b}_{k,\mu}^{[\mathrm{D},\nu](q_\nu)}=0}}^{Q^{[\mathrm{D},\nu]}} \left(\max_{\forall q_{\bar{\nu}} \in \mathbb{D}_{q_\nu}^{[\mathrm{D},\nu]}}{}^{\star} \left(\tilde{\alpha}_{t,k}(\mathcal{D}^{-1}(q_1,q_2)) + \tilde{\beta}_{t,k}(\mathcal{D}^{-1}(q_1,q_2)) \right) - \frac{1}{2}\mathsf{L}_{\mathrm{CD}}^{[\mathrm{ext}]}(b_{t,k,\mu}^{[\mathrm{D},\nu]}) \right) \\
&\quad - \max_{\substack{q_\nu=1 \\ \bar{b}_{k,\mu}^{[\mathrm{D},\nu](q_\nu)}=1}}^{Q^{[\mathrm{D},\nu]}} \left(\max_{\forall q_{\bar{\nu}} \in \mathbb{D}_{q_\nu}^{[\mathrm{D},\nu]}}{}^{\star} \left(\tilde{\alpha}_{t,k}(\mathcal{D}^{-1}(q_1,q_2)) + \tilde{\beta}_{t,k}(\mathcal{D}^{-1}(q_1,q_2)) \right) + \frac{1}{2}\mathsf{L}_{\mathrm{CD}}^{[\mathrm{ext}]}(b_{t,k,\mu}^{[\mathrm{D},\nu]}) \right).
\end{aligned}$$

(G.38)

AK1-NOPT

The temporal forward recursion required in the AK1-NOPT algorithm in the logarithmic domain is given by

$$\tilde{\alpha}_{t,k}^{[\mathrm{tim}]}(q) = \tilde{\gamma}_{t,k}^{[\mathrm{D},1]}(\mathcal{D}_1(q)) + \tilde{\gamma}_{t,k}^{[\mathrm{D},2]}(\mathcal{D}_2(q)) + \tilde{\alpha}_{t,k}^{[\mathrm{pos}]}(q) + \tilde{\beta}_{t,k}^{[\mathrm{pos}]}(q) + \max_{\tilde{q}=1}^{Q\star} \left(\widetilde{\mathsf{Pr}}\{I_{t,k}=q | I_{t-1,k}=\tilde{q}\} + \tilde{\alpha}_{t-1,k}^{[\mathrm{tim}]}(\tilde{q}) \right) , \quad \text{(G.39)}$$

with $\tilde{\alpha}_{t,k}^{[\mathrm{tim}]}(q) \doteq \ln \alpha_{t,k}^{[\mathrm{tim}]}(q)$, $\tilde{\alpha}_{t,k}^{[\mathrm{pos}]}(q) \doteq \ln \alpha_{t,k}^{[\mathrm{pos}]}(q)$, and $\tilde{\beta}_{t,k-1}^{[\mathrm{pos}]}(q) \doteq \ln \beta_{t,k-1}^{[\mathrm{pos}]}(q)$. Besides the temporal recursion, spatial forward and backward recursions are required. In the logarithmic domain, these can be written as

$$\tilde{\alpha}_{t,k}^{[\mathrm{pos}]}(q) = \max_{\tilde{q}=1}^{Q\star} \left(\tilde{\gamma}_{t,k-1}^{[\mathrm{D},1]}(\mathcal{D}_1(\tilde{q})) + \tilde{\gamma}_{t,k-1}^{[\mathrm{D},2]}(\mathcal{D}_2(\tilde{q})) + \tilde{\alpha}_{t,k-1}^{[\mathrm{pos}]}(\tilde{q}) + \widetilde{\mathsf{Pr}}\{I_{t,k}=q | I_{t,k-1}=\tilde{q}\} \right) \quad \text{(G.40)}$$

$$\tilde{\beta}_{t,k-1}^{[\mathrm{pos}]}(q) = \max_{\tilde{q}=1}^{Q\star} \left(\tilde{\gamma}_{t,k}^{[\mathrm{D},1]}(\mathcal{D}_1(\tilde{q})) + \tilde{\gamma}_{t,k}^{[\mathrm{D},2]}(\mathcal{D}_2(\tilde{q})) + \tilde{\beta}_{t,k}^{[\mathrm{pos}]}(\tilde{q}) + \ln \mathsf{Pr}\{I_{t,k}=\tilde{q} | I_{t,k-1}=q\} \right) . \quad \text{(G.41)}$$

Using (G.39), (G.40), and (G.41) the extrinsic information is given by

$$\mathsf{L}_{\mathrm{SD}}^{[\mathrm{ext}]}(b_{t,k,\mu}^{[\mathrm{D},\nu]}) = \max_{\substack{q_\nu=1 \\ \bar{b}_{k,\mu}^{[\mathrm{D},\nu](q_\nu)}=0}}^{Q^{[\mathrm{D},\nu]}\star} \left(\max_{\forall q_{\bar{\nu}} \in \mathbb{D}_{q_\nu}^{[\mathrm{D},\nu]}} \left(\tilde{A}'''_{t,k}(q_1,q_2) \right) - \frac{1}{2} \mathsf{L}_{\mathrm{CD}}^{[\mathrm{ext}]}(b_{t,k,\mu}^{[\mathrm{D},\nu]}) \right) - \max_{\substack{q_\nu=1 \\ \bar{b}_{k,\mu}^{[\mathrm{D},\nu](q_\nu)}=1}}^{Q^{[\mathrm{D},\nu]}\star} \left(\max_{\forall q_{\bar{\nu}} \in \mathbb{D}_{q_\nu}^{[\mathrm{D},\nu]}} \left(\tilde{A}'''_{t,k}(q_1,q_2) \right) + \frac{1}{2} \mathsf{L}_{\mathrm{CD}}^{[\mathrm{ext}]}(b_{t,k,\mu}^{[\mathrm{D},\nu]}) \right) , \quad \text{(G.42)}$$

with the auxiliary variable

$$\tilde{A}'''_{t,k}(q_1,q_2) \doteq \tilde{\alpha}_{t,k}^{[\mathrm{pos}]}(\mathcal{D}^{-1}(q_1,q_2)) + \tilde{\beta}_{t,k}^{[\mathrm{pos}]}(\mathcal{D}^{-1}(q_1,q_2) + \tilde{\alpha}_{t,k}^{[\mathrm{tim}]}(\mathcal{D}^{-1}(q_1,q_2)) . \quad \text{(G.43)}$$

H

Source Compression System Configurations

In this appendix, the different system configurations of the irregular bit mapping component and the irregular channel coding component of the system depicted in Fig. 5.3 (page 108) used for producing the simulation results in Fig. 5.6 (page 116) are given. The source correlation coefficients amount to $\rho = 0$ and $\delta = 0.9$ (intra-frame correlation). The single parameters are scalar-quantized using a $Q = 16$ *Lloyd-Max Quantizer* (LMQ). The bit mapping and the convolutional codes are selected as described in Sec. 5.2 (page 108). No channel noise is present, i.e., $E_\mathrm{s}/N_0 \to \infty$. At the receiver, AK1-INTRA SDSD is employed. The optimization of the transmitter is performed using the non-linear optimization formulated in Sec. 5.1.3 (page 108). Different values are obtained by varying the offset vector $\mathbf{o}$ in the constraint (5.19). For each different offset vector, the resulting number of bits N_E/N_I for each index is given along with the parameters $N_I^{(j)}$ and $N_X^{(\chi)}$ required for setting up the transmitter (and receiver). The system configurations are given for $N_I = 10000$. Settings for different values of N_I can be easily derived by appropriate scaling and rounding as the optimization is independent of N_I. In what follows the system configurations, sorted in ascending order by N_E/N_I, are given.

- $N_E/N_I = 2.6563$:

Irregular bit mapping

j	1	2	6	7	11
$r_\mathrm{BM}^{(j)}$	$\frac{4}{5}$	$\frac{4}{6}$	$\frac{4}{10}$	$\frac{4}{11}$	$\frac{4}{15}$
$N_I^{(j)}$	4704	4756	194	116	230

Irregular convolutional code

χ	4	5	9
$r_\mathrm{CC}^{(\chi)}$	2	2.5	5
$N_X^{(\chi)}$	47594	2704	8424

- $N_E/N_I = 2.6834$:

Irregular bit mapping

j	1	2	11
$r_\mathrm{BM}^{(j)}$	$\frac{4}{5}$	$\frac{4}{6}$	$\frac{4}{15}$
$N_I^{(j)}$	3307	6343	350

Irregular convolutional code

χ	4	5	6	9
$r_\mathrm{CC}^{(\chi)}$	2	2.5	3	5
$N_X^{(\chi)}$	48217	1186	1215	9225

- $N_E/N_I = 2.7118$:

Irregular bit mapping			
j	1	2	11
$r_{\mathrm{BM}}^{(j)}$	$\frac{4}{5}$	$\frac{4}{6}$	$\frac{4}{15}$
$N_I^{(j)}$	2010	7770	220

Irregular convolutional code				
χ	1	4	5	9
$r_{\mathrm{CC}}^{(\chi)}$	1.25	2	2.5	5
$N_X^{(\chi)}$	1684	46154	1335	10797

- $N_E/N_I = 2.7396$:

Irregular bit mapping			
j	1	2	11
$r_{\mathrm{BM}}^{(j)}$	$\frac{4}{5}$	$\frac{4}{6}$	$\frac{4}{15}$
$N_I^{(j)}$	91	9851	58

Irregular convolutional code				
χ	1	4	8	9
$r_{\mathrm{CC}}^{(\chi)}$	1.25	2	4	5
$N_X^{(\chi)}$	4285	41584	5314	9248

- $N_E/N_I = 2.7680$:

Irregular bit mapping			
j	2	3	11
$r_{\mathrm{BM}}^{(j)}$	$\frac{4}{6}$	$\frac{4}{7}$	$\frac{4}{15}$
$N_I^{(j)}$	9860	114	26

Irregular convolutional code			
χ	1	4	9
$r_{\mathrm{CC}}^{(\chi)}$	1.25	2	5
$N_X^{(\chi)}$	4527	42984	12837

- $N_E/N_I = 2.7972$:

Irregular bit mapping		
j	2	3
$r_{\mathrm{BM}}^{(j)}$	$\frac{4}{6}$	$\frac{4}{7}$
$N_I^{(j)}$	8994	1006

Irregular convolutional code			
χ	1	4	9
$r_{\mathrm{CC}}^{(\chi)}$	1.25	2	5
$N_X^{(\chi)}$	5980	40610	14416

- $N_E/N_I = 2.8277$:

Irregular bit mapping		
j	2	3
$r_{\mathrm{BM}}^{(j)}$	$\frac{4}{6}$	$\frac{4}{7}$
$N_I^{(j)}$	8335	1665

Irregular convolutional code					
χ	1	2	3	4	9
$r_{\mathrm{CC}}^{(\chi)}$	1.25	1.5	1.75	2	5
$N_X^{(\chi)}$	7847	514	1535	34752	17017

- $N_E/N_I = 2.8594$:

Irregular bit mapping		
j	2	3
$r_{\mathrm{BM}}^{(j)}$	$\frac{4}{6}$	$\frac{4}{7}$
$N_I^{(j)}$	7815	2185

Irregular convolutional code					
χ	1	2	3	4	9
$r_{\mathrm{CC}}^{(\chi)}$	1.25	1.5	1.75	2	5
$N_X^{(\chi)}$	10187	2717	3908	24418	20955

- $N_E/N_I = 2.8914$:

Irregular bit mapping		
j	2	3
$r_{\mathrm{BM}}^{(j)}$	$\frac{4}{6}$	$\frac{4}{7}$
$N_I^{(j)}$	7309	2691

Irregular convolutional code					
χ	1	2	3	4	9
$r_{\mathrm{CC}}^{(\chi)}$	1.25	1.5	1.75	2	5
$N_X^{(\chi)}$	12449	4569	6179	14930	24564

- $N_E/N_I = 2.9234$:

Irregular bit mapping		
j	2	3
$r_{\mathrm{BM}}^{(j)}$	$\frac{4}{6}$	$\frac{4}{7}$
$N_I^{(j)}$	6815	3185

Irregular convolutional code					
χ	1	2	3	4	9
$r_{\mathrm{CC}}^{(\chi)}$	1.25	1.5	1.75	2	5
$N_X^{(\chi)}$	14629	6057	8341	6318	27840

- $N_E/N_I = 2.9556$:

Irregular bit mapping		
j	2	3
$r_{\mathrm{BM}}^{(j)}$	$\frac{4}{6}$	$\frac{4}{7}$
$N_I^{(j)}$	6314	3686

Irregular convolutional code				
χ	1	2	3	9
$r_{\mathrm{CC}}^{(\chi)}$	1.25	1.5	1.75	5
$N_X^{(\chi)}$	16581	6599	10206	30300

- $N_E/N_I = 2.9841$:

Irregular bit mapping		
j	2	3
$r_{\mathrm{BM}}^{(j)}$	$\frac{4}{6}$	$\frac{4}{7}$
$N_I^{(j)}$	1614	8386

Irregular convolutional code					
χ	1	2	4	8	10
$r_{\mathrm{CC}}^{(\chi)}$	1.25	1.5	2	4	6
$N_X^{(\chi)}$	19221	2243	9055	25557	12310

- $N_E/N_I = 3.0151$:

Irregular bit mapping		
j	2	3
$r_{\mathrm{BM}}^{(j)}$	$\frac{4}{6}$	$\frac{4}{7}$
$N_I^{(j)}$	1196	8804

Irregular convolutional code					
χ	1	2	4	8	10
$r_{\mathrm{CC}}^{(\chi)}$	1.25	1.5	2	4	6
$N_X^{(\chi)}$	21121	2685	4463	29717	10818

- $N_E/N_I = 3.0463$:

Irregular bit mapping		
j	1	3
$r_{\mathrm{BM}}^{(j)}$	$\frac{4}{5}$	$\frac{4}{7}$
$N_I^{(j)}$	418	9582

Irregular convolutional code					
χ	1	2	4	8	10
$r_{\mathrm{CC}}^{(\chi)}$	1.25	1.5	2	4	6
$N_X^{(\chi)}$	22980	2659	752	33610	9163

- $N_E/N_I = 3.0781$:

Irregular bit mapping		
j	1	3
$r_{\text{BM}}^{(j)}$	$\frac{4}{5}$	$\frac{4}{7}$
$N_I^{(j)}$	100	9900

Irregular convolutional code				
χ	1	2	8	11
$r_{\text{CC}}^{(\chi)}$	1.25	1.5	4	8
$N_X^{(\chi)}$	24521	1238	38674	5367

- $N_E/N_I = 3.1105$:

Irregular bit mapping	
j	3
$r_{\text{BM}}^{(j)}$	$\frac{4}{7}$
$N_I^{(j)}$	10000

Irregular convolutional code					
χ	1	2	8	10	11
$r_{\text{CC}}^{(\chi)}$	1.25	1.5	4	6	8
$N_X^{(\chi)}$	25562	456	36849	5938	1195

- $N_E/N_I = 3.1453$:

Irregular bit mapping		
j	1	3
$r_{\text{BM}}^{(j)}$	$\frac{4}{5}$	$\frac{4}{7}$
$N_I^{(j)}$	357	9643

Irregular convolutional code			
χ	1	8	9
$r_{\text{CC}}^{(\chi)}$	1.25	4	5
$N_X^{(\chi)}$	26322	36051	6913

- $N_E/N_I = 3.1835$:

Irregular bit mapping		
j	1	3
$r_{\text{BM}}^{(j)}$	$\frac{4}{5}$	$\frac{4}{7}$
$N_I^{(j)}$	321	9679

Irregular convolutional code				
χ	1	5	8	9
$r_{\text{CC}}^{(\chi)}$	1.25	2.5	4	5
$N_X^{(\chi)}$	27364	265	29842	11887

- $N_E/N_I = 3.2242$:

Irregular bit mapping		
j	1	3
$r_{\text{BM}}^{(j)}$	$\frac{4}{5}$	$\frac{4}{7}$
$N_I^{(j)}$	535	9465

Irregular convolutional code				
χ	1	5	8	9
$r_{\text{CC}}^{(\chi)}$	1.25	2.5	4	5
$N_X^{(\chi)}$	28312	2985	17428	20205

- $N_E/N_I = 3.2642$:

Irregular bit mapping		
j	1	3
$r_{\text{BM}}^{(j)}$	$\frac{4}{5}$	$\frac{4}{7}$
$N_I^{(j)}$	748	9252

Irregular convolutional code				
χ	1	5	8	9
$r_{\text{CC}}^{(\chi)}$	1.25	2.5	4	5
$N_X^{(\chi)}$	29247	5660	5220	28377

I

Deutschsprachige Zusammenfassung

Die Einführung des drahtlosen Telegraphen durch Guglielmo Marconi stellt einen Meilenstein für die Entwicklung des modernen Informationszeitalters dar. Der schnelle Austausch aller Art von Informationen, unabdingbar für das Funktionieren der heutigen Volkswirtschaft, wäre ohne drahtlose Kommunikation erschwert. Der Trend zu mehr Mobilität im aktuellen Wirtschaftsleben verlangt nach praktisch überall verfügbarer mobiler und drahtloser Sprach- und Datenkommunikation.

Die Einführung des *Global System for Mobile Communications* (GSM) Standards markierte einen bedeutenden Durchbruch in der drahtlosen mobilen Telefonie. Infolge einer raschen Marktdurchdringung wurde mobile Telefonie plötzlich einer großen Anzahl an Personen zugänglich. Am Ende des Jahres 2009 gab es weltweit ungefähr 4,6 Milliarden Mobilfunkverträge, entsprechend 67% der weltweiten Population. Seit 2006 ist die Anzahl der Mobilfunkverträge in Deutschland sogar höher als die Anzahl der Einwohner. Die Marktdurchdringung übertrifft mittlerweile sogar in den Entwicklungsländern die 50% Marke.

Nach dem Erfolg der mobilen Telefonie zeichnete sich schnell der Wunsch ab, den mobilen Internetzugang weit verfügbar anzubieten, einhergehend mit dem Verlangen jederzeit und überall online zu sein. Die Erweiterung des GSM-Netzwerkes mit GPRS und EDGE war ein erster Schritt zum mobilen Internet mit Endgeräten wie Mobiltelefonen, PDAs oder Notebooks. Die Einführung des *Universal Mobile Telecommunications System* (UMTS) Netzes und der zukünftigen Erweiterung *Long Term Evolution* (LTE) versucht die Schere zwischen Angebot und Nachfrage nach einem schnellen Zugang zum mobilen Internet zu schließen. Der dadurch erreichte Anstieg der verfügbaren Datenrate hat die Übertragung der immer wichtiger werdenden multimedialen Inhalte, wie z.B. Audio und Video, ermöglicht.

Die erzielbaren Raten einer Mobilfunkverbindung sind leider begrenzt durch die von Claude Shannon formulierten fundamentalen Grenzen. Diese Grenzen basieren auf informationstheoretischen Überlegungen und geben die maximal erzielbare Übertragungsrate auf gestörten Kanälen an, allerdings ohne zu zeigen wie diese erreicht werden kann. Nach der Veröffentlichung von Shannons bahnbrechendem Artikel dauerte es mehr als vier Jahrzehnte bis die wissenschaftliche Gemeinschaft ein praktikables Codierverfahren entwickeln konnte, welches es erstmalig ermöglichte, mit begrenztem Aufwand eine Übertragung dicht an der fundamentalen Grenze zu realisieren.

Diese wichtige Entdeckung, von ihren Erfindern Turbo-Codes genannt, hat zu komplett neuen Codier- und Decodierparadigmen geführt, welche alle auf dem iterativen Austausch so genannter *extrinsischer* Information basieren.

Das Austauschen extrinsischer Information mittels Turbo-Prinzip ist nicht nur auf das Gebiet der Kanalcodierung limitiert, es wurde auch erfolgreich auf andere Komponenten des Empfängers angewandt. Ein Beispiel ist die iterative Auswertung von Quellendecodierung und Kanaldecodierung, genannt *Iterative Source-Channel Decoding* (ISCD). ISCD beruht auf dem Fakt, dass die meisten praktischen Quellencodierer das Quellensignal nicht komplett dekorrelieren können. Dies ist eine direkte Konsequenz aus praktischen Randbedingungen bezüglich Komplexität und Verzögerung des Algorithmus. Die im codierten Quellensignal dadurch enthaltene Restredundanz kann zusammen mit eventuell hinzugefügter künstlicher Redundanz (z.B. durch das *Bit-Mapping*) verwendet werden, um extrinsische Information zu berechnen. Diese Information kann anschließend iterativ in einer Schleife zwischen Quellen- und Kanaldecoder verbessert werden. Nach einer bestimmten Anzahl an Iterationen kann eine verbesserte Schätzung (gegenüber dem nicht-iterative Fall) des übertragenen audiovisuellen Signals durchgeführt werden.

In dieser Dissertation wird das ISCD-Konzept im Hinblick auf eine flexible und praktische Anwendung in heterogenen Netzwerken ergänzt und erweitert. Die verfügbare Rechenleistung in mobilen Terminals steigt, wie durch das Mooresche Gesetz vorhergesagt, exponentiell an. Dieser exponentielle Anstieg ermöglicht die Implementierung komplexer Empfänger wie ISCD, wodurch sowohl der Durchsatz als auch die Netzabdeckung der Mobilfunknetze erhöht werden kann. Somit lassen sich indirekt die Investitionen der Mobilfunkanbieter reduzieren. Obwohl das ISCD-Konzept im Allgemeinen bekannt ist, ist die Implementierung immer noch eine Herausforderung. Ein großer Teil der vorliegenden Dissertation befasst sich mit der Behebung der Schwierigkeiten, die bei der Implementierung praktischer Systeme mit ISCD auftreten können. Diese Schwierigkeiten beinhalten beispielsweise die unpräzise Konvergenzvorhersage, die Suboptimalität des Quellendecoders in Systemen mit Beschränkungen hinsichtlich der Verzögerung, der Bedarf an ungleichmäßigem Fehlerschutz, sowie die Reduktion des *Error-Floors*, welcher nicht vernachlässigbare Symbolfehlerraten bei guten Kanälen zur Folge hat. Das Ausnutzen inkrementeller Redundanz ermöglicht die effiziente Erhöhung des Durchsatzes und damit indirekt die Erhöhung der Anzahl an Nutzern, die bei gegebener Bandbreite innerhalb einer Funkzelle bedient werden können.

Da reale Übertragungssysteme im Allgemeinen nicht dem vereinfachten Basisbandmodell, welches in frühen Veröffentlichungen zu ISCD betrachtet wurde, entsprechen, wurde die Erweiterung von ISCD auf *Multiple Description Coding* (MDC) betrachtet. MDC ist ein Konzept zur Quellencodierung welches häufig bei zu erwartenden Paketverlusten in heterogenen Netzwerken verwendet wird. Weiterhin wurde eine auf ISCD basierende robustere und flexiblere Alternative zu Entropiecodes untersucht. Entropiecodes werden beispielsweise häufig in Quellencodierern für Audio-, Bild- und Videocodierung verwendet.

Obwohl die verfügbare Rechenleistung in mobilen Endgeräten exponentiell ansteigt, folgt die Batteriekapazität leider nicht diesem Anstieg. Dieser Umstand, zusammen

mit der steigenden Ressourcenknappheit, erfordert die Untersuchung von Ansätzen zur Komplexitätsreduktion. Diese beinhalten sowohl die Begrenzung der am Empfänger durchzuführenden Iterationen als auch den Einsatz von komplexitätsreduzierten Empfängerbausteinen.

Optimierung und Erweiterung der iterativen Quellen-Kanaldecodierung

Kernthema der vorliegenden Arbeit ist die iterative Quellen-Kanaldecodierung (*Iterative Source-Channel Decoding* (ISCD)). ISCD wurde in Kapitel 2 in seinem historischen Kontext eingeführt. ISCD bezeichnet die Realisierung eines Turbo-ähnlichen Empfängers bestehend aus der Verkettung von Quellen- und Kanaldecodierung. Neben einer Systembeschreibung auf abstrakter Ebene wurde anhand eines Beispiels der Einsatz von ISCD in Übertragungssystemen mit modernen Multimediacodecs gerechtfertigt. Da ISCD auf dem Konzept der Turbo-Codes beruht, wurden diese zusammen mit dem generalisierten Konzept der Turbo-ähnlichen Codes eingeführt. Anhand von Simulationsergebnissen konnte die überragende Leistungsfähigkeit von Turbo- und Turbo-ähnlichen Codes gegenüber konventionellen Verfahren gezeigt werden. Weiterhin wurde die Konvergenzanalyse mittels *EXtrinsic Information Transfer* (EXIT) Charts eingeführt. EXIT-Charts erlauben eine präzise Analyse der Konvergenz von Turbo- und Turbo-ähnlichen Codes und stellen ein wertvolles Hilfsmittel zum Systementwurf dar.

Abbildung I.1 zeigt das abstrakte Basisband-Systemmodell eines Senders und Empfängers mit ISCD. Dieses Modell bildet die Grundlage für die meisten Untersuchungen in dieser Dissertation. Das ISCD-System basiert auf einer rahmenweisen Verarbeitung. Zum diskreten Zeitpunkt t extrahiert die Signalanalyse eines Quellencodierers aus dem audiovisuellen Signal $\mathbf{s}_t$ einen Satz an Parametern, mit deren Hilfe das Signal am Empfänger rekonstruiert werden kann. Diese Parameter werden in einem Vektor $\mathbf{u}_t$ gespeichert und quantisiert. Das so genannte *Bit-Mapping* weist den einzelnen

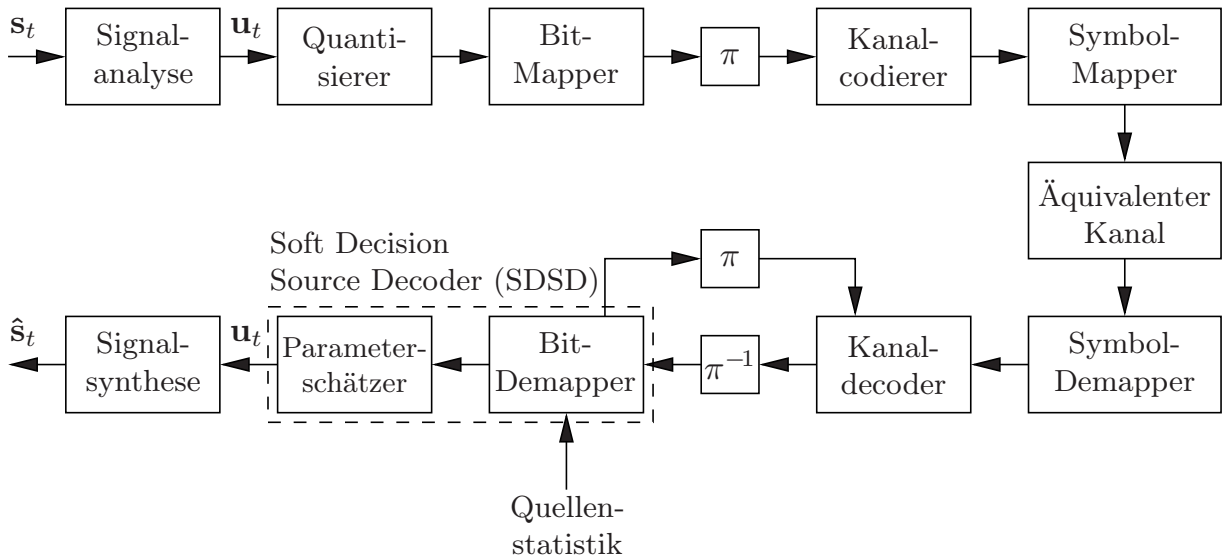

Abbildung I.1: Basisband-Blockschaltbild eines Übertragungssystems mit iterativer Quellen-Kanaldecodierung.

Quantisierungsindizes ein Bitmuster zu. Die gruppierten Bitmuster werden mittels einer Permutation (*Interleaver*) verwürfelt und anschließend wird mit dem Kanalcodierer gezielt Redundanz zum Schutz gegenüber Übertragungsfehlern zugefügt. Der kanalcodierte Bitstrom wird vom *Symbol-Mapper* auf (komplexe) Signalraumpunkte abgebildet und über ein äquivalentes Basisbandkanalmodell übertragen.

Empfangsseitig rekonstruiert der *Symbol-Demapper* die Bitsequenz aus den empfangenen, gestörten Signalraumpunkten und generiert idealerweise so genannte *Soft-Information*, d.h. Zuverlässigkeitsinformation über die einzelnen Bits. Die eigentliche iterative Quellen- und Kanaldecodierung findet in der folgenden Stufe statt. Ein *Soft Input Soft Output* (SISO) Kanaldecoder tauscht iterativ extrinsische Information mit einem *Soft Decision Source Decoder* (SDSD) aus. Neben der Struktur des Bit-Mappings und dem vom Kanaldecoder gelieferten Wissen nutzt der SDSD außerdem die natürliche Restredundanz der Parameter aus, um verbessertes extrinsisches Wissen zu generieren. Nach einer festgelegten Anzahl an Iterationen werden mithilfe der geschätzten *a posteriori* Wahrscheinlichkeiten die Codecparameter rekonstruiert.

Mit einem Simulationsbeispiel sollen nachfolgend die mittels ISCD erzielbaren Gewinne gegenüber konventionellen Übertragungssystemen gezeigt werden. Ein Rahmen besteht in diesem Beispiel aus 250 statistisch unabhängigen Parametern, welche allerdings zeitlich korreliert sind, d.h. es besteht eine Abhängigkeit der Parameter zweier zeitlich benachbarter Rahmen. Die einzelnen Parameter werden jeweils mit einer Gauss-Markov Quelle mit Korrelationskoeffizient $\rho = 0.9$ modelliert. Solche Korrelationskoeffizienten werden typischerweise bei den Verstärkungsfaktoren und LSF-Parametern von CELP-Sprachcodecs oder bei den Verstärkungsfaktoren vom MP3-Codec beobachtet. Die einzelnen Parameter werden anschließend mit einem skalaren Lloyd-Max Quantisierer mit $Q = 16$ Quantisierungsstufen quantisiert. In einem ersten Beispiel wird ein konventionelles, nicht redundantes *Natural-Binary*-Bit-Mapping durchgeführt und der so erhaltene Bitstrom mit einem rekursiv-systematischen Faltungscode der Einflusslänge $J + 1 = 4$ geschützt. Die Übertragung wird beispielhaft mithilfe einer BPSK-Modulation und AWGN modelliert. Der Faltungscode wird am Empfänger mittels MAP-Algorithmus decodiert und die Parameter werden in einem ersten Versuch mit harter Entscheidung (*Hard-Decision*) und Nachschlagen des Codebucheintrages rekonstruiert. Abbildung I.2 zeigt das erzielbare Parameter-SNR (Signal-Rausch-Verhältnis) in Abhängigkeit der Kanalqualität E_s/N_0 ($\triangle$). Wird der Hard-Decision-Decoder durch einen SDSD ersetzt welcher die Korrelation der zeitlich benachbarten Parameter ausnutzt (AK1, $\Diamond$), so ergibt sich ein Gewinn bezüglich der Kanalqualität von $\approx 2\,\mathrm{dB}$, d.h. um das gleiche Parameter-SNR zu erreichen, kann die Kanalqualität $\approx 2\,\mathrm{dB}$ schlechter sein als im Fall mit Hard-Decision-Decodierung. Andererseits kann bei gleichem gegebenen E_s/N_0 die Rekonstruktionsqualität um bis zu $8\,\mathrm{dB}$ verbessert werden.

Wird der Faltungscode durch den in der Originalarbeit von Berrou *et. al.* vorgeschlagenen Turbo-Code ersetzt, kann die Rekonstruktionsqualität gegenüber dem Fall mit Faltungscodierung signifikant verbessert werden. Die Ergebnisse in Abb. I.2 zeigen, dass mit Turbo-Code und Hard-Decision-Decodierung ($\bigtriangledown$) ein Parameter SNR von $\approx 20\,\mathrm{dB}$ schon bei $E_\mathrm{s}/N_0 = -1,5\,\mathrm{dB}$ erreicht werden kann. Allerdings sind die Ge-

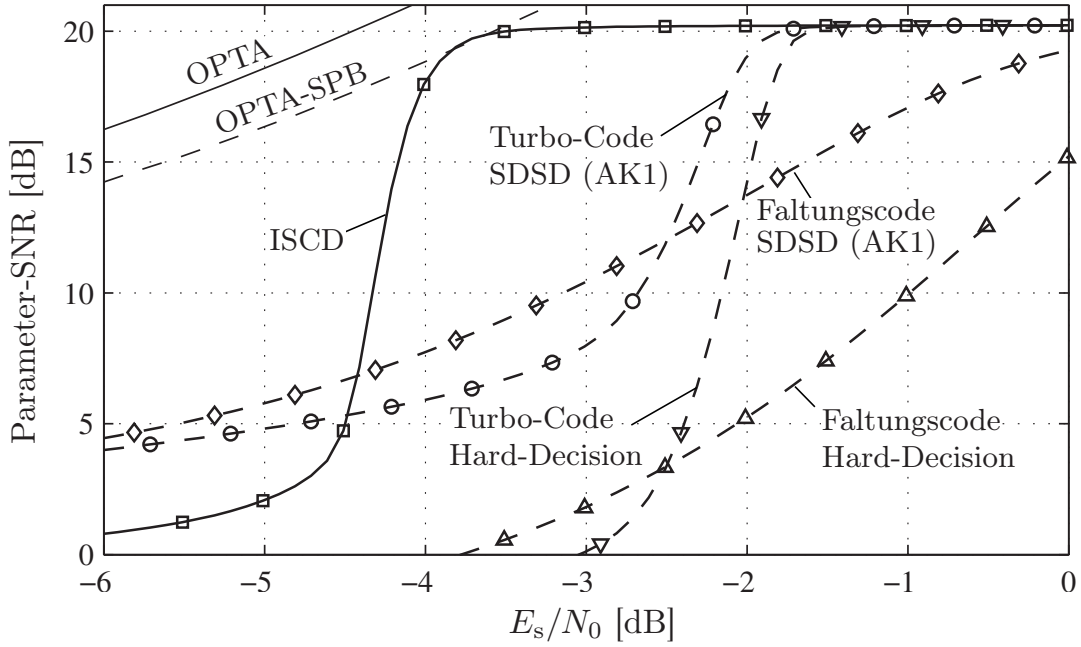

Abbildung I.2: Vergleich zwischen konventionellen Verfahren mit Faltungscodes oder Turbo-Codes zur Kanalcodierung und Hard-Decision Rekonstruktion oder SDSD mit Ausnutzung von *a priori* Wissen 1. Ordnung (AK1), und ISCD mit Wiederholungs-Bit-Mapping und Rate $r_{\mathrm{CC}} = 1$ Faltungscodierung, zeitliche Korrelation $\rho = 0.9$, $N_I = 250$ Parameter pro Rahmen.

winne die mit SDSD unter Ausnutzung der zeitlichen Korrelation (AK1) erzielt werden (◯), geringer als mit reiner Faltungscodierung (△, ◇). Wird iterative Quellen-Kanaldecodierung (ISCD) verwendet und wird die Korrelation der Quelle während des Systementwurfs berücksichtigt, ergibt sich folgendes System: die den Quantisierungsindizes zugehörigen Bitmuster werden durch einen Wiederholungscode geschützt, der gesamte resultierende Bitstrom mit einer pseudozufälligen Permutation verwürfelt und anschließend mit einem Faltungscodierer der Rate $r_{\mathrm{CC}} = 1$ codiert. Falls am Empfänger 25 Iterationen zwischen Quellen- und Kanaldecoder durchgeführt werden, ergibt sich die in Abb. I.2 mit "ISCD" bezeichnete Kurve (□). Verglichen mit der Konfiguration mit Turbo-Code und SDSD (AK1) ist nun ein Gewinn von $\approx 1,5\,\mathrm{dB}$ bis 2 dB bezüglich der Kanalqualität E_s/N_0 möglich. Bei einer Zielrekonstruktionsqualität von $\approx 20\,\mathrm{dB}$ kann mit diesem System sogar die theoretische Grenze unter Berücksichtigung der begrenzten Blockgröße (OPTA-SPB) erreicht werden. Die theoretische Grenze für unendlich große Blöcke ist mit OPTA bezeichnet.

In Kapitel 3 der vorliegenden Dissertation wurde das ISCD Basissystem grundlegend erweitert. Eine erste wichtige Erweiterung ist die Verbesserung der Konvergenzanalyse mittels EXIT-Charts. Falls die Quellenparameter Korrelation zwischen benachbarten Rahmen aufweisen, kann das herkömmliche EXIT-Chart nicht präzise die benötigte Anzahl an Iterationen vorhersagen. Daher wurde die so genannte *EXIT Trajectory Bound* (ETB) als Lösung vorgeschlagen. Die ETB erlaubt eine untere Abschätzung der benötigten Iterationen und damit einen präziseren Systementwurf. Weiterhin wurde gezeigt wie mithilfe der EXIT-Charts die Symbolfehlerrate nach Decodierung geschätzt werden kann.

Da aufgrund von Randbedingungen bezüglich der maximalen Systemverzögerung keine Information aus zukünftigen Rahmen zur Decodierung verwendet werden kann, ist das ISCD-System, welches Korrelation zwischen benachbarten Rahmen ausnutzt, nicht in der Lage, die maximal mögliche Decodiereffizienz zu erzielen. Daher wurde in dieser Arbeit eine neuartige Empfängerarchitektur vorgestellt, die eine verbesserte Nutzung der Zusammenhänge zwischen aufeinander folgenden Rahmen ermöglicht, ohne eine zusätzliche Verzögerung zu verursachen. Die erzielbaren Gewinne durch den neuartigen Empfänger konnten mithilfe eines Simulationsbeispiels quantifiziert werden.

Ein Großteil der Optimierungsansätze von ISCD-Systemen basiert auf der sorgfältigen Auswahl eines Bit-Mappings. Da mit redundanten Bit-Mappings, d.h., Bit-Mappings die gezielt künstliche Redundanz hinzufügen, Systeme mit der größten Leistungsfähigkeit entworfen werden können, bilden diese ein Kernthema dieser Dissertation. Basierend auf irregulären redundanten Bit-Mappings wurde ein leistungsfähiges ISCD-System vorgestellt. Irregulär bedeutet in diesem Kontext, dass die Zuordnung der Bitmuster zu den einzelnen Quantisierungsindizes von Parameter zu Parameter unterschiedlich sein kann. Irreguläre redundante Bit-Mappings erlauben eine elegante Systemoptimierung mittels EXIT-Charts. Das Konzept der Irregularität bildet die Grundlage für die meisten in dieser Arbeit vorgestellten Innovationen. Es wurde weiterhin gezeigt, dass sich mit irregulären Bit-Mappings gezielt ungleichmäßiger Fehlerschutz realisieren lässt. Ungleichmäßiger Fehlerschutz ist wichtig in praktischen Anwendungen wo manche Parameter des Quellencodierers einen höheren Einfluss auf die Qualität des rekonstruierten Signals haben als andere.

Ein Nachteil von einigen bekannten ISCD-Systemen mit guter Leistungsfähigkeit im so genannten Wasserfallbereich ist der beobachtbare hohe *Error-Floor*. Dieser Error-Floor wird größtenteils durch die Distanzeigenschaften des Bit-Mappings beeinflusst. Es wurde in der vorliegenden Arbeit gezeigt, dass der Error-Floor durch eine sorgfältige Wahl des Bit-Mappings reduziert werden kann. Da diese Bit-Mappings oft eine Verschlechterung der Leistungsfähigkeit im Wasserfallbereich mit sich ziehen, wird ein irregulärer Kanalcode mit geringer Decodierkomplexität vorgestellt, der diese Verschlechterung größtenteils aufhebt. Dieser irreguläre Kanalcode kann beispielsweise effizient im *FlexCode* Quellen-Kanalcodierer zur robusten Übertragung der Transformationskoeffizienten eingesetzt werden.

Im Falle des Einsatzes von Quantisierungscodebüchern mit nur wenigen Einträgen, ist es oft nicht möglich, optimierte Bit-Mappings zu verwenden. Aus diesem Grund wurde in dieser Dissertation eine innovative Sender- und Empfängerarchitektur vorgestellt, die den Error-Floor weiter verringern kann. Die vorgestellte Lösung, *Multi-Dimensional Bit Mappings* (MDBMs) genannt, gruppiert mehrere aufeinander folgende Quantisierungsindizes zu einem so genannten Super-Index. Diese Gruppierung erlaubt den Einsatz von Bit-Mappings mit verbesserten Distanzeigenschaften. Neben einer detaillierten Beschreibung des neuartigen Senders wurde gezeigt, wie der Empfänger beim Einsatz von MDBMs modifiziert werden muss. Die Reduktion des Error-Floors wurde mithilfe eines Simulationsbeispiels bestätigt.

Da die Konvergenz des ISCD-Empfängers sowohl von den aktuellen Kanalbedingungen als auch vom Systementwurf abhängt, ist es vorteilhaft, die Anzahl der benötigten Iterationen automatisch zu kontrollieren. Es wurden mehrere Verfahren verglichen, welche die Konvergenz des Empfängers erkennen und nur so viele Iterationen zulassen, wie auch benötigt werden. Ein vorteilhaftes Verfahren für ISCD mit redundanten Bit-Mappings basiert auf der Auswertung der so genannten Paritätsprüfmatrix des Bit-Mappings. Mit einem Simulationsbeispiel konnte gezeigt werden, dass das vorgeschlagene Verfahren eine geringere Anzahl an Iterationen benötigt, als die meisten bekannten heuristischen Ansätze.

Aufbauend auf den Abbruchkriterien wurden zwei ISCD-basierte *Hybrid Automatic Repeat reQuest* (HARQ) Schemata realisiert. Falls der Empfänger den aktuellen Rahmen nicht fehlerfrei decodieren kann, wird ein *Not-Acknowledge* (NACK) Signal über einen Rückkanal zum Sender geschickt. In diesem Fall wiederholt der Sender den Rahmen nicht wie bei herkömmlichen ARQ-Verfahren, sondern überträgt inkrementell kleinere Pakete, welche zusätzliche Paritätsbits enthalten. Mit dieser zusätzlichen Paritätsinformation kann der Empfänger eine verbesserte Decodierung durchführen. Es wurden zwei verschiedenartige Realisierungen eines solchen HARQ-Systems verglichen, welche auf effiziente Art und Weise den Durchsatz, und damit die Anzahl an bedienbaren Nutzern, erhöhen können.

Komplexitätsreduktion des *Soft Decision Source Decoders*

In Kapitel 4 der vorliegenden Dissertation wurden mehrere Ansätze zur Komplexitätsreduktion des SDSD vorgestellt. Diese können mit bekannten Ansätzen aus dem Gebiet der Kanalcodierung kombiniert werden, um einen Empfänger mit insgesamt reduzierter Komplexität zu realisieren. Der erste vorgestellte Ansatz basiert auf einer sendeseitigen Modifikation des Quantisierers. Durch diese Modifikation kann ein Abgleich zwischen Komplexität und Quantisierungsrauschen erzielt werden. Der vorgestellte bedingte Quantisierer (*conditional quantizer*) wurde gründlich untersucht und es wurde festgestellt, dass die Anzahl der benötigten SDSD-Operationen um einen bestimmten Faktor reduziert werden kann, falls ein gewisser Verlust der Rekonstruktionsqualität tolerierbar ist. Es wurde außerdem gezeigt, dass durch den Einsatz des bedingten Quantisierers die Entropie der Quantisierungsindizes verringert wird. Zudem wurde beobachtet, dass die bedingte Quantisierung zusätzlich implizit Redundanz hinzufügt, welche als Verringerung der Code-Rate des Quellencodierers aufgefasst werden kann.

Das zweite Verfahren zur Komplexitätsreduktion basiert auf einem bekannten Ansatz aus dem Gebiet der Kanaldecodierung: Die unzuverlässigsten Übergänge im SDSD werden nicht weiter berücksichtigt, da deren Einfluss auf das Decodierergebnis vernachlässigbar ist. Mithilfe eines Beispiels wurde gezeigt, wie viele Übergänge vernachlässigt werden können, ohne das Konvergenzverhalten und die Rekonstruktionsqualität maßgeblich zu verschlechtern. Der resultierende Algorithmus wurde in Analogie zu den bekannten Verfahren M-SDSD genannt.

Beide Verfahren konnten in einem dritten Schritt kombiniert werden, um die Komplexität des Empfängers weiter zu verringern. Im Falle einer Beschränkung der zur

Verfügung stehenden Rechenressourcen kann der Einsatz der komplexitätsreduzierten Algorithmen vorteilhaft sein. Da mehr Iterationen ausgeführt werden können, kann ein höheres Signal-Rausch-Verhältnis der rekonstruierten Parameter über einen breiten Bereich von Kanalverhältnissen erzielt werden.

Zusätzlich zur genauen Beschreibung der Algorithmen wurde eine detaillierte Komplexitätsanalyse der verschiedenen Verfahren durchgeführt und die Anzahl der benötigten Rechenleistung genau quantifiziert. Dabei wurden alle Verfahren im Hinblick auf eine günstige Implementierung im logarithmischen Bereich untersucht.

Turbo-Quellencodierung basierend auf ISCD

Kapitel 5 der vorliegenden Dissertation befasst sich mit der fehlertoleranten Komprimierung der Parameter des Quellencodierers. Die Komprimierung erfolgt in diesem Fall durch die Konfiguration des Senders aus Abb. I.1 so, dass die Anzahl der zu übertragenden Bits minimiert wird und die Rekonstruktion am Empfänger weiterhin gewährleistet ist. Auch in diesem Fall hat sich das Konzept der Irregularität als leistungsfähiges und vielseitiges Hilfsmittel zur Realisierung der angepeilten Ziele herausgestellt. Es wurde gezeigt, dass entweder ein irreguläres Bit-Mapping oder ein irregulärer Kanalcode durch numerisches Lösen eines linearen Optimierungsproblems mit Nebenbedingungen so eingestellt werden kann, dass die Anzahl der codierten Bits minimiert wird. Zudem wurde gezeigt, wie ein irreguläres Bit-Mapping und ein irregulärer Kanalcode gemeinsam optimiert werden können. Es hat sich herausgestellt, dass dieser letztere Fall die vielseitigsten Möglichkeiten bietet und das resultierende System sowohl gute Komprimierungsraten als auch gute Konvergenzeigenschaften besitzt. Der relevante Teil des Senders eines Übertragungssystems mit irregulären Bit-Mappings und irregulären inneren Codes ist in Abb. I.3 dargestellt. Die einzelnen Quantisierungsindizes innerhalb eines Blockes werden in $M_{\mathcal{B}}$ Sub-Blöcke aufgeteilt, welche mit jeweils einem unterschiedlichen Bit-Mapping codiert werden. Die einzelnen Bit-Mappings besitzen üblicherweise verschiedene Raten. Der resultierende Bitstrom wird seinerseits nach Permutation durch den Interleaver π in $M_{\mathcal{E}}$ Sub-Bitströme aufgeteilt, die jeweils mit einem unterschiedlichen Kanalcode mit eigener Rate codiert werden.

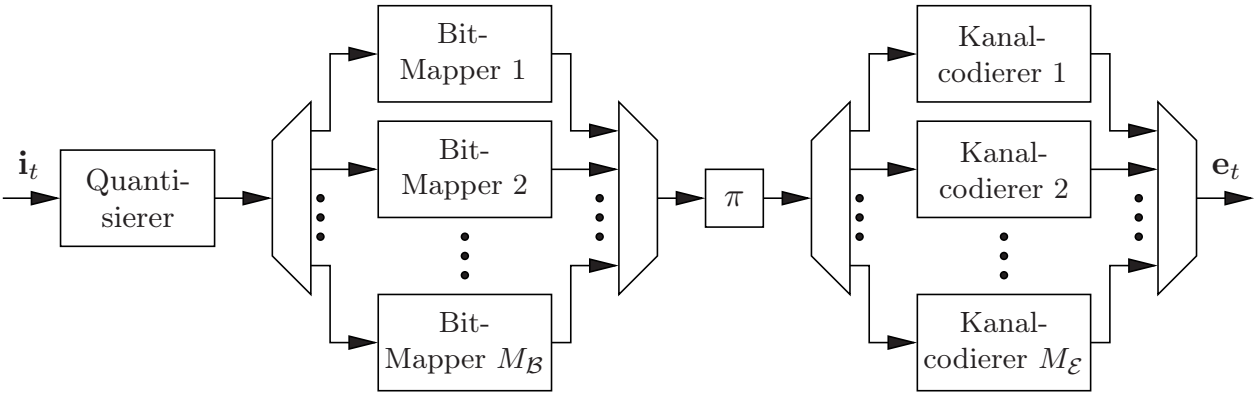

Abbildung I.3: Basisband-Blockschaltbild eines Senders mit irregulären Bit-Mappings und irregulärem inneren Kanalcode.

Alle eingeführten Optimierungsansätze wurden in einem Beispiel verglichen. Dabei wurde festgestellt, dass mit der gemeinsamen Optimierung die (theoretisch) besten Komprimierungsraten erzielt werden können. Es wurde in einem Simulationsbeispiel gezeigt, dass insbesondere bei großen Blockgrößen, das durch die bedingte Entropie vorgegebene theoretische Maximum fast erreicht werden kann. Das vorgeschlagene Verfahren kann bessere Ergebnisse liefern als konventionelle Entropiecodierschemata, wie z.B. Huffmann-Codes oder arithmetische Codes. Der Hauptvorteil des neuartigen Konzeptes liegt in der Robustheit gegenüber Übertragungsfehlern, da die Optimierung veränderte Kanalbedingungen direkt berücksichtigen kann. Weiterhin wird das Problem des Verlustes der Synchronisierung und der damit einhergehenden Fehlerfortpflanzung, die bei konventionellen Entropiecodierverfahren auftritt, vermieden.

Iterative Quellen-Kanaldecodierung von *Multiple-Descriptions*

Der letzte Teil der vorliegenden Dissertation befasst sich mit der Anwendung von *Soft Decision Source Decoder* (SDSD) und ISCD auf *Multiple Description Coding* (MDC). Das MDC-Konzept erlangt insbesondere in heterogenen Netzen immer größere Bedeutung. In solchen Netzen können nicht nur Paketverluste, sondern auch Bitfehler auftreten. In Kapitel 6 der vorliegenden Arbeit wurde gezeigt, dass sich mit der Anwendung eines SDSD auf MDC Gewinne bezüglich der Rekonstruktionsqualität erzielen lassen, falls die Quellenparameter eine gewisse Menge an Restredundanz enthalten. Die Gewinne sind nicht nur beobachtbar falls Bitfehler oder Kanalrauschen auftritt, sondern auch im Falle von Paketverlusten, d.h. falls eine oder mehrere Beschreibungen ausgelöscht werden. Die Anwendung von SDSD auf MDC ist somit immer vorteilhaft wenn Bitfehler oder Paketverluste auf dem Übertragungsmedium zu erwarten sind. Eine detaillierte Analyse der erzielbaren Gewinne wurde für verschiedene Arten von *a priori* Wissen in dieser Arbeit durchgeführt. Dabei zeigte sich, dass schon eine geringe Korrelation der Parameter signifikante Gewinne bezüglich der Rekonstruktionsqualität ermöglicht.

Weiterhin wurde in der vorliegenden Arbeit ein bekanntes iteratives MDC Decodierverfahren so verallgemeinert, dass *a priori* Wissen zur Decodierung verwendet werden kann. Das *a priori* Wissen berücksichtigt sich in diesem Fall eine mögliche Ungleichverteilung und/oder Korrelation zwischen benachbarten Quantisierungsindizes. Das resultierende MDC-basierte ISCD-System ermöglicht die Rekonstruktion der quantisierten Parameter bei sehr schlechten Übertragungsverhältnissen, nahe der theoretischen Grenze, bei der eine Rekonstruktion überhaupt noch möglich ist. Das Basisband-Blockschaltbild dieses Systems ist in Abb. I.4 dargestellt. Im Gegensatz zum System aus Abb. I.1 generiert ein zusätzlicher Block namens "MD-Indexzuweiser" (*Multiple Description Index Assignment* (MDIA)) zwei Beschreibungen jedes Quantisierungsindizes. Jeder dieser Beschreibungen wird getrennt ein Bitmuster zugewiesen. Die resultierenden Bitströme werden verwürfelt, getrennt kanalcodiert und über zwei unabhängige Kanäle übertragen. Auf den Kanälen können neben Bitfehlern auch komplette Paketverluste (d.h. Auslöschungen) auftreten. Auf Empfangsseite werden beide Beschreibungen getrennt kanaldecodiert und das jeweilige extrinsische Wissen (nach *Deinterleaving*) dem gemeinsamen Bit-Demapper zugeführt. Dieser berücksichtigt neben der Quellenstatistik auch die Struktur der MD-Indexzuweisung und das

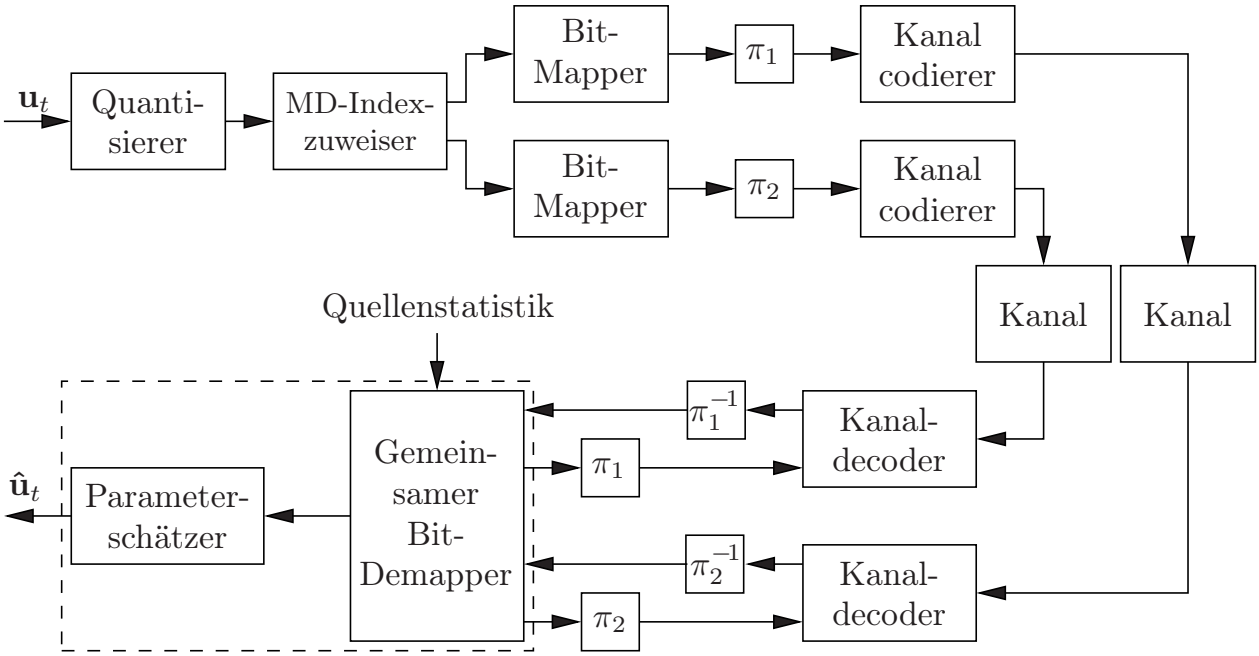

Abbildung I.4: Basisband-Blockschaltschild eines Übertragungssystems mit Multiple-Description-Coding und iterativer Quellen-Kanaldecodierung.

(eventuell redundante) Bit-Mapping, um extrinsisches Wissen für den iterativen Prozess und *a posteriori* Wahrscheinlichkeiten zur Parameterschätzung zu bestimmen.

In der vorliegenden Arbeit wurde die Konvergenzanalyse mittels EXIT-Charts dahingehend angepasst, dass das neuartige MDC-ISCD-System berücksichtigt werden kann. Die resultierenden neuartigen EXIT-Charakteristiken stellen ein wertvolles Hilfsmittel zur Konvergenzanalyse und -prädiktion dar. Basierend auf dem EXIT-Chart wurde in dieser Dissertation eine weitere Systemvariante vorgestellt, bei welcher keine explizite Bitrate durch einen Kanalcode hinzugefügt wird. Gegenüber konventionellen *Multiple-Description*-Ansätzen lässt sich mit dem neuartigen System eine verbesserte Rekonstruktionsqualität über eine breite Spanne an Kanalverhältnissen erzielen.

Schlussendlich wurde ein innovatives neuartiges Konzept zur Generierung von *Multiple-Descriptions* untersucht. Bei diesem Konzept werden die einzelnen Beschreibungen nicht sofort nach der Quantisierung durch ein *Index-Assignment* erzeugt, sondern unmittelbar vor der Übertragung durch einen Faltungscodierer. Das Entwicklungsziel dieses Konzeptes, genannt *Multiple Descriptions by Channel Coding* (MDCC), bestand darin, die in den Quellenparametern enthaltene Restredundanz insoweit auszunutzen, dass das Signal auch im Falle wo nur eine Beschreibung am Empfänger verfügbar ist, komplett rekonstruiert werden kann. In einer detaillierten Analyse wurde die notwendige Restredundanz zur Erfüllung dieses Entwurfszieles quantifiziert. Verglichen mit konventionellen MDC-Systemen ergibt sich mit dem neuen Ansatz eine verbesserte Rekonstruktionsqualität über einen weiten Bereich von Paketverlustwahrscheinlichkeiten. Sogar im Falle von zusätzlichem AWGN-Rauschen kann eine hervorragende Rekonstruktionsqualität mit dem neuen System gewährleistet werden.

Bibliography

[3GP01] 3GPP TS 26.190. "AMR Wideband Speech Codec; Transcoding Functions", 2001. available at http://www.3gpp.org.

[3GP07] 3GPP, TSG Services and System Aspects. "Packet-Switched Conversational Multimedia Applications; Performance Characterisation of Default Codecs". Technical report, TR 26.935, 2007.

[AAC+06] M. Adrat, M. Antweiler, T. Clevorn, B. Korall, and P. Vary. "EXIT-Optimized Quantizer Design for Iterative Source-Channel Decoding". *International Symposium on Turbo Codes & Related Topics and International ITG Conference on Source and Channel Coding (SCC)*, Munich, Germany, April 2006.

[AAS+10] M. Adrat, M. Antweiler, L. Schmalen, P. Vary, and T. Clevorn. "On the Overshooting Effect in EXIT Chart of Iterative Source-Channel Decoding". *IEEE International Conference on Communications (ICC)*, Cape Town, South Africa, May 2010.

[Abb07] A. Abbasfar. *Turbo-like Codes: Design for High Speed Decoding*. Springer, 2007.

[ABCV05] M. Adrat, J. Brauers, T. Clevorn, and P. Vary. "The EXIT-Characteristic of Softbit-Source Decoders". *IEEE Communications Letters*, vol. 9, no. 6, pp. 540–542, June 2005.

[ACBV06] M. Adrat, T. Clevorn, J. Brauers, and P. Vary. "Minimum Terms of Residual Redundancy for Successful Iterative Source-Channel Decoding". *IEEE Communications Letters*, vol. 10, no. 11, pp. 778–780, November 2006.

[ACS08] M. Adrat, T. Clevorn, and L. Schmalen. "Iterative Source-Channel Decoding & Turbo DeCodulation". R. Martin, U. Heute, and C. Antweiler, editors, *Advances in Digital Speech Transmission*, chapter 13, pp. 365–398. John Wiley & Sons, Ltd., January 2008.

[Adr03] M. Adrat. *Iterative Source-Channel Decoding for Digital Mobile Communications*. Aachener Beiträge zu Digitalen Nachrichtensystemen (ABDN) (ed. P. Vary), RWTH Aachen University, 2003. ISBN 3-86073-835-6.

[AGM07] J. G. Andrews, A. Ghosh, and R. Muhamed. *Fundamentals of WiMAX: Understanding Broadband Wireless Networking*. Prentice Hall, 2007.

[AHV02] M. Adrat, R. Haenel, and P. Vary. "On Joint Source-Channel Decoding for Correlated Sources". *International Conference on Acoustics, Speech, and Signal Processing (ICASSP)*, Orlando, FL, USA, May 2002.

[AKtB02] A. Ashikhmin, G. Kramer, and S. ten Brink. "Code Rate and the Area Under Extrinsic Information Transfer Curves". *IEEE International Symposium on Information Theory (ISIT)*, p. 115, June 2002.

[AKtB04] A. Ashikhmin, G. Kramer, and S. ten Brink. "Extrinsic Information Transfer Functions: Model and Erasure Channel Properties". *IEEE Transactions on Information Theory*, vol. 50, no. 11, pp. 2657–2673, November 2004.

[AL07a] A. Antoniou and W.-S. Lu. *Practical Optimization – Algorithms and Engineering Applications*. Springer, New York City, NY, USA, 2007.

[AL07b] B. Asadi and F. Lahouti. "An Efficient MMSE Decoder for Differential Source Coders with Adaptive Quantizer: A Joint Source Channel Coding Perspective". *IEEE International Conference on Signal Processing and Communications (ICSPC)*, pp. 1187–1190, Dubai, United Arab Emirates, November 2007.

[AM84] J. Anderson and S. Mohan. "Sequential Coding Algorithms: A Survey and Cost Analysis". *IEEE Transactions on Communications*, vol. 32, no. 2, pp. 169–176, February 1984.

[And89] J. B. Anderson. "Limited Search Trellis Decoding of Convolutional Codes". *IEEE Transactions on Information Theory*, vol. 35, no. 5, pp. 944–955, September 1989.

[APF96] F. Alajaji, N. Phamdo, and T. Fuja. "Channel Codes that Exploit the Residual Redundancy in CELP-encoded Speech". *IEEE Transactions on Speech and Audio Processing*, vol. 4, no. 5, pp. 325–336, September 1996.

[APV01] M. Adrat, J.-M. Picard, and P. Vary. "Softbit-Source Decoding based on the TURBO-Principle". *IEEE Vehicular Technology Conference (VTC-Fall)*, Atlantic City, NJ, USA, October 2001.

[APV04] M. Adrat, J.-M. Picard, and P. Vary. "Efficient Near-Optimum Softbit Source Decoding for Sources with Inter- and Intra-Frame Redundancy". *ICASSP*, pp. 653–656, Montreal, Canada, may 2004.

[Ari09] E. Arikan. "Channel Polarization: A Method for Constructing Capacity-Achieving Codes for Symmetric Binary-Input Memoryless Channels". *IEEE Transactions on Information Theory*, vol. 55, no. 7, pp. 3051–3073, July 2009.

[ASHV00] M. Adrat, J. Spittka, S. Heinen, and P. Vary. "Error Concealment by Near Optimum MMSE-Estimation of Source Codec Parameters". *IEEE Workshop on Speech Coding*, Delavan, WI, USA, September 2000.

[AV04a] M. Adrat and P. Vary. "Turbo Error Concealment of Mutually Independent Source Codec Parameters". *International ITG Conference on Source and Channel Coding (SCC)*, Erlangen, Germany, January 2004.

[AV04b] M. Adrat and P. Vary. "Iterative Source-Channel Decoding with Code Rates near r=1". *IEEE International Conference on Communications (ICC)*, Paris, France, June 2004.

[AV05] M. Adrat and P. Vary. "Iterative Source-Channel Decoding: Improved System Design Using EXIT Charts". *EURASIP Journal on Applied Signal Processing (Special Issue: Turbo Processing)*, vol. 2005, pp. 928–941, May 2005.

[AvAV03] M. Adrat, U. von Agris, and P. Vary. "Convergence Behavior of Iterative Source-Channel Decoding". *International Conference on Acoustics, Speech, and Signal Processing (ICASSP)*, Hongkong, China, April 2003.

[AVC05] M. Adrat, P. Vary, and T. Clevorn. "Optimized Bit Rate Allocation for Iterative Source-Channel Decoding and its Extension towards Multi-Mode Transmission". *14th IST Mobile and Wireless Communications Summit*, Dresden, Germany, June 2005.

[AVS01] M. Adrat, P. Vary, and J. Spittka. "Iterative Source-Channel Decoder Using Extrinsic Information from Softbit-Source Decoding". *International Conference on Acoustics, Speech, and Signal Processing (ICASSP)*, Salt Lake City, UT, USA, May 2001.

[BA04] D. Bokolamulla and T. M. Aulin. "A New Stopping Criterion for Iterative Decoding". *IEEE International Conference on Communications (ICC)*, Paris, France, June 2004.

[Bal97] V. B. Balakirsky. "Joint Source-Channel Coding with Variable Length Codes". *IEEE International Symposium on Information Theory (ISIT)*, Ulm, Germany, June 1997.

[BCJR74] L. Bahl, J. Cocke, F. Jelinek, and J. Raviv. "Optimal Decoding of Linear Codes for Minimizing Symbol Error Rate". *IEEE Transactions on Information Theory*, vol. 20, no. 2, pp. 284–287, March 1974.

[BCK07] E. Bodden, M. Clasen, and J. Kneis. "Arithmetic Coding Revealed - A Guided Tour from Theory to Praxis". Technical Report SABLE-TR-2007-5, Sable Research Group, School of Computer Science, McGill University, Montreal, Canada, May 2007.

[BCW90] T. C. Bell, J. G. Cleary, and I. H. Witten. *Text Compression*. Prentice Hall, Inc., 1990.

[BDMP97] S. Benedetto, D. Divsalar, G. Montorsi, and F. Pollara. "A Soft-Input Soft-Output APP Module for Iterative Decoding of Concatenated Codes". *IEEE Communications Letters*, vol. 1, no. 1, pp. 22–24, January 1997.

[BDMP98a] S. Benedetto, D. Divsalar, G. Montorsi, and F. Pollara. "Analysis, Design, and Iterative Decoding of Double Serially Concatenated Codes with Interleavers". *IEEE Journal on Selected Areas in Communications*, vol. 16, no. 2, pp. 231–244, February 1998.

[BDMP98b] S. Benedetto, D. Divsalar, G. Montorsi, and F. Pollara. "Serial Concatenation of Interleaved Codes: Performance Analysis, Design, and Iterative Decoding". *IEEE Transactions on Information Theory*, vol. 44, no. 3, pp. 909–926, May 1998.

[Bee10] M. Beermann. "Design and Optimization of LDPC and Turbo Codes for High Speed Mobile Networks". Diploma thesis, Institute of Communications Systems and Data Processing (IND), RWTH Aachen University, May 2010.

[Ber71] T. Berger. *Rate-Distortion Theory: A Mathematical Basis for Data Compression*. Prentice Hall, 1971.

[Ber03] C. Berrou. "The Ten-Year-Old Turbo Codes Are Entering into Service". *IEEE Communications Magazine*, vol. 41, no. 8, pp. 110–116, August 2003.

[BFF+09] S. Bruhn, M. Flierl, S. Flierl, V. Grancharov, W. B. Kleijn, J. Klejsa, M. Li, J. Plasberg, H. Pobloth, S. Ragot, and A. Vasilache. "Deliverable D-1.3: Video Coder Pilot Study". Technical report, European Union, March 2009. http://www.flexcode.eu.

[BG96] C. Berrou and A. Glavieux. "Near Optimum Error Correcting Coding and Decoding: Turbo-Codes". *IEEE Transactions on Communications*, vol. 44, no. 10, pp. 1261–1271, October 1996.

[BGK+08a] S. Bruhn, V. Grancharov, W. B. Kleijn, J. Klejsa, M. Li, J. Plasberg, H. Pobloth, S. Ragot, and A. Vasilache. "Deliverable D-1.1: Baseline Source Coder". Technical report, European Union, February 2008. http://www.flexcode.eu.

[BGK+08b] S. Bruhn, V. Grancharov, W. B. Kleijn, J. Klejsa, M. Li, J. Plasberg, H. Pobloth, S. Ragot, and A. Vasilache. "Deliverable D-1.2: Final Source Coder". Technical report, European Union, October 2008. http://www.flexcode.eu.

[BGK+08c] S. Bruhn, V. Grancharov, W. B. Kleijn, J. Klejsa, M. Li, J. Plasberg, H. Pobloth, S. Ragot, and A. Vasilache. "The FlexCode Speech and Audio Coding Approach". *ITG Conference on Speech Communication*, Aachen, Germany, October 2008.

[BGO+07] C. Berrou, A. Graell i Amat, Y. Ould-Cheikh-Mouhamedou, C. Douillard, and Y. Saouter. "Adding a Rate-1 Third Dimension to Turbo Codes". *IEEE Information Theory Workshop*, pp. 156–161, Lake Tahoe, CA, USA, September 2007.

[BGOS09] C. Berrou, A. Graell i Amat, Y. Ould-Cheikh-Mouhamedou, and Y. Saouter. "Improving the Distance Properties of Turbo Codes Using a Third Component Code: 3D Turbo Codes". *IEEE Transactions on Communications*, vol. 57, no. 9, pp. 2505–2509, September 2009.

[BGT93] C. Berrou, A. Glavieux, and P. Thitimajshima. "Near Shannon Limit Error-Correcting Coding and Decoding: Turbo-Codes (1)". *IEEE International Conference on Communications (ICC)*, pp. 1064–1070, May 1993.

[BH00] R. Bauer and J. Hagenauer. "Iterative Source-Channel Decoding Using Reversible Variable Length Codes". *Data Compression Conference (DCC)*, Snowbird, UT, USA, March 2000.

[BHG02] J. Barros, J. Hagenauer, and N. Görtz. "Turbo Cross Decoding of Multiple Descriptions". *IEEE International Conference on Communications (ICC)*, pp. 1398–1402, April 2002.

[BIV10] T. Breddermann, S. Iwelski, and P. Vary. "Bad Parameter Indication for Error Concealment in Wireless Multimedia Communication". *IEEE Vehicular Technology Conference (VTC-Fall)*, Ottawa, Canada, September 2010.

[BLV+10] T. Breddermann, H. Lüders, P. Vary, I. Aktas, and F. Schmidt. "Iterative Source-Channel Decoding with Cross-Layer Support for Wireless VoIP". *International ITG Conference on Source and Channel Coding (SCC)*, Siegen, Germany, January 2010.

[BM96a] S. Benedetto and G. Montorsi. "Serial Concatenation of Block and Convolutional Codes". *Electronics Letters*, vol. 32, no. 10, pp. 887–888, May 1996.

[BM96b] S. Benedetto and G. Montorsi. "Iterative Decoding of Serially Concatenated Convolutional Codes". *Electronics Letters*, vol. 32, no. 13, pp. 1186–1188, June 1996.

[BMD03] S. Benedetto, G. Montorsi, and D. Divsalar. "Concatenated Convolutional Codes with Interleavers". *IEEE Communications Magazine*, vol. 41, no. 8, pp. 102–109, August 2003.

[Bro98] A. E. Brouwers. "Bounds on Linear Codes". V. S. Pless and W. C. Huffmann, editors, *Handbook of Coding Theory*, pp. 265–461. Elsevier, 1998.

[Bro06] D. C. Brock, editor. *Understanding Moore's Law: Four Decades of Innovation*. Chemical Heritage Press, 2006.

[BSMH05] I. N. Bronstein, K. A. Semendjajew, G. Musiol, and H.Mühlig. *Taschenbuch der Mathematik*. Verlag Harri Deutsch, 6th edition, 2005.

[BSTW86] J. L. Bentley, D. D. Sleator, R. E. Tarjan, and V. K. We. "A Locally Adaptive Data Compression Scheme". *Communications of the ACM*, vol. 29, no. 4, pp. 320–330, April 1986.

[BSV11] M. Beermann, L. Schmalen, and P. Vary. "Improved Decoding of Binary and Non-Binary LDPC Codes by Probabilistic Shuffled Belief Propagation". *IEEE International Conference on Communications (ICC)*, Kyoto, Japan, June 2011.

[Bun08] Bundesnetzagentur für Elektrizität, Gas, Telekommunikation, Post und Eisenbahnen. "Jahresbericht", 2008.

[BV10] T. Breddermann and P. Vary. "Complexity-Reduced Iterative Source-Channel Decoding Using Inner Irregular Insertion Convolutional Codes". *ITG Conference on Speech Communication*, Bochum, Germany, October 2010.

[BW94] M. Burrows and D. Wheeler. "A Block Sorting Lossless Data Compression Algorithm". Technical Report 124, Digital Equipment Corporation, 1994.

[CAV06] T. Clevorn, M. Adrat, and P. Vary. "Turbo DeCodulation using Highly Redundant Index Assignments and Multi-Dimensional Mappings". *International Symposium on Turbo Codes & Related Topics and International ITG Conference on Source and Channel Coding (SCC)*, Munich, Germany, April 2006.

[CBAV05] T. Clevorn, J. Brauers, M. Adrat, and P. Vary. "Turbo DeCodulation: Iterative Combined Demodulation and Source-Channel Decoding". *IEEE Communications Letters*, vol. 9, no. 9, pp. 820–822, September 2005.

[CC84] R. A. Comroe and D. J. Costello, Jr. "ARQ Schemes for Data Transmission in Mobile Radio Systems". *IEEE Journal on Selected Areas in Communications*, vol. 2, no. 4, pp. 472–481, July 1984.

[CD09] R. Chrabieh and Ö. Dural. "Multi-Dimensional Constellations for Coded Transmission in Fading Channels". *IEEE Vehicular Technology Conference (VTC-Spring)*, Barcelona, Spain, April 2009.

[CF02] J. Chen and M. P. C. Fossorier. "Near Optimum Universal Belief Propagation Based Decoding of Low-Density Parity Check Codes". *IEEE Transactions on Communications*, vol. 50, no. 3, pp. 406–414, March 2002.

[CFR01] G. Colavolpe, G. Ferrari, and R. Raheli. "Reduced-State BCJR-Type Algorithms". *IEEE Journal on Selected Areas in Communications*, vol. 19, no. 5, pp. 848–859, May 2001.

[CFRU01] S.-Y. Chung, G. D. Forney, Jr., T. Richardson, and R. Urbanke. "On the Design of Low-Density Parity-Check Codes Within 0.0045 dB of the Shannon Limit". *IEEE Communications Letters*, vol. 5, no. 2, pp. 58–60, February 2001.

[CGV04] T. Clevorn, S. Godtmann, and P. Vary. "EXIT Chart Analysis of Non-Regular Signal Constellation Sets for BICM-ID". *International Symposium on Information Theory and its Applications (ISITA)*, Parma, Italy, October 2004.

[CGV06] T. Clevorn, S. Godtmann, and P. Vary. "Optimized Mappings for Iteratively Decoded BICM on Rayleigh Channels with IQ Interleaving". *IEEE Vehicular Technology Conference (VTC-Spring)*, Melbourne, Australia, May 2006.

[CHG03] C. Cardinal, D. Haccoun, and F. Gagnon. "Iterative Threshold Decoding Without Interleaving for Convolutional Self-Doubly Orthogonal Codes". *IEEE Transactions on Communications*, vol. 51, no. 8, pp. 1274–1282, August 2003.

[CHGB98] C. Cardinal, D. Haccoun, F. Gagnon, and N. Batani. "Convolutional Self Doubly Orthogonal Codes for Iterative Decoding Without Interleaving". *IEEE International Symposium on Information Theory (ISIT)*, Cambridge, MA, USA, 1998.

[CHH06] C. Cardinal, D. Haccoun, and Y.-C. He. "Reduced-Complexity Convolutional Self-Doubly Orthogonal Codes for Efficient Iterative Decoding". *IEEE Vehicular Technology Conference (VTC-Spring)*, vol. 3, pp. 1372–1376, Melbourne, Australia, May 2006.

[CHIW98] D. J. Costello, Jr., J. Hagenauer, H. Imai, and S. B. Wicker. "Applications of Error-Control Coding". *IEEE Transactions on Information Theory*, vol. 44, no. 6, pp. 2531–2560, Oct. 1998.

[Cle06] T. Clevorn. *Turbo DeCodulation: Iterative Joint Source-Channel Decoding and Demodulation*. Aachener Beiträge zu Digitalen Nachrichtensystemen (ABDN) (ed. P. Vary), RWTH Aachen University, 2006. ISBN 3-86130-650-6.

[COV05] T. Clevorn, F. Oldewurtel, and P. Vary. "Combined Iterative Demodulation and Decoding using very short LDPC Codes and Rate-1 Convolutional Codes". *Conference on Information Sciences and Systems (CISS)*, Baltimore, MD, USA, March 2005.

[CPS92] R. W. Cottle, J.-S. Pang, and R. E. Stone. "The Linear Complementarity Problem". *Computer Science and Scientific Computing*. Academic Press, 1992.

[CR01] A. Chindapol and J. A. Ritcey. "Design, Analysis, and Performance Evaluation for BICM-ID with Square QAM Constellations in Rayleigh Fading Channels". *IEEE Journal on Selected Areas in Communications*, vol. 19, no. 5, pp. 944–957, May 2001.

[CRU01] S.-Y. Chung, T. J. Richardson, and R. L. Urbanke. "Analysis of Sum-Product Decoding of Low-Density Parity-Check Codes Using a Gaussian Approximation". *IEEE Transactions on Information Theory*, vol. 47, no. 2, pp. 657–670, February 2001.

[CRWC05] I. Chatzigeorgiou, M. R. D. Rodrigues, I. J. Wassell, and R. Carrasco. "Punctured Binary Turbo-Codes with Optimized Performance". *IEEE Vehicular Technology Conference (VTC-Fall)*, pp. 1965–1969, Dallas, TX, USA, September 2005.

[CSS+06] T. Clevorn, B. Schotsch, L. Schmalen, P. Vary, and M. Adrat. "Separation of Recursive Convolutional Codes into Sub-Codes using Galois Field Arithmetic". *Conference on Information Sciences and Systems (CISS)*, Princeton, NJ, USA, March 2006.

[CSV03] G. Caire, S. Shamai, and S. Verdú. "Universal Data Compression With LDPC Codes". *International Symposium on Turbo Codes & Related Topics*, Brest, France, September 2003.

[CSVA06] T. Clevorn, L. Schmalen, P. Vary, and M. Adrat. "On The Optimum Performance Theoretically Attainable for Scalarly Quantized Correlated Sources". *International Symposium on Information Theory and its Applications (ISITA)*, Seoul, South Korea, October 2006.

[CSVA08a] T. Clevorn, L. Schmalen, P. Vary, and M. Adrat. "On Redundant Index Assignments for Iterative Source-Channel Decoding". *IEEE Communications Letters*, vol. 12, no. 7, pp. 514–516, July 2008.

[CSVA08b] T. Clevorn, L. Schmalen, P. Vary, and M. Adrat. "Iterative Source-Channel Decoding: Design of Redundant Index Assignments". *ITG Conference on Speech Communication*, Aachen, Germany, October 2008.

[CSVA10] T. Clevorn, L. Schmalen, P. Vary, and M. Adrat. "Hybrid ARQ with Incremental Redundant Index Assignments for Iterative Source-Channel Decoding". *IEEE International Conference on Communications (ICC)*, Cape Town, South Africa, May 2010.

[CT06] T. M. Cover and J. A. Thomas. *Elements of Information Theory.* John Wiley & Sons, Inc., 2006.

[CTB98] G. Caire, G. Taricco, and E. Biglieri. "Bit-Interleaved Coded Modulation". *IEEE Transactions on Information Theory*, vol. 44, no. 3, pp. 927–946, May 1998.

[Cui08] Y. Cui. "Iterative Source-Channel Decoding Using Multiple Description Coding". Diploma thesis, Institute of Communications Systems and Data Processing (IND), RWTH Aachen University, July 2008.

[CV05] T. Clevorn and P. Vary. "The Box-Minus Operator and its Application to Low-Complexity Belief Propagation". *IEEE Vehicular Technology Conference (VTC-Spring)*, Stockholm, Sweden, May 2005.

[CVA06a] T. Clevorn, P. Vary, and M. Adrat. "Iterative Source-Channel Decoding using Short Block Codes". *ITG Conference on Speech Communication*, Kiel, Germany, April 2006.

[CVA06b] T. Clevorn, P. Vary, and M. Adrat. "Iterative Source-Channel Decoding using Short Block Codes". *International Conference on Acoustics, Speech, and Signal Processing (ICASSP)*, Toulouse, France, May 2006.

[CVA06c] T. Clevorn, P. Vary, and M. Adrat. "Parameter SNR Optimized Index Assignments and Quantizers based on First Order A Priori Knowledge for Iterative Source-Channel Decoding". *Conference on Information Sciences and Systems (CISS)*, Princeton, NJ, USA, March 2006.

[DB05a] L. Dinoi and S. Benedetto. "Design of Fast Prunable S-Random Interleavers". *IEEE Transactions on Wireless Communications*, vol. 4, no. 5, pp. 2540–2548, September 2005.

[DB05b] L. Dinoi and S. Benedetto. "Variable Size Interleaver Design for Parallel Turbo Decoder Architectures". *IEEE Transactions on Communications*, vol. 53, no. 11, pp. 1833–1840, November 2005.

[DDP98a] S. Dolinar, D. Divsalar, and F. Pollara. "Code Performance as a Function of Block Size". TMO Progress Report 42-133, Jet Propulsion Laboratory, Pasadena, CA, USA, May 1998.

[DDP98b] S. Dolinar, D. Divsalar, and F. Pollara. "Turbo Code Performance as a Function of Code Block Size". *IEEE International Symposium on Information Theory (ISIT)*, Cambdrige, MA, USA, August 1998.

[DDP00] D. Divsalar, S. Dolinar, and F. Pollara. "Low Complexity Turbo-Like Codes". *International Symposium on Turbo Codes & Related Topics*, pp. 78–80, Brest, France, September 2000.

[DDPM95] D. Divsalar, S. Dolinar, F. Pollara, and R. J. McEliece. "Transfer Function Bounds on the Performance of Turbo Codes". TDA Progress Report 42-122, Jet Propulsion Laboratory, Pasadena, CA, USA, August 1995.

[DGGH06] N. Dütsch, S. Graf, J. Garcia-Frias, and J. Hagenauer. "Source Model Aided Lossless Turbo Source Coding". *International Symposium on Turbo Codes & Related Topics and International ITG Conference on Source and Channel Coding (SCC)*, Munich, Germany, April 2006.

[DJB95] C. Douillard, M. Jézéquel, and C. Berrou. "Iterative Correction of Intersymbol Interference: Turbo Equalization". *European Transactions on Telecommunications (ETT)*, vol. 6, pp. 507–511, September 1995.

[DJM98] D. Divsalar, H. Jin, and R. J. McEliece. "Coding Theorems for "Turbo-like" Codes". *Allerton Annual Conference on Communication, Control and Computing*, pp. 201–210, Monticello, IL, USA, September 1998.

[DK09] P. Duhamel and M. Kieffer. *Joint Source-Channel Decoding: A Cross-Layer Perspective with Applications in Video Broadcasting over Mobile and Wireless Networks*. Academic Press, September 2009.

[DM98] M. C. Davey and D. MacKay. "Low-Density Parity Check Codes Over GF(q)". *IEEE Communications Letters*, vol. 2, no. 6, pp. 165–167, February 1998.

[DMW82] D. Daut, J. Modestino, and L. Wismer. "New Short Constraint Length Convolutional Code Constructions for Selected Rational Rates". *IEEE Transactions on Information Theory*, vol. 28, no. 5, pp. 794–800, September 1982.

[Dob63] R. L. Dobrushin. "General Formulation of Shannon's Basic Theorems of Information Theory". *AMS Translation*, vol. 33, pp. 323–438, 1963.

[DP95a] D. Divsalar and F. Pollara. "Multiple Turbo Codes for Deep-Space Communications". *JPL TDA Progress Report*, vol. 42, no. 121, pp. 66–77, May 1995.

[DP95b] D. Divsalar and F. Pollara. "Turbo Codes for PCS Applications". *IEEE International Conference on Communications (ICC)*, Seattle, WA, USA, June 1995.

[DP97] D. Divsalar and F. Pollara. "Hybrid Concatenated Codes and Iterative Decoding". TDA Progress Report 42-130, Jet Propulsion Laboratory, Pasadena, CA, USA, August 1997.

[DPSB08] E. Dahlmann, S. Parkvall, J. Sköld, and P. Berning. *3G Evolution - HSPA and LTE for Mobile Broadband*. Academic Press, 2nd edition, 2008.

[Düt06] N. Dütsch. "Code Optimisation for Lossless Compression of Binary Memoryless Sources based on FEC Codes". *European Transactions on Telecommunications (ETT)*, vol. 17, no. 2, pp. 219–229, March 2006.

[EH99] M. Eroz and A. R. Hammons Jr. "On the Design of Prunable Interleavers for Turbo Codes". *IEEE Vehicular Technology Conference (VTC-Spring)*, Houston, TX, USA, July 1999.

[Eli55] P. Elias. "Coding for Noisy Channels". *IRE Convention Record, Part IV*, pp. 37–46, 1955.

[Erd05] C. Erdmann. *Hierarchical Vector Quantization: Theory and Application to Speech Coding*. PhD thesis, Aachener Beiträge zu Digitalen Nachrichtensystemen (ABDN) (ed. P. Vary), July 2005.

[ETS09a] ETSI. "Digital Video Broadcasting (DVB); Second generation framing structure, channel coding and modulation systems for Broadcasting, Interactive Services, News Gathering and other broadband satellite applications (DVB-S2)". Technical report, EN 302 307 V1.2.1, August 2009.

[ETS09b] ETSI. "Digital Video Broadcasting (DVB); Frame structure channel coding and modulation for a second generation digital terrestrial television broadcasting system (DVB-T2)". Technical report, EN 302 755 V1.1.1, September 2009.

[FA98] V. Franz and J. B. Anderson. "Concatenated Decoding with a Reduced-search BCJR Algorithm". *IEEE Journal on Selected Areas in Communications*, vol. 16, no. 2, pp. 186–195, February 1998.

[Far90] N. Farvardin. "A Study of Vector Quantization for Noisy Channels". *IEEE Transactions on Information Theory*, vol. 36, no. 4, pp. 799–809, July 1990.

[FC06] M. Fresia and G. Caire. "Combined Error Protection and Compression with Turbo Codes for Image Transmission using a JPEG2000-Like Architecture". *IEEE International Image Processing Conference (ICIP)*, pp. 821–824, Atlanta, GA, USA, October 2006.

[FC10] M. Fresia and G. Caire. "A Linear Encoding Approach to Index Assignment in Lossy Source-Channel Coding". *IEEE Transactions on Information Theory*, vol. 56, no. 3, pp. 1322–1344, March 2010.

[FF03] T. Fazel and T. Fuja. "Robust Transmission of MELP-compressed Speech: An Illustrative Example of Joint Source-Channel Decoding". *IEEE Transactions on Communications*, vol. 51, no. 6, pp. 973–982, June 2003.

[FGL+84] G. D. Forney, Jr., R. G. Gallager, G. R. Lang, F. M. Longstaff, and S. U. Qureshi. "Efficient Modulation for Band-Limited Channels". *IEEE Journal on Selected Areas in Communications*, vol. 2, no. 5, pp. 632–647, September 1984.

[FH95] A. Franchi and R. A. Harris. "On the Error Burst Properties of the "Standard" K=7, Rate-1/2 Convolutional Code with Soft-Decision Viterbi Decoding". *European Transactions on Telecommunications (ETT)*, vol. 6, no. 3, pp. 337–351, May 1995.

[FHCS02] T. Fingscheidt, T. Hindelang, R. V. Cox, and N. Seshadri. "Joint Source-Channel (De-)Coding for Mobile Communications". *IEEE Transactions on Communications*, vol. 50, no. 2, pp. 200–212, February 2002.

[FHV99] T. Fingscheidt, S. Heinen, and P. Vary. "Joint Speech Codec Parameter and Channel Decoding of Parameter Individual Block Codes (PIBC)". *IEEE Workshop on Speech Coding*, pp. 75–77, June 1999.

[Fin98] T. Fingscheidt. *Softbit-Sprachedecodierung in digitalen Mobilfunksystemen*. Aachener Beiträge zu Digitalen Nachrichtensystemen (ABDN) (ed. P. Vary), RWTH Aachen University, 1998. ISBN 3-86073-438-5.

[Fin08] T. Fingscheidt. "Parameter Models and Estimators in Soft Decision Source Decoding". R. Martin, U. Heute, and C. Antweiler, editors, *Advances in Digital Speech Transmission*, chapter 10, pp. 311–328. John Wiley & Sons, Ltd., January 2008.

[For70] G. D. Forney, Jr. "Convolutional Codes I: Algebraic Structure". *IEEE Transactions on Information Theory*, vol. 16, no. 6, pp. 720–738, November 1970.

[For73] G. D. Forney, Jr. "The Viterbi Algorithm". *Proceedings of the IEEE*, vol. 61, no. 3, pp. 268–278, March 1973.

[FPPV10] M. Fresia, F. Pérez-Cruz, H. V. Poor, and S. Verdú. "Joint Source and Channel Coding – Proposing a Low-Density Parity-Check Code". *IEEE Signal Processing Magazine*, vol. 27, no. 6, pp. 104–113, November 2010.

[Fri96] B. Friedrichs. *Kanalcodierung*. Springer, 1996.

[FSB02] M. Ferrari, F. Scalise, and S. Bellini. "Prunable S-Random Interleavers". *IEEE International Conference on Communications (ICC)*, New York City, NY, USA, April 2002.

[FV87] N. Farvardin and V. Vaishampayan. "Optimal Quantizer Design for Noisy Channels: An Approach to Combined Source - Channel Coding". *IEEE Transactions on Information Theory*, vol. 33, no. 6, pp. 827–838, November 1987.

[FV91] N. Farvardin and V. Vaishampayan. "On the Performance and Complexity of Channel-Optimized Vector Quantizers". *IEEE Transactions on Information Theory*, vol. 37, no. 1, pp. 155–160, January 1991.

[FV01] T. Fingscheidt and P. Vary. "Softbit Speech Decoding: A New Approach to Error Concealment". *IEEE Transactions on Speech and Audio Processing*, vol. 9, no. 3, pp. 240–251, March 2001.

[GA03] J.-L. Gailly and M. Adler. "The GNU zip (gzip) Home Page". http://www.gzip.org, July 2003. version 1.2.4.

[Gal63] R. G. Gallager. *Low-Density Parity-Check Codes*. M.I.T. Press, Cambridge, MA, USA, 1963.

[GBB05] N. Gresset, J. J. Boutros, and L. Brunel. "Multidimensional Mappings for Iteratively Decoded BICM on Multiple-Antenna Channels". *IEEE Transactions on Information Theory*, vol. 51, no. 9, pp. 3337–3346, September 2005.

[GEGP09] D. Gündüz, E. Erkip, A. Goldsmith, and H. V. Poor. "Source and Channel Coding for Correlated Sources Over Multiuser Channels". *IEEE Transactions on Information Theory*, vol. 55, no. 9, pp. 3927–3944, September 2009.

[Ger79] A. Gersho. "Asymptotically Optimal Block Quantization". *IEEE Transactions on Information Theory*, vol. IT-25, no. 4, pp. 373–380, July 1979.

[GFGR01] A. Guyader, E. Fabre, C. Guillemot, and M. Robert. "Joint Source-Channel Turbo Decoding of Entropy-Coded Sources". *IEEE Journal on Selected Areas in Communications*, vol. 19, no. 9, pp. 1680–1696, September 2001.

[GGF02] T. Guionnet, C. Guillemot, and E. Fabre. "Soft Decoding of Multiple Descriptions". *IEEE International Conference on Multimedia and Expo (ICME)*, Lausanne, CH, August 2002.

[GLAV08] S. Godtmann, H. Lüders, G. Ascheid, and P. Vary. "A Bit-Mapping Strategy for Joint Iterative Channel Estimation and Turbo-Decoding". *IEEE Vehicular Technology Conference (VTC-Fall)*, Calgary, Canada, September 2008.

[GMW81] P. E. Gill, W. Murray, and M. H. Wright. *Practical Optimization*. Academic Press, London, 1981.

[GMW91] P. E. Gill, W. Murray, and M. H. Wright. *Numerical Linear Algebra and Optimization*, vol. 1. Addison Wesley, Redwood City, 1991.

[GN98] R. M. Gray and D. L. Neuhoff. "Quantization". *IEEE Transactions on Information Theory*, vol. 44, no. 6, pp. 2352–2383, October 1998.

[Goy01] V. K. Goyal. "Multiple Description Coding: Compression Meets the Network". *IEEE Signal Processing Magazine*, vol. 18, no. 5, pp. 74–93, September 2001.

[GP68] H. Gish and J. Pierce. "Asymptotically Efficient Quantization". *IEEE Transactions on Information Theory*, vol. 14, no. 5, pp. 676–683, September 1968.

[GPH+07] S. Godtmann, A. Pollok, N. Hadaschik, G. Ascheid, and H. Meyr. "On the Influence of Pilot Symbol and Data Symbol Positioning on Turbo Synchronization". *IEEE Vehicular Technology Conference (VTC-Spring)*, pp. 1723–1726, Dublin, Ireland, April 2007.

[Gra53] F. Gray. "Pulse Code Modulation". United States Patent Office, US patent 2,632,058, March 1953.

[GS05] C. Guillemot and P. Siohan. "Joint Source-Channel Decoding of Variable-Length Codes with Soft Information: A Survey". *EURASIP Journal on Applied Signal Processing (Special Issue: Turbo Processing)*, vol. 2005, pp. 906–927, May 2005.

[GZ02] J. Garcia-Frias and Y. Zhao. "Compression of Binary Memoryless Sources Using Punctured Turbo Codes". *IEEE Communications Letters*, vol. 6, no. 9, pp. 394–396, September 2002.

[Gör00] N. Görtz. "Iterative Source-Channel Decoding Using Soft-In/Soft-Out Decoders". *IEEE International Symposium on Information Theory (ISIT)*, p. 173, Sorrento, Italy, June 2000.

[Gör01a] N. Görtz. "A Generalised Framework for Iterative Source-Channel Decoding". *Annals of Telecommunications, Special Issue on Turbo Codes*, pp. 435–446, July 2001.

[Gör01b] N. Görtz. "On the Iterative Approximation of Optimal Joint Source-Channel Decoding". *IEEE Journal on Selected Areas in Communications*, vol. 19, no. 9, pp. 1662–1670, September 2001.

[Gör03] N. Görtz. "Optimization of Bit Mappings for Iterative Source-Channel Decoding". *International Symposium on Turbo Codes & Related Topics*, Brest, France, September 2003.

[Gör07] N. Görtz. *Joint Source-Channel Coding of Discrete-Time Signals with Continuous Amplitudes*. Imperial College Press, September 2007. ISBN 1-86094-845-6.

[HA08] S. Heinen and M. Adrat. "Optimal MMSE Estimation for Vector Sources with Spatially and Temporally Correlated Elements". R. Martin, U. Heute, and C. Antweiler, editors, *Advances in Digital Speech Transmission*, chapter 11, pp. 311–328. John Wiley & Sons, Ltd., January 2008.

[HAFH07] T. Hindelang, M. Adrat, T. Fingscheidt, and S. Heinen. "Joint Source and Channel Coding: From the Beginning until the 'Exit'". *European Transactions on Telecommunications (ETT)*, vol. 18, no. 8, pp. 851–858, April 2007.

[Hag88] J. Hagenauer. "Rate-Compatible Punctured Convolutional Codes (RCPC codes) and their Applications". *IEEE Transactions on Communications*, vol. 36, no. 4, pp. 389–400, April 1988.

[Hag95] J. Hagenauer. "Source-Controlled Channel Decoding". *IEEE Transactions on Communications*, vol. 43, no. 9, pp. 2449–2457, September 1995.

[Hag04] J. Hagenauer. "The EXIT Chart - Introduction To Extrinsic Information Transfer in Iterative Processing". *European Signal Processing Conference (EUSIPCO)*, Vienna, Austria, September 2004.

[HCC01] J. Heo, K. Chung, and K. M. Chugg. "Simple Stopping Criterion for Min-sum Iterative Decoding Algorithm". *Electronics Letters*, vol. 37, no. 25, pp. 1530–1531, December 2001.

[HEA01] X.-Y. Hu, E. Eleftheriou, and D.-M. Arnold. "Progressive Edge-Growth Tanner Graphs". *IEEE Global Telecommunications Conference (GLOBECOM)*, pp. 995–1001, San Antonio, TX, USA, November 2001.

[HEA05] X.-Y. Hu, E. Eleftheriou, and D. M. Arnold. "Regular and Irregular Progressive Edge-Growth Tanner Graphs". *IEEE Transactions on Information Theory*, vol. 51, no. 1, pp. 386–398, January 2005.

[Hei01a] S. Heinen. "An Optimal MMSE-Estimator for Source Codec Parameters Using Intra- and Inter-Frame Correlation". *IEEE International Symposium on Information Theory (ISIT)*, Washington, D.C., USA, June 2001.

[Hei01b] S. Heinen. *Quellenoptimierter Fehlerschutz für digitale Übertragungskanäle.* Aachener Beiträge zu Digitalen Nachrichtensystemen (ABDN) (ed. P. Vary), RWTH Aachen University, 2001. ISBN 3-86073-833-X.

[HEM99a] J. Hokfelt, O. Edfors, and T. Maseng. "Interleaver Design for Turbo Codes Based on the Performance of Iterative Decoding". *IEEE International Conference on Communications (ICC)*, pp. 93–97, Vancouver, Canada, June 1999.

[HEM99b] J. Hokfelt, O. Edfors, and T. Maseng. "Interleaver Structures for Turbo Codes with Reduced Storage Memory Requirement". *IEEE Vehicular Technology Conference (VTC-Fall)*, pp. 1585–1589, Amsterdam, Nederlands, September 1999.

[HEM01] J. Hokfelt, O. Edfors, and T. Maseng. "A Turbo Code Interleaver Design Criterion Based on the Performance of Iterative Decoding". *IEEE Communications Letters*, vol. 5, no. 2, pp. 52–54, February 2001.

[HFSC00a] T. Hindelang, T. Fingscheidt, N. Seshadri, and R. V. Cox. "Combined Source/Channel (De-)Coding: Can A Priori Information Be Used Twice?". *IEEE International Symposium on Information Theory (ISIT)*, p. 266, June 2000.

[HFSC00b] T. Hindelang, T. Fingscheidt, N. Seshadri, and R. V. Cox. "Combined Source/Channel (De-)Coding: Can A Priori Information Be Used Twice?". *IEEE International Conference on Communications (ICC)*, pp. 1208–1212, June 2000.

[HG03] J. Hagenauer and N. Görtz. "The Turbo Principle in Joint Source-Channel Coding". *IEEE Information Theory Workshop*, pp. 275–278, March 2003.

[HH09] J. Huber and T. Hehn. "The Lowest-Possible BER and FER for any Discrete Memoryless Channel with Given Capacity". *IEEE Transactions on Communications*, vol. 57, no. 10, pp. 2849–2852, October 2009.

[HHSX00] T. Hindelang, J. Hagenauer, M. Schmautz, and W. Xu. "Channel Coding Techniques for Adaptive Multi Rate Speech Transmission". *IEEE International Conference on Communications (ICC)*, vol. 2, pp. 744–748, New Orleans, LA, USA, June 2000.

[HHVH00] T. Hindelang, S. Heinen, P. Vary, and J. Hagenauer. "Two Approaches to Combined Source-Channel Coding: A Scientific Competition in Estimating Correlated Parameters". *International Journal of Electronics and Communications (AEÜ)*, vol. 54, no. 6, pp. 364–378, December 2000.

[Hin01] T. Hindelang. *Source-Controlled Channel Encoding and Decoding for Mobile Communications*. PhD thesis, Munich University of Technology, 2001. ISBN 3-18-369510-3.

[HK07] J. Hagenauer and C. Kuhn. "The List-Sequential (LISS) Algorithm and Its Application". *IEEE Transactions on Communications*, vol. 55, no. 5, pp. 918–928, May 2007.

[HKH+00] T. Hindelang, M. Kaindl, J. Hagenauer, M. Schmautz, and W. Xu. "Improved Channel Coding and Estimation for Adaptive Multirate (AMR) Speech Transmission". *IEEE Vehicular Technology Conference (VTC-Spring)*, pp. 1210–1214, Tokyo, Japan, May 2000.

[HLY02] L. Hanzo, T. H. Liew, and B. L. Yeap. *Turbo Coding, Turbo Equalisation and Space-Time Coding for Transmission over Fading Channels*. John Wiley & Sons, Ltd., 2002.

[HN02] A. Hedayat and A. Nosratinia. "On Joint Iterative Decoding of Variable-Length Source Codes and Channel Codes". *Allerton Annual Conference on Communication, Control and Computing*, Montecello, IL, USA, October 2002.

[HNL+07] C. Herzet, N. Noels, V. Lottici, H. Wymeersch, M. Luise, M. Moeneclaey, and L. Vandendorpe. "Code-Aided Turbo Synchronization". *Proceedings of the IEEE*, vol. 95, no. 6, pp. 1255–1271, June 2007.

[Hoc98] B. Hochwald. "Tradeoff Between Source and Channel Coding on a Gaussian Channel". *IEEE Transactions on Information Theory*, vol. 44, no. 7, pp. 3044–3055, November 1998.

[HOP96] J. Hagenauer, E. Offer, and L. Papke. "Iterative Decoding of Binary Block and Convolutional Codes". *IEEE Transactions on Information Theory*, vol. 42, no. 2, pp. 429–445, March 1996.

[HT06] H. Holma and A. Toskala, editors. *HSDPA/HSUPA for UMTS:High Speed Radio Access for Mobile Communications*. John Wiley & Sons, Inc., Chichester, UK, 2006.

[Hu64] G. D. Hu. "On Shannon Theorem and its Converse for Sequence of Communication Schemes in the Case of Abstract Random Variables". *3rd Prague Conference on Information Theory, Statistical Decision Functions, Random Processes*, pp. 285–333, Prague, Czechoslovakia, 1964.

[Huf52] D. A. Huffman. "A Method for the Construction of Minimum Redundancy Codes". *Proceedings of the IRE*, vol. 40, pp. 1098–1101, 1952.

[HV05] S. Heinen and P. Vary. "Source-Optimized Channel Coding for Digital Transmission Channels". *IEEE Transactions on Communications*, vol. 53, no. 4, pp. 592–600, April 2005.

[HZ97] B. Hochwald and K. Zeger. "Tradeoff Between Source and Channel Coding". *IEEE Transactions on Information Theory*, vol. 43, no. 5, pp. 1412–1424, September 1997.

[IEE09] IEEE. "IEEE Standard for Information technology–Telecommunications and information exchange between systems–Local and metropolitan area networks–Specific requirements Part 11: Wireless LAN Medium Access Control (MAC) and Physical Layer (PHY) Specifications Amendment 5: Enhancements for Higher Throughput|". Technical report, Std 802.11n-2009, 2009.

[ITU06] ITU-T. *Recommendation ITU-T G.729.1: G.729 Based Embedded Variable Bit-Rate Coder: An 8-32 kbit/s Scalable Wideband Coder Bitstream Interoperable with G.729*, 2006.

[ITU08] ITU-T. *Recommendation ITU-T G.718: Frame Error Robust Narrow-Band and Wideband Embedded Variable Bit-Rate Coding of Speech and Audio from 8-32 kbit/s*, June 2008.

[ITU10] ITU-D. "Measuring the Information Society", 2010.

[Jin01] H. Jin. *Analysis and Design of Turbo-Like Codes*. PhD thesis, California Institute of Technology, Pasadena, CA, USA, May 2001.

[JKM00] H. Jin, A. Khandekar, and R. J. McEliece. "Irregular Repeat-Accumulate Codes". *International Symposium on Turbo Codes & Related Topics*, Brest, France, September 2000.

[JN84] N. S. Jayant and P. Noll. *Digital Coding of Waveforms: Principles and Applications to Speech and Audio*. Prentice-Hall, 1984.

[Jos99] N. M. Josuttis. *The C++ Standard Library: A Tutorial and Reference Guide*. Addison-Wesley, 1999.

[JV08] X. Jaspar and L. Vandendorpe. "Joint Source-Channel Codes Based on Irregular Turbo Codes and Variable Length Codes". *IEEE Transactions on Communications*, vol. 56, no. 11, pp. 1824–1835, November 2008.

[JZ99] R. Johannesson and K. S. Zigangirov. *Fundamentals of Convolutional Coding*. IEEE Press, 1999.

[KG01] J. Kliewer and N. Görtz. "Soft-Input Source Decoding for Robust Transmission of Compressed Images Using Two-Dimensional Optimal Estimation". *International Conference on Acoustics, Speech, and Signal Processing (ICASSP)*, vol. 4, pp. 2565–2568, May 2001.

[KG02] J. Kliewer and N. Görtz. "Iterative Source-Channel Decoding for Robust Image Transmission". *International Conference on Acoustics, Speech, and Signal Processing (ICASSP)*, vol. 3, pp. 2173–2176, May 2002.

[KG05] J. Kliewer and N. Görtz. "Two-Dimensional Soft-Input Source Decoding for Robust Transmission of Compressed Images". *Electronics Letters*, vol. 41, no. 4, pp. 184–185, February 2005.

[KGM04a] J. Kliewer, N. Görtz, and A. Mertins. "Iterative Source-Channel Decoding for Error-Resilient Image Transmission Using a Markov Random Field". *International ITG Conference on Source and Channel Coding (SCC)*, pp. 305–310, Erlangen, Germany, January 2004.

[KGM04b] J. Kliewer, N. Görtz, and A. Mertins. "On Iterative Source-Channel Image Decoding with Markov Random Field Source Models". *International Conference on Acoustics, Speech, and Signal Processing (ICASSP)*, vol. 4, pp. 661–664, May 2004.

[KGM06] J. Kliewer, N. Görtz, and A. Mertins. "Iterative Source-Channel Decoding With Markov Random Field Source Models". *IEEE Transactions on Signal Processing*, vol. 54, no. 10, pp. 3688–3701, October 2006.

[KHC06] J. Kliewer, A. Huebner, and D. J. Costello, Jr. "On the Achievable Extrinsic Information of Inner Decoders in Serial Concatenation". *IEEE International Symposium on Information Theory (ISIT)*, pp. 2680–2684, July 2006.

[KK03] H. Kfir and I. Kanter. "Parallel Versus Sequential Updating for Belief Propagation Decoding". *Physica A: Statistical Mechanics and its Applications*, vol. 330, no. 1-2, pp. 259–270, December 2003.

[KK09] J. Klejsa and W. B. Kleijn. "Rate Distribution Between Model and Signal for Multiple Descriptions". *International Conference on Acoustics, Speech, and Signal Processing (ICASSP)*, pp. 2489–2492, Taipei, Taiwan, April 2009.

[KKK08] J. Klejsa, M. Kuropatwinski, and W. B. Kleijn. "Adaptive Resolution-Constrained Scalar Multiple-Description Coding". *International Conference on Acoustics, Speech, and Signal Processing (ICASSP)*, pp. 2945–2948, Las Vegas, NV, USA, March 2008.

[KLK10] J. Klejsa, M. Li, and W. B. Kleijn. "FlexCode – Flexible Audio Coding". *International Conference on Acoustics, Speech, and Signal Processing (ICASSP)*, Dallas, TX, USA, March 2010.

[KM02] M. A. Kousa and A. H. Mugaibel. "Puncturing Effects on Turbo Codes". *IEE Proceedings-Communications*, vol. 149, no. 3, pp. 132–138, June 2002.

[KM04] J. Kliewer and A. Mertins. "Soft-Input Reconstruction of Binary Transmitted Quantized Overcomplete Expansions". *IEEE Signal Processing Letters*, vol. 11, no. 11, pp. 899–903, November 2004.

[KM05] J. Kliewer and A. Mertins. "Low Latency Joint Source-Channel Coding Using Overcomplete Expansions and Residual Source Redundancy". *IEEE Global Telecommunications Conference (GLOBECOM)*, St. Louis, MO, USA, December 2005.

[KO07] W. B. Kleijn and A. Ozerov. "Rate Distribution Between Model and Signal". *IEEE Workshop on Applications of Signal Processing to Audio and Acoustics*, pp. 243–246, New Paltz, NY, USA, October 2007.

[Kon04] A. M. Kondoz. *Digital Speech – Coding for Low Bit Rate Communication Systems*. John Wiley & Sons, Inc., 2nd edition, 2004.

[KST04] R. Koetter, A. C. Singer, and M. Tüchler. "Turbo Equalization". *IEEE Signal Processing Magazine*, vol. 21, no. 1, pp. 67–80, January 2004.

[KT02a] J. Kliewer and R. Thobaben. "Combining FEC and optimal soft-input source decoding for the reliable transmission of correlated variable-length encoded signals". *Data Compression Conference (DCC)*, pp. 83–91, Snowbird, UT, USA, April 2002.

[KT02b] J. Kliewer and R. Thobaben. "On the utilization of residual source redundancy for iterative joint source-channel decoding of variable-length codes". *IEEE International Symposium on Information Theory (ISIT)*, Lausanne, Switzerland, June 2002.

[KT03] J. Kliewer and R. Thobaben. "Parallel Concatenated Joint Source-Channel Coding". *Electronics Letters*, vol. 39, no. 23, pp. 1664–1666, November 2003.

[KT05] J. Kliewer and R. Thobaben. "Iterative Joint Source-Channel Decoding of Variable-Length Codes Using Residual Source Redundancy". *IEEE Transactions on Wireless Communications*, vol. 4, no. 3, pp. 919–929, May 2005.

[Lar73] K. Larsen. "Short Convolutional Codes with Maximal Free Distance for Rates 1/2, 1/3 and 1/4". *IEEE Transactions on Information Theory*, vol. 19, no. 3, pp. 371–372, May 1973.

[LC88] C. R. Laymeyer and K. M. Cheung. "Long Decoding Runs for Galileo's Convolutional Codes". Telecommunications and Data Acquisition Progress Report 42-95, Jet Propulsion Laboratory, Pasadena, CA, USA, July 1988.

[LC04] S. Lin and D. J. Costello, Jr. *Error Control Coding*. Prentice Hall, 2nd edition, 2004.

[LCC00] G. Lanzetta, H. A. Cabral, and D. J. Costello, Jr. "Soft-Input/Soft-Output Sequential Decoding". *International Symposium on Information Theory and its Applications (ISITA)*, Honolulu, HI, USA, November 2000.

[LESV09] H. Lüders, B. Eschbach, L. Schmalen, and P. Vary. "OFDM Turbo DeCodulation with EXIT Optimized Bit Loading and Signal Constellations". *International Conference on Acoustics, Speech, and Signal Processing (ICASSP)*, pp. 2589–2592, Taipei, Taiwan, April 2009.

[LHHH05] I. Land, S. Huettinger, P. A. Hoeher, and J. B. Huber. "Bounds on Information Combining". *IEEE Transactions on Information Theory*, vol. 51, no. 2, pp. 612–619, February 2005.

[LK01] F. Lahouti and A. Khandani. "Approximating and Exploiting the Residual Redundancies – Applications to Efficient Reconstruction of Speech over Noisy Channels". *International Conference on Acoustics, Speech, and Signal Processing (ICASSP)*, May 2001.

[LK03] X. Liu and S. N. Koh. "Simplification of Soft-bit Speech Decoding and Application to MELP Encoded Speech". *Electronics Letters*, vol. 39, no. 3, pp. 332–333, February 2003.

[LK04] F. Lahouti and A. K. Khandani. "Reconstruction of Predictively Encoded Signals Over Noisy Channels Using a Sequence MMSE Decoder". *IEEE Transactions on Communications*, vol. 52, no. 8, pp. 1292–1301, August 2004.

[LK07] M. Li and W. B. Kleijn. "A Low-Delay Audio Coder with Constrained-Entropy Quantization". *IEEE Workshop on Applications of Signal Processing to Audio and Acoustics*, pp. 191–194, October 2007.

[Llo82] S. P. Lloyd. "Least Squares Quantization in PCM". *IEEE Transactions on Information Theory*, vol. 28, no. 2, pp. 129–137, March 1982.

[LR97] X. Li and J. A. Ritcey. "Bit-Interleaved Coded Modulation with Iterative Decoding". *IEEE Communications Letters*, vol. 1, no. 6, pp. 169–171, November 1997.

[LR99] X. Li and J. A. Ritcey. "Bit-Interleaved Coded Modulation with Iterative Decoding". *IEEE International Conference on Communications (ICC)*, Vancouver, BC, Canada, June 1999.

[LSV08] H. Lüders, L. Schmalen, and P. Vary. "Approximating EXIT Characteristics of Soft Demodulators in OFDM BICM-ID Systems for Time Variant Frequency Selective Fading Channels". *International ITG Conference on Source and Channel Coding (SCC)*, Ulm, Germany, January 2008.

[LTV05] K. Lakovic, T. Tian, and J. Villasenor. "Iterative Decoder Design for Joint Source-Channel LDPC Coding". *International Conference on Computer as a Tool (EUROCON)*, pp. 486–489, Belgrade, Serbia and Montenegro, November 2005.

[LV02] K. Lakovic and J. Villasenor. "Combining Variable Length Codes and Turbo Codes". *IEEE Vehicular Technology Conference (VTC-Spring)*, pp. 1719–1723, Birmingham, AL, USA, May 2002.

[LW07] F.-M. Li and A.-Y. Wu. "On the New Stopping Criteria of Iterative Turbo Decoding by Using Decoding Threshold". *IEEE Transactions on Signal Processing*, vol. 55, no. 11, pp. 5506–5516, November 2007.

[Mac99] D. J. C. MacKay. "Good Error-Correcting Codes Based on Very Sparse Matrices". *IEEE Transactions on Information Theory*, vol. 45, no. 2, pp. 399–431, March 1999.

[Man74] D. M. Mandelbaum. "An Adaptive-Feedback Coding Scheme Using Incremental Redundancy". *IEEE Transactions on Information Theory*, vol. 20, no. 3, pp. 388–389, May 1974.

[Mar04] C. Martinez. "Partial Quicksort". *ACM-SIAM Workshop on Analytic Algorithmics and Combinatorics (ANALCO)*, New Orleans, LA, USA, January 2004.

[Max60] J. Max. "Quantizing for Minimum Distortion". *IEEE Transactions on Information Theory*, vol. 6, no. 1, pp. 7–12, March 1960.

[MB02] P. Mitran and J. Bajcsy. "Turbo Source Coding: A Noise-Robust Approach to Data Compression". *Data Compression Conference (DCC)*, p. 465, Snowbird, UT, USA, April 2002.

[MC78] J. L. Melsa and D. L. Cohn. *Decision and Estimation Theory.* McGray-Hill, 1978.

[MH09a] R. G. Maunder and L. Hanzo. "Concatenated Irregular Variable Length Coding and Irregular Unity Rate Coding". *IEEE Vehicular Technology Conference (VTC-Spring)*, pp. 1–5, Barcelona, Spain, April 2009.

[MH09b] R. G. Maunder and L. Hanzo. "Near-Capacity Irregular Variable Length Coding and Irregular Unity Rate Coding". *IEEE Transactions on Wireless Communications*, vol. 8, no. 11, pp. 5500–5507, November 2009.

[MIF06] P. A. Martin, M. Isaka, and M. P. C. Fossorier. "Serial Concatenation of Linear Block Codes and a Rate-1 Convolutional Code". *International Symposium on Turbo Codes & Related Topics and International ITG Conference on Source and Channel Coding (SCC)*, Munich, Germany, April 2006.

[MN77] F. MacWilliams and N.Sloane. *The Theory of Error-Correcting Codes.* North Holland, 1977.

[MN96] D. J. C. MacKay and R. M. Neal. "Near Shannon Limit Performance of Low Density Parity Check Codes". *Electronics Letters*, vol. 32, no. 18, July 1996.

[MN97] D. J. C. MacKay and R. M. Neal. "Near Shannon Limit Performance of Low Density Parity Check Codes". *Electronics Letters*, vol. 33, no. 6, pp. 457–458, March 1997.

[Moo05] T. K. Moon. *Error Correction Coding - Mathematical Methods and Algorithms*. John Wiley & Sons, Inc., 2005.

[Mur88] K. G. Murty. "Linear Complementarity, Linear and Nonlinear Programming". *Sigma Series in Applied Mathematics*, vol. 3. Heldermann Verlag, 1988.

[MWN+07] R. G. Maunder, J. Wang, S. X. Ng, L.-L. Yang, and L. Hanzo. "Iteratively Decoded Irregular Variable Length Coding and Trellis Coded Modulation". *IEEE Workshop on Signal Processing Systems (SiPS)*, pp. 222–227, Shanghai, China, October 2007.

[MWN+08] R. G. Maunder, J. Wang, S. X. Ng, L.-L. Yang, and L. Hanzo. "On the Performance and Complexity of Irregular Variable Length Codes for Near-Capacity Joint Source and Channel Coding". *IEEE Transactions on Wireless Communications*, vol. 7, no. 4, pp. 1338–1347, April 2008.

[NA94] NTT-AT. "Multi-Lingual Speech Database for Telephonometry", 1994. http://www.ntt-at.com/products_e/speech/index.html.

[NB08] H. H. Nguyen and T. Q. Bui. "Bit-Interleaved Coded OFDM With Iterative Decoding in Impulsive Noise". *IEEE Transactions on Power Delivery*, vol. 23, no. 2, pp. 640–649, April 2008.

[NEO+08] Nasruminallah, M. El-Hajjar, N. S. Othman, A. P. Quang, and L. Hanzo. "Over-Complete Mapping Aided, Soft-Bit Assisted Iterative Unequal Error Protection H.264 Joint Source and Channel Decoding". *IEEE Vehicular Technology Conference (VTC-Fall)*, pp. 1–5, Calgary, Canada, September 2008.

[NH08] Nasruminallah and L. Hanzo. "Short Block Codes for Guaranteed Convergence in Soft-bit Assisted Iterative Joint Source and Channel Decoding". *Electronics Letters*, vol. 44, no. 22, pp. 1315–1316, October 2008.

[NH09a] Nasruminallah and L. Hanzo. "Convergence Behaviour of Iteratively Decoded Short Block-Codes in H.264 Joint Source and Channel Decoding". *IEEE Vehicular Technology Conference (VTC-Spring)*, pp. 1–5, Barcelona, Spain, April 2009.

[NH09b] Nasruminallah and L. Hanzo. "EXIT-Chart Optimized Short Block Codes for Iterative Joint Source and Channel Decoding in H.264 Video Telephony". *IEEE Transactions on Vehicular Technology*, vol. 58, no. 8, pp. 4306–4315, October 2009.

[NHD+03] N. Noels, C. Herzet, A. Dejonghe, V. Lottici, H. Steendam, M. Moeneclaey, M. Luise, and L. Vandendorp. "Turbo Synchronization: An EM Algorithm Interpretation". *IEEE International Conference on Communications (ICC)*, pp. 2933–2937, Anchorage, AK, USA, May 2003.

[NW06] J. Nocedal and S. Wright. *Numerical Optimization*. Springer, 2006.

[OEA+09] N. S. Othman, M. El-Hajjar, O. Alamri, S. X. Ng, and L. Hanzo. "Iterative AMR-WB Source and Channel Decoding Using Differential Space-Time Spreading-Assisted Sphere-Packing Modulation". *IEEE Transactions on Vehicular Technology*, vol. 58, no. 1, pp. 484–490, January 2009.

[OEAH07] N. S. Othman, M. El-Hajjar, O. Alamri, and L. Hanzo. "Soft-Bit Assisted Iterative AMR-WB Source-Decoding and Turbo-Detection of Channel-Coded Differential Space-Time Spreading Using Sphere Packing Modulation". *IEEE Vehicular Technology Conference (VTC-Spring)*, pp. 2010–2014, Dublin, Ireland, April 2007.

[OSI96] OSI. *Information Technology – Open Systems Interconnection – Basic Reference Model: The Basic Model*, June 1996. ISO/IEC 7498-1.

[OV09] P. Ojala and A. Vasilache. "FlexCode Deliverable 4.3 - Report on FlexCode Hardware Demonstration". Technical report, European Union, June 2009. http://www.flexcode.eu.

[PDL+90] S. S. Pietrobon, R. H. Deng, A. Lafanechere, G. Ungerboeck, and D. J. Costello, Jr. "Trellis-Coded Multidimensional Phase Modulation". *IEEE Transactions on Information Theory*, vol. 36, no. 1, pp. 63–89, January 1990.

[PDLF05] C. Poulliat, D. Declercq, C. Lamy-Bergot, and I. Fijalkow. "Analysis and Optimization of Irregular LDPC Codes for Joint Source-Channel Decoding". *IEEE Communications Letters*, vol. 9, no. 12, pp. 1064–1066, December 2005.

[PE10] D. Persson and T. Eriksson. "On Multiple Description Coding of Sources with Memory". *IEEE Transactions on Communications*, vol. 58, no. 8, pp. 2242–2251, August 2010.

[Pea88] J. Pearl. *Probabilistic Reasoning in Intelligent Systems: Networks of Plausible Inference*. Morgan Kaufmann, 1988.

[PKH01] R. Perkert, M. Kaindl, and T. Hindelang. "Iterative Source and Channel Decoding for GSM". *International Conference on Acoustics, Speech, and Signal Processing (ICASSP)*, pp. 2649–2652, Salt Lake City, UT, USA, May 2001.

[Poo00] H. V. Poor. "Turbo Multiuser Detection: An Overview". *International Spread Spectrum Techniques and Applications Symposium (ISSTAS)*, pp. 583–587, Parsippany, NJ, USA, September 2000.

[Poo04] H. V. Poor. "Iterative Multiuser Detection". *IEEE Signal Processing Magazine*, vol. 21, no. 1, pp. 81–88, January 2004.

[PPR04] S. S. Pradhan, R. Puri, and K. Ramchandran. "n-Channel Symmetric Multiple Descriptions - Part I: (n, k) Source-Channel Erasure Codes". *IEEE Transactions on Information Theory*, vol. 50, no. 1, pp. 47–61, January 2004.

[PR99] R. Puri and K. Ramchandran. "Multiple Description Source Coding Using Forward Error Correction Codes". *Asilomar Conference on Signals, Systems and Computers*, Pacific Grove, CA, USA, October 1999.

[Pro00] J. G. Proakis. *Digital Communications*. McGraw Hill, 4th edition, 2000.

[PU02] A. Papoulis and S. Unnikrishna Pillai. *Probability, Random Variables and Stochastic Processes*. McGraw Hill, international edition, 2002.

[PYH07] A. Q. Pham, L. L. Yang, and L. Hanzo. "Joint Optimization of Iterative Source and Channel Decoding Using Over-Complete Source Mapping". *IEEE Vehicular Technology Conference (VTC-Fall)*, Baltimore, MD, USA, September 2007.

[PYOH08] A. Q. Pham, L. L. Yang, N. S. Othman, and L. Hanzo. "EXIT-Chart Optimized Block Codes for Wireless Video Telephony". *IEEE Transactions on Circuits and Systems for Video Technology*, vol. 18, no. 12, pp. 1671–1680, December 2008.

[Ree54] I. Reed. "A Class of Multiple-Error-Correcting Codes and the Decoding Scheme". *IRE Professional Group on Information Theory*, vol. 4, no. 4, pp. 38–49, September 1954.

[Rei06] J. Reimes. "Entwicklung eines generischen Kanalmodells für digitale Kommunikationssysteme". Diploma thesis, Institute of Communications Systems and Data Processing (IND), RWTH Aachen University, April 2006.

[Rot06] R. M. Roth. *Introduction to Coding Theory*. Cambridge University Press, 2006.

[RS60] I. S. Reed and G. Solomon. "Polynomial Codes over Certain Finite Fields". *Journal of the Society for Industrial and Applied Mathematics (SIAM)*, vol. 8, no. 2, pp. 300–304, June 1960.

[RSU01] T. J. Richardson, M. A. Shokrollahi, and R. L. Urbanke. "Design of Capacity-Approaching Irregular Low-Density Parity-Check Codes". *IEEE Transactions on Information Theory*, vol. 47, no. 2, pp. 619–637, February 2001.

[RVH95] P. Robertson, E. Villebrun, and P. Hoeher. "A Comparison of Optimal and Sub-Optimal MAP Decoding Algorithms Operating in the Log Domain". *IEEE International Conference on Communications (ICC)*, pp. 1009–1013, Seattle, WA, USA, June 1995.

[SA05] L. Schmalen and M. Adrat. "An Iterative, Turbo-like Approach to Convolutional Decoding". *9th International Student Conference on Electrical Engineering (POSTER 2005)*, Prague, Czech Republic, May 2005.

[SACV11] L. Schmalen, M. Adrat, T. Clevorn, and P. Vary. "EXIT-Chart Based System Design for Iterative Source-Channel Decoding with Fixed-Length Codes". *IEEE Transactions on Communications*, 2011. accepted for publication.

[Sam04] J. Samuelsson. "Waveform Quantization of Speech Using Gaussian Mixture Models". *International Conference on Acoustics, Speech, and Signal Processing (ICASSP)*, vol. 1, Montreal, Canada, May 2004.

[SB91] K. Sayood and J. Borkenhagen. "Use of Residual Redundancy in the Design of Joint Source/Channel Coders". *IEEE Transactions on Communications*, vol. 39, no. 6, pp. 838–846, June 1991.

[Sch05] L. Schmalen. "Innovative Algorithmen zur effizienten Decodierung von Faltungscodes". Diploma thesis, Institute of Communications Systems and Data Processing (IND), RWTH Aachen University, April 2005.

[Sch06] B. Schotsch. "Turbo DeCodulation with LDPC Codes: Joint Source Decoding, Channel Decoding and Demodulation based on Graphs". Diploma thesis, Institute of Communications Systems and Data Processing (IND), RWTH Aachen University, May 2006.

[Sch08] T. Schlien. "Iterative Quellen-Kanal Decodierung für die flexible Übertragung von Audio und Sprache". Diploma thesis, Institute of Communications Systems and Data Processing (IND), RWTH Aachen University, August 2008.

[SCV07] L. Schmalen, T. Clevorn, and P. Vary. "Iterative Source-Coded Equalization: Turbo Error Concealment for ISI Channels". *IEEE Workshop on Signal Processing Advances in Wireless Communications (SPAWC)*, Helsinki, Finland, June 2007.

[Sew08] J. Seward. "A Program and Library for Data Compression. Bzip2 and libbzip2". http://www.bzip.org, 2008. version 1.0.5.

[Sha48] C. E. Shannon. "A Mathematical Theory of Communication". *The Bell System Technical Journal*, vol. 27, pp. 379–423, 623–656, July and October 1948.

[Sha59] C. E. Shannon. "Probability of Error for Optimal Codes in a Gaussian Channel". *The Bell System Technical Journal*, vol. 38, pp. 611–656, May 1959.

[Sha61] C. E. Shannon. "Two-Way Communication Channels". *Berkeley Symposium on Mathematics, Statistics, and Probability*, vol. 1, pp. 611–644, 1961.

[SLF99] R. Y. Shao, S. Lin, and M. P. C. Fossorier. "Two Simple Stopping Criteria for Turbo Decoding". *IEEE Transactions on Communications*, vol. 47, no. 8, pp. 1117–1120, August 1999.

[SM06] L. Schmitt and H. Meyr. "Turbo Decoding as an Approximative Iterative Solution to Maximum Likelihood Sequence Detection". *International Symposium on Turbo Codes & Related Topics and International ITG Conference on Source and Channel Coding (SCC)*, Munich, Germany, April 2006.

[SM09] P. M. Szecówka and T. Mandrysz. "Towards Hardware Implementation of bzip2 Data Compression Algorithm". *International Conference on Mixed Design of Integrated Circuits and Systems*, Łódź, Poland, June 2009.

[SMB+09] M. R. Stoufs, A. Munteanu, J. Barbarien, J. Cornelis, and P. Schelkens. "Optimized Scalable Multiple-Description Coding and FEC-based Joint Source-Channel Coding: A Performance Comparison". *Workshop on Image Analysis and Multimedia Interactive Services (WIAMIS)*, London, United Kingdom, May 2009.

[Sri99] M. Srinivasan. "Iterative Decoding of Multiple Descriptions". *Data Compression Conference (DCC)*, Snowbird, UT, USA, March 1999.

[SSA99] A. Shibutani, H. Suda, and F. Adachi. "Reducing Average Number of Turbo Decoding Iterations". *Electronics Letters*, vol. 35, no. 9, pp. 70–71, April 1999.

[SSJ+08] L. Schmalen, B. Schotsch, M. Jeub, P. Vary, and T. Clevorn. "The FlexCode Channel Coding Approach". *ITG Conference on Speech Communication*, Aachen, Germany, October 2008.

[SSV08] L. Schmalen, T. Schlien, and P. Vary. "FlexCode Deliverable 2.3 - Final Channel Coder". Technical report, European Union, October 2008. http://www.flexcode.eu.

[SSV10] L. Schmalen, T. Schlien, and P. Vary. "The FlexCode Source-Channel Coding Approach for Audio and Speech Transmission". *International ITG Conference on Source and Channel Coding (SCC)*, Siegen, Germany, January 2010.

[SSVC08] B. Schotsch, L. Schmalen, P. Vary, and T. Clevorn. "Graph-Based Turbo DeCodulation with LDPC Codes". *IEEE Vehicular Technology Conference (VTC-Spring)*, pp. 772–776, Singapore, May 2008.

[STPM09] M. Sybis, P. Tyczka, S. Papaharalabos, and P. T. Mathiopoulos. "Reduced-Complexity Algorithms for Near-Optimal Decoding of Turbo TCM Codes". *Electronics Letters*, vol. 45, no. 5, pp. 278–279, February 2009.

[SV07] B. Schotsch and P. Vary. "FlexCode Deliverable 2.1 - BISO Channel Model". Technical report, European Union, July 2007. http://www.flexcode.eu.

[SV09] L. Schmalen and P. Vary. "Near-Lossless Compression and Protection by Turbo Source-Channel (De-)Coding Using Irregular Index Assignments". *International Conference on Acoustics, Speech, and Signal Processing (ICASSP)*, pp. 2485–2488, Taipei, Taiwan, April 2009.

[SV10a] L. Schmalen and P. Vary. "Error Resilient Turbo Compression of Source Codec Parameters Using Inner Irregular Codes". *International ITG Conference on Source and Channel Coding (SCC)*, Siegen, Germany, January 2010.

[SV10b] L. Schmalen and P. Vary. "Reconstruction of Multiple Descriptions by MMSE Estimation". *ITG Conference on Speech Communication*, Bochum, Germany, October 2010.

[SVA08] L. Schmalen, P. Vary, and M. Adrat. "Reduced-Search Source Decoders for Iterative Source-Channel Decoding". *ITG Conference on Speech Communication*, Aachen, Germany, October 2008.

[SVAC07] L. Schmalen, P. Vary, M. Adrat, and T. Clevorn. "On the EXIT Characteristics of Feed Forward Convolutional Codes". *IEEE International Symposium on Information Theory (ISIT)*, pp. 2686–2690, Nice, France, June 2007.

[SVAC08] L. Schmalen, P. Vary, M. Adrat, and T. Clevorn. "Complexity-Reduced Iterative Source-Channel Decoding by Conditional Quantization". *International Symposium on Turbo Codes & Related Topics*, pp. 327–332, Lausanne, Switzerland, September 2008.

[SVC07] B. Schotsch, P. Vary, and T. Clevorn. "Adaptive Exploitation of Residual Redundancy in Iterative Source-Channel Decoding". *IEEE International Symposium on Personal, Indoor, and Mobile Radio Communications (PIMRC)*, Athens, Greece, September 2007.

[SVC08] L. Schmalen, P. Vary, and T. Clevorn. "FlexCode Deliverable 2.2 - Baseline Channel Coder". Technical report, European Union, February 2008. http://www.flexcode.eu.

[SVCA10] L. Schmalen, P. Vary, T. Clevorn, and M. Adrat. "Turbo Source Compression with Jointly Optimized Inner Irregular and Outer Irregular Codes". *IEEE Vehicular Technology Conference (VTC-Fall)*, Ottawa, Canada, September 2010.

[SVCS08] L. Schmalen, P. Vary, T. Clevorn, and B. Schotsch. "Efficient Iterative Source-Channel Decoding Using Irregular Index Assignments". *International ITG Conference on Source and Channel Coding (SCC)*, Ulm, Germany, January 2008.

[SWBM05] F. Simoens, H. Wymeersch, H. Bruneel, and M. Moeneclaey. "Multi-dimensional Mapping for Bit-Interleaved Coded Modulation with BPSK/QPSK Signaling". *IEEE Communications Letters*, vol. 9, no. 5, pp. 453–455, May 2005.

[SWM04] F. Simoens, H. Wymeersch, and M. Moeneclaey. "Spatial mapping for MIMO systems". *IEEE Information Theory Workshop*, San Antonio, TX, USA, October 2004.

[SWM05] F. Simoens, H. Wymeersch, and M. Moeneclaey. "Multi-dimensional Mapping for Bit-Interleaved Coded Modulation". *IEEE Vehicular Technology Conference (VTC-Spring)*, Stockholm, Sweden, May 2005.

[SY05] U. Samarawickrama and P. Yahampath. "Joint Source-Channel Decoding of Multiple Descriptions". *Canadian Conference on Electrical and Computer Engineering (CCECE)*, Saskatoon, Canada, May 2005.

[tB99a] S. ten Brink. "Convergence of Iterative Decoding". *Electronics Letters*, vol. 35, no. 10, pp. 806–808, May 1999.

[tB99b] S. ten Brink. "Convergence of Iterative Decoding". *Electronics Letters*, vol. 35, no. 13, pp. 1117–1119, June 1999.

[tB00a] S. ten Brink. "Rate One-Half Code for Approaching the Shannon Limit by 0.1 dB". *Electronics Letters*, vol. 36, no. 15, pp. 1293–1294, July 2000.

[tB00b] S. ten Brink. "Design of Serially Concatenated Codes based on Iterative Convergence". *International Symposium on Turbo Codes & Related Topics*, Brest, France, September 2000.

[tB00c] S. ten Brink. "Design of Serially Concatenated Codes based on Iterative Decoding Convergence". *International Journal of Electronics and Communications (AEÜ)*, vol. 54, no. 6, pp. 389–398, December 2000.

[tB01a] S. ten Brink. *Design of Concatenated Coding Schemes based on Iterative Decoding Convergence*. PhD thesis, University of Stuttgart, April 2001.

[tB01b] S. ten Brink. "Code Doping for Triggering Iterative Decoding Convergence". *IEEE International Symposium on Information Theory (ISIT)*, p. 235, June 2001.

[tB01c] S. ten Brink. "Convergence Behavior of Iteratively Decoded Parallel Concatenated Codes". *IEEE Transactions on Communications*, vol. 49, no. 10, pp. 1727–1737, October 2001.

[tB01d] S. ten Brink. "Exploiting the Chain Rule of Mutual Information for the Design of Iterative Decoding Schemes". *Allerton Annual Conference on Communication, Control and Computing*, Monticello, IL, USA, October 2001.

[TDB07] A. Tarable, L. Dinoi, and S. Benedetto. "Design of Prunable Interleavers for Parallel Turbo Decoder Architectures". *IEEE Communications Letters*, vol. 11, no. 2, pp. 167–169, February 2007.

[TH02] M. Tüchler and J. Hagenauer. "EXIT Charts of Irregular Codes". *Conference on Information Sciences and Systems (CISS)*, Princeton, NJ, USA, March 2002.

[Tho07a] R. Thobaben. "A New Transmitter Concept for Iteratively-Decoded Source-Channel Coding Schemes". *IEEE Workshop on Signal Processing Advances in Wireless Communications (SPAWC)*, pp. 1–5, Helsinki, Finland, June 2007.

[Tho07b] R. Thobaben. "EXIT Functions for Randomly Punctured Systematic Codes". *IEEE Information Theory Workshop*, pp. 24–29, Lake Tahoe, CA, USA, September 2007.

[Tho07c] R. Thobaben. *Iterative Quellen- und Kanaldecodierung für Codes variabler Länge*. PhD thesis, Christian-Albrechts-Universität zu Kiel, 2007.

[TK03] R. Thobaben and J. Kliewer. "Robust decoding of variable-length encoded Markov sources using a three-dimensional trellis". *IEEE Communications Letters*, vol. 7, no. 7, pp. 320–322, July 2003.

[TK05] R. Thobaben and J. Kliewer. "Low-Complexity Iterative Joint Source-Channel Decoding for Variable-Length Encoded Markov Sources". *IEEE Transactions on Communications*, vol. 53, no. 12, pp. 2054–2064, December 2005.

[TK06] R. Thobaben and J. Kliewer. "Design Considerations for Iteratively-decoded Source-Channel Coding Schemes". *Allerton Annual Conference on Communication, Control and Computing*, Monticello, IL, USA, September 2006.

[TK09] R. Thobaben and J. Kliewer. "An Efficient Variable-length Code Construction for Iterative Source-Channel Decoding". *IEEE Transactions on Communications*, vol. 57, no. 7, pp. 2005–2013, July 2009.

[TKS02] M. Tüchler, R. Koetter, and A. C. Singer. "Turbo Equalization: Principles and New Results". *IEEE Transactions on Communications*, vol. 50, no. 5, pp. 754–767, May 2002.

[TM01] D. S. Taubmann and M. W. Marcellin. *JPEG2000: Image Compression Fundamentals, Standards, and Practices*. Kluwer Academic Publishers, 2001.

[TN04] N. H. Tran and H. H. Nguyen. "Improving the Performance of QPSK BICM-ID by Mapping on the Hypercube". *IEEE Vehicular Technology Conference (VTC-Fall)*, Los Angeles, CA, USA, September 2004.

[Tsc11] M. Tschauner. "Turbo Source Coding for an Efficient Packet-Based Transmission of Multimedia Signals". Diploma thesis, Institute of Communications Systems and Data Processing (IND), RWTH Aachen University, March 2011.

[TSV08] R. Thobaben, L. Schmalen, and P. Vary. "Joint Source-Channel Coding with Inner Irregular Codes". *IEEE International Symposium on Information Theory (ISIT)*, pp. 1153–1157, Toronto, Canada, July 2008.

[TtBH02] M. Tüchler, S. ten Brink, and J. Hagenauer. "Measures for Tracing Convergence of Iterative Decoding Algorithms". *International ITG Conference on Source and Channel Coding (SCC)*, pp. 53–60, Berlin, Germany, January 2002.

[Tüc02] M. Tüchler. "Convergence Prediction for Iterative Decoding of Threefold Concatenated Systems". *IEEE Global Telecommunications Conference (GLOBECOM)*, pp. 1358–1362, November 2002.

[Tüc03] M. Tüchler. "Design of Serially Concatenated Systems for Long or Short Block Lengths". *IEEE International Conference on Communications (ICC)*, pp. 2948–2952, May 2003.

[Tüc04] M. Tüchler. "Design of Serially Concatenated Systems Depending on the Block Length". *IEEE Transactions on Communications*, vol. 52, no. 2, pp. 209–218, February 2004.

[Vai93] V. A. Vaishampayan. "Design of Multiple Description Scalar Quantizers". *IEEE Transactions on Information Theory*, vol. 39, no. 3, pp. 821–834, May 1993.

[Vit67] A. J. Viterbi. "Error Bounds for Convolutional Codes and an Asymptotically Optimum Decoding Algorithm". *IEEE Transactions on Information Theory*, vol. 13, no. 2, pp. 260–269, April 1967.

[VM06] P. Vary and R. Martin. *Digital Speech Transmission – Enhancement, Coding and Error Concealment*. John Wiley & Sons, Inc., Chichester, UK, 2006. ISBN 0-471-56018-9.

[Vol09] M. Volmer. "Massively Parallel Implementation of Modern Communication Algorithms Using Graphic Cards". Diploma thesis, Institute of Communications Systems and Data Processing (IND), RWTH Aachen University, December 2009.

[VVS94] S. Vembu, S. Verdú, and Y. Steinberg. "When Does the Source-Channel Separation Theorem Hold". *IEEE International Symposium on Information Theory (ISIT)*, Trondheim, Norway, June 1994.

[VVS95] S. Vembu, S. Verdú, and Y. Steinberg. "The Source-Channel Separation Theorem Revisited". *IEEE Transactions on Information Theory*, vol. 41, no. 1, pp. 44–54, January 1995.

[VY00] B. Vucetic and J. Yuan. *Turbo Codes: Principles and Applications*. Kluwer Academic Publishers, 2000.

[WB94] S. B. Wicker and V. K. Bhargava, editors. *Reed-Solomon Codes and their Applications*. IEEE Press, 1994.

[WDW04] X. Wu, S. Dumitrescu, and Z. Whang. "Monotonicity-Based Fast Algorithms for MAP Estimation of Markov Sequences Over Noisy Channels". *IEEE Transactions on Information Theory*, vol. 50, no. 7, pp. 1539–1544, July 2004.

[Wei87] L.-F. Wei. "Trellis Coded Modulation with Multidimensional Constellations". *IEEE Transactions on Information Theory*, vol. 33, no. 4, pp. 483–501, July 1987.

[Wei01] C. Weiß. *Error Correction with Tail-Biting Convolutional Codes*. PhD thesis, TU München, December 2001.

[Wic95] S. B. Wicker. *Error Control Systems for Digital Communication and Storage*. Prentice Hall, Englewood Cliffs, NJ, USA, 1995.

[WKM10] T. C. Wong, H. M. Kwon, and A. Mukherjee. "Hybrid Multi-Dimensional Modulation for Gaussian and Fading Channels". *IEEE Vehicular Technology Conference (VTC-Fall)*, Ottawa, Canada, September 2010.

[WM04] K. K. Y. Wong and P. J. McLane. "Bi-directional Soft-output M-algorithm for Iterative Decoding". *IEEE International Conference on Communications (ICC)*, vol. 2, pp. 792–797, Paris, France, June 2004.

[WR61] J. Wozencraft and B. Reiffen. *Sequential Decoding*. MIT Press, Cambridge, MA, USA, 1961.

[WW06] X. Wu and X. Wang. "Joint Source-Channel Decoding of Multiple Description Quantized Markov Sequences". *Data Compression Conference (DCC)*, Snowbird, UT, USA, March 2006.

[WWE00] Y. Wu, B. D. Woerner, and W. J. Ebel. "A Simple Stopping Criterion for Turbo Decoding". *IEEE Communications Letters*, vol. 4, no. 8, pp. 258–260, August 2000.

[WWW09] X. Wu, X. Wang, and Z. Wang. "Resource-Scalable Joint Source-Channel MAP and MMSE Estimation of Multiple Descriptions". *IEEE Transactions on Signal Processing*, vol. 57, no. 1, pp. 279–288, January 2009.

[YS05] P. Yahampath and U. Samarawickrama. "Joint Source-Channel Decoding of Convolutionally Encoded Multiple-Descriptions". *IEEE Global Telecommunications Conference (GLOBECOM)*, St. Louis, MO, USA, November 2005.

[Zeh92] E. Zehavi. "8-PSK Trellis Codes for a Rayleigh Channel". *IEEE Transactions on Communications*, vol. 40, no. 5, pp. 873–884, May 1992.

[ZF02] J. Zhang and M. P. C. Fossorier. "Shuffled Belief Propagation Decoding". *Asilomar Conference on Signals, Systems and Computers*, 2002.

[ZG90] K. Zeger and A. Gersho. "Pseudo-Gray Coding". *IEEE Transactions on Communications*, vol. 38, no. 12, pp. 2147–2158, December 1990.

[Ziv85] J. Ziv. "On Universal Quantization". *IEEE Transactions on Information Theory*, vol. 31, no. 3, pp. 344–347, May 1985.

[ZKK09] G. Zhang, J. Klejsa, and W. B. Kleijn. "Analysis of K-Channel Multiple Description Quantization". *Data Compression Conference (DCC)*, pp. 53–62, Snowbird, UT, USA, March 2009.

[ZL77] J. Ziv and A. Lempel. "A Universal Algorithm for Sequential Data Compression". *IEEE Transactions on Information Theory*, vol. 23, no. 3, pp. 337–343, May 1977.

[ZPBF04] E. Zimmermann, P. Pattisapu, P. K. Bora, and G. Fettweis. "Reduced Complexity LDPC Decoding Using Forced Convergence". *International Symposium on Wireless Personal Multimedia Communications (WPMC)*, Abano Terme, Italy, September 2004.

[ZSN08] D. Zhao, J. Samuelsson, and M. Nilsson. "On Entropy-Constrained Vector Quantization Using Gaussian Mixture Models". *IEEE Transactions on Communications*, vol. 56, no. 12, pp. 2094–2104, December 2008.